NUCLEAR INSTRUMENTS & METHODS

A JOURNAL ON ACCELERATORS, INSTRUMENTATION
AND TECHNIQUES IN NUCLEAR PHYSICS

EDITOR: K. SIEGBAHN – UPPSALA

VOLUME 11

JANUARY 1961 — MAY 1961

NORTH-HOLLAND PUBLISHING COMPANY — AMSTERDAM

PRINTED IN THE NETHERLANDS
DRUKKERIJ MEIJER N.V. WORMERVEER AND AMSTERDAM

NUCLEAR INSTRUMENTS AND METHODS

EDITORIAL BOARD:

J. B. ADAMS (CERN)
F. A. ALSINA (Buenos Aires)
E. AMALDI (Rome)
H. L. ANDERSON (Chicago)
K. T. BAINBRIDGE (Cambridge, Mass.)
P. R. BELL (Oak Ridge)
R. E. BELL (Montreal)
A. BERTHELOT (Saclay)
H. BRINKMAN (Groningen)
E. H. COOKE–YARBOROUGH (Harwell)
S. DE BENEDETTI (Pittsburgh)
M. DE HEMPTINNE (Louvain)
A. DE-SHALIT (Rehovoth)
M. DEUTSCH (Cambridge, Mass.)
S. DU TOIT (Pretoria)
B. S. DŽELEPOV (Leningrad)
W. GENTNER (Heidelberg)
P. C. GUGELOT (Amsterdam)
H. HALBAN (Paris)
O. HAXEL (Heidelberg)
P. HUBER (Basel)
S. KIKUCHI (Tokyo)
J. KOCH (Copenhagen)
M. S. KOZODAEV (Moscow)
S. LIVINGSTON (Cambridge, Mass)
E. M. MCMILLAN (Berkeley)
M. G. MEŠČERJAKOV (Moscow)
P. B. MOON (Birmingham)
M. L. OLIPHANT (Canberra)
W. PAUL (Bonn)
A. S. RAO (Bombay)
G. SALVINI (Rome)
P. SAVIĆ (Belgrade)
P. SCHERRER (Zürich)
CH. SCHMELZER (CERN)
R. TANGEN (Oslo)
D. TAYLOR (Northampton)
V. I. VEKSLER (Moscow)
G. VON DARDEL (CERN)
O. WERNHOLM (Stockholm)
R. R. WILSON (Cornell)
S. D. WINTER (Saclay)

JANUARY 1961
(Conference Issue)

VOLUME 11 (1961) No. 1

GREGG M. SINCLAIR LIBRARY
UNIVERSITY OF HAWAII
8-7-63

NUCLEAR INSTRUMENTS & METHODS

A JOURNAL ON ACCELERATORS, INSTRUMENTATION
AND TECHNIQUES IN NUCLEAR PHYSICS

EDITOR: K. SIEGBAHN - UPPSALA

PROCEEDINGS
of the
SECOND ACCELERATOR CONFERENCE

AMSTERDAM, OCTOBER 4–6, 1960

This Conference was sponsored by:
HIGH VOLTAGE ENGINEERING CORPORATION AND HIGH VOLTAGE ENGINEERING (EUROPA) N.V.

NORTH-HOLLAND PUBLISHING COMPANY – AMSTERDAM

NUCLEAR INSTRUMENTS AND METHODS

A journal on accelerators, instrumentation and techniques in nuclear physics

EDITOR: K. SIEGBAHN, UPPSALA

EDITORIAL BOARD:

J. B. ADAMS (CERN)
F. A. ALSINA (Buenos Aires)
E. AMALDI (Rome)
H. L. ANDERSON (Chicago)
K. T. BAINBRIDGE (Cambridge, Mass.)
P. R. BELL (Oak Ridge)
R. E. BELL (Montreal)
A. BERTHELOT (Saclay)
H. BRINKMAN (Groningen)
E. H. COOKE-YARBOROUGH (Harwell)
S. DE BENEDETTI (Pittsburgh)
M. DE HEMPTINNE (Louvain)
A. DE-SHALIT (Rehovoth)
M. DEUTSCH (Cambridge, Mass.)
S. DU TOIT (Pretoria)
B. S. DŽELEPOV (Leningrad)
W. GENTNER (Heidelberg)
P. C. GUGELOT (Amsterdam)
H. HALBAN (Paris)
O. HAXEL (Heidelberg)
P. HUBER (Basel)
S. KIKUCHI (Tokyo)
J. KOCH (Copenhagen)
M. S. KOZODAEV (Moscow)
S. LIVINGSTON (Cambridge, Mass.)
E. M. MCMILLAN (Berkeley)
M. G. MEŠČERJAKOW (Moscow)
P. B. MOON (Birmingham)
M. L. OLIPHANT (Canberra)
W. PAUL (Bonn)
A. S. RAO (Bombay)
G. SALVANI (Rome)
P. SAVIĆ (Belgrade)
P. SCHERRER (Zürich)
CH. SCHMELZER (CERN)
R. TANGEN (Oslo)
D. TAYLOR (Northampton)
V. I. VEKSLER (Moscow)
G. VON DARDEL (CERN)
O. WERNHOLM (Stockholm)
R. R. WILSON (Cornell)
S. D. WINTER (Saclay)

INSTRUCTIONS FOR CONTRIBUTORS

Contributions may be sent to the Editor, Professor K. Siegbahn, Institute of Physics, University of Uppsala, Sweden, either directly or through the intermediation of one of the members of the Editorial Board. Contributions may be written in English, French or German but should always, except for very short papers, be supplied with a brief abstract in English. Figures should be inked original drawings or glossy prints and they should be sufficiently large. Contributors should make sure that important details in drawings and photographs will show up clearly in the diminished copy used by the publisher.

Books for review should be sent to Professor Siegbahn.

Objective and descriptive material on endeavours and product developments from the industry for the section "Spotlight on Industry" should be sent directly to the publishers, North-Holland Publishing Company, P.O. Box 103, Amsterdam.

Nuclear Instruments and Methods is published monthly. The subscription price of a volume of about 360 pages is $ 17.00 (130 s), postage free.

Subscriptions should be sent to the publishers, North-Holland Publishing Company, P.O. Box 103, Amsterdam, or to any subscription-agent.

No part of this issue may be reproduced in any form, by print, photoprint, microfilm or any other means without written permission from the publisher.

PROCEEDINGS

of the

SECOND ACCELERATOR CONFERENCE

The discussions were compiled and edited by

HIGH VOLTAGE ENGINEERING (EUROPA) N.V.

PROCEEDINGS
of the
SECOND ACCELERATOR CONFERENCE

AMSTERDAM — 4-6 OCTOBER 1960

EDITOR: K. SIEGBAHN – UPPSALA

1961

NORTH-HOLLAND PUBLISHING COMPANY – AMSTERDAM

NO PART OF THIS ISSUE MAY BE REPRODUCED IN ANY FORM BY PRINT, PHOTOPRINT,
MICROFILM OR ANY OTHER MEANS WITHOUT WRITTEN PERMISSION FROM THE PUBLISHER

The Second Accelerator Conference has been organized and sponsored by the High Voltage Engineering Corporation, Burlington, Massachusetts, U.S.A. together with High Voltage Engineering (Europa) N.V., Amersfoort, The Netherlands.

In addition to the regular subscription distribution of NUCLEAR INSTRUMENTS AND METHODS, *participants* of the Second Accelerator Conference will receive a personal copy with the compliments of High Voltage Engineering Corporation. A limited number of extra copies will be sent upon letterhead.

N. TUFTS, Jr.
High Voltage Engineering Corporation
So. Bedford Street
Burlington, Massachusetts, U.S.A.

PRINTED IN THE NETHERLANDS

PREFACE

This issue of Nuclear Instruments and Methods is devoted entirely to the conference on low energy accelerators which was held in Amsterdam on October 4, 5 and 6, 1960. The conference was organized by the High Voltage Engineering Corporation to the great satisfaction of all the participants. In a joint effort the contributors, the publisher, and the editor have tried to speed up the publication of this issue as much as possible. A lot of interesting information was presented during the conference concerning accelerator designs, techniques, and applications in different fields of current interest. The present conference report thus gives a fairly comprehensive picture of the present situation of this branch of nuclear physics. It is with a great pleasure that I use this opportunity, on behalf of the members of the conference, to thank the President of the High Voltage Engineering Corporation, Dr. Denis Robinson, and his organizing committee for their excellent way of arranging this very successful conference.

THE EDITOR

It was a distinct pleasure for our company to have sponsored the Second Accelerator Conference in Amsterdam. The value of this exchange of information on accelerators, low energy physics and radiation research was demonstrated by the high caliber of the presented lectures and the enthusiastic response of the participants.

We are indebted to the speakers for their excellent papers, to the Session Chairmen for their stimulating support, to Professor Siegbahn for his editorial effort and to the North-Holland Publishing Company for devoting a special issue of Nuclear Instruments and Methods to the Proceedings.

DENIS M. ROBINSON
President,
High Voltage Engineering Corporation

Organizing Committee:

Dr. Denis M. Robinson, *President High Voltage Engineering Corporation*
Ir. J. S. Woldringh, *Managing Director High Voltage Engineering (Europa) N.V.*
N. Tufts Jr., *High Voltage Engineering Corporation*
J. M. Hartogh, *Adviesbureau voor Public Relations, Rotterdam*

Chairmen of the Sessions:

Professor H. Brinkman, *University of Groningen, The Netherlands*
Professor H. H. Staub, *University of Zürich, Switzerland*
Professor K. Siegbahn, *University of Uppsala, Sweden*
Professor A. Charlesby, *Royal Military College of Science, England*

CONTENTS

Nuclear Physics 1–46

P. M. Endt, Resonance Reactions 3

L. Katz and K. H. Lokan, The Generation of Positrons in a Thick Target Bombarded by Fast Electrons 7

L. Katz, Desirable Linear Electron Accelerator Characteristics for Nuclear Research 14

T. Huus, Coulomb Excitation 19

G. Goldring, Experiments using Ultra-Fast Pulse Techniques 29

E. Cotton, Durées de Vie Nucléaires 39

A. Schoch, A Discussion of Colliding Beam Techniques 40

Particle Research 47–135

P. H. Rose, The Three-Stage Tandem Accelerator 49

H. E. Gove, Current Experimentation with the Tandem Accelerator at the Chalk River Laboratories 63

K. W. Allen, Recent Research in Nuclear Reactions using the Aldermaston Tandem Generator 93

R. Fleischmann, Sources of Polarized Ions (for Protons and Similar Particles) . . . 112

R. J. Connor, Millimicrosecond Pulsing 122

J. C. Nygard and R. F. Post, Recent Advances in High Power Microwave Electron Accelerators for Physics Research 126

Physics and Radiation Research (I)

Physics 137–184

U. Gonser and K. Lücke, The Use of Van de Graaff Accelerators for High Intensity Neutron Irradiation of Metals 139

K. H. Beckurts, Reactor Physics Research with Pulsed Neutron Sources 144

F. Amman, The KS-3MeV Van de Graaff Injector of the Frascati Electron Synchrotron 169

J. Kistemaker, On Ion Sources with High Efficiency and Intensity 179

Physics and Radiation Research (II)

RADIATION RESEARCH AND INDUSTRIAL APPLICATION 185–253

J. W. OTVOS, V. P. GUINN, H. R. LUKENS, Jr. and C. D. WAGNER, Photoactivation and Photoneutron Activation Analysis 187

P. BARUCH, The Use of the Electron Accelerator in Solid State Physics. 196

W. HUBER, High Energy Radiation for Research in Biochemistry and Microbiology 210

S. H. PINNER and W. T. H. DAVISON, The Development of Radiation Process Applications 227

D. MOORE, Neutrons, Electrons and X-ray Beams used for Radiation Research from a Van de Graaff Generator 238

D. A. TRAGESER, Future Accelerators: Intense Sources for Processing 248

List of Accelerators 254

Left to right: Prof. Dr. A. Charlesby, *Royal Military Academy of Science, England.* Dr. D. M. Robinson, *President, High Voltage Engineering Corporation U.S.A.* Prof. Dr. P. M. Endt, *University of Utrecht, The Netherlands.* Prof. Dr. W. Gentner, *Max-Planck Institute, Heidelberg, Germany.* Prof. Dr. R. Fleischmann, *University of Erlangen, Germany.*

Banquet speech by Professor Casimir. From left to right: Mrs. Woldringh, Prof. Dr. H. B. G. Casimir, *Director of the Philips' Laboratories,* Dr. D. M. Robinson, *President of the High Voltage Engineering Corporation,* Prof. Dr. P. M. Endt, *University of Utrecht.*

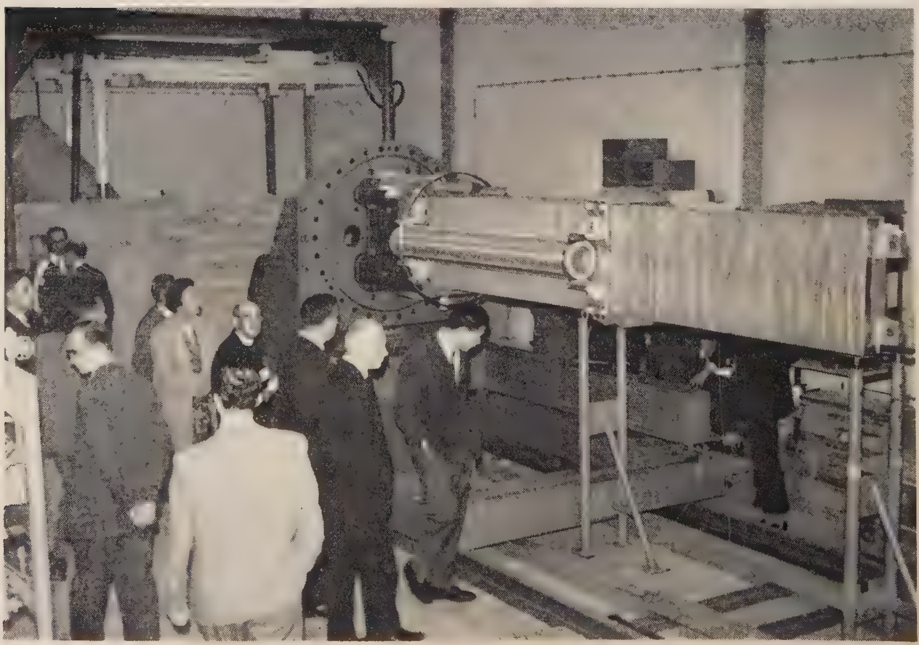

Visit of participants to the new High Voltage Engineering factory in Amersfoort.

NUCLEAR PHYSICS

(October 4, 1960) pp. 1-46

Chairman: H. Brinkman

University of Groningen, The Netherlands

CONTENTS

Endt, P. M. Resonance Reactions . . . 3

Katz, L. and Lokan, K. H. The Generation of Positrons in a Thick Target Bombarded by Fast Electrons . . . 7

Katz, L. Desirable Linear Electron Accelerator Characteristics for Nuclear Research . . . 14

Huus, Torben Coulomb Excitation . . . 19

Goldring, G. Experiments using Ultra-Fast Pulse Techniques . . . 29

Cotton, E. Durées de Vie Nucléaires . . . 39

Schoch, A. A Discussion of Colliding Beam Techniques . . . 40

NUCLEAR INSTRUMENTS AND METHODS **11** (1961) 3–6; NORTH-HOLLAND PUBLISHING CO.

RESONANCE REACTIONS

P. M. ENDT

Fysisch Laboratorium der Rijksuniversiteit Utrecht

The experimental conditions are discussed for the observation of reactions proceeding through narrow isolated resonances. This includes a survey of gamma-ray resonant scattering or absorption techniques, making use of accelerator produced radiation.

This general introduction is followed by some examples of recent Utrecht work on resonance reactions. The ^{23}Na(p,γ)^{24}Mg reaction has been investigated at six resonance levels in the $E_{\mathrm{p}} = 300$–800 keV region. The gamma-ray branching has been determined of these levels and of twelve lower levels in ^{24}Mg. Gamma-ray angular distributions have been measured at nine resonances in the ^{24}Mg(α,γ)^{28}Si reaction, from which resonance spins and parities can be determined in a unique way. Isotopic spin selection rules explain the relative weakness of observed E1 and M1 transitions compared to E2 transitions. From yield measurements in the ^{27}Al(p,γ)^{28}Si, ^{27}Al(p,α)^{24}Mg, and ^{24}Mg(α,γ)^{28}Si reactions the partial widths have been obtained for the decay of the relevant ^{28}Si resonance levels.

Reactions proceeding through resonances offer ideal opportunities for nuclear spectroscopy. The theoretical description of such reactions is relatively easy, because of the fact that the intermediate compound state has a well defined spin and parity.

It seems appropriate to discuss here in some detail the experimental conditions suitable for the observation of narrow isolated resonances. The main requirement is that the compound nucleus should not be too highly excited, or in other words, that the binding energy of incoming and outgoing particles should be relatively small. This generally excludes the use of deuterons, tritons or He^3 nuclei as either incoming or outgoing particles. The only choice for the latter is thus protons, neutrons, alpha particles or gamma quanta. The possibility of observing resonances in heavy ion bombardements will be discussed tomorrow by Gove.

To start with we shall only consider resonance reactions initiated through protons or alpha particles. This is clearly the ideal field for low energy Cockcroft-Walton or electrostatic generators. The maximum machine energy limits the region of nuclides to be investigated. With a 1 MeV machine one might observe proton resonances in nuclides up to $Z = 20$, while alpha-particle resonances below 1 MeV have only been found in lithium and boron. A 3 MeV machine would allow the observation of proton resonances at least up to $Z = 35$, and of alpha particle resonances up to $Z = 20$. For a given target nucleus the resonance region also has a high energy limit, where resonances become broad and close, and thus start to overlap. Generally one can say, that any resonance work becomes impossible above 6 MeV incoming particle energy. For medium weight nuclei the high energy limit is much lower than this because resonances, although narrow, have an average spacing smaller than, or comparable with, the available energy resolution. Much recent resonance work has only been possible just because of improvements in energy resolution. Small beam energy spread, and good energy stability and reproducibility are imperative for those investigations. It is interesting to speculate on the possibilities for generators yielding high currents at very good energy resolution, say 1 in 10000 or better. They would be extremely useful e.g. for resonance work in the high Z region, for the measurement of resonance total widths, and for neutron spectroscopy through the ^{7}Li(p,n) reaction.

Neutron resonance spectroscopy will not be treated here. Some aspects will be discussed by other speakers.

Resonant scattering and absorption of gamma radiation has recently become a powerful tool for the investigation of both virtual and bound nuclear states. The ultracentrifuge and high temperature techniques have proved to be of rather limited scope, applicable only to low energy radiation from high Z sources. Three new methods, however, have appreciably widened the applicability.

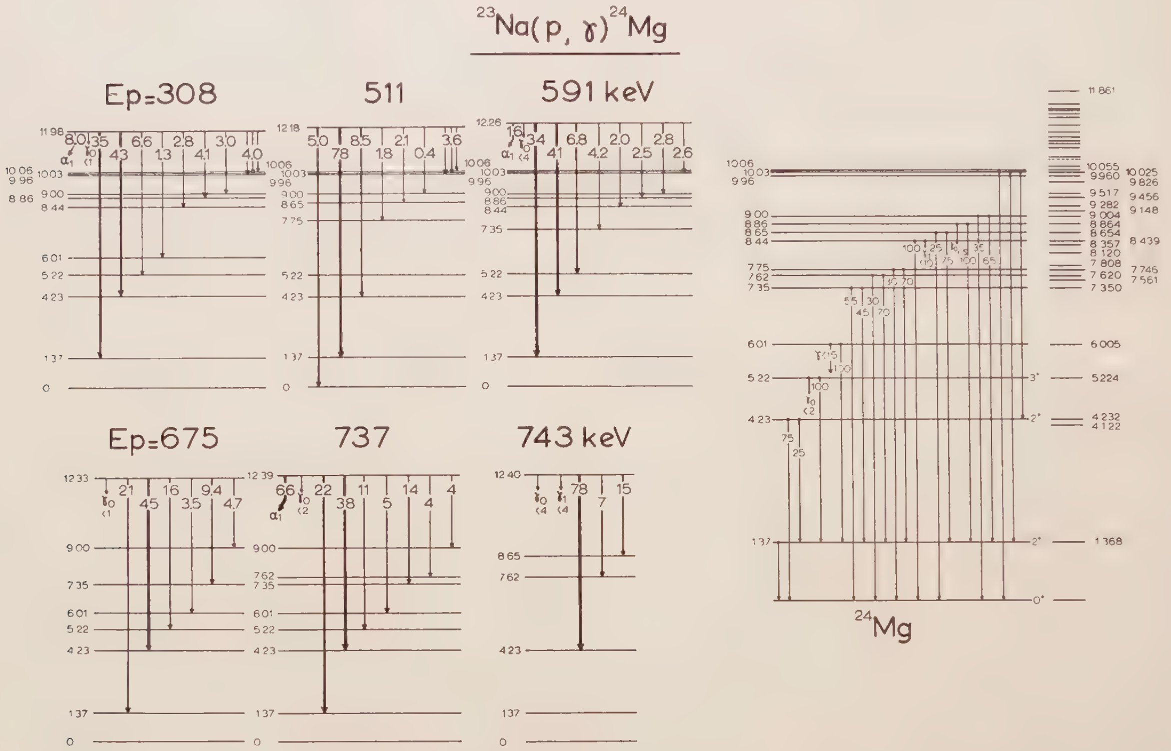

Fig. 1. Decay of six ^{23}Na(p,γ)^{24}Mg resonance levels and of twelve ^{24}Mg lower levels, as determined by Glaudemans.

The first method makes use of gamma radiation Doppler-shifted in energy through preceding proton capture, and proceeds through the observation of resonant absorption rather than of resonant scattering[1,2]. The radiation widths and sometimes total widths of a number of highly excited states in light nuclei have been determined in this way. Even "cross-shooting" has been achieved, in which the radiation from the ^{13}C(p,γ)^{14}N reaction was used to excite the 9.19 MeV level in ^{11}B [3]).

In the second method resonant scattering has been observed of gamma radiation Doppler-broadened through preceding particle emission in reactions like (d,pγ) or (p,p$'\gamma$) [4]). The method has succesfully been used for the determination of radiation widths of bound states in several light and medium weight nuclei.

Finally, electron accelerators can be used for achieving resonant scattering[5]). The radiation resonantly scattered from a sample placed in the continuous X-ray beam of the machine is detected with a scintillation counter. It seems probable that this rather universal method

[1]) P. B. Smith, Proceedings of the 1957 Rehovoth Conference on Nuclear Structure (North Holland Publ. Co., Amsterdam, 1958) p. 587;

P. B. Smith and P. M. Endt, Phys. Rev. **110** (1958) 397 and 1442.

[2]) S. S. Hanna and L. Meyer-Schützmeister, Phys. Rev. **108** (1957) 1644 (L), and (1959) 115, 986.

[3]) L. Meyer-Schützmeister and S. S. Hana, Bull. Am. Phys. Soc. **3** (1958) 188.

[4]) See e.g. Metzger, Swann and Rasmussen, Nucl. Phys. **16** (1960) 568.

[5]) See e.g. E. Hayward and E. G. Fuller, Phys. Rev. **106** (1957) 991;

V. J. Vanhuyse and G. Vanpraet, private communication.

will find a wider application in the future.

Photo-reactions like (γ,p), (γ,n) or (γ,α) show broad giant resonances, but apart from those there should exist narrow single level resonances close above threshold, corresponding to the low energy particle capture resonances. The "breaks" recently found in yield curves provide proof of these levels, but the lack of strong monoenergetic gamma-ray sources, variable in energy over a wide range, has prevented a detailed investigation of those narrow resonances.

The experimental work in Utrecht has centered recently on the investigation of some even-even self-conjugated nuclei, like ^{24}Mg and ^{28}Si, through the use of particle capture reactions.

Results of an investigation of the ^{23}Na(p,γ)^{24}Mg reaction by Glaudemans[6]) are shown in fig. 1. It gives the decay of six resonance levels in the E_p = 300–800 keV region and of some twelve lower levels in ^{24}Mg as observed from single and coincidence scintillation spectra.

Analogous work had been done previously on the ^{27}Al(p,γ)^{28}Si reaction[7]). The analysis of recent gamma-ray angular distribution and correlation measurements is in progress. The analysis is quite involved because up to five continuous mixing parameters may occur in the theoretical expression for a (p,$\gamma\gamma$) angular correlation. They are: the channel spin mixing parameter, two orbital momentum mixing parameters (one for each channel), and two E2/M1 radiation mixing parameters (one for each gamma transition). Measurements have to be performed in at least five different "geometries". The mixing parameters can then be found by least-squares analysis with the use of an electronic computing machine.

To provide more information on the ^{28}Si levels in the E_x = 11–13 MeV region an investigation was started of the ^{24}Mg (α,γ)^{28}Si reaction. A

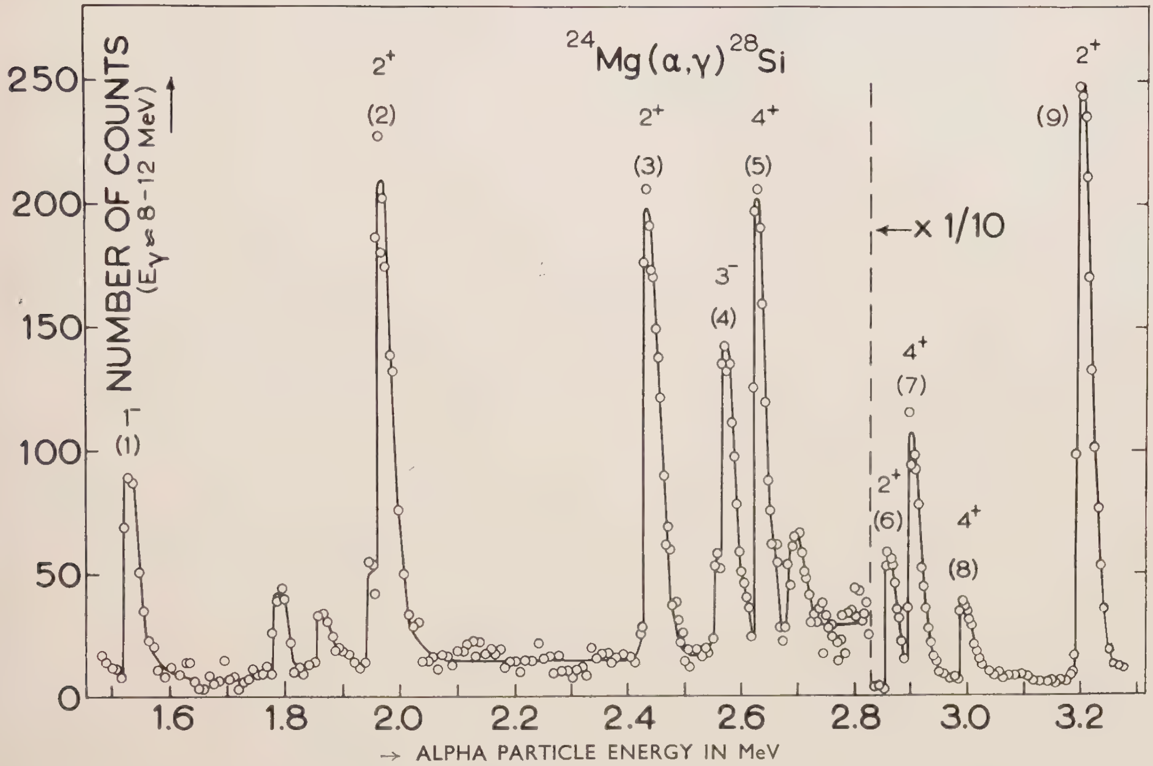

Fig. 2. Yield curve of the ^{24}Mg(α,γ)^{28}Si reaction in the E_α = 1.5–3.3 MeV region.

---

[6]) P. W. M. Glaudemans, to be published.

[7]) P. M. Endt and A. Heyligers, Physica 26 (1960) 230.

preliminary report of this work has been submitted at the Kingston conference[8]), but since then new data have been obtained. In fig. 2 the gamma-ray yield is given as a function of the alpha-particle energy. A natural magnesium target was used, but the gamma-ray spectra measured at the resonances numbered 1 through 9 show without doubt that those resonances all stem from the predominant ^{24}Mg isotope.

At those ten resonances gamma-ray angular distributions were measured of either the ground-state transition or of the transition to the ^{28}Si first excited state. In contrast to what was said above on the ^{27}Al(p,γ)^{28} reaction, these angular distributions are extremely easy to interpret because both ^{24}Mg and the alpha particle are spinless. Only E2/M1 radiation mixing can occur, and actually this is only found at one resonance (number 2). At all other resonances the transitions investigated are either pure E1 or pure E2. Characteristic angular distributions for ground-state transitions at 1^- and 2^+ resonances, and first excited state transitions at 3^- and 4^+ resonances are shown in fig. 3. The very large anisotropies should be noted, especially for the ground-state transition at 1^- and 2^+ resonances.

Another notable feature is the relative weakness of E1 and M1 transitions compared to E2 transitions. This might be explained by assuming that isotopic spin in ^{28}Si is still a good quantum number even at excitation energies as high as 12 MeV. Because the ground states of both ^{24}Mg and ^{4}He have $T = 0$ the resonances excited in ^{28}Si also have $T = 0$. Dipole transitions to ^{28}Si states below 9 MeV (which all have $T = 0$) are then forbidden.

Most of the resonance levels found in the latter investigation can also be excited in the Al^{27}(p,α)Mg^{24} reaction. Yields for this reaction have been determined in Utrecht[9]) and in Oslo[10]).

Some ^{28}Si resonance levels are excited in all three reactions ^{27}Al(p,γ)^{28}Si, ^{27}Al(p,α)^{24}Mg and ^{24}Mg(α,γ)^{28}Si. The yields of these reactions are proportional to $\Gamma_p\Gamma_\gamma/\Gamma$, $\Gamma_p\Gamma_\alpha/\Gamma$ and $\Gamma_\alpha\Gamma_\gamma/\Gamma$ respectively, where Γ_p, Γ_γ, and Γ_α are the widths for emission of a proton, gamma radiation and an alpha particle, and where $\Gamma = \Gamma_p + \Gamma_\alpha + \Gamma_\gamma$ represents the total width. Measurements of the yields of these three reactions clearly provide an easy way to determine the three relevant widths. This has now been done for the resonances corresponding to proton energies of 504, 631, and 731 keV. Planned extensions of the yield measurements should make it possible to apply this method to a much larger number of ^{28}Si resonances.

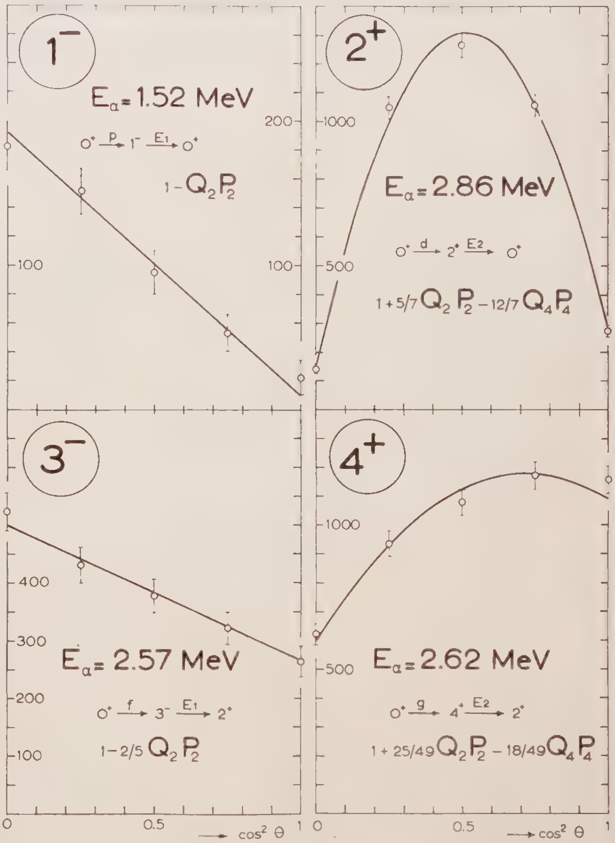

Fig. 3. Gamma-ray angular distributions observed in the ^{24}Mg(α,γ)^{27}Si reaction. Ground-state transitions were measured at 1^- and 2^+ resonances, and first excited state transitions at 3^- and 4^+ resonances. Drawn curves are theoretical, with the proper solid angle attenuation factors Q_2 and Q_4 inserted.

---

[8]) Smulders, Smith and Endt, Proceedings of the International Conference on Nuclear Structure, Kingston (1960).

[9]) J. Kuperus and P. B. Smith, submitted to Physica.

[10]) T. Holtebekk *et al.*, private communication.

NUCLEAR INSTRUMENTS AND METHODS **11** (1961) 7–13; NORTH-HOLLAND PUBLISHING CO.

THE GENERATION OF POSITRONS IN A THICK TARGET BOMBARDED BY FAST ELECTRONS

L. KATZ

University of Saskatchewan, Saskatoon, Saskatchewan

and

K. H. LOKAN

United Kingdom Atomic Energy Authority, Atomic Energy Research Establishment, Harwell, Didcot, Berks.

An approximate analytical solution is developed for the distributions in energy and angle of positrons generated by fast electrons incident on a thick radiator (≈ 0.2 radiation lengths). For small angles, the positron energy spectrum may be expressed generally as a function of target thickness, incident electron energy, and a generalised shape function which is tabulated. Numerical estimates of the energy distributions in the forward direction, arising from 25 and 100 MeV electrons incident on a radiator of thickness 0.2 radiation lengths are made, and compared with spectra measured at these energies; the agreement is satisfactory.

1. Introduction

In general, calculations of electron densities in a low energy ($\lesssim$ 100 MeV) shower are handled by Monte Carlo methods (e.g. Wilson 1951[1]) since the simplifying approximations available at extreme relativistic energies (Janossy 1950[2]) are not valid in this energy region. Unfortunately, the labour involved in deriving energy and angular distributions of reasonable precision in this way is enormous, and they are not at present available in the literature. Moreover, this process is currently of some interest, since with the advent of high intensity electron accelerators, it offers a potential source of resolved positrons of ample intensity for experimental purposes.

In section 2 of the calculation an expression is found for the bremsstrahlung spectrum at a depth t within the target. In section 3 this is combined with the pair production cross-section to yield the positron spectrum integrated over angle. The dependence of the final angular distribution on the bremsstrahlung angular distribution, the intrinsic pair distribution, and the angular spread introduced by multiple scattering of the positrons is discussed in section 4 and an expression is derived for the energy and angular distributions. From these an empirical expression is found for the positron spectrum in the forward direction, as a function of target thickness, incident electron energy, and a shape function which is tabulated. Finally numerical estimates are made of the forward spectrum generated by 25 and 100 MeV electrons incident on 0.2 radiation lengths of tungsten, and compared with measurements made at these energies.

2. The Bremsstrahlung Spectrum

We consider a stream of electrons of energy $U_0 = E + m_0c^2$ incident on a plane target of thickness t radiation lengths† (see fig. 1). In penetrating a thickness t' of the target, electrons lose energy principally by radiation, and their energy distribution is modified accordingly. The probability that an electron has an energy in an interval defined by $\mathrm{d}y$ is (Heitler 1954[3]), p. 378)

---

[1] R. R. Wilson, Phys. Rev. **84** (1951) 100.

[2] Janossy, Cosmic Rays (Oxford University Press, 1950).

[3] W. Heitler, The Quantum Theory of Radiation (Oxford University Press, 1954).

† It is convenient to measure thickness in units of radiation length. For tungsten, the case we consider in detail, 1 radiation length = 6.2 g/cm^2.

$$\omega(y, t')\,\mathrm{d}y = \frac{\mathrm{e}^{-y}\, y^{\left(\frac{t'}{\ln 2} - 1\right)}}{\Gamma\left(\frac{t'}{\ln 2} - 1\right)}\,\mathrm{d}y \qquad (1)$$

where $y = \ln (U_0/U)$, U = electron energy.

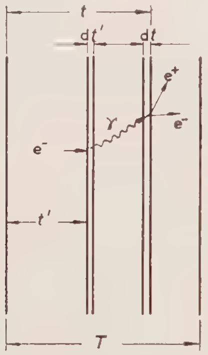

Fig. 1. Target parameters.

Now, the probability that an electron of energy U emits a photon from a layer $\mathrm{d}t'$ (see fig. 1) of energy between k and $k + \mathrm{d}k$ is

$$\psi_{\mathrm{rad}}\,\mathrm{d}v\,\mathrm{d}t' = \frac{1}{v}\left[1.20 - \left(\frac{1}{2} + \frac{5}{U}\right) v\right] \mathrm{d}v\,\mathrm{d}t' \qquad (2)$$

where

$$v = \frac{k}{U}$$

and

$$\psi_{\mathrm{rad}} = \frac{1}{v}\left[1.20 - \left(\frac{1}{2} + \frac{5}{U}\right) v\right]$$

is a good approximation to the Bethe-Heitler bremsstrahlung spectrum (Rossi 1952)[4]) for $0.2 \lesssim v \lesssim 0.8$ and $10 \lesssim U \lesssim 100$ MeV (see fig. 2).

Then the number of photons in an interval k and $k + \mathrm{d}k$ from $\mathrm{d}t'$, generated by electron between y and $y + \mathrm{d}y$ is

$$\mathrm{d}N = \frac{\mathrm{d}k}{k}\left[1.20 - \left(\frac{1}{2} + \frac{5}{U}\right)\frac{k\,\mathrm{e}^{y}}{U_0}\right] \frac{\mathrm{e}^{-y}\, y^{\left(\frac{t'}{\ln 2} - 1\right)}}{\Gamma\left(\frac{t'}{\ln 2} - 1\right)}\,\mathrm{d}y\,\mathrm{d}t' \qquad (3)$$

where we neglect the weak U-dependence of the term $(\frac{1}{2} + 5/U)$. Integrating over all values of y which can contribute to k, we obtain after some manipulation

$$k\,\frac{\mathrm{d}N}{\mathrm{d}k} = \mathrm{d}t'\, {y_0}^{\frac{t'}{\ln 2}} \left[\psi_{\mathrm{rad}} - 1.20\, y_0\, \frac{t'}{\ln 2} \cdot \left\{ \frac{1}{1 + \frac{t'}{\ln 2}} - y_0 \frac{1}{2 + \frac{t'}{\ln 2}} + {y_0}^2 \frac{1}{3 + \frac{t'}{\ln 2}} \cdots\cdots \right\}\right] \qquad (4)$$

where

$$y_0 = \ln (U_0/k)\ .$$

In traversing the remaining $(t - t')$ of target material, photons are attenuated by a factor $\mathrm{e}^{-\lambda(t-t')}$ so that the bremsstrahlung spectrum at a depth t is

$$k\,\frac{\mathrm{d}N}{\mathrm{d}k} = \int_0^t \mathrm{d}t'\, {y_0}^{\frac{t'}{\ln 2}} \left[\psi_{\mathrm{rad}} - 1.20\, y_0\, \frac{t'}{\ln 2} \cdot \left\{ \frac{1}{1 + \frac{t'}{\ln 2}} - y_0 \frac{1}{2 + \frac{t'}{\ln 2}} + {y_0}^2 \frac{1}{3 + \frac{t'}{\ln 2}} \cdots \right\}\right] \mathrm{e}^{-\lambda(t-t')}$$

which to order t^2 reduces to

$$k\,\frac{\mathrm{d}N}{\mathrm{d}k} = \psi_{\mathrm{rad}}\, t - \left[\psi_{\mathrm{rad}}\, \frac{\lambda}{2} - \frac{\ln y_0\, \psi_{\mathrm{rad}}}{2 \ln 2} + \frac{1.20\, y_0}{2 \ln 2} \left\{ 1 - \frac{y_0}{4} + \frac{{y_0}^2}{18} - \frac{{y_0}^3}{96} \right\}\right] t^2 . \qquad (5)$$

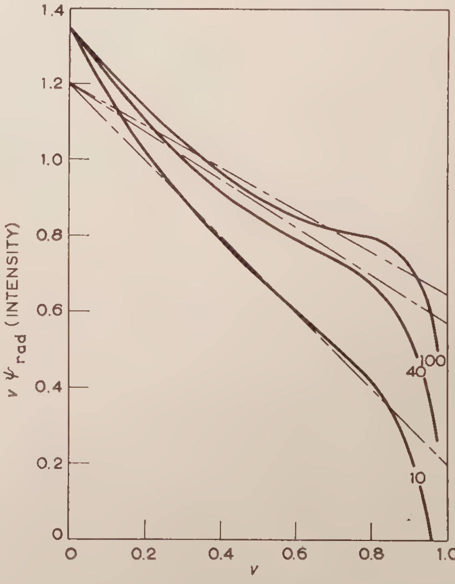

Fig. 2. Bremsstrahlung distribution for U = 10, 40, and 100 MeV. The dotted lines represent fits to these, used in the calculation (eq. (2)).

---

[4]) B. Rossi, High Energy Particles (Prentice Hall, Inc., N.Y., 1952).

We have evaluated the correction term in t^2 for $U_0 = 30$ and $U_0 = 100$ MeV as a function of v; the result is shown in fig. 3. We fit these functions linearly in v, to obtain

$$\psi_{\text{corr}} \approx -[0.65 + \gamma_v]$$

where $\gamma = 0.5$ and 0.8 at $U_0 = 30$ and 100 MeV respectively. Thus the total bremsstrahlung distribution at a depth t is given by

$$v \frac{\mathrm{d}N}{\mathrm{d}v} = k \frac{\mathrm{d}N}{\mathrm{d}k} = \psi_{\text{rad}}\, t + \psi_{\text{corr}}\, t^2 . \tag{6}$$

In section 4 it is shown that the angular distribution of the bremsstrahlung may be adequately represented by a gaussian of mean square angle $< \theta^2 >$ given by

$$< \theta^2 > = \frac{1.34 + 17t}{U_0{}^2}$$

where t = thickness in radiation lengths, U_0 = electron energy in MeV. However, for targets so thick that the electron energy is changed significantly, with depth we must replace U_0 by a mean value. Following Lanzl (Lanzl 1951[5])) we write for the mean energy at depth t

$$U(t) = (0.92 + 0.162\, U_0) \frac{\mathrm{e}^{-0.162t}}{0.162}$$

then, taking for the average energy, the mean energy at $\frac{1}{2}t$, we obtain

$$U^2 = \frac{U_0{}^2}{1 + \left(1 + \dfrac{5.7}{U_0}\right) t} .$$

Thus we may write for the central intensity

$$v \frac{\mathrm{d}N}{\mathrm{d}v} = \frac{\psi_{\text{rad}}\, t + \psi_{\text{corr}}\, t^2}{< \theta^2 >} =$$

$$= \frac{(\psi_{\text{rad}}\, t + \psi_{\text{corr}}\, t^2)\, U_0{}^2}{(1.34 + 17t)\left(1 + \left(1 + \dfrac{5.7}{U_0}\right) t\right)} . \tag{7}$$

We may compare this equation directly with Lanzl's experimental determination of the t dependence at $U_0 = 17$ MeV and $v \approx 0.84$. The calculated variation of yield with thickness for the forward direction (eq. (7)) and the total integrated over angle (eq. (6)) are shown, together with Lanzl's experimental data, in fig. 4. The significant feature of this analysis, for the generation of positrons, is that there is no increase in central yield once the target has reached a thickness of ≈ 0.2 rad. lengths; this conclusion, which applies equally well up to 100 MeV, implies that the optimum target thickness for positron production will be of this order.

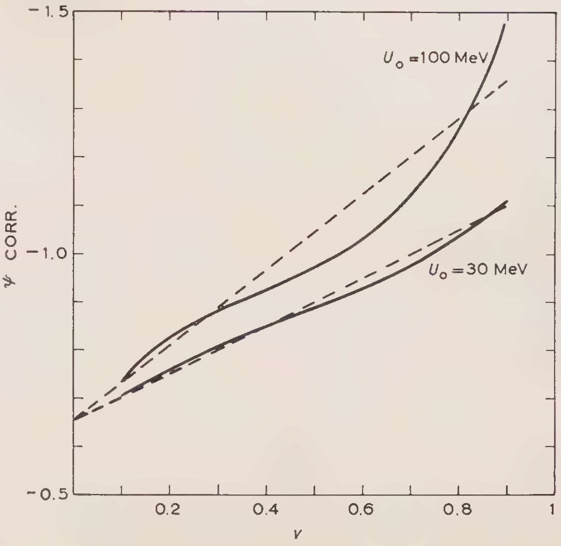

Fig. 3. The bremsstrahlung correction functions ψ_{corr} for $U_0 = 30$ MeV and $U_0 = 100$ MeV.

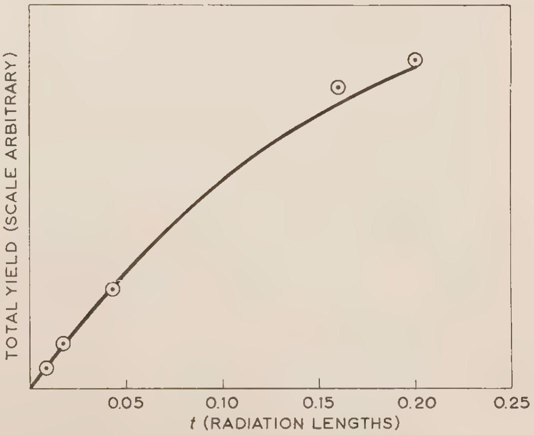

Fig. 4 (a).

Total bremsstrahlung yield versus target thickness for $U_0 = 17$ MeV, $k \approx 14$ MeV. The solid line is obtained from eq. (6), the experimental points are due to Lanzl and Hanson[5]).

---

[5]) Lanzl and Hanson, Phys. Rev. 83 (1951) 959.

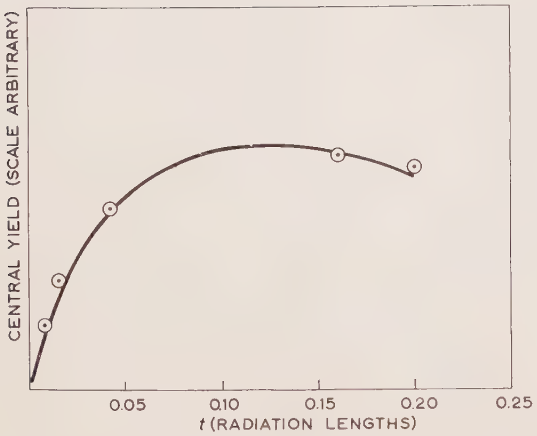

Fig. 4 (b).
Central bremsstrahlung yield versus target thickness for $U_0 = 17$ MeV, $k \approx 14$ MeV. The solid line is obtained from eq. (7), the experimental points are due to Lanzl and Hanson[5]).

3. The Generation of Positrons

The differential pair production cross-section, shown in fig. 5, is very nearly flat for $0.2 < U_+/k < 0.8$ and $10 < k < 100$ MeV, where U_+ is the positron energy. Its dependence on k is given by

$$\psi_{\text{pair}}\,\mathrm{d}k = 0.146\,[\ln k - 0.308]\,\mathrm{d}k$$

where ψ_{pair} is the total probability per radiation length of generating a positron. Making the approximation that the differential cross-section is constant, the positrons generated by photons of energy k will be distributed uniformly over the available energy k, the number of positrons between U_+ and $U_+ + \mathrm{d}U_+$ is

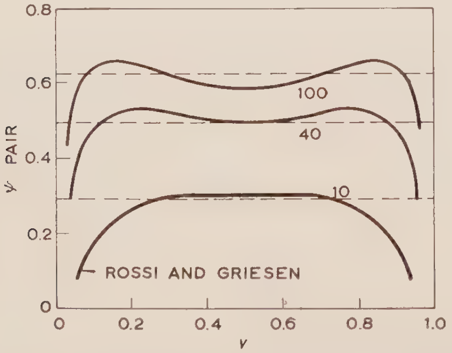

Fig. 5. The differential pair production cross-section for $k = 10$, 40, and 100 MeV. The dotted lines represent fits used in the calculation.

$$\mathrm{d}\mathscr{N} = \int_0^T \int_{v_{\min}}^{v_{\max}} 0.146\,(\ln k - 0.308)\,\frac{\mathrm{d}N}{\mathrm{d}v}\,\mathrm{d}v\,\mathrm{d}t\,\frac{\mathrm{d}U_+}{k}\,\cdot$$

or writing $k = U_0 v$

$$\frac{\mathrm{d}\mathscr{N}}{\mathrm{d}U_+} = \frac{0.146}{U_0}\int_0^T \int_{v_{\min}}^{v_{\max}} (\ln U_0\,v - 0.308)\,\frac{\mathrm{d}N}{\mathrm{d}v}\,\frac{\mathrm{d}v}{v}\,\mathrm{d}t\,. \quad (8)$$

The limits of integration are

$$v_{\min} = \frac{U_+ + m_0c^2}{U_0} \quad \text{and} \quad v_{\max} = \frac{U_0 - m_0c^2}{U_0}$$

or writing $U_+/U_0 = \alpha$, and neglecting m_0c^2/U_0 compared to 1,

$$\frac{\mathrm{d}\mathscr{N}}{\mathrm{d}U_+} = \frac{0.146}{U_0}\int_0^T \int_\alpha^1 (\ln U_0\,v - 0.308)\,(\psi_{\text{rad}}\,t + \psi_{\text{corr}}\,t^2)\,\frac{\mathrm{d}v}{v^2}\,\mathrm{d}t\,. \quad (9)$$

4. Angular Distribution

The angular distribution of the emergent positrons is compounded from the distributions for the bremsstrahlung, the intrinsic positron distribution, and the distribution generated by multiple scattering of the positrons after they are formed. The angular distribution of photons emerging from a target of thickness t has been calculated (Muirhead 1952[6])) to be

$$\frac{U_0^2}{\text{cons.}}\left[-E_{\mathrm{i}}\left(-\frac{U_0^2\theta^2}{450t}\right) + E_{\mathrm{i}}\left(-\frac{U_0^2\theta^2}{\gamma\, m_0c^2}\right)\right]$$

where $-E_{\mathrm{i}}\,(-x)$ is the incomplete gamma function, and $\gamma = 1.781$. In calculating this equation Muirhead *et al.* used the electron scattering theory of Rossi and Greisen (Rossi 1941[7])). Following Lanzl and Hanson[5]) we use Moliere's scattering theory (Moliere 1948[8])) to derive the effective mean electron scattering angle for tungsten, and introduce this into the above expression to obtain a distribution†

---

† The constant 250 in this expression is the constant C in the expression for the mean square scattering angle $< \theta^2 > = ct/u^2$. In fact C is not strictly constant with respect to t, and the value $C = 250$ is an average value of C which varies slowly over the range $t = 0$–$t = 0.3$ radiation lengths.

[6]) Muirhead, Spicer and Lichtblau, Proc. Phys. Soc. A **65** (1952) 59.

[7]) Rossi and Greisen, Rev. Mod. Phys. **13** (1941) 240.

[8]) Moliere, Z.f. Naturforschung **39** (1948) 78.

$$\frac{U_0^2}{\text{cons.}}\left[-E_\mathrm{i}\left(-\frac{U_0^2\theta^2}{250t}\right)+E_\mathrm{i}\left(-\frac{U_0^2\theta^2}{\gamma\, m_0c^2}\right)\right]. \quad (10)$$

It is convenient for our purposes to write this distribution as a gaussian; graphical analysis of eq. (10) shows it to be a symmetric distribution with a full width at half height of

$$U_0^2\,\theta_{\frac{1}{2}}^2 = 0.94 + 12t\,.$$

Thus we may write for the distribution per unit solid angle of photons not too far from the center $\mathrm{e}^{-0.693\theta^2/\theta_{\frac{1}{2}}^2}$ or using the small angle approximation (element of solid angle $= 2\theta\,\mathrm{d}\theta = \mathrm{d}\theta^2$) and normalising appropriately, the number of photons between θ and $\theta + \mathrm{d}\theta$ is

$$\Theta\,\mathrm{d}\theta = \mathrm{e}^{-\frac{U_0^2\theta^2}{1.34+17t}}\,\frac{U_0^2\,2\theta\,\mathrm{d}\theta}{1.34+17t}\,. \quad (11)$$

The mean square angle between the original photon direction and the direction of emission of the positron formed is given by Stern (Rossi 1952[4]) as

$$<\psi^2> = \left(q\ln\frac{k}{m_0c^2}\right)^2 \quad (12)$$

where

$$q \sim \tfrac{1}{4}\left(1+\frac{3}{2}\,\frac{k}{U_+}\right)$$

so that we may write the angular distribution in gaussian form as

$$\Psi\,\mathrm{d}\psi = \mathrm{e}^{-\psi^2/<\psi^2>}\,\frac{2\psi\,\mathrm{d}\psi}{<\psi^2>}\,. \quad (13)$$

Finally, on leaving the target the positrons have to traverse a thickness $(T - t)$ of target material in which they suffer multiple scattering. The mean square scattering angle for this process is given (see footnote p. 10) by

$$<\varphi^2> = \frac{250\,(T-t)}{U_+^2}$$

and the angular distribution, written as a gaussian becomes

$$\Phi\,\mathrm{d}\varphi = \mathrm{e}^{-\varphi^2/<\varphi^2>}\,\frac{2\varphi\,\mathrm{d}\varphi}{<\varphi^2>}\,. \quad (14)$$

These three independent gaussians may be combined in the usual way, to give for the final angular distribution a gaussian

$$X\,(\chi)\,\mathrm{d}\chi = \mathrm{e}^{-\chi^2/<\chi_2>}\,\frac{2\chi\,\mathrm{d}\chi}{<\psi^2>} \quad (15)$$

where

$$<\chi^2> = <\theta^2> + <\varphi^2> + <\psi^2>$$

$$= \frac{250\,(T-t)}{U_+^2} + \frac{1.34+17t}{U_0^2} + <\psi^2>\,. \quad (16)$$

In eq. (16), except for $t \approx T$ the intrinsic pair distribution is negligible compared with the other two, and may be neglected.

Thus we may write

$$<\chi^2> = A + Bt \quad (17)$$

where

$$A = \frac{1}{U_0^2}\left(1.34+\frac{250T}{\alpha^2}\right) \text{ and } B = \frac{1}{U_0^2}\left(17-\frac{250}{\alpha^2}\right).$$

Combining expressions (15) and (9) we obtain for the energy and angular distribution

$$\frac{\mathrm{d}}{\mathrm{d}\chi}\left(\frac{\mathrm{d}\mathcal{N}}{\mathrm{d}U_+}\right)\mathrm{d}\chi = \frac{1}{U_0}\int_0^T\int_\alpha^1 \psi_\text{pair}\,(\psi_\text{rad}\,t +$$

$$+\,\psi_\text{corr}\,t^2)\,\frac{\mathrm{d}v}{v^2}\,\mathrm{e}^{-\chi^2/<\chi^2>}\,\frac{2\chi\,\mathrm{d}\chi}{<\chi^2>}\,. \quad (18)$$

Integrating over v

$$\frac{\mathrm{d}}{\mathrm{d}\chi}\left(\frac{\mathrm{d}\mathcal{N}}{\mathrm{d}U_+}\right)\mathrm{d}\chi = \int_0^T\{\,f\,(\alpha,\,U_0)\,t +$$

$$+\,h\,(\alpha,\,U_0)\,t^2\,\}\,\mathrm{e}^{-\frac{\chi^2}{A+Bt}}\,\frac{2\chi\,\mathrm{d}\chi}{A+Bt} \quad (19)$$

where

$$f\,(\alpha,\,U_0) = \int_\alpha^1 \psi_\text{pair}\,\psi_\text{rad}\,\frac{\mathrm{d}v}{v^2}\,,$$

$$h\,(\alpha,\,U_0) = \int_\alpha^1 \psi_\text{pair}\,\psi_\text{corr}\,\frac{\mathrm{d}v}{v^2}\,. \quad (20)$$

To find the number of positrons emitted into a forward cone of half angle η we integrate next over χ to obtain

$$\frac{\mathrm{d}\mathcal{N}}{\mathrm{d}U_\mathrm{C}} = \int_0^T\{\,f(\alpha,\,U_0)\,t + h(\alpha,\,U_0)\,t^2\,\}\,(1-\mathrm{e}^{-\frac{\eta^2}{A+Bt}})\,\mathrm{d}t$$

$$= f(\alpha,\,U_0)\,\eta^2\int_0^T\frac{t\,\mathrm{d}t}{A+Bt} + h(\alpha,\,U_0)\,\eta^2\int_0^T\frac{t^2\,\mathrm{d}t}{A+Bt}$$

for $\dfrac{\eta^2}{A+Bt} << 1\,,$

$$= f(\alpha,\,U_0)\,g_1\,(\eta,\,T) + h(\alpha,\,U_0)\,g_2\,(\eta,\,T) \quad (21)$$

where

$$g_1 = \eta^2 \int_0^T \frac{t\,\mathrm{d}t}{A + Bt} - \frac{\eta^2}{B}\left(\frac{A}{B}\right)\left[\frac{BT}{A} - \ln\left(1 + \frac{BT}{A}\right)\right]$$

$$g_2 = \eta^2 \int_0^T \frac{t^2\,\mathrm{d}t}{A + Bt} = \frac{\eta^2}{2B}\left(\frac{A}{B}\right)^2 \left[\left(\frac{BT}{A} - 1\right)\left(\frac{BT}{A} - 3\right)\right.$$

$$\left. + 3 + 2\ln\left(1 + \frac{BT}{A}\right)\right] \qquad (22)$$

and the functions $f(\alpha, U_0)$ and $h(\alpha, U_0)$, defined by eqs. (20) are

$$f(\alpha, U_0) = \frac{0.146}{U_0}\left[1.20\left(\frac{1-\alpha}{\alpha}\right)(0.692 + \ln U_0) + \right.$$

$$\left. + \frac{1.20 \ln\alpha}{\alpha} + \left(\frac{1}{2} + \frac{5}{U_0}\right)\ln\alpha\,(\ln\alpha\,U_0 - 0.308)\right]$$

$$h(\alpha, U_0) = -\frac{0.146}{U_0}\left[0.65\left(\frac{1-\alpha}{\alpha}\right) + \left(\frac{0.65}{\alpha} - \frac{\gamma}{2}\ln\alpha\right)\right.$$

$$\left. \ln\alpha + \left(\frac{0.65}{\alpha}(1 - \ln\alpha) - \gamma\ln\alpha\right)(\ln\alpha - 0.308)\right]$$

with

$\gamma = 0.5$ at $U_0 = 30$ MeV and $\gamma = 0.8$ at $U_0 = 100$ MeV . (23)

In developing eq. (21) we have assumed that the differential pair cross-section is completely flat. In fact it falls off rapidly at both wings and our calculation will therefore overestimate the number of high energy positrons.

We correct for this by choosing a closer fit to the crosssection shape and write

$$f_{\mathrm{corr}}(\alpha, U_0) = \int_\alpha^1 \psi_{\mathrm{pair}}\psi_{\mathrm{rad}}\, q(v)\frac{\mathrm{d}v}{v^2}$$

where

$$q(v) = 1 \text{ for } \frac{U_+}{k} < 0.8\text{ , i.e. } v > \frac{\alpha}{0.8}$$

$$q(v) = 5\left(1 - \frac{\alpha}{v}\right) \text{ for } v < \frac{\alpha}{0.8}$$

(see fig. 5).

Then

$$f_{\mathrm{corr}}(\alpha, U_0) = \int_\alpha^{\alpha/0.8} \psi_{\mathrm{pair}}\psi_{\mathrm{rad}}\, q(v)\frac{\mathrm{d}v}{v^2} +$$

$$+ \int_{\alpha/0.8}^1 \psi_{\mathrm{pair}}\psi_{\mathrm{rad}}\frac{\mathrm{d}v}{v^2}\,.$$

Writing

$$\int_\alpha^{\alpha/0.8} \psi_{\mathrm{pair}}\psi_{\mathrm{rad}}\, q(v)\frac{\mathrm{d}v}{v^2} \approx \tfrac{1}{2}\int \psi_{\mathrm{pair}}\psi_{\mathrm{rad}}\frac{\mathrm{d}v}{v^2}$$

we obtain

$$\text{for } \alpha < 0.8\ f_{\mathrm{corr}}(\alpha, U_0) = \tfrac{1}{2}\left[f(\alpha, U_0(+ f\left(\frac{\alpha}{0.8}, U_0\right)\right]$$

while for $\alpha > 0.8$

$$f_{\mathrm{corr}}(\alpha, U_0) = \tfrac{1}{2} f(\alpha, U_0)\,. \qquad (24)$$

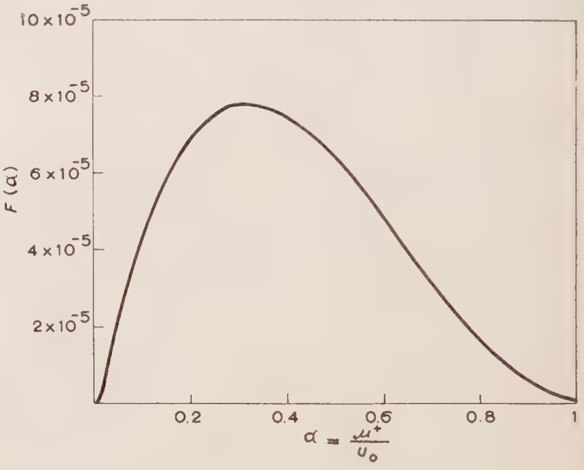

Fig. 6. The function $F(\alpha)$.

Since the correction is fairly crude, we do not apply it to the $h(\alpha)$ function.

TABLE 1
The function $F(\alpha)$

α	$F(\alpha)(\times\ 10^{-5}$
0.1	4.43
0.2	6.98
0.3	7.78
0.4	7.46
0.5	6.34
0.6	4.96
0.7	3.24
0.8	1.54
0.9	0.62
1	0

Using eqs. (22) and (24) we have computed the forward positron spectra for $U_0 = 30$ MeV and $U_0 = 100$ MeV and $T = 0.2$ radiation lengths. It turns out that the shapes of these are very similar, with both showing a broad maximum at $\alpha = 0.3$. Indeed the calculation may be finally summarised in terms of a general empirical equation for the number of positrons per MeV interval per unit solid angle in the forward direction per incident electron, given by

$$\frac{\mathrm{d}\mathcal{N}}{\mathrm{d}U_+} = F(\alpha)\, U_0\, (\ln U_0 - 0.58)\, T\, (1 - T) \qquad (25)$$

for $10 \leqslant U_0 \leqslant 100$ MeV, $T \leqslant 0.3$ radiation lengths.

$F(\alpha)$, the shape function is shown in fig. 6 and is given in tabular form in table 1.

5. Comparison with Experiment

To check the calculations, we have measured the positron spectrum in the forward direction, for incident electrons of 25 and 100† MeV. The results are shown in fig. 7, where they are compared with the calculated values given by eq. (25), and the exact calculations given by eqs. (22) and (24). At both energies the absolute scale is probably not reliable to closer than a factor of two, and the 100 MeV measurement contains a normalising factor of 1.5 to bring the experimental points into agreement with the calculated shape. The close agreement in the 25 MeV case is perhaps fortuitous. Certainly, however, the calculations agree reasonably well with experiment, and indicate that eq. (25) is a fair representation of the positron spectrum.

One of the authors (L.K.) would like to express his appreciation to the U.K. AEA and particularly Dr. E. Bretscher for the opportunity to spend a year at the Research Establishment, Harwell, where these calculations were carried out.

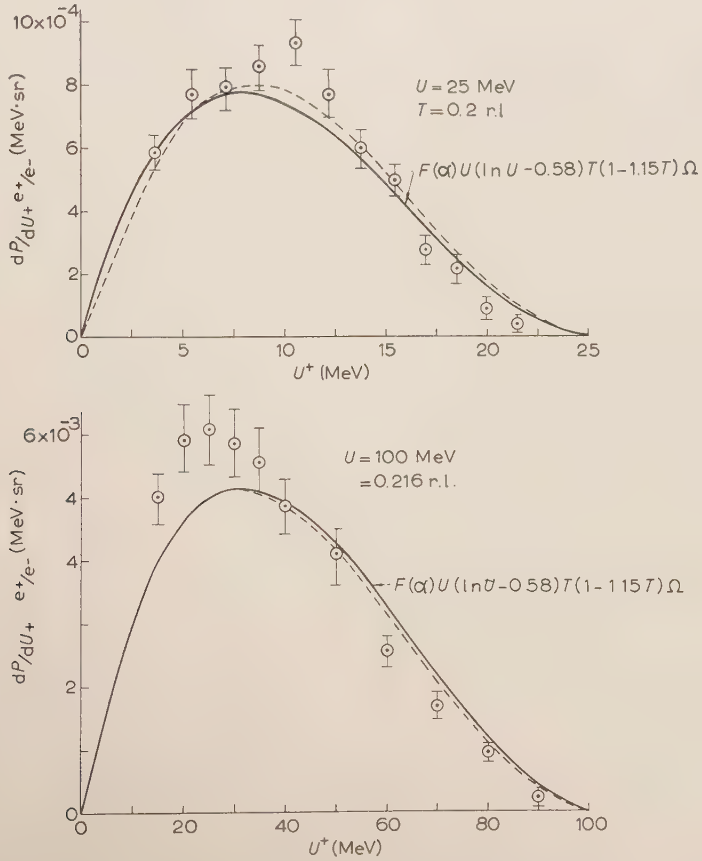

Fig. 7. Positron spectra for $U_0 = 25$ MeV and $U_0 = 100$ MeV. The solid and dotted lines are calculated from eq. (25) and eqs. (22) and (24) respectively. The 100 MeV measurement contains an arbitrary normalising factor of 1.5.

---

† The 100 MeV measurements were performed in collaboration with J. E. Leiss and R. E. Taylor at the Laboratoire Des Hautes Énergies, École Normale Supérieure, Orsay, France.

NUCLEAR INSTRUMENTS AND METHODS **11** (1961) 14–18; NORTH-HOLLAND PUBLISHING CO.

DESIRABLE LINEAR ELECTRON ACCELERATOR CHARACTERISTICS FOR NUCLEAR RESEARCH

L. KATZ

University of Saskatchewan, Saskatoon, Saskatchewan

A brief discussion is given of the desirable linear electron accelerator characteristics for nuclear research. The varies research projects possible with such machines are outlined and the machine characteristics desirable for this research are indicated.

1. Introduction

Having written the paper on the generation of positrons, I now find that I would rather discuss another topic today and would refer you to the proceedings of this conference for further information on positron generation.

During the past few months I have been devoting considerable time to the question of what physics research projects could be most effectively attacked with the aid of a linear electron accelerator or conversely, what are the main characteristics which I would like to see in such an accelerator if I were to purchase one for such research? I would now like to share some of these ideas with you.

To give this problem a proper setting I must first state that if I were to acquire one of these accelerators for research, it would probably be the only one I would have for a long time to come. Furthermore, Canada is not such an affluent country that I could have two or more of these, each tailored for a particular research project. Thus the accelerator I consider would have to serve a multiplicity of research programs. It is particularly because of its versatility that I think the linear electron accelerator is the ideal research tool for such a relatively small institute as the University of Saskatchewan.

With these few points in mind let us then ask specifically what are the research projects which one can undertake with a high energy beam of electrons and what features should be incorporated into the machine delivering this beam?

First of all I must say that the accelerator should be a machine that "likes" to work. I think research equipment in general and particle accelerators in particular can be classed as machines that "like" to work and those that don't. If well designed and properly engineered the linear electron accelerator should "like" to work. To date I know of only one such machine, the 15 MeV linear accelerator at Harwell. It could be operated day after day, for 24 hours per day, without any trouble and with remarkable stability.

A machine which is continually breaking down or continually in need of adjustment is often worse than no machine at all; since it occupies valuable space, wastes valuable time, depletes financial resources while giving only meager experimental results in return.

Thus I would place reliability at the head of my requirements. I want to be able to flip a switch to turn the machine *on*, then go ahead with the research. Perhaps this is a little too much to hope for, but any near approach to this ideal would be acceptable — say one operator at the control — with his eyes glued to the meters and his hands fiddling knobs for less than 50 % of his time!

To discuss other machine characteristics I must now give reference to the research for which it will be used.

2. Neutrons

Suppose we want a copious supply of neutrons for ordinary time of flight work. These neutrons are obtained from photoneutron or photofission reactions. As we know the cross section for both these reactions goes through a maximum $\approx$ 13–20 MeV and the integrated cross section is

$$\int_0^{E_0} \sigma \, \mathrm{d}k \approx 0.015\, A \text{ MeV-barn.}$$

Thus, to produce neutrons from a given electron current we use high Z targets, preferably uranium to take advantage of the extra fission neutrons. As the electron energy of the incident beam is increased above the reaction threshold the number of neutrons per kW of beam power increases rapidly. Barber and Dodge (Phys. Rev. **116** (1959) 1551) have shown that this is still true at electron energies of 36 MeV. At this energy the rate of increase is $\approx 3\%$ per kW, MeV; that is for a given incident beam power, 3% more electrons are obtained at 36 MeV than at 35 MeV.

One may ask how long this trend persists. Calculations in this intermediate energy region are very difficult to carry out. At higher energies however, one may use shower theory (Richard Wilson, Cambridge Electron Accelerator Project, report CEA-73). For neutrons of a few tens of MeV, or less the calculation may proceed as follows: A track length $\pi(E_0,k)\mathrm{d}k$ is defined in shower theory which is the total path length of photons in the interval k to $k + \mathrm{d}k$ in the shower produced by an electron of energy E_0. Theory (Rossi, High Energy Particles Physics) tells us that $\pi(E_0,k) = 0.6\ E_0/k^2$.

Then assuming that the photonuclear cross section is concentrated at energy k we can immediately calculate the neutron yield per electron as

$$Y = 0.013\ N_0\ X_0 \frac{E_0}{k^2} \times 10^{-24}\,.$$

Where N_0 is Avogadros number and X_0 is the radiation length of the material in g/cm^2.

Consider a lead target as an example, $X_0 = 6$, $k \sim 14$, $N_0 = 6 \times 10^{23}$.

$$Y \approx 2.4 \times 10{-4}\ E_0 \text{ neutrons/electron}$$
$$\approx 1.5 \times 10^{12} \text{ n/kW}\,.$$

Thus at very high energy we find the neutron yield to be directly proportional to the beam power and independent of machine energy.

Barber and George find experimentally the yield from lead to be 1.6×10^{12} n/kW at 34 MeV and still increasing with electron energy.

Considering the crudeness of our calculations the agreement is excellent.

Thus we conclude that to generate a maximum of neutrons we want a high beam power; also per kW of power the number of neutrons is still increasing with electron energy at 36 MeV but levels off at very high energy. From this point of view we wish to optimize machine design to get the most MeV per kW for a given cost.

If these neutrons are to be used in a conventional time of flight set-up we also want the neutron burst to be very short. How short?

The usual arguments go as follow:

(a) The resolution in a given time of flight arrangement varies as $(\Delta t/L)\sqrt{E_\mathrm{n}}$ where Δt is the pulse width, E_n, the neutron energy and L the length of the flight path.

(b) The neutrons per unit area at the end of the flight path in a time Δt varies as $(\Delta t/L^3)\sqrt{E_\mathrm{n}}$.

Thus for a given resolution and beam power the neutrons at the sample varies as $1/L^2$.

Then it is advantageous to use short path lengths, but to get good resolutions Δt must be small. How short a pulse duration is feasible?

I think you will agree that 10 nanoseconds can be almost considered standard laboratory practice and 1 nsec is now quite practical. Garg (Nucl. Instr. and Methods **6** (1959) 72) has recently built a neutron detector for time of flight work with a response of 0.65 nsec and an American company is offering an instrument off the shelf with $\frac{1}{4}$ nsec resolution for time interval measurements.

Not to be dated in our thinking, linear electron accelerators now being designed for neutron time of flight work should consider pulses of $\frac{1}{10}$ nsec duration with a repetition rate of $\approx 10^5$ pps.

Why stop here—let us take full advantage of the linear accelerator capabilities: The S band machine operates at 3×10^9 cps in the r.f. and the electrons are bunched on the wave crest of each r.f. cycle with a phase spread of 20°. This means that the individual electron bunches would pass a point in 2×10^{-11} sec ($\frac{1}{50}$ nsec). Why not bring out these pulses individually? This type of operation would also be desirable in other fields of research.

Just how good a neutron source is an electron machine? The following table is for a feasible machine.

1 keV neutrons

	Chopper	Linear acc.
	Neutron flux 3×10^{13} n/cm^2 sec	50 kW at 100 MeV nat. U target 0.1 μsec pulses
Flight path (meter)	120	10
Neutrons in gate (n/cm^2 sec)	0.001	250
Resolution $\Delta E/E$	0.02	0.02
Resolution nsec/m	10	10

10 MeV neutrons

	Linear elec. acc.	
	50 kW at 100 MeV	
Pulse length (nsec)	10	1
Flight path (meter)	100	10
Neutrons in gate (n/cm^{2}sec)	0.6	60
Resolution $\Delta E/E$	0.02	0.02
Resolution (nsec/meter)	0.1	0.1

3. Electrons

Except for the generation of a copious beam of photons or positrons one is usually interested in an electron beam with a very low energy spead. This is most readily obtained by resolving the electron beam momentum wise. It results, however, in throwing away a large fraction of the initial electron current.

Thus to obtain a 20 keV energy spread at 20 MeV from a beam with an initial energy spread of 5 % will necessitate discarding 96 % of the initial beam. Reducing the initial energy spread by a factor of 2 is equivalent to raising the machine power by a factor of two. Need I say more on energy spread?

At the present time the electron beams are so copious that throwing away 99 % of the beam still leaves much more current than has been available in the past, and, usually much more current than is required for the experiments contemplated. For example, first class electron scatter experiments have been performed with fractional microampere beams while the accelerator I am talking about has mean currents of tens of mA. However, looking into the future I am certain we will quickly run out of intensity.

I would certainly strive for a low energy spread in the electron beam. Is it too much to ask for $\Delta E/E \approx 0.01$?

There are other advantages to be gained from a small energy spread—and some difficulties arise. With a small $\Delta E/E$ it is much easier to design achromatic magnetic systems to bend the beam, on the other hand if it is energy analyzed, one needs good energy stability ($E \approx$ const.) in order that the analyzed beam does not vary erratically in intensity. I would suggest as a minimum that the energy drift over periods of hours, or from pulse to pulse be fraction-wise $\approx \frac{1}{2} \Delta E/E$.

Electron scatter from nuclei has hardly been explored. The work of Leiss and Taylor at Orsay (Karlsrühe Photonuclear Conference, 1960) have indicated the great wealth of nuclear information which can be gained from such experiments. Virtual photons transferred to nuclei in such scatter experiments can have their energy and momentum varied independently. A most interesting study is the cross section as a function of the momentum transfer at each energy.

If short duration beam pulses are used, electron scatter or X-rays bursts may be used to study the life times of excited states in stable or neutron deficient nuclei. Life times of 10^{-10} sec or better could be examined by this means. The X-rays will excite mostly states requiring low spin change, while electron scatter can lead to high spin states.

One limitation on this type of work; indeed on much of the work with fast pulses, is the dark current and late electrons which follow the main beam pulse. Work at MIT with fast pulses show that the out of pulse current should be down by at least a factor of 10^{-6}. To be specific, let me ask that the current density 2 pulse width ($2 \times \frac{1}{50}$ nsec) after the pulse be down by 10^{-6}. I will not attempt to place a limitation on the total number of electrons between pulses but such limitation is of interest.

4. Photons

In the usual type of photonuclear experiment the electron beam is used to generate bremsstrahlung. Again the electron beam needs to have a well defined energy in order to specify the maximum energy of the bremsstrahlung.

A resolution of 10 keV at 20 MeV from a machine delivering 5 kW with an energy spread of 5 % still results in 100 times the bremsstrahlung intensity presently available from betatrons.

In this type of research and in many other studies it is imperative that the electron beam energy be continuously variable from its maximum value to ≈ 1 or 2 MeV. Since many experiments require frequent changes of energy, the control should be simple and easily performed.

In studying photoneutron reactions, much can be learned from an analysis of the energies of the emitted neutrons. Recent work by Bertozzi and Demos (Nuclear Structure Conferences, Kingston, 1960) at MIT has demonstrated the value of such studies. They measured the neutron energies from the $Be^9(\gamma,n)Be^8$ and $Be^9(\gamma,n)Be^4$ reactions by time of flight. Here short duration pulses are essential, certainly 1 nsec or shorter. The $\frac{1}{50}$ nsec pulses would be ideal for this work.

5. Positrons

The shower created when a stream of fast electrons are incident on a thick target contains many positrons. The number of such positrons within a forwardly directed cone of small half angles has been calculated by Lokan and myself. These calculations have been confirmed by experiment. We find the maximum number of positrons have energies at $\approx \frac{1}{3}$ of the initial electron energy. The number of positrons per MeV energy interval per kW of electron beam varies as $\ln(E_0)$. Thus again, as in the neutron case this output is almost independent of initial electron energy.

Two methods are open to us to create a stream of positrons:

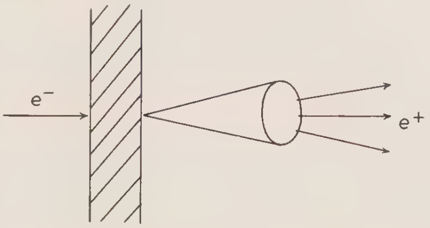

Fig. 1.

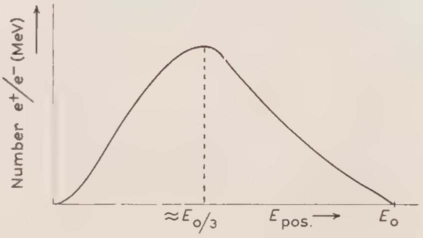

Fig. 2.

(a) Make them at the end of the linear accelerator, realizing that useful intensities are available to only 0.7 of the initial electron energy.

(b) Use a small high intensity machine to generate low energy positrons then inject these into another machine for acceleration to higher energy.

Rough calculations indicate that the first scheme is preferable from the point of view of cost per positron obtained. This is largely governed by the small acceptance angle of the second accelerating section.

With presently designed machines, a 100 MeV accelerator will give a 30 MeV positron beam of 1 MeV energy spread with intensities comparable to the electron intensities now available from a good betatron.

The positron beam can be energy analyzed and allowed to fall on a low Z target. Anihilation of the positrons in flight will give rise to a photon spectrum which looks something like this:

The width of the spike depends on the energy spread of the anihilated positron beam, the thickness of the anihilation target and the forward angle into which photons are collected.

Useful photon beams have been obtained at Saclay in France by Tzara and by Fultz at Livermore in the U.S.A.

To keep the spike width narrow machines of high electron beam power are necessary and to cover the photonuclear energy range (at least ≈ 5 to 35 MeV) a machine of at least 100 MeV is desirable.

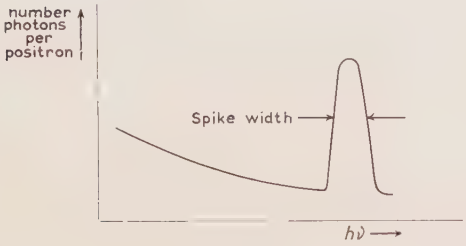

Fig. 3.

Since in many of the experiments which I have mentioned it is necessary to conduct the electron beam over long distances, (up to 50 meters) it is important that the beam leaving the machine have a very small cross sectional area and a very low angular divergence. I would suggest as 1 sq.cm and 1 milliradian as desirable values for these parameters.

A large angular divergence leads to expensive large aperture magnets and the use of troublesome quadruple lenses.

Let me summarize the desirable characteristic as follows

6. Summary

1. *Reliability*—without this the most wonderful machine just hobbles along. I mean reliability in performance.

2. *Variable energy*—a fixed energy machine is like a centipeed with all but one of its legs tied behind its back.

3. *Intensity*—so that sufficient beam current is left after it is analyzed for high resolution experiments—for some experiments low energy spread is equivalent to high intensity.

4. *Very short pulses*—to open a region of research which has been hardly explored.

5. *Large duty cycle*—who has ever had a machine with a sufficiently high duty cycle?

6. *Low cost*—so I can afford one of these machines.

NUCLEAR INSTRUMENTS AND METHODS **11** (1961) 19–28; NORTH-HOLLAND PUBLISHING CO.

COULOMB EXCITATION

TORBEN HUUS

Institute for Theoretical Physics, University of Copenhagen, Denmark

Recent work on Coulomb excitation is surveyed by means of reproductions of a table and several figures which have appeared in papers published within the last year, or were available in the form of preprints. The table summarizes the various approximations which have been employed in the theoretical description of the process. The figures illustrate the information obtained from the excitation of collective nuclear states.

In the Coulomb excitation process, nuclei are excited as a consequence of the electromagnetic interaction with the projectiles when these pass by close to the surface of the nuclei. The electromagnetic interaction is very well understood and the theory for the process can therefore be worked out in great detail.

The cross section for Coulomb excitation is most conveniently expressed in terms of the Rutherford cross section $\mathrm{d}\sigma_{\mathrm{R}}$ for elastic scattering, i.e.

$$\mathrm{d}\sigma_{\mathrm{C.E.}} = P\{\lambda, \vartheta, \eta_0, \eta_{\mathrm{f}}, B^{\lambda}_{0\mathrm{f}}\}\,\mathrm{d}\sigma_{\mathrm{R}}\ ,$$

where P is the probability that the nucleus is excited when it deflects the projectile through an angle ϑ in the C.M. system. The probability P depends on the multipolarity λ of the excitation, on the deflection angle ϑ, and on the collision index

$$\eta = \frac{Z_1 Z_2 e^2}{\hbar v}\ ,$$

which measures to what extent the projectile can be described as moving along a classical trajectory. The indices 0 and f indicate that the value to be inserted for the relative velocity v should correspond to the situation before the collision, and after the excitation of the nucleus to the various final states f, respectively.

The cross section is proportional to the reduced transition probability $B^{\lambda}_{0\mathrm{f}}$ which depends only on the structure of the nucleus, and which is the nuclear parameter one wants to extract from the measurements.

For cases where the probabilities P are small for all the levels of a nucleus, it is possible to calculate their values on the basis of perturbation theory. In the semi-classical case, i.e. for

$$\eta_0 >> 1\ ,$$

which experimentally is of very great importance, one finds that the cross sections under these circumstances to a good approximation depend on the η_{f}'s through the adiabadicity parameter

$$\xi = \eta_{\mathrm{f}} - \eta_0\,.$$

Multiple excitation becomes important when some of the P's are no longer small compared to unity, i.e. in one and the same collision the projectile produces a so-to-speak stepwise excitation of the higher lying levels. Perturbation theory naturally breaks down under these conditions, which can be characterized by

$$\chi >> 1\ ,$$

where the strength parameter χ is defined by

$$\chi = \sqrt{P^{(1)}_{0\mathrm{f}}}\ .$$

Here $P^{(1)}_{0\mathrm{f}}$ are the values which result for the probabilities if one employs the 1. order perturbation formulae in spite of the fact that this approximation is no longer valid; hence χ can become larger than unity. For these conditions the cross sections have recently been calculated by Alder and Winther[1]) in the so-called "sudden approximation", i.e. for

$$\xi << 1\ .$$

---

[1]) Alder and Winther, Mat. Fys. Medd. Dan. Vid. Selsk. **32**, no. 8 (1960).

With respect to the total cross sections (i.e. dσ integrated over ϑ) the present situation is summarized in Table 1, which has been reproduced from the paper referred to above.

TABLE 1

Survey of different limiting cases of the characteristic parameters η, ξ, and χ. In the table is indicated the kind of approximation which is appropriate for the various cases and the values of λ for which computations have been performed (cf. ref. [1]).

	η arbitrary	$\eta >> 1$ semi-classical
ξ arbitrary	$\chi << 1$ 1. order perturbation $\lambda = 1, 2$	$\chi < 1$ 1. and 2. order perturbation $\lambda = 1, 2, 3, 4$
$\xi << 1$ sudden approximation	$\chi << 1$ 1. order perturbation $\lambda = 3, 4$	χ arbitrary multiple excitation $\lambda = 2$

Because of interference terms, the differential cross sections are more elaborate to evaluate, and until recently they were only known for the single excitations in the semi-classical approximation. For the electric quadrupole excitation they have now been evaluated by J. Bang[2]) for arbitrary η_0, but only in the limit $\xi \rightarrow 0$ and $\chi \ll 1$. For small η-values the distributions become isotropic, but for $\eta \geqslant 4$ the deviations from the semi-classical limit is less than 2 per cent.

These results are important because the most precise measurements of the cross sections have been carried out by detecting the inelastically scattered projectiles. The yield of these particles is of course independent of the decay mode and therefore a good measure of the excitation cross section, but the measurements are difficult to perform in the forward directions where the background conditions are unfavourable. To obtain the total cross sections one must therefore to some extent rely on the theoretical distributions.

Bernstein and Skurnik[3]) have recently made a new experimental check of the angular distributions by investigating the scattering from Sm^{152}. Their results agree well with the theory for an E2 excitation, as is seen from fig. 1. The multipolarity can also be infered from the excitation functions shown in fig. 2. It is evident from the figure that, if one wants to employ this well established method for a determination of the multipolarity of the excitation, care should be taken to compare the particles of different A/Z at different bombarding energies, since for equal

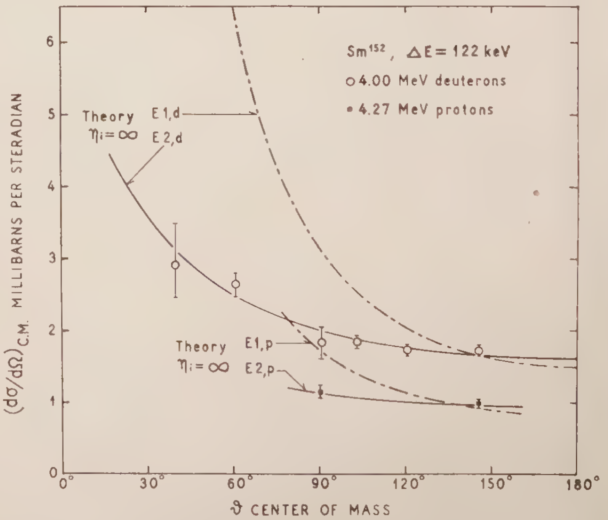

Fig. 1. Comparison between experimental and theoretical angular distributions of the scattered particles. The figure is reproduced from ref.[3]). In the present paper η_i is denoted by η_0.

---

[2]) J. Bang, Mat. Fys. Medd. Dan. Vid. Selsk. **32**, no. 5 (1960).

[3]) Bernstein and Skurnik, Phys. Rev. (to be published).

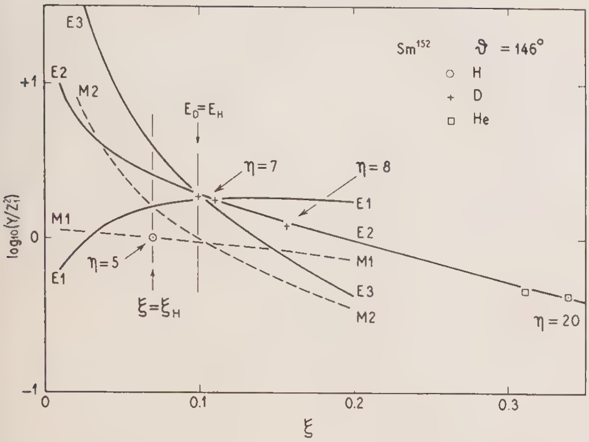

Fig. 2. Excitation functions measured by Bernstein and Skurnik[3]). The yields are denoted by Y and normalized relative to the proton point which corresponds to a bombarding energy of 4.2 MeV. The curves represent the theoretical excitation functions for projectiles with a mass to charge ratio $A_1/Z_1 = 2$. They are calculated for $\eta = \infty$ and are all normalized relative to the proton point.

energies the excitation functions (at small ξ-values) do not discriminate uniquely between the various possibilities. The experimental points, which correspond to η-values ranging from 5 to 20, are, as expected, in good agreement with the E2 curve for $\eta = \infty$.

The technique of measuring the inelastically scattered projectiles in a heavy particle spectrometer has been employed extensively by Elbek *et al.*[4]) for a precision determination of the cross sections for excitation of the rotational states of nuclei in the rare earth region. Their results with some later additions are shown in fig. 3. The isotopes of osmium have not yet been measured by this method, and the points shown for this element correspond to results obtained by studying the gamma rays[5]) and the conversion electrons[6]) emitted in the decay of the excited states. Rester *et al.*[6]) conclude from the apparent discrepancy that the theoretical conversion coefficients employed in the evaluation of the two sets of data possibly are about 30% too low for these transitions.

In fig. 3 the measured B-values have been interpreted in terms of nuclear deformations represented by the intrinsic quadrupole moments

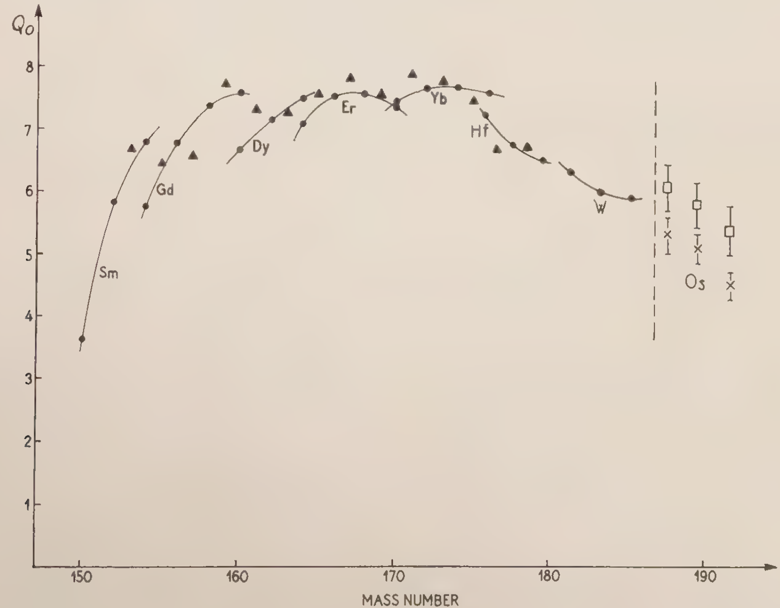

Fig. 3. Intrinsic quadrupole moments Q_0 measured in barns. The figure is reproduced from ref.[4]) with the addition of results for Hf and W obtained later with the same heavy particle spectrograph[4a]). The Os points represent cross section measurements on gamma rays (crosses, from ref.[5])) and conversion electrons (squares, from ref.[6])).

---

[4]) Elbek, Olesen and Skilbreid, Nucl. Phys. (to be published).

[4a]) Hansen, Olesen, Skilbreid and Elbek, (to be published).

[5]) McGowan and Stelson, Phys. Rev. **109** (1958) 901.

[6]) Rester, Moore, Durham and Class, Nucl. Phys. (to be published).

Q_0 measured in barns. As is well known[7]), the experimental values for Q_0 agree well with the theoretical expectations and it seems likely that the fine structure exhibited by the more precise measurements can be accounted for by an incorporation of pairing effects in the theoretical description, even though a detailed calculation on this line has not yet been carried through.

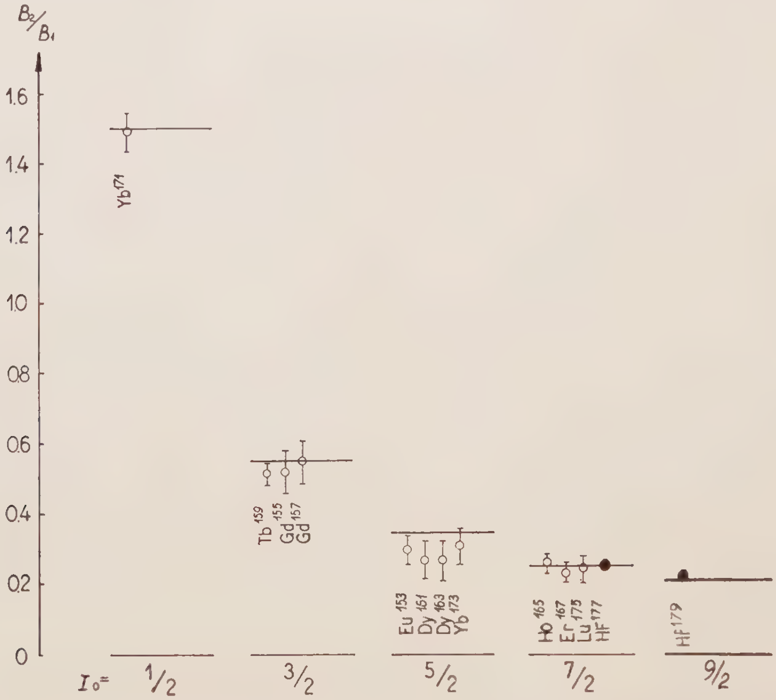

Fig. 4. Comparison between experimental and theoretical ratios of B-values corresponding to E2 transitions from the ground state to the second and first rotational state, respectively. The figure is reproduced from ref.[8]), with some later additions from ref.[4a]).

The justification for interpreting the B-values measured in these experiments in terms of Q_0 comes in particular from the studies of the odd-A nuclei for which it is possible to excite the two first rotational states, and thus to check the intensity rules derived from the rotational description. Fig. 4 shows such a comparison for the ratio between the B-values measured for the second and first excited states by detecting the inelastically scattered particles[8]).

Detection of the scattered particles yields the most precise results, but it gives no information about the decay. Additional testing of the intensity rules can therefore be obtained from the gamma ray and conversion electron experiments. The cascade decay of the second rotational state can proceed through mixed E2–M1 transitions and the degree of mixing can be infered from the measured conversion coefficients, or from the gamma ray angular distribution and polarization, which for pure E2 transitions have been shown[5,9]) to agree well with Coulomb excitation theory. By a model-independent analysis of such data, Bernstein and Graetzer[10]) have determined the relative B(E2)-values for the cross-over and cascade transitions, as well as the relative B(M1)-values for the two cascade transitions. The agreement with theory is satisfactory (cf. figs. 5 and 6), and one can therefore have some confidence in the gyro-magnetic factors extracted from a comparison of the data with the ground state magnetic moments. The gyromagnetic factor g_K for the last odd nucleon depends mainly on the values for the magnetic moment, whereas the collective gyro-magnetic ratio g_R depends more sensitively on the B(M1) values. The improved accuracy of the measurements has therefore in particular led to more reliable values for g_R. Our present knowledge about g_R values in the rare earth region is summarized in fig. 7, which has been reproduced from a recent paper by Bernstein and de Boer[11]). The difference between the g_R-values for odd-Z and odd-N nuclei indicate that the last odd nucleon is less exposed to the residual interactions. This

---

[7]) cf. e.g. Alder *et al.*, Rev. Mod. Phys. **28** (1956) 432.

[8]) Olesen and Elbek, Nucl. Phys. **15** (1960) 134.

[9]) Martin, Marmier and de Boer, Helv. Phys. Acta **31** (1958) 435.

[10]) Bernstein and Graetzer, Phys. Rev. **119** (1960) 1321.

---

[11]) Bernstein and de Boer, Nucl. Phys. **18** (1960) 40.

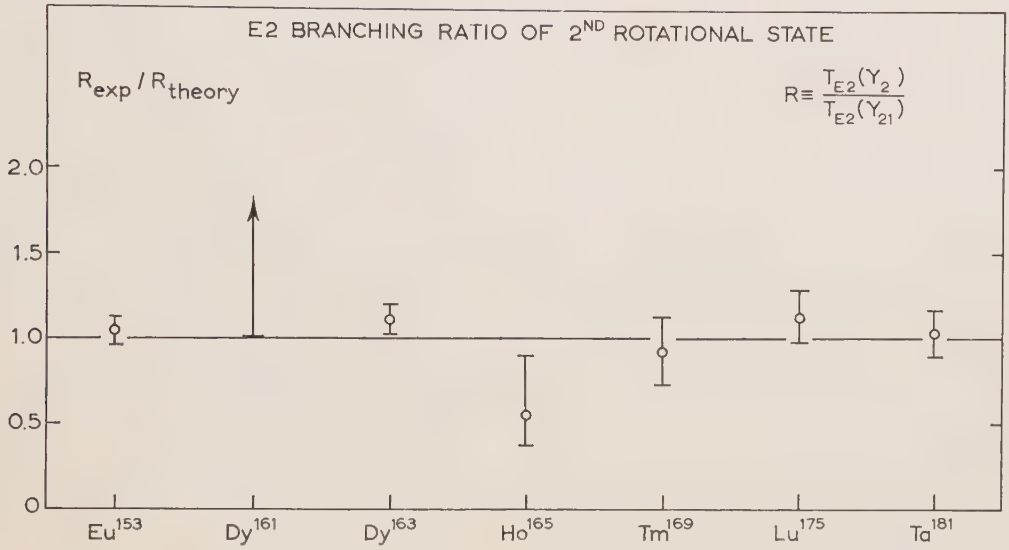

Fig. 5. Comparison between the experimental and theoretical B-values corresponding to E2 transitions from the second rotational state to the ground state and the first rotational state, respectively. The figure is reproduced from ref.[10]).

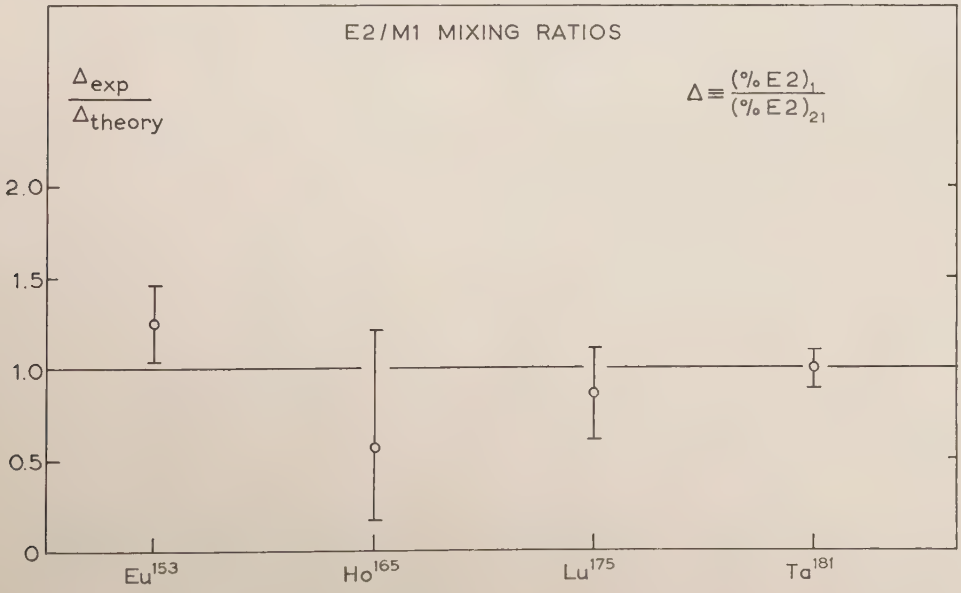

Fig. 6. Comparison between the experimental and theoretical ratios of E2/M1 mixing for the lower and the upper cascade transitions from the decay of the second rotational state. The figure is reproduced from ref.[10]).

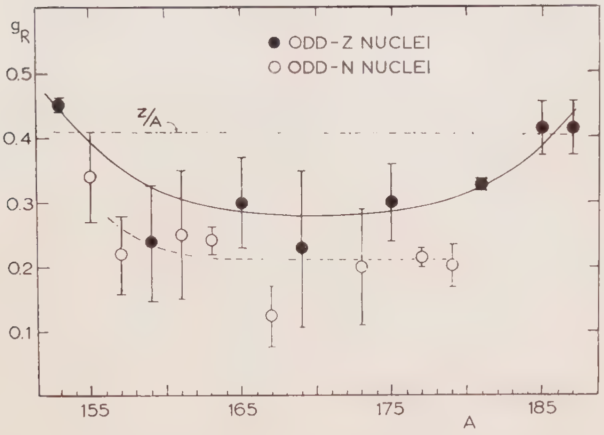

Fig. 7. Gyro-magnetic ratio g_R for collective rotation. The figure is reproduced from ref.[11]).

is already known to be the case from the fact that the odd-*A* nuclei have comparatively large moments of inertia[13]).

In a way it is an advantage that in most Coulomb excitation experiments only a few levels are populated, because it allows a clearcut interpretation, but it is of course also a very severe limitation. It is therefore very fortunate that the interaction with heavy ions as projectiles becomes sufficiently strong to permit multiple excitations of collective states. A convincing demonstration of this effect has been reported about a year ago by Stephens *et al.*[12]), who bombarded Th^{232} and U^{238} by 190 MeV argon ions and thereby obtained the gamma ray spectra shown in fig. 8. The observed peaks correspond to the cascade decay of rotational states which are excited up to the fifth or sixth level. For the conditions employed one calculates that $\chi_{0\to 2}$ $(\vartheta = \pi)$ = 3.5, and the experimental results are therefore in accordance with the theoretical values, shown in fig. 9, for the primary population probabilities. In obtaining the gamma ray spectra shown, the authors have exploited the large excitation probabilites by counting the gamma rays in coincidence with the backward scattered particles. This makes the spectra appear cleaner with a moderate loss in counting rate. It will be of great value if the experimental technique can be improved sufficiently to allow a detailed test of the theory, so that this very important method can be used for quantitative studies. The rotational transitions are the ones best suited for such a purpose, as they are comparatively well understood, and it will be interesting to confirm the predictions of fig. 9, which e.g. implies that the lower states are already depopulated in the primary process itself. In this context it should be mentioned that the rotational bands are expected to break off rather suddenly as a consequence of the pairing force. This suggestion is due to Mottelson and Valatin[14]) who from a preliminary calculation estimate that the break off in a heavy nucleus like Th^{232} should take place somewhere in the vicinity of the eighth rotational state of the ground state band.

Th^{232} and U^{238} have recently been further investigated by means of bombardments with O^{16}

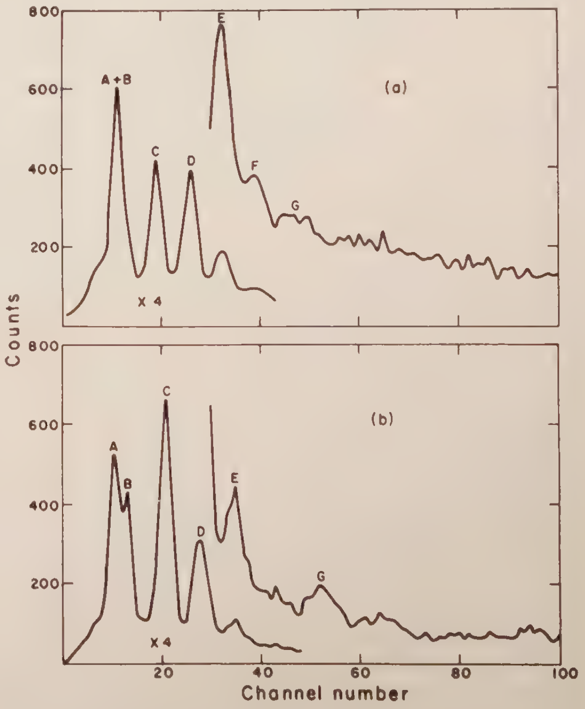

Fig. 8. De-excitation gamma ray spectrum of (a) U^{238} and (b) Th^{232}, irradiated with 190 MeV A^{40} ions. A, B, C, D, E, and F correspond to K X-rays, $4^+ \to 2^+$, $6^+ \to 4^+$, $8^+ \to 6^+$, $10^+ \to 8^+$, and $12^+ \to 10^+$ transitions, respectively, and G is a pile-up peak. The figure is reproduced from ref.[12]).

---

[12]) Stephens, Diamond and Perlman, Phys. Rev. Letters **3** (1959) 435.

[13]) cf. e.g. Mottelson and Nilsson, Mat. Fys. Skr. Dan. Vid. Selsk, **1**, no. 8 (1959)

[14]) B. R. Mottelson and Valatin, Phys. Rev. Letters (to be published).

ions (Diamond *et al.*[15])). Here E3 excitations of odd parity states were observed, as demonstrated by fig. 10. In the interpretation of the data it must be kept in mind that multiple excitations occur between the rotational bands built on the two states in question, and the authors therefore also investigated the conversion electrons which can be measured with a higher resolution. From detailed studies on these lines it should be possible to extract the octupole parameters for heavy nuclei.

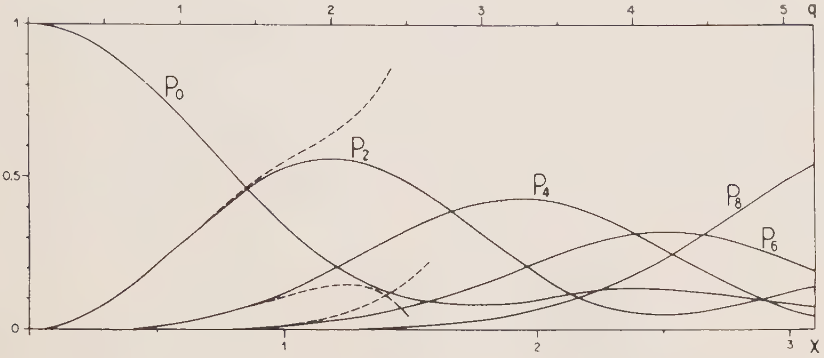

Fig. 9. Theoretical population probabilities for multiple excitation of a rotational band built on a 0^+ ground state. The probabilities P_2, P_4, etc. refer to the 2^+, 4^+, etc. rotational states and P_0 to the probability for no excitation. The broken curves represent perturbation calculations. The figure is reproduced from ref.[1]).

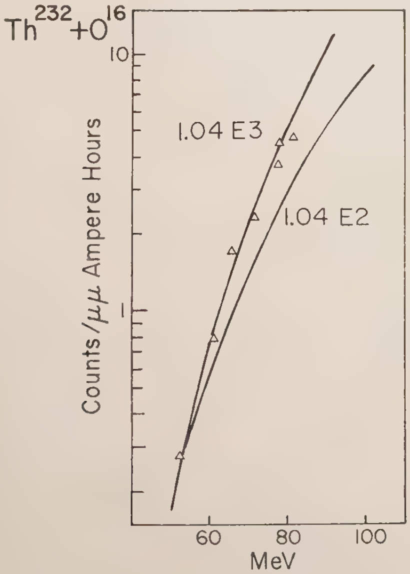

Fig. 10. Yield function for O^{16} induced E3 excitations of odd parity states at 1.04 MeV in Th^{232}. The figure is reproduced from ref.[15]).

In the same experiments also E2 vibrations were excited. In the case of Th^{232}, detailed studies of these excitations have recently been reported by other workers who employed α-particles or protons as projectiles. The gamma rays have been investigated by McGowan and

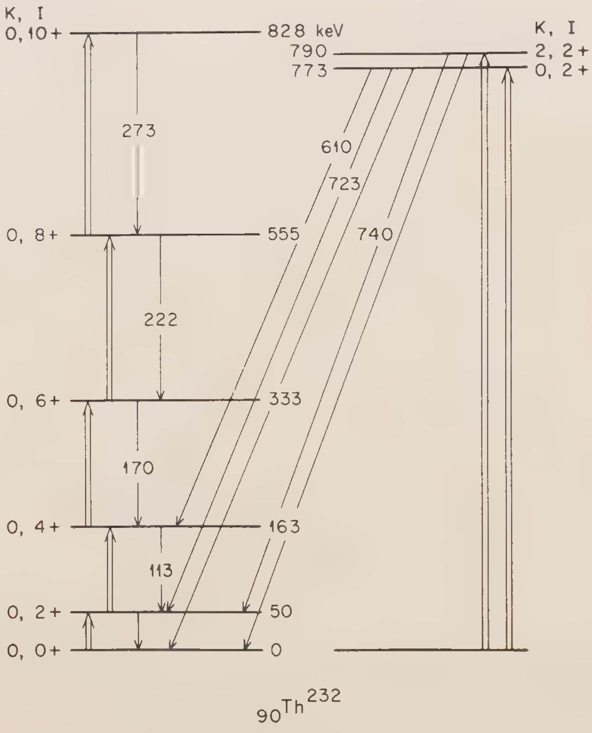

Fig. 11. Level diagram for Th^{232}. The figure is reproduced from ref.[16]).

[15] Diamond, Elbek, Igo and Stephens, reported at the Kingston Conference in Canada, Sept. 1960.

Stelson[16]), who interpret their data in accordance with the level diagram shown in fig. 11. The construction of this decay scheme was only possible by incorporation of the conversion electron data obtained by Rester *et al.*[6]). The interpretation is in particular facilitated by the identification of the strong monopole transitions which, of course, only show up in the electron spectra.

Stelson and McGowan[17]) have also recently reported gamma ray studies of even-even medium weight spherical nuclei for which one can hope to identify near harmonic E2 vibrations. Such states should be characterized by a first excited 2^+ state and a $0^+2^+4^+$ triplet situated at about twice the energy of the first state and decaying through that state by cascade E2 transitions. If the vibrations were very nearly

---

[16]) McGowan and Stelson, (to be published).

[17]) Stelson and McGowan (to be published).

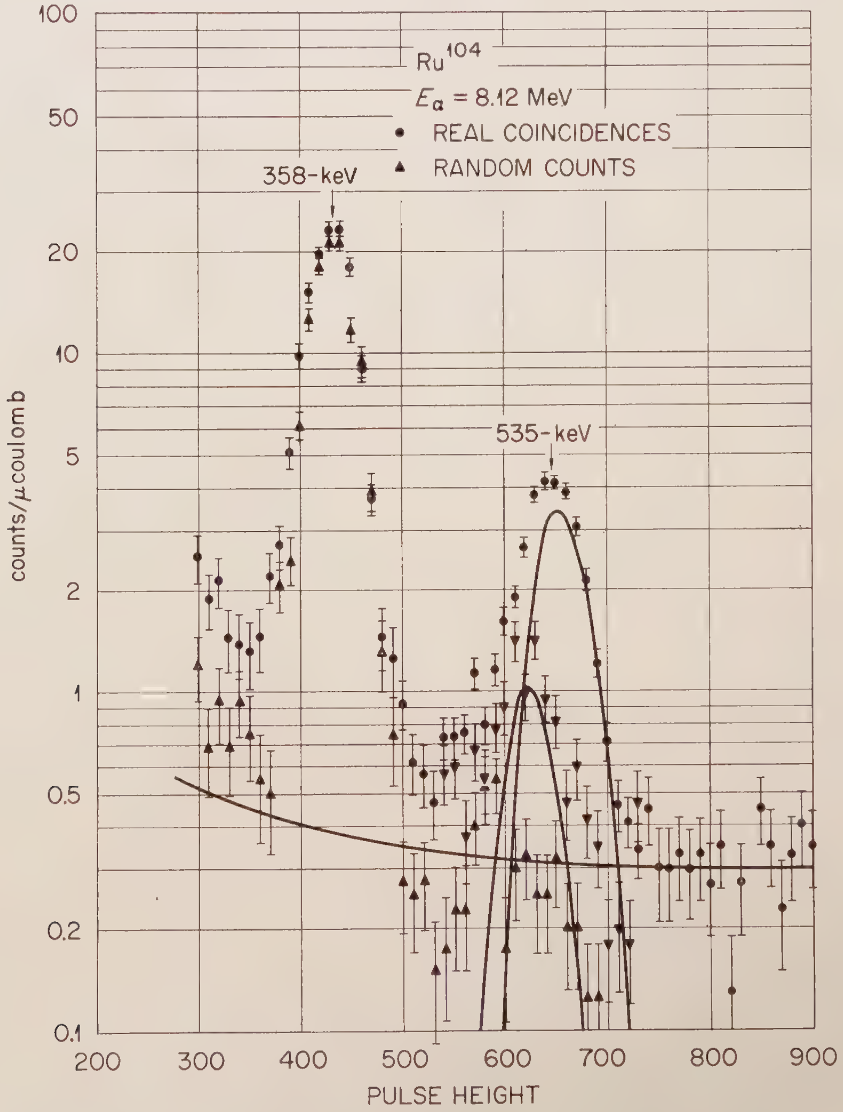

Fig. 12. Coincidence spectrum for the cascade gamma rays emitted in the decay of the second excited state of Ru^{104}. The direct excitation of the first 2^+ state at 358 keV is seen to give rise to random coincidences. The other peak exhibited by the random counts is caused by annihilation radiation from light element contaminations. The figure is reproduced from ref.[17]).

harmonic, it would be extremely hard to observe normal Coulomb excitation of any member of the triplet, because even for the second 2^+ state, which at least can be E2 excited, the cross-over B-value would be negligible; in addition to this, the cascade gamma ray would be coincident in energy with the gamma rays from the direct population of the first 2^+ state. This is, however, not quite the case and it has therefore been possible to detect the cascade gamma rays by recording them in coincidence with each other, as is illustrated by fig. 12. With α-particles of 9 MeV, the background conditions prevent observation of gamma rays from the second state unless they are recorded in coincidence, and for this reason no cross-over gamma rays were observed. In order to obtain the B-values related to the second excited state, one then has to rely on branching ratios found in β-decay investigations of transitions which are supposed to be identical with those studied in the Coulomb excitation experiments. This uncertainty has been avoided by Nathan and Popov[18]) who employ the technique of recording the gamma rays in coincidence with the scattered α-particles. This allows employment of higher bombarding energies because the α-coincidences discriminate against proper nuclear reactions of the type $(\alpha, n\gamma)$ etc., which in the $\gamma-\gamma$ measurements are responsible for the bothersome background effect of genuine coincidences from cascade gamma rays. Hence it was possible in a few cases to measure both cross-over and cascade gamma rays.

One way of testing the nuclear models is to measure the relative strength of the transitions $2' \rightarrow 2$ and $2 \rightarrow 0$, where $2'$ stands for the second 2^+ state. The 2 and the $2'$ states represent in the harmonic approximation one and two "phonon" excitations, respectively, and the ratio between the B-values for the above mentioned transitions should thus be 2. The experimental ratios reported in the refs.[17]) and [18]) are shown in fig. 13, from which at least can be concluded that the $2' \rightarrow 2$ transition is enhanced about as much as the $2 \rightarrow 0$ transition is.

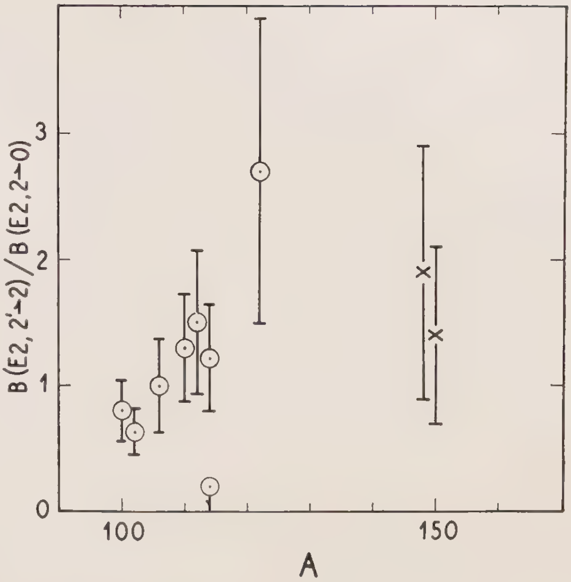

Fig. 13. Experimental ratios of B-values for the cascade transitions in spherical even-even nuclei. For harmonic oscillations the predicted ratio is 2. The points correspond to data obtained by Stelson and McGowan[17]) (circles) and by Nathan and Popov[18]) (crosses).

The vibrational states of nuclei are still far from being as well established as is the case for the rotational states. However, it has been demonstrated[15–18]) that means are now available for detailed investigations when the experimental conditions are chosen such that relatively large χ-values can be obtained. The most promising technique appears to be experiments on multiple excitations carried out by employment of heavy ions which are counted in triple coincidence with the cascade radiations, thus allowing one to combine the advantages of the various methods described above.

For this purpose it will be desirable to have the theoretical angular distributions for the decay radiations tabulated as functions of the deflection angle for the particles, not because this in itself yields any new information about the process, but because technical problems like the background conditions make it more practical to use the backward scattering angles for the coincidence measurements.

The fact that in multiple excitations more levels are excited, and the fact that some of these are expected to decay by $0 \rightarrow 0$ or other monopole transitions, makes it likely that the employment of β-spectrometers in conjunction with particle accelerators will be more frequent in the future than at present. For this reason it will be important to develop new broad range β-spectrometers with a reasonable transmission, and it appears that the wedge-gap spectrometer (i.e. a single "orange" gap) represents the type of instrument which is most promising in this respect.

---

[18]) Nathan and Popov, Nucl. Phys. (to be published).

In a few cases, excitations of single-particle states have been observed (cf. e.g. ref.[10]). With some further improvements of the background conditions such states should now become more generally accessible.

NUCLEAR INSTRUMENTS AND METHODS **11** (1961) 29–38; NORTH-HOLLAND PUBLISHING CO.

EXPERIMENTS USING ULTRA-FAST PULSE TECHNIQUES

G. GOLDRING

The Weizmann Institute of Science, Israel

Lifetime measurements were carried out at the Weizmann Institute for low-lying levels of a number of odd-A nuclei in the rare earth region. The mean lives are in the range of $(3–20) \times 10^{-11}$ sec and a special method was developed for the measurement of these short times. This consists of a microwave beam pulsing device which chops the charged particle beam producing the excited level at a frequency of 2500 Mc/sec, and a combination of a beta-ray spectrometer and a microwave cavity modulating the energy of the electrons and acting as a timed shutter for conversion electrons emitted in the decay of the excited state. The time resolution in these experiments was 7×10^{-11} sec. The ultimate time resolution that can be achieved is determined by the optical properties of the particle beam and the power available for the microwave deflection.

A method for measuring mean lives in the range $\tau \geqslant 3 \times 10^{-11}$ seconds has recently been developed at the Weizmann Institute, and a series of measurements of lifetimes of low lying levels in odd A rotational nuclei was carried out early this year by A. E. Blaugrund, Y. Dar and G. Goldring. A full report of these measurements will be published shortly, and in the present account the aim is mainly to describe in detail the method as such and to discuss its potentialities and its limitations.

This method consists of a combination of a high frequency beam chopper producing short bursts of charged particles impinging on a target and a shutter like device which is capable of selecting conversion electrons according to their time of emission from the target. Both the beam chopping and the electromagnetic shutter action are produced by microwave fields in suitably designed microwave cavities.

The general experimental arrangement is shown in the first figure: thin targets of odd A rare earth isotopes are bombarded by 2.5 MeV protons from a 3 MV High Voltage Engineering Corp. Van de Graaff accelerator, and conversion electrons following Coulomb excitation are observed in a lens type β-ray spectrometer. An oscillating transverse momentum is imparted to the proton beam by means of a microwave field of 2500 Mc/sec produced in a cavity shown in detail in figs. 2–4. In the narrow region between the reentrant post and the opposite wall a strong field is produced and it can be shown that provided the dimensions of the narrow region are small compared to the microwave wave length, the action of the field on the protons is equivalent to the action of an oscillating electric field between condenser plates of the same shape. After the protons traverse the deflection magnet they strike an aperture, and as the beam is swept across the aperture short bursts emerge made up of those protons which have acquired zero transverse momentum in the sweeping cavity. The target is located behind the aperture and the nuclear reactions are produced in regular, short time intervals.

The conversion electrons emerging from the target are timed by means of another cavity which modulates the electron energy and which is shown in figs. 5 and 6. If the conversion electrons show up as a sharp line in the spectrum and if the spectrometer field is adjusted to the peak of this line then the modulating action of the cavity throws the electrons out of focus and only those electrons will be registered which have passed the cavity at a moment when the field was zero, and whose energy therefore remained unchanged. In this way both the proton beam initiating the reaction and the emerging conversion electrons are timed, the protons which hit the target and the electrons which are registered are those which have passed the respective cavities at phases corresponding to zero field. By changing the relative phase between the cavities, a variable time scale is established between the production of the excited nuclear state and its decay. In practice the relative phase is kept constant and the velocity of the protons is varied, thereby changing their time of flight t between the sweeping cavity and the target. A velocity change of the protons Δv is equivalent to a phase change $\Delta\varphi$ given by:

$$\Delta\varphi = \omega t \frac{\Delta v}{v}$$

where ω is the angular frequency of the micro-wave field.

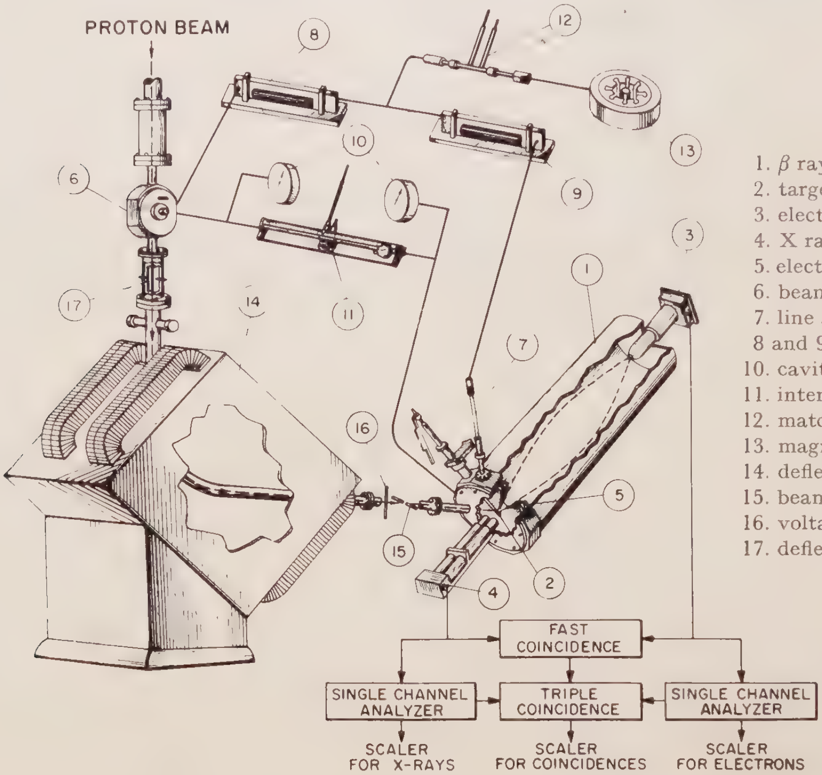
PROTON BEAM
FAST COINCIDENCE
SINGLE CHANNEL ANALYZER
TRIPLE COINCIDENCE
SINGLE CHANNEL ANALYZER
SCALER FOR X-RAYS
SCALER FOR COINCIDENCES
SCALER FOR ELECTRONS
1
2
3
4
5
6
7
8
9
10
11
12
13
14
15
16
17

1. β ray spectrometer;
2. target;
3. electron counter;
4. X ray counter;
5. electron energy modulating cavity;
6. beam sweeping cavity;
7. line stretcher;
8. and 9. unilines;
10. cavity power monitors;
11. interferometer;
12. matching transformer;
13. magnetron;
14. deflection magnet;
15. beam chopping slits;
16. voltage stabilizing slits;
17. deflection plates.

Fig. 1. General experimental arrangement.

Fig. 7 shows how the counting rate is expected to vary with phase difference in an idealized case. The full line is assumed to be the response to prompt radiation, i.e. radiation from a level having an infinitely short mean life. The broken lines represent the response for two transitions having finite mean lives, one with $\tau = 1/\omega$ and one with $\tau = 2/\omega$. It would obviously be of advantage to observe the prompt response directly but this is rather difficult since there are no conversion electron transitions fast enough to serve as prompt-radiations, the transitions measured being among the fastest in this energy

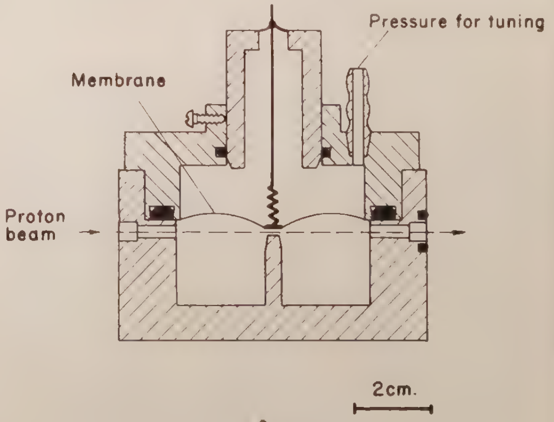
Pressure for tuning
Membrane
Proton beam
2cm.

Fig. 2. Beam sweeping cavity.

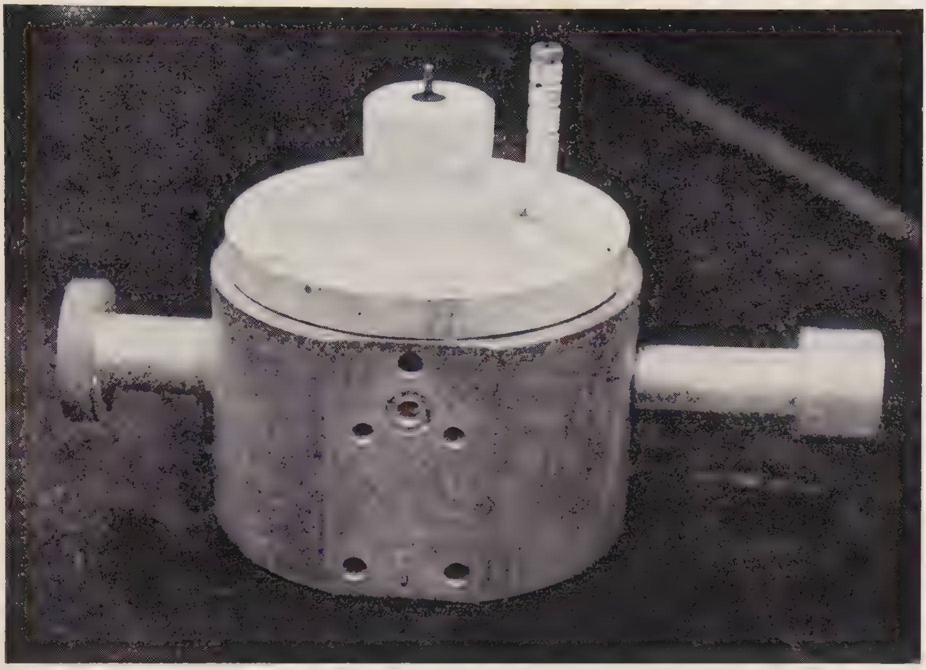

Fig. 3. Beam sweeping cavity.

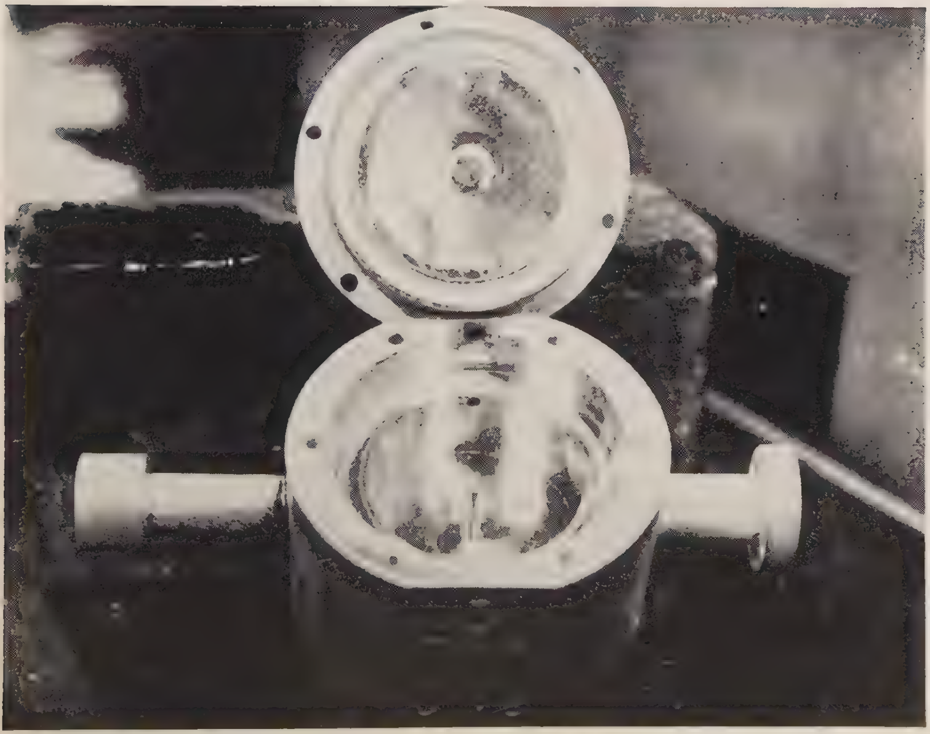

Fig. 4. Beam sweeping cavity (opened up).

region. We observe however that the various lines in this graph depend on the quantity $\omega\tau$, the curves getting steeper as $\omega\tau$ is reduced; the "prompt" curve corresponds to $\omega\tau = 0$. It is therefore clear that one may observe the prompt response curve not only in cases for which $\tau = 0$ but also in measurements with transitions having finite τ, but with $\omega = 0$.

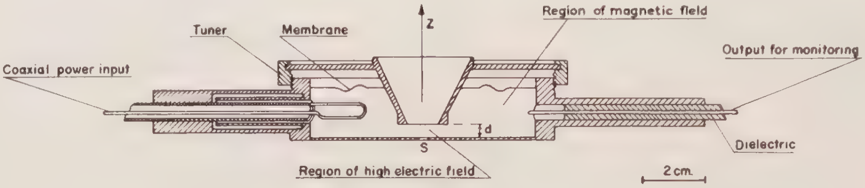

Fig. 5. Electron energy modulating cavity.

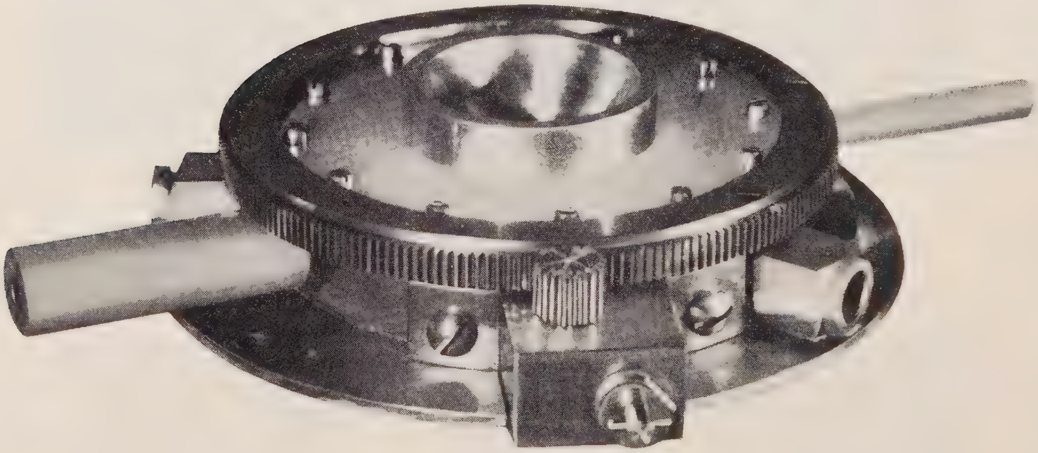

Fig. 6. Electron energy modulating cavity.

Measurements of this nature were carried out for all the transitions investigated by sweeping the beam with a 50 cycles field between two condenser plates and by modulating the spectrometer current at the same frequency. The two measurements ($\omega \neq 0, \tau \rightarrow 0$ and $\tau \neq 0, \omega \rightarrow 0$) are identical insofar as phase width is concerned i.e. phase broadening due to the finite amplitude of modulation, the slit width and the spectrometer resolution. The two measurements differ however in that for finite ω and $\tau = 0$ there may also be a broadening due to a genuine time spread, notably in the time of flight of the protons from the cavity to the target. We therefore expect a mesurement for finite ω and $\tau = 0$ to yield a response curve somewhat broader than a measurement with $\omega \rightarrow 0$.

In drawing the curves in this figure, it has been assumed that the only electrons emitted from the target are conversion electrons. This is generally not true since there is always some source of background radiation. We shall now discuss the modification in the distribution function brought about by background counts. We consider first some prompt ($\tau = 0$) radiation which has a spectrum $S(E)$ (this is the spectrum *as measured in the spectrometer*). If we set the spectrometer to some value E_0 and apply the modulating fields to the protons and electrons, the number of counts as a function of phase angle will be given by:

$$N_0(E_0, \varphi) = \tfrac{1}{2}\left[S(E_0 - \Delta \sin\varphi) + S(E_0 + \Delta \sin\varphi)\right] .$$

where Δ is the voltage (integral of the electric field across the gap) amplitude of the microwave field. We have assumed for simplicity that the proton pulse is infinitely narrow. The two terms in the relation given above derive from the fact that the beam and the electron pulses have a recurrence phase of π. It is evident that if $S(E)$ exhibits a narrow symmetric peak (narrow with respect to $\triangle$ and symmetric with respect to E_0) than the peak will be reproduced practically unchanged in the "φ spectrum":

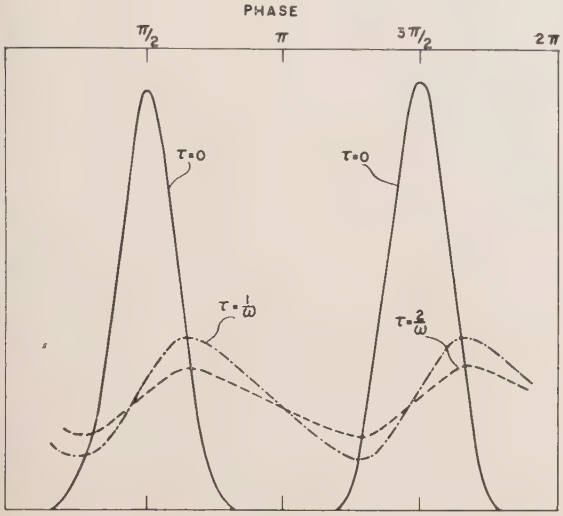

Fig. 7. $N_0(E_0,\varphi)$ for idealized case.

$$N_0(E_0,\varphi) \sim S(E_0 + \Delta\varphi)\,.$$

If however $S(E)$ represents some slowly varying function of energy, such as are typical for most "background" radiations, then $N_0(E_0,\varphi)$ will be in effect a "symmetrized" version of $S(E)$ and as a result $N_0(E_0,\varphi)$ will be very nearly a constant.

If the radiation with spectrum $S(E)$ is decaying with mean life τ than the observed φ spectrum will be given by:

$$N_\tau(E_0,\varphi) = \frac{1}{\omega\tau}\int_{-\infty}^{\varphi} N_0(E_0,\varphi')\,\mathrm{e}^{-\frac{\varphi-\varphi'}{\omega\tau}}\,\mathrm{d}\varphi'\,.$$

We now consider a case where the spectrum $S(E)$ is made up of several different parts: a "line" (around E_0) $\overline{S}(E)$, decaying with mean life τ, and a number of "background" radiations $S^{(i)}(E)$, decaying with mean lives τ_i, where one of the τ_i may vanish and another may conceivably be equal to τ; we only assume that all $N_0^{(i)}(E_0,\varphi)$ corresponding to the $S^{(i)}(E)$ are constants. If the $N_0^{(i)}(E_0,\varphi)$ are folded with the proper exponentials to give $N_{\tau_i}^{(i)}(E_0,\varphi)$ one finds that: $N_{\tau_i}^{(i)}(E_0,\varphi) = N_0^{(i)}(E_0,\varphi)$ and the complete distribution function measured in a microwave modulation experiment is given by:

$$\begin{aligned} N_{\text{delayed}}(E_0,\varphi) &= \sum N_{\tau_i}^{(i)}(E_0,\varphi) + \overline{N}_\tau(E_0,\varphi) \\ &= \sum N_0^{(i)}(E_0,\varphi) + \overline{N}_\tau(E_0,\varphi) \end{aligned}$$

where $\overline{N}_\tau(E_0,\varphi)$ is the delayed distribution function for the line represented by $\overline{S}(E)$. A "prompt" measurement would yield the distribution function:

$$N_{\text{prompt}}(E_0,\varphi) = \sum N_0^{(i)}(E_0,\varphi) + \overline{N}_0(E_0,\varphi)\,.$$

We therefore expect the prompt distribution to exhibit a line $\overline{N}_0(E_0,\varphi)$ superimposed on a constant background, and this background can be subtracted from the delayed distribution function—without having to inquire into the time dependence of the background radiation—to yield the delayed distribution function $\overline{N}_\tau(E_0,\varphi)$ corresponding to the prompt distribution function $\overline{N}_0(E_0,\varphi)$.

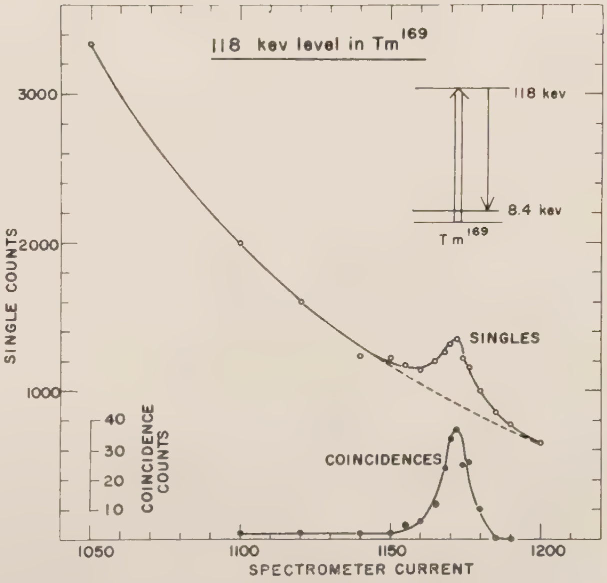

Fig. 8. Spectrum of Tm^{169} near conversion line of 110 keV transition.

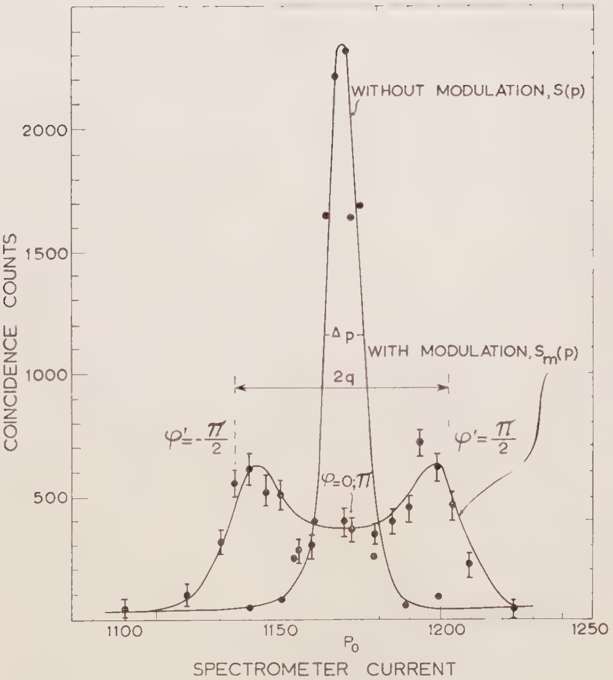

Fig. 9. Momentum spectrum of electrons with and without modulation.

As an illustration to the way in which information is obtained in a real experiment we consider in detail the measurement of the mean life of the second excited level (118 keV) in Tm^{169}. The observed transition is the 110 keV transition to the 8 keV level. In fig. 8 we see the electron spectrum in the neighbourhood of the K conversion line of the 110 keV transition. The rather large background is due to δ-ray emission from the target. In order to decrease this background a NaI crystal counter was placed behind the targets and coincidence counts were registered between K X ray counts in the crystal and electron counts in the spectrometer. The spectrum (as a function of electron momentum) of these coincidence counts is shown in the lower line. The great reduction in the background level is due to the fact that at these energies and in this range of Z the great majority of δ-ray electrons are emitted from outer shells. The effect of the energy modulation on the electrons is seen in fig. 9 where one curve represents again the spectrum of electrons from the Tm^{169} transition in coincidence with K X rays and the other curve shows the spectrum obtained (counts vs. spectrometer current) with the electron energy modulation cavity in operation (and with a steady unmodulated beam). The conversion line is broadened by the modulation and in this broadened spectrum there is now a definite phase relationship between momentum and phase. In particular the electrons observed at the position of the unmodulated peak value p_0 correspond to the phase 0 and π.

The effect of the beam sweeping cavity is similarly shown in figs. 10 and 11, were the beam profile is shown without and with the beam sweeping cavity in operation.

In fig. 12 we see the combined effect of the two cavities. The coincidence counting rate is here plotted as a function of phase difference between the cavities. The "prompt" curve similarly represents the coincidence counting rate in a 50 cycle modulation measurement. The 50 cycle distribution function exhibits the fact

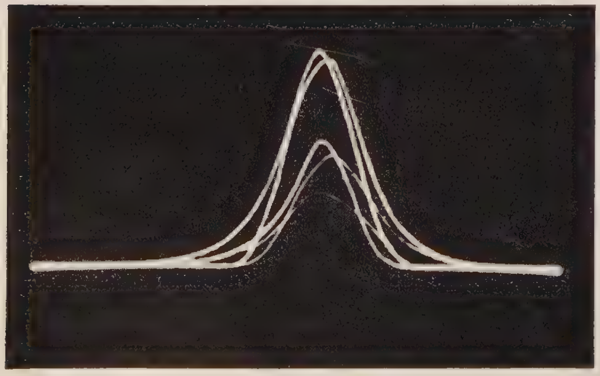

Fig. 10. Beam profile.

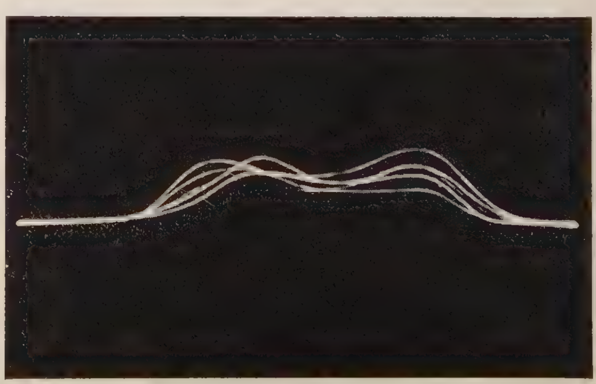

Fig. 11. Beam profile with beam sweeping cavity in operation.

that the background is very nearly constant, and as was pointed out before, it is possible to subtract the background quite accurately from the microwave distribution function. The prompt distribution function (after background subtraction) vanishes over an appreciable range, $0.2 \times T \approx 8 \times 10^{-11}$ sec, and we expect the delayed distribution function to exhibit a pure exponential decay in this region. In fig. 13 we see the microwave distribution function after background subtraction plotted on a logarithmic scale, and the exponential decay is quite evident. The slope of the decay curve corresponds to a mean life τ of $(9.0 \pm 0.4) \times 10^{-11}$ sec. The time scale is established in a very accurate and straightforward manner: the phase periodicity is observed experimentally (as in fig. 12) and enables one to calibrate the time scale directly in terms of the microwave period.

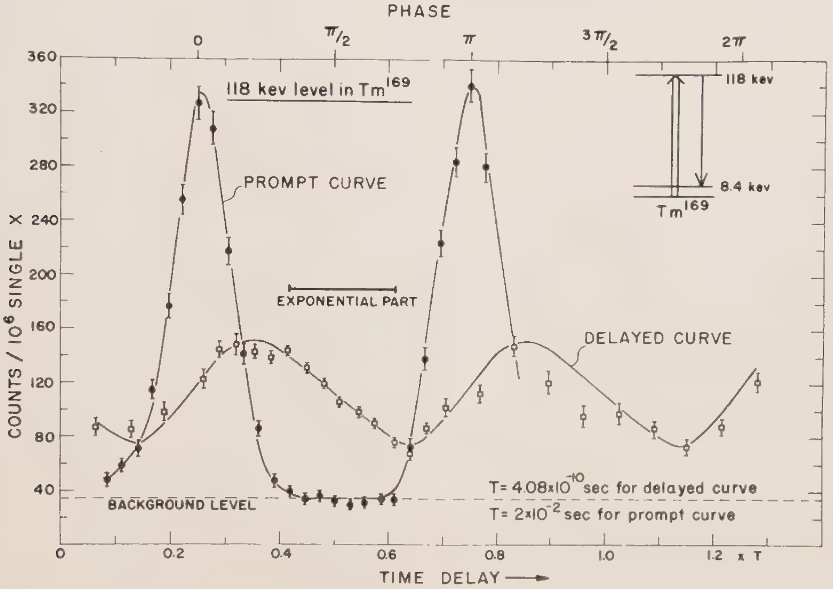

Fig. 12. Prompt and delayed distribution functions for the 110 keV transition in Tm^{169}.

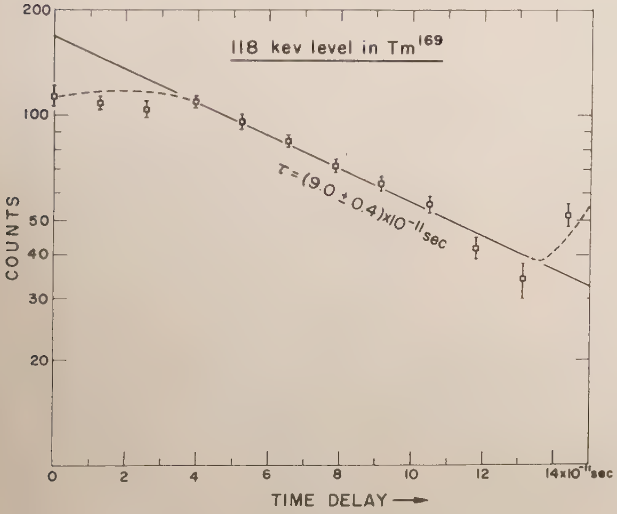

Fig. 13. Delayed distribution function for the 110 keV transition in Tm^{169} after background subtraction.

Similar measurements have been carried out for the transitions from the first excited state to the ground state in Lu^{175}, Hf^{177}, Hf^{179}, Ta^{181}, Re^{185}, and Re^{187}. The mean lives of these states were found to be:

$$\tau(\mathrm{Lu}^{175}) = (14.6 \pm 1) \times 10^{-11}\ \mathrm{sec}$$

$$\tau(\mathrm{Hf}^{179}) = (5.4 \pm 0.4) \times 10^{-11}\ \mathrm{sec}$$

$$\tau(\mathrm{Ta}^{181}) = (6.0 \pm 0.5) \times 10^{-11}\ \mathrm{sec}\,.$$

The mean life of Hf^{177} was found to be rather too long for a convenient measurement with the present microwave system (fig. 14) and the mean lives of the first excited states in the two Re isotopes were found to be too short for an accurate measurement (fig. 15) The limits found for Hf^{177} on the one hand and for Re^{185}, Re^{187} on the other hand constitute indeed the limits of applicability of the present timing system ((3–50) × 10^{-11} sec).

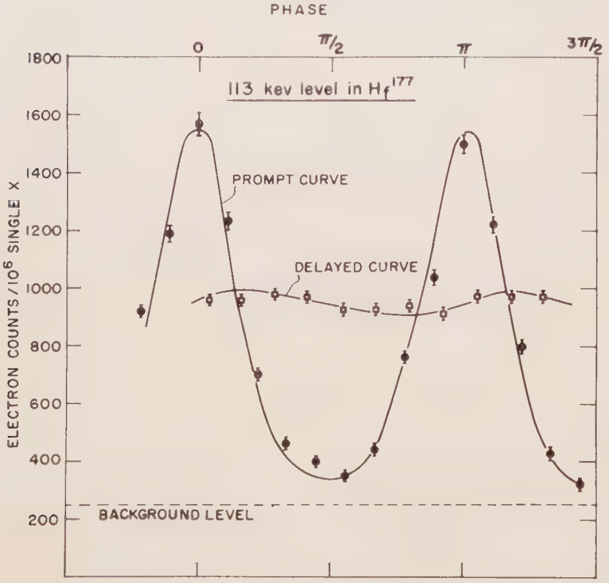

Fig. 14. Prompt and delayed distribution functions for Hf^{177}.

The restriction on longer lifetimes could easily be removed by reducing the frequency of the modulation system. This seems however of doubtful value since measurements in this range can now be carried out much more easily with conventional electronic timing methods. The restriction on short times is due to the limited time resolution of the modulation system, and this will now be considered in detail.

It has already been observed that the width of the prompt pulse distribution function is made up of two parts: a phase broadening and a time broadening due to time inhomogeneity in the proton beam. The phase broadening can be decreased in principle in a straightforward way by increasing either the amplitude or the frequency of the modulating fields. The time spread in the proton beam on the other hand poses a much more severe restriction and it constitutes indeed the fundamental limitation in this type of measurement. One can get estimates of the magnitude of this time spread in a number of ways.

a. In the idealized picture in fig. 7 the minima and the maxima of the delayed distribution curves lie on the prompt distribution curve. In fig. 12 the two curves were so shifted with respect to each other that the minimum of the delayed (microwave) modulation curve lies on the prompt (50 cycle) modulation curve. The maximum of the delayed curve is seen to be removed from the prompt curve indicating that the "true prompt" curve is somewhat broader. From the shift in the position of the maximum one estimates the time spread to be about 3 × 10^{-11} sec.

b. It is well known that one may obtain a measure of the mean life by comparing the prompt and the delayed distribution functions. This relationships may be used to derive the width of the true prompt distribution function in the four cases for which the mean life has been measured by observation of the exponential decay. Comparing these widths with the widths of the 50 cycle distribution functions one obtains consistently an additional inherent time spread of (3 ± 1) × 10^{-11} sec. This figure is also con-

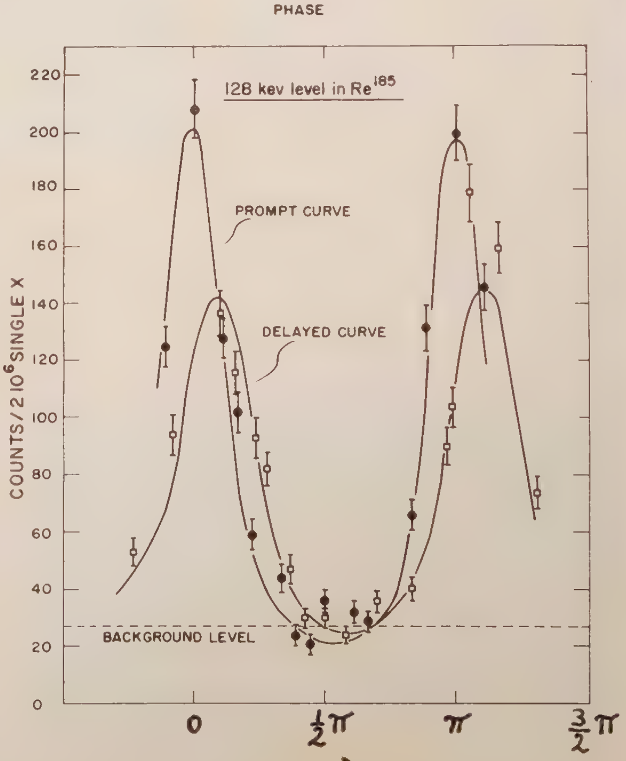

Fig. 15. Prompt and delayed distribution functions for Re^{185}.

sistent with the difference in widths in the 50 cycles and microwave distribution functions for the fast transitions in Re^{185}, Re^{187}.

We now examine the causes of this time spread; the time of flight of the protons from the sweeping cavity to the target is given by: $t = l/v$. In our arrangement: $l = 230$ cm, $v = 2.5 \times 10^9$ cm/sec and therefore: $t \approx 10^{-7}$ sec. If there is an inhomogeneity in either the path length or in the velocity of the protons, a time spread $\mathrm{d}t$ will be produced:

$$\mathrm{d}t = \left(\frac{\mathrm{d}l}{l} - \frac{\mathrm{d}v}{v}\right) t \,.$$

A velocity spread is always present in the proton beam, and one also has a path length spread $\mathrm{d}l$ because the beam entering the sweeping cavity has a finite width. Both effects may be minimized by suitable geometrical synchronization arrangements. By placing the target at an angle one can make use of the fact that after the deflection magnet the proton path and therefore l are a function of the velocity v. One can then find an angle for which the differential:

$$\frac{\mathrm{d}l}{l} - \frac{\mathrm{d}v}{v} = \left(\frac{1}{l}\frac{\mathrm{d}l}{\mathrm{d}v} - \frac{1}{v}\right) \mathrm{d}v$$

vanishes. Similarly the $\mathrm{d}l$ spread may be compensated for by having the target at a suitable distance from the point where the beam converges to a focus. Closer inspection reveals that the total time spread due to the two effects mentioned can be reduced only to a degree depending on the optical quality of the beam, i.e. the quantity $\Delta x\, \Delta\theta$ where Δx is the width and $\Delta\theta$ the angular spread of the beam at the position of the target. The minimum time spread that can be achieved is given by:

$$\Delta t = K \frac{\sqrt{l\, \Delta x\, \Delta\theta}}{v} \,.$$

K is a numerical constant depending somewhat on the geometrical details. It is always close to unity and in our particular arrangement:

$$K \approx 1.5 \,.$$

In our experiments we had $\Delta x \approx 0.3$ mm, $\Delta\theta \approx 3 \times 10^{-4}$ (and as mentioned before: $l = 230$ cm, $v = 2.5 \times 10^9$ cm/sec). The minimum spread that can be achieved with such a beam according to the formula given above is:

$$\Delta t \approx 2 \times 10^{-11} \text{ sec} \,.$$

The observed spread: $\Delta t = (3 \pm 1) \times 10^{-11}$ sec is seen to be not very far from this limiting value.

An alternative method would be to place the sweeping cavity *after* the deflection magnet. This would completely eliminate the path length spread $\mathrm{d}l$, and the velocity spread which for a tilted target (at an angle α) arrangement is given by $(\Delta x/v) \tan\alpha$ could also be reduced by reducing Δx (at the expense of $\Delta\theta$). However in this system other limitations appear. These have been stated explicity and analyzed at length in a recent publication by T. K. Fowler and W. M. Good¹). In this work it is pointed out that the sweeping action itself introduces an energy spread in the beam and with it a time spread is produced. There is therefore a limiting pulse duration which is given by:

$$\Delta t' = \frac{\sqrt{l\, \Delta x\, \Delta\theta}}{v} \,.$$

In the case discussed above, the sweeping cavity being situated before the deflection magnet, the time spread produced by the induced energy spread is cancelled by the synchronizing action of the deflection magnet and tilted target combination.

It is a remarkable fact that although the nature of the basic limitations is quite different in the two situations discussed above, the final limitation on the pulse duration is essentially the same for both.

In concluding these remarks on the limitations of the time resolution it should be pointed out that the resolution may also be improved quite significantly by placing an accelerating cavity in a position intermediate between the sweeping cavity and the target. In this way the protons may be bunched and the total time spread reduced in a manner completely analogous to the combined sweeping and bunching systems

---

¹) T. K. Fowler and W. M. Good, Nucl. Instr. and Meth. 7 (1960) 245.

now being constructed for RF beam modulation.

The most severe restriction on this type of measurement is probably not any limitation on beam timing accuracy, but rather the fact that for timing the decay one needs conversion electrons for the microwave field manipulations. The requirement of reasonably high conversion coefficients limits the scope of this timing method to low energy transitions in medium and heavy nuclei. For most of these transitions the mean lives are expected to be larger than 10^{-11} sec and these should definitely be measurable as far as timing precision is concerned.

Even though the scope of this type of measurement is thus severely restricted, there are still large and important groups of nuclear levels for which these methods are expected to be very suitable. In particular two such groups should be pointed out here: the first comprises the first two excited levels in odd A rotational nuclei. The levels so far studied by this method are first excited levels from this group and measurements of mean lives of the second excited levels in the same nuclei are now being planned. Such a combined precise evaluation of the M1 transition probabilities for two transitions within the same rotational band is of interest because it would test one of the fundamental and far reaching predictions of the theory of collective rotation, namely that all reduced M1 transition probabilities within one rotational band are related to each other in a purely geometrical manner.

The second group consists of the 4^+ rotational levels in even nuclei (decaying to the 2^+ level). These can now be excited in tandem machines accelerating highly ionized oxygen ions. Such measurements would be of importance since in most of these, the simplest rotational nuclei, only one E2 quantity is known at present; this is the E2 transition probability in the transition $2^+ \rightarrow 0^+$. Here again the evaluation of the transition probability for the $4^+ \rightarrow 2^+$ transition would make it possible to relate the measurements to a prediction of the collective motion theory: the geometric relationship between the E2 transition probabilities in a purely rotational band.

DISCUSSION

Speaker adressed: G. Goldring (*Rehovoth*)

Question by: L. Katz (*Saskatoon*)

Question: Do I understand you to have some reservations in regard to efforts for very short pulses from linear electron accelerators?

Answer: I do not consider it at all impossible. I only think that one would have to look very carefully into effects similar to those discussed here, especially since the requirements on "optics" appear to be so stringent.

NUCLEAR INSTRUMENTS AND METHODS **11** (1961) 39; NORTH-HOLLAND PUBLISHING CO.

DUREES DE VIE NUCLEAIRES

E. COTTON

C.E.N., Saclay, Gif-sur-Yvette (S & O)

A short review is given of general trends and experimental results of methods used in recent works to get nuclear widths and lifetimes, especially in the case of electromagnetic transitions. Resonance curves of charged particles and neutrons, resonance fluorescence of X-rays, Doppler methods, direct measurements of lifetimes by delayed coincidences with or without pulsed beams are successively examined.

L'exposé a consisté en un rappel des principales méthodes utilisées pour déterminer, soit les temps de vie, soit les largeurs de niveaux des états nucléaires, illustré par des résultats récents mais déjà publiés ou en cours de publication; il ne m'a donc pas semblé utile d'en publier le texte intégral. Je donnerai seulement ici un tableau des méthodes utilisées avec les références aux exposés généraux et aux résultats récents cités en exemple (excluant ceux obtenues par radioactivité).

Largeurs

Courbes de résonance (pour mémoire).
Résonance de fluorescence[1]
— $(p,\alpha\,\gamma)$
— $(p,p'\,\gamma)$[2]
— (p,γ)[3,4]
— (γ,γ) avec rayonnement de freinage[5,6,7]
avec effet Mössbauer (pour mémoire)
Elargissement Doppler[8,9]
Déplacement Doppler

Temps

Mesures directes par coïncidences γ—γ[10–13]
par coïncidences avec faisceau pulsé[14–18]

Mesure directe des éléments de matrice
(Excitation coulombienne[19])

Les régions de recouvrement des diverses méthodes se sont étendues au cours des deux dernières années, ainsi que les précisions obtenues. L'accord semble en général très bon et permet de comparer les valeurs avec les différentes prévisions des modèles nucléaires. Des mesures encore plus précises seraient cependant fort utiles dans les domaines où elles sont techniquement possibles.

[1] Metzger, Progr. nucl. Phys. **7** (1959) 54.

[2] V. K. Rasmussen, F. R. Metzger et C. P. Swann, Nucl. Phys. **13** (1959) 95.

[3] S. S. Hanna et L. Meyer-Schützmeister, Phys. Rev. **115** (1959) 986.

[4] W. L. Mouton et P. B. Smith, Nucl. Phys. **16** (1960) 206.

[5] E. L. Garwin, Phys. Rev. **114** (1959) 143.

[6] A. Bussière de Nercy et M. Langevin, Proc. Inter. Conf. Nucl. Structure, Kingston 1960, Eds. D. A. Bromley and E. W. Vogt (University of Toronto Press, 1960) p. 937; J. Phys. Rad. **21** (1960) 293; C. R. **250** (1960) 1252.

[7] P. Paul et U. Stierlin, Nucl. Phys. **13** (1960) 576.

[8] S. Devons, Proc. Rehovoth Conf. Nucl. Structure, 1957, p. 542.

[9] A. E. Litherland, B. M. Adams et J. L. Yates Proc., Intern. Conf. Nucl. Structure Kingston 1960, Eds. D. A. Bromley and E. W. Vogt (University of Toronto Press, 1960) p. 953.

[10] S. Gorodetzky, R. Richert, R. Manquenouille et A. Knipper, Nucl. Phys. **17** (1960) 684.

[11] S. Gorodetzky, R. Richert, R. Manquenouille et A. Knipper, C. R. **251** (1960) 944.

[12] S. Gorodetzky, A. Knipper, R. Manquenouille et R. Richert, Communication privée.
^{25}Mg $(p,\gamma)^{26}$Al ^{26}Al(412 keV:E2) 1.6×10^{-9}s
cible isotopique.   2e niveau excité.

[13] R. Bell et M. H. Jorgensen, Nucl. Phys. **12** (1959) 413.

[14] A. T. G. Fergusson, M. A. Grace et I. D. Newton, Nucl. Phys. **17** (1960) 1.

[15] A. T. G. Fergusson, M. A. Grace et I. D. Newton, Nucl. Phys. **17** (1960) 9.

[16] Birk, G. Goldring et Wolfson, Phys. Rev. **116** (1959) 730.

[17] A. E. Blaugrund, Y. Dar et G. Goldring, Phys. Rev. (à paraître).

[18] G. Goldring, These Proceedings, p. 29.

[19] R. K. Sheline, H. L. Nielsen et A. Sperduto, Nucl. Phys. **16** (1960) 518.

NUCLEAR INSTRUMENTS AND METHODS **11** (1961) 40–46; NORTH-HOLLAND PUBLISHING CO.

A DISCUSSION OF COLLIDING BEAM TECHNIQUES

A. SCHOČH

CERN, Geneva

Colliding beam techniques require ultra-high vacuum and particle currents and densities exceeding substantially those available in present-day accelerators. Accumulation of pulses of accelerated particles in storage devices is commonly considered a way of obtaining the particle numbers necessary. Design proposals for such devices and knowledge on the problems involved are due mainly to groups of the M.U.R.A., and of Princeton University, and to groups in Moscow. The principal difficulties arising are: the limitations to phase space compression imposed by Liouville's theorem, and gas scattering and other statistical effects tending to reduce density and lifetime of beams. In the case of relativistic electrons, orbit radiation helps to overcome these difficulties, and a storage ring system designed for the study of e–e interactions will be tested at Stanford University in the near future.

Colliding beam experiments with protons, in conjunction with recently completed Multi-GeV proton synchrotrons, might be feasible if beam stacking can be effected with maximum phase space economy. A low-energy model study planned at CERN is hoped will contribute to answering the question of feasibility.

1. Introduction

The idea of studying particle interactions by the use of colliding beams has met with growing interest during the last years. Devices for trying this technique are in an advanced state of construction at Stanford University and in the laboratory of the MURA group. The technique of colliding beams can therefore be expected to play a part in high energy physics as from next year.

The idea has been thought of for quite some time already. But it could not be taken serious before a way of obtaining high particle densities could be seen. The proposition was taken up in more detail by D. Kerst[1]) and collaborators in 1956, when the idea had appeared of accumulating and storing pulses of particles, of moderate intensity each, until the required densities were achieved. Experiments on beam storage were first made by Crawford and Stubbins in 1956 using the Synchrocyclotron at Berkeley[2]). Subsequently, understanding of the problems involved and design studies of possible devices had been promoted particularly by groups of the Midwestern Universities Research Association (MURA)[1,3]) and of Princeton University[4]) in the U.S., and by a Russian group[5]). The situation, as it presented itself at the end of 1959, was summarized by papers given and discussions held at the second conference on high energy accelerators in Geneva[6]).

---

[1]) D. W. Kerst, F. T. Cole, H. R. Crane, L. W. Jones, L. J. Laslett, T. Ohkawa, A. M. Sessler, K. R. Symon, K. M. Terwilliger and N. Vogt-Nilsen, Attainment of very high energy by means of intersecting beams of particles, Phys. Rev. **102** (1956) 590;

D. W. Kerst, Properties of an intersecting beam accelerating system, CERN Symposium on high energy accelerators, Geneva 1956, Proc. p. 36.

[2]) F. S. Crawford and W. F. Stubbins, Beam storage in the 184-inch cyclotron, UCRL report 3463 (1956).

[3]) K. R. Symon and A. M. Sessler, Methods of radiofrequency acceleration in fixed field accelerators with application to high current and intersecting beam accelerators, CERN Symposium on high energy accelerators, Geneva 1956, Proc. p. 44;

L. W. Jones, C. H. Pruett, K. R. Symon and K. M. Terwilliger, Comparison of experimental results with the theory of radio-frequency acceleration processes in FFAG accelerators, Internat. Conf. on high energy accelerators, Geneva 1959, Proc. p. 58;

MURA Staff, The MURA two-way electron accelerator, Internat. Conf. on high energy accelerators, Geneva 1959, Proc. p. 71;

L. W. Jones, Experimental utilisation of colliding beams, Internat. Conf. on high energy accelerators, Geneva 1959 Proc. p. 15.

[4]) G. K. O'Neill, Storage-ring Synchrotron, Device for high-energy physics Research, Phys. Rev. **102** (1956) 1418;

G. K. O'Neill, The storage ring synchrotron, CERN Symposium on high energy accelerators, Geneva 1956, Proc. p. 64;

E. J. Woods and K. G. O'Neill, Concentric storage rings, Bull. Amer. Phyc. Soc., Ser. II, **3** (1958) 169.

G. K. O'Neill, Experimental methods for colliding beams, Int. Conf. on high energy accelerators, Geneva 1959, Proc. p. 23;

G. K. O'Neill, Storage rings for electrons and protons, Int. Conf. on high energy accelerators, Geneva 1959, Proc. p. 125.

The present paper reviews very briefly (i) the interest in colliding beam experiments, (ii) the requirements on beams and vacuum for such experiments to be feasible, (iii) the basic features of the devices that have been suggested for storage and intersection of beams, (iv) the theoretical limitations on accumulation of particles, and (v) some considerations regarding studies being made at CERN.

2. Interest of Colliding Beams

If particles of equal and opposite momentum collide, the centre of mass is at rest. Thus, the energy available for reactions in the centre of mass frame is the sum of the energies of the incident particles, whereas for a particle of the same energy colliding with a target particle at rest, a part of the energy is wasted on centre of mass motion and therefore not available for reactions.

For particles of equal masses M, the total centre of mass energy, in units of rest energy of one particle, is

$$\frac{E_{\mathrm{C.M.}}}{Mc^2} = (2(\gamma + 1))^{\frac{1}{2}}\,,$$

if the incident particle has γ times rest energy, and the target particle is at rest. So for highly relativistic particles, $E_{\mathrm{C.M.}}$ increases only as the square root of the laboratory energy of the incident particle. Two examples may be quoted for illustration: The 25-GeV protons provided by the CERN proton synchrotron make available about 7 GeV in the centre of mass in proton-nucleon collisions, with target at rest, as compared to 50 GeV in a colliding beam experiment. Electrons of 500 MeV (the particle energy envisaged for the colliding beam experiment at Stanford) produce ≈ 22 MeV in the centre of mass, against the 1000 MeV in colliding beams. Conversely, in order to obtain 50 GeV in p–p, and 1000 MeV in e–e collisions with targets at rest, particles accelerated to 1300 GeV and 1000 GeV, respectively, would be necessary. It is obvious that accelerators for these energies would represent daring enterprises at the present stage of development, to say the least.

Colliding beam experiments with presently available energies may therefore be of incontestable value for exploratory studies at appreciably lower cost. The fact that this method provides interactions between free particles may also be of value. It is a different question how interesting the energies made available by colliding beams will be from a physics of view. There is little doubt as far as electron collision experiments, like the one being prepared at Stanford University [4,7]), are concerned, which may reveal fundamental information on the structure of the electron. As for proton interactions, it is difficult to anticipate whether any treasures are hidden in the domain opened by this technique.

3. Feasibility Requirements on Beams and Vacuum

For colliding beam experiments to be feasible the rate of beam-beam reactions must (i) exceed the rate of interactions of beam particles with residual gas sufficiently to be well detectable, (ii) be sufficient in absolute value. The reaction rates, per cm^3 of interaction volume and second, are for

beam-beam reactions: $\mathrm{R.R.}_{\mathrm{bb}} = 2c\,\sigma_{\mathrm{bb}} n_{\mathrm{b}}^2$

beam-gas reactions: $\mathrm{R.R.}_{\mathrm{bg}} = 2c\,\sigma_{\mathrm{bg}} n_{\mathrm{b}} n_{\mathrm{g}}\,,$

---

[5]) V. A. Petukov, Concerning the possibility of an experimental investigation of the structure of the electron, J. Exp. Th. Physics USSR **32** (1957) 379;

A. A. Kolomenski, A symmetric circular phasotron with oppositely directed beams, J. Exp. Th. Physics USSR **33** (1957) 298;

V. N. Kanunnikov, A. A. Kolomenskii, A. N. Lebedev, E. P. Ouchinnikov, A. M. Stolov, V. A. Titov, A. P. Fatew and B. N. Yablokov, Investigations connected with the design of accelerators of the ring phasotron type, Int. Conf. on high energy accelerators, Geneva 1959, Proc. p. 89.

[6]) See the Proceedings quoted under [3]) and [4]).

[7]) W. C. Barber, B. Richter, W. K. H. Panofsky, G. K. O'Neill and B. Gittelmann, An experiment on the limits of quantum electrodynamics, High Energy Physics Laboratory report, Stanford University (1959).

where for relativistic particles the velocity is the velocity c of light, σ_{bb} and σ_{bg} are the relevant interaction cross sections, and n_b, n_g are the number densities of beam and gas particles.

For an order of magnitude estimate, we take, in the case of electrons, the cross sections for wide angle Coulomb scattering. Large angle deflection of fast electrons by residual gas is produced by atomic nuclei rather than by atomic electrons. The number density of nuclei in a diatomic residual gas is $n_g = 7 \times 10^{16} p_{\mathrm{Torr}}$, p being the gas pressure in Torr. Thus we find for the ratio

$$\frac{\mathrm{R.R.}_{bb}}{\mathrm{R.R.}_{bg}} = \frac{\sigma_{bb} n_b^2}{\sigma_{bg} n_b n_g} \approx \frac{n_b}{Z^2 \times 7 \times 10^{16} p}.$$

Assuming that a pressure of $p = 10^{-9}$ Torr can be achieved—which appears feasible with recent vacuum techniques—and a residual gas with nuclear charge $Z \approx 7$, the ratio is $\geqq 1$ if

$$n_b \gtrsim 3.5 \times 10^9 \text{ electrons/cm}^3 .$$

In the case of protons in the Multi-GeV range, the Coulomb interaction cross sections are negligible in comparison with the nuclear cross section. The total proton-nucleon cross section at several GeV is $\simeq 40$ mb, without strong energy dependence. Taking now for n_g the number of nucleons per cm^3, we find for protons

$$\frac{\mathrm{R.R.}_{bb}}{\mathrm{R.R.}_{bg}} = \frac{\sigma_{bb} n_b^2}{\sigma_{bg} n_b n_g} \simeq \frac{n_b}{A \cdot 7 \times 10^{16} p},$$

where A the nucleon number per atom. With $A \simeq 15$ and the same pressure p as before, this ratio is $\geqq 1$ for

$$n_b \gtrsim 10^9 \text{ protons/cm}^3 .$$

The absolute reaction rates resulting under these conditions are for electrons $\mathrm{R.R.}_{bb} = 2c\, \sigma_{bb} n_b^2 \gtrsim 1.5\, (10^5/\gamma^2)$ cm^{-3} s^{-1} where γ = electron energy in units of rest mass. For $\gamma \simeq 1000$ (Stanford experiment) this gives ~ 0.1 events/cm^3 s.

For protons $\mathrm{R.R.}_{bb} \gtrsim 2 \times 10^3$ cm^{-3} s^{-1}.

These figures are not impossibly small, provided that other background can be kept small by means of shielding, selective detection etc.

We have to compare the beam densities required with those of present day accelerators, i.e. $\approx 10^7$ particles/cm^3 for both high energy electrons and protons (corresponding to current densities of ≈ 50 mA/cm^2). There is probably no fundamental difficulty preventing improvement of these figures by a factor of 3 to 10. What is needed is, however, a factor of 100 or more in beam density. Thus 100 or more pulses of presently available intensity have to be accumulated and superimposed on a storage orbit in order to make beam against beam experiments possible—unless vacuum can be improved considerably with respect to our assumptions, or the beam can be compressed in order to raise density.

It should be kept in mind that there are additional requirements referring to beam quality: For measurements of differential cross sections, magnitude and direction of primary momenta must be defined to a certain precision. E.g., for a 1% accuracy in momenta, the angular resolution must be $\approx 10^{-2}$ radian, and the momentum spread of the beam must not exceed 1%. The interaction volume may be permitted a substantial extension, if the angular selection of secondary particles is effected by appropriate beam optics. It will be realized that the detection of secondary particles may be problematic at small angles with the primary beams. There is evidence, confirmed by recent experiments with the CERN proton synchrotron, that the secondary particles in high energy nucleon-nucleon interactions are strongly peaked, in the centre of mass system, in the direction of the primaries except if the multiplicity of particle production is high⁸).

4. Basic Features of Storage Devices for Intersecting Beams

The device generally considered consists of two "storage rings"—annular magnets providing guide fields for the particles to be stored on circular orbits—with a common section where the particles can interact. The storage rings have to be filled by injection from a separate accelerator. The apparatus constructed by Stanford and Princeton Universities as a joint project, already mentioned here several times, is of this type[4,7]).

---

[8]) International Conf. on high energy physics, Rochester 1960.

An interesting alternative had been suggested by Ohkawa[9]) and Kolomenski[5]). They showed that a radial sector type of machine, in which there is symmetry between positive and negative magnetic field sectors can accomodate orbits in opposite senses. These orbits intersect in a number of points. Such an accelerator has been built as a model for 40 MeV electrons at the MURA laboratory and is in its early stage of tests. Unfortunately, this type of machine would become monstrous and uneconomic in the GeV range.

In both types of devices the beam has to be moved from the injection orbit to a storage orbit, where it can stay circulating without being perturbed by the injection of additional pulses. The displacement must be obtained by some means acting selectively on the new pulse only and affecting as little as possible the stored beam. This feature is provided in the first line by a R.F. acceleration or deceleration voltage, which acts only on particles whose frequency of revolution in synchronous with the R.F. frequency. In a guide field configuration in which the revolution frequency depends on energy (as in a synchrotron type of field), beam orbits can therefore be displaced by appropriate frequency modulation.

Another possibility for beam displacement is to make use of the energy loss suffered by a beam due to radiation on curved trajectories. This is, however, only practical for high energy electrons. An accelerating field (R.F. of constant frequency) has then to be provided for maintaining the energy of the stored beam. If the electrons are injected at slightly higher energy they drop by radiation into the maintaining "bucket".

The injected beam needs a kick (by an inflecting field) in order to stay in the storage chamber. Even in the 500 MeV electron case, radiation loss per turn and shrinkage of orbits are too small to move the beam fast enough away from the inflecting field. The inflecting field must therefore either be switched on and off fast enough to admit one single turn. Or a few turns, if the beam is injected off its equilibrium orbit such that it oscillates radially, thus avoiding the inflector for a few turns. Also in the case of R.F. displacement, one revolution time is in practice never enough to move the beam to a sufficient distance from the inflector. Pulsed inflectors designed to avoid perturbation of already stored beam, are therefore essential components[10]).

5. Theoretical Limitations to Accumulation and Storage of Beams

We have seen that it is important not only to store a large number of particles, but also to store them with a high density. Unfortunately, there are limitations to this:

1. Liouville's theorem states that density in phase space stays constant (if the particles obey Hamiltonian equations). Denoting transverse coordinates (with respect to the ideal trajectory) by $x, y; p_x, p_y$; and longitudinal coordinates by z, p_z, the phase space volume $\Delta x\, \Delta y\, \Delta z\, \Delta p_x\, \Delta p_y\, \Delta p_z$ enclosing a given bunch of particles remains therefore constant throughout its history. If no coupling exists between transverse and longitudinal motion, singly

$$\Delta x\, \Delta y\, \Delta p_x\, \Delta p_y = \text{const.}, \quad \Delta z\, \Delta p_z = \text{const.}$$

In a storing process, successive bunches can therefore not occupy the same phase space volume, but can only be stacked one beside the other. They can, e.g. fill the same transverse phase space, and pile up in longitudinal phase space; this happens in R.F. stacking. Or, they can occupy the same longitudinal phase space and pile up in transverse phase space; this happens, e.g., in a multiturn injection process.

The restrictive influence of Liouville's theorem for beam storage seems to have been emphasised first by E. Wigner[1]). The systematic theory of beam accumulation by R.F. has been developed by Symon and Sessler of MURA[3]).

What matters for collision rates, is beam density in ordinary space. Therefore, the bunches stacked by R.F., which because of Liouville's theorem, must all have slightly different momenta, should not differ much in transverse position. The relevant figure characterizing the relation between orbit radius r and momentum p is the "momentum compaction" factor α defined by

---

[9]) T. Ohkawa, A scaled radial sector FFAG for intersecting beams, MURA report TO-6 (1956);

T. Ohkawa, Two-beam fixed field alternating gradient accelerator, Rev. Sci. Instr. **29** (1958) 108.

[10]) G. K. O'Neill and V. Korenman, The delay-line inflector, Princeton-Pennsylvania Accelerator Project report (1957).

$$\frac{\delta r}{r} = \alpha \frac{\delta p}{p} .$$

α is greater than, but close to 1 for weak focusing, and smaller than 1 for strong focusing (values as low as $\alpha = \frac{1}{1000}$ might be considered in this case). As long as the radial width of a beam due to momentum spread is much smaller than the width due to transverse oscillations, the particle density can be increased by R.F. stacking. It may be noted that the ratio of these widths is about 1 : 30 in the CERN proton synchrotron at 25 GeV†, and that it may be difficult to do much better. For this reason, a suggestion, put forward by Terwilliger[11]), for "achromatic" orbit focusing in the beam intersection region deserves attention: By an appropriate perturbation in the focusing field the equilibrium orbits can be made to go through one selected point independent of momentum. This local cancellation of radial displacement with momentum has to be paid for by doubled displacement of other parts of the orbit.

If dissipative effects, like orbit radiation, enter, Liouville's theorem does no longer hold (since the equations of motion become non-Hamiltonian). Radiation can cause the phase space occupied by a bunch of particles to shrink indefinitely, thereby increasing particle density indefinitely. In physical terms: radiation can damp transverse and longitudinal oscillations (betatron- and phase oscillations). This effect is therefore very useful for electron storage rings; in fact, it plays an essential part in the design of the Stanford e–e experiment. It had been suggested[4]) to obtain similar damping of protons by making them traverse tapered foils. However, it was shown[12]) later that the multiple scattering connected with the energy loss in a foil kills the idea. Although there may exist other ways of effecting non-Liouvillean damping of oscillations, it appears essential at the present stage that any waste of phase space must be avoided in the storage of protons, if it is to succeed satisfactorily.

2. A second limitation of particle density is due to scattering by residual gas and other perturbations of the "random noise" type like quantum fluctuations of radiation and bremsstrahlung (of importance in the case of electrons only), noise in R.F. accelerating gaps etc. These effects may either cause loss of stored particles or at least widen transverse amplitude and energy spread. Wide angle scattering leads to loss in one event; multiple scattering causes gradual blow-up of transverse oscillations.

In the case of Multi-GeV protons, scattering due to nuclear forces causes heavier losses than Coulomb scattering. Using the figures of section 3 for reaction rates and residual gas pressure, one arrives at a decay of a proton beam to e^{-1} of its initial density in $\approx 10^6$ seconds, which is a comfortable life time.

The case of high energy electrons is more favourable if the storage ring is of such a design that betatron oscillations are damped by radiation. This is the case for the Stanford storage ring, and at 500 MeV, radiation damping (time constant ≈ 1 ms) beats multiple scattering growth of oscillation amplitudes and keeps amplitudes stationary at very low values.

At energies of 50 MeV or less, radiation damping (which is $\approx \gamma^3$ for a given orbit radius) does not help much against scattering, and a useful lifetime of beam is defined by a maximum tolerable amplitude. At 10^{-9} Torr, one arrives at a few hundred seconds for 50 MeV, and less for lower energies (lifetime roughly proportional to γ^2).

Not only betatron amplitudes but also energy spread is increased by random perturbations like scattering, quantum fluctuations of orbit radiation and of bremsstrahlung. The latter effects are most serious in the Stanford storage rings, and require a very high R.F. voltage for maintenance against radiation loss, operated at small phase angle.

---

† for "debunched" R.F. structure of the beam, when the $\delta p/p < 10^{-4}$.

[11]) K. M. Terwilliger, Achieving higher beam densities by superimposing equilibrium orbits, Int. Conf. on high energy accelerators, Geneva 1959, Proc. p. 53.

[12]) D. B. Lichtenberg, P. Stehle and K. R. Symon, Modification of Liouville's theorem required by the presence of dissipative forces, MURA report DBL/PS/KRS-1, (1956).

3. Space charge effects are in general not a serious limitation at highly relativistic energies. Difficulties for orbit stability may arise, however, from space charge forces between interacting beams.

6. Considerations regarding a Model Study of Beam Storage

In view of the potential possibilities of colliding beam experiments in conjunction with the new 25-GeV proton synchrotron, the problems of beam stacking have attracted attention in CERN for some time. It was felt that experience with some kind of model would be desirable before one would feel confident to contemplate a large-scale device for use with the proton synchrotron.

Since a FFAG 2-way electron device along the lines of MURA[9,3]) has many features making it attractive for a model (no separate accelerator, no beam transfer, wide radial aperture), the design problems involved were studied in the hope that a model could be arrived at which would not only serve for studying the dynamics of beam stacking, but would also be useful for electron collision experiments[13]). However, this type of machine presents formidable technological difficulties (due to excessive radiation loss, complexity of magnet, R.F., and vacuum systems) if one approaches electron energies of 100 MeV. It has also certain disadvantages for e−e interaction experiments (limited angular range for secondary particles which furthermore traverse a complicated magnetic field on their way out of the machine; difficulty of achieving transverse oscillation damping by radiation).

Confining a first step to tests of the feasibility of efficient multi-pulse stacking, a simpler model was therefore considered more adequate. It is planned to be a storage ring, with a vacuum chamber of relatively small aperture ($\approx 10 \times 5$ cm^2), permitting the use of small bending magnets and focusing lenses, and designed for R.F. stacking experiments with electrons (and eventually with protons) of energies as low as 1… 2 MeV[†]. Thus, tests can be made in the absence of orbit radiation, i.e. under the restrictions by Liouville's theorem as they would apply to proton stacking. Even in this modest from of a model, quite a few non-trivial problems arise: (i) a vacuum better than 10^{-9} Torr is vital for a sufficient life time of low energy beams; (ii) a high precision magnetic field; (iii) a pulsed inflector with millimicrosecond performance; (iv) for accomodating a large number of pulses in the stack, an injector providing enough current within a very small "beam emittance"[††], and extremely good stability of beam characterstics is essential; it is hoped that these requirements can be met by a pulsed Van de Graaff accelerator as injector.

There is a number of additional problems, as possible instabilities due to space charge forces causing undesired bunching of beams[14]), and space charge interaction between separate filaments of beam[15]). Phenomena like these, which play a part in injection into any circular accelerator, are likely to require a first stage of studies on the model. Oddly enough, several of the complications encountered in a model would be absent in a large-scale storage system for high energy protons.

[†] Presently working on this model in CERN is a group whose members are: H. G. Hereward, K. Johnsen, M. Pentz, C. J. Zilverschoon, F. A. Ferger, E. Fischer, P. T. Kirstein, F. Schneider, A. Susini, D. A. Swenson.

[††] = product of $\frac{1}{2}$ beam diameter $\times$ $\frac{1}{2}$ angle of beam divergence, which is a measure of transverse phase space.

[13]) M. Barbier, F. A. Ferger, E. Fischer, P. T. Kirstein, G. L. Munday, M. Morpurgo, M. J. Pentz, A. Schoch, A. Susini and N. Vogt-Nilsen, Studies of an experimental beam-stacking electron accelerator, Int. Conf. on high energy accelerators, Geneva 1959, Proc. p. 100.

[14]) C. E. Nielsen, A. M. Sessler and K. R. Symon, Longitudinal instabilities in intense relativistic beams, Int. Conf. on high energy accelerators, Geneva 1959, Proc. p. 239.

[15]) G. Gendreau, H. Bruck, A. Gabet, M. Goutefangeas, J. Hamelin, R. Levy-Mandel, A. Nakach, G. Rastoix, G. Rommel, R. Schoen and R. Vienet, Mise en évidence de pertes de particules par charge d'espace et d'une anomalie de plan médian dans le synchrotron Saturne, Saclay Preprint 1960, to be published in J. de Physique et le Radium.

DISCUSSIONS

Speaker adressed: A. Schoch, (*CERN*)

Question by: V. J. Vanhuyse (*Utrecht*)

Question: I should like to know where the factor 2 is coming from in the expression for the reaction rate. (The relative velocity of the two beams being still c)?

Answer: Figure below shows volume of opposite beam (shaded), intercepted by a particle cross section σ. Where particle moves by vt, this volume is 2 vt.

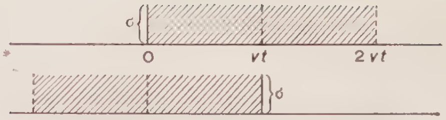

There is no need of the concept of relative velocity. Of course, using it, the same result is obtained with the proper Lorentz transformation.

Speaker adressed: A. Schoch (*CERN*)

Question by: N. F. Verster (*Philips*)

Question: You stated that the phase volume reduces in the case of radiation damping. Does this mean that part of the phase volume is taken up by the coordinates of the radiation field?

Answer: The equations of motion, with radiation loss terms included, are non-Hamiltonian. If you are looking for a Hamiltonian formulation, the electromagnetic field should be included in the system, and your statement is probably correct.

PARTICLE RESEARCH

(October 5, 1960) pp. 47 - 135

Chairman: H. H. Staub

University of Zürich, Switzerland

CONTENTS

Rose, P. H.	The Three-Stage Tandem Accelerator	49
Gove, H. E.	Current Experimentation with the Tandem Accelerator at the Chalk River Laboratories	63
Allen, K. W.	Recent Research in Nuclear Reactions using the Aldermaston Tandem Generator	93
Fleischmann, R.	Sources of Polarized Ions (for Protons and Similar Particles)	112
Connor, Richard J.	Millimicrosecond Pulsing	122
Nygard, J. C. and Post, R. F.	Recent Advances in High Power Microwave Electron Accelerators for Physics Research	126

NUCLEAR INSTRUMENTS AND METHODS **11** (1961) 49–62; NORTH-HOLLAND PUBLISHING CO.

THE THREE-STAGE TANDEM ACCELERATOR

P. H. ROSE

High Voltage Engineering Corporation, Burlington, Massachusetts, U.S.A.

The position of this new accelerator among the tools of nuclear physics is yet to be determined. Beam currents of 10 mA and energies as high as 30 MeV are probably achievable within the next ten years. The accelerator has all the advantages of constant voltage acceleration.

Two forms of the accelerator are described, one with negative ion injection and the other with neutral beam injection. Of the two, neutral beam injection has not only the virtue of having been tried successfully but has the greatest potential for the future. The technical problems associated with the vacuum and ion optics are described and it is pointed out that from an initial 10 mA of positive ions a target current of 191 μA of energetic protons is theoretically possible.

Tests with a three stage tandem accelerator are described which show the various loss mechanisms involved in the accelerator. A small beam of 0.3 mμA was obtained, however, at an energy of 15 MeV and with the excellent energy stability of ± 1 in 100000. Results of experiments in which a neutral helium beam was injected into a tandem accelerator are also mentioned.

In conclusion it is shown that neither the vacuum nor the optical problem pose any insoluble problems. Current high vacuum techniques should insure pressures of 10^{-7} torr in the accelerator. Injection of a converging neutral beam should solve the optical problem and high currents will eventually be obtained.

1. Introduction

The place of this new accelerator in the tools of nuclear physics is yet to be seen. It is almost certain that with this accelerator, protons with energies up to 30 MeV will be obtained within the next ten years and currents perhaps of milliamperes with the energy uniformity and properties associated with constant potential acceleration. Further, if required, the properties of the D.C. machine can be enhanced by a controlled pulsing of the output beam. In this paper the properties of this little known accelerator[1]) will be explored. The discussion should be of help to those nuclear physicists examining the properties of the various accelerators which cover this energy range.

The three-stage tandem accelerator takes two forms shown in fig. 1 and 2. The first figure illustrates a machine made up from two standard HVEC components—a 5.5 MeV CN vertical negative ion injector and a tandem 12-MeV EN accelerator. The final beam has a rated maximum energy of 17.5 MeV and a current in excess of 4 μA is expected from the first models. Considerably higher currents can be expected in the future. Fig. 2 shows a more sophisticated version of the three-stage accelerator in which the ion source is kept at ground potential and the negative ion beam is formed in the terminal of the first generator by charge-exchange from a fast neutral beam. The main advantage of the second version, once the initial design difficulties have been overcome, lies in having the ion source at ground potential. Accessibility is assured and unlimited power may be poured in the source (and dissipated by coolants, if necessary) to achieve the wanted beam intensities. When sources of polarized protons are developed, the first stage of the accelerator will be particularly adaptable for their use. If polarized negative ions ever prove to be feasible, the full potential of the machine may be realized. HVEC has considered the construction of such an accelerator with a rated energy of 22 MeV and an analyzed beam current of 0.5 μA.

The ground potential ion source makes the formation of a wide variety of negative ions relatively simple. See fig. 3 for a list of some of the feasible ions. The effective *Z* after stripping in the second terminal will be large because of the higher energies of the incident negative ion and the final energy per nucleon will be correspondingly increased. The neutral injection tandem presents more interesting technical features than the more conventional three-stage machine and has a greater potential performance. For these reasons the remainder of this paper will be devoted to this type of accelerator and to a description of the results of successful tests carried out with it up to energies of 15 MeV.

---

[1]) R. J. Van de Graaff, Tandem Electrostatic Accelerators, Proceedings of the 1958 Accelerator Conference, sponsored by High Voltage Engineering Corporation, October 14–16, 1958;

P. H. Rose, R. P. Bastide, A. B. Wittkower, D. L. Webb, C. H. Goldie and J. Shaw, Injection of Fast Neutral Beams into the Three-Stage Tandem Accelerator, Rev. Sci. Instr. **31** (1960) 1052.

Standard models of neither of the accelerators described above have yet been built, but it is confidently expected that in the near future HVEC will start construction of both these types of accelerators.

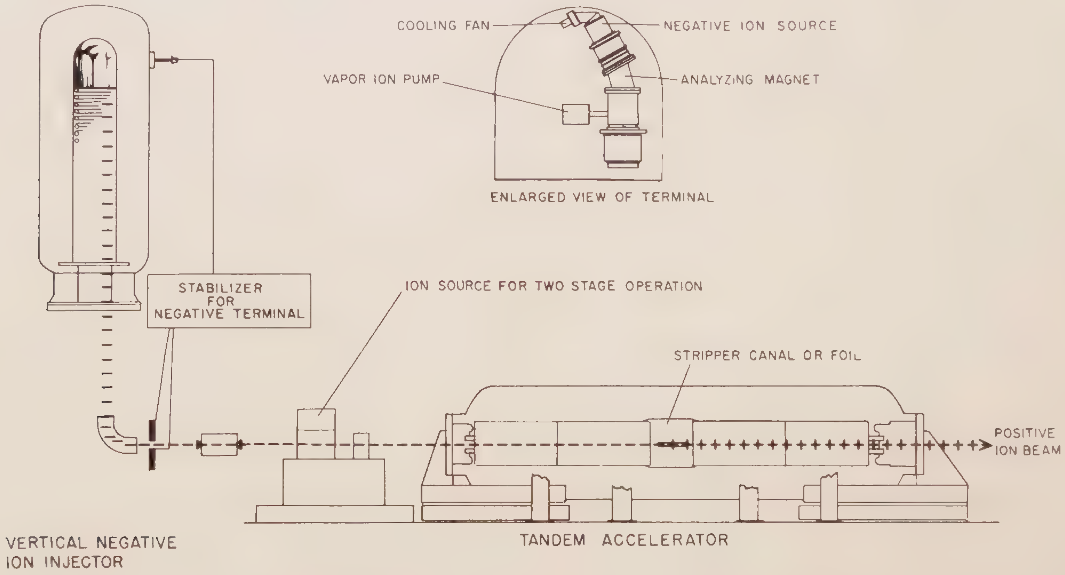
COOLING FAN
NEGATIVE ION SOURCE
VAPOR ION PUMP
ANALYZING MAGNET
ENLARGED VIEW OF TERMINAL
STABILIZER FOR NEGATIVE TERMINAL
ION SOURCE FOR TWO STAGE OPERATION
STRIPPER CANAL OR FOIL
POSITIVE ION BEAM
VERTICAL NEGATIVE ION INJECTOR
TANDEM ACCELERATOR

Fig. 1. The three-stage tandem with vertical negative ion injection.

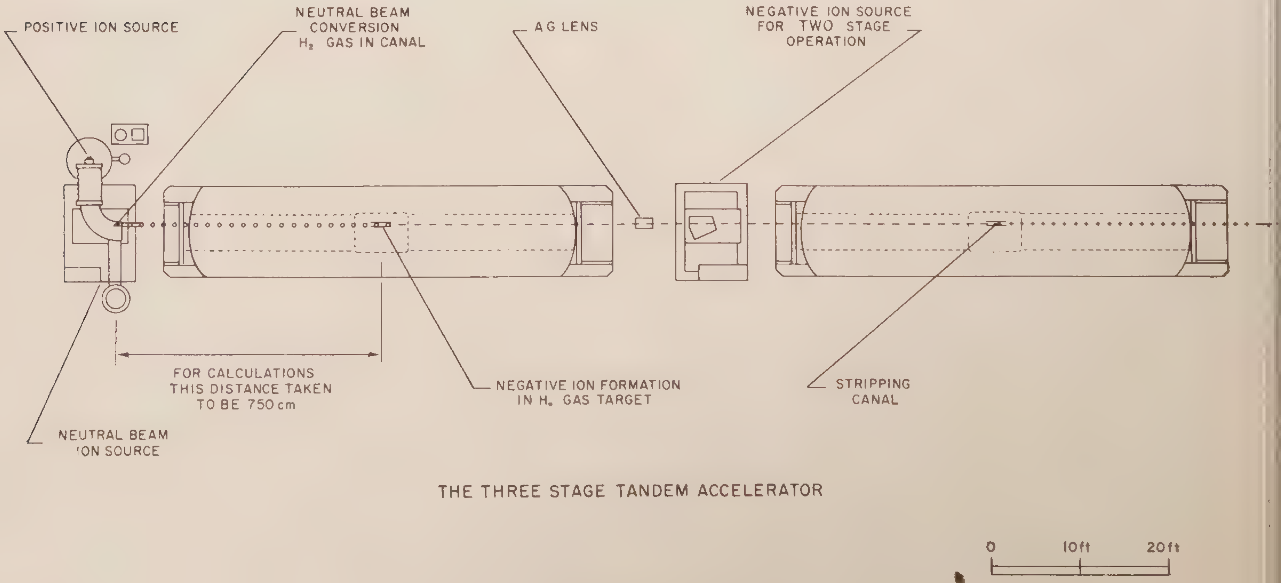
POSITIVE ION SOURCE
NEUTRAL BEAM CONVERSION H_2 GAS IN CANAL
A G LENS
NEGATIVE ION SOURCE FOR TWO STAGE OPERATION
FOR CALCULATIONS THIS DISTANCE TAKEN TO BE 750 cm
NEGATIVE ION FORMATION IN H_2 GAS TARGET
STRIPPING CANAL
NEUTRAL BEAM ION SOURCE
THE THREE STAGE TANDEM ACCELERATOR
0
10ft
20ft

Fig. 2. The three-stage tandem with neutral beam injection.

2. General Discussion

Before proceeding to examine some of the problems of the three-stage tandem accelerator in detail, it is interesting to examine the optimum performance which can be expected from the accelerator after the three charge-exchange processes required. For this purpose all the other phenomena involved will be ignored. Positive ions are generated in an ion source at the front end of the accelerator. Let the intensity of these ions be I_0^+ and the energy ≈ 13 keV, which is the optimum for negative ion formation in hydrogen gas. Charge-exchange in the first region will produce a neutral beam of intensity 0.87 I_0^+ (fig. 4), the neutral beam will drift to the terminal of the first accelerator in a special vacuum tube where charge-exchange to negative ions occurs. The charged components formed at the same time as the neutral beam are separated from the neutral beam by a magnet before entry into the high voltage region. Of the incident neutral beam 2.2% will be converted into negative ions—fig. 5.

OBSERVED ATOMIC NEGATIVE IONS
(NUMBERS GIVE THE RELIABLE① AFFINITIES)

	I	II	III	IV	V	VI	VII	VIII
1	H^- 0.754							
2	Li^-		B^-	C^- 1.13	N^- ⊖	O^- 1.48	F^- 3.62	
3	Na^-		Al^-	①	P^-	S^- 2.07	Cl^- 3.82	
4	K^-					Cr^-		
	Cu^-				As^-	Se^-	Br^- 3.54	
5	Rb^-							
	Ag^-				Sb^-	Te^-	I^- 3.23	
6	Cs^-							
	Au^-		Tl^-		Bi^-			

① Si^- SHOULD BE QUITE STABLE-NOT YET LOOKED FOR.

Fig. 3. Table of stable negative ions.

The ions formed will be accelerated to ground potential, drift between the machines and enter the second tandem where they will be accelerated to the terminal and pass through the third and last charge-exchange region. In this region there will be negligible loss of beam because at these high energies the stripping cross-section will be orders of magnitude larger than the competing attachment cross-sections.

The final current on the target will therefore be 0.0191 I_0^+. If the initial positive ion beam is assumed to be 10 mA, a positive ion current which can easily be achieved, the target current will be as high as 191 μA. Of course, it will not be possible to achieve this efficiency in practice, but the numbers do show how favorable the charge-exchange processes are.

As will be seen, two other phenomena enter into the problem and they are, the degree of vacuum and the optics of the beam and accelerating systems. In an experiment with standard EN accelerators, the residual gas and ion optical deficiencies reduced the beam by a factor of 10^6 from that just estimated as possible. (See table 1.) Obviously then, the problems of beam formation by charge-exchange are only a small part of the whole. In the experiments at

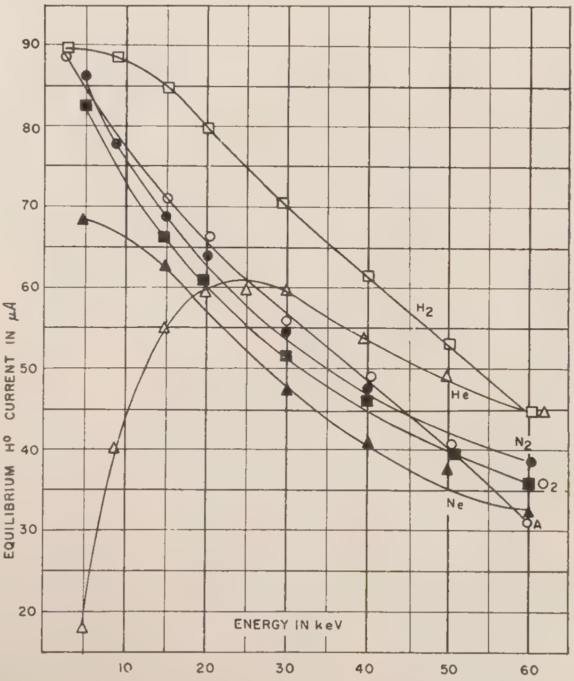

Fig. 4. Equilibrium H^0 current after charge-exchange in different gases (100 μA incident beam).

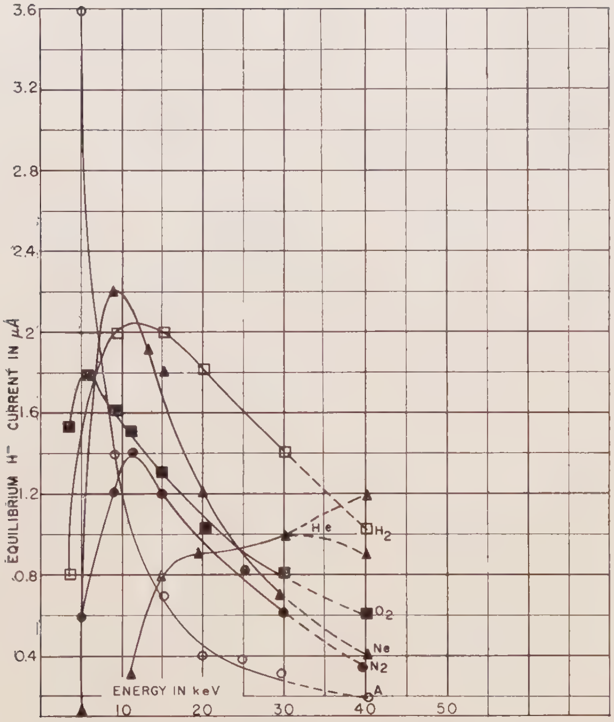

Fig. 5. Equilibrium negative ion currents produced in different gases (100 μA incident beam).

HVEC, which are described later, it has been found that the vacuum and the optics were about equally to blame for the beam loss.

Before proceeding to discuss experiments with this system of acceleration a brief study will be made of the beam loss by charge-exchange. This will be followed by an introduction to the concepts of acceptance of an accelerator and beam emittance, two quantities which emphasize the critical nature of the ion optical problem in the three-stage accelerator.

3. Beam Loss by Charge-Exchange†

Charge-exchange which occurs intentionally in the charge-exchange canals of the tandem accelerator also occurs undesirably in the intermediate drift and acceleration regions—fig. 2. The residual gases in the vacuum system are the cause of the unwanted electron exchange processes. Neutral beams generated at the source must pass to the terminal of the first accelerator a distance of at least 750 cm. In this region two cross-sections determine the loss of neutral beam σ_{01} and σ_{0-1}, the ionization and electron capture cross-sections for the neutral beam. The fraction of beam lost may be estimated from

$$\frac{I^{+} + I^{-}}{I^{\circ}} = e^{-nL\hat{P}(\sigma_{01} + \sigma_{0-1})}$$

where

$\frac{I^{+} + I^{-}}{I^{\circ}}$ = the fraction of beam loss

n = the number of atoms per cc at 1 torr

$\hat{P}$ = the average pressure in the region, torr

L = the path length, cm.

The most likely molecules in this region are air, mercury vapor, polyvinyl acetate, and araldite. Except for air and mercury the cross-sections σ_{01}, σ_{0-1} are unknown. To add to the uncertainty, the pressure gauges employed are not reliable with the presence of organic contaminants. The cross-sections of the complex organic molecules are estimated to be a factor of 5 higher than for air. The pressure near the terminal of a tandem accelerator is known to be in the region 10^{-4} torr, so that the intensity of a 40-keV neutral beam would be down by two orders of magnitude on reaching the terminal. The loss is illustrated graphically in fig. 6). The ordinate gives the fraction of beam lost at different pressures for varying total attenuation cross-sections.

In the region between the adder canal of the first accelerator and the stripper in the second, the loss of negative ions will be energy dependent, decreasing with increasing energy. The cross-section σ_{-10} varies as $1/E^{x}$, x lying between 0.5 and 1.0 for different gases. The pressure as well as the energy vary with z so that the attenuation must be determined from

$$I^{-}/I_{0}^{-} = n_{0} \int \sigma_{-10}\, E(z) P(z) \mathrm{d}z\,.$$

For example, in the first meter of acceleration tube, an average pressure is 10^{-4} torr, causing a beam loss of 50%, a loss which is obviously prohibitively high.

Elimination of this high loss, as a result of

---

† The cross-sections quoted are taken from the review by S. K. Allison[2]).

[2]) S. K. Allison, Rev. Mod. Phys. 30 (1958) 1137.

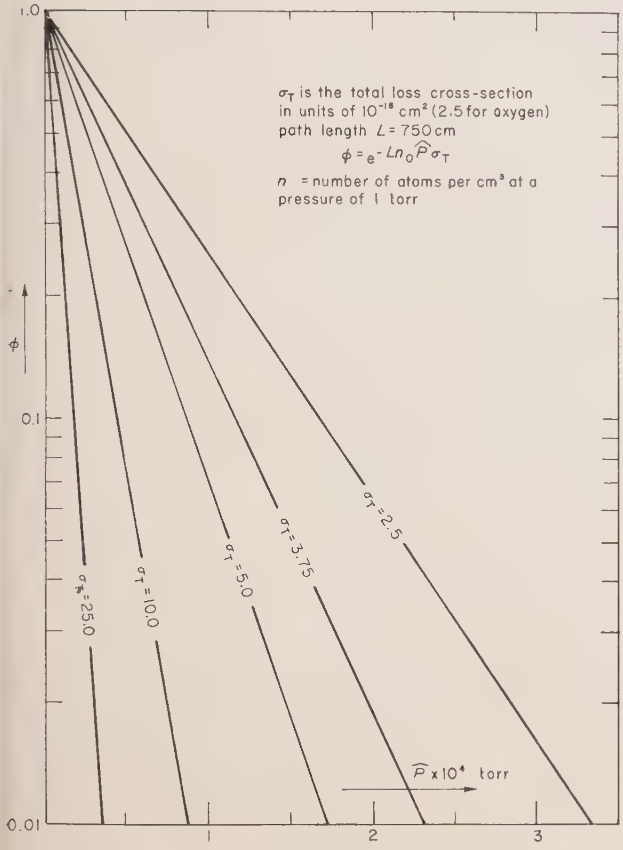

Fig. 6. Beam loss by charge-exchange in residual gas.

residual gas and vapors, does not represent a serious vacuum problem. A pressure of 5×10^{-7} torr would be quite adequate to eliminate loss by charge-exchange with the residual gas and this is not nowadays regarded as a difficult pressure to reach. A metal gasketed system using adequately trapped diffusion pumps or vapor ion pumps with partial baking out of the system should be adequate. It is worth mentioning that some HVEC acceleration tubes similar in construction to those in the tandem accelerator reach pressures of 5×10^{-7} torr in permanently sealed systems.

4. The Acceptance of an Accelerating system †

The motion of particles through an electromagnetic system can be represented by forming the classical Hamiltonian provided radiation effects are not considered. The momentary state of a particle can be described completely by a position vector in a six dimensional phase space, the components of which are three-space coordinates and the canonically conjugate momenta. Neglecting particle interactions, space-charge for example, the Hamiltonian separates into a sum of terms each involving a pair of canonically conjugate variables. In rotationally symmetric ion optical systems a particle is completely specified in the two dimensional phase space— the radius r and the radial momentum p_r. Because the ion beam may be represented by a Hamiltonian, the well-known invariants of Lagrange and Liouville hold true and may immediately be applied.

If r_i, p_{r_i} are the initial radius and momentum of a particle before entering an optical system, then the emergent ray may be specified by

$$\begin{bmatrix} r_f \\ p_{r_f} \end{bmatrix} = \begin{bmatrix} a_{11} & a_{12} \\ a_{21} & a_{22} \end{bmatrix} \begin{bmatrix} r_i \\ p_{r_i} \end{bmatrix}. \tag{1}$$

The expression is a linear transformation between a given initial and final plane and is true for all particles. Generally the quantities a_{jk} are functions of the radius and momentum of the initial ray. For a constant momentum across the beam and for small radii, the a_{jk} are very nearly constant. This region includes the paraxial region which in Gaussian optics is defined by the equality

$$\tan\theta \approx \theta \quad \text{or} \quad p_r \approx p\,\frac{\mathrm{d}r}{\mathrm{d}z}$$

where p is the total momentum of the particle.

There will be a region defined by the integral curve

$$F(r_i\,, p_{r_i}) = 0 \tag{2}$$

which will map all those initial rays which can reach the point (r_f, p_{r_f}). In this case F is determined from the canonical transformation equation (1) above. This gives the relationship

---

† The concepts introduced in the two following sections are also discussed by D. L. Judd, H. G. Hereward, and P. A. Sturrock, and others[3]).

[3]) D. L. Judd, Conceptual Advances in Accelerators, Annual Review of Nuclear Science 8 (1958) 181. (Annual Reviews, Inc.);

H. G. Hereward, K. Johnsen and P. Lapostolle, Problems of Injection, CERN Symposium, 1956;

P. A. Sturrock, Static and Dynamic Electron Optics (Cambridge University Press, Cambridge, 1955).

$$r_f\, p_{r_i} - r_i\, p_{r_f} = a_{12}\, p_{r_i}^2 + (a_{11} - a_{22})\, r_i\, p_{r_i} - a_{21}\, r_i^2. \tag{3}$$

The right hand side obviously represents a conic section in the (r_i, p_i) plane. The left hand side has the general form of a Lagrange invariant representing the same trajectory at two different time intervals. Consequently it can be seen that the left hand side of (3) is the function F.

Let the area of each conic section F be denoted by a. Then there will be a maximum value of a, $a_{\max}$, above which some particles entering the system will not arrive at the exit plane. The area $a_{\max}$ might well be called the maximum acceptance of the system. Another quantity a_p can be defined for those particles passing through the system for which the a_{jk} are a constant. This quantity defines those rays entering the tube which will map points on the exit plane corresponding to points on the entrance plane without distortion.

The importance of the concept of acceptance is now obvious, it determines, for example, how much of the aperture of an acceleration tube can be used. In order to determine a_p, the field in an acceleration tube has been calculated by solving the Laplacian for a very close representation of the tube geometry by using difference equations. Particle trajectories were determined through the acceleration tube by solving the relativistic ray equation which may be written in the form

$$r'' = \frac{1 + r'^2}{2Q}\left(\frac{\partial Q}{\partial r} - r'\,\frac{\partial Q}{\partial z}\right).$$

where

$$Q = -2\,\frac{e\phi}{M_0\, c^2} + \left(\frac{e\phi}{M_0\, c^2}\right)^2$$

and ϕ is the potential at the point r, z. The other quantities have their usual meaning.

Typical trajectories are shown in fig. 7, and they illustrate the behavior of particles entering an acceleration tube with a narrow aperture. The acceptance diagram for this acceleration tube is shown in fig. 8. From the diagram it is easy to see how little of the tube aperture can be used by the beam.

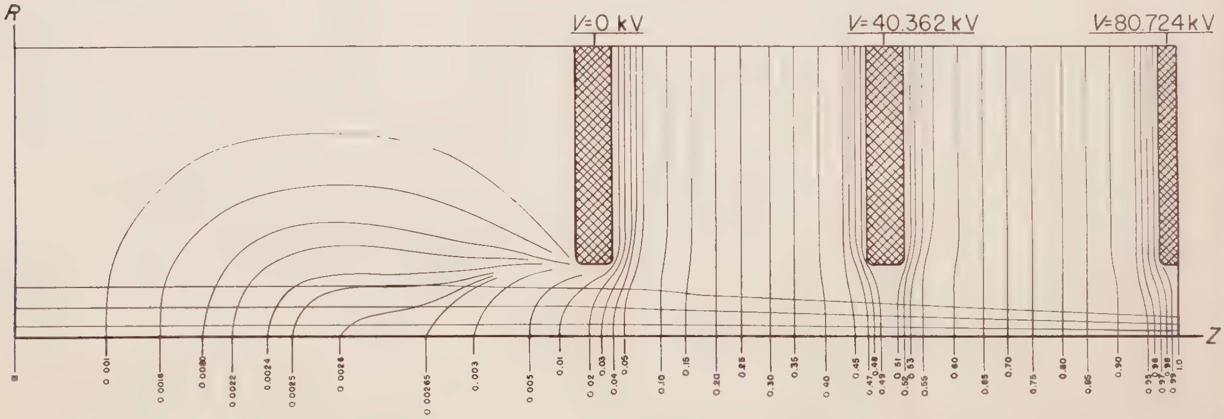

Fig. 7. Diagram showing particle trajectories and equipotentials in entrance of an acceleration tube.

Bore dia. — ½ in. Injection energy — 20 kV
Electrode spacing — 1.0 in. Electrode thickness — ⅛ in.

ray	initial r	initial r_z	final r	final r_z
1	0.170	0	— 0.0661	— 0.0354
2	0.100	+ 0.001	— 0.0418	— 0.0204
3	0.040	+ 0.001	— 0.0181	— 0.00805

The exact calculations also give directly the cardinal points of the lens system, which can be compared with first order theories. The aberrations of the tube can easily be examined by selecting suitable rays and running them on the computer.

5. The Emittance of an Ion Beam

By Liouville's theorem, the motion of points representing ions in phase space is like the motion of an incompressible fluid. The ions occupy at some instant a certain volume inside a

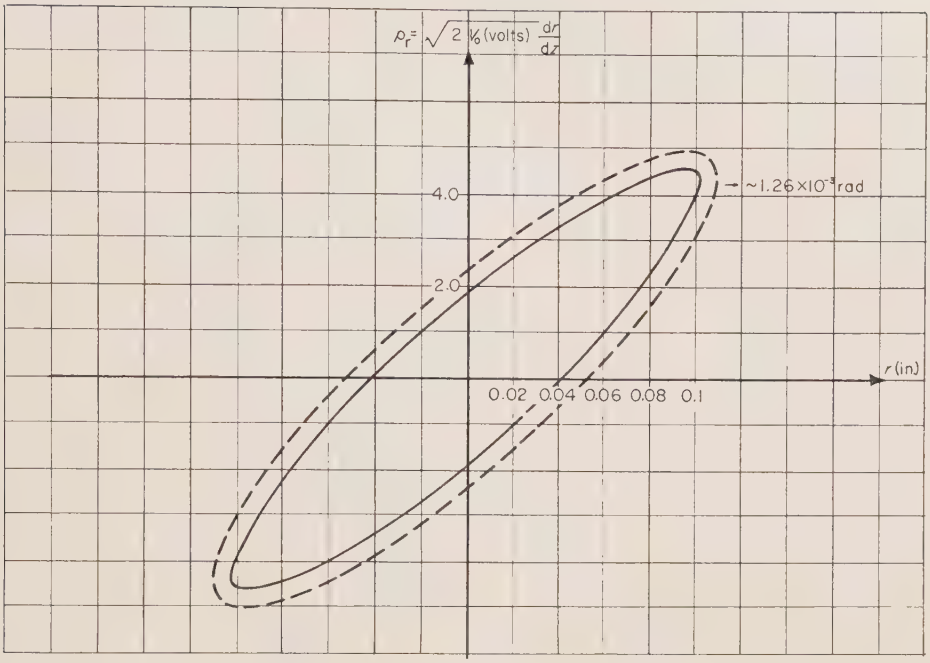

Fig. 8. The acceptance diagram of a $\frac{1}{2}''$ diameter acceleration tube ($V_0 = 53.3$ keV).

closed surface. At any other instant they will occupy the same volume, and this volume is consequently an invariant of motion. Analytically, the equivalence of

$$\oint p_{r_i}\, \mathrm{d}r_i = \oint p_{r_f}\, \mathrm{d}r_f$$

implies that the determinant of the general relationship between (r_i, p_{r_i}) and (r_f, p_{r_f}) namely

$$\begin{vmatrix} a_{11} & a_{12} \\ a_{21} & a_{22} \end{vmatrix}$$

is equal to unity.

The surface area embraced by the line integral in phase space may be defined as the emittance of the beam of particles represented in the diagram. The beam is completely defined if intensity contours are included in the diagram. See fig. 9. The measurement of beam emittance which is the complementary quantity to acceptance is of utmost importance in accelerator design. For this reason a beam scanner has been developed which can measure the position, direction of motion, and emittance of a beam. The emittance of ion beams is often quoted in units of radian centimeters, and when this is done it must be made clear how much of the beam is included in the area quoted and beam energy should be stated. The beam scanner is shown schematically in fig. 10. It can be seen that the two displays give all the information required except the emittance. This can be measured by scanning the

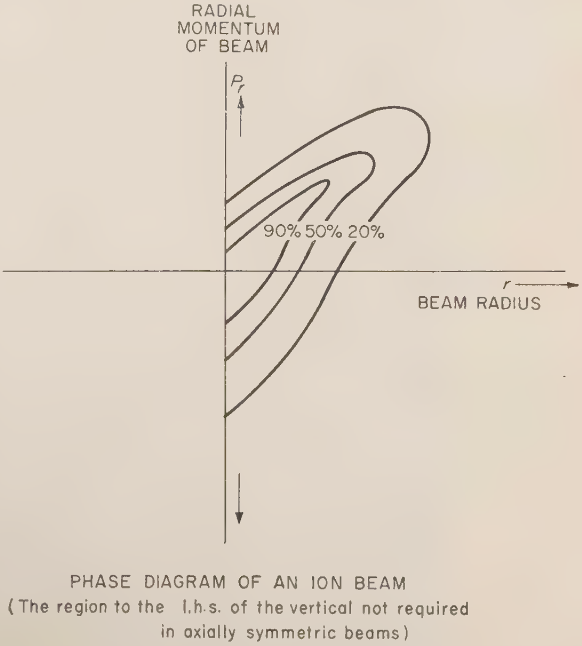
RADIAL MOMENTUM OF BEAM
P_r
90% 50% 20%
r
BEAM RADIUS
PHASE DIAGRAM OF AN ION BEAM
(The region to the l.h.s. of the vertical not required in axially symmetric beams)

Fig. 9. A phase diagram showing intensity countours.

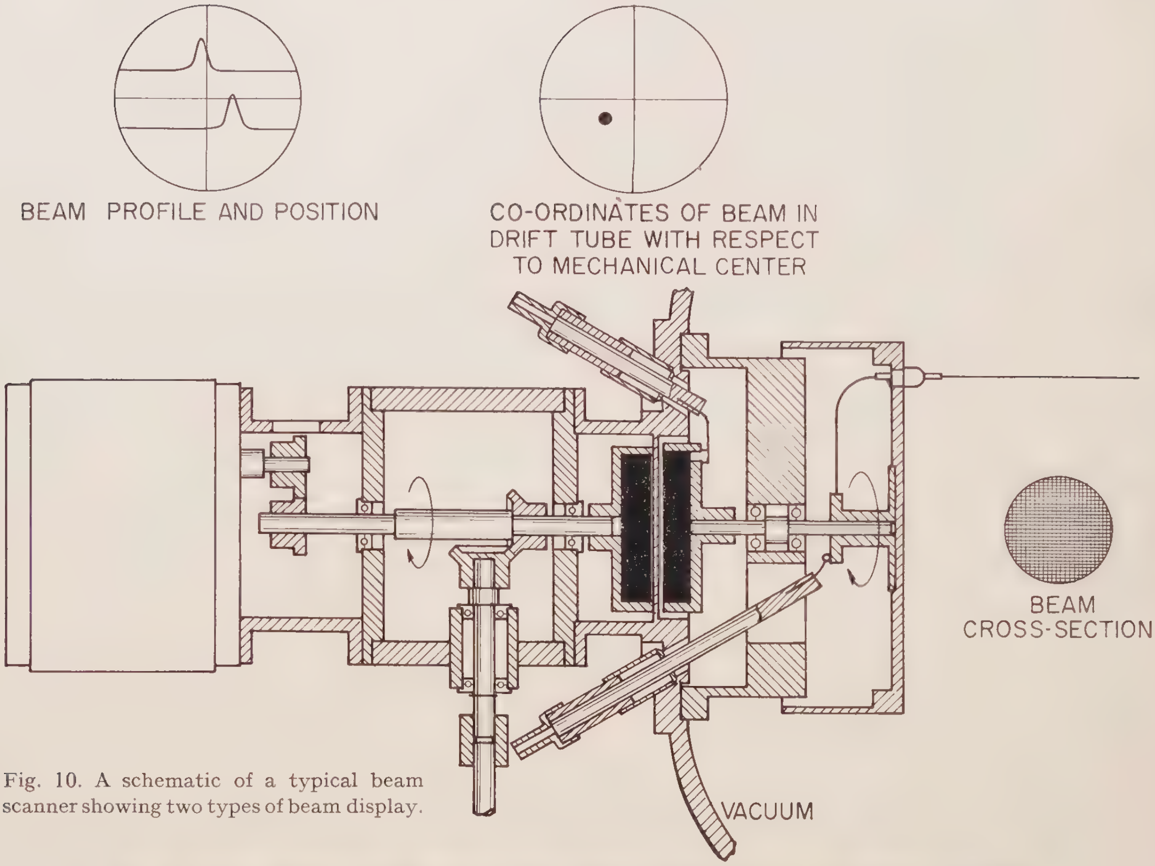
BEAM PROFILE AND POSITION
CO-ORDINATES OF BEAM IN DRIFT TUBE WITH RESPECT TO MECHANICAL CENTER
BEAM CROSS-SECTION
VACUUM

Fig. 10. A schematic of a typical beam scanner showing two types of beam display.

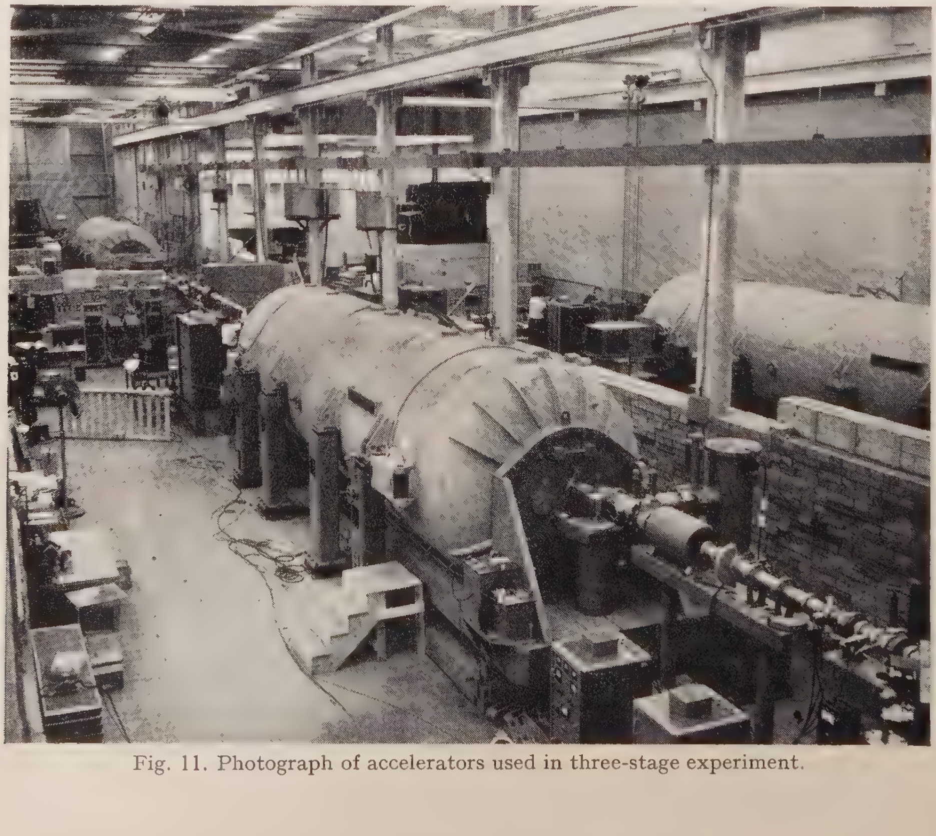

Fig. 11. Photograph of accelerators used in three-stage experiment.

beam after it has passed through a series of small apertures.

Care must be used in this type of measurement when the beams are intense and comparatively low in energy. The beam emittance has been found to be sensitive to the surrounding geometry and, as is well known, to the residual gas pressure[4]). This category of ion beams more properly fall into a different class. The particle interactions become important (perveances $\sim 10^{-7}$ amp/volt$^{\frac{3}{2}}$) and destroy the applicability of the Liouville theorem. The measurement becomes good for the plane of the measurement only and elaborate calculations are required to take into account the space charge and neutralization phenomena.

6. Experiments with a Three-Stage Tandem Accelerator

The design of these more complicated accelerators is being assisted by a series of tests being undertaken in the HVEC factory. Early this year, two 12-MeV tandem accelerators were built on a common axis to permit a full scale test of the neutral injection three-stage tandem principle. Fig. 11 is a photograph of the accelerators as they appeared during the tests. Fig. 12 is a plan view of the accelerators giving the scale of the installation and showing the large distance between the accelerators. The distance was governed by factory requirements and was unavoidable.

The neutral beam was obtained from a standard negative ion source located on the axis of the accelerator. The source is shown in cross-section in fig. 13. The charged components formed in the source were removed from the beam by a small magnet beyond the source.

The neutral beam was measured at the base of the tank and also in the terminal by calorimeters which could be inserted into the beam. One milliampere of beam was measured inside a $\frac{1}{4}''$ diameter circle three feet from the source. This intensity fell to 100 μA six feet further on. The beam measured in the terminal with the terminal grounded was reduced to 5 μA, and of this only 1–2 μA was found to be neutral. Charge-exchange between the drifting beam and residual gas accounts for the charged components observed in the terminal and for a large part of the beam loss.

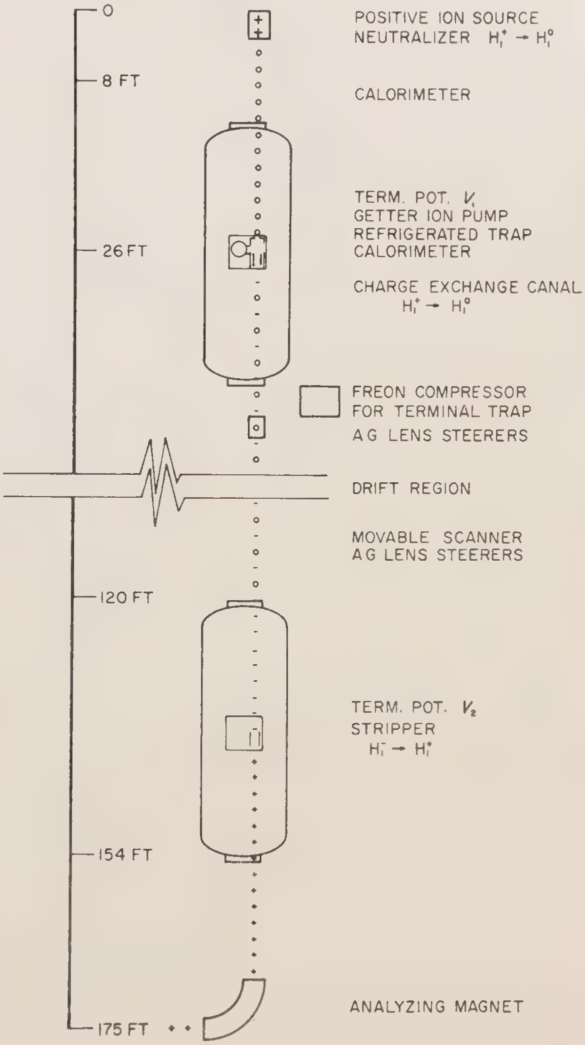
0
8 FT
26 FT
120 FT
154 FT
175 FT
POSITIVE ION SOURCE
NEUTRALIZER $H_1^+ \rightarrow H_1^0$
CALORIMETER
TERM. POT. V_1
GETTER ION PUMP
REFRIGERATED TRAP
CALORIMETER
CHARGE EXCHANGE CANAL
$H_1^+ \rightarrow H_1^0$
FREON COMPRESSOR
FOR TERMINAL TRAP
AG LENS STEERERS
DRIFT REGION
MOVABLE SCANNER
AG LENS STEERERS
TERM. POT. V_2
STRIPPER
$H_1^- \rightarrow H_1^+$
ANALYZING MAGNET

Fig. 12. Schematic of three-stage tandem.

The beam intensity could be made to show a definite peak of intensity $\sim \frac{1}{4}''$ in diameter at the terminal by a critical adjustment at the focus control of the ion source. The emittance of the neutral beam from the ion source was

---

[4]) See, for example, Electromagnetic Isotope Separators and Applications of Electromagnetically Enriched Isotopes, Ed. J. Koch (North-Holland Publishing Co., Amsterdam, 1958).

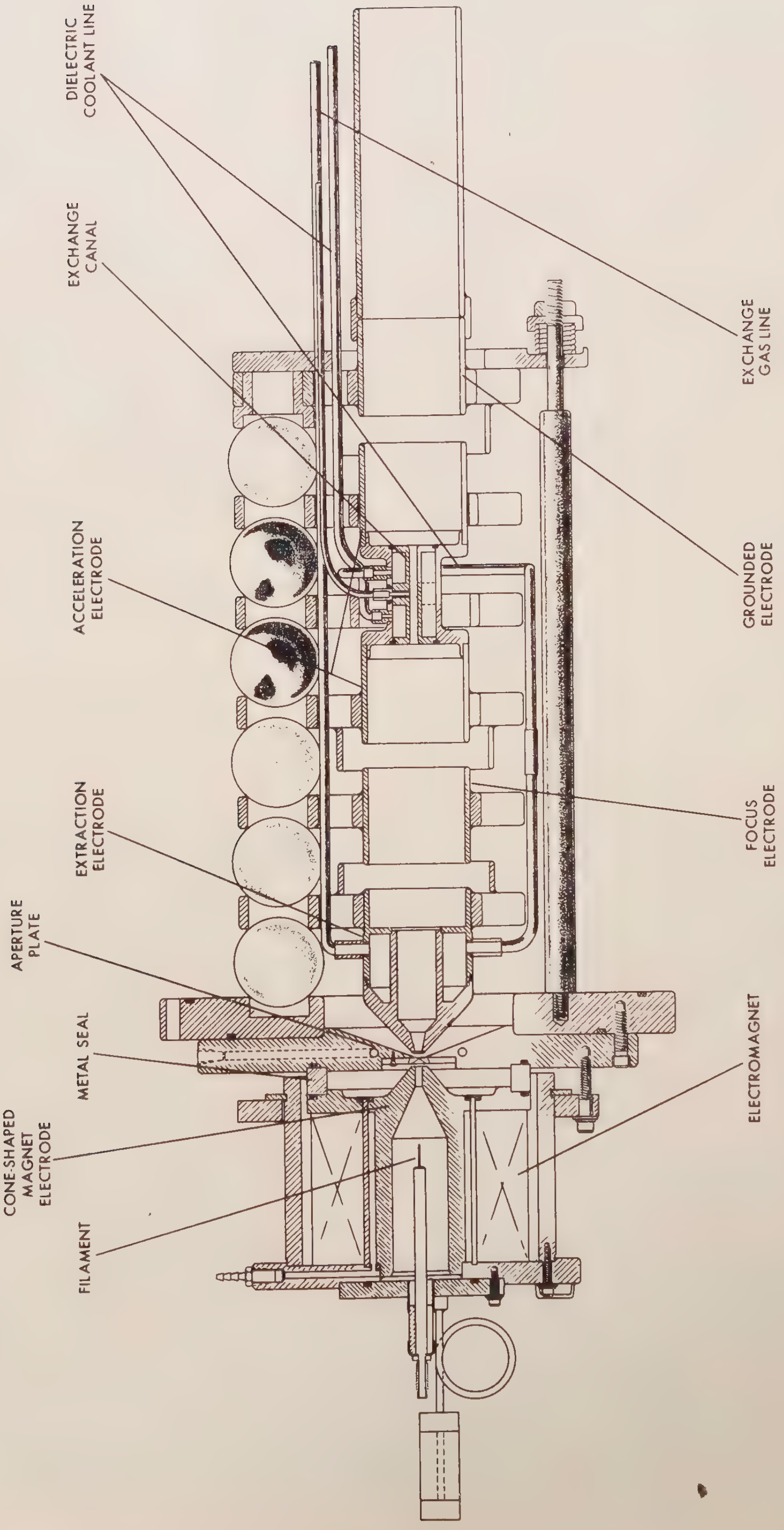
DIELECTRIC COOLANT LINE
EXCHANGE CANAL
ACCELERATION ELECTRODE
EXTRACTION ELECTRODE
APERTURE PLATE
METAL SEAL
CONE-SHAPED MAGNET ELECTRODE
FILAMENT
EXCHANGE GAS LINE
GROUNDED ELECTRODE
FOCUS ELECTRODE
ELECTROMAGNET

Fig. 13. Neutral beam source assembly.

c. 0.005 radian cm for a 45-keV neutral beam. Maximum beam intensities were observed in the terminal for beam energies higher than the optimum for neutral atom production. This was presumably because of the $1/E^{\frac{1}{2}}$ dependence of the beam emittance outweighed any changes in the charge-exchange cross-sections.

The pressure in the terminal region was $\approx 10^{-4}$ torr with the terminal at ground potential when these measurements were made. A vapor ion pump was installed in the terminal and this reduced the pressure to 2×10^{-5} torr after 48 hours pumping. Under these conditions a neutral beam of 2–3 μA was observed in the terminal. The neutral beam was observed beyond the first terminal along the ion path up to the second accelerator. A beam scan at the entrance of the second accelerator showed an intensity of c. 10 mμA and a width at half height of $\frac{1}{2}''$.

The analyzed negative ion beam accelerated from the first terminal was maximized to 30 mμA with very similar source conditions to those when 2–3 μA of neutral beam was observed in the terminal. This result shows that there was remarkably little loss in the accelerating region and drift section. Depending on the initial positive ion beam composition (H_1^+, H_2^+, H_3^+) about 2% of the neutral beam should be converted into negative ions in good agreement with the results. Shortly after these measurements were made, the power supply to the vapor ion pump failed and the negative ion beam obtainable fell to c. 1.0 mμA, presumably as a result of the increased pressure.

It was with this small beam the remaining stages of acceleration were accomplished. The presence of the neutral beam in the vacuum extension between the two accelerators was a serious nuisance. The neutral beam made it impossible to use the normal scanning technique. The beam was scanned instead with a thin lithium strip and the neutrons from the high energy protons were counted. A typical result of a scan in the vertical and horizontal directions is shown in fig. 14. The beam is noticeably asymmetric as a result of focusing by the AG lens. Apparently the axis of this lens and the beam did not coincide. Maximum transmission through both accelerators was obtained by using both AG lenses shown in fig. 12 and also some steering. The beam from the second accelerator was analyzed and measured in a Faraday cage. A neutron count was used to verify that the

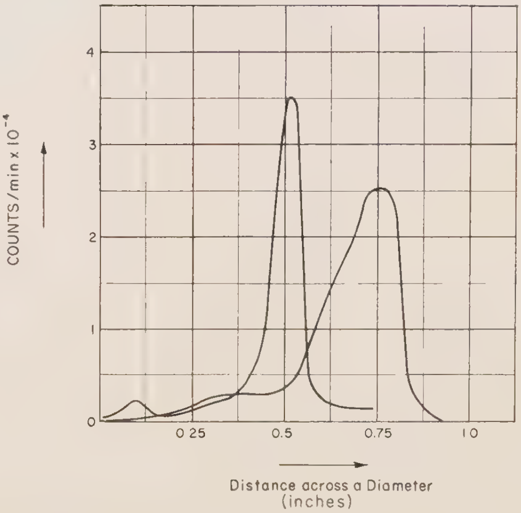

Fig. 14. Profile of the high energy negative ion beam taken with a lithium strip. A vertical and a horizontal scan are shown.

TABLE 1

Results of tests on the three-stage tandem[a]

V_1 (mV)	I^- (10^{-9} amp)	V_2 (mV)	I^+ (10^{-9} amp)	E (MeV)	ΔE (eV)
2.50	1.6[b]	4.6	0.33	11.7	. . .
2.50	1.6	6.25	0.15	15.0	700

[a] V_1 and V_2 are the terminal potentials, I^- the negative ion current between accelerators, and I^+ the analyzed proton current.

[b] The pump in the first terminal (see fig. 12) failed and as a result I^- fell to $\frac{1}{10}$ th of earlier yields.

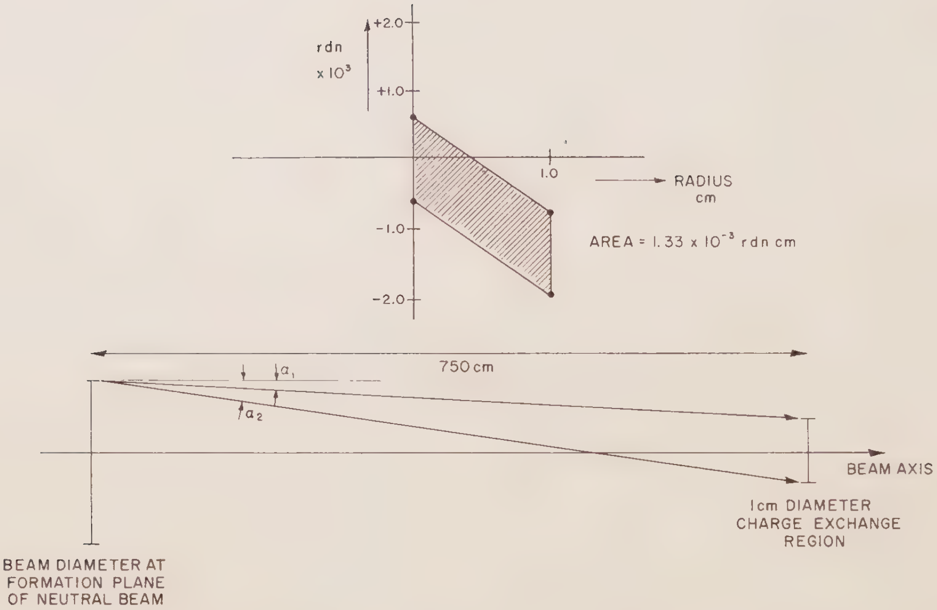
rdn
x 10^3
+2.0
+1.0
-1.0
-2.0
1.0
RADIUS
cm
AREA = 1.33 x 10^{-3} rdn cm
750 cm
a_1
a_2
BEAM AXIS
1cm DIAMETER
CHARGE EXCHANGE
REGION
BEAM DIAMETER AT
FORMATION PLANE
OF NEUTRAL BEAM

Fig. 15. Estimated emittance diagram for a three-stage tandem accelerator.

beam was indeed a proton beam. Both accelerators were stabilized. The first with a negative terminal was stabilized by a 50 point corona control which proved very effective. The second machine was stabilized in the normal manner from the signal from the image slits of the analyzing magnet. Table 1 gives the results of the experiment.

An important conclusion can be drawn from the results and it is that most of the beam is lost in the neutral drift section. The results also showed that the degree of vacuum and the neutral beam emittance are the two parameters controlling the beam loss.

7. Neutral Beam Formation

Clearly there emerges from the preceding discussion and experimental description one outstanding problem. It is the study and improvement of the emittance of the neutral beam injected into the accelerator. The acceptance of the accelerating system can be estimated very simply. In fig. 15 the flight path of a hypothetical beam is shown. The beam originates from a 750 cm away from the first terminal where the beam must not have a diameter greater than 1 cm if excessive gas or vapor flows in the terminal are to be avoided. The beam shown is convergent and has a 2 cm diameter at the

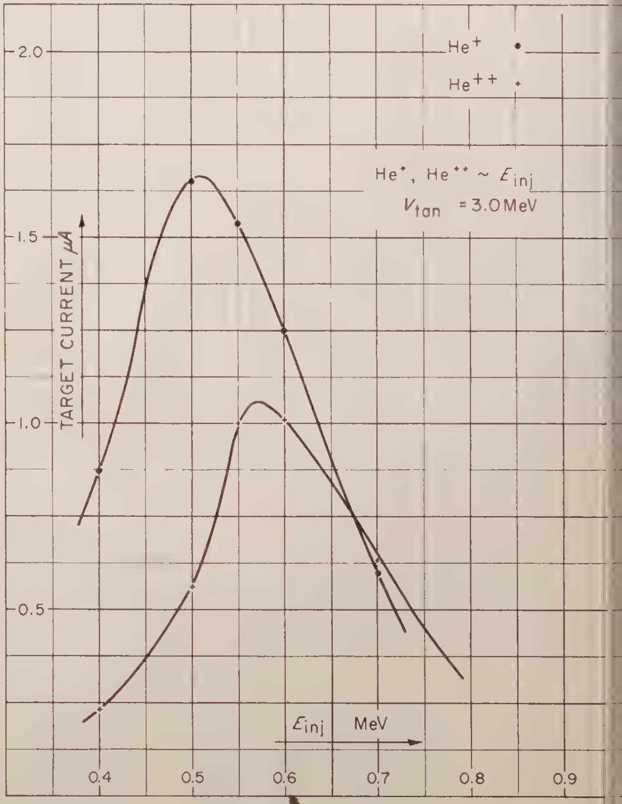

Fig. 16. Helium production by injection of a neutral beam.

plane of the neutralizing region. The area of the diagram is 2×10^{-3} rdn cm and therefore the acceptance of the acceleration tube must be this or greater is all the beam is to pass through.

Table 2

Beam emittances e calculated from the ideal case shown in fig. 15

r_0	r	α_1	α_2	$e = r_0 (\alpha_1 - \alpha_2)$
0.1	0.5	+ 0.00052	— 0.0008	0.00013
0.2	0.5	+ 0.0004	— 0.00093	0.00026
0.5	0.5	— 0.0	— 0.0013	0.00068
0.8	0.5	— 0.0004	— 0.00175	0.00108
1.0	0.5	— 0.00033	— 0.002	0.0017

r_0, r measured in cm

The neutral beam obtained after charge-exchange will have the emittance of the positive ion beam forming it, modified by the scattering introduced by the charge-exchange process. Positive ions beams of intensities in the 10 mA or above region are produced regularly at HVEC from duoplasmatron sources. The measured emittance of these beams is c. 0.004 rdn cm[†] not too far removed from the emittances required of the neutral beam. Charge-exchange introduces a mean scattering angle of 3×10^{-4} rdn for hydrogen in hydrogen gas at 40-keV5)). This increases the emittance of the neutral beam to

$$\approx r\,(\alpha + \bar{\alpha}_s) \text{ rdn cm}\,.$$

Unfortunately the beam through an acceleration tube for a fixed image size is a function of the incident beam diameter as is shown in table 2. The positive ion beams available do not make it possible to utilize a small radius at the neutralizer. A beam diameter of 2–4 cm appears to be required. With this diameter beam, multiple scattering will have small effect. Multiple scattering, in fact, makes the utilization of beams with a small α_1 and α_2 an impossibility. The minimum positive ion beam emittance worth striving for appears to be above 0.001 rdn cm.

8. Conclusions

The success of the elementary experiments with neutral injection to a three-stage tandem described above taken together with the results of the injection of fast neutral helium beams—see fig. 16 emphasizes the flexibility and general validity of this method of neutral injection. The beam from the accelerator has all the energy homogeniety of the conventional electrostatic machine and is free from background contamination. The results of the AECL group at Chalk River with heavy ions should serve to increase the interest in three-stage acceleration with a neutral beam ion source.

Acknowledgements

The author wishes to express his thanks to Dr. R. J. Van de Graaff for many helpful discussions, without whose inventive genius this paper would not have been possible.

[†] Measured at 40 keV.

5) M. Johnson, MS Thesis 1960, Electrical Engineering Department, Massachusetts Institute of Technology.

DISCUSSIONS

Speaker adressed: P. H. Rose (*H.V.E.C.*)

Question by: K. W. Allen (*A.W.R.E.*)

Question: You mentioned that the attenuation of the neutral beam was 1 in 1000. Can you say how much attenuation there is in the negative ion beam when the machine is running normally?

Answer: The attenuation by charge exchange has been measured and found to be negligible.

Speaker adressed: P. H. Rose (*H.V.E.C.*)

Question by: H. E. Gove (*Chalk River*)

Question: Did you really mean an energy stability of one part in 10^5 in the three stage tandem tests and, if so, how was it measured?

Answer: Yes. I was talking about the *short*-term stability and it was measured by changing the magnetic field in the analysing magnet and in this way moving the beam from the high energy to low energy image slits. The frequency change of the proton resonance meter was recorded and from the geometry of the system ΔE was determined. The result is the average of measurements made in a half hour period.

Speaker adressed: P. H. Rose (*H.V.E.C.*)

Question by: G. Toraldo di Francia (*Florence*)

Question: In your application of Liouville's theorem you made use of only the radial degree of freedom. What about the azimuthal degree of freedom? Can the beam have an exact cylindrical symmetry? What about astigmatism?

Answer: The discussion was limited to cases of cylindrical symmetry. Measurements show that this is a very close approximation to the truth. P_θ was taken to be zero.

Speaker adressed: P. H. Rose (*H.V.E.C.*)

Question by: N. F. Verster (*Philips*)

Question: 1. Is the acceptance ellips the result of amplitude limitations in all individual lenses of the tube?

2. Do you have adjustable lenses in the H.V. terminals in order to match the beam to the tube acceptance?

Answer: 1. The area of the acceptance ellipse is reduced, in the case shown, by the perturbations of the electrodes forming the tube. The ellipse itself is of course a general consequence of Hamiltonian dynamics.

2. In the experiment described we did not have lenses. Such lenses will be necessary in a three stage machine.

NUCLEAR INSTRUMENTS AND METHODS **11** (1961) 63–92; NORTH-HOLLAND PUBLISHING CO.

CURRENT EXPERIMENTATION WITH THE TANDEM ACCELERATOR† AT THE CHALK RIVER LABORATORIES

H. E. GOVE

Physics Division, Atomic Energy of Canada Limited, Chalk River, Ontario, Canada

The tandem accelerator began operation at Chalk River in February 1959 and the total fraction of operating time in the 18 month period since then has been about 80%. The installation and major experimental apparatus is described and a brief summary of the experimental program is given. This is followed by a more detailed description of two aspects of this program. The first concerns the interaction between beams of heavy ions such as C^{12}, N^{14} and O^{16} with targets of nitrogen, oxygen, fluorine, neon, magnesium, aluminium and silicon. In this investigation narrow resonance structure was observed in the $C^{12} + C^{12}$ reaction. The second concerns measurements of spins of levels in even-even nuclei lying between O^{16} and Ca^{40}. A particle in, particle out-reaction such as inelastic proton scattering is employed to excite the levels and gamma-gamma correlations are measured in different geometries. The spins of 18 levels have been assigned to date.

I would like to describe today the Chalk River tandem accelerator¹) installation and the instrumentation we have developed, to be used with the accelerator, and to describe in outline some of the experiments which have been carried out since the machine first came into operation and then to give a more detailed account of two particular fields of research which have been occupying our time for the past year.

Fig. 1 shows a plan view of the tandem accelerator installation at Chalk River showing the machine room which is approximately 153 feet long and 32 feet wide. The present accelerator is shown in position and behind it another accelerator tank is shown in dotted outline. We have left sufficient room in this area for the second installation if occasion arises to require it at some future date. The 90° deflecting magnet is located 25 feet from the accelerator tank and a quadrupole lens is used to focus the beam on the exit slits of this magnet. These exit slits provide a signal which stabilizes the terminal potential. Following the 90° magnet is a small ± 25° deflecting magnet which allows the beam to be sent into any one of three experimental positions. The gap in the shield wall is completely filled with concrete with holes for the beam tubes to pass through. The target room is about 38 feet long by 50 feet wide and has a ceiling height of 32 feet. In addition to the main target room there is a second experimental area marked here as the gamma cave, which is a specially shielded low background area for gamma ray measurements. The gamma cave has been constructed of iron-loaded concrete which has a very low potassium content and therefore a low background of 1.46 MeV gamma rays from K^{40}. In addition to this, the cave is surrounded on all sides by about 15 feet of earth to eliminate another source of background which we experience at Chalk River. This is radioactive argon from the reactors, which is emitted from the reactor cooling stacks. A small building located in the upper right hand side of the figure contains the gas storage tank for the insulating gas of the tandem accelerator and the equipment for handling the exchange of this gas. The control room is connected to the main building by a passageway and contains both the controls for the accelerator and the experimental equipment.

The accelerator commenced operation at Chalk River in February of 1959 and has operated on a 2-shift a day, five-day week basis ever since then. The total fraction of operating time

---

† Designed and built by High Voltage Engineering Corporation, Burlington, Massachusetts for Atomic Energy of Canada Limited, Chalk River, Ontario.

¹) J. L. Danforth, Can. Electron. Engr. 2 (1958) 18.

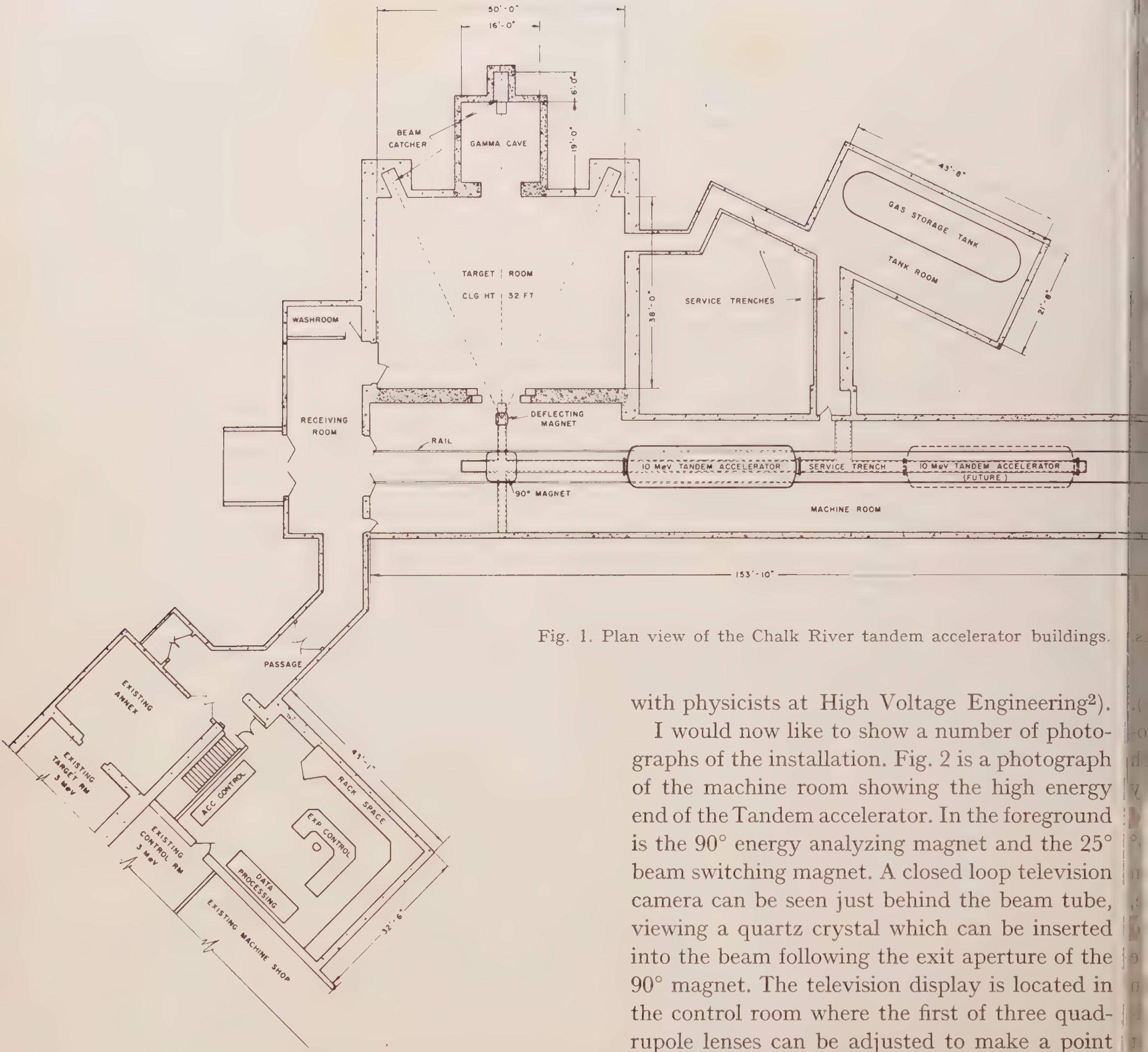
50'-0"
16'-0"
6'-0"
19'-0"
BEAM CATCHER
GAMMA CAVE
43'-8"
GAS STORAGE TANK
TANK ROOM
21'-8"
TARGET ROOM
CLG HT 32 FT
38'-0"
SERVICE TRENCHES
WASHROOM
RECEIVING ROOM
DEFLECTING MAGNET
RAIL
10 MeV TANDEM ACCELERATOR
SERVICE TRENCH
10 MeV TANDEM ACCELERATOR (FUTURE)
90° MAGNET
MACHINE ROOM
153'-10"
PASSAGE
EXISTING ANNEX
EXISTING TARGET RM 3 MeV
ACC CONTROL
43'-1"
RACK SPACE
EXP CONTROL
EXISTING CONTROL RM 3 MeV
DATA PROCESSING
EXISTING MACHINE SHOP
32'-6"

Fig. 1. Plan view of the Chalk River tandem accelerator buildings.

in the 18-month period since then has been 80 % which is, I think, some kind of a record for a machine of new design. Prior to its operation at Chalk River it was tested at the High Voltage Engineering Plant in Burlington, Massachusetts, where a number of preliminary experiments to measure (p,n) thresholds were performed by Chalk River physicists in collaboration with physicists at High Voltage Engineering[2]).

I would now like to show a number of photographs of the installation. Fig. 2 is a photograph of the machine room showing the high energy end of the Tandem accelerator. In the foreground is the 90° energy analyzing magnet and the 25° beam switching magnet. A closed loop television camera can be seen just behind the beam tube, viewing a quartz crystal which can be inserted into the beam following the exit aperture of the 90° magnet. The television display is located in the control room where the first of three quadrupole lenses can be adjusted to make a point focus at the exit aperture of this 90° magnet. There is a second quadrupole lens located on the target room side of the shield wall between the target room and the machine room and this takes as its object, the point focus at the exit

[2]) H. E. Gove, J. A. Kuehner, A. E. Litherland, E. Almqvist, D. A. Bromley, A. J. Ferguson, P. H. Rose, R. P. Bastide, N. Brooks and R. J. Connor, Phys. Rev. Letters 1 (1958) 251.

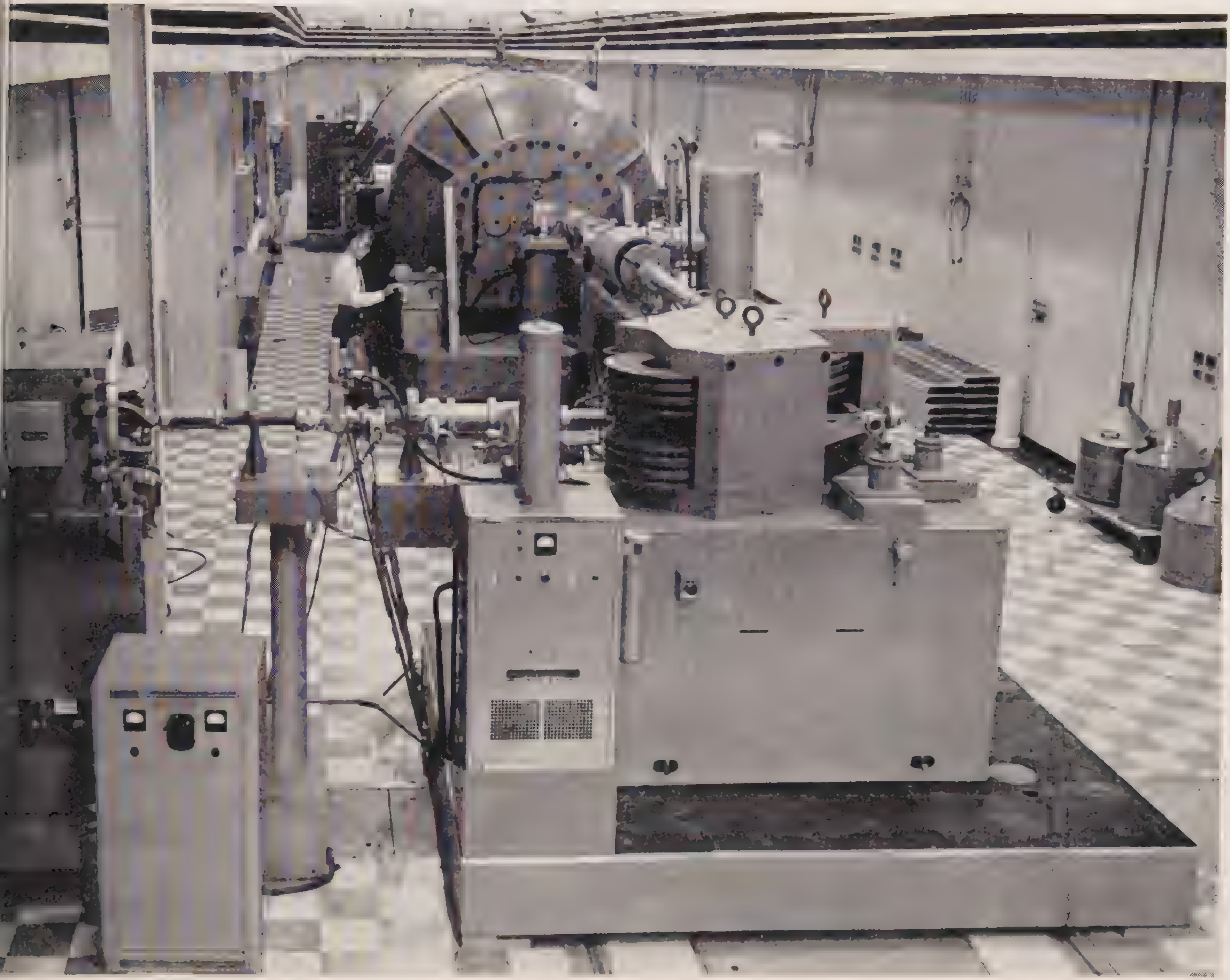

Fig. 2. Photograph of the machine from the high energy end.

aperture of the 90° magnet, and focusses it to an image approximately in the center of the target room. The third quadrupole lens is located just at the entry to the gamma cave and this allows the beam to be focussed in the center of the gamma cave. At each of the focal points a quartz can be remotely inserted into the beam and a television camera can examine the spot size at these focal points. When a change in potential is made on the tandem accelerator terminal, the quadrupole lenses must be re-focussed sequentially and this operation can be carried out quite quickly with this remote viewing system. Around the walls of both the machine room and the target room are trays which carry the wiring from the control room to the machine or target room. This enables new wires to be added quite conveniently and is particularly important in the case of the experimental wiring which must be constantly modified.

Fig. 3 is another view, again taken from the high energy end of the machine. Fig. 4 shows the ion source end of the accelerator. This comprises an rf ion source for producing positive ions. These ions are accelerated through a potential of about 40 kilovolts and pass into an exchange canal emerging unchanged in charge or as neutral or negative ions. In the case of hydrogen about 1 % of the beam passing into the exchange canal emerges as negative ions. The machine has been used to date to accelerate protons and deuterons, as well as a number of heavy ions, including

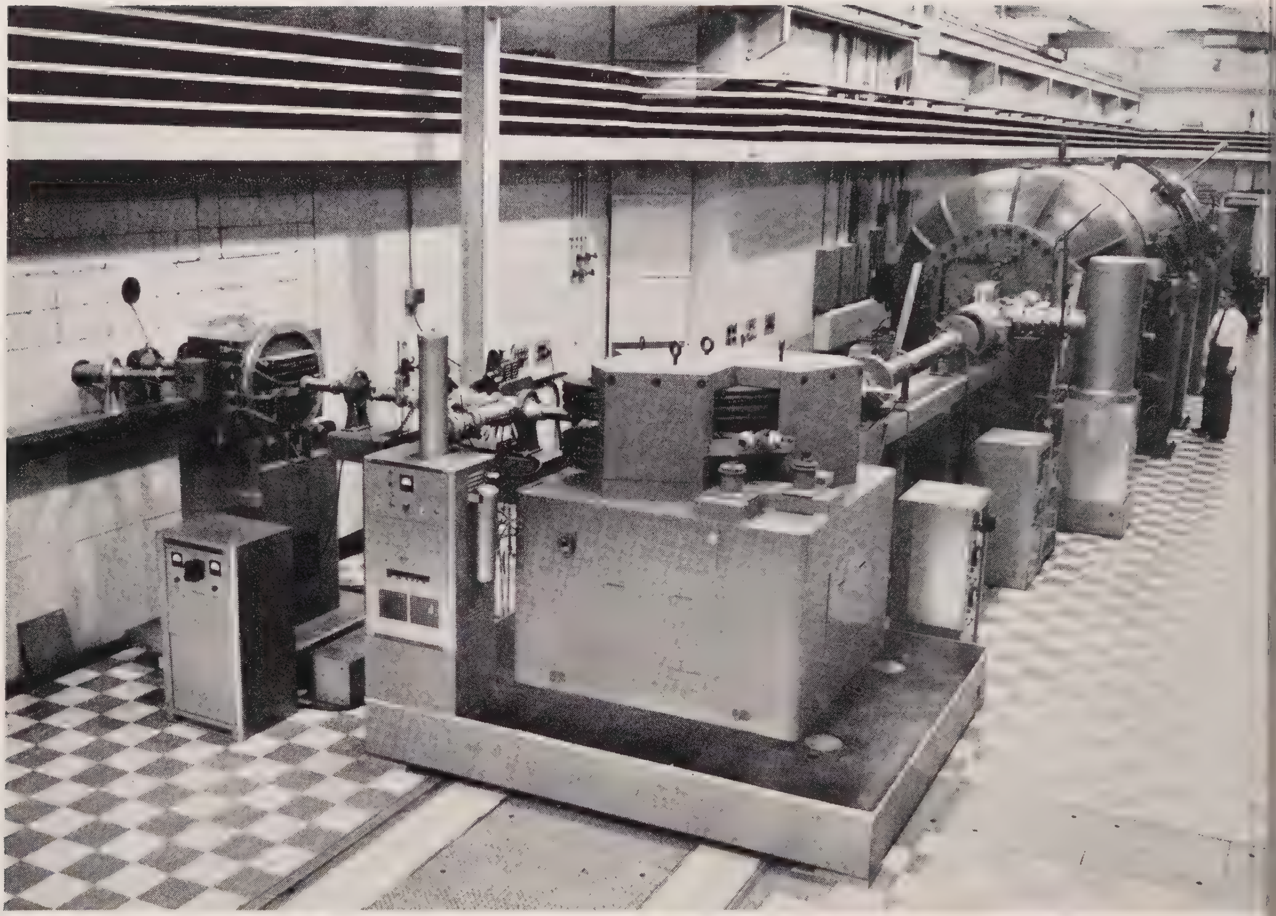

Fig. 3. Another view of the high energy end of the accelerator.

oxygen, carbon, nitrogen, fluorine and even Cl^{35}. These latter ions were accelerated to an energy of 48 MeV. Since this photograph was taken we have added an alpha-particle ion source which consists of a 1-MeV positive ion Van de Graaff accelerator with a helium ion source in its terminal. These singly-charged helium ions are accelerated to about 0.4 MeV in this accelerator, and then pass into the exchange canal where they are neutralized. The neutral beam is then drifted through the first half of the tandem machine and passed into the stripper canal in the high voltage terminal, where a high fraction of the neutral He ions are doubly ionized. The doubly ionized He ions are then accelerated through the second half of the machine to a potential corresponding to twice the terminal voltage. This installation has just been completed and tested and will shortly be used for experimental work.

Fig. 5 is a rather old photograph of the target room showing the central beam tube only, emerging from the shield wall between the target and the machine room. The experimental apparatus shown in this photograph was that used for making (p,n) threshold measurements[3]) and consists of the modified long counter and a thermal neutron counter, both placed at 0° to the incident beam. The experimental wiring which runs along the trays on the wall is carried out on booms and brought to the experimental apparatus. Fig. 6 is another view of the target room looking toward the gamma ray cave which

---

[3]) D. A. Bromley, A. J. Ferguson, H. E. Gove, J. A. Kuehner, A. E. Litherland, E. Almqvist and R. Batchelor, Can. J. Phys. **37** (1959) 1514.

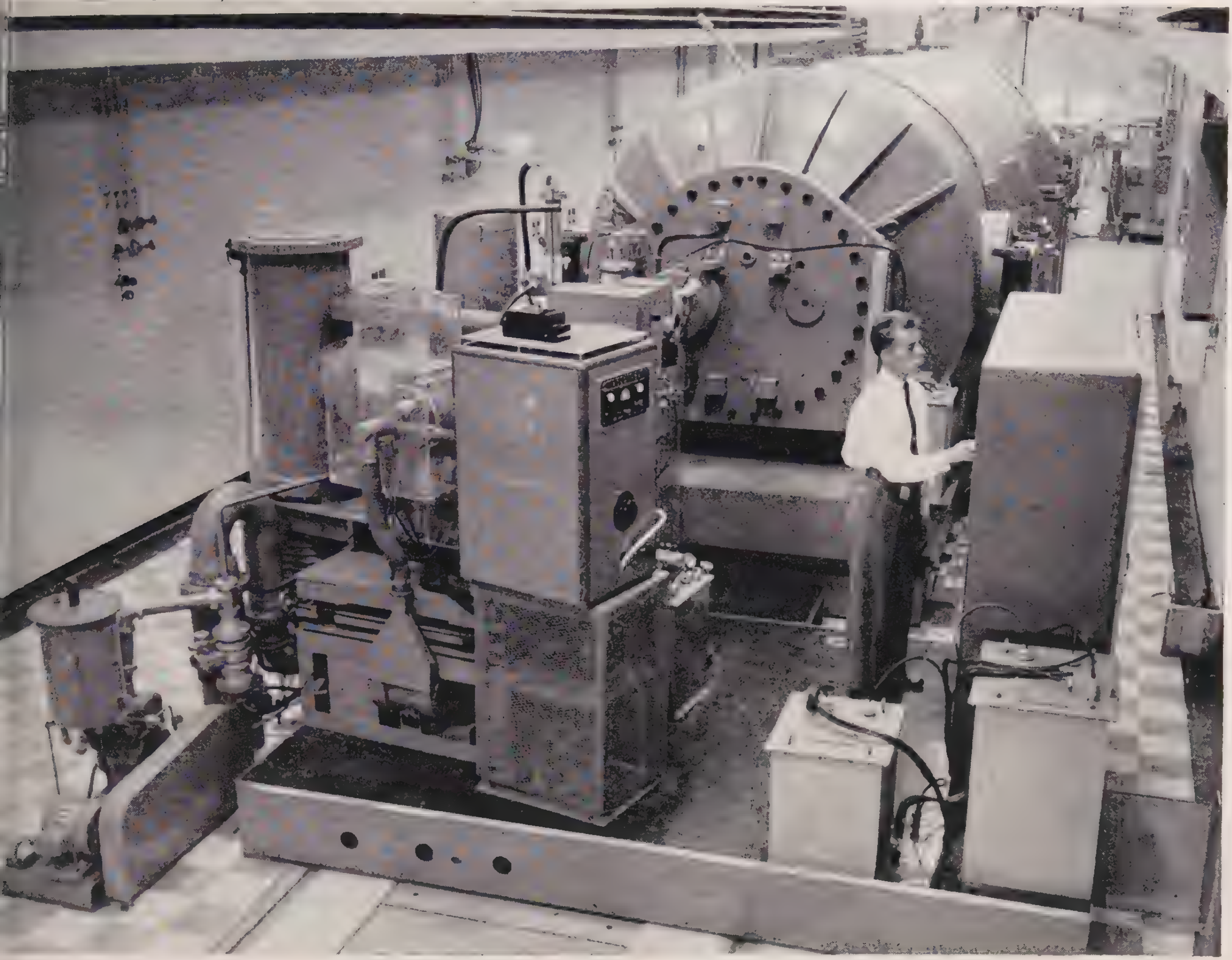

Fig. 4. The ion source end of the accelerator.

is shown in the background. The circular hole in the back wall of this cave is a shielded location for a beam catcher.

Fig. 7 is a view of the control room showing the experimental control console and electronics for experimental purposes. The electronics are located in racks along the wall and the experiments are conducted from the console where runs can be started and stopped and counters can be moved in angle. Included among the electronics are two 100-channel transistor pulse amplitude analyzers[4]). The contents of these analyzers is printed automatically by an electric typewriter and also punched on a paper tape. The tape can be used either to feed into an automatic plotter for plotting the spectrum, or it can be used for analyzing the data on a computer. In addition to the contents of these two multi-channel analyzers a number of other pieces of information are also recorded automatically at the end of each run. These include the date, the run number, the length of the run, the sensitivity of the integrator which measures the total charge striking the target during the run, a number corresponding to the physicist who is conducting the experiment, and also the contents of a number of single-channel scalers. One of these scalers is used for recording the length of the run and another records the frequency of a proton resonance fluxmeter which measures the magnetic

---

[4]) Developed by the Electronics Branch, Atomic Energy of Canada Limited.

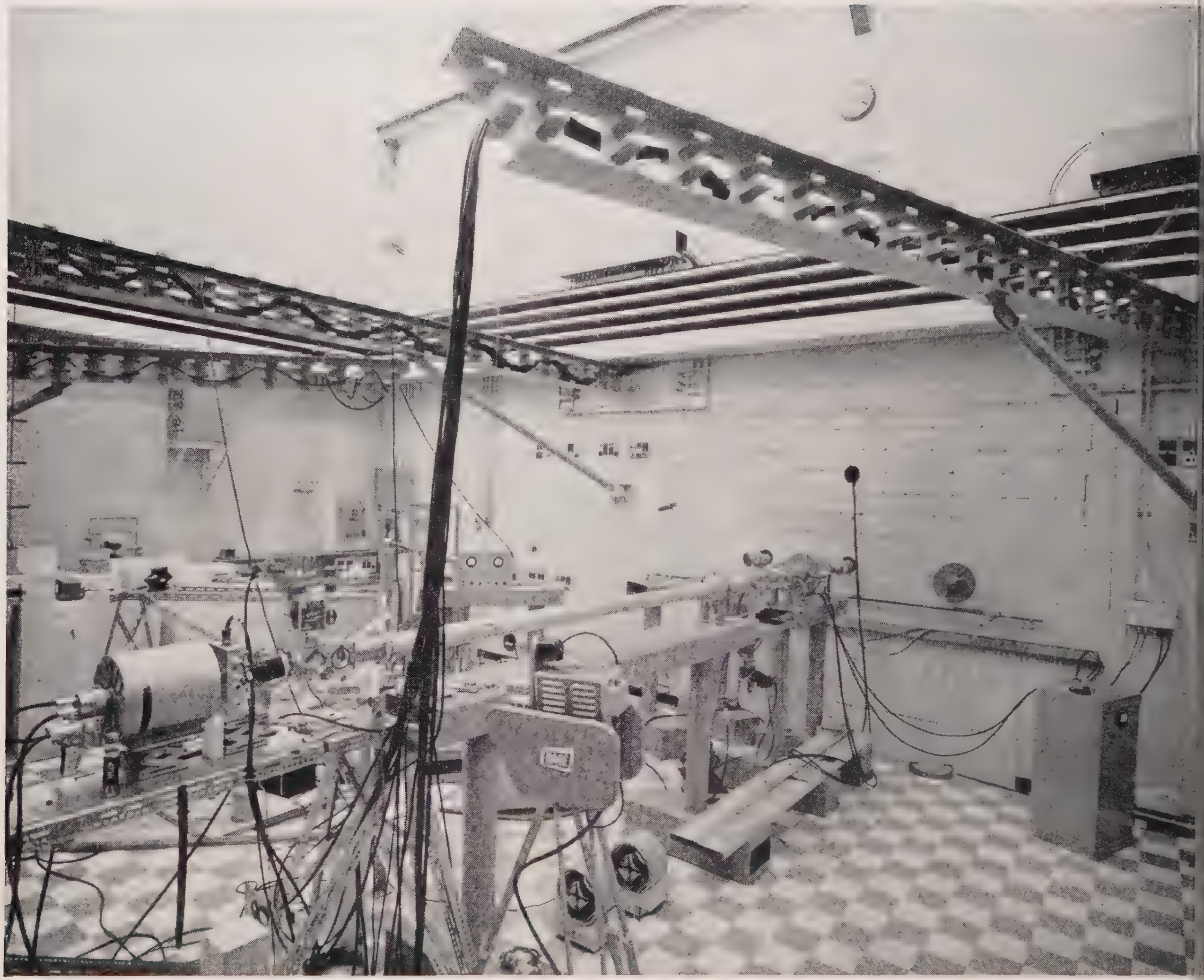

Fig. 5. The main target room looking toward the three foot thick shield wall between the machine and target rooms.

field in the 90° beam analyzing magnet and therefore gives a measure of the machine energy. We will be putting into operation shortly in addition to this, a system for recording the angle at which counters are set during the experiment. In this system the counter angle is measured on a digitizer which converts angle information into digital information and this in turn can be recorded by the print-out mechanism. The aim here is to go as far as possible in the direction of making the recording of all pertinent information automatic so that the person conducting the experiment can spend more time considering the implications of the results and deciding what experiments should follow the one that has just been performed.

Fig. 8 is a photograph of the accelerator control console. This is similar to control consoles used on standard Van de Graaff accelerators except for the greater complexity of the ion source controls. On the extreme right hand panel the receiver for the remote closed loop television system can be seen and it is actually viewing one of the windows beyond which is located the retractable quartz plate.

I would like to turn now to a description of some of the experimental apparatus which we have put into operation. This comprises princi-

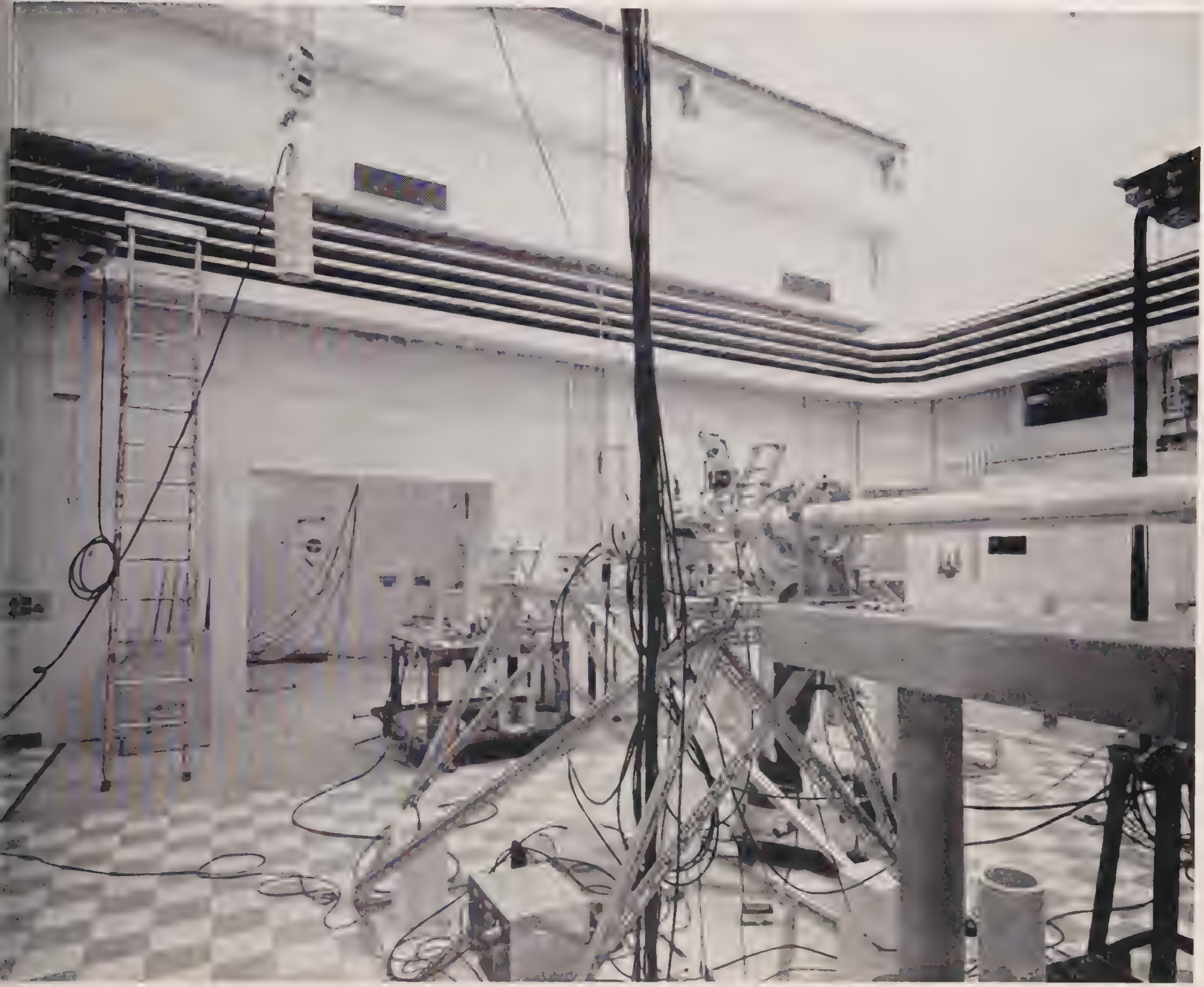

Fig. 6. The main target room looking toward the gamma cave.

pally three major pieces of equipment and the first of these is shown in fig. 9. This is a broad range magnetic spectrograph, manufactured for us by High Voltage Engineering. It is of a similar design to that described by Browne and Beuchner[5]) at M.I.T. The photographic plate covers a range of particle energies of a factor of 2.4 and the magnet is capable of handling protons of energies up to 35 MeV. This magnet has one additional interesting feature which is due to Enge[6]) at M.I.T. and that is a device for converting it from a spectrograph to a spectrometer. In the spectrometer operation a single element of a magnetic quadrupole lens is employed to increase the solid angle by a factor of approximately 8 and in this mode of operation the magnet is rotated about a central axis through 90°. This magnet has now been tested with alpha particles from a natural radioactive source, and appears to meet the specifications which were originally set for it. It has an energy resolution of about 1 part in 10^3 and a solid angle when operating as a spectrograph of 1 part in 10^4 of a sphere. In the spectrometer operation the solid angle is approximately 1 part in 10^3.

---

[5]) C. P. Browne and W. W. Buechner, Rev. Sci. Instr. **27** (1956) 899.

[6]) H. A. Enge, Rev. Sci. Instr. **29** (1958) 885.

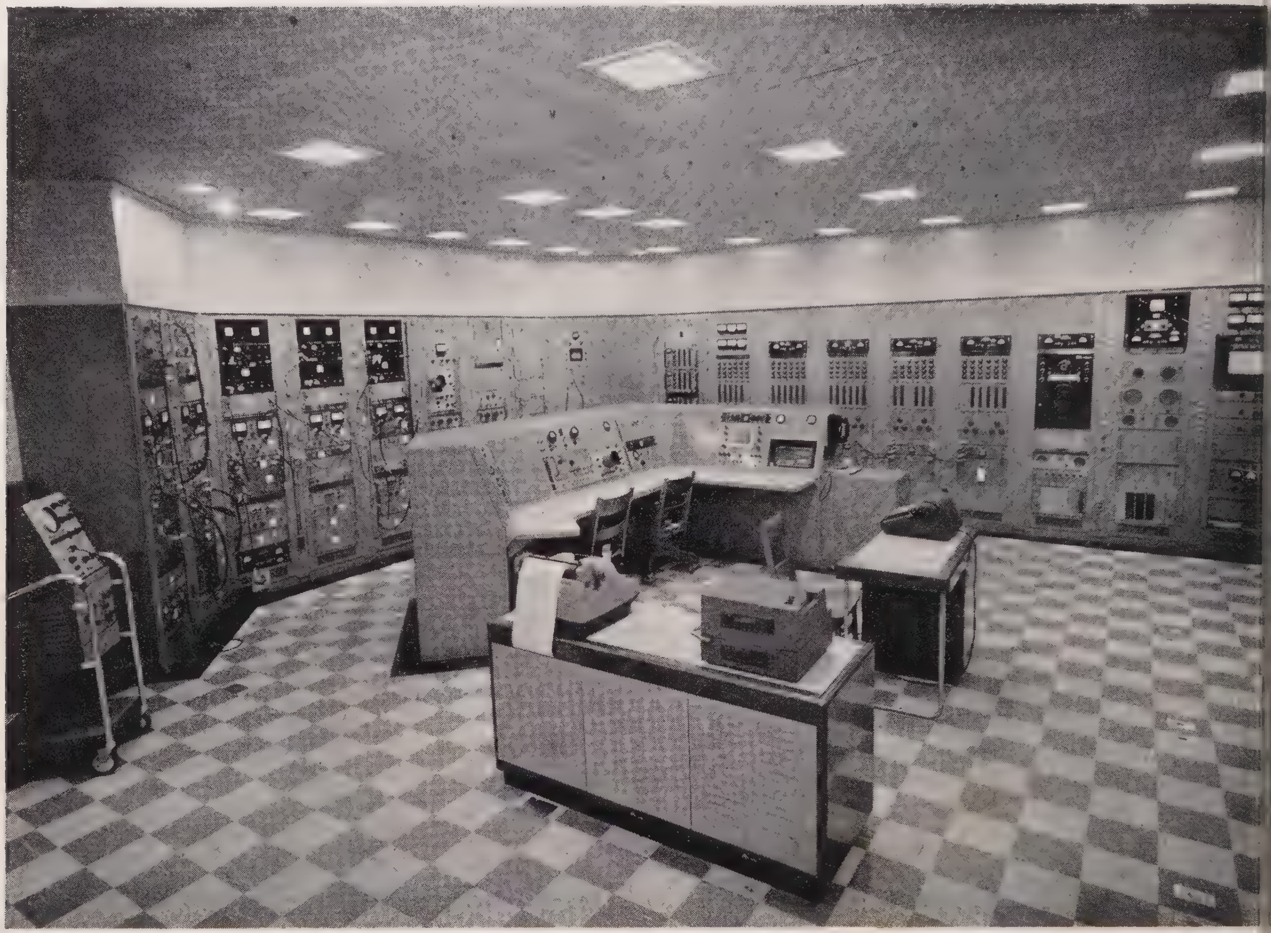

Fig. 7. The experimental area of the control room.

Fig. 10 shows the second piece of apparatus which is a large scattering chamber. This chamber was designed to allow detectors of various kinds to rotate about a target placed in the center. The target arrangement is such that a number of targets can be accommodated and these can be brought into position and the angle between the target and the beam can be varied both in the horizontal and the vertical planes. The detectors themselves can be rotated either in a horizontal or vertical plane containing the beam, or a vertical plane perpendicular to the beam.

Fig. 11 shows some apparatus located in the gamma-ray cave. This is an azimuthal gamma-ray table. Two large NaI crystals are mounted on the apparatus, one on an arm which can move in the horizontal plane containing the beam about the target center and the other which can be moved over the surface of the hemisphere which is centered at the target center. This second detector is mounted on a carriage which in turn moves on the semicircular beam. This beam is pivoted through a vertical axis which passes through the target center and so by combining the two motions this counter can be moved anywhere over a hemisphere with its base in the horizontal plane. I will describe later some experiments which employ this apparatus. The distance between the counters and the target center can be adjusted over a wide range and the three angles, one for the counter moving in the horizontal plane and two angles for the second counter, are controlled remotely at the experimental console in the control room. Again you can see a television

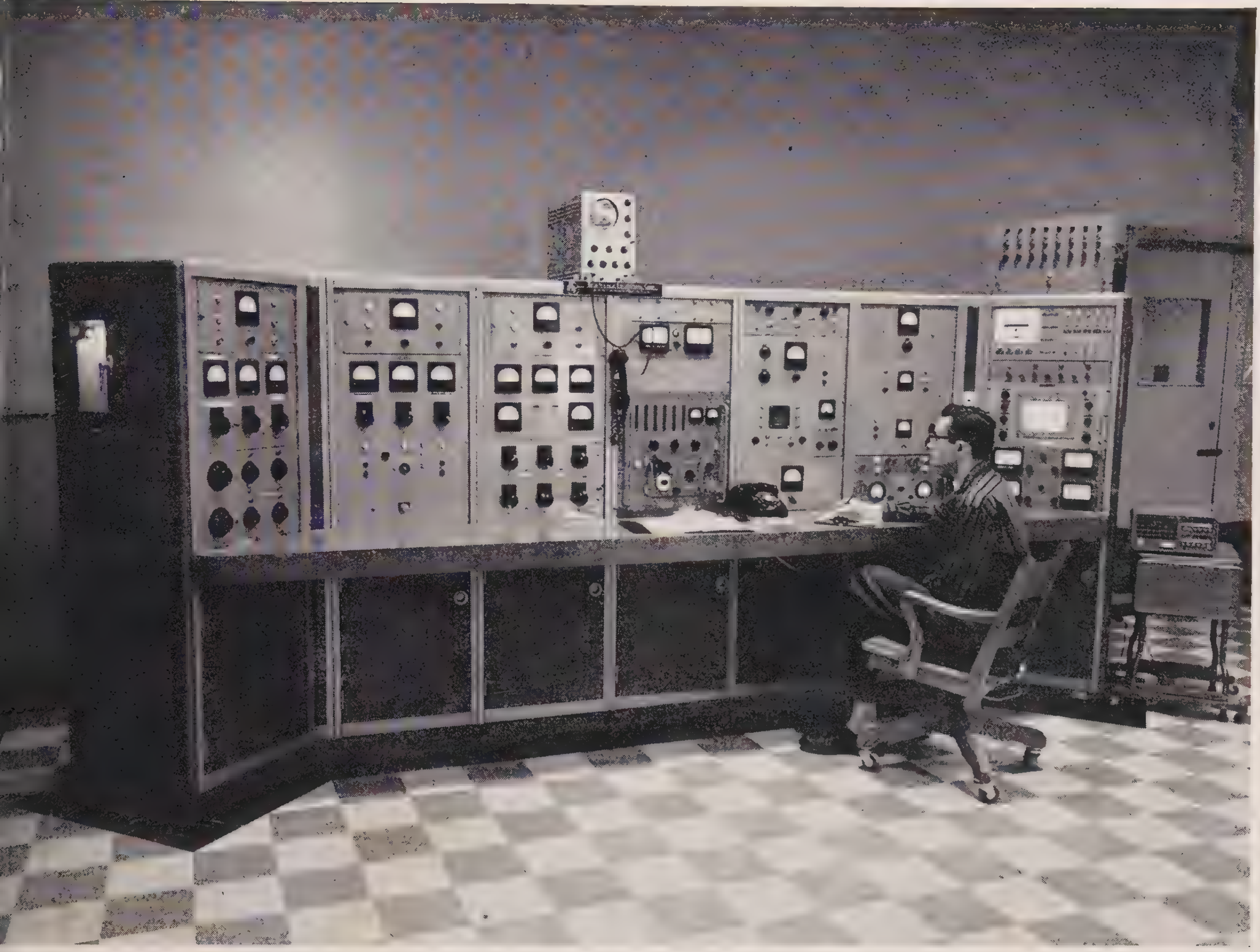

Fig. 8. The tandem accelerator control console.

camera which views a quartz plate inserted in the beam part way along this beam tube and in this way the focus at the target can be examined.

I will now outline briefly the experiments that we have performed on this machine since beginning operation February 1959 and follow this with details of two particular experimental programs. Table 1 outlines the research program with the machine. The first experiments we performed were (p,n) threshold measurements and yields and these covered a machine energy range of about 1.8 to 10.5 MeV[3]).

The second experiment involved study of capture gamma rays from the giant resonance region in light nuclei. This is an experiment which is a very obvious one to try on a tandem accelerator and provides some information that, until the tandem accelerator came into operation, was really not available[7]).

The next experiment involved the measurement of total proton cross sections on a number of target elements[8]).

Listed in this table are a number of experiments of the type (particle-particle, γ–γ) and these are one of the groups of experiments which I will discuss later in greater detail.

[7]) H. E. Gove, A. E. Litherland and R. Batchelor, Phys. Rev. Letters **3** (1959) 177; also Proceedings of the Intern. Conference on Nuclear Structure, Kingston, Canada, 1960, Eds. D. A. Bromley and E. W. Vogt (University of Toronto Press and North-Holland Publishing Company, 1960) p. 944.

[8]) E. Almqvist, D. A. Bromley, J. A. Kuehner and E. W. Vogt, Proceedings of the International Conference on Nuclear Structure, Kingston, Canada, Eds. D. A. Bromley and E. W. Vogt (University of Toronto Press and North-Holland Publishing Company, 1960) p. 736.

TABLE 1

Summary of the first year's research program with the Chalk River tandem accelerator.

Topic	Particle energy (MeV)	Work done by
(1) (pn) thresholds and yields	1.8 → 10.5	Bromley, Ferguson, Gove, Kuehner, Litherland, Almqvist and Batchelor
(2) Giant resonance in C^{12}, Si^{28} and Mg^{24}	2.6 → 11.4	Gove, Litherland and Batchelor
(3) Total proton cross sections on Mg, Al, Ti, Fe, Co, Ni, Ni^{58}, Cu and Zn	4 → 12.9	Almqvist, Bromley and Kuehner
(4) $Mg^{24}(pp'\gamma\gamma)$ spin of 4.24 level	4.9 → 6	Batchelor, Ferguson, Gove and Litherland
(5) (d,n) and (d,n,γ) on B^{10}, B^{11} and C^{12}	5.0 and 8.0	Ferguson, Gove, Litherland and Batchelor
(6) (d,p) and (d,pγ) on O^{16}, Al^{27} and Si^{28}	6 → 10.7	Kuehner, Almqvist and Bromley
(7) $H^3(O^{16}p\gamma\gamma)O^{18}$ spin of 3.65 and 3.93 levels	14	Litherland, Batchelor, Ferguson and Gove
(8) Coulomb excitation with O^{16} ions on Mg^{24}, Al^{27}, Si^{28}, Fe^{56}, Ni^{58} and Ni^{60}	16 → 35	Broude, Gove and Litherland
(9) Elastic scattering of O^{16} by C^{12}, Al^{27} and Mg^{24} and C^{12} by C^{12}	10.27 and 31.9	Bromley, Kuehner and Almqvist
(10) $Si^{30}(pp'\gamma\gamma)$ spin of 3.51 and 3.79 levels	5.0 → 5.6	Broude and Gove

There were a number of experiments performed on (d,n) and (d,nγ) reactions measuring angular distributions[9]) and also (d,p) and (d,pγ) reactions. The latter were designed to test the reaction mechanism involved in the (d,p) process and specifically to discover whether a plane wave or a distorted wave approximation was needed to describe the reaction[10]). Then, there have been a very extensive series of experiments performed using a variety of heavy ions from the accelerator. One group of these involved Coulomb excitation measurements[11]) and the other group involved the study of elastic and reaction scattering of heavy ions, like C^{12} and O^{16} from various light nuclei, and this is the second group of experiments which I will discuss in some detail.

This original experimental program was designed to test the capabilities of the machine and to cover a fairly broad range of fields in order to see just what were the most interesting things to pursue in more detail and hence this explains the rather large variety of work shown in this table.

Turning now to a more detailed examination of two items in the research program, I would like to begin by describing some heavy ion experiments which were performed by E. Almqvist, D. A. Bromley and J. A. Kuehner[12]).

[9]) A. J. Ferguson, H. E. Gove, A. E. Litherland and R. Batchelor, Bull. Am. Phys. Soc. Series II, **5** (1960) 45; and also Proceedings of the International Conference on Nuclear Structure, Kingston, Canada, 1960, Eds. D. A. Bromley and E. W. Vogt (University of Toronto Press and North-Holland Publishing Company, 1960) p. 364.

[10]) J. A. Kuehner, E. Almqvist and D. A. Bromley, Phys. Rev. Letters **4** (1960) 132; and also Proceedings of the International Conference on Nuclear Structure, Kingston, Canada, 1960, Eds. D. A. Bromley and E. W. Vogt (University of Toronto Press and North-Holland Publishing Company, 1960) pp. 349, 352, 375 and 378.

[11]) H. E. Gove and C. Broude—Proceedings of the Second Conference on Reactions Between Complex Nuclei, Gatlinburg, Tennessee, May (1960) Eds. A. Zucker, E. C. Halbert and F. T. Howard (John Wiley & Sons, 1960); and also Proceedings of the International Conference on Nuclear Structure, Kingston, Canada, Eds. D. A. Bromley and E. W. Vogt (University of Toronto Press and North-Holland Publishing Company, 1960) p. 943.

[12]) E. Almqvist, Proceedings of the International Conference on Nuclear Structure ,Kingston, Canada, (1960)—Eds. D. A. Bromley and E. W. Vogt (University of Toronto Press and North-Holland Publishing Company) p. 255—this was a report of contributions No. 6, 7, 43 and 146 to the International Conference on Nuclear Structure, Kingston, Canada, August (1960); See also D. A. Bromley, J. A. Kuehner and E. Almqvist, Phys. Rev. Letters **4** (1960) 367; E. Almqvist, D. A. Bromley and J. A. Kuehner, Phys. Rev. Letters **4** (1960) 515; and Proceedings of the Second Conference on Reactions Between Complex Nuclei, Gatlinburg, Tennessee, May 1960, Eds. A. Zucker E. C. Halbert and F. T. Howard (John Wiley & Sons, 1960).

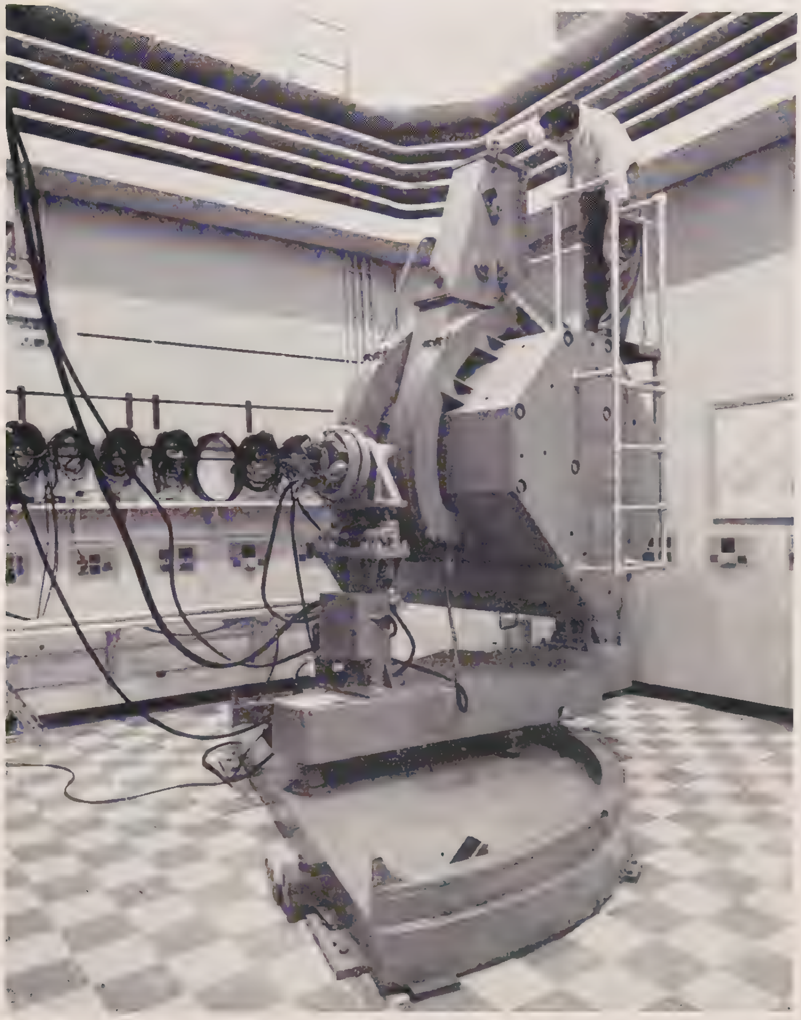

Fig. 9. The 65 cm magnetic spectrograph with spectrometer conversion.

These experiments involved a study of the elastic scattering of heavy ions and of nuclear reactions initiated by heavy ions and in the course of the experiments a number of very interesting phenomena were discovered.

The elastic scattering of C^{12} ions by C^{12}, O^{16} and Si^{28} and of O^{16} ions by O^{16}, Mg^{24}, Al^{27} and Si^{28} has been studied in the energy range below 36 MeV using heavy ion beams from the tandem accelerator and Au-Si surface barrier detectors. Fig. 12 shows excitation curves measured at 90° in the center of mass system for elastic scattering of C^{12} by C^{12}, O^{16} by O^{16} and C^{12} by O^{16}. The smooth curve through the data at lower energies and extended by a dotted curve is the Coulomb prediction. As can be seen this prediction is in complete accord with the experimental data at energies below the Coulomb barrier. At energies above the Coulomb barrier striking differences in the behaviour are found. In the first place, the experimental points break sharply away from predicted Coulomb curves, at a point corresponding approximately to the barrier and in the case of the scattering of C^{12} by C^{12}, pronounced structure is observed. Such structure is also observed in the scattering of O^{16} by C^{12}, but at much higher energies above the barrier, while in the case of elastic scattering of O^{16} by O^{16}, no resonance structure is observed at all.

Angular distributions have been measured in

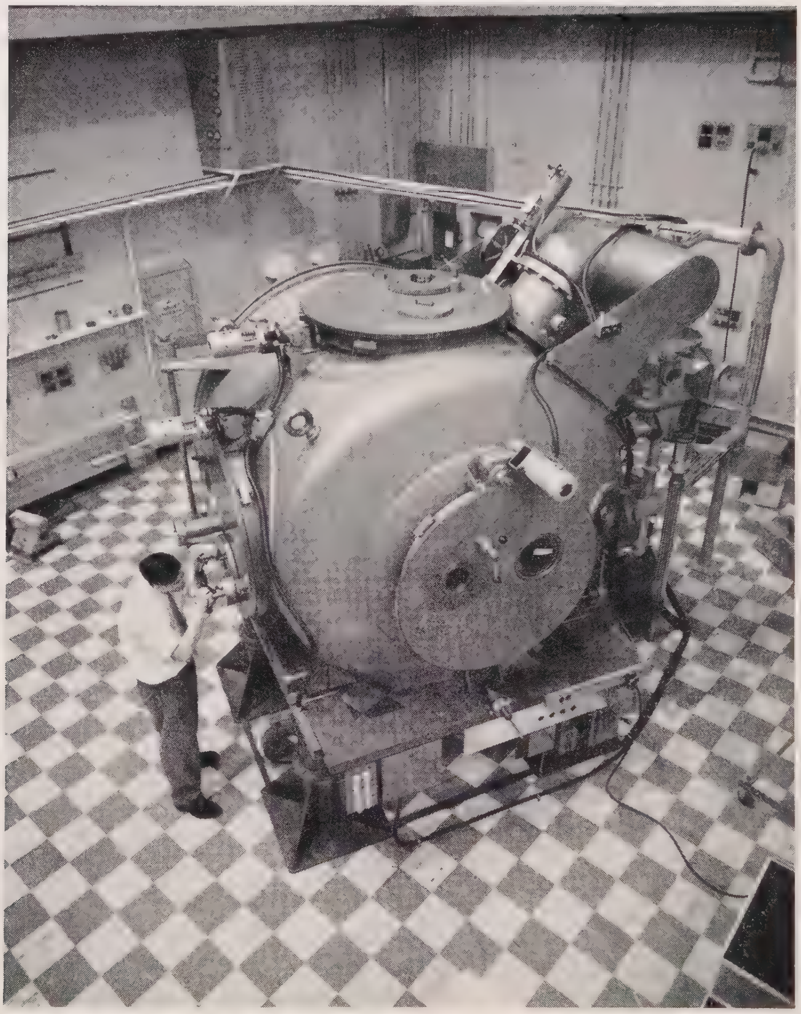

Fig. 10. Large scattering chamber.

all three cases at a number of energies and some of these are shown in fig. 13. On the upper left hand diagram is shown the elastic scattering of C^{12} by C^{12} at 5 MeV energy in the center of mass system and one sees here the characteristic quantum interference modulation which is observed in identical particle scattering. The smooth solid curve is that predicted for classical Coulomb scattering between identical particles while the dotted curve is the Mott quantum-mechanical prediction and as one can see, there is remarkably good agreement between this and the observed experimental points. This energy of 5 MeV is well below the Coulomb barrier for C^{12} and C^{12}. Similarly, in the case of O^{16} elastic scattering by O^{16} at 8.8 MeV in the center of mass system which is again below the Coulomb barrier for these two particles, one sees very good agreement between the experimental data and the Mott prediction. In this case, one sees that the frequency of modulation has increased over the C^{12} by C^{12} scattering and this is a consequence of the greater mass of the O^{16} ions. At center of mass energies above the Coulomb barrier, shown on the two lower curves, the elastic scattering as a function of center of mass angle departs in a marked manner from that predicted for Mott scattering which is shown by the dotted curve in both the case of C^{12} by C^{12} and O^{16} by O^{16} scattering. The data on the elastic scattering of various combinations of heavy ions plotted as a function of energy as

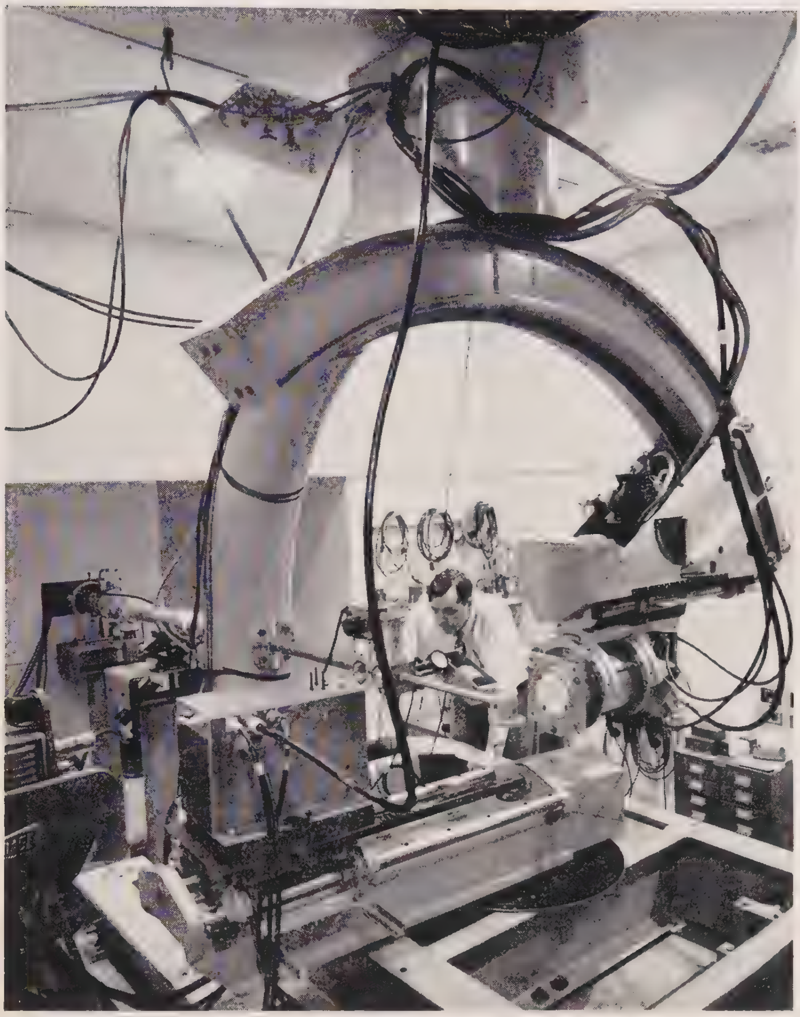

Fig. 11. Azimuthal gamma-ray table located in gamma cave.

shown in fig. 13, can be used to estimate the nuclear radii of these ions. In this estimate, one employs the Blair[13]) quarter-point formula in which one assumes that the sum of the two radii are approximately equal to the classical apsidal distance if one evaluates this at the energy for which the experimental cross section is one-quarter of the corresponding Coulomb cross section. In this way, the radii shown in table 2 have been obtained. The formula for the radius is shown on the upper part of the table and the values of R and r_0 for various combinations of heavy ions are given in the right hand column. It is to be observed that these values of r_0 are approximately constant and equal to about 1.62 fermis† except for the case of C^{12} scattering by C^{12} where the value seems to be appreciably larger, namely 1.75 fermis. I shall return to this point later in this paper.

Table 2

Interaction radii for various combinations of heavy ions and targets.

$$R = r_0 (A_1^{\frac{1}{3}} + A_2^{\frac{1}{3}}) \text{ fermi}^{\dagger}$$

	R	r_0
O^{16} on Al^{27}	9.05	1.64
O^{16} on Mg^{24}	8.76	1.62
C^{12} on Si^{28}	8.53	1.60
C^{12} on O^{16}	7.84	1.63
O^{16} on O^{16}	8.22	1.63
C^{12} on C^{12}	8.02	1.75

† 1 fermi = 10^{-13} cm.

---

[13]) J. S. Blair, Phys. Rev. **95** (1954) 1218.

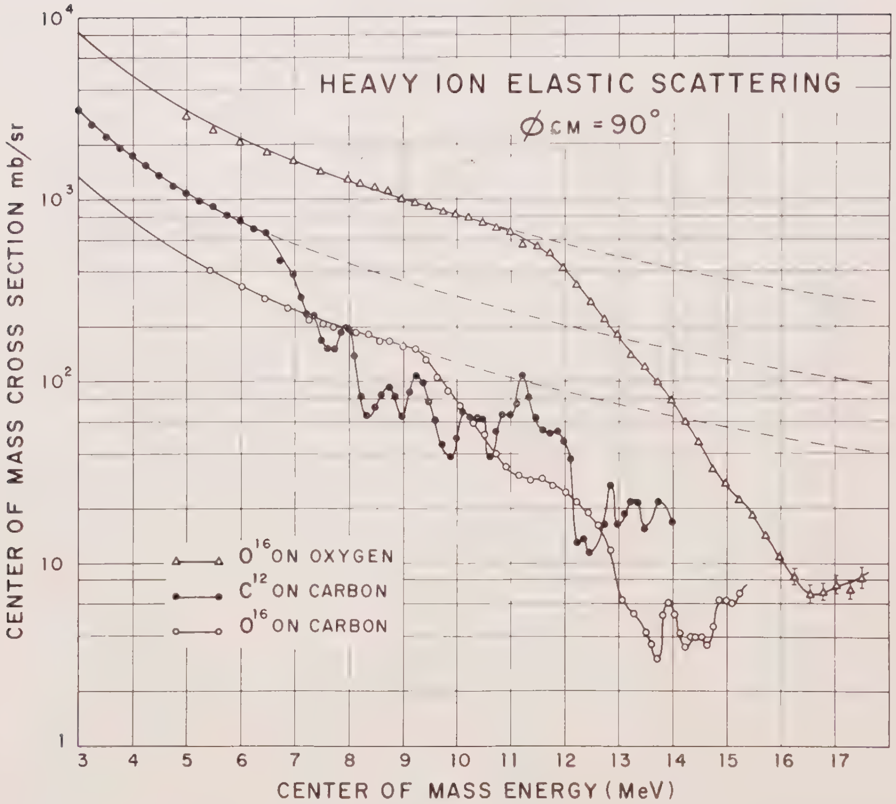

Fig. 12. Cross section for elastic scattering of O^{16} by oxygen C^{12} by carbon and O^{16} by carbon at 90° in the center of mass as a function of center of mass energy.

With the discovery of this marked resonance structure in the elastic scattering of carbon by carbon above the Coulomb barrier, it was a natural step to investigate the yield of reaction particles, both below and above the Coulomb barrier for the C^{12} on C^{12} system and for other combinations of heavy ions. Excitation curves were measured for all gamma radiation of energy greater than 600 kilovolts in the case of C^{12} bombardment of C^{12}, N^{14}, O^{16}, F^{19} and Ne^{20}, and O^{16} bombardment of O^{16} and Ne^{20}, and with N^{14} bombardment of N^{14}. These measurements approximate those for the total reaction cross section. In addition, excitation curves for alpha particles, protons and neutrons have been measured for the $C^{12} + C^{12}$ system, and alpha particles for the $O^{16} + O^{16}$ system.

In the case of the $C^{12} + C^{12}$ system, isolated resonances were observed at energies below the Coulomb barrier in all excitation curves and at all angles. In order to obtain the resonance parameters a differentially-pumped target system was used to permit the use of gaseous targets such as methane for C^{12}, N^{14}, O^{16}, sulphur hexafluoride for F^{19} and finally Ne^{20}. Fig. 14 shows the results of the bombardment of methane by C^{12}. On the left hand side is a spectrum of gamma rays from the reaction of C^{12} on C^{12} ions and this shows a prominent peak at 1.63 MeV corresponding to the compound system emitting alpha particles to the first excited state of Ne^{20}. On the right hand side of the figure are shown yield curves taken under various conditions. The upper curve shows the yield of this 1.63 MeV gamma ray, using a gas target which was 60 kilovolts thick to the carbon ions. The curve below this shows the yield of all gamma rays > 1 MeV from a 60 kilovolt thick target and then the lowest curve shows the yield of gamma rays above 1 MeV from a 30 kilovolt target.

The fact that the excitation curve for 1.63 MeV gamma radiation is identical to that for all radiations of energy >1.0 MeV indicates that the resonances are an entrance channel phenomena. By using successively thinner targets it is shown that the upper of the three resonances is in fact a doublet and the resonances occur at energies of 5.65, 5.98, 6.32 and 6.50 MeV respectively in the center of mass system and have widths of the order of 130 kilovolts. By assuming

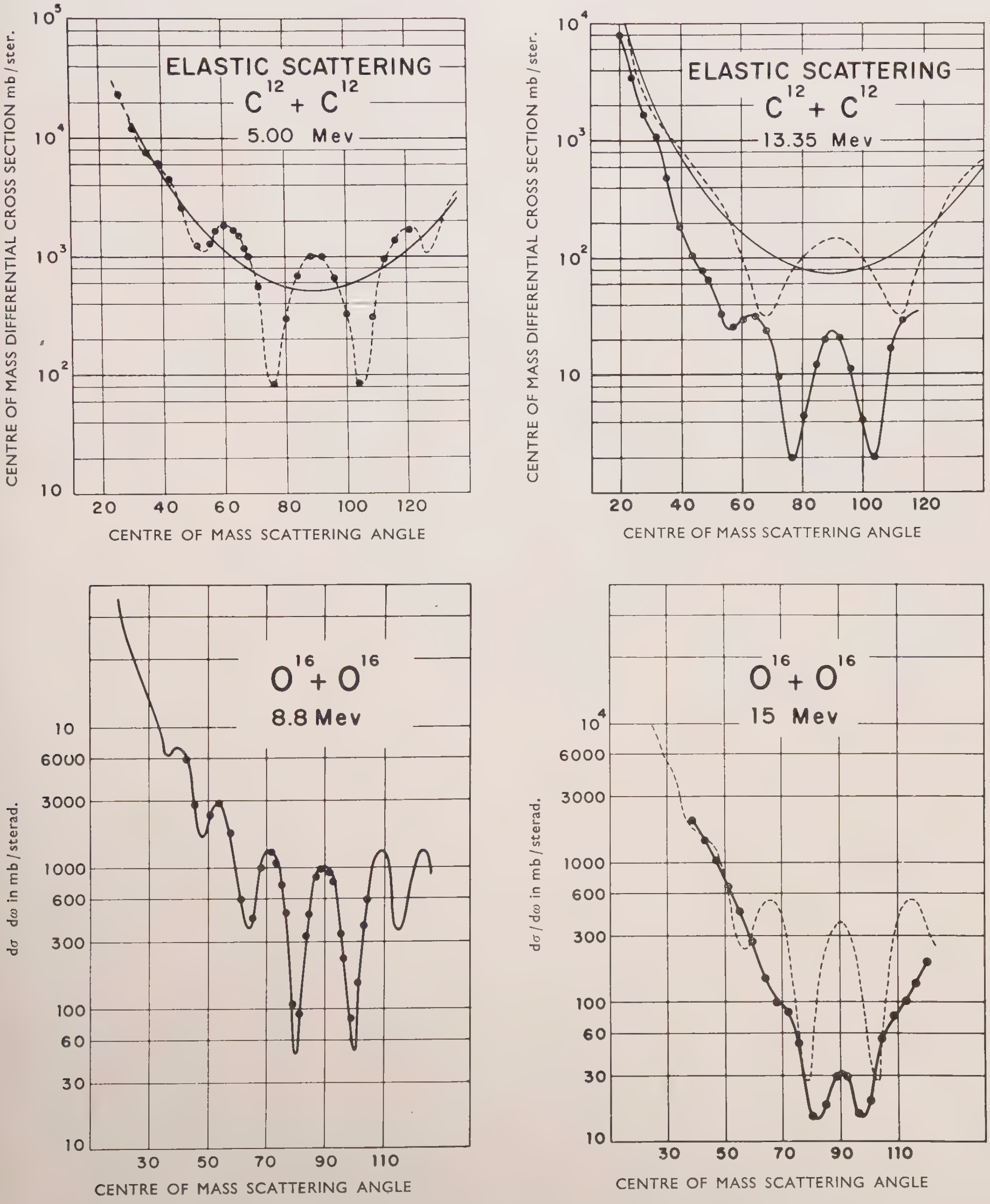

Fig. 13. Elastic scattering angular distributions.

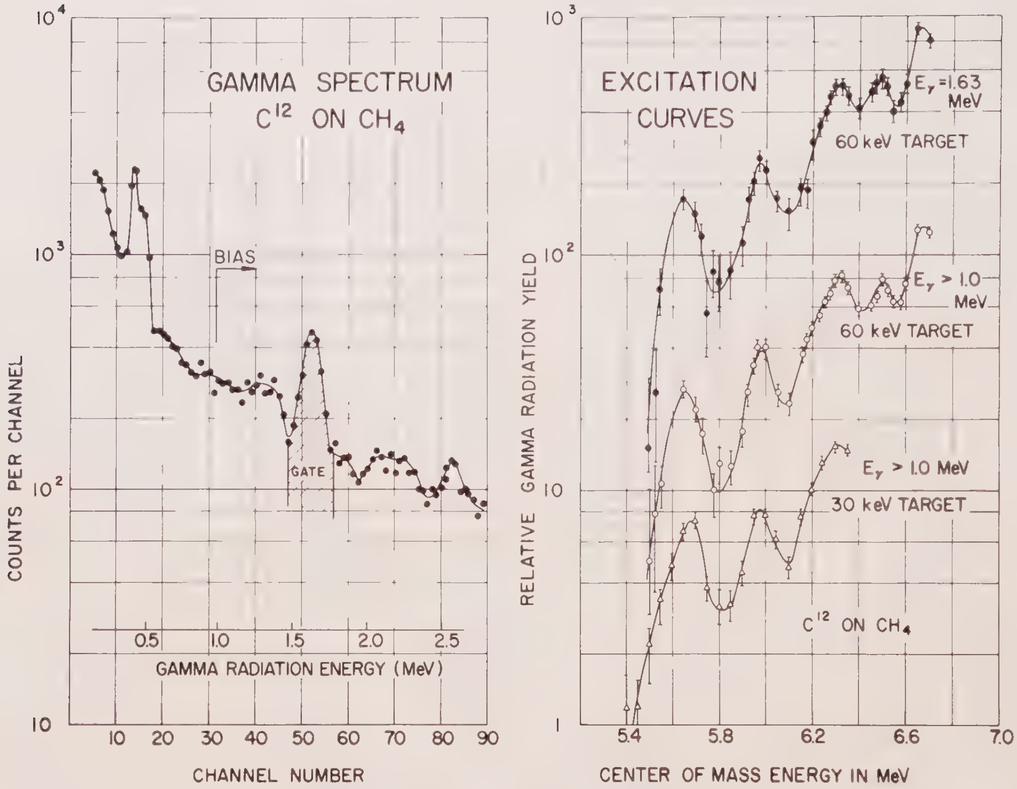

Fig. 14. Reaction yields from C^{12} on carbon below the coulomb barrier. A gas target was used so that the target thickness could be readily varied.

a smooth curve, for the continuum underlying the resonance peaks and subtracting it, one finds that within a factor of 2 all peak cross sections are the same. Normalizing the yield to the cross section data for charge particles and neutrons, and assuming isotropic angular distributions, an estimate of 60 millibarns is obtained for the total reaction cross section at resonance in each case. Application of the single level Breit-Wigner resonance formula for spinless particles then yields the result that the partial width for break-up into carbon ions is $> 5\ \%$ of the Wigner limit for orbital angular momenta $\leqq 8$. This is a surprisingly large value and its significance will be assessed later. The corresponding excitation curves for O^{16} on O^{16} show no resonance structure. Measurements for C^{12} ions on N^{14}, O^{16}, F^{19} and Ne^{20}, and for O^{16} ions on Ne^{20} show only a smooth increase with energy attributable to penetrability effects for energies below the barrier. In the single case of $C^{12} + O^{16}$ residual resonance structure is observed at energies several MeV above the barrier corresponding to the structure observed in the elastic scattering of these ions. In the case of the gamma radiation yield associated with $N^{14} + N^{14}$ shown in fig. 15, only a single resonance peak is observed some 2.0 MeV below the barrier. The difference between the carbon and nitrogen systems may in part reflect the operation of the selection rule, allowing only even orbital momenta in the carbon case with a resulting greater level density in the nitrogen case, smearing out any structure near the barrier.

In order to obtain a better understanding of the structure of the compound system which is occurring at these narrow resonances in the case of the reaction yields of C^{12} bombardment of a C^{12} target it is of considerable interest to try to determine the spins of these resonances. Two approaches have been used to elucidate these spins. The obvious one would appear to be an experiment in which the angular distribution of alpha particles leading to the ground state of Ne^{20} was measured as a function of energy over these resonances. Since all of the particles in this case involved in the reaction have spin 0, one would have thought that the angular distribution would uniquely determine the spin. I will show, however, in a moment that this is apparently not the case.

These experiments were carried out using Si

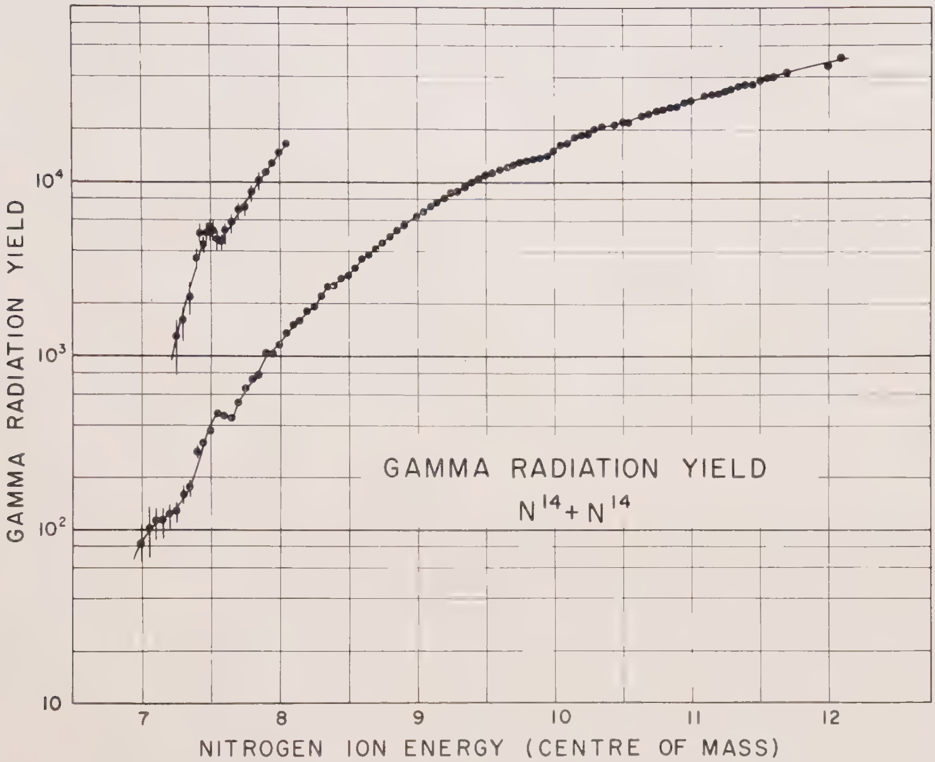

Fig. 15. Reaction yield from N^{14} on nitrogen.

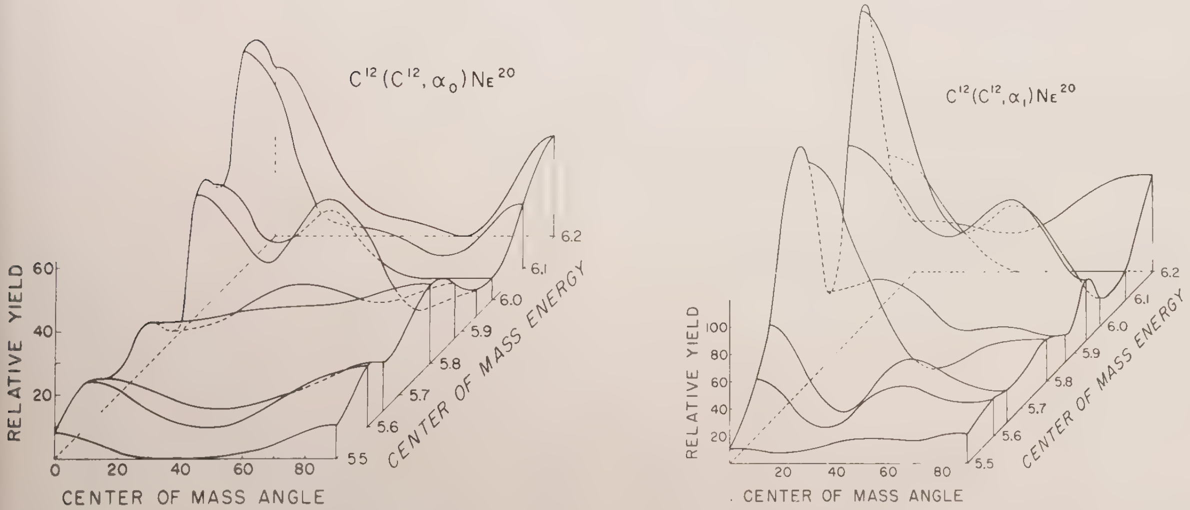

Fig. 16. Angular distributions of alpha particles leading to the ground state (α_0) and first excited state (α_1) of Ne^{20} from C^{12} ($C^{12}\alpha$) Ne^{20}.

p–n junction detectors and angular distributions and excitation functions were measured for the alpha particle groups leading to the ground and first excited state of Ne^{20}.

Fig. 16 shows the angular distributions plotted on a three-dimensional diagram with the relative yield shown on one axis, the center of mass angle on the other and the center of mass energy at which each measurement was made on the third. These measurements indicate that the situation is much more complex than had been anticipated with interference terms between resonant and background amplitudes and between various background amplitudes playing important roles. In fig. 17, the yield of the alpha particles is shown. In the upper curve the measurement is that of alpha particles with energies > 7 MeV for a laboratory angle of 52°. This measurement is typical of many made at different angles of observation, all of which show essentially the same energy dependence. This is in contrast to the situation for the differential excitation functions for a selected alpha particle group. These latter measurements again suggest large interference terms. It should be noted that in accordance with the earlier interpretation of these resonances as being specifically in the entrance channel only when a large number of exit channels are summed do the resonances appear undistorted.

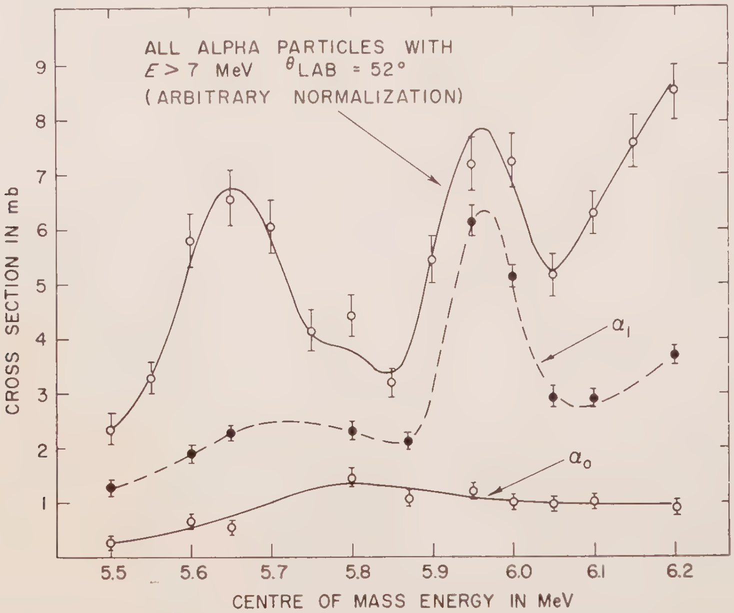

Fig. 17. Differential cross sections for the yield of alpha particles from $C^{12}(C^{12}\alpha)Ne^{20}$.

The lower two curves of this figure give the total cross section and energy dependence for the ground and first excited state reactions. In these curves since interference between states of unlike spin and parity does not contribute to the total cross section, we have a measure of the alpha particle width for the exit channels. One must conclude that the reason why no resonance appears for either reaction at 5.65 MeV and for the ground state reaction at 5.98 MeV is that the partial width for alpha emission for these cases is unobservably small. Because the ground state of Ne^{20} has spin zero it is only the angular distribution of alpha particles leading to it which can be simply interpreted. Since the yield of these alpha particles does not show the resonances this method cannot be employed for spin assignment.

The second possibility for determining the spins of these resonances lies in an examination of the elastic scattering below the Coulomb barrier. As mentioned previously, the excitation function measurements for reaction products have yielded values of 130 kilovolts for the width of the resonance and 60 millibarns for the total reaction cross section at the peak of each of the resonances at 5.65 and 5.98 MeV. From the one level Breit-Wigner expression one can solve for the partial width for emission of C ions for any assumed value of orbital angular momentum. The parameters thus found can be inserted in the expression for the elastic scattering differential cross section for spin zero bosons in the region of an isolated resonance. This theoretical expression can then be compared to the experimental data.

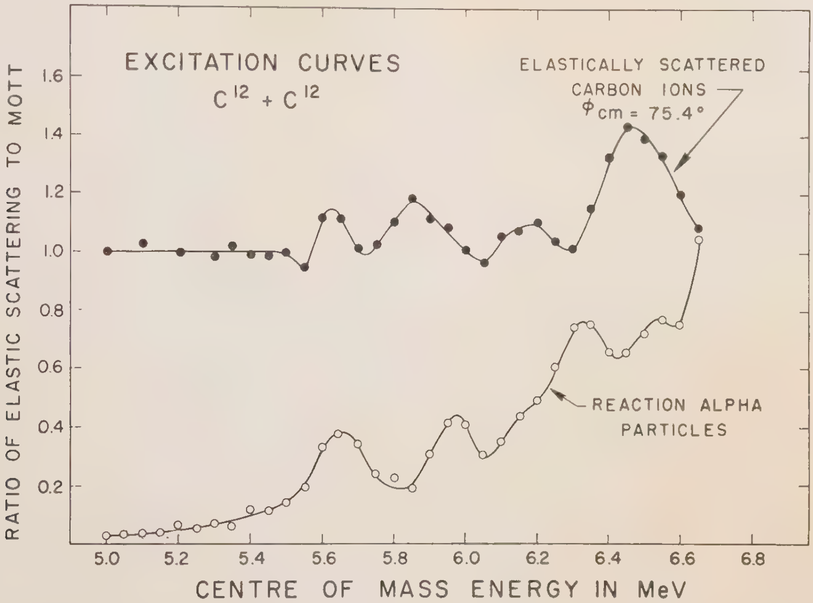

Fig. 18. Elastic scattering and reaction yields from C^{12} on carbon below the Coulomb barrier.

A typical measurement is shown in fig. 18 for center of mass angle of 75.4°. The elastic scattering differential cross section has been divided by the Mott cross section. For comparison and to locate the reaction resonances, the simultaneous yield of reaction alpha particles has also been included. At this angle, fluctuations of about 20% are observed for each of the resonances at 5.65 and 5.98 MeV. Since this angle of 75.4° is one at which the Legendre polynomial of order 6 vanishes one can immediately eliminate $l = 6$ for both these resonances.

Fig. 19 shows curves of the predicted magnitude of fluctuations in the elastic scattering cross section as a function of angle for different assumed angular momenta. Included on these curves are the measured magnitudes for the resonance at 5.98 MeV. The best fit to the measurements is given by the $l = 4$ curve. As well as this agreement in magnitude with the $l = 4$ predictions, good agreement is obtained regarding the detailed shape of the fluctuation for each of the angles measured. In the case of the 5.65 MeV resonance, a qualitatively good fit is given with $l = 8$. In this case, however, the magnitudes are not given as well. Since penetrability arguments would tend to rule out higher angular momenta than considered here, this disagreement may reflect contributions from other resonances. An $l = 8$ assignment to the resonance at 5.65 MeV is untenable on the normal compound nucleus picture because of penetrability considerations.

The observation of marked resonance structure in the elastic scattering of C^{12} by C^{12} above the Coulomb barrier as well as this less marked evidence for structure below the Coulomb barrier, the evidence that the radius of $C^{12} + C^{12}$

is larger than for other heavy ions, the evidence that the resonances observed in reaction yields occur in entrance channels, the large ratio of the width for C^{12} emission to the Wigner limit, and these large values of orbital angular momenta associated with the resonances below the Coulomb barrier led Almqvist *et al.*[12]) to postulate a quasi-molecular interaction mechanism depending critically on the nuclear structure of the ions involved. The question then arises as to why such a quasi-molecule is observed in the C^{12} on C^{12} system and not in the case of O^{16} on O^{16}, or in any other combination of heavy ion interactions with the possible exception of that involving N^{14} bombardment by N^{14}.

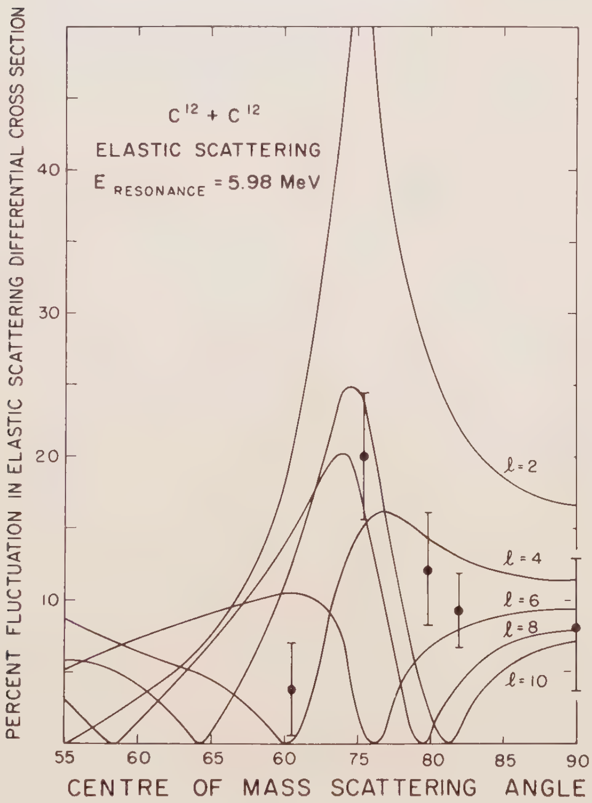

Fig. 19.

Comparison between the theoretical percent fluctuation in the elastic scattering differential cross section (solid lines) for various orbital angular momenta and the experimental values (closed circles) for the resonance at 5.98 MeV.

It was first suggested by Vogt and McManus[14]) that this difference could be explained on the basis of the greater deformability of a carbon ion compared to an oxygen ion. In this picture when the two carbon nuclei come into contact there is a mode of surface vibration in which every part of the system simultaneously stretches or contracts at constant density along the axis joining the two C^{12} nuclei, the surfaces remaining in contact. The motion in this low energy breathing mode can be approximated by assuming that for each value of separation of the mass centers of the C^{12} nuclei the nuclear surfaces will deform adiabatically to a minimum potential energy of the system. This has the effect that as the system dilates the nuclear attraction increases for a given radial separation of the mass centers because the mass motion of the nuclei drags the nuclear potential with it. This is balanced by the energy required to deform the C^{12} nuclei. At large separations of the mass centers the repulsive energy will be predominant. At large separations before contact is made a spherical shape is preferred for the two C^{12} droplets. As the nuclei approach the distance of about 10 fermis at which the deformed potential crosses the Coulomb barrier for the spherical case the deformed shape is energetically preferred. At very much shorter distances the droplets tend to be absorbed into normal states of a Mg^{24} nucleus. The motion is clearly reminiscent of fission. At small distances as the nuclei coalesce, one cannot suppose that the C^{12} really retain their identities. The motion, however, at large distances sets up a highly correlated motion involving a large number of particles in the p-shell. As the nuclei coalesce, this correlated motion creates a re-arrangement energy barrier against absorption into normal Mg^{24} compound states. This, together with the centrifugal barrier, prevents rapid absorption into compound states leading to nucleon emission. The higher the angular momentum the less likely is the absorption to occur and the motion may persist for several vibrational periods. From the observed widths a lifetime of about 5 vibrational periods is required. The rigidity of O^{16} on the other hand, not only narrows the molecular potential and increases the absorption width of the molecular states but it also strongly decreases the formation probability for such states which require shape fluctuations enabling the nuclei to touch and deform when this is energetically advantageous. This is reflected in the lack of structure in the O^{16} + O^{16} data. An explanation based on an optical model potential has been given by Davis15). Experimental work on this very interesting aspect of nuclear structure is continuing at Chalk River by Almqvist and Kuehner.

---

[14]) E. W. Vogt and H. McManus, Proceedings of the Second Conference on Reactions Between Complex Nuclei, Gatlinburg, Tennessee, May 1960, Eds. A. Zucker, E. C. Halbert and F. T. Howard (John Wiley & Sons, 1960); and also Phys. Rev. Letters **4** (1960) 518.

I will turn now to a second project involving the Chalk River tandem accelerator. About one year ago a program was begun with this accelerator to measure the total angular momentum of levels in nuclei in the 1d-2s shell, that is, elements in the periodic table lying between O^{16} and Ca^{40}. Because of certain simplifying features of nuclei with an even number of protons and neutrons, the initial effort has been concentrated on these. A great deal of the research effort of the Chalk River accelerator group during the past few years has involved study of the elements in this region of the periodic table. In particular, the nuclei Al^{25} and Mg^{25} 16) have been extensively investigated, and this resulted in the application of the collective model of Bohr and Mottelson17) for the first time to this region, an application which has proven quite useful for a number of other nuclei in the vicinity of mass 25. It therefore seemed natural to try to devise a technique which would permit a systematic identification of the properties of as many levels in nuclei between O^{16} and Ca^{40} as possible. The essence of such a technique was first suggested by A. E. Litherland and it has now been applied with various refinements to a number of levels in even-even nuclei in the 1d-2s shell by Batchelor *et al.*18), Litherland *et al.*19) and Broude and Gove[20] as I shall show later. I propose to describe now the general features of the method, to show how the experiments are performed and to present experimental data on a level in Si^{28} and two levels in Ne^{20}, and then at the end, to review the status of the work to the present time.

The energy of charged particles, particularly protons from the tandem accelerator permit the excitation of levels up to energies approaching 10 MeV in light nuclei. These excited states in turn decay to the ground state by emission of gamma-rays, either a direct transition to the

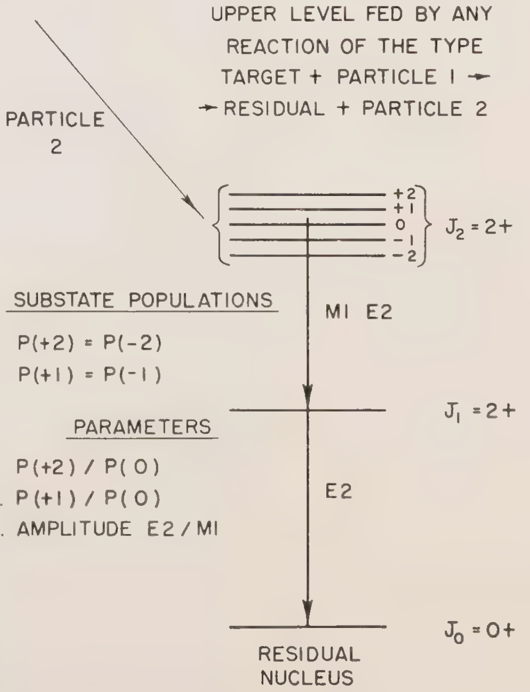

Fig. 20. Schematic diagram for the gamma-gamma coincidence correlation method for measuring spins.

---

15) R. H. Davis, Proceedings of the Second Conference on Reactions Between Complex Nuclei, Gatlinburg, Tennessee, May 1960, Eds. A. Zucker, E. C. Halbert and F. T. Howard (John Wiley & Sons, 1960); and also Phys. Rev. Letters **4** (1960) 521.

16) A. E. Litherland, E. B. Paul, G. A. Bartholomew and H. E. Gove, Phys. Rev. **102** (1956) 208;
A. E. Litherland, H. McManus, E. B. Paul, D. A. Bromley and H. E. Gove, Can. J. Phys. **36** (1958) 378.

17) A. Bohr and B. R. Mottelson, Mat. Fys. Medd. Dan. Vid. Selsk. **27**, No. 16 (1953).

18) R. Batchelor, A. J. Ferguson, H. E. Gove and A. E. Litherland, Nucl. Phys. **16** (1960) 38.

19) A. E. Litherland, R. Batchelor, A. J. Ferguson and H. E. Gove, (to be published).

20) C. Broude and H. E. Gove, Proceedings of the International Conference on Nuclear Structure, Kingston, Canada, 1960, Eds. D. A. Bromley and E. V. Vogt (University of Toronto Press and North-Holland Publishing Company, 1960) p. 471.

ground state or by a cascade of two or more gamma rays through intermediate levels. Such a cascade de-excitation is illustrated schematically in fig. 20. A particular example has been chosen here of an even-even residual nucleus with a spin zero ground state and a spin 2 first excited state, both with even parity. Consider now an excited state above this, which also has spin 2 and even parity and which is fed by some nuclear reaction of the general type shown. If only gamma-ray angular distributions are measured with respect to the incident particle beam then details of the nuclear reaction which feed the state J_2 can be ignored. One can instead consider the nucleus in state J_2 as an aligned nucleus with symmetric magnetic substate populations, that is, the population of the $m = +2$ substate is equal to that of the $m = -2$ and similarly for $m = \pm 1$. The relative substate populations can be treated as parameters which are to be determined in the experiment. The only other possible parameter then will be the amplitude ratio of the multipole radiation between J_2 and J_1. The final transition between J_1 and J_0 terminates with a spin zero state and so no multipole mixing occurs. In the example shown here then, only three parameters are required when $J_2 = 2+$. If J_2 were 0 there are no parameters, while values for J_2 greater than 2 increases the number of parameters. Hence, if one measures a coincidence angular correlation between the two gamma transitions with respect to the incident beam direction in a sufficient number of different geometries one would expect to determine a rather large number of parameters, and in fact, to overdetermine the number which can ever occur. In addition, there is a possibility of measuring the direct correlation between the first gamma ray and the incident beam. If there is a cross-over transition between J_2 and J_0 its angular distribution with respect to the incident beam can also be measured[21]).

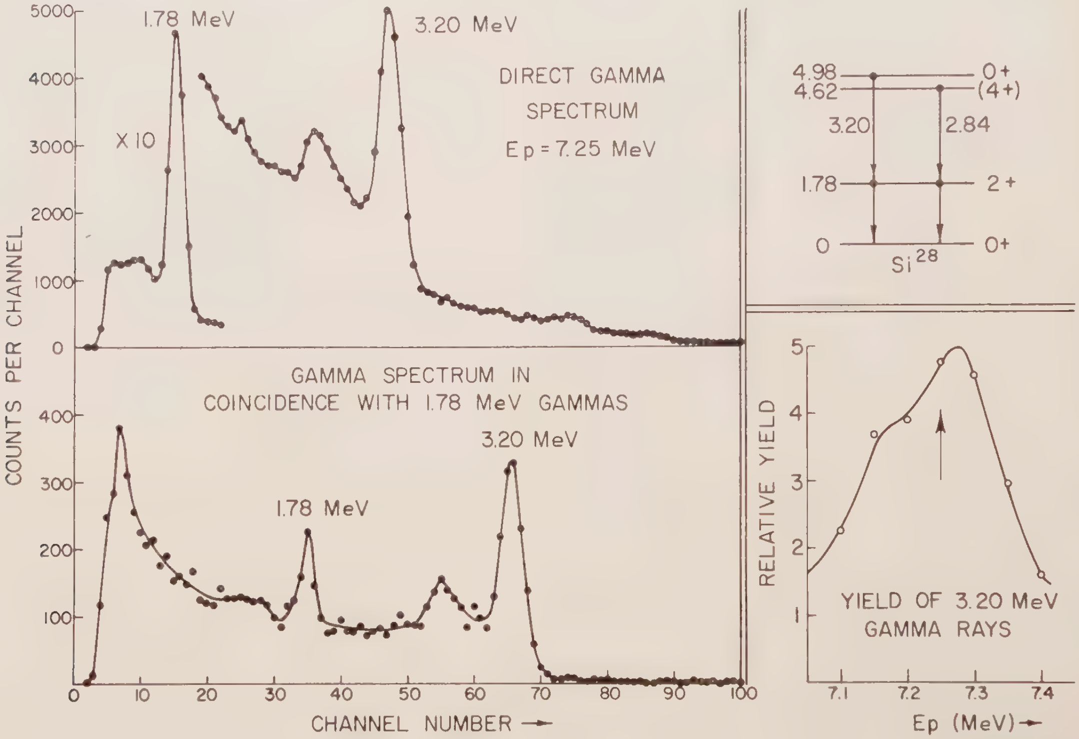

Fig. 21. Details of direct and coincidence gamma spectra and yield for the study of the 4.98 MeV level in Si^{28}.

---

[21]) A general discussion of the theory of such direct and

As I mentioned above, it is essential that the coincidence correlation between the two gamma rays be measured in a number of different geometries. In order to do this, it must be possible to move one of the gamma-ray detectors out of the plane defined by the incident beam and the axis of the second gamma detector. I have already shown earlier in this paper, a photograph of the apparatus for performing such an experiment. It was the azimuthal gamma-ray table which you will recall had two counters, one mounted on an arm which could be rotated in the horizontal plane about the intersection between the beam and the target and the other which was mounted on a carriage allowing it to be moved anywhere over the surface of a vertical hemisphere with its center at the beam spot center on the target. (See fig. 11.)

In the experiments carried out to date, the target element is evaporated on a backing, usually Au, of sufficient thickness to completely stop the beam. The size of the beam spot on the target is about $\frac{1}{8}''$ in diameter, the NaI crystal moving in the hemisphere is 5″ in diameter and 6″ long, while the other crystal is 5″ in diameter by 4″ long. Let me illustrate the use of this equipment by discussing the measurement on the level in Si^{28} at 4.98 MeV carried out by Broude and Gove^{20}). Except for the ground state and first excited states none of the levels below 10 MeV in Si^{28} have spin assignments. In fact, until just recently, the positions of the energy levels were not even known very accurately. Some details of the experiment are shown in fig. 21. In the upper right hand corner is a level diagram showing the first three excited states of Si^{28}. At the time we began the experiment, the level at 4.98 MeV was not known and it was our

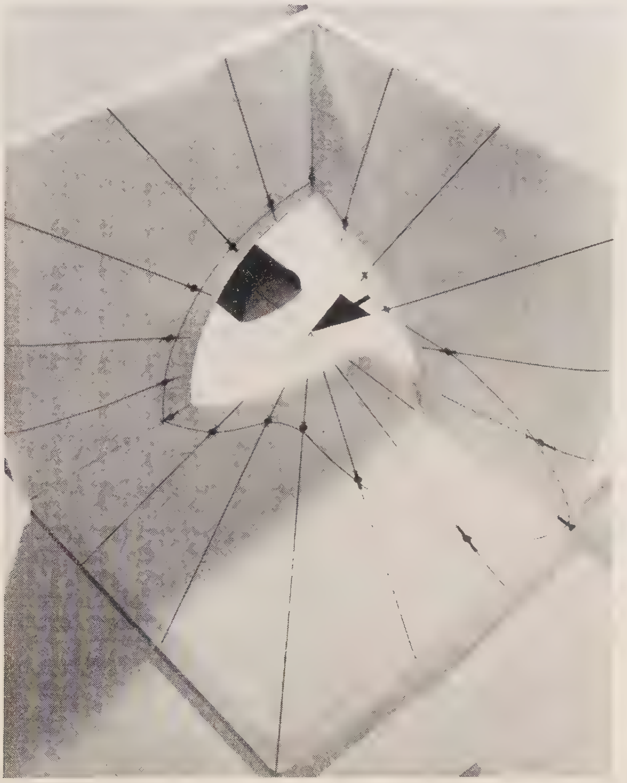

Fig. 22. Model of the gamma-gamma coincidence correlation measurement. The solid points are the experimental values for a 0–2–0 spin sequence measured for the 4.98 MeV level in Si^{28}.

coincidence angular correlation measurements will be published by A. E. Litherland and A. J. Ferguson.

intention to measure the spin of the level at 4.62 MeV. A series of direct gamma-ray spectra were measured at intervals of about 50 kilovolts in proton energy. At 7.25 MeV the direct spectrum was measured as shown in the upper left hand corner of the figure. Two prominent peaks appear, corresponding to gamma ray energies of 1.78 and 3.20 MeV. The yield of the 3.2 MeV gamma ray in the vicinity of 7.25 MeV proton energy is shown on the lower right.

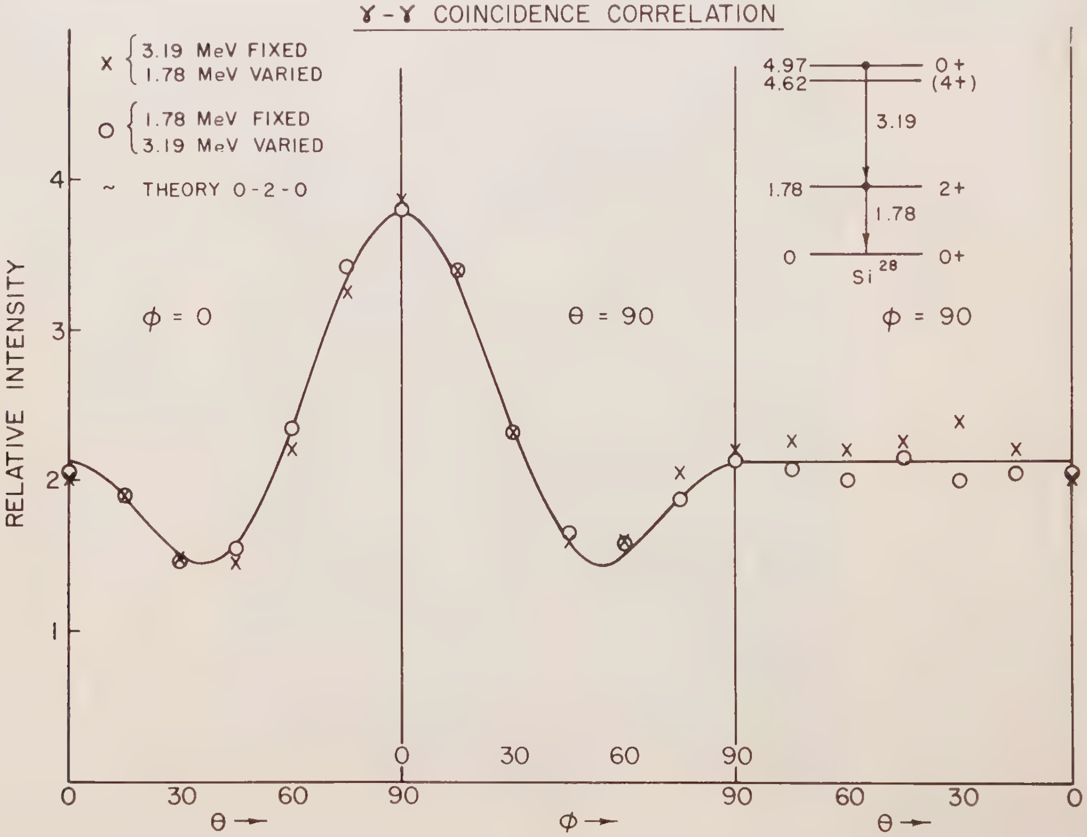

Fig. 23. Conventional way of plotting the data of fig. 22.

When a voltage window was set on one crystal to include only the peak of 1.78 MeV, the gamma spectrum measured in the second crystal in coincidence with this 1.78 MeV peak was measured as shown on the lower left. This proves that the 3.2 MeV gamma rays and some of the 1.78 MeV arise from the decay of a level at 4.98 MeV in Si^{28}. The existence of this level has since been confirmed by Hinds and Middleton[22] at Aldermaston. In the coincidence correlation experiment the voltage window is set on the 1.78 MeV peak in both detectors and the corresponding coincidence spectrum from both is recorded simultaneously. Fig. 22 is a photograph of a three-dimensional model of the coincidence correlation between the 3.2 and 1.78 MeV gamma rays. The arrow indicates the incident beam impinging on the target. One of the counters shown as a half cylinder, is fixed in the horizontal plane at 90° to the beam direction. The second counter is then moved over the edges of an octant. The solid circles with error flags are the experimentally measured values for the coincidence counts and the solid curve through the points is the theoretical prediction if the 4.97 MeV level has spin zero. This is a rather interesting case since spin zero for the first state means that there is no alignment of the nucleus and the coincidence correlation should depend only on the angle between the two gamma detectors. When the second counter is moved in the vertical plane containing the beam the angle between the two counters is fixed at 90° and the coincidence correlation does not vary in intensity with angle. In the other two planes the correlations are identical since the angle between the two counters is varying in the same way in both cases. Furthermore, in this case of a $0 \rightarrow 2 \rightarrow 0$ correlation, both radiations are pure E2 and it then does not matter which gamma-ray is measured in the moving detector, the coincidence correlation is the same in both cases. A more conventional way of plotting these data is shown in fig. 23, and in this case both correlations are displayed and it can be seen that they are virtually identical. In addition to these correlations, the direct distribution of the 3.2 MeV gamma ray with respect to the beam was measured and it was spherically symmetric, further proof that the initial state at 4.97 MeV has spin zero. Finally, no evidence for a direct transition between the 4.97 MeV level and the ground state was observed and this is again consistent with spin zero. In a similar fashion the level at 4.62 MeV was measured and a fit to the experimental data establishes its spin to be 4 20).

---

[22] S. Hinds and R. Middleton, (private communication).

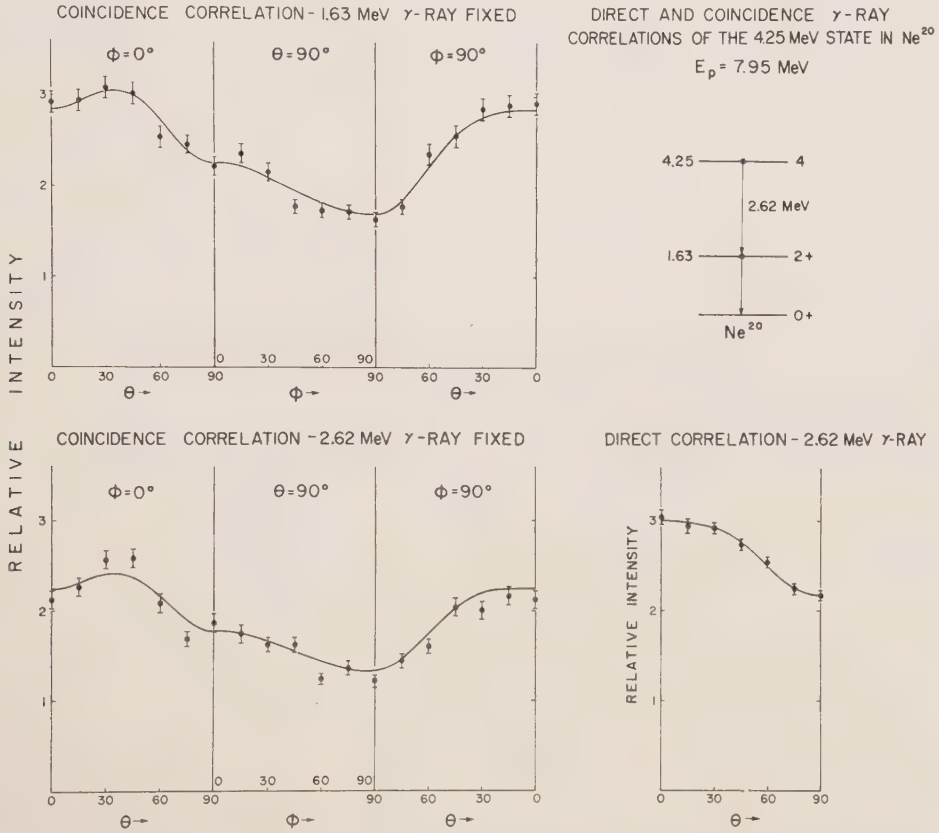

Fig. 24. Direct and coincident correlation measurements of the 4.25 MeV level in Ne^{20}.

Another example of the measurements made by Broude and Gove 20) is shown in the next figures and consist of studies of levels in Ne^{20}. There are three levels in this nucleus above the first excited state at 1.63 MeV whose positions have been very accurately measured but whose spin assignments are unknown. Fig. 24 shows the angular correlation measurements on gamma rays from the decay of the 4.25 MeV level in Ne^{20}. This level decays through the 1.63 MeV state of $J = 2+$ and the coincidence correlations measured in the two geometries are shown on the curves on the left hand side of the diagram. In addition, the direct correlation of the 2.62 MeV gamma ray has been measured and this is shown on the lower right. The solid curves through the experimental points in all three cases are least square fits to the results assuming a spin 4 for the 4.25 level. Any other spin assignment which one would be inclined to make to this level will not fit the experimental data.

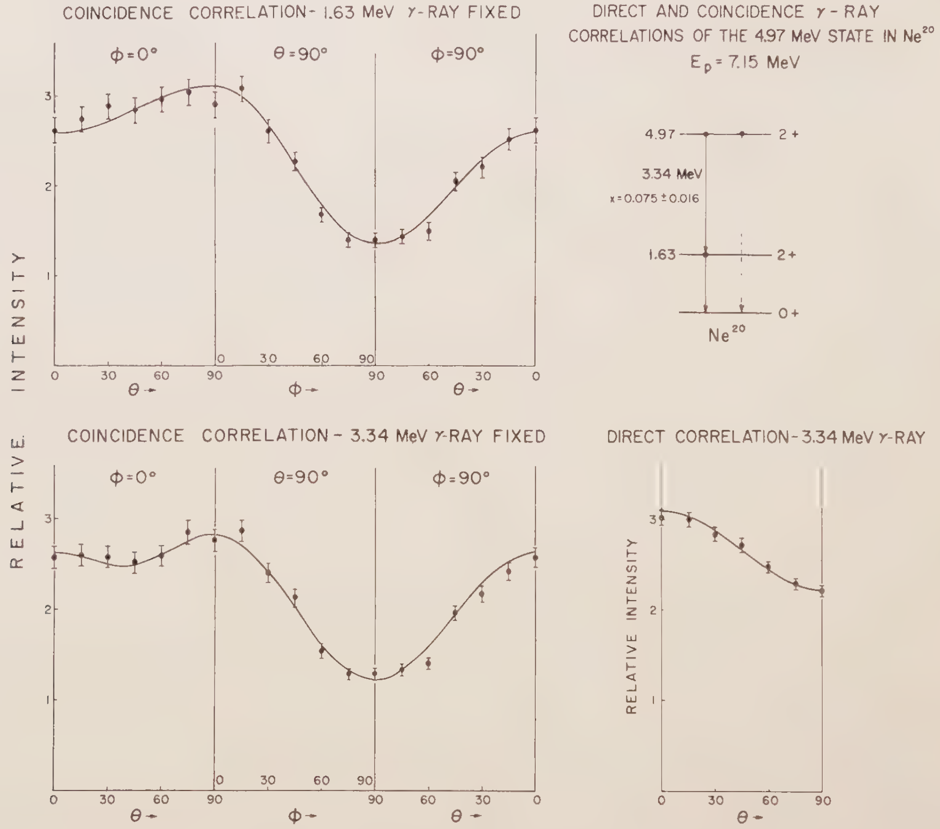

Fig. 25. Direct and coincident correlation measurements of the 4.97 MeV level in Ne^{20}.

Fig. 25 shows the experimental results for the decay of the 4.97 MeV level in Ne^{20}. Again on the left hand side of the diagram the coincidence correlations are displayed and on the lower right, the direct correlation of the primary gamma ray between the 4.97 and the 1.63 MeV levels. The solid curves through the experimental points are again least square fits to the experimental data assuming a spin of 2 + for the 4.97 MeV level. In this case the parameter which measures the E2 to M1 amplitude ratio in the first radiation is given as the quantity $x = +0.075 \pm 0.016$.

Fig. 26 shows the complete level diagram for Ne^{20} with the spin assignments we have made for the two levels at 4.25 and 4.97 included. The level at 5.63 MeV was searched for but no evidence in the gamma-ray spectrum was found for it and one must, therefore, assume that it breaks up into alpha particles to the ground state of O^{16} and therefore has a spin and parity combination of the type even plus or odd minus. That is, it has what is called "natural" parity. The other levels from 6.7 MeV up to 9 MeV have had their spin assignments made by elastic alpha scattering and the references to this work have been summarized by Ajzenberg-Selove and Lauritsen[23]). It should be noted that although this nucleus appears now to be very well measured, only states of natural parity have been

[23]) F. Ajzenberg-Selove and T. Lauritsen, Nuclear Physics **11** (1959) 1.

observed. These are the only states that would be seen in elastic alpha scattering on the even-even nucleus O^{16} and so one might well expect to find additional levels here which have unnatural parity and these have not yet been studied. We have so far been unable to devise any method for measuring the spin of the level at 5.63 MeV.

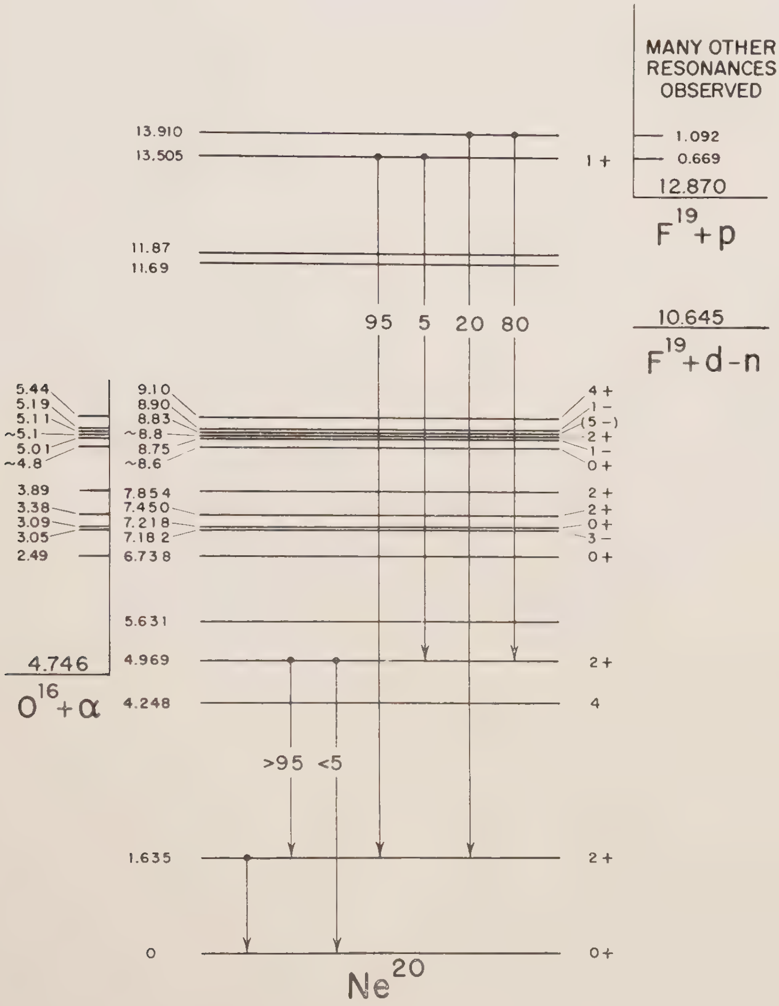
MANY OTHER RESONANCES OBSERVED
1.092
0.669
12.870
F19 + p
10.645
F19 + d - n
13.910
13.505
1 +
11.87
11.69
95
5
20
80
5.44
5.19
5.11
~5.1
5.01
~4.8
3.89
3.38
3.09
3.05
2.49
4.746
O16 + α
9.10
8.90
8.83
~8.8
8.75
~8.6
7.854
7.450
7.218
7.182
6.738
5.631
4.969
4.248
1.635
0
4 +
1 -
(5 -)
2 +
1 -
0 +
2 +
2 +
0 +
3 -
0 +
2 +
4
>95
<5
2 +
0 +
Ne20

Fig. 26. Level scheme for Ne^{20}.

Another nucleus in this region which is of great interest to study is the nucleus Mg^{24}. The latest results on this are shown in fig. 27. The level at 4.23 MeV has been measured by Batchelor *et al.*[18]) at Chalk River and Broude and Gove[20]) have measured the levels at 5.22, 6.0 and the possible level at 6.4 MeV. The level positions in this nucleus have been determined with considerable precision by Hinds and Middleton[24]). The gamma-ray branching ratio of the 4.23 MeV state is about three to one in favour of the ground state transition and both radiations are virtually pure E2. The E2 to M1 amplitude ratio in the transition to the first excited state is 23 ± 9. The level at 5.22 MeV decays virtually completely to the first excited state and is a pure E2

[24]) S. Hinds and R. Middleton, Proceedings of the International Conference on Nuclear Structure, Kingston, Canada, 1960, Eds. D. A. Bromley and E. W. Vogt (University of Toronto Press and North-Holland Publishing Company, 1960) p. 947; and private communication.

transition. Using the model of Davydov and Fillipov25) of a triaxial ellipsoid, Batchelor *et al.*18) calculate gamma, the parameter which describes the inequality of the two minor axes of the ellipsoid, to be 21.9° from the energy ratio of the first and second 2 + levels. Using this value of gamma and the Davydov-Fillipov expression for the branching ratio of the second 2 + state, a value of 0.88 is obtained compared to the experimental value of 2.8. The Davydov-Fillipov model predicts the M1 transitions are forbidden. One can, however, take a somewhat more general point of view which assumes that there is mixing between two bands, one with $K = 0$ (the ground state rotational band) and one with $K = 2$ (a gamma vibrational band). The branching ratio of the second 2 + state then permits a measure of the parameter "z"26) equal to 0.1, which implies an admixture of the $K = 2$ in the $K = 0$ band of only 0.1 % in intensity. If one then assumes that there is a gyromagnetic ratio g_k associated with the intrinsic motion of the $K = 2$ band, one can calculate the quantity g_k–g_r to be 0.03 from the observed M1/E2 mixture in the 2 + transition. From this, one can predict that the M1/E2 intensity ratio of the 3 + to 2 + transition should be 3×10^{-4} and experimentally it is found to be zero. It therefore seems quite reasonable to assume that the levels at 1.37 and 4.12 are the 2 + and 4 + members of a ground state band with $K = 0$ and the levels at 4.23, 5.22, 6.00 with spins 2 +, 3 + and 4 + are members of a vibrational band with $K = 2$. This figure also shows the predicted positions of levels in the $K = 0$ and $K = 2$ bands using the parameters A and B, determined from the $0 \rightarrow 2 \rightarrow 4$ spacing and the standard equation

$$E = A\,[J\,(J+1)\,] + B\,[J\,(J+1)\,]^2$$

and assuming that the second 2 + level is located as observed. Agreement with the positions of the 3 + and 4 + states are not too bad although it does appear that the spacing which is observed experimentally is substantially smaller than that predicted theoretically. This implies a smaller value of the parameter A and therefore a larger value of the moment of inertia for the $K = 2$ band. The 6 + state associated with the ground state band comes at 9.2 MeV and would be well worth looking for experimentally. Calculations of the energy positions made by Preston27) assuming that the Mottelson $K = 0$ to $K = 2$ mixing as well as mixing with assumed higher two phonon states, yields a value of the parameter $z = 0.2$ compared to 0.1 from the branching ratio but gives the energy positions shown on the left hand side of the figure, which are in even poorer agreement with those observed experimentally. One should not, however, take this energy calculation too seriously since it is very model dependent. Recent calculations by Banerjee *et al.* applicable to nuclei in the 1d-2s shell and in particular to Mg^{24} show very great promise28).

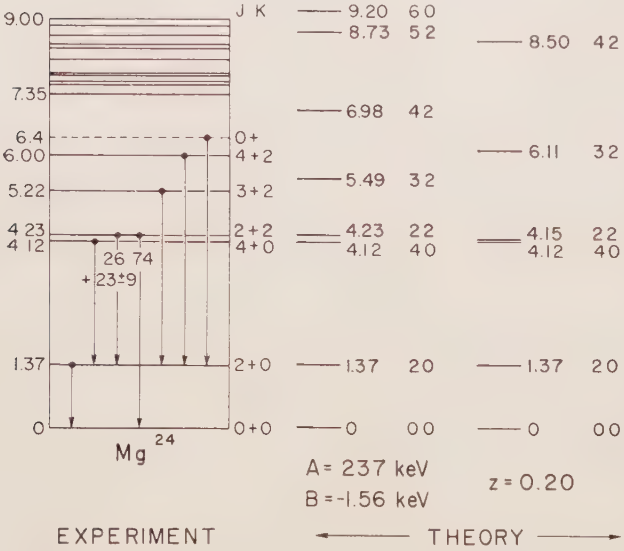

Fig. 27. Level scheme for Mg^{24} and comparison with theory.

---

25) A. S. Davydov and G. F. Fillipov, Nucl. Phys. **8** (1958) 237.

26) B. R. Mottelson, (private communication—see note added in proof in reference 18), see also Hansen, Nielsen and Sheline, Nucl. Phys. **12** (1959) 389.

27) The author is indebted to M. A. Preston for deriving expressions for the M1-E2 branching ratios and the level positions for the $K = 0$ and $K = 2$ band mixing situation.

28) M. K. Banerjee, Proceedings of the International Conference on Nuclear Structure, Kingston, Canada, (1960) Eds. D. A. Bromley and E. W. Vogt (University of Toronto Press and North-Holland Publishing Company, (1960) p. 461. This was a report of the work of Banerjee, Levinson, Meshkov and Pal.

Finally, I would like to summarize the present status of information about spins and parities of levels in the even-even nuclei lying between O^{16} and Ca^{40} and this is shown in fig. 28. The spin assignments enclosed in square brackets are those which have been measured using the gamma-gamma correlation technique I have just described. The levels in O^{18} were studied by bombarding a tritium target with O^{16} ions and observing the gamma rays emitted following proton emission. Again the straightforward gamma-gamma technique was applied and the results have been described by Litherland *et al.*[19]). The level, as I have mentioned, at 4.24 MeV in Mg^{24} has been measured by Batchelor *et al.*[18]). The other levels enclosed in the square boxes have had their spin assignments made by Broude and Gove[20]). In this connection I should mention that in order to obtain these spin assignments it is necessary that the data be analysed on an electronic computer. One program for this analysis was devised by A. J. Ferguson and this has been supplemented by a second program devised by C. Broude. In this program it is attempted to make a fit to the experimental data for spin assignments of 0, 1, 2, 3 and 4 to the particular excited state and to then examine the results to see which corresponds most closely to the experimental data. In all but one case that we have investigated so far, the technique gives a unique spin assignment.

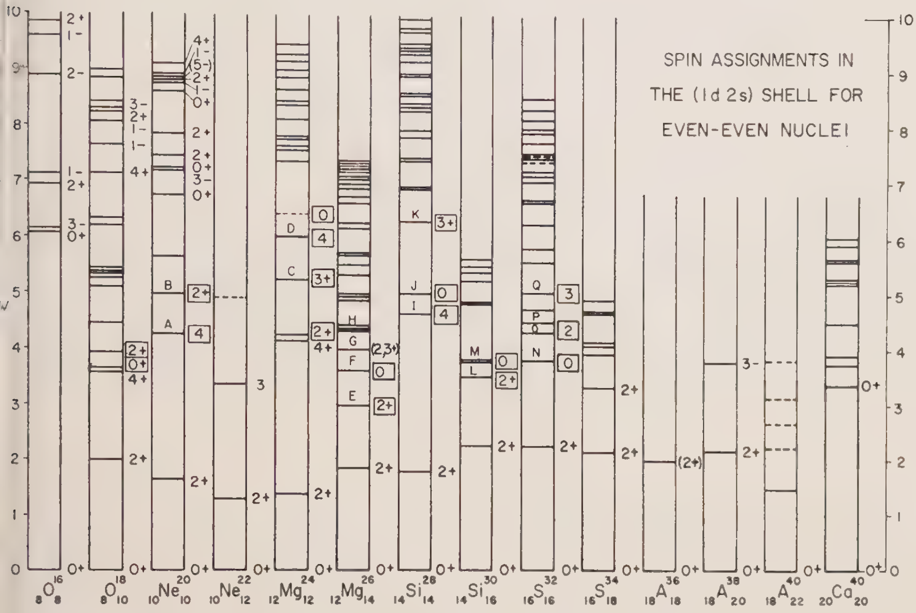

LEVEL	QUADRUPOLE / DIPOLE AMPLITUDE TO 2+ LEVEL	CROSS OVER TO GROUND
A	∞	NO
B	+0.08 ± 0.02	NO
C	∞	NO
D	∞	NO
E	+0.1	YES
F	∞	NO
G	NOT MEASURED	NO
H	TRIPLET	
I	∞	NO
J	∞	NO
K	-0.14 ± 0.07	NO
L	-0.2 ± 0.05	YES
M	∞	NO
N	∞	NO
O	NOT MEASURED	YES
P	NOT ANALYZED	NO
Q	0	NO

Fig. 28. Summary of information on level spins in even-even nuclei between O^{16} and Ca^{40}. The assignment in square boxes are measurements made at Chalk River by the gamma- gamma correlation technique.

Some general comments can be made about the systematics of levels shown on this diagram although, in all fairness, one should remark that more spin assignments are required than shown here to really determine any empirical regularities in the positions of levels of the same spin and parity. Despite this, however, the situation is very much better than it was a year ago when scarcely any of the levels shown here had been measured. In the first place, of all the levels having spin 2 or 3 only those in Mg^{24} show practically pure E2 transitions to the first excited state. In O^{18} for example, the 2+ level is practically a pure M1 transition to the first excited 2+ state so that despite the appearance of a 0–2–4 triplet, suggestive of a weak coupling collective model, the M1 character of this radiation denies the validity of that model because it would predict the radiation to be pure E2. Second, there is a very pronounced difference between the levels in Mg^{24} and those of Mg^{26} and in this connection I should remark that the odd A nuclei following Mg^{24} and Mg^{26}, namely, Al^{25}, Mg^{25}, Al^{27} and Si^{27} all show very well-defined rotational structure which illustrates the ability of a single particle to apparently produce a permanent nuclear deformation. Third, in all the nuclei with the exception of Ne^{20}, Ne^{22} which has not been very carefully studied and Mg^{24}, a relatively low-lying $0+$ state is observed. The situation beyond S^{34}, of course, has scarcely been investigated. Fourth, while Mg^{24} looks like it may be explained on a strong coupling rotational model, as was shown in the previous figure Mg^{26} seems to possess some aspects of a vibrational model.

In conclusion, I will just remark that there are two nuclei here, namely, Ne^{22} and S^{34} both of which are of very low isotopic abundance which, however, can be studied using alpha particles. In such an experiment, for example, to study Ne^{22} one would bombard F^{19}, which has a spin of $\frac{1}{2}$, with alpha particles of spin 0. The protons emitted in this reaction feed levels in Ne^{22}. Protons have a spin $\frac{1}{2}$ and Ne^{22} is again an even-even nucleus and the situation then is exactly the same as far as measuring gamma-gamma correlations are concerned as for the case of inelastic proton scattering from an even-even nucleus. Similarly, in the case of S^{34} one would bombard P^{31}, which has a spin of $\frac{1}{2}$, with alpha particles and the outgoing protons would feed the levels in S^{34}. It is expected to try these reactions shortly using the newly-installed alpha particle source on the Chalk River tandem accelerator.

DISCUSSIONS

Speaker adressed: H. E. Gove (*Chalk River*)

Question by: P. M. Endt (*Utrecht*)

Question: Is anything known at present on the lowest $T = 1$ state in Mg^{24}?

Answer: Not that I know of. In our measurements we did not look at levels much higher than 6.4 MeV in excitation in Mg^{24}.

Speaker adressed: H. E. Gove (*Chalk River*)

Question by: W. M. Jones (*A.W.R.E.*)

Question: What is the effect on the resolution of your Brueckner type spectrograph of transforming it into a spectrometer by use of a quadrupole lens?

Answer: The resolution appeared to be unaffected by this change from the spectrograph to the spectrometer mode, that is, it remained at about 1 part in 10^3 for $\Delta E/E$.

Speaker adressed: H. E. Gove (*Chalk River*)

Question by: H. H. Staub (*Zürich*)

Question: Have the pairs in the $0^+ \to 0^+$ transition of Mg^{24} at about 6 MeV been observed? This would give a unique assignment of 0^+ to this level.

Answer: They have not been observed. The 0–2–0 angular distributions measured as I have described are unique and provide an unambiguous spin assignement. It would, of course, be of interest to measure the competition between pair emission and gamma decay.

NUCLEAR INSTRUMENTS AND METHODS **11** (1961) 93–111; NORTH-HOLLAND PUBLISHING CO

RECENT RESEARCH IN NUCLEAR REACTIONS USING THE ALDERMASTON TANDEM GENERATOR

K. W. ALLEN

Atomic Weapons Research Establishment, Aldermaston, Berks.

The Aldermaston Tandem and 6 MV electrostatic generators are being used for the study of nuclear reactions produced by protons, deuterons, tritons and He^3 ions in the bombarding energy range up to 12 MeV. The angular distributions of the emitted charged particles are measured with large magnetic analysers, which include a multi-channel broad range spectrograph with twenty four gaps. The results show that at the higher bombarding energies, the reactions proceed predominately by a direct mechanism.

Oxygen ions accelerated in the Tandem generator to energies in the range 10 MeV to 40 MeV have been used for Coulomb excitation of energy levels in both rotational and vibrational nuclei and for the measurement of nuclear lifetimes by Doppler shift methods. As a consequence of the large momentum transfer from the incident ions to the target and residual nuclei, Doppler shifts of the emitted γ-rays may be up to an order of magnitude greater than in light particle reactions, and the technique is useful for measuring lifetimes in the range 10^{-14} to 10^{-11} second.

Methods of producing ion beams of higher energy by combinations of electrostatic generators are also discussed briefly.

1. Introduction

One of the principal aims of experimental work in the field of nuclear structure is the provision of data for a wide range of nuclei, which can be compared with calculations using appropriate nuclear models. The measurements required include

(i) precise location of energy levels,

(ii) spin and parity assignment to the levels, determination of nucleon reduced widths, and studies of γ-ray branching ratios,

(iii) determination of nuclear lifetimes.

The purpose of this paper is to give a short account of some of the experimental apparatus in use with the Aldermaston Tandem accelerator, and to illustrate by examples the type of experimental programme that is being carried out. This programme falls naturally into two parts

(i) study of nuclear reactions produced by "conventional" particles such as protons, deuterons, tritons and He^3 ions which lead to locations of energy levels and measurements of reduced widths,

(ii) study of nuclear reactions and Coulomb excitation produced by heavy ions which can lead to determination of transition probabilities and nuclear lifetimes.

The Tandem accelerator produces *steady* beams of energetic ions, and in this respect is superior to the cyclotron and the linear accelerator, whose outputs are pulsed at the R.F. frequency. Since many experiments involve coincidence counting techniques, a pulsed beam is a serious disadvantage.

2. Light Particle Reactions

2.1. DIRECT REACTIONS

The importance of the deuteron stripping reaction as a tool in nuclear spectroscopy is now well established. The early experiments with the Liverpool 37″ cyclotron in which the angular distributions of the emitted protons[1]) and neutrons[2]) were studied for deuteron bombarding energies of about 9 MeV i.e. well above the potential barrier for most of the elements studied, showed that the orbital angular momentum taken into the nucleus by the captured particle, according to simple stripping theory[3]), was in agreement with shell model expectations whenever a firm prediction could be made. In these experiments, and indeed in almost all experiments at reasonably high bombarding energies (and occasionally at lower energies[4]), the simple Butler or Born approximation plane wave stripping theory gives a good fit to the angular distribution of the emitted particles in the region of the stripping peak. This is true even when it is known that the emitted particles are polarized, a result which is clearly incompatible with *plane* waves. Fig. 1 shows some measurements of the angular distribution of the ground state protons in the $C^{12}(d,p)C^{13}$ reaction obtained by Barbara Adams with the Aldermaston Tandem generator. It is known[5]) that the protons are polarized at bombarding energies of 6 to 9 MeV. Note, however, the well defined $l = 1$ stripping peak at all energies, also the fluctuations at large angles, a frequently observed feature of (d,p) angular distributions.

---

[1]) See, for example, J. R. Holt and T. N. Marsham, Proc. Phys. Soc. A **66** (1953); 249; and subsequent papers in this series; also the review article by R. Huby, Progress in Nuclear Physics **3** (1953) 177, for an account of early deuteron stripping experiments.

[2]) R. Middleton, F. A. El Bedewi and C. T. Tai, Proc. Phys. Soc. A **66** (1953) 95.

[3]) S. T. Butler, Proc. Roy. Soc. A 208 (1951) 559; Bhatia, Huang, Huby and Newns, Phil. Mag. **43** (1952) 485.

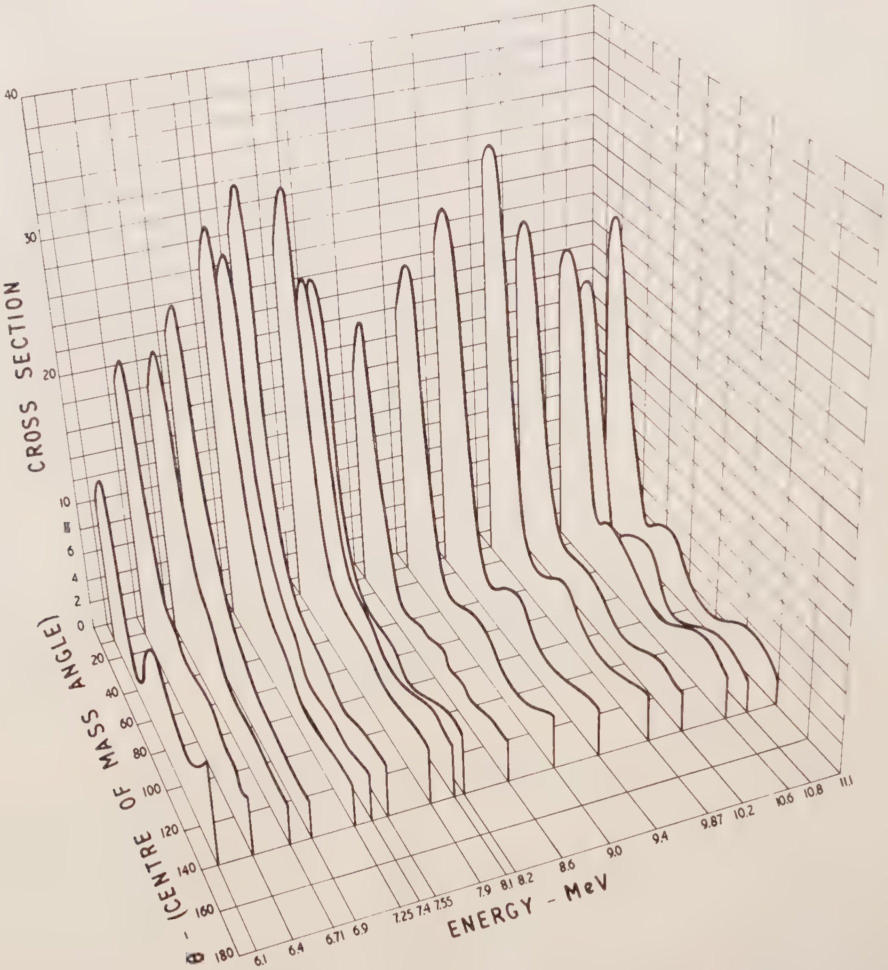

Fig. 1. Angular distribution of the ground state protons emitted in the reaction $^{12}C(d,p)C^{13}$, shown as a function of deuteron bombarding energy.

During the last few years, considerable effort has been devoted to the formulation of a more rigorous stripping theory in which proper account is taken of the distortion of the particle waves by nuclear and Coulomb forces[6]). The availability of the Tandem generator, with its well focussed beam and precisely controlled and readily adjustable energy, makes possible the detailed experimental test of the predictions of these more sophisticated theories.

---

[4]) D. H. Wilkinson, Phil. Mag. **3** (1958) 1185;
J.P.F. Sellschop, Phys. Rev. Letters **3**, (1959) 346.

[5]) P. Hillman, Phys. Rev. **104** (1950) 176;
Bokhari, Cookson, Hird and Weesaknl, Proc. Phys. Soc. A **72** (1958) 88.

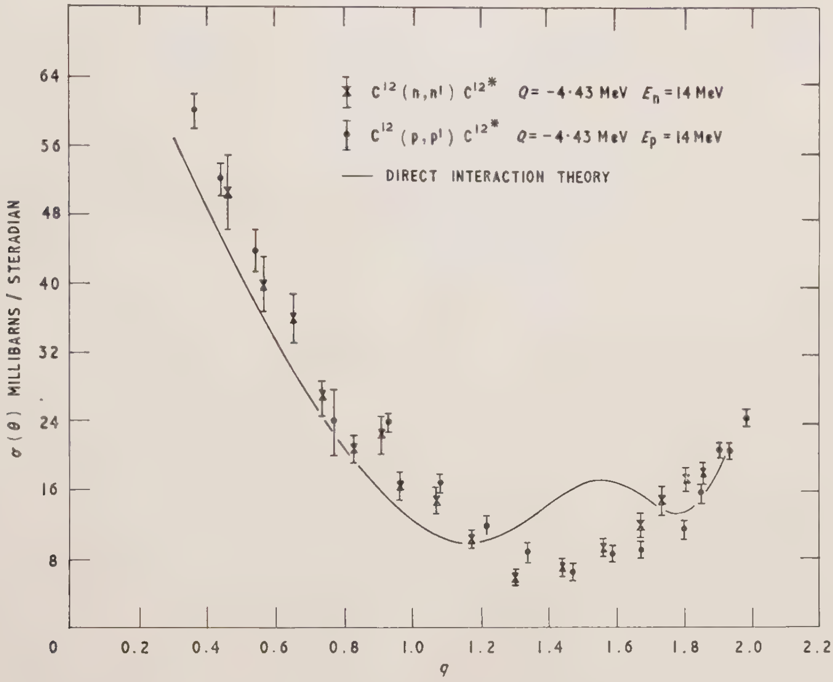

Fig. 2. Angular distribution of protons and neutrons inelastically scattered from the first excited state of C^{12} at 4.43 MeV. The solid line is calculated from a distorted wave direct interaction theory. The abscissa q is the momentum transfer in units of $\hbar$ (1.4×10^{-13} cm).

At Chalk River, Kuehner, Almqvist and Bromley[7]) have examined the reaction $Si^{28}(dp)Si^{29}$ over the energy range 6 to 10 MeV. They have measured angular distributions, excitation functions, and the (d,p,γ) angular correlations associated with first two excited states of Si^{29}. They find evidence for distorted wave effects at the lower energies, but little departure from plane wave theory for bombarding energies above about 7 MeV. These results are encouraging, for they suggest that the values of reduced widths extracted from data on (d,p) reactions at reasonably high energies are likely to be reliable. Nevertheless one should proceed with caution, since it has been shown[8]) that distortions of the initial and final particle waves may cancel out as regards their effects on angular distributions, whereas they may reinforce each other in their effects on reaction cross sections (and hence reduced widths) and on the polarization of the outgoing particles. In this connection it is interesting to note that angular distributions in (pp′) and (nn′) reactions at energies of 10–20 MeV show much larger deviations from the plane wave approximation than do deuteron stripping reactions. For example, fig. 2 shows the angular distributions of 14 MeV neutrons and protons[9]) inelastically scattered from C^{12}. The angular distributions are similar in shape, as expected from charge symmetry considerations (the proton energy is well above the potential barrier), but both differ markedly from the simple plane wave direct interaction prediction,

[6]) J. Horowitz, and A. M. L. Messiah, Journ. Phys. et Rad. **14** (1953) 695;
W. Tobocman and M. H. Kalos, Phys. Rev. **97** (1955) 132;
R. Huby, I. Rafai and G. R. Satchler, Nuclear Physics **9** (1958) 94;
W. Tobocman, Phys. Rev. **115** (1959) 98;
G. R. Satchler and W. Tobocman, Phys. Rev. **188** (1960) 1566.

[7]) J. A. Kuehner, E. Almqvist and D. A. Bromley, Phys. Rev. Letts. **4** (1960) 132.

[8]) G. R. Satchler, Nuclear Physics **18** (1960) 110.

[9]) Anderson, Gardner, McClure, Nakada and Wong, Phys. Rev. **111** (1958) 572.

which would go to zero as $q \rightarrow 0$ in this case. However they can be fitted by a distorted wave calculation[10]), also shown in fig. 2. The large distortion effects arise presumably because the neutron or proton passes through the nucleus and is therefore considerably influenced by the nuclear potential, whereas deuteron reactions occur out at the edge of the nucleus before the distortion can become fully effective.

The well established direct nature of deuteron induced reactions leads us to enquire whether triton and He^3 reactions might show similar features. The advantages (high Q values, multiplicity of reactions emitting charged particles, ease of reaching otherwise inaccessible nuclei etc.) associated with these reactions are well known, and the possibility of using angular distributions to obtain nuclear spectroscopic information is a subject which has interested us a great deal at Aldermaston during the past three years. However before passing to a discussion of some of the more recent data, a short account will be given of the apparatus and techniques being used in this programme.

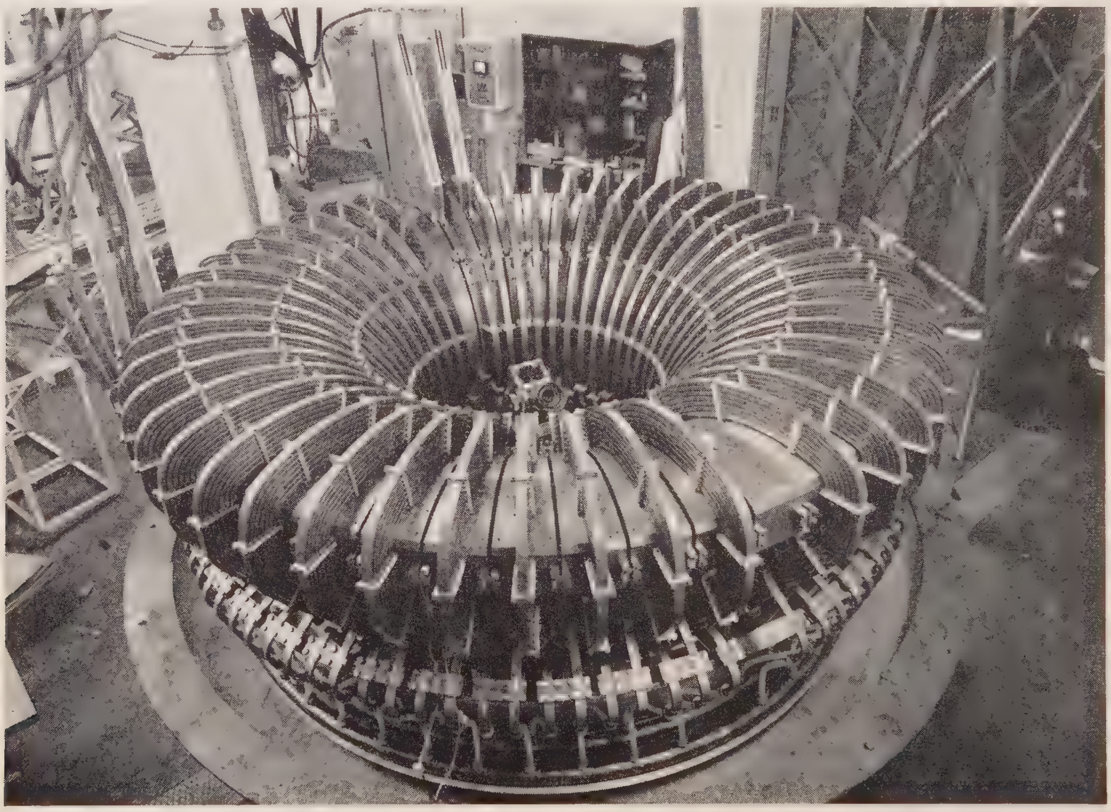

Fig. 3. The magnetic circuit of the 24 gap multi-channel spectrograph, shown during assembly.

2.2. MAGNETIC SPECTROGRAPHS AND PARTICLE ANALYSERS

To take full advantage of the inherent precision of electrostatic generators, it is necessary to provide magnets of high resolution for analysing the products of nuclear reactions. For although not all experiments call for the ultimate in resolution, it is always desirable to have precise knowledge of nuclear level schemes—to know, for example, that an apparently single level is, in fact, a close doublet, may considerably affect the interpretation of γ-ray spectra measured with relatively low resolution NaI spectrometers.

---

[10]) C. A. Levison and M. K. Banerjee, Ann. Phys. 2 (1957) 471.

With these and other considerations in mind, Middleton and Hinds[11]) have designed a multichannel broad range magnetic spectrograph for use with the Tandem accelerator. This type of instrument, first proposed by Buechner and Enge of M.I.T., has evolved from the single channel broad range spectrographs which have been in use for some years at M.I.T.[12]) and Aldermaston[13]). The energy resolution of the single channel instrument, which is limited in practice by target thickness and beam energy spread, is adequate for most experiments, and its principal limitations are encountered in the measurements of angular distributions. These limitations arise, firstly, from the physical size and design of the magnet, which prevent measurements at large backward angles and, secondly, from the difficulty of producing targets which are sufficiently thin to give good energy resolution yet able to withstand the long bombardments required to provide data at many angles.

In the multi-channel spectrograph, shown during assembly in fig. 3, the magnetic circuit consists of a ring of low carbon steel formed from 48 segments. The diameter of the ring is 200 cm and the mean radius of curvature of particles traversing the gaps is 50 cm. Precision brass spacers are used to separate the segments in the first and third quadrants of the ring to form 24 radial air gaps, each 0.95 cm wide. These gaps cover the angular range from 5° to 175° in two banks. Thus the entire angular range can be covered in a single bombardment. The magnet is energised by 30 coils, each consisting of 7 turns of hollow copper conductor. Current is supplied by a 1200 ampere, 60 kW generator, and is stabilised electronically to better than 1 part in 10^4.

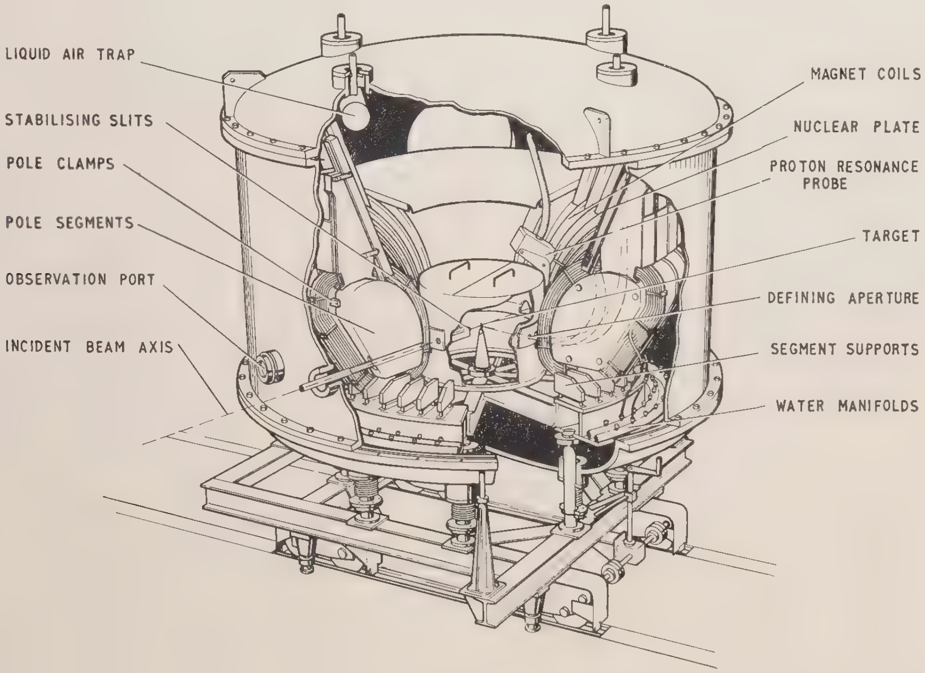

Fig. 4. Diagram of the multi-channel spectrograph.

Charged particles are recorded on long strips of photographic emulsion as in the single channel spectrograph, and the entire assembly of magnet, coils, and plate holders is contained in an aluminium alloy chamber 10 feet in diameter

[11]) S. Hinds and R. Middleton, Proceedings Kingston Conference on Nuclear Structure (1960).

[12]) C. P. Browne and W. W. Buechner, Rev. Sci. Inst. **27** (1956) 899.

[13]) S. Hinds and R. Middleton, Proc. Phys. Soc. A **74** (1959) 196.

and 8 feet high which is evacuated by a 24″ oil diffusion pump to better than 10^{-4} mm. A diagram of the complete instrument is shown fig. 4.

The ion beam enters the magnet through a $1\frac{1}{2}$″ diameter hole in the iron yoke and is defined by a slit system placed just ahead of the central target. The slits also provide the error signal for stabilising the voltage of the Tandem generator.

After calibration and location of the focal planes in the usual way with α-particles from a source of thorium active deposit, the first reaction to be studied with the new spectrograph was $Mg^{24}(dp)Mg^{25}$ at a bombarding energy of 10.10 MeV. At the time of presenting this paper, twenty angular distributions had been measured. Some examples of $l = 2$ angular distributions are shown in fig. 5. Note that the measurements extend over almost the entire angular range from 0° to 180°. Distorted wave analyses of some of these data are being undertaken by Dr. P. E. Hodgson's group at the Clarendon Laboratory as part of a joint Oxford-Aldermaston programme. Further measurements on the elastic scattering of deuterons by Mg^{24} and of protons by Mg^{25} are planned in order to assist in the choice of distorting potentials to be used in the calculations.

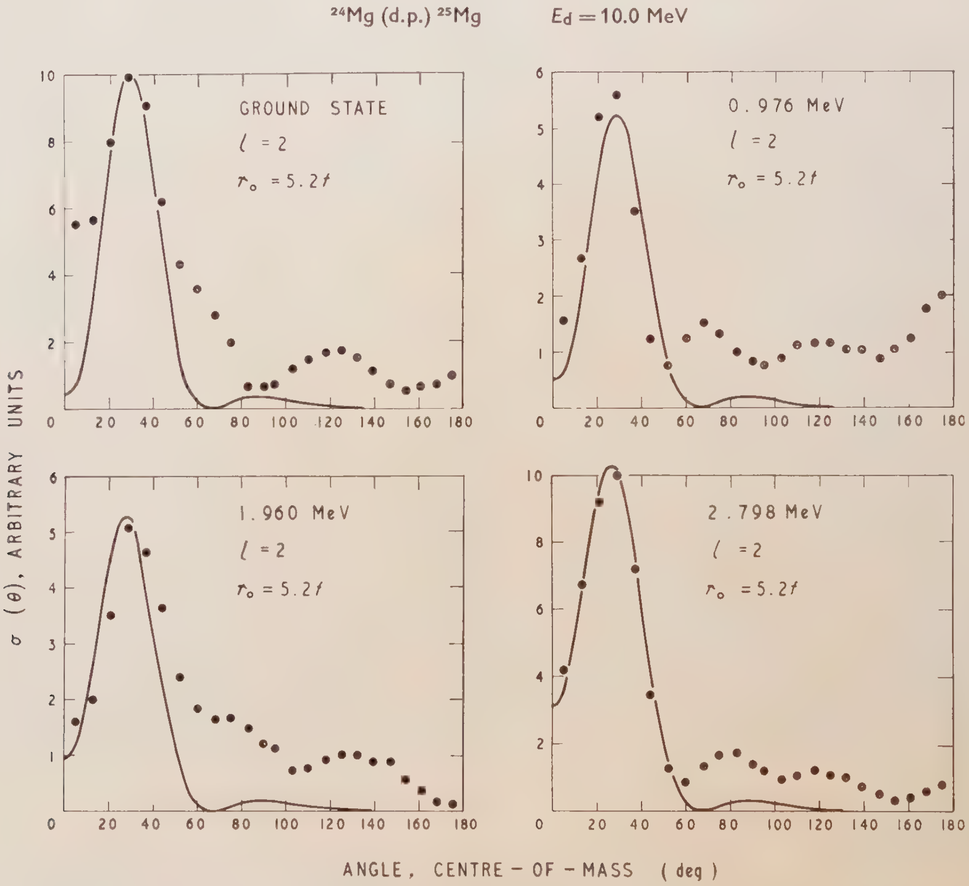

Fig. 5. Some angular distributions from the reaction $Mg^{24}(d,p)Mg^{25}$ obtained with the multi-channel spectrograph.

To follow up the data on energy levels obtained with the multi-channel spectrograph, experiments using coincidence counting techniques are required, particularly for the study of γ-ray branching ratios. A typical experiment involves the measurement of the γ-ray spectrum in coincidence with a particular proton group from, for example, a (pp′) reaction. For experiments of this type, A. V. Cohen and J. A. Cookson are using a large 180° deflection double focussing magnet[14]) shown in fig. 6. The magnet weighs 13 tons, the mean radius of curvature is 60 cm and protons with energies up to 20 MeV may be analysed. The solid angle is about 0.007 steradian and the energy resolution for 10 MeV protons is 0.12%. The magnet is currently being used in a study of γ-ray branching ratios in Mg^{24} and Si^{28}.

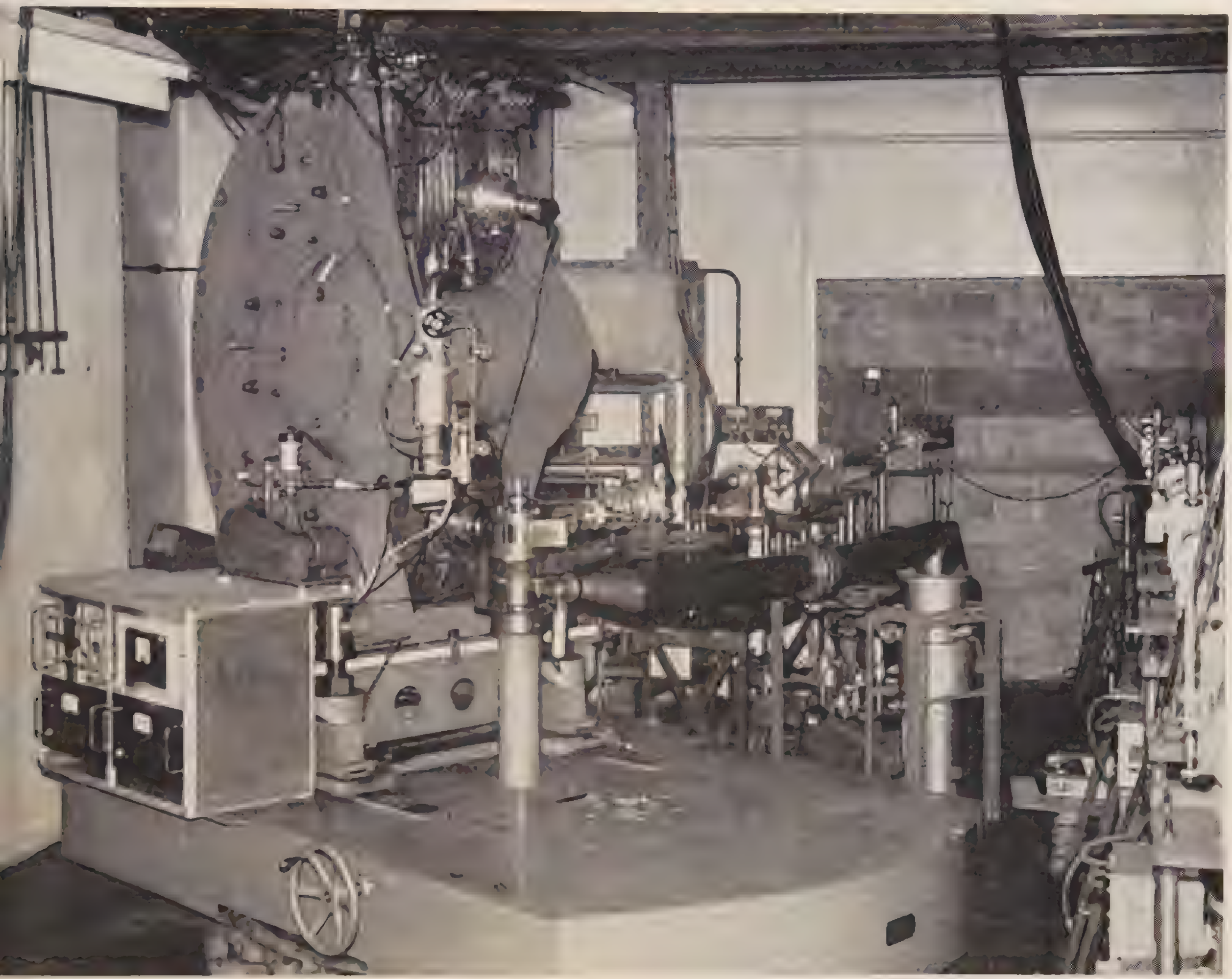

Fig. 6. The large 180° deflection double focussing particle spectrometer used with the Tandem generator.

2.3. He^3 AND T REACTIONS

In recent studies of He^3 and triton reactions, doubly ionized He^3 beams (energy range 6–11 MeV) produced in our 6 MV electrostatic generator and tritons with energies of about 10 MeV accelerated in the Tandem generator have been used.

Our Tandem generator is particularly suited to the acceleration of tritons since the gas consumption of the ion source is quite modest. Fig. 7 shows a schematic diagram of the gas recovery system which is based on the system first developed at Chalk River[15]). Since we have several stages of differential pumping at the injector, very little tritium gets into the main accelerating tubes. Also, because the Aldermaston Tandem is vertical, the injector is located 80 feet above the ground; thus in the event of an accident, tritium would be discharged harmlessly into the atmosphere at a high level.

---

[14]) A. V. Cohen and J. Cookson, Proceedings of Kingston Conference on Nuclear Structure (1960).

[15]) K. W. Allen and E. Almqvist. Rev. Sci. Inst. **24** (1953) 70.

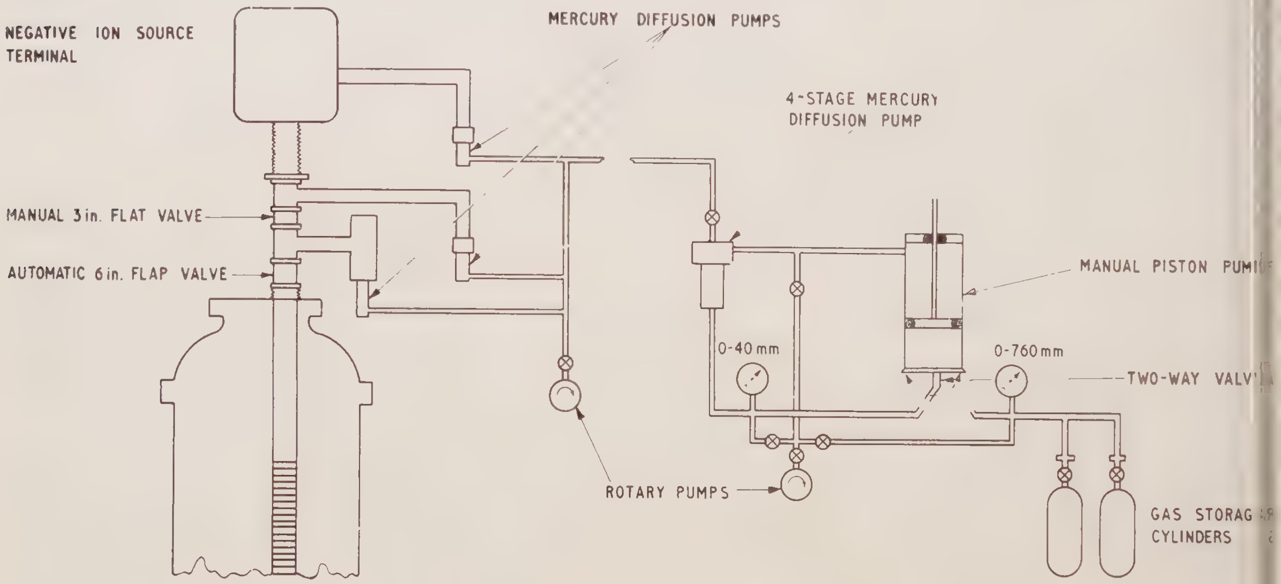

Fig. 7. Gas recovery system installed on the Tandem generator.

To obtain useful yields of doubly ionized helium from our 6 MV generator, we have inserted a gas stripper tube[16]) into the accelerating column as shown in fig. 8. Since the electron temperature in almost all commonly used ion sources is too low for appreciable double ionization of He, this seemed to us to be the simplest procedure. The singly charged He$^+$ ions are pre-accelerated to about 400 keV; at this energy the equilibrium concentration of He^{++} ions is about 20%[17]). Since the ion beam is focussed through the stripper, it is necessary to add an additional electrostatic lens at the base of the accelerating tube to refocus the diverging beam on to the target. Beam intensities of 0.5 to 1.0 microampere have been obtained on a target of area about 5 mm^2, and the He^{++} beam has a unique momentum to charge ratio which allows it to be separated from extraneous ion beams arising from traces of impurity in the ion source.

In studies of He^3 induced reactions by magnetic analysis, many interesting results have been obtained. It is generally found that (He^3,d) reactions are well behaved and show good stripping angular distributions. For example, fig. 9 shows some angular distributions obtained by Hinds and Middleton for the reaction $B^{11}(He^3,d)C^{12}$ at a bombarding energy of 9.84 MeV[18]) and similar results have been obtained in several other reactions[19]).

Even at a lower bombarding energy of about 5 MeV, good stripping patterns are still obtained.

In double stripping reactions of type (He^3,p) and (t,p) however, the situation appears to be more complicated. For $O^{16}(He^3,p)F^{18}$ and $O^{16}(t,p)O^{18}$, the angular distributions[20]) (fig. 10, fig. 11) have the typical shape expected of a

[16]) J. W. Bittner, Rev. Sci. Inst. **25** (1954) 1058.

[17]) S. K. Allison, Rev. Mod. Phys. **30** (1958) 1137.

[18]) S. Hinds and R. Middleton, Proceedings of Kingston Conference on Nuclear Structure (1960).

[19]) P. D. Forsyth *et al.*, Proc. Phys. Soc. **75** (1960) 291;
S. Hinds and R. Middleton Proc. Phys. Soc. **75** (1960) 444, 960;
ibid. **75** (1960) 745; **75** (1960) 745.

[20]) S. Hinds and R. Middleton, Proc. Phys. Soc. **74** (1959) 762;
S. Hinds, A. E. Litherland, R. Middleton and D. Pullen, Proceedings Kingston Conference on Nuclear Structure (1960).

direct reaction, and the assignments of transferred angular momentum are in accord with shell model expectations[21]). On the other hand, the angular distributions in $Be^9(t,p)Be^{11}$ and $^{12}C(t,\alpha)B^{11}$ (figs. 12 and 13) show strong backward angle contributions[22]). These latter data, all of which were taken with the multi-channel spectrograph, demonstrate the importance of studying the full angular range.

These few examples, taken from a large amount of data, will perhaps indicate the interesting stage reached in current research on nuclear reactions. Without going into detail, it is evident that for light nuclei, and for bombarding energies in the 10 MeV region, the direct reaction mechanism is always very prominent. With the advent of really large computers to speed up the handling of distorted wave calculations, we can expect to see rapid progress in extracting accurate information of nuclear structure interest from measured angular distributions.

3. Heavy Ion Reactions

At Aldermaston, oxygen ions in the energy range 10 to 40 MeV have been used for Coulomb excitation of nuclear levels, and for the measurement of nuclear lifetimes by methods based on the measurement of the Doppler shift of γ-rays emitted by the residual nucleus.

3.1. COULOMB EXCITATION

In Coulomb excitation[23]), the projectile does not enter the nucleus as in a conventional nuclear reaction but excites it "en passant" through the action of the long range Coulomb field. It is convenient to define certain parameters as follows:

(i) Half the distance of closest approach, a, given by

$$a = \frac{Z_1 Z_2 e^2}{m_1 v_i v_f}$$

where $Z_1 Z_2$ are the nuclear charges of the projectile and target nucleus, m is the reduced projectile mass, and v_i, v_f are the initial and final relative velocities.

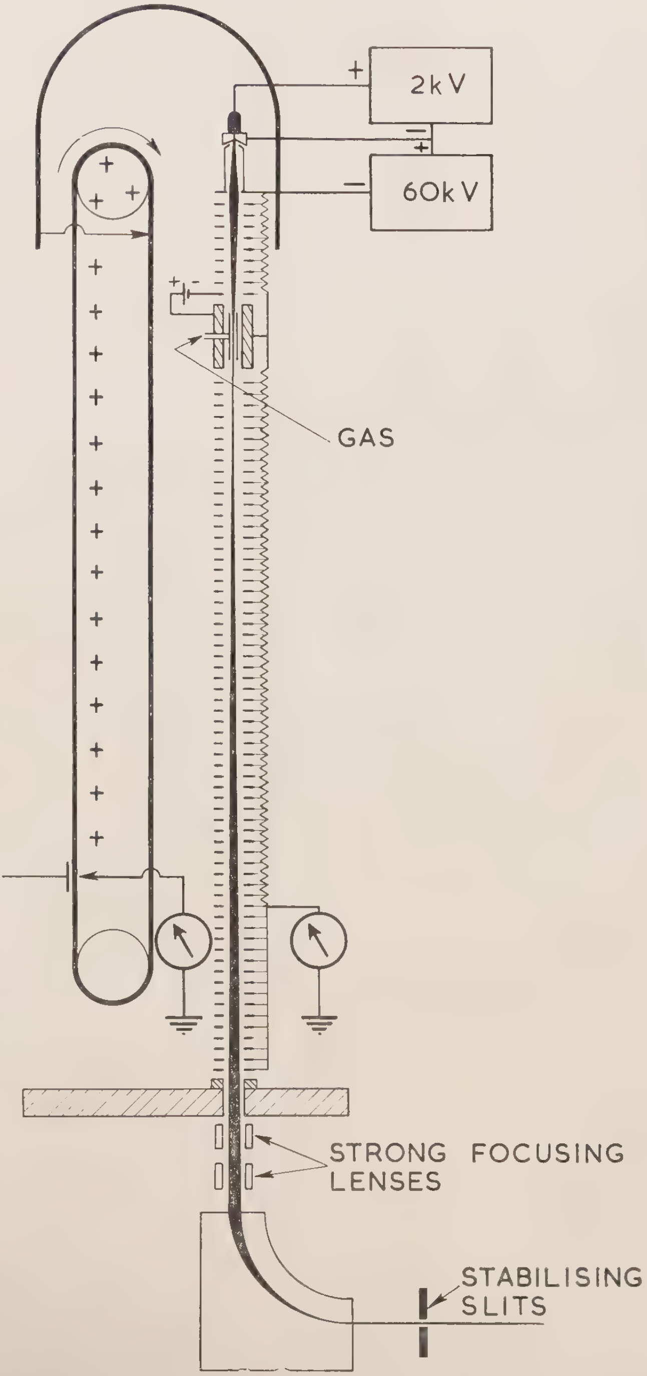

Fig. 8. Diagram showing the arrangement of the gas stripper tube installed in the accelerating tube of the 6 MV generator.

---

[21]) J. P. Elliott and B. H. Flowers, Proc. Roy. Soc. 229 (1955) 536.

[22]) S. Hinds, A. E. Litherland R. Middleton and D. Pullen, Proceedings Kingston Conference on Nuclear Structure (1960).

[23]) K. Alder, A. Bohr, T. Huus, B. Mottelson and A. Winther, Rev. Mod. Phys. 28 (1958) 432.

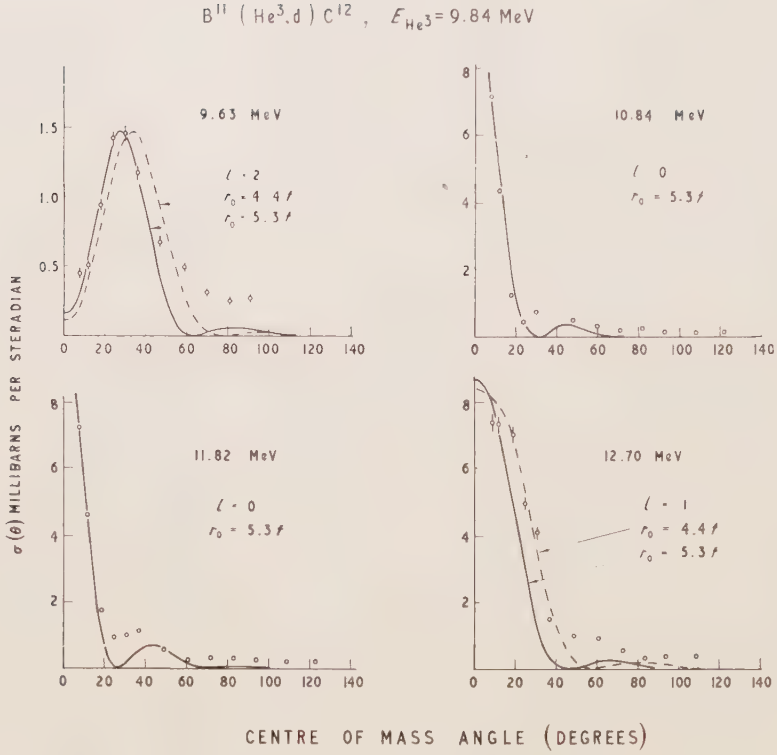

Fig. 9. Some angular distributions measured in the reaction $B^{11}(He^3,d)C^{12}$ for a bombarding energy of 9.84 MeV. The deuteron groups are assocaited with levels in C^{12} at 9.63, 10.84, 11.82 and 12.70 MeV.

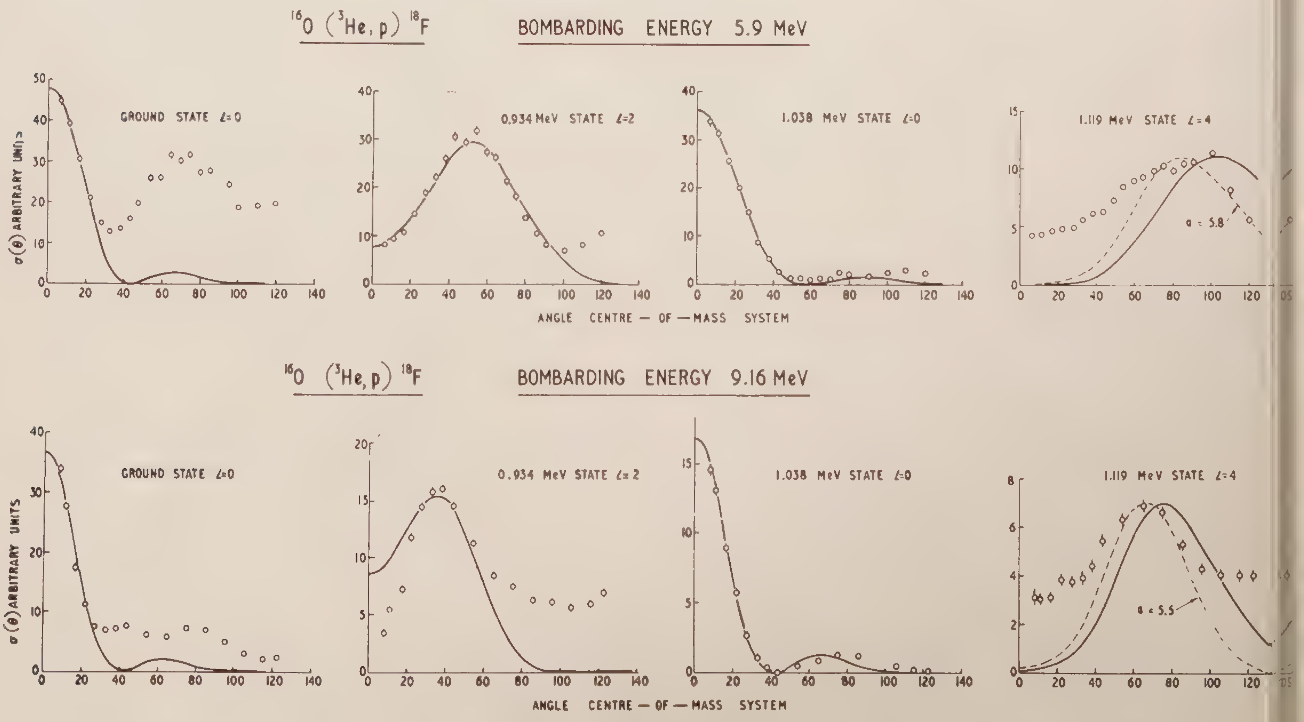

Fig. 10. Some angular distributions measured in the reaction $O^{16}(He^3,p)F^{18}$ at bombarding energies of 5.9 and 9.16 MeV.

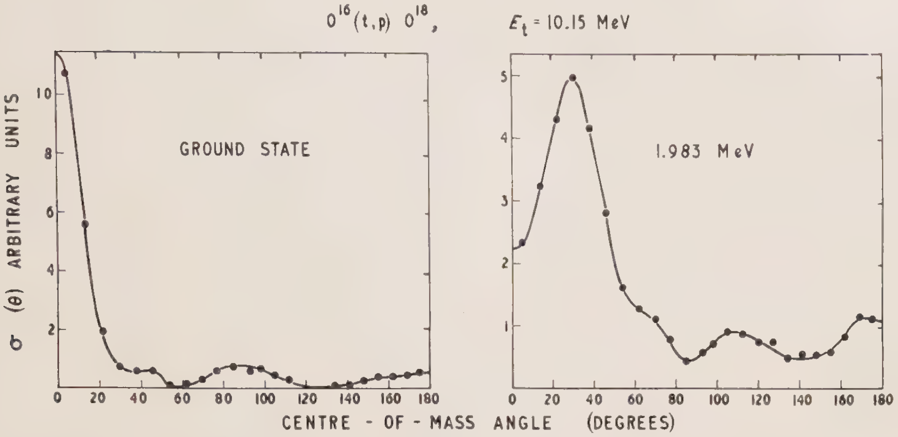

Fig. 11. Angular distribution of proton groups in the reaction $O^{16}(t,p)O^{18}$.

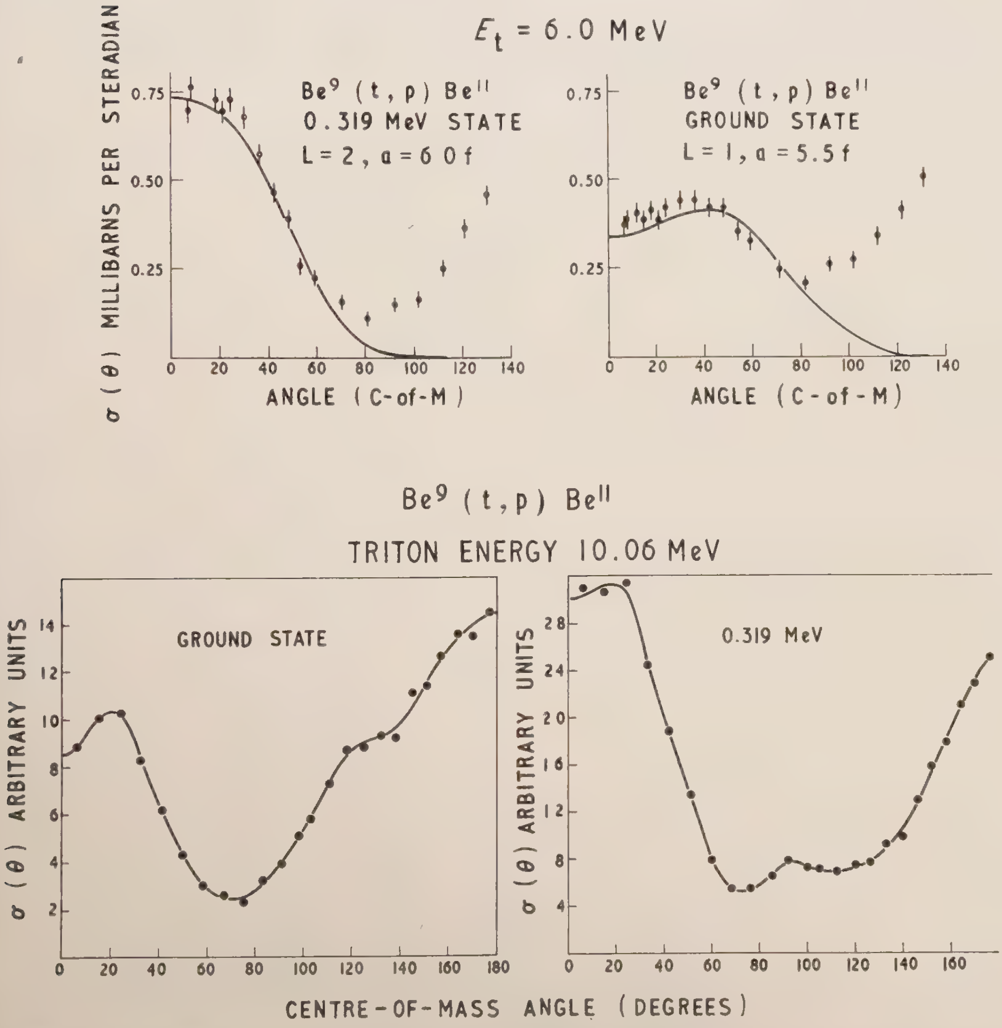

ig. 12. Angular distribution of the ground state and first excited state proton groups in the reaction $Be^9(t,p)Be^{11}$ obtained at bombarding energies of 6.0 and 10.06 MeV.

(ii)

$$\eta = \frac{\text{half the distance of closest approach}}{\text{particle wavelength}}$$

$$= \frac{Z_1 Z_2 e^2}{\hbar v_i} .$$

For a classical theory of the orbit to be valid, $\eta >> 1$.

(iii)

$$\xi_\varepsilon = \frac{\text{Collision time}}{\text{nuclear period}} \text{ where the orbit eccentricity,}$$

$$\varepsilon = \operatorname{cosec} \tfrac{1}{2}\theta .$$

also,

$$\xi = \eta_f - \eta_i \simeq \eta \frac{\Delta E}{2E} .$$

For good excitation, ξ should be small so that the nucleus experiences a strong electric shock. Small ξ and large η require $\Delta E/E$ to be small, which is also the condition for the *mean* orbit to be a good approximation.

For 35 MeV oxygen ions bombarding a medium mass nucleus, we find η about 50, ξ about 0.1–0.3, so that the semi-classical theory, in which the motion of the projectile is treated classically and the excitation quantum mechanically, would be expected to hold accurately. In addition, the γ-ray background from nuclear processes is much less with heavy ions, and there is the possibility of observing excitation of high lying states and also multiple excitations. Multiple excitation was first observed by Newton and Stephens[24]) using high energy heavy ions produced by the Berkeley linear accelerator,

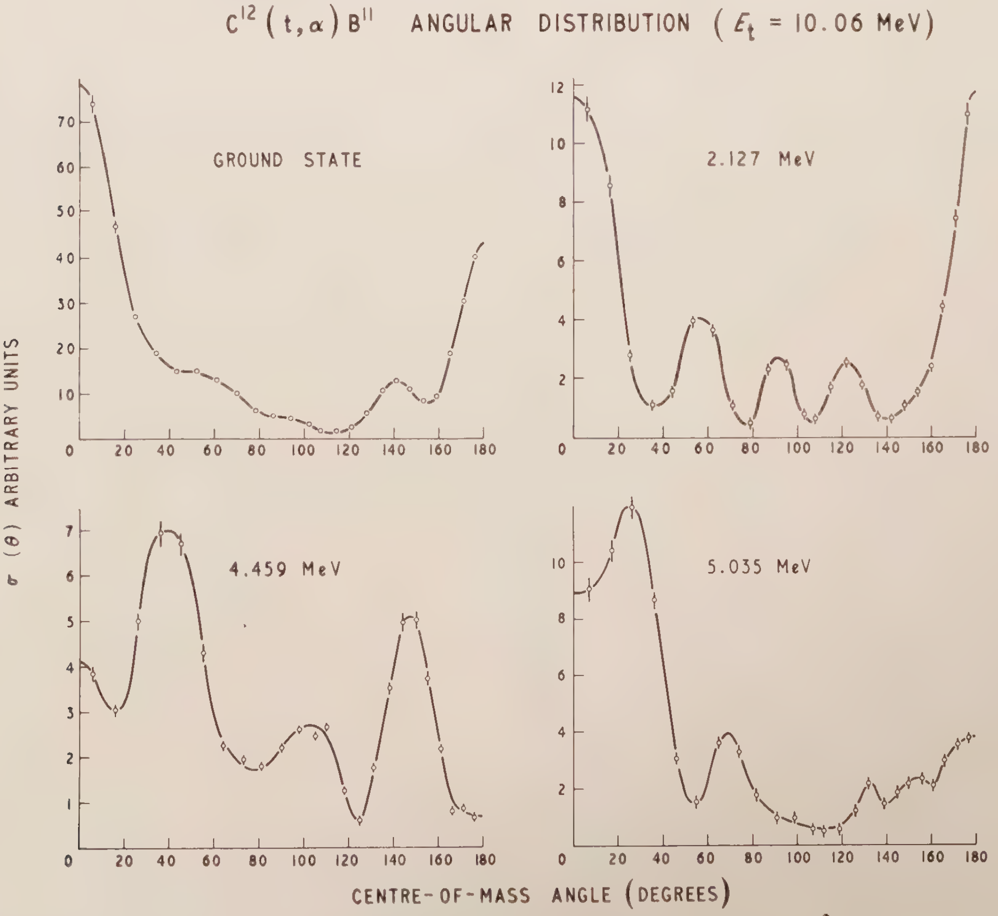

Fig. 13. Some angular distributions measured in the reaction $C^{12}(t,\alpha)\,B^{11}$ for a triton bombarding energy of 10.06 MeV.

---

[24]) J. O. Newton and F. R. Stephens. Phys. Rev. Letts. 1 (1958) 63.

and is of interest partly because it offers the opportunity of checking the theory to higher orders of approximation and also because it is possible to obtain information about nuclear states not accessible in first order excitation processes.

I would now like to illustrate some of these features of heavy ion Coulomb excitation by examples from recent work by Eccleshall, Adams and Yates[25]).

Fig. 14 shows the difference in background effects between the excitation of V^{51} by 9 MeV α-particles and 36.5 MeV oxygen ions. The 323 keV γ-ray arises from E2 excitation of the first excited state of V^{51}. The values of ξ are approximately equal to 0.1 for the two cases, but the background is obviously much greater for the α-particle bombardment. Both spectra were observed with the same NaI crystal in the same target geometry.

Fig. 15 shows γ-ray spectrum from the bombardment of a thick natural Sm target with 35.6 MeV oxygen ions. The Sm isotopes occur in a region where the nuclear distortion is changing rapidly with neutron number, so that the level schemes of Sm^{152} and Sm^{154} are well separated e.g. the first 2^+ state of Sm^{152} is at 123 keV and the corresponding state in Sm^{154} is at 80 keV. With samarium, it is therefore possible to obtain unambiguous information without the use of separated isotopes.

Fig. 16 shows the result of a (γ-γ) coincidence experiment in which the γ-ray spectrum in coincidence with the 123 keV transition in Sm^{152}

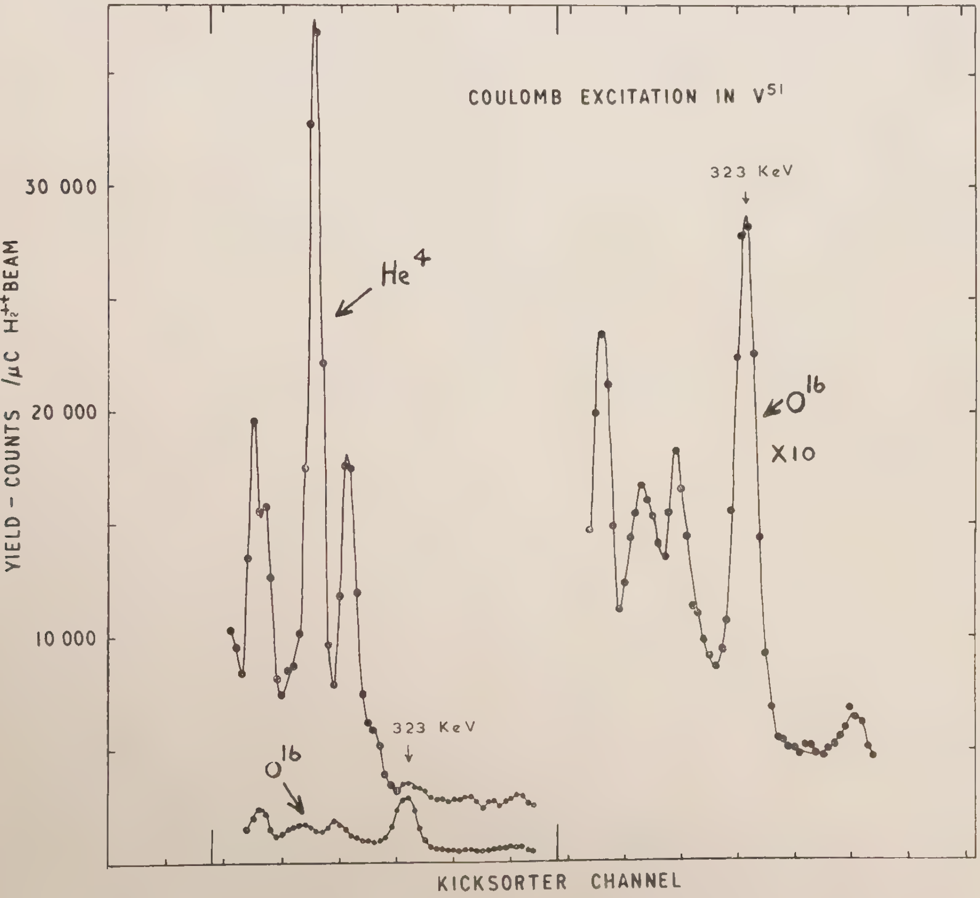

Fig. 14. γ-rays from the bombardment of V^{51} by 9 MeV α-particles and 36.5 MeV oxygen ions. The lower curve in the left hand portion of the diagram is due to oxygen ions and the 323 keV line arises from Coulomb excitation.

---

[25]) D. Eccleshall, B. Adams and M. J. L. Yates, Proceedings of Gatlinburg Conference on Heavy Ion Reactions (1960).

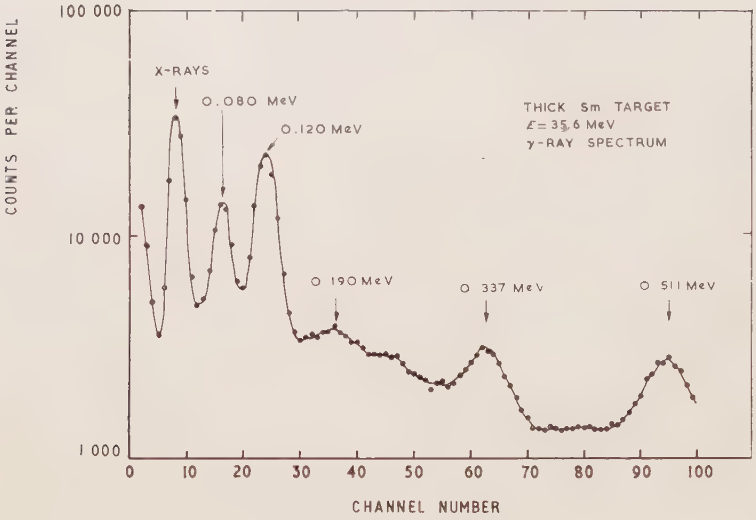

Fig. 15. γ-rays from the bombardment of a thick Sm target with 35.6 MeV oxygen ions.

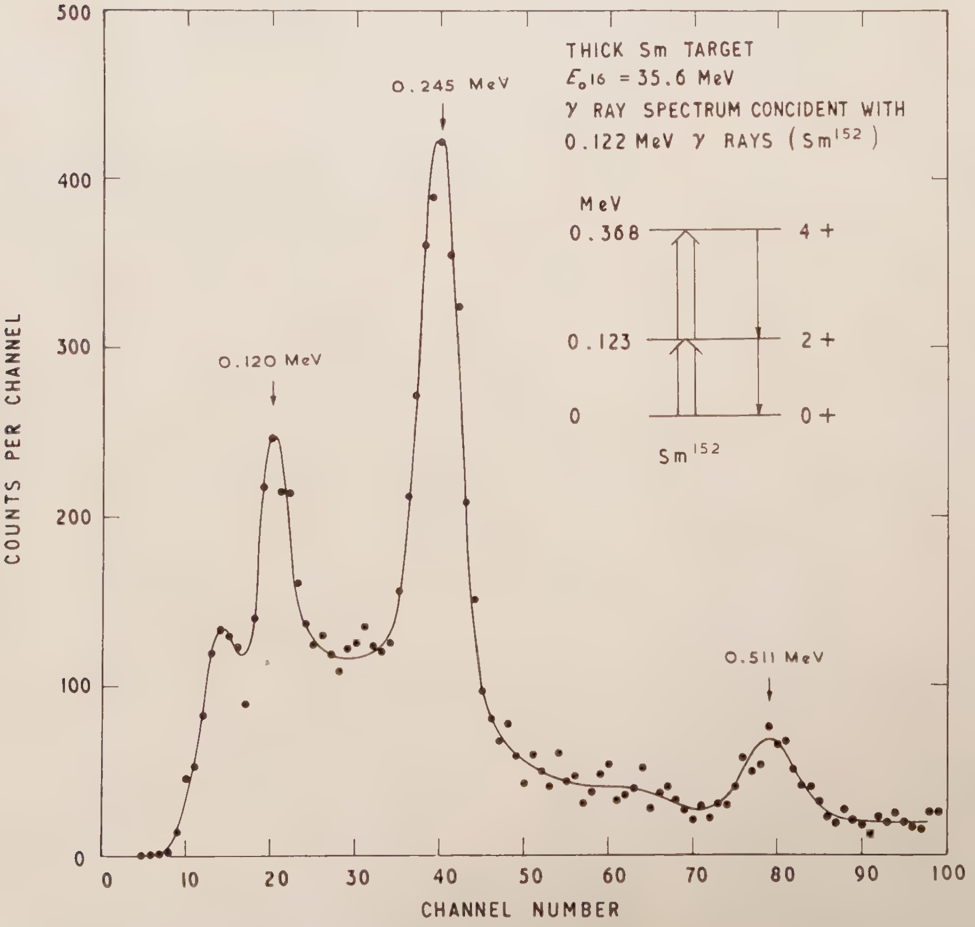

Fig. 16. γ-ray spectrum in coincidence with 123 keV γ-rays from the decay of the first excited state of Sm^{152}. The 245 keV γ-ray arises from double excitation of the 4^+ level at 368 keV.

was observed. The strong 245 keV line arises from double Coulomb excitation of the 4^+ level at 368 keV. Fig. 17 shows the γ-ray spectrum in coincidence with back scattered ions, and again the 245 keV γ-ray arising from double excitation is clearly seen.

Fig. 18 shows an example of double excitation in a vibrational nucleus, Pd^{108}. The γ-ray spectrum observed in coincidence with the 430 keV transition shows lines at 600 keV and 513 keV, with the former arising from double excitation to the level at 1.03 MeV which, from the decay of Ag^{108}, is thought to have a 0^+ assignment. However the observed coincidence yield and the angular correlation of the cascade γ-rays suggest that an unresolved 4^+ level is also present at the same energy.

In comparing the observed γ-ray yields from second order processes with theory, some care is necessary. Calculations may be made using second order perturbation theory, but it is important to bear in mind that the probability of first order excitation may be high enough to invalidate a perturbation treatment. For example, the probability of excitation of the first 2^+ state of a rotational nucleus such as W^{186} or Sm^{154} may be as much as 50% with 35 MeV oxygen ions. Alder and Winther have carried out higher order calculations using the sudden approximation ($\xi = 0$), but this is not always sufficiently accurate. For example, in vibrational nuclei such as Pd^{108} referred to above, where $\xi = 0.25$, the sudden approximation gives results greater by a factor two than second order

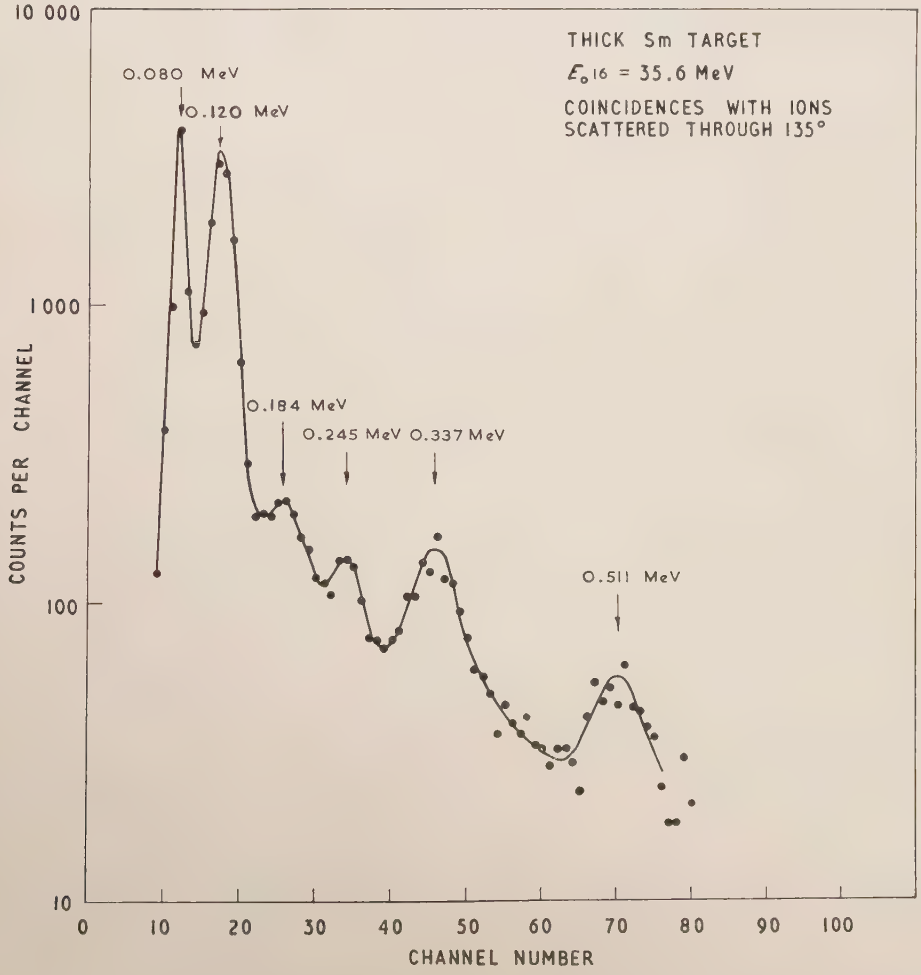

Fig. 17. γ-ray spectrum from a thick Sm target in coincidence with back scattered oxygen ions.

perturbation theory, which should be a good approximation in this case since the first order excitation probability is only about 20%. The sudden approximation should be useful for the interpretation of experiments with higher energy heavy ions, particularly when the γ-rays are observed in coincidence with back scattered ions.

These mathematical difficulties are, however, not of a fundamental nature. and the importance of Coulomb excitation processes is that reduced transition probabilities may be extracted with good accuracy directly from the data. Since these transition probabilities reflect the contribution of collective effects in nuclei, the data obtained are often complementary to the information obtained from nuclear reactions of the direct type in which the intrinsic or single particle states are preferentially excited.

3.2. NUCLEAR LIFETIMES FROM HEAVY ION REACTIONS

A characteristic feature of heavy ion induced reactions is the large amount of linear momentum transferred to the residual nucleus from the bombarding particle. Thus the Doppler shift of γ-rays emitted from the residual nucleus may be quite large, and this fact is being exploited by Litherland, Adams, Eccleshall and Yates[26]) to measure the lifetimes of some excited states of light nuclei. The technique is in general similar of that developed by Devons and his collaborators[27]), but the present experiments have the advantage that the velocities of the recoiling nuclei can be up to an order of magnitude greater.

Fig. 19 shows the principle of an experiment used to determine the half-life of the 1.98 MeV level in O^{18}. The nuclear reaction is $T(O^{16},p)O^{18}$, and with an oxygen ion bombarding energy of 13.5 MeV, the O^{18} nuclei are concentrated around the edges of a cone of half angle 8.4°. γ-rays are observed at 45° and 135° with a 5″ × 6″ NaI

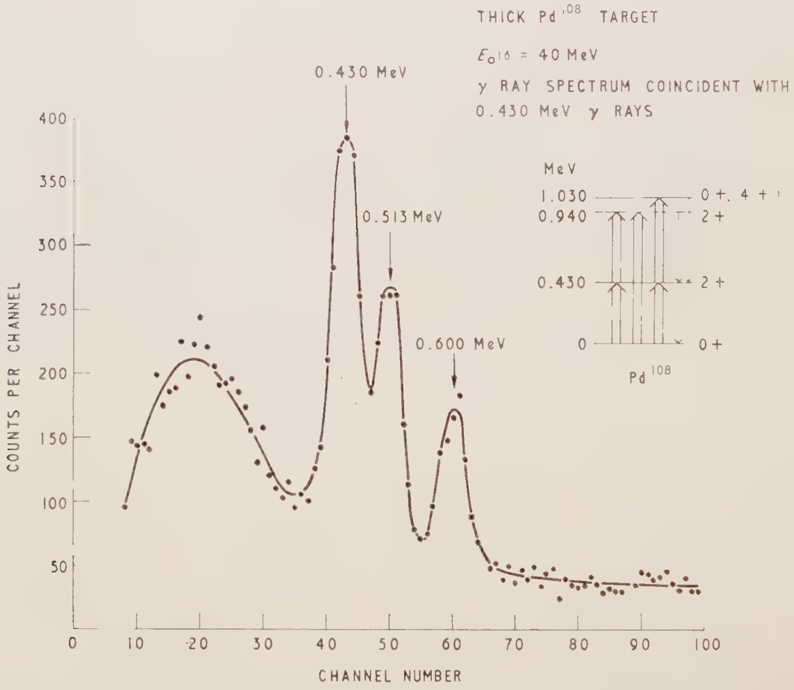

Fig. 18. Coulomb excitation of Pd^{108} by 40 MeV oxygen ions. The γ-ray spectrum observed in coincidence with 430 keV γ-rays from the decay of the first excited state of Pd^{108}.

---

[26]) A. E. Litherland, B. Adams D. Eccleshall and M. J. L. Yates, Proceedings Kingston Conference on Nuclear Structure (1960).

[27]) S. Devons, G. Manning and D. St. P. Bunburg, Proc. Phys. Soc. A **68** (1955) 18.

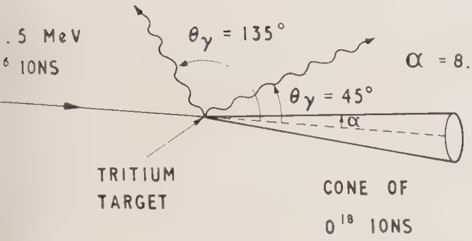
.5 MeV
6 IONS
θ_γ = 135°
θ_γ = 45°
α = 8.4°
α
TRITIUM TARGET
CONE OF
O18 IONS

AN VELOCITY ~ 1.1 × 10^9 cm sec^{-1}
XIMUM DOPPLER SHIFT 5.2%
ASURED DOPPLER SHIFT 1.0%
LF-LIFE OF 1.98 MeV EXCITED STATE OF O^{18}
× 10^{-12} SECOND

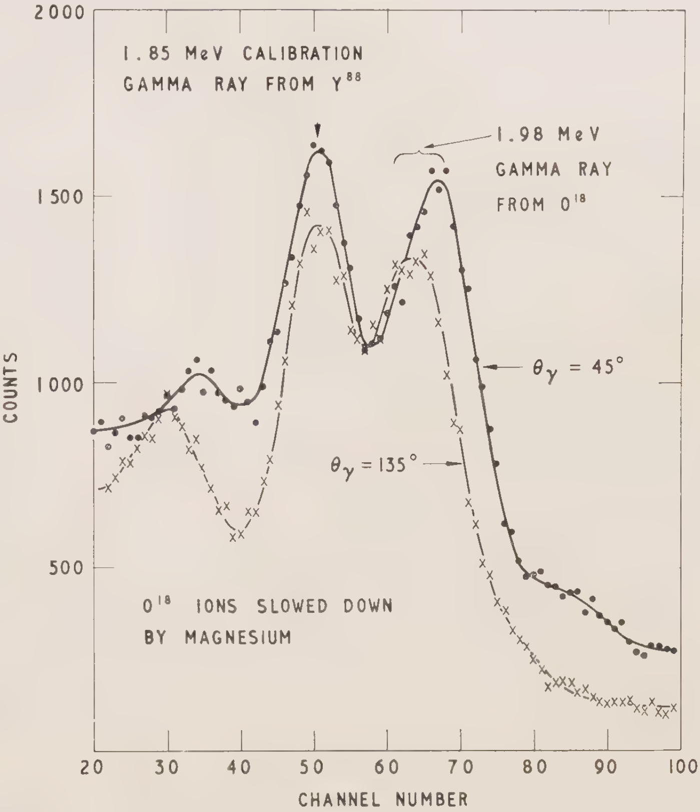

g. 19. Doppler shift of the 1.85 MeV γ-ray from the cay of the first excited state of O^{18}, produced in e bombardment of a tritium target by 13.5 MeV oxygen ions.

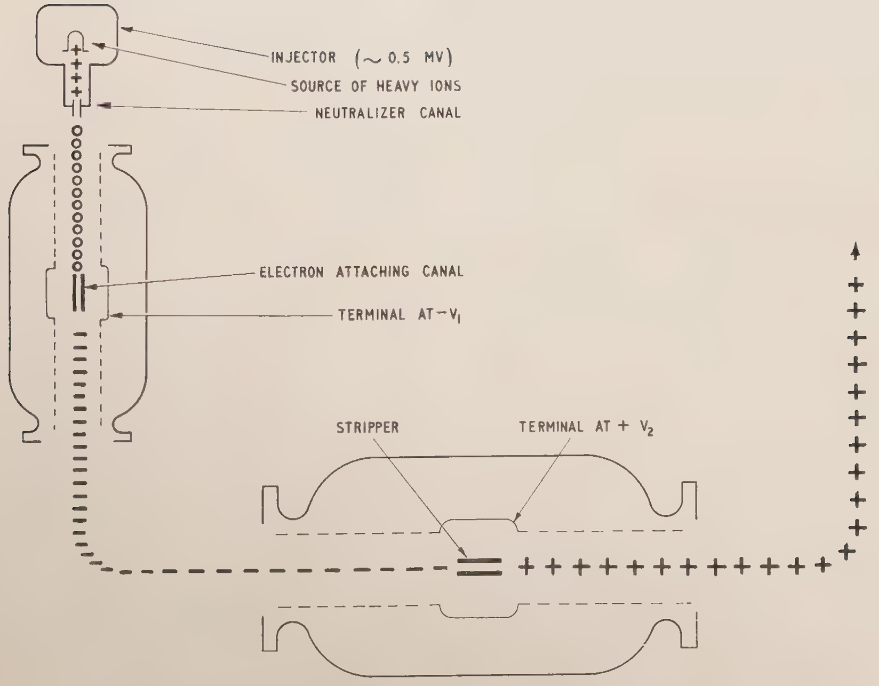
INJECTOR (~ 0.5 MV)
SOURCE OF HEAVY IONS
NEUTRALIZER CANAL
ELECTRON ATTACHING CANAL
TERMINAL AT − V1
STRIPPER
TERMINAL AT + V2

Fig. 20. A possible combination of Van de Graaff generators to give high energy heavy ion beams.

crystal spectrometer, and the 1.85 MeV γ-ray from Y^{88} is used as a comparison standard. The curves shown in fig. 18 were obtained with a tritium target on a magnesium backing, and the observed Doppler shift was approximately 20% of the maximum possible value. With a copper backing, the shift was observed to be only about 10% of the maximum possible. These data yield a value of about 1.4×10^{-12} second for the half life of the 1.98 MeV state in O^{18}.

With this experimental arrangement, approximate values for the lifetimes of about 10 states in O^{18} and F^{18} have been obtained.

This technique is clearly a very valuable method of measuring nuclear lifetimes, since it covers the important range from 10^{-11} to about 10^{-14} second. Given a Tandem generator with a flexible injector capable of producing a variety of heavy ions, and accurate data on energy loss, the method is capable of considerable extension and refinement.

4. Production of Heavy Ions of High Energies

To exploit the potentialities of heavy ions as nuclear projectiles, higher energies are required than are available from currently operating Tandem generators, although it is important to retain all the well known advantages associated with electrostatic generators. How should this be achieved?

One possibility is to inject into a Tandem generator high energy negative ions produced by an electrostatic generator of conventional single-ended design. This is clearly satisfactory for hydrogen ions since a source of negative hydrogen (or deuterium or tritium) ions can be quite simple and robust, and can be expected to operate satisfactorily in the terminal of a pressurized accelerator.

For heavy ions, this solution is perhaps not so satisfactory since it is desirable to have available a variety of ions and this may involve the use of more than one type of ion source. For this reason it would be preferable to have the source of ions at ground potential outside the pressure tank of the accelerator, so that two Tandem generators in series, as proposed by Van de Graaff[28]) at the last accelerator conference, might be better. A typical arrangement is shown in fig. 20.

To assist us in assessing the design requirements of a neutral atom injector for such a combination, Sweetman and Riviere have recently begun experiments on the physics of the interaction of beams of heavy ions with the common gases, using apparatus similar to that described by Sweetman in a recent article on the dissociation of molecular hydrogen ions[29]).

In order that the neutral beam shall pass through the electron donor tube in the high voltage terminal, the divergence of the neutral beam must be very small ($\gtrsim 3 \times 10^{-4}$ radian), and such a small divergence is only likely to be produced in a charge exchange process. Since charge exchange cross sections decrease rapidly with increasing energy, the optimum injection energy is likely to be in the region of a few hundred kilovolts. It cannot be fixed until more data on atomic cross sections are available. A preliminary investigation using a beam of 230 keV neutral oxygen atoms did, however, show an acceptably small divergence.

Acknowledgements

Many of the results and some of the techniques mentioned in this paper have not previously been published, and I am greatly indebted to my colleagues at Aldermaston, in particular A. V. Cohen, D. Eccleshall, S. Hinds, A. E. Litherland and R. Middleton, for much helpful discussion, and for allowing me to mention some of their more recent experiments.

It is also a pleasure to acknowledge the very important contributions made by F. A. Julian, V. Shepherd and P. Hammond in the design and operation of the accelerators, and also the work of our engineering design group led by A. J. Marriott.

---

[28]) R. J. Van de Graaff, Proceedings of the 1958 Accelerator Conference, Cambridge, Mass.

[29]) D. R. Sweetman, Proc. Roy. Soc. A **256** (1960) 416.

DISCUSSIONS

Speaker addressed: K. W. Allen (*A.W.R.E.*).

Question by: J. P. F. Sellschop (*Johannesburg*)

Question: In the reaction $O^{16}(He^3,p)F^{18}$ (ground state) you have shown as an angular distribution with, besides the expected peak, a prominent but simple structure at about 70°—have you an explanation for its appearance?

Answer: It has been considered that the complex structure in the angular distribution of the ground state proton group could be associated with alpha state admixture in the ground state of F^{18}. However the effect is larger than would be expected and since the angular distribution changes with energy it is, perhaps, more likely due to distorted wave effects.

Speaker addressed: K. W. Allen (*A.W.R.E.*)

Question by: J. P. E. Sellschop (*Johannesburg*)

Question: Did you mean to imply that as a general rule in simple (d,p) reactions, better agreement will be obtained at higher and higher energies?

Answer: I would generally expect that agreement with plane wave stripping theory would be better at the higher bombarding energies. However as pointed out by Wilkinson and confirmed by some of your own measurements, it is possible to get good plane wave stripping patterns at quite low bombarding energies for a limited range of Q values.

NUCLEAR INSTRUMENTS AND METHODS 11 (1961) 112–121; NORTH-HOLLAND PUBLISHING CO.

SOURCES OF POLARIZED IONS (FOR PROTONS AND SIMILAR PARTICLES)

R. FLEISCHMANN

Physikalisches Institut der Universität, Erlangen

The possible methods for the production of polarized protons (or similar particles) are discussed. Probably the most promising schemes are:

1. To send a beam of atomic hydrogen through an inhomogeneous magnetic field (4-pol or 6-pol) and to separate one substate in a weak field.

2. To separate two substates commonly in a strong field. In this case 50% polarized protons can be obtained.

3. A radio frequency transition between substates can be effected too. Then 75% polarized particles can be produced (but 100%, if every disturbance is avoided).

4. Setups similar to a Rabi apparatus should also give a 100% polarized atomic beam.

A serious difficulty is the residual gas pressure in the ionization section, which is to be overcome by differential pumping and by the use of very strong atomic beams. Ionization yields are very small until now.

Several other possible methods are discussed and important aspects of apparatus built by several research groups are mentioned.

1. Introduction

The methods will be discussed that come into question today for the production of polarized protons. These methods can also be used for the production of polarized deuterons and of helium 3. Perhaps it will even be possible in the future to produce polarized H^- ions in an analogical way.

The following groups of methods for the production of polarized particles are to be mentioned.

1. The production of polarized particles by scattering,

2. The production of polarized particles by means of nuclear reactions.

I do not wish to go into further details concerning these two groups, because in the important energy region of 0–10 MeV it does not appear possible to produce beams of sufficient intensity in that way. Further methods are:

3. The production of polarized protons by means of atomic or molecular beams, and

4. Making use of the Lambshift.

I would like to restrict myself to these two methods, since only these render a rather constant and parallel beam of polarized protons.

The principal scheme for the production of polarized protons starts with atomic hydrogen produced by the dissociation of hydrogen molecules in a discharge. Then an atomic beam is formed and split up into partial beams in passing it through an inhomogeneous magnetic field. This dividing of the states will lead to nuclei, the spin of which is either parallel or anti-parallel to the magnetic field. I will refer to these as spin-up and spin-down. Such nuclei are called polarized.

After leaving the magnetic field, these atoms will be ionized and the ions will be accelerated and fed into an accelerator machine. This principal scheme is used in all molecular beam or atomic beam devices for the production of a beam of polarized particles.

2. Principles of Separation

Now I would like to discuss the individual steps of this method and the different variants used by different workers:

The basis for splitting the atomic beam in an inhomogeneous field is the level scheme of the hydrogen atom. Fig. 1 shows the splitting of the different states of the hydrogen atom in the ground state as a function of the magnetic field, that is to say the Zeeman effect of the hyperfine structure of the hydrogen atom. The spin of the electron is indicated by an arrow, the spin of the proton by a broken line arrow.

The states 1 and 3, that is the states with the magnetic quantum number $m_F = +1$ and $m_F = -1$ are pure states. In state 1 both spins are parallel to the magnetic field and in 3 anti-parallel. The states 2 and 4 (with $m_F = 0$) are mixed states. In a weak magnetic field these states are the sum or the difference of the two configurations: electron spin up, proton spin down, and electron spin down, proton spin up. Both configurations have $m_F = 0$. In the strong magnetic field however there is almost only one configuration present in these mixed states. In a strong field the electron and proton spins are decoupled and it is the spin state of the electron, which principally determines the magnetic moment. The slope of the curves renders the effective magnetic moment.

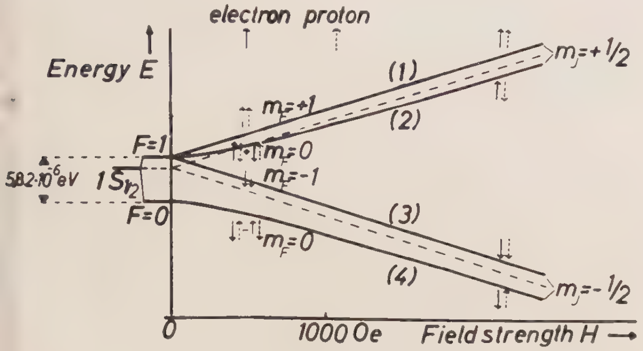

Fig. 1. Zeeman-effect of hfs splitting of atomic hydrogen (ground state).

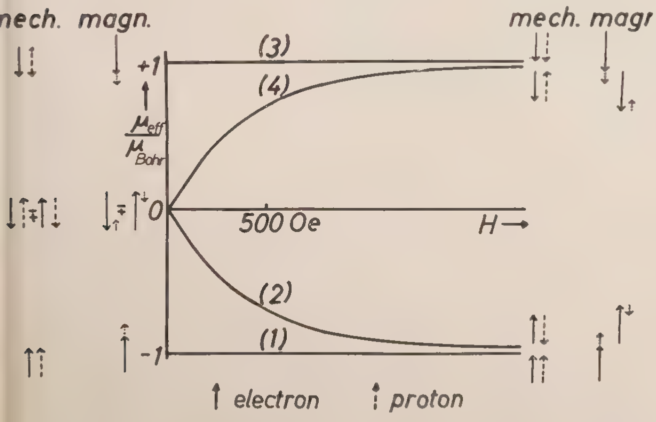

Fig. 2. Magnetic moment of hydrogen vs. magnetic field strength.

In fig. 2 the magnetic moment is shown as a function of the magnetic field strength; it is constant for the states 1 and 3.

I would like to point to the well known fact that the *spin* of the nucleus of the hydrogen atom and the spin of the electron are equal, namely $\frac{1}{2}\hbar$. The *magnetic moment* of the electron is, however, approximately a thousand times greater than that of the proton and this is the reason for the relatively good deflectability of an atomic beam of hydrogen compared with a H_2 molecular beam.

The deflectability in an inhomogeneous field depends on the absolute value of the magnetic moment μ_{eff}. If therefore the magnetic field is *weak* enough, the components 2 and 4 will not be deflected at all; the state 1, however, will be deflected in one direction and state 3 in the opposite direction. If we use a cylindrical symmetric field arrangement, e.g. a 4-pole or 6-pole field, this means that one is repelled from the axis and the other attracted to it. In a *weak* magnetic field, which is strongly inhomogeneous, it is therefore possible to select one single state (which contains $\frac{1}{4}$ of all atoms). The atoms which have been thus selected are 100% polarized.

In a *strong* magnetic field (Stern-Gerlach type) the components 1 and 2 or the components 3 and 4 can be deflected commonly. In these pairs of states the spins of the *electrons* have the *same* direction. If a pair of these states, e.g. 1 and 2 is commonly deflected, the *protons* of state 1, while in a strong magnetic field, have 100% of their spins *up*, but the protons of state 2 have almost 100% of their spins *down*. Therefore, while they are in a strong magnetic field, the nuclei of the commonly deflected beam are *unpolarized*.

If however the atoms, e.g. of state 1, pass onto a region of *low* (almost zero) field strength, the protons of this state remain 100% polarized, those in state 2 however become a mixture of 50% parallel, 50% anti-parallel with net polarization zero.

If state 1 and state 2 are commonly deflected in a strong field, and are brought into a weak field and ionized there, one obtains 50% polarized protons according to the relationship for the degree of polarization

$$P = \frac{N_p - N_a}{N_p + N_a} = \frac{(50 + 25) - 25}{100} = 0.5 ;$$

$$\text{that means } \frac{N_p}{N_a} = \frac{3}{1} .$$

Here N_p is the number of parallel, N_a the number of antiparallel particles.

Let us start again with a beam containing the commonly separated states 1 and 2. By use of RF a transition can be produced between different substates. The energy differences and the associated frequencies can be taken from fig. 1. If it were possible to transfer all atoms of substate 2 into substate 4 and the ionization would take place in a *strong* magnetic field, we would obtain 100% polarized protons and the ionization in such a field should be more efficient. But in an atomic beam having a Maxwellian distribution of velocity, only 75% proton polarization can be obtained, but cf.[16]).

In order to induce transitions only between component 2 and 4, but not however between component 1 and 3, which would need the same frequency at high field strength, the transition is made in a medium field strength of approximately 200–300 oerstedt.

To summarize: For the separation of the substates of the atomic beam we may use:

weak field: One component is separated, the intensity is $\frac{1}{4}$ of the total beam and the degree of polarization is 100%

strong field for the separation, but ionization in a weak field, the intensity is $\frac{1}{2}$ of the total beam, degree of polarization 50%

strong field for the separation, followed by RF transition and then ionization in a strong field. The intensity is $\frac{1}{2}$ of the total beam, degree of polarization 75%. (Perhaps it can be increased.)

3. Geometry of Field Forms

Now I want to discuss the different geometrical forms of magnetic fields, which can be used for separation. On a particle with the magnetic moment μ there acts a force

$$\boldsymbol{F} = \text{grad}\,(\boldsymbol{\mu}\cdot\boldsymbol{H}) = \mu_{\text{eff}}\,\text{grad}\,|\boldsymbol{H}| .$$

It is expedient to have a field with a circular symmetry and an inhomogeneity as high as possible. For this we can use

1. A 4-pole field. In this case $|\boldsymbol{H}| \sim r$

$$\frac{\partial|\boldsymbol{H}|}{\partial r} = \text{const} .$$

The particles of state 1 will be deflected towards the axis and those of state 3 will be deflected away from the axis. Although the direction of the magnetic field strength varies in the azimuth and changes very much around the center (fig. 3), the force on the atom only depends on r.

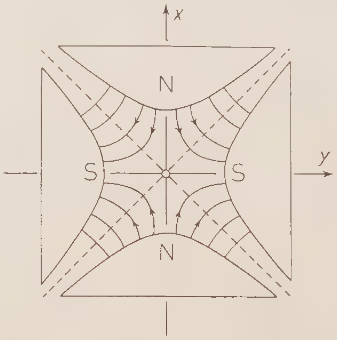

Fig. 3. Field lines in a 4-pole field.

The path of an atom starting from the axis corresponds to a parabola of a projectile. Atoms which start from one point of the axis with equal angle and equal velocity will be refocussed into one point.

2. Secondly we have the 6-pole field. In this case

$$|\boldsymbol{H}| \sim r^2$$

$$\frac{\partial|\boldsymbol{H}|}{\partial r} \sim r .$$

A particle of state 1 starting from the axis will make harmonic oscillations.

If a beam of polarized particles leaves the inhomogeneous 4 or 6-pole field and enters a region of a homogeneous magnetic field, the spins of the nuclei will be turned into the direction of the field. The particles do not suffer depolarization by Umklapp-processes (spin flip) in a usual experimental arrangement of usual design. This has been checked in Erlangen by Clausnitzer, who showed that 90 ± 10% of the particles retain their state of polarization. For this he used one 4-pole field as a polarizer, one as an analyser.

A 4-pole magnet with *continuously decreasing field strength* is being built by Keller[1]). The annular atomic beam enters the 4-pole field at the strong field end and leaves the magnet at the weak field end.

In fig. 4 the trajectories of the states 1 and 2 are drawn. Keller has calculated the slope of the particle path as a function of the velocity of the particles. Since the beam particles have a Maxwellian distribution, Keller also calculated the envelope of the trajectories for the different velocities. He found that by inserting a sufficiently long cylindrical tube at the end of the 4-pole field, it is possible to separate the (whole) Maxwellian distribution of one substate. All atoms of component 2 will sooner or later hit the cylindrical tube since their amplitude of oscillation is larger than that of the substate. This scheme has the disadvantage that the field has to be of considerable length and that the beam is rather wide spread behind the magnetic field. Therefore it is difficult to ionize the beam.

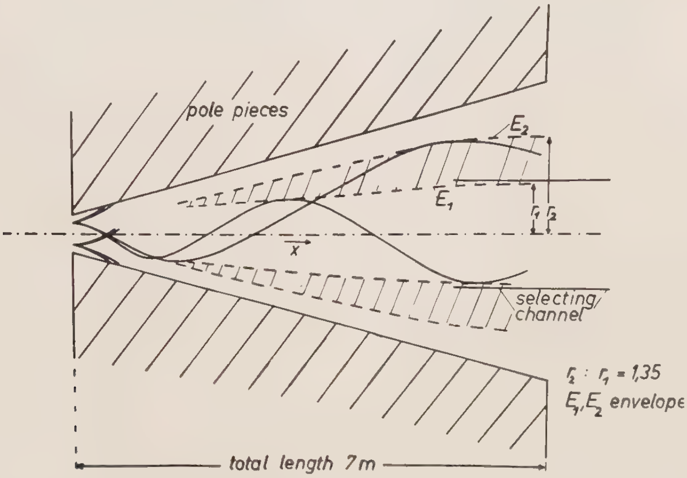
pole pieces
E_2
E_1
r_1 r_2
x
selecting channel
$r_2 : r_1 = 1{,}35$
E_1, E_2 envelope
total length 7m

Fig. 4. 4-pole field arrangement by Keller.

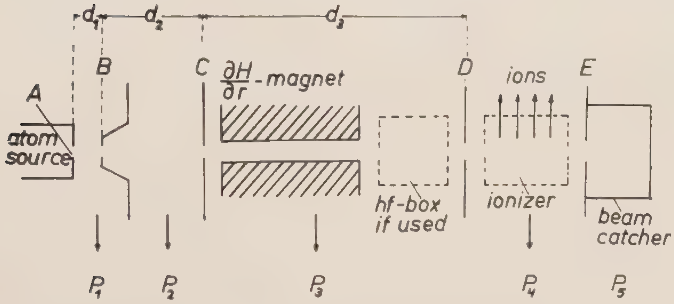
d_1
d_2
d_3
A
B
C
$\frac{\partial H}{\partial r}$-magnet
D
ions
E
atom source
hf-box if used
ionizer
beam catcher
P_1
P_2
P_3
P_4
P_5

Fig. 5.

A. Entrance diaphragm.
B. Intermediate diaphragm.
C. Beam defining aperture.
D. Selecting aperture.
E. Beam exit.
$P_{1 \cdots 5}$. Pumps.

4. Atomic Beam Conditions and Vacuum Requirements

We now come to the discussion on the conditions for obtaining an atomic beam and the requirements for the vacuum system.

All the schemes discussed so far make use of an apparatus, which has approximately the following design (fig. 5).

In this figure A is a *circular hole*. An atomic beam will be produced only if the width of this hole is of the same order of magnitude as the length of the mean free path of the outflowing gas. This means that at a pressure of 0.5 Torr a diameter of 0.3 mm for the circular opening is permissible.

---

[1]) R. Keller, CERN-Reports 3141/f; and 60–2; and Basel Symposium 1960.

If one wishes to have a higher particle flux, A may be *annular* in shape. If and when the width of the annular slit is comparable in size to the mean free path of the gas, the particle flux will increase with the area of the opening. Instead of a single opening at the point of A, a glass collimator consisting of a *large number* of capillary *channels* can also be used and this is done by Dickson and Craddock²) of Harwell. In this case most of the outflowing gas is directed to the axis; this at the same time reduces the pumping requirements between A and B. In the region beyond B there must be a vacuum of about 10^{-6} Torr; separate high speed pumps are needed for the different sections; between A and B the pressure should be below 10^{-3} Torr and the distance between A and B should be small. In practice, one will obtain an atomic beam behind B even if the pressure in the source is about 10 times higher than the pressure permitted by the atomic beam condition, if and when a pressure increase behind A is prevented by strong pumping.

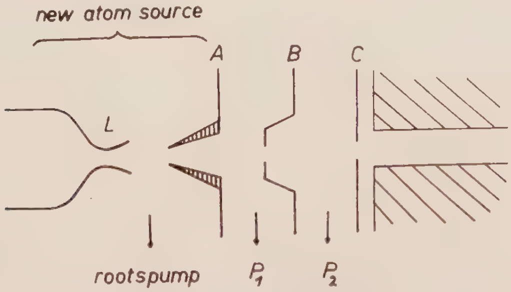

Fig. 6. A. Entrance diaphragm = "Abschäler" with critical angle behind the nozzle. L. Laval nozzle.

In order to obtain as powerful as possible an atomic beam a Laval nozzle can be used within which the speed of sound is attained from a certain critical pressure onwards. If the pressure is increased, the density is increased but not the velocity. When using a Laval nozzle, the Abschäler (pealer) fig. 6 takes the place of the entrance diaphragm of a usual atomic beam apparatus. Between L and A very strong pumps (Rootspumps in preference) are required.

If the pressure

between A and B is	about 10^{-3} Torr
between B and C	about 10^{-4} Torr
behind C	about 10^{-6} Torr
behind D smaller than	about 10^{-8} Torr

and if the diaphragms have a diameter of a few tenths of a mm, gas will diffuse from left to right and tend to increase the partial pressure behind D.

In order to diminish this undesired diffusion, channels can be used between the sections instead of simple diaphragms and more differential pumping stages could be included³).

The diffusing gas causes a disturbance especially in the ionization section. If the ionization is accomplished by electron bombardment, protons will also be produced there from undissociated molecular H_2 present in the ionization region. These protons are, of course, not polarized. Even at a pressure of 10^{-7} Torr and confinement of bombarding electrons to a volume as small as possible, the number of protons produced in the residual gas is relatively high. Therefore oil pumps and rubber gaskets should be avoided. Preference is therefore given to mercury pumps and for the ionization section to getter pumps, e.g. Vacion pumps. In addition, it might be desirable for the walls of the ionization section to be bakable.

5. Dissociation

Three methods are in use for dissociation:

1. Wood's discharge
2. Arc discharge
3. Radio frequency discharge.

In order to keep the recombination low, which at small pressures will take place at the wall only, glass vessels are used. Sometimes the inner surface is coated with methyltrichlorisilane (CH_3SiCl_3)²). In any case it is desirable to keep the distance between the region of dissociation and the entrance diaphragm as short as possible.

The Wood's discharge presupposes a rather

---

²) Dickson and Craddock, Basel Symposium, 1960.

³) cf. N. F. Ramsey *et al.*, Rev. Sci. Instr. **29** (1958) 935.

low pressure of a few tenths of a Torr. The source has the advantage of a dissociation of almost 100% but the particle flux is very limited. For the dissociation, a radio frequency discharge can also be used (e.g. Keller 20 Mc/s 1 kW at a pressure of 1–2 Torr). If the pressure is to be increased much higher, one can use also radio frequency, but the frequency should be higher too.

Thus it is possible to dissociate hydrogen of atmospheric pressure almost 100% by a frequency of 2400 Mc/s (electronic torch). At such a high pressure, however, the volume recombination increases strongly, and this volume recombination is accompanied by an undesired increase of the temperature of the gas.

Desirable in an atomic beam is a large product of particle flux times degree of dissociation.

If the pressure is rather high in the source also, an arc discharge can be used (Clausnitzer); as electrodes for the arc a pierced plate of tungsten (at the same time serving as a nozzle) and a tungsten electrode inside the source can be applied. The high temperature of the gas is a disadvantage, since particles of high velocity are much harder to deflect.

6. Ionization

The ionization takes place by electron bombardment. For this purpose the electrons from heated cathodes are accelerated and sent across the atomic beam one or several times. Until now the yield of ionized atoms is rather low, only 10^{-4} or 10^{-3} is usual.

To increase the electron current density Thirion[4]) makes use of space charge compensation by ions of a metal vapour in a low voltage arc and uses titanium vapour. A strong magnetic field (13000 gauss) is superimposed. The arc can be operated at rather low pressures. The metal vapour does not spoil the vacuum. Moreover it is condensed when striking the wall thus forming a getter surface.

In principle ionization by collisions of the second kind of excited atoms (e.g. He) is possible too, but has not been used so far.

7. Production of Polarized Deuterons

For the production of polarized *deuterons* the same arrangement in principle can be used as in the production of polarized protons. Since, however, deuterons have a nuclear spin 1, the deflection pattern is more complicated. There are 4 plus 2 substates instead of 3 plus 1 which are shown in figs. 1 (and 2).

In a strong field, atoms with quantum numbers

$$m_e = \tfrac{1}{2} \text{ and } m_d = +1, 0, -1$$

will be deflected towards the axis to a circular cylindrical region. After the selection by an apperture the nuclei of the deuterium atoms have a spin population of $\frac{4}{3}, \frac{4}{3}, \frac{1}{3}$ for $m_d = +1, 0, -1$ respectively.

Such a separation has been accomplished by Baumgartner, Brown, Huber, Rudin and Striebel[5]) in Basel. A small part of the separated deuterons was ionized and accelerated to 100 keV by an electric field. They then hit a tritium target. The neutrons out of reaction T (d,n) He^4 have an inhomogeneous angular distribution if the deuterons are polarized. The ratio $\sigma(0)/\sigma(\theta)$ for three angles is simultaneously measured with four scintillation detectors. The necessary correction could be taken into account by comparing the neutron counting rates produced by deuterons from the atomic beam and from molecular gas admission. The population ratio of spin state 0 to the sum of the state + 1 and — 1 is called G; this is a convenient parameter. G is expected to be $\frac{4}{5}$.

Experimentally $G = 0.706 \pm 0.014$ was found. The current of polarized deuterons was about 0.01 mA. That means 6×10^{10} polarized deuterons/sec were produced. In the Basel apparatus 500 neutrons per minute have been counted with the beam on.

The advantage in the production of polarized deuterons compared with that of protons is that the residual gas pressure caused by rubber

[4]) J. Thirion, Basel Symposium, 1960; and private communication.

[5]) E. Baumgartner *et al.*, Phys. Rev. Lett. 5 (1960) 154; and Basel Symposium, 1960.

gaskets, oil diffusion pumps and water vapour has no influence, since these contain only light hydrogen and no neutrons can be produced from them in tritium. The apparatus cannot be baked out. Although it consists of seven sections separately pumped, polarized protons could *not* be produced in it because far too many protons are present in the residual gas.

8. Production of Polarized H⁻ Ions

If it were possible to produce a sufficiently strong current of polarized protons, one could accelerate them by 5–10 kV and produce from them H^- ions by charge exchange. The dependence of the charge exchange cross-section on the energy is known from the revelant literature. There should be no depolarization since there is only a pure Coulomb interaction.

Perhaps it is even possible to add electrons to the neutral atoms in a Duoplasmatron.

9. Lamb Shift

Based on the famous paper by Lamb and Retherford⁶), Savoiskiik⁷) has made the suggestion to use the Lamb shift. The $2^2S_{\frac{1}{2}}$ state of the hydrogen atom is metastable. If it is possible to excite a sufficient number of hydrogen atoms into this metastable state, 50% polarized protons can be obtained in the following manner:

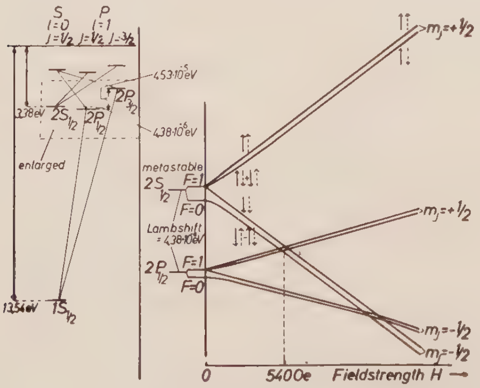

Fig. 7. Zeeman effect of hfs exited state ($n = 2$) of atomic hydrogen.

Fig. 7 shows the level scheme and the energy of the neighbouring substates as a function of the magnetic field. It can be seen that two of the hyperfine levels of the $2^2S_{\frac{1}{2}}$ state and two of the hfs levels of the $2^2P_{\frac{1}{2}}$ state cross each other at a certain magnetic field (the better value is 585 Oe). If there is also a weak electrical field present, a mixture of states occurs (Stark effect). Near the crossover a few volts/cm will suffice for this mixture. A transition will take place from the lower two substates of the *metastable* S-level to the corresponding substates of the *non metastable* P-level. This state will immediately decay to the ground state. Only the 2 higher substates will remain in the metastable state. For the spin and the magnetic moment the same relationships apply as for the corresponding substates in the ground state (as shown in figs. 1 and 2).

The atoms remaining in the metastable state, if ionized in a *weak* magnetic field, will give 50% polarized protons. No atomic beam would be needed and for the ionization of the metastable atom 3.38 eV would be adequate. For the ionization, light quanta of sufficient energy (or may be collisions of the second kind by excited atoms) should be possible. Hydrocarbons, H-atoms and H_2 molecules would thus produce no protons. The life time of the metastable S state is in absence of electrical fields about $\frac{1}{10}$ of a second. Thus those atoms with thermal velocities can travel hundreds of meters before de-excitation, the P state however has a lifetime of only 10^{-9} sec.

The idea behind this scheme is very good, however experience shows that it is hardly possible to excite a sufficient fraction of H-atoms into the metastable state. Under the usual conditions (as in the measurements of Lambshift) this fraction is at a maximum 10^{-4}.

Madansky and Owen⁸) (Johns Hopkins) have prepared experiments to increase the yield in the production of the metastable state $2^2S_{\frac{1}{2}}$. They hope to obtain this by means of charge exchange

---

⁶) W. Lamb and R. C. Retherford, Phys. Rev. **79** (1950) 549.

⁷) E. K. Savoiskiik, J. Exp. Theor. Phys. U.S.S.R. **32** (1957) 731.

⁸) L. Madansky and G. E. Owen Phys. Rev. Lett. **2** (1959) 209; and private communication.

⁹) R. L. Garwin, Rev. Sci. Instr. **29** (1958) 374.

between low energy protons and lithium vapour atoms. Because of the similarity of the wave functions of the electrons of lithium and hydrogen the yield of the metastables should be increased 1000 times beyond the yield in a usual source. It is, however, very difficult to produce protons of such small energy in sufficient intensity. However, even at higher proton energies the yield of metastables should be higher.

10. Molecular Hydrogen

It has been suggested by Garwin[9]) that a beam of hydrogen molecules be sent through a very strong inhomogeneous field. Molecules which have their nuclei *both* parallel or *both* antiparallel to the magnetic field are deflected by the magnet in opposite directions, while those molecules in which the nuclear spins have opposite direction (one nuclear spin up, one down) remain undeflected. Here the *nuclear* magnetic moments are responsible for the deflection. Therefore the deflection is much smaller than in the case of atoms, where the high magnetic moments of the electrons are involved. Therefore very strong magnetic fields and also very narrow slits are needed. On the other hand Garwin argued convincingly that the molecules with polarized nuclei can be stored[10]) for some tenths of a second without depolarization. If such stored amounts of polarized gas molecules are ionized, they can be fed into an accelerator with pulsed operation.

11. Optical Pumping[11])

In the ground state of atomic hydrogen one could succeed in depopulating the hyperfine state with $m = -\frac{1}{2}$ by optical pumping and populating the one with $m = +\frac{1}{2}$. This could be accomplished by *circularly polarized light* of the Lyman-α-line with $h\nu = 10.15$ eV. If this radiation is absorbed by an hydrogen atom in the $m = -\frac{1}{2}$ state, it will make a transition to the $2^2P_{\frac{1}{2}}$ state but only into such substates, in which m is greater by 1. *Two* thirds of the subsequent transitions to the ground state will end in an $m = +\frac{1}{2}$ state, *one* third to $m = -\frac{1}{2}$ state. In due time all the atoms would be in the $m = +\frac{1}{2}$ ground state. This means that we would have achieved the same as in the atomic beam strong field separating method. By ionization in a weak field one can again obtain 50% polarized protons. Unfortunately there is no possibility of producing circularly polarized light of the Lyman-α-line in sufficient intensity.

12. Characteristics of Different Setups

Finally some of the more important aspects of the different apparatuses that were built by various research teams will be mentioned. I follow in general the information given at the Basel conference, July 1960.

In *Erlangen*[12]) most measurements of the intensity are made by the colour change of the molybdenum oxide. If one uses a Wood's discharge (containing water vapour) 10^{14} atoms/cm² sec will give the first indication of blueing after 1 min.

In order to obtain a much stronger atomic beam and a better ratio of beam-to-background signal, experiments were made with a Laval nozzle up to a source pressure of 200 Torr. For the dissociation an arc discharge or RF is needed. In the case of the arc a higher temperature cannot be avoided.

In Erlangen an arrangement is now in operation for dissociation at the last instant prior to the outflow of the particles. Between a cylindrical electrode immediately behind the annular opening, and an annular electrode in front of this opening, a high frequency discharge burns through the nozzle. Thus the recombination is minimalized.

CLAUSNITZER[13]) (Minneapolis) uses a tapered 6-pole field, 25 cm long and an arc discharge for the dissociation. The degree of dissociation is 10–20%. The measurements on the selection of substates were taken with molybdenum oxide or by means of an ionization manometer. These gave the result of 2 × 10^{16} atoms/sec entering the magnet. The polarized atoms travel in an insulated column into 500 kV potential of the intake side of the linac, are ionized there in a weak magnetic field and fed into a linac, whose efficiency is not too high (10^{-5}; i.e. duty cycle 10^{-2}, transmission 10^{-3}).

---

[10]) For the storing of polarized H-atoms cf. N. F. Ramsey *et al.*, Phys. Rev. Lett. **5** (1960) 361.

[11]) A. Kastler, Physica **17** (1951) 191.

[12]) G. Clausnitzer, R. Fleischmann and H. Schopper, Z. Phys. **144** (1956) 336;
G. Clausnitzer, Z. Phys. **153** (1959) 609;
R. Fleischmann, Basel Symposium, 1960.

[13]) G. Clausnitzer, Annual Progress Report, U. of Minnesota (Nov. 1958) and (Nov. 1959); and Basel Symposium, 1960.

KELLER (CERN)[1]) effected the dissociation by means of RF (20 megacycles, 1 kW) in a glass vessel with a glass nozzle, which is cooled by compressed air. Besides the 4-pole field referred to previously, which is designed for the 600 MeV cyclotron, a *second apparatus* has been built. This is a 4-pole weak field model with a narrow atomic beam similar to that in Erlangen. A single component was separated. The atoms of this narrow beam were fed into a small cyclotron, the dees of which were cooled by liquid air. This cooling effectively reduced the water and oil vapour contents of the residual gas. At the centre of the cyclotron the beam is ionized. The cyclotron accelerates the protons to 4.4 MeV. Their polarization is analyzed by elastic scattering in helium. The analyzing power P_2 is taken from papers on double scattering experiments and by means of measuring the scattering asymmetry, which gives the product P_1P_2, the degree of polarization P_1 is determined.

DICKSON and CRADDOCK[2]) (Harwell) accomplished in their experiments the dissociation by an inductively coupled RF (20 megacycles/sec and 400 W) in a glass tube. A prominent characteristic of their apparatus is the before mentioned multichannel collimator glass nozzle. The 6-pole magnet (40 cm long) is as close as possible to the source and the magnet chamber is divided into 4 separately pumped sections. The most striking external feature is the pumping system: 6 oil diffusion pumps are arranged round the main vacuum vessel, containing the magnet and ionizer. The RF device for a transition between component 2 and 4 can be built in later. 1 – 5 × 10^{15} polarized atoms/sec leave the magnet. These are, however, spread over 9 mm diameter. The ionizer efficiency is small, the linac efficiency rather high (8 × 10^{-4}). It is expected that around 2 × 10^{8} protons/sec can be utilized. The experimental scheme gives 50% polarization. From measurements of the ion current with the atomic beam on and off the unpolarized proton background is determined. Taking this and other corrections into account, the protons should be 39% polarized.

The work of the Basel group has already been referred to (section 7). In their work the ionizer efficiency was 10^{-5}.

For the selection of substates a Rabi apparatus can be used. In an ordinary Rabi setup the A-magnet and the B-magnet have antiparallel gradients. If no radio frequency is applied in the C-field all particles are transmitted. One can also use a A- and B-magnet with parallel gradients. Without radiofrequency in the C-field no particles are transmitted at all. With an RF field in the C-magnet transitions into other substates can be effected and atoms are transmitted.

V. HUGHES[14]) (Yale) uses such an apparatus to flop in one substate of deuterium. He has very strong and short permanent magnets. His A-field is 2 cm, C-field 11 cm and B-field 6 cm. The distance between source and detector is only 36 cm. In the Wood's discharge 60–90% of the molecules are dissociated.

SHERWOOD[15]) (Oak Ridge) uses the same type of apparatus but he wants to separate hydrogen. Radio frequency transitions are effected in the C-field between components 2 and 3 and 3 and 2 respectively. This means that both components are flopped in. Thus these 2 components are separated off and ionized in a strong field to give almost 100% polarized protons.

THIRION[4]) (Saclay) uses and RF source for dissociation similar to that of Keller, a tapered 6-pole field, and an RF transition from 2 to 4. His scheme is based on a proposal by Abragam and

---

[14]) V. Hughes, Brookhaven Conference, 1959; and Basel Symposium, 1960.

[15]) J. E. Sherwood and Overshain, private communication.

Winter[16]), the object of which is to cause the radio frequency to induce only transitions from component 2 to 4, but not from 4 to 2. The polarization (of the neutral atoms) attained was checked by a strong Stern-Gerlach field behind the separator magnet. The beam intensity decreases at the transition frequency of component 2. From this a degree of polarization of atoms of 62 ± 5% could be calculated. The beam is measured by an ionization manometer, the compression factor of which is 70. His ionization method which uses a titanium low voltage arc is already mentioned in Sect. 6.

These are the experiments made. Only the future can prove which way is the best to get polarized protons with sufficient intensity.

DISCUSSION

Speaker adressed: R. Fleischmann (*Erlangen*)

Question by: H. E. Gove (*Chalk River*)

Question: What are the possibilities for producing polarized negative ion beams for tandem accelerator use?

Answer: If a sufficiently strong beam of polarized protons is produced, these protons can be accelerated to the order of about 20 keV and then a part of them transformed by charge exchange into H⁻ions and fed into a tandem.

---

[16] A. Abragam and J. M. Winter, Phys. Rev. Lett. **1** (1958) 374.

NUCLEAR INSTRUMENTS AND METHODS 11 (1961) 122–125; NORTH-HOLLAND PUBLISHING CO.

MILLIMICROSECOND PULSING

RICHARD J. CONNOR

High Voltage Engineering Corporation, Burlington, Massachusetts, U.S.A.

Apparatus for the production of short intense bursts of positive ions is in an early test stage at Burlington.

The positive ion pulses are generated in the terminal of a 3 MV accelerator by deflecting a D.C. beam across a small aperture. The pulses after acceleration are swept across a Mobley type compression magnet.

The pulses generated in the terminal are of 1 mA intensity and 10 mμs duration: on traversing the post acceleration compression magnet the pulses will be compressed in time by a factor of 10 with the resultant increase in beam intensity to 10 mA.

Some of the design considerations and anticipated problem areas are discussed.

In recent years there has been increasing interest in the generation of intense bursts of neutrons of short time duration for many diverse applications in nuclear physics. In general the neutron pulse should be of the shortest practical duration and accordingly there is a desire for high intensity during the pulse and a minimization of events between pulses for greater ease in interpretation of the data.

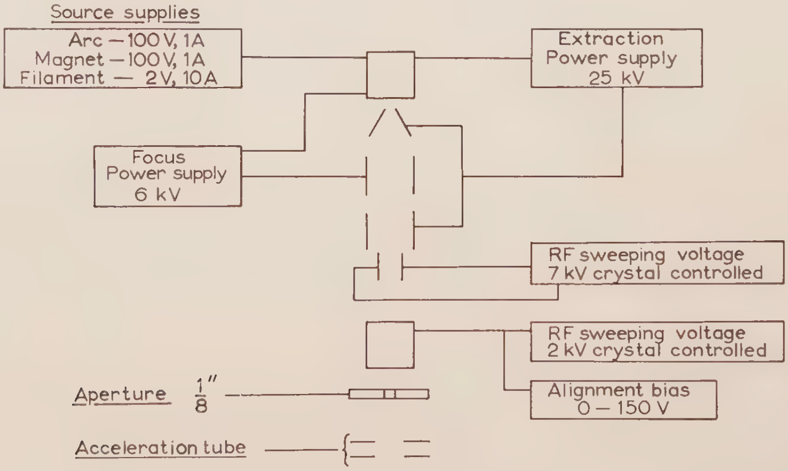
Source supplies
Arc — 100 V, 1A
Magnet — 100 V, 1A
Filament — 2V, 10A
Extraction
Power supply
25 kV
Focus
Power supply
6 kV
RF sweeping voltage
7 kV crystal controlled
RF sweeping voltage
2 kV crystal controlled
Alignment bias
0 — 150 V
Aperture $\frac{1}{8}''$
Acceleration tube

Fig. 1. Terminal deflection pulsing.

Considerable work has been carried out in pulsing the various ion sources used in accelerators; however, the production of ion bursts of duration shorter than a few microseconds involves increasingly complex electronics of prohibitively great power consumption in the generally inaccessible high voltage terminal. This technique must also become limited when the pulse duration required becomes comparable to the plasma formation time.

A technique that has enjoyed considerable success is to deflect a D.C. beam across a suitable aperture after acceleration to high energies and this post acceleration chopping of the beam will doubtless continue to enjoy great popularity.

As the bombarding energy is increased and especially in those cases using deuterium as the projectile, the question of the large background between pulses assumes increasing importance and eventually a point is reached where the deuterium imbedded in the limiting aperture under bombardment creates an intolerable background between pulses. Additionally, the intensity during the pulse is limited to the D.C. operating value of the accelerator.

A second method is to generate the pulses by chopping an intense D.C. beam in the high voltage terminal at low energies (approx. 30 keV) and then to accelerate the bursts to high energy. This technique should allow the generation of pulses of considerably greater intensity with quite free backgrounds. Fig. 1 schematically illustrates this technique. There are, however, limitations on the system.

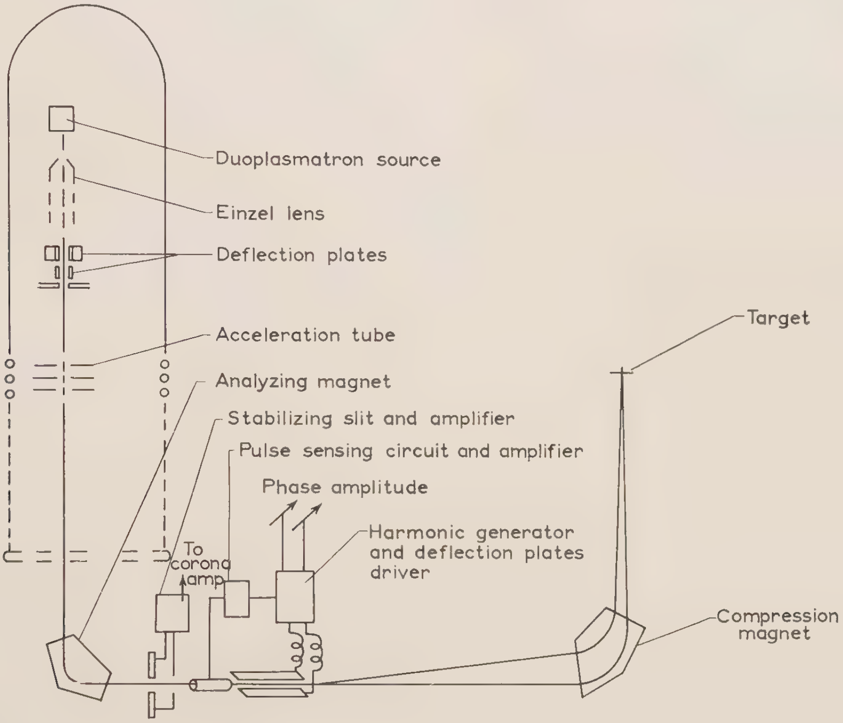
Duoplasmatron source
Einzel lens
Deflection plates
Acceleration tube
Analyzing magnet
Stabilizing slit and amplifier
Pulse sensing circuit and amplifier
Phase amplitude
Harmonic generator and deflection plates driver
To corona amp
Target
Compression magnet

Fig. 2. Schematic diagram of millimicrosecond pulsing equipment.

Under D.C. conditions, a particle experiences zero net space charge force along the optic axis. When the beam is chopped, however, the leading and trailing boundary of the pulse experience forces tending to accelerate the former and retard the latter. The velocity spread tends to lengthen the pulse in its travel through the accelerator. The effect is negligible for pulses in the microsecond region but becomes serious for pulses in the millimicrosecond region. At the energy of formation of the pulses, say 30 keV, a millimicrosecond proton pulse has an axial dimension of approximately 1 cm. In principle, the space charge effects can be calculated. In practice, the influence of electrons in the beam region presents a serious unknown and the calculations are of dubious validity. Experience would indicate, however, that space charge effects are present and while calculations always give a pessimistic answer, the space charge forces set an upper limit to the pulse intensity for a given pulse duration. Practice would indicate that a 10 mμsec pulse is limited to 1–2 mA.

In view of the above considerations, the system originally suggested, in essentially its present form by Cranberg¹), has been adopted.

To produce intense bursts, it is contemplated that terminal deflection pulsing will produce relatively long bursts of ions of intensity such that the space charge pulse lengthening may be avoided. The bursts after acceleration are shortened by post acceleration compression.

¹) L. Cranberg, Private communication.

Systems such as Klystron bunching involve, at the energies under consideration, inordinately long apparatus as well as introducing considerable energy spread into the beam. The alternative is to sweep the pulse over the face of a Mobley[2]) type compression magnet where the leading surface of the pulse traverses a longer path than the trailing surface and is brought to the target in time considerably shorter than the pulse duration produced at the terminal. Such a system is shown in fig. 2.

It is necessary that the ion burst arrives at the deflection plates with a certain phase relationship to the deflection wave form. While synchronization can be obtained by employing a signal derived from the terminal oscillator, the problems involved in transmitting this signal and in variation in pulse arrival time at the deflection plates due to variation in particle species and energy would complicate the design.

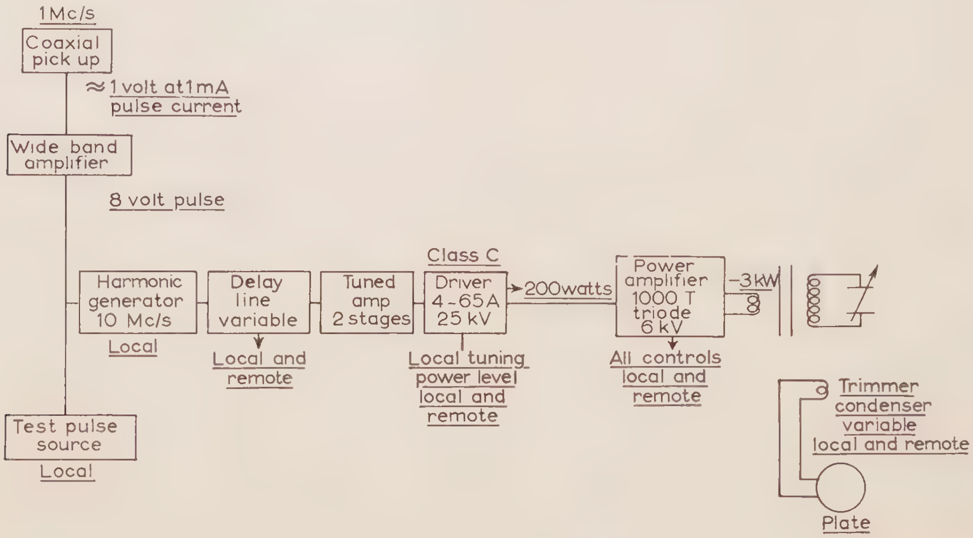
1 Mc/s
Coaxial pick up
≈1 volt at 1 mA pulse current
Wide band amplifier
8 volt pulse
Harmonic generator 10 Mc/s
Local
Delay line variable
Local and remote
Tuned amp 2 stages
Class C
Driver 4-65A 25 kV
Local tuning power level local and remote
200 watts
Power amplifier 1000 T triode 6 kV
All controls local and remote
-3 kW
Trimmer condenser variable local and remote
Plate
Test pulse source
Local

Fig. 3. Deflection voltage generating circuit.

The deflection and sensing elements are shown in fig. 3.

A signal is derived from a coaxial pick-up positioned just prior to the deflection system. The signal is amplified and triggers a harmonic generator.

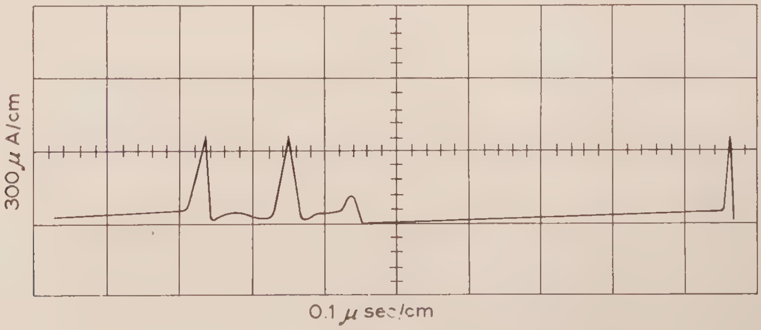

Fig. 4.

The decaying sinusoidal signal from the harmonic generator is fed to a variable delay line for proper phasing with the ion beam pulse and amplified to drive the deflection plates.

A saw tooth wave form would, of course, be most desirable; however, the generation of this wave shape at the high voltages required would require an enormous expenditure of power. To avoid this, a sinusoidal wave form has been chosen with the beam deflected either side of the axis when the sine wave is approximately linear. At the frequency chosen, 10 Mc/s, the maximum departure from linearity of the used portion of the sine wave will be 4% for a period of 10 millimicroseconds. As an example, a peak R.F. potential of 45 kV applied to deflector plates 20 cm long and separated by 1 cm will deflect a 3 MeV proton beam $\pm 2\frac{1}{4}°$. A 90° double focusing symmetrical magnet of 30″ radius of curvature with object and image at 60″ from the magnet face will then compress a 10 millimicrosecond pulse to 1 millimicrosecond.

---

[2]) P. C. Mobley, Phys. Rev. **88** (1952) 360.

The desirability of analysis of the ion beam prior to compression is illustrated in fig. 4. The oscillograph display is a 10 millimicrosecond pulse from a test apparatus at 25 kV. The velocity separation of the 3 components of the hydrogen beam should be noted and since the atomic and molecular components are approximately equal in magnitude, the two pulses will generate erroneous signals and cause difficulties in the operation of the deflection circuits. The oscilloscope used in this test has a rise time comparable to the pulse duration and the pulses are smeared in time.

An example of the pulse obtained with the entire system is shown in fig. 5. The upper pulse is with a small RF potential on the deflecting plates, the lower with near optimum RF voltage, beam energy 3 MeV. The rise time of the sampling oscilloscope is 0.4 millimicroseconds.

The compression achieved will depend in large measure on the beam quality and size in the region of the deflection plates and this has been exhaustively studied by Fowler and Good[3]) and by Neiler and Good[4]).

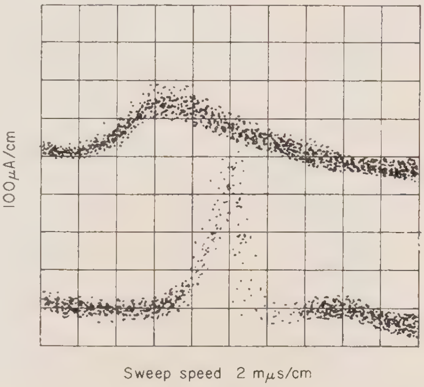

Fig. 5.

In general there is an energy spread introduced by the sweeping voltage that depends on the beam quality sweeping amplitude and energy spread that under unfavorable conditions may approach 10 keV for a 3 MeV particle.

[3]) T. K. Fowler and W. M. Good, Nucl. Instr. and Meth. 7 (1960) 245.

[4]) J. H. Neiler and W. M. Good, Time of-Flight Techniques, in Fast Neutron Physics, Part 1, Eds. J. B. Marion, J. L. Fowler, p. 509–621.

NUCLEAR INSTRUMENTS AND METHODS **11** (1961) 126–135; NORTH-HOLLAND PUBLISHING CO.

RECENT ADVANCES IN HIGH POWER MICROWAVE ELECTRON ACCELERATORS FOR PHYSICS RESEARCH

J. C. NYGARD

High Voltage Engineering Corporation

and

R. F. POST

University of California, U.S.A.

There have been some large steps forward in the microwave electron linear accelerator art. More power, precision and versatility than heretofore are now available for use in the search for further fundamental knowledge in nuclear structure. A number of very high current linear accelerators of great precision are described, among which are the following 1. a 10-MeV synchrotron injector having 200 mA of pulse current with an energy spread of 1 % and a divergence of less than 1 milliradian; 2. a 35-MeV with pulse currents up to 500 mA and 30 microsecond pulse length offering 2×10^{12} neutrons *per pulse*; 3. a very new 130-MeV linear accelerator for the U.S. National Bureau of Standards. A breakthrough in the problem of "beam blow-up" and its possible origin in TM 110 mode excitation is described. New accelerating structures have been employed to advantage in the elimination of this problem. A new and potentially useful R.F. power tube called the Amplitron is just emerging, and its attractive features are described. Techniques are now available for microwave linear accelerators of arbitrarily great precision and power output.

There have been some significant steps forward in the microwave accelerator art, which is fortunate, for the electron linear accelerator is an ideal tool for neutron and photonuclear physics in the energy range from 15 to about 200 MeV.

The search for further fundamental knowledge in the fields of nuclear, atomic and molecular structure continues with increasing demands for experimental versatility, precision and power. Much of the existing useful data in this energy range has been taken with orbital accelerators of limited power output. As a consequence of this, the experimental substantiation of theoretical understanding of photonuclear interactions and other interactions is lacking in detail. To obtain data indicating more than general effects requires at least *one order of magnitude* improvement in accelerator precision, and *several orders of magnitude* improvement in experimental yield or power output from the accelerator.

Several high power electron accelerators now under construction, including one for Yale University, one for Rensselaer Polytechnic Institute, and for the U.S. National Bureau of Standards, are well suited to meet such requirements. The features of some of these recent machines may be of interest.

Fig. 1 shows a single section accelerator 5 feet long which was constructed as an injector for the electron synchrotron at Cornell university in the U.S. It operates at a wavelength of 23 cm. As a synchrotron injector it was required to pass its beam through an aperture 6 mm in diameter with a beam divergence of less than 1 *milliradian.* It was to operate at 10 MeV and have ac pulse current of 200 mA within a total energy spread of 1 %. It has met and *exceeded* all of these requirements. The nominal pulse length is one microsecond. At shorter pulse lengths this accelerator design has produced pulse currents in excess of 2 *amperes!* Other points of interest in this picture are the 200 kV injector, and the R.F. power input, and the R.F. water load. The rectangular R.F. waveguide shown is pressurized with freon.

Fig. 2 shows a five section accelerator now in operation at the university of California, U.S.A. It produces a beam pulse intensity of up to 500

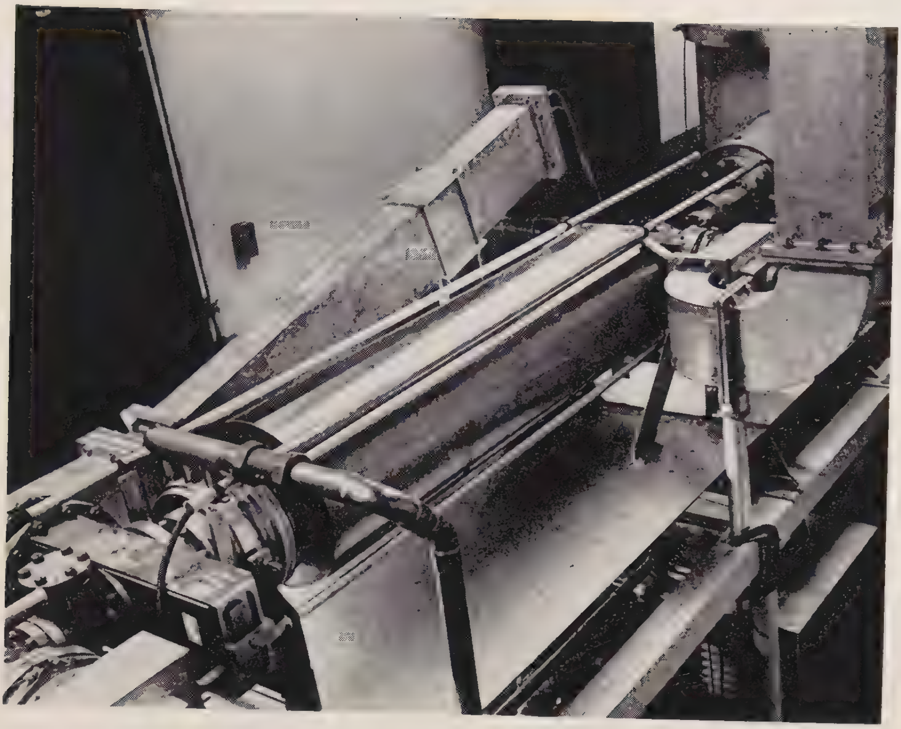

Fig. 1.

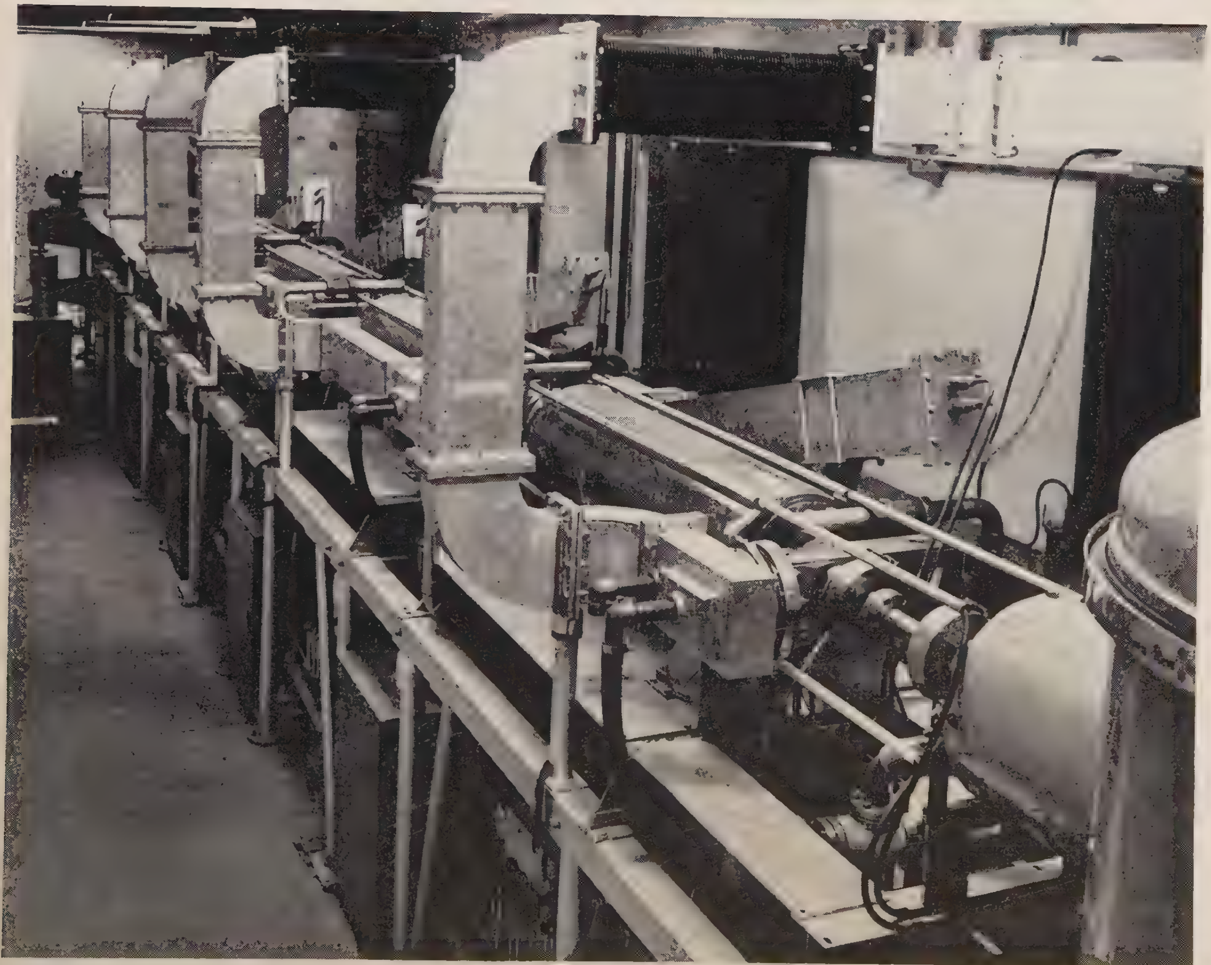

Fig. 2.

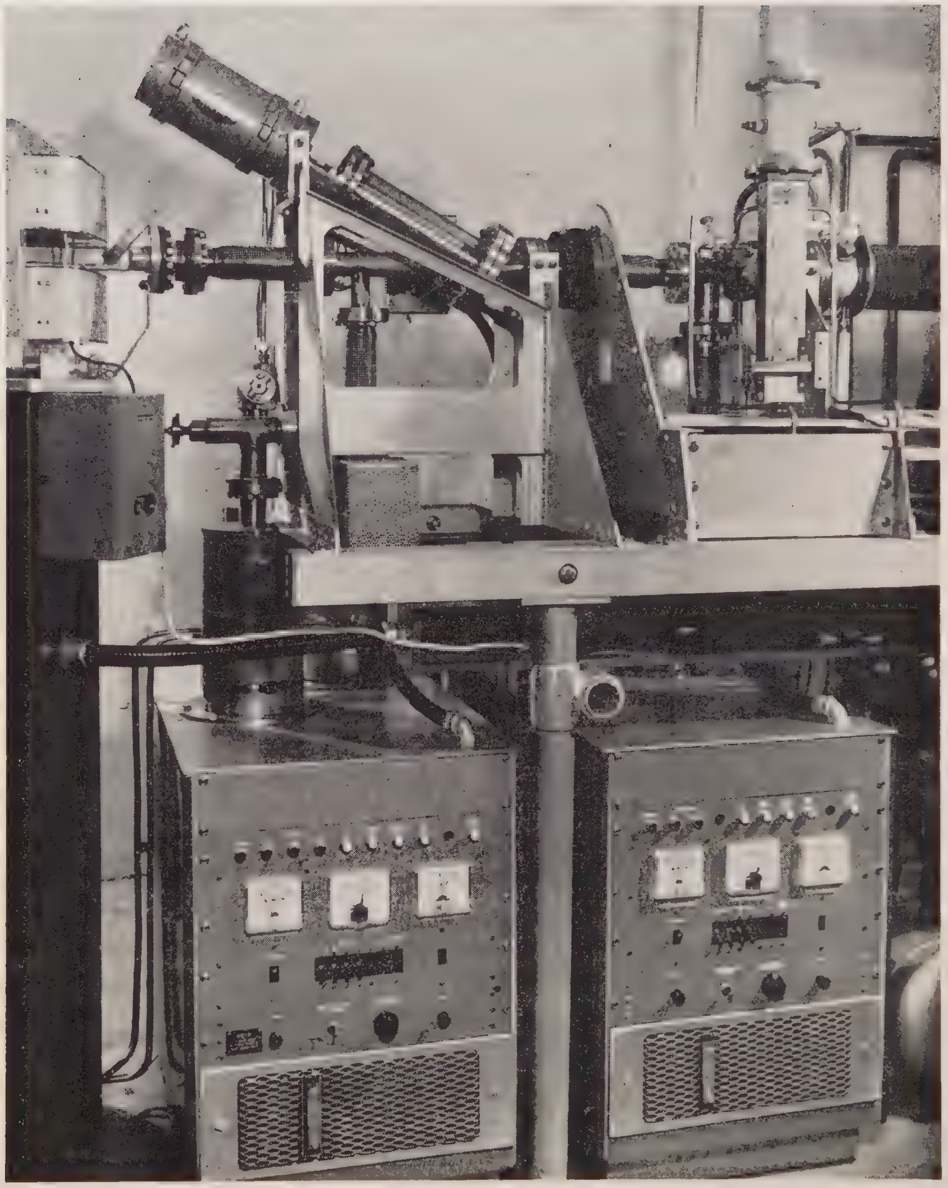

Fig. 3.

milliamperes at a pulse length of 30 *microseconds.* The energy is 35 MeV. It is believed that this is the longest pulse duration of any electron microwave linear accelerator in existence. With suitable targets a yield of more than 2 × 10^{12} neutrons *per pulse* is to be had. As a gamma source, more than 50 roentgens *per pulse* at 1 meter is to be had.

Another accelerator, similar to the one shown, for Yale university, is presently under factory test. It has already produced long pulse currents in excess of 500 mA, and short pulse currents well in excess of *one ampere* at an energy of 60 MeV.

Some of the structural details may be seen. The 200 kV injector is in the lower righthand corner. The output end of this accelerator far to the rear is shown more clearly in fig. 3.

Fig. 3 shows an essential component of any linear accelerator used in an experimental research program. It is a quick closing, *all*

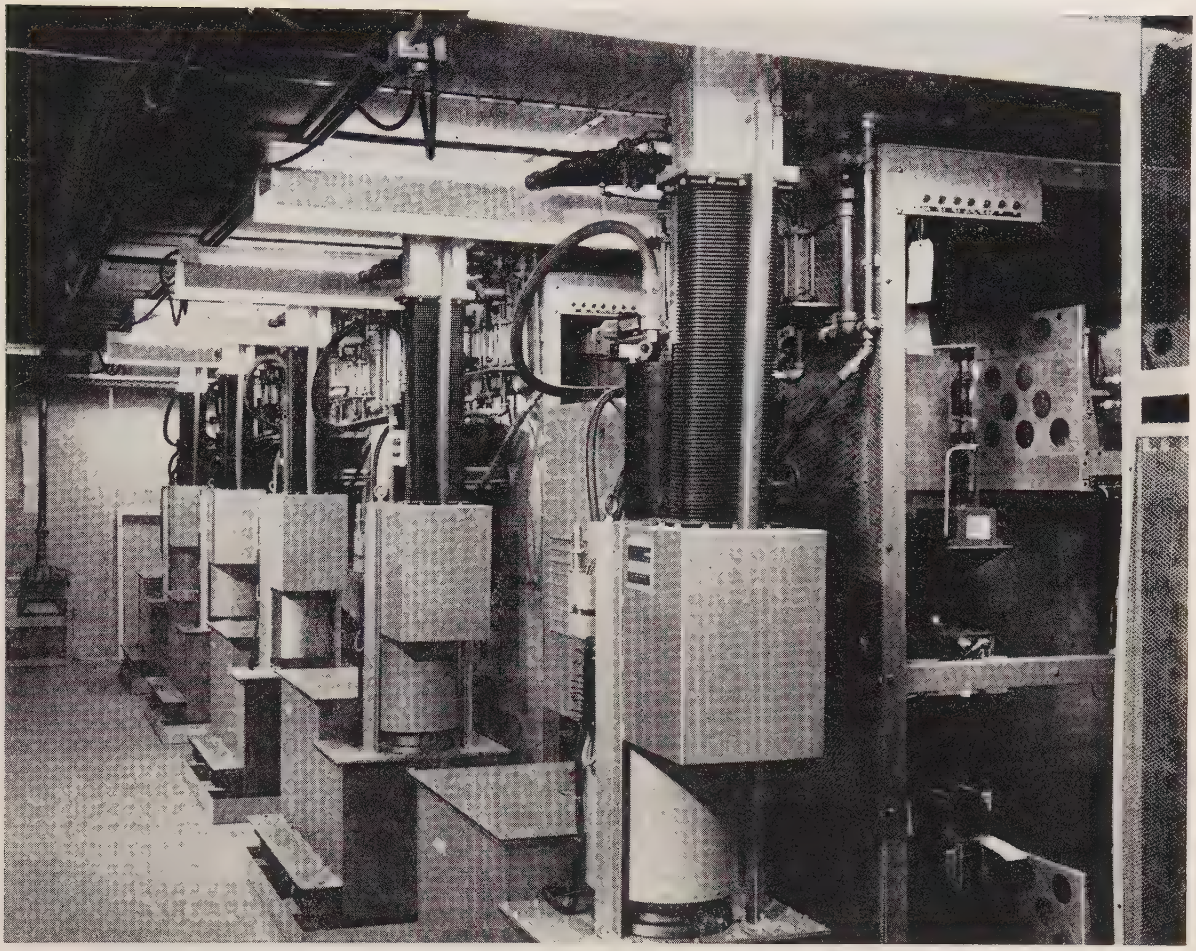

Fig. 4.

metallic, vacuum valve. Its function is the rapid close-off of the accelerator vacuum system in the event of vacuum loss in the users experimental apparatus. In this connection it might be emphasized that the entire vacuum systems for the accelerators shown are metal including gaskets. *No organic gaskets are used whatever*. This is absolutely essential to the attainment of vacua better than 10^{-7} mm of mercury.

Fig. 4 shows the high power klystron and modulator room for the accelerator previously shown. The enclosure is completely filtered and double screens form minimum leakage of pulse and R.F. interference, Sensitive users instrumentation is often jammed by pulse interference from high power electron linacs unless great care is taken in system design.

Fig. 5 gives one a closer look at one of the klystrons and high power modulators within the screened enclosure. The number of capacitors shown give an indication of the energy storage required in the 30 microsecond pulse forming networks. A large number of sections, and great care in the trimming of the pulse forming network is *essential* for the attainment of pulses flat to better than *one percent*.

Fig. 6 shows the "klystron alley" for another very large physics research linear accelerator just entering its test phase. It is a nine section machine for Rensselaer Polytechnic Institute at Troy, New York. Each of the klystron units are similar to the one in fig. 5.

Fig. 7 is the control console for the same accelerator. When completed, the R.P.I. accelerator

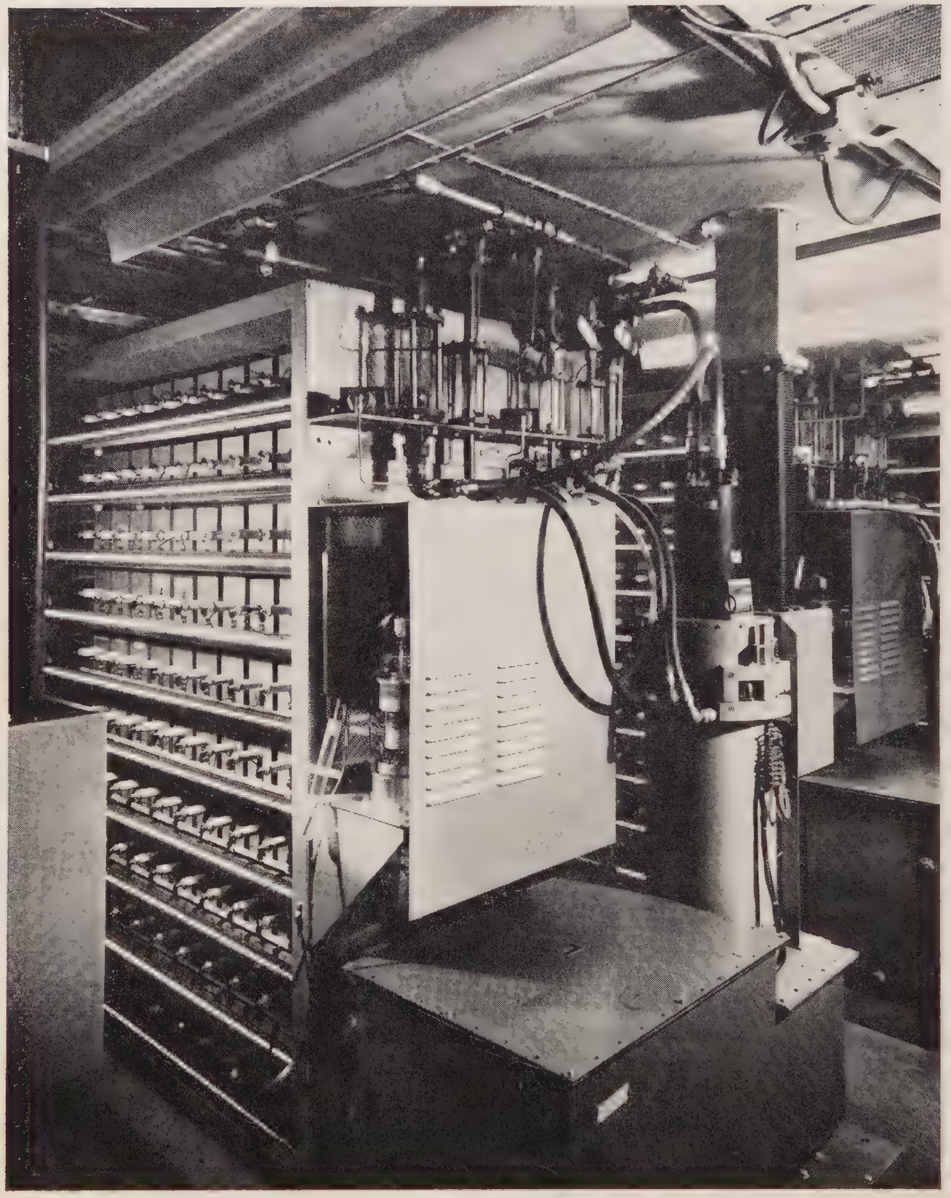

Fig. 5.

tor is expected to be one of the most powerful electron lineacs in the world for several years. With a beam power of 60 kilowatts it will be superseded only by the accelerator for the U.S. National Bureau of Standards now being designed.

Fig. 8 is a drawing of the installation of the 130 MeV electron linear accelerator now under design for the U.S. National Bureau of Standards, and to be installed at the Bureau's new site at Gaithersburg, Maryland. The objective specifications for this accelerator assure its future role as one of the worlds most powerful and important research tools. It will be initially powered by twelve R.F. power tubes of advanced design, and will have an overall length of nearly 100 feet.

The achievement of such performance specifications discussed, and particularly those for the new N.B.S. accelerator, requires careful design,

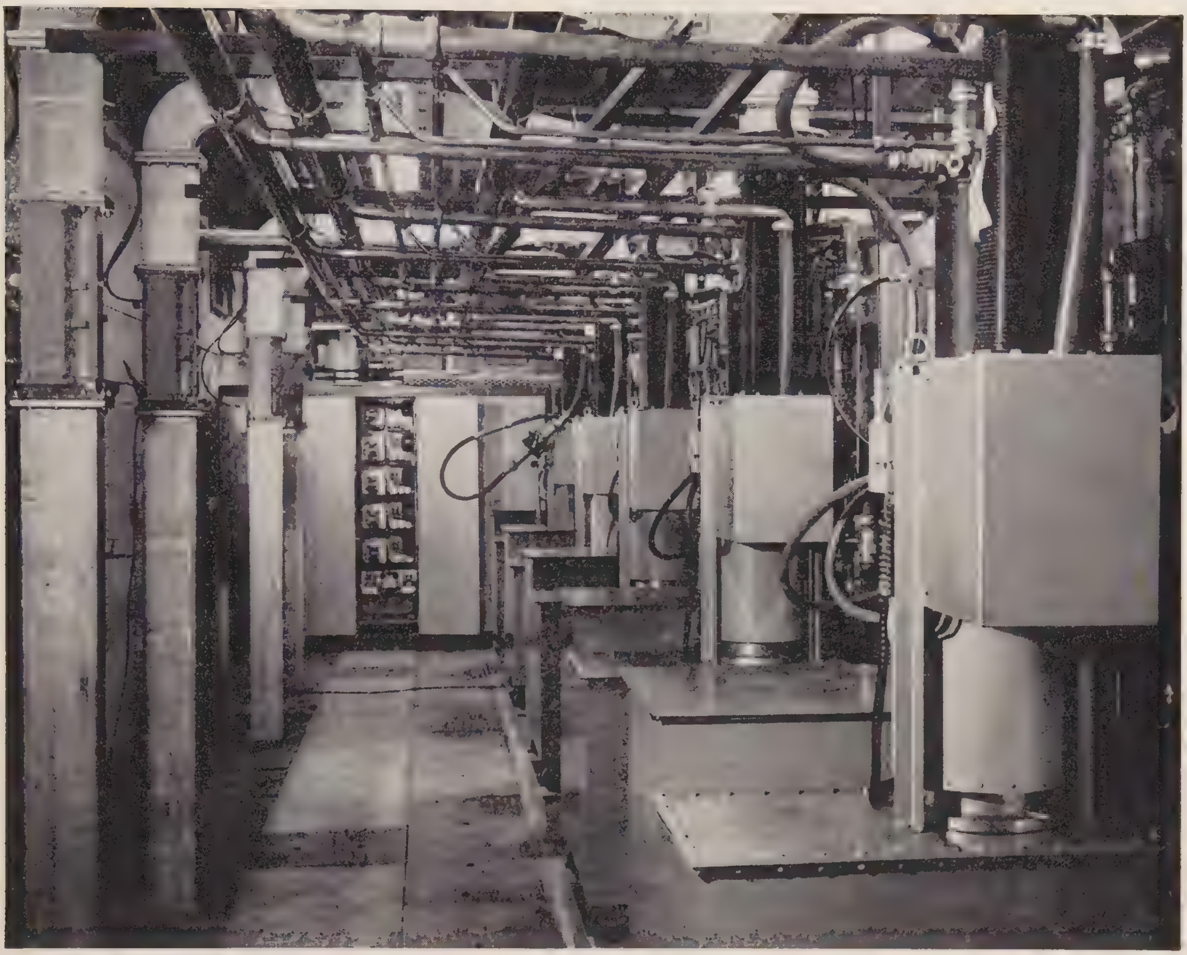

Fig. 6.

and it might be interesting to review some of the requirements.

The inherent energy spread of *any* accelerator, in order to be useful, must be minimized. The general objective for physics research is for as large a fraction of the total electron beam as possible to be contained in an energy "bin" of 1% or less. In a large linear accelerator, one of the major contributors to energy spread, is excessive phase spread of the electron "bunches" on the R.F. wave. Less than 10 degrees is essential. A number of techniques employed for the compression of phase, inclusing a unique chopper-bunches-system, are available. Ideally one would like to compress the phase spread to the point, where, for computational purposes, the electron bunches could be considered as *one fat electron!*

The Chopper-buncher system mentioned is expected to do just this. Fundamentally it consists of an injector system which supplies tightly bunched pulses at the microwave frequency to the first section of the accelerator instead of the usual continuous current. Briefly it consists, in one configuration, of a klystron velocity type bunches system, followed by a "chopper section" which rejects all electrons outside established phase limits. Trajectory computations from the differential equations of motion for such a system have been made using an IBM 650 digital computer. All of the various parameters have been carefully explored, and it is possible to obtain phase *acceptance* over more than 250 degrees, and phase compression to bunches which are *remarkably* small. These analytical

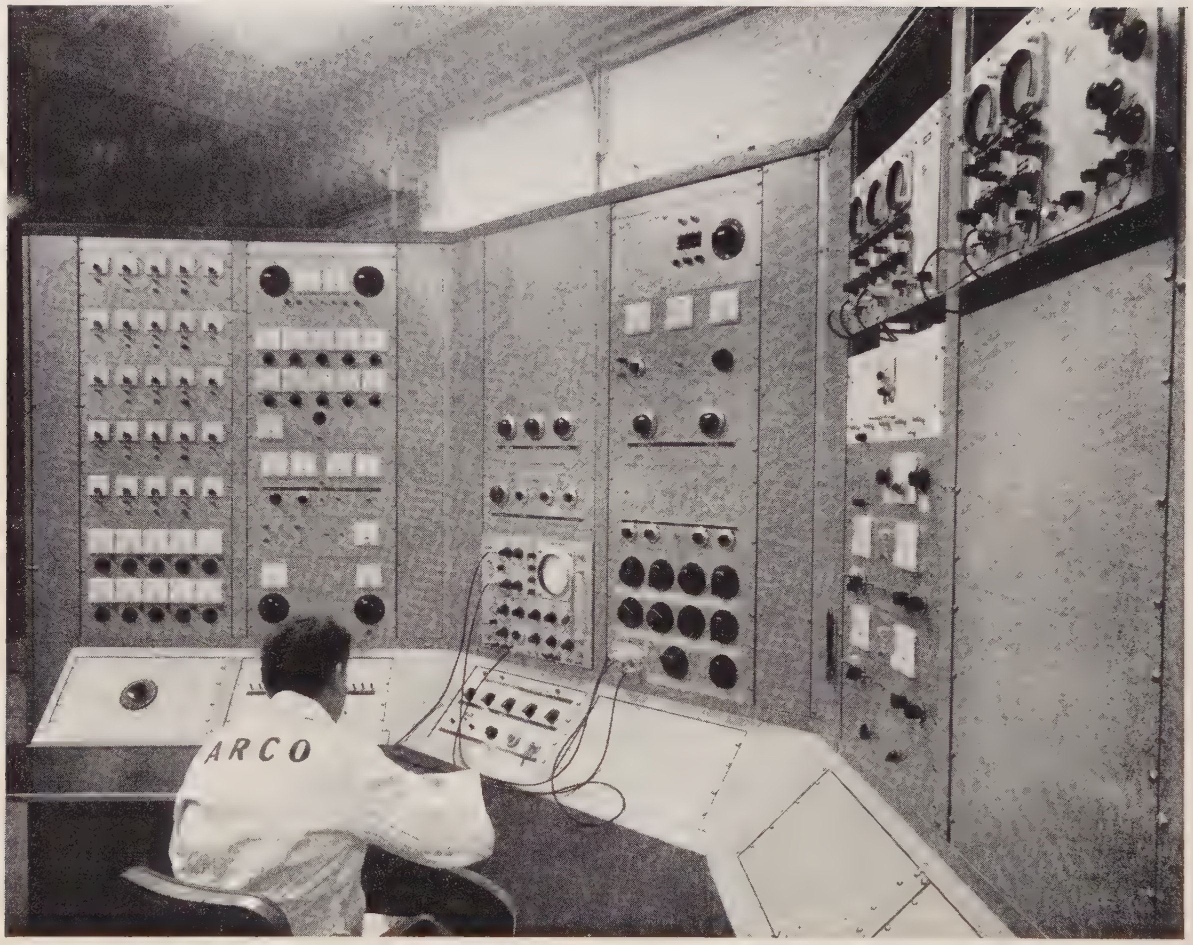

Fig. 7.

determinations are soon to be substantiated experimentally on an injector test stand now under construction for the N.B.S. linac program.

There is one other method for the reduction of energy spread due to phase spread by a post acceleration de-bunching method reported in the in the literature, but this will not be discussed in this paper.

Another major contributor to linac energy spread is electric field modulation or variations. These result from *R.f.power variations* during the pulse, *phase modulation* during the pulse, and *beam current transients*. In order to minimize these effects, beam and R.F. pulses of exceptional flatness—better than a small fraction of 1% are required. Often supplementary electronic regulation to pulse forming networks is utilized to further minimize pulse ripple and droop. The N.B.S. pulsers will additionally employ a system using inverse current feedback control on the R.F. power tube itself, assuring the best pulse flatness that present electronic art will permit.

Equally essential to experimental precision is *long period stability*. The system average stability must be as good as or better than the stability conditions during the pulse. Meaningful experiments of many hours duration require a stabilization of mean energy and current to much better than 1% if an overall resolution approaching 1% is sought. Aside from the expected stabilization of all voltages and currents previously mentioned, a very high order of stability over long periods for *frequency*, *temperature* of waveguide and *line voltage* is required. Frequency

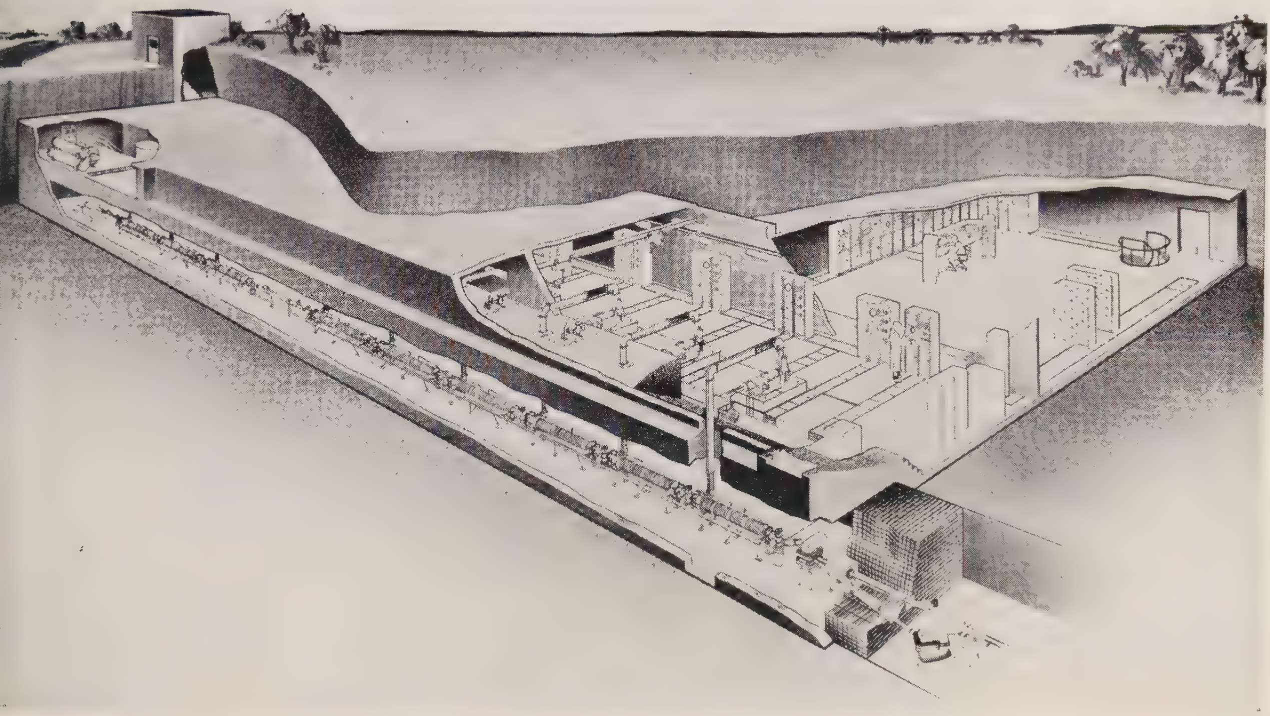

Fig. 8.

and temperature variations lead to phase slip between the electron bunch and the R.F. wave. A stable C.W. frequency source with an average variation of a few parts per million with automatic frequency control is indispensable. A waveguide water temperature control system holding temperature variations to less than 0.5 degrees with excellent response time is also a must since temperature and frequency variations are indistinguishable in effect. Transient surges in main line power lead to disruptive beam variations without careful regulation. A system affording complete isolation and a high order of regulation employing rotating machinery is presently utilized on the high power accelerators mentioned earlier.

The reliability and stability of microwave linear accelerators is also influenced by the accelerator frequency or wavelength. Out of necessity the linear accelerator art has been very much dependent upon the development of the high power radar art for many of its components, particularly the very large radio frequency power tubes.

Commercial microwave linear accelerators have been built with operating wavelengths of 3 cm, 10 cm and 23 cm. These have been called X, S and L bands respectively. While high power accelerators for physics will clearly not be built on X band, the choice between S and L band is not always an obvious one. There are *substantial* advantages to L band accelerators, one of which is a higher electron trapping efficiency at the input end of the accelerator, resulting in more of the injected current being usefully accelerated. Another advantages lies in the increased beam aperture available as compared to shorter wavelength accelerators, which makes possible the acceleration of very high pulse currents. As was mentioned, short pulse peak currents well over 2 amperes have been measured. It is *not known* how *far* this technique may be extended since the limitations observed to date have all arisen in the electron gun itself, and *not* in the accelerating structure of its focussing system.

All of the scaling laws, by which one would expect to predict L band performance, have been

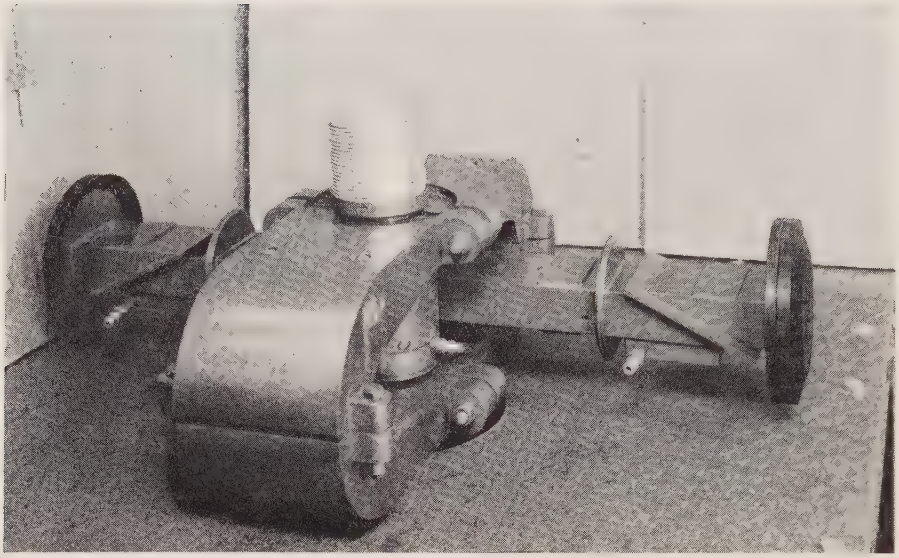

Fig. 9.

checked. Most of these behave as expected particularly the trapping efficiency. Others exhibit anomolies.

A disadvantage of longer wavelength accelerators lies in the reduced shunt impedances in the resonant structure that are obtainable. However this is more than offset *at present* by the greater R.F. Peak Power available at L band frequencies.

It is well known that for a given peak R.F. power that the maximum electron energy increases as the fourth root of the frequency, therefore as reliable R.F. power sources of *equal* capability are developed, one would expect a trend toward *higher* frequencies where *energy* is a prime requirement. Where *peak pulse current intensity* is a prime requirement, the *longer wavelength* accelerators will always be superior. The rapidly closing gap of R.F. power sources, and superior accelerating structures, may yet favor some *other* frequency in the future which may lie intermediate between L and S band.

A linear accelerator of high average and peak beam power demands microwave R.F. power tubes having *substantial* mean R.F. power as well as *high* peak pulse power output. Early linear accelerators were powered by magnetrons having peak power output of 1 to 2 megawatts and mean power outputs of 1 to 2 kilowatts. More recently S band accelerators have utilized klystrons with peak powers of 2 to 5 megawatts and mean powers of up to 10 kilowatts. *Outstanding* klystrons offering 10 megawatts peak power and 15 kilowatts average power are presently employed on several new powerful L band accelerators, which you have seen. This year, culminating more than six years of develop-, ment, there has emerged another R.F. microwave power tube called the Amplitron. Its characteristics seem to be ideally suited to high power research accelerators. One S band Amplitron with a peak power capability of 3 to 5 megawatts, and a mean power of 15 kilowatts is presently employed in several new accelerators. L band amplitrons rated at 10 megawatts peak power and 20 kilowatts average power are presently undergoing life tests, and are under consideration for use in the N.B.S. accelerator. A high power research accelerator requires a number of such R.F. power tubes, and the efficiency with which dc power is converted to R.F. power is one important consideration in maximizing performance as a function of accelerator cost. Where klystron efficiency is characteristically 30 to 40 percent, the efficiency of the Amplitron is 60 to 80 percent.

Fig. 9 shows a 10 cm Amplitron rated at 3 megawatts peak power and 15 kilowatts average power. Contrast its physical size to any 15 kilowatt klystron and it appears deceptively simple.

Another efficiency of importance to the linear accelerator art is that with which R.F. microwave power is converted to electron beam power in the acceleration process. This figure has been typically 40 to 50 percent in the past. Several *new* accelerating structures have been investigated and two new designs having *substantially* lower losses are now employed, permitting accelerator designs having a conversion efficiency of 75 to 80 percent if desired.

Having mentioned new accelerating structures, there is what would appear to be a *substantial breakthrough* in the problem of linear accelerator beam instability. It can be shown that the theoretical maximum efficiency in the conversion of microwave energy to electron beam power is realized when the beam current magnitude is such as to "load" the accelerator energy down to one-half the energy at vanishing current. This efficiency has only been demonstrated on L band accelerators to date. Maximum power obtainable on S band has previously been *limited* by a phenomenon known as "beam blow-up" or as referred to by early British linear accelerator designers "beam stalling". This phenomenon has been the subject of much conjectural thought, and mathematical analysis. While direct evidence is still lacking, supporting evidence and analysis strongly suggests the *Beam Blow-up is caused by the accelerator oscillating as a backward wave oscillator of the transverse type in the TM 110 mode.* Two new accelerators, operating at S-band, have been built using a *new accelerating structure* believed to be incapable of supporting this mode, and have *successfully* demonstrated the achievement of theoretical maximum efficiency *without any limitation* imposed by radial beam instability. Mode suppressors for conventional accelerating structure are also possible and are under investigation.

Now a final word about the reliability. An electron accelerator with power output capability of 30 to 100 kilowatts produces a very intense gamma and neutron flux as is its purpose. This environment brings about radiation damage and access problems. The structure becomes radioactive, radioactive atmospheric gases are produced, organic materials disintegrate, electronic components fail, etc. To say that a several million dollar instrument such as an accelerator must be characterized by a high degree of reliability is an understatement. However, the means to its attainment is not necessarily clear. One thing is certain. Adequate component and circuit design margins are *vital.* Present advanced accelerators through experience in component design are demonstrating reliability to a degree previously unrealized in highly specialized research equipment. That techniques are now available for linear accelerators of arbitrarily great precision and power output is evidenced in the proposed accelerator, two miles in length, soon to begin in construction at Stanford University.

Acknowledgements

The Authors are indebted to Dr. R. L. Khyle of M.I.T. for the analytical study leading to the suspicion of the TM 110 mode in the beam blow-up problem.

We are also indebted to the staff of the Applied Radiation Corporation, without whose assistance this paper would not have been possible.

PHYSICS AND RADIATION RESEARCH (I)

(October 6, 1960) pp. 137-184

PHYSICS

Chairman: K. SIEGBAHN

University of Uppsala, Sweden

CONTENTS

GONSER, U. AND LÜCKE, K. The Use of Van de Graaff Accelerators for High Intensity Neutron Irradiation of Metals 139

BECKURTS, K. H. Reactor Physics Research with Pulsed Neutron Sources 144

AMMAN, FERNANDO The KS-3 MeV Van de Graaff Injector of the Frascati Electron Synchrotron 169

KISTEMAKER, J. On Ion Sources with High Efficiency and Intensity 179

NUCLEAR INSTRUMENTS AND METHODS **11** (1961) 139–143; NORTH-HOLLAND PUBLISHING CO.

THE USE OF VAN DE GRAAFF ACCELERATORS FOR HIGH INTENSITY NEUTRON IRRADIATION OF METALS

U. GONSER and K. LÜCKE

Institut für Reaktorwerkstoffe der Kernforschungsanlage Jülich und Institut für Allgemeine Metallkunde und Metallphysik der Technischen Hochschule Aachen

In order to study the nature of radiation damage in solids provoked by neutron irradiation, a 3 MeV Van de Graaff accelerator delivering a d^+ beam of 400 mμA has been installed. With the help of a Be-target this apparatus is expected to give a total neutron output of 3×10^{12} n/sec leading to a flux density of about 2×10^{11} n/sec/cm^2 if the specimen is fixed at a distance of 1 cm of the target. This flux density is comparable with that of the reactors in which the more fundamental studies of neutron damage in solids are made.

Because of the easier access to the neutron source, an accelerator has many advantages to a reactor, especially if, as it is planned, the experiments will be conducted at liquid helium temperature. This type of experiment, which leads to difficulties inside of a reactor, is of great importance since only then recovery of some of the defects during irradiation can be avoided. Another advantage is that in the case of an accelerator the neutrons are unidirectional and much better monochromatic than in a reactor.

With the event of the first successful controlled-chain-reaction the question of how reactor-materials (fuels, moderators, construction-materials, screening-materials etc.) behave in the radiation field of a reactor became of extreme importance. Although this problem of change of properties of materials under irradiation at first sight appears to be one which is primarily technical in nature, the further investigation of this question has also given a strong impetus to solid state physics. As early as 1942 E. P. Wigner had already recognized that high energy radiation is able to displace an atom from its equilibrium position if a threshold displacement energy (E_d) is transferred to the atom. The quantitative measurements of the number and dynamics of displaced atoms, the investigation of the atomistic structure and the spacial distribution of the radiation induced lattice defects and of their annealing are the main object of the more fundamental studies in this field. However, phenomena such as phase-transformation, precipitation, corrosion, change of mechanical properties etc. under irradiation are also of great interest.

An ever increasing number of papers in this field of radiation damage has been published in the last few years, so that today it is practically impossible for someone to follow this field closely in its entire range. This is a result of the variety of experimental parameters involved, such as type of bombarding particles (α, β, γ, p, d, n, etc.), variation of energy, intensity and temperature of radiation, methods of detection of imperfections or the kind of observed properties and also type of the investigated materials (metals, alloys, semiconductors, covalent crystals, ionic crystals etc.). One of the most important problems in this field is the neutron irradiation of metals, since reactors can be run with great safety only after these radiation damage problems are understood. However, in this field very little useful fundamental work has been done, as the experimental work in the core of a reactor leads to many difficulties.

First there are the difficulties connected with the fact that the core of the reactor is surrounded in a complicated way by moderating and absorbing materials and that only little space is available for the apparatus. Also the whole apparatus, not only the specimen, must be able to stand strong radiation, which may change its properties or will make handling difficult after irradiation.

The difficulties are very much increased if one plans to do the experiments at liquid helium temperature, mainly because of the large amount of γ-heating to be conducted away. Liquid helium temperature, however, must be reached in radiation experiments if one wants to detect the primary radiation induced imperfections and so deduce an appropriate model of radiation damage. Otherwise, the experimental data may lead to an incorrect model since some of the imperfections are very mobile at higher temperatures and may anneal out already during irradiation.

Finally, there is the important question of the energy spectrum of the neutrons during irradiation. This spectrum must be known in order to interpret correctly the experimental results. Its measurement is again very difficult, especially since the introduction of an experimental apparatus often causes considerable change of the spectrum. Only in a few cases one has here relatively clear conditions, i.e. in a graphite reactor, where one has in first approximation a $1/E$ spectrum, or by surrounding the sample with a convertor, so that one can hope for a fission spectrum.

In most cases, however, one has only a rough estimate of the neutron spectrum in the neighborhood of the specimen. Therefore, the integrated flux, mostly used in the literature for characterizing the dosage of radiation, is only very approximate in value. The damaging effect of a neutron strongly depends on its energy, a fact which is usually not considered sufficiently in the values normally given for the integrated flux. Often this fact is taken into account only by cutting off the energy spectrum at some specified place, i. e. at 25 keV or at the threshold energy value of a special detector.

It can be seen immediately, that most of these difficulties would disappear if one would use for the radiation experiments a neutron source other than a reactor. The question then arises whether one can obtain a neutron flux comparable with that given by reactors with the help of a relatively simple particle accelerator. Another question of importance is which acceleration principle is more applicable, Van de Graaff or Cockroft-Walton machine? At this time the Van de Graaff machine appears to be superior, because this kind of accelerator, for the energy range of a few MeV, is less expensive and has already proven an effective tool. Cyclotrons present more technical difficulties and are much more expensive to operate.

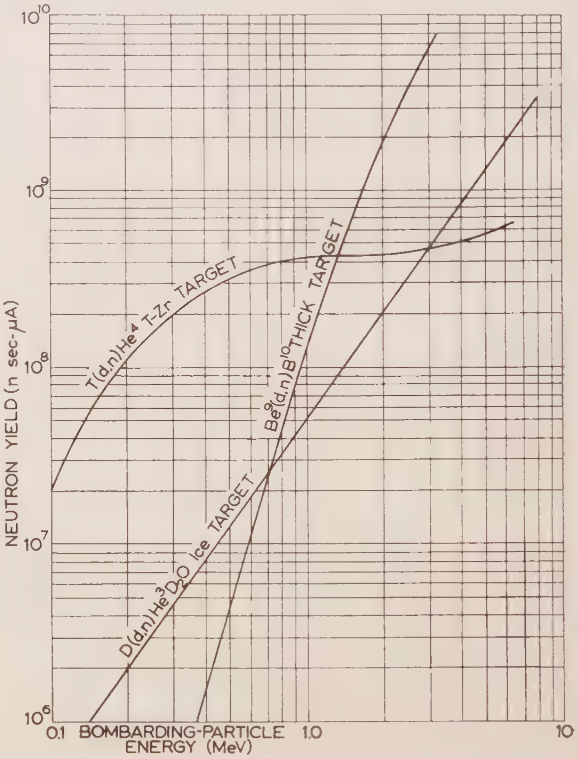

Fig. 1. Neutron yields *vs* bombarding energy for three different reactions.

There are quite a number of nuclear reactions which give neutrons ((p,n), (d,n), (t,n), (γ,n)) and which are accessible with medium high voltage generators (some MeV)1). Since for most radiation damage experiments and especially those on metals a high neutron flux is necessary, only nuclear reactions with high cross-sections are useful. In fig. 1 the yield of fast neutrons as a function of primary particle energy is plotted for three different reactions2). The reaction of primary interest is

$$\mathrm{Be}^{9} + \mathrm{d}^{2} = \mathrm{B}^{10} + \mathrm{n}^{1} + 4.360\ \mathrm{MeV}\,. \qquad (1)$$

1) S. W. Ross, USNRDL–TR–15.

2) High Voltage Engineering Corporation, Bulletin.

Measurements of the energy distribution and angular distribution of the neutrons in this reaction have been carried out for primary particles of different energy³). The energy diagram of B^{10} has been investigated by Ajzenberg and Lauritsen⁴).

In the following, the amount of radiation damage obtained in reactors and that expected to be obtained with accelerator-installations will be compared.

If a crystal is exposed to high energy neutron irradiation, some of the atoms are hit by the neutrons and displaced from their lattice sites. Most of these primary knock-on atoms have enough energy to displace other atoms, so that the number of displaced atoms increases in a cascade fashion. The fraction of the primary knock-ons is given by⁵,⁶)

$$n_{\mathrm{d}} = \phi \, \sigma_{\mathrm{d}} \, t \qquad (2)$$

and the total fraction of displaced atoms from all cascade processes by

$$N_{\mathrm{d}} = \phi \, \sigma_{\mathrm{d}} \, \bar{\nu} \, t \qquad (3)$$

where ϕ is the number of bombarding particles (neutrons) traversing 1 cm²/sec, t the radiation time in seconds, σ_{d} the cross section per atom for collisions between lattice atoms and bombarding particles (neutrons) which produce displacements, and $\bar{\nu}$ the average number of displaced atoms per primary knock-on of a certain knock-on spectrum. The value of these parameters shall now be discussed.

Flux density ϕ: The Oak Ridge graphite research reactor in which many of the fundamental radiation damage experiments with neutrons on metals are made, has a neutron flux of $\phi = 1.7 \times 10^{11}$ neutrons/cm² sec with energies above 25 keV. In comparison we consider a deuteron-accelerator with 3 MeV and 400 μ amp and with a beryllium target. According to figure 1 a neutron flux of 3×10^{12} neutrons/sec should be obtained. Since low temperature irradiation ($\approx 4°$K) must be performed with the sample in a cryostat, the distance from target to specimen cannot be chosen smaller than one centimeter. Therefore, a flux density of

$$\phi = \frac{1}{4\pi} \times 3 \times 10^{12} \approx 2.4 \times 10^{11} \text{ n/cm}^2 \text{ sec}$$

reaches the specimen. This estimate is a lower limit because of the assumption of isotropic neutron distribution; in reality the forward scattering of neutrons is somewhat preferred.

Cross section σ_{d} *for displacement collisions between neutrons with lattice atoms*: This quantity is dependent on the neutron energy and becomes smaller for faster neutrons. Also, for fast neutrons the elastic scattering shows greater deviation from hard sphere collisions, so that the anisotropy of the scattering of the displaced lattice atoms is more pronounced. Measurements of the differential cross-section of the elastic scattering of neutrons on copper have been made for several energies of the neutrons (1 MeV and 2.9 MeV)⁷,⁸), however, the data are not sufficient to allow a quantitative comparison between the numbers of displacements after reactor and accelerator irradiation. All that can be said is, that because of its higher average neutron energy a lower value for σ_{d} must be assumed in the case of an accelerator.

Number of displaced atoms per primary knock-on $\bar{\nu}$: This quantity increases with increasing energy of the neutrons but again no quantitative data are available. Therefore, it is assumed for the following that the decrease of σ_{d} for higher neutron energies is nearly compensated for by this increase in $\bar{\nu}$. This would mean that the product $\sigma_{\mathrm{d}}\bar{\nu}$ is about the same for reactor and accelerator.

Irradiation time t: Because of the above assumption, one has to compare only the product ϕt of eq. (3). In order to obtain an integrated flux of 10^{17} neutrons/cm² an irradiation time of 6×10^5 seconds (approx. 7 days) is necessary for the reactor and 4.3×10^5 seconds (approx.

---

³) A. I. Shpetnyi, Soviet Physics JETP **5** (1957) 357.

⁴) F. Ajzenberg and T. Lauritsen, Rev. Mod. Phys. **27** (1955) 77.

⁵) F. Seitz and J. S. Koehler, Solid State Physics, Vol. 2 (Academic Press, Inc., New York, 1956) 305.

⁶) G. J. Dienes and G. H. Vineyard, Radiation Effects in Solids, Vol. 2 (Interscience Publishers, New York, 1957).

⁷) M. Walt and H. H. Barschall, Phys. Rev. **93** (1954) 1062.

⁸) V. I. Popov, J. Nuclear Energy **9** (1959) 9.

5 days) for the accelerator. Since modern Van de Graaff generators are capable of running over long periods of time, it should be possible to conduct weekly experiments and to obtain with them an amount of radiation damage corresponding to an integrated flux of 10^{17} neutrons/cm^2.

In order to get an idea of the amount of damage which can be reached in copper, one may either introduce the appropriate quantities into eq. (3) or analyze the experimental results. In applying the first method one obtains $N_d \approx 10^{-4}$ for the fraction of displaced atoms with $\phi t = 10^{17}$n/cm^2 and the approximate values (for reactor neutrons) $\sigma_d \approx 2.7 \times 10^{-24}$ and $\bar{\nu} \approx 350$. With the second method a value smaller by a factor of approximate 5 results. The origin of this discrepancy can be discussed on the basis of correlated collision processes (dynamical crowdions and focusons[9,10]).

In either case, however, the fraction of displaced atoms turns out to be relatively small and it will be difficult to increase. Therefore, for dosages very much higher than 10^{17}n/cm^2 only reactors can at present be used. On the other side, for many fundamental studies dosages up to 10^{17}n/cm^2 are sufficient, as experiments with reactor irradiations have shown. In these cases, as has already been mentions, accelerators may have some advantages, which may be summerized as follows:

1) An accelerator installation is less expensive and simpler to operate than a reactor.

2) A Van de Graaff accelerator has great versatility since deuterons or protons as well as neutrons can be used for the irradiation. With minor changes electrons can be accelerated.

3) In contrast to a reactor the spectrum of the neutrons produced by an accelerator installation is relatively well known and for our purpose practically monochromatic. It can be altered through the use of different target materials.

4) In contrast to the reactor the neutrons are unidirectional so that the crystallographic orientation of the irradiated specimen can be taken into consideration.

5) The difficulties connected with placing the sample and part of the apparatus in the core of a reactor are avoided.

6) It is a relatively easy task to measure the neutron damage at the lowest temperatures with the aid of an accelerator installation while in a reactor additional technical difficulties arise. There is not only the problem of γ-heating mentioned above but also the danger of cryostat explosions inside of a reactor as have occurred repeatedly in the past.

7) There are many radiation experiments which, because of their special requirements, are not feasable at all inside of reactors but can be easily arranged around accelerators. An example is the investigation of correlated collision processes by neutron irradiation, the study of which becomes increasingly important with respect to modern theories of radiation damage[11]).

Finally, some special comments with respect to the Aachen Installation will be made. The chosen accelerator is a 3 MeV Van de Graaff generator in horizontal position which is able to produce an ion current of 400 μA d$^+$. The deuterium beam is scanned over an area of 1 cm^2 when it hits a water cooled Be-target. As already shown above, the total neutron yield should be under these conditions 3×10^{12} n/sec. The specimen is planned to be at a 1 cm distance from the target surface even when it is cooled to liquid helium temperature so that a neutron flux density of 2.4×10^{11} n/sec/cm^2 can be expected.

Since a hill-side was available for the building it was possible to construct target room and accelerator underground while the control room and the laboratories are above ground. The target room is 3 × 3 × 3 meters so that the measuring equipment can well be accomodated there. The interior of the target room wall is built from replacable cement blocks some 25 cm in thickness. In addition, the room is covered by Hydrobord plates (W. Mallinson and Sons, Ltd., 130 Hackney Road, London). This material has a large boron content and the neutrons which are

---

[9]) R. H. Silsbee, J. Appl. Phys. **28** (1957) 1246.

[10]) G. Leibfried, J. Appl. Phys. **30** (1959) 1388.

[11]) M. W. Thompson, Phil. Mag. **4** (1959) 139.

thermalized and scattered in the concrete, should be absorbed in this material before activating any equipment in the target room. The use of structural steel in the concrete walls was minimized to avoid any possibility of activation of cobalt even after years of use.

At present the total neutron output and also the energy distribution and angular distribution of the neutrons at 3 MeV is being measured. The radiation damage experiments are expected to start within a few months. It is planned to start with some fundamental studies of neutron damage in copper, the metal mostly used for such investigations. Therefore, measurements of the change of electrical resistivity, stored energy and megacycle damping during irradiation at 4.2° K and of their recovery during a subsequent annealing treatment are being prepared. Also an investigation of correlated collision processes in uranium and of the change of precipitation kinetics in some alloy systems under neutron irradiation is planned.

NUCLEAR INSTRUMENTS AND METHODS **11** (1961) 144–168; NORTH-HOLLAND PUBLISHING CO.

REACTOR PHYSICS RESEARCH WITH PULSED NEUTRON SOURCES

K. H. BECKURTS

Kernforschungszentrum, Karlsruhe

For the past 6 years pulsed neutron sources have been successfully used for studies of the kinetic behavior of neutrons in matter. Three main fields of interest have been particularly stressed: neutron lifetime measurements in moderators; reactivity measurements on reactor systems; and neutron spectra measurements by time-of-flight techniques. A number of most important results has been obtained, particularly in the field of neutron thermalisation research. The present status of pulsed source techniques and some of the more relevant results will be discussed.

1. Introduction

The first pulsed accelerator to be used for neutron research was the 36″ Berkeley cyclotron, as reported by Alvarez[1]). This author obtained bursts of neutrons from a (d,n)-reaction by modulation of the cyclotron acceleration voltage. By placing detectors at different distances from a paraffin moderator surrounding the target, effects of neutrons of different velocities could be studied. During the past twenty years, the art has considerably improved and expanded; there are more than 60 pulsed sources in use today in different branches of neutron and reactor physics. Their main uses may be classified as follows:

1.1. SPECTROMETRY OF SLOW AND INTERMEDIATE ENERGY NEUTRONS

These spectrometers make use of the enormous neutron burst intensities available from high-current electron linear accelerators (using mostly uranium targets) or from high-energy proton accelerators. The fast neutrons, which are primarily produced, are slowed down into the intermediate and slow energy region by a small hydrogenous moderator close to the target; energy analysis is done by the time-of-flight technique using flight path lengths up to more than 150 meters. Resolutions better than 0.01 μs/m (corresponding to $\Delta E/E = 2.8\%$ at $E = 10$ keV) have been reported. These spectrometers are used for total and partial neutron cross section measurements; they have hitherto delivered a wealth of cross section data and will certainly continue to do so for many years. The main representatives at present are the Saclay[2]) and Harwell[3]) linear accelerator spectrometers, the Nevis synchrocyclotron spectrometer[4]) and the KAPL betatron spectrometer[5]). Some Russian machines have been described[6]). Yale University and Rensselear Polytechnic Institute will soon obtain powerful electron linear accelerators which may outdo today's sources by a factor of 10 in intensity (see Nucleonics **18**, 8 (1960) 57).

In spite of the fact that these spectrometers contribute very important basic nuclear data to reactor physics, they are considered outside the scope of this paper and will not be discussed further.

1.2. FAST NEUTRON SPECTROMETRY

As it is known, fast neutrons of practically any desired energy can be obtained from (p,n)— or (d,n)— reactions on suitable targets bombarded with protons or deuterons from van de Graaff-generators. Therefore, for many cross-section measurements the time-of-flight technique involving a pulsed source is not necessary. It has however succesfully been used

---

[1]) L. W. Alvarez, Phys. Rev. **54** (1938) 609.

[2]) P. Billaud *et al.*, Geneva 1958 P/1186.

[3]) M. J. Poole and E. R. Wiblin, Geneva 1958 P/59.

[4]) J. Rainwater *et al.*, Rev. Sci. Instr. **31** (1960) 481.

[5]) M. L. Yeater, E. R. Gärttner and G. C. Baldwin, Rev. Sci. Instr. **28** (1957) 514.

[6]) V. V. Vladimirski and V. V. Sokolovski, Geneva 1958 P/2041.

- to study the spectrum of outgoing neutrons from a nuclear reaction (e.g. inelastic neutron scattering, fission neutron spectrum)[7])
- to improve the signal-to-noise-ratio in capture and fission cross section measurements[8])
- to improve the energy resolution of a $Li^7(p,n)$ neutron source in the keV region[9]).

In order to obtain good resolution, pulse widths have to be of the order of millimicroseconds and many experimental problems of detecting the neutrons and timing the events arise. An excellent review of the associated problems of fast neutron spectroscopy is given in the corresponding chapters of Marion and Fowler's recent book[10]); see also Rybakov and Sydorov[11]). No further treatment of this subject is intended here.

1.3. Investigation of thermal neutron diffusion parameters in moderators by measurement of neutron lifetimes.

1.4. Reactivity measurements on reactor systems by measurements of prompt reactor periods.

1.5. Measurements of neutron spectra from moderator and reactor systems by the time-of-flight method.

In the following we shall deal with items 1.3, 1.4. and 1.5. which are essentially all applications of pulsed source techniques to reactor physics. We intend to give a general review of the methods which have been developed and of some of the more relevant results. We do not plan to give details of the reactor theory underlying many of the measurements. Reference is made to the orginal articles quoted in the text and especially to two excellent review articles covering all work done up to early 1958:

"Diffusion measurements with pulsed neutron sources" by G. F. v. Dardel and N. G. Sjöstrand[12]).

"The measurement and theory of reactor spectra" by M. J. Poole, M. S. Nelkin and R. S. Stone[13]).

2. Investigations of Thermal Neutron Diffusion Parameters in Moderators

2.1. GENERAL

If a burst of fast neutrons is fed into a moderator a slowing down and thermalisation of the neutron field occurs until an asymptotic state is established in which a characteristic neutron distribution in space and energy exists. This distribution is called a "thermal neutron flux", it will decay exponentially with a time constant $\alpha(\sec^{-1})$; $1/\alpha$ is the "effective thermal neutron lifetime". If the geometrical dimensions of the moderator are characterized by its "buckling" B^2 (see fig. 1), the experimentally observed decay constants can be fitted in the following way:

$$\alpha = \alpha_0 + D_0 B^2 - C B^4 + \text{higher terms} . \qquad (2.1)$$

α_0 is the decay constant which would be observed in an infinite medium ($B^2 = 0$) and is entirely due to absorption; for $1/v$–absorption we have just

$$\alpha_0 = v_0 \, \Sigma_a \, (v_0) . \qquad (2.2)$$

The remaining terms describe the neutron leakage from a finite moderator. If this could

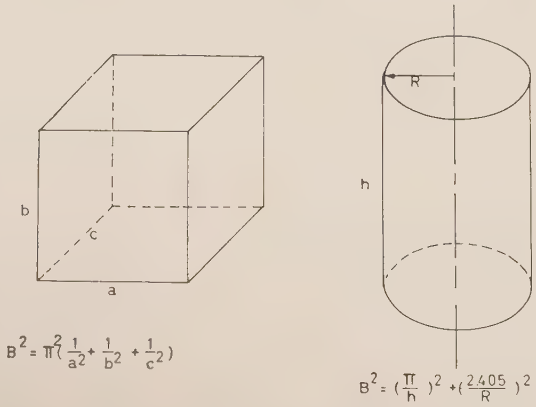
R
b
c
a
h
$B^2 = \pi^2(\frac{1}{a^2}+\frac{1}{b^2}+\frac{1}{c^2})$
$B^2 = (\frac{\pi}{h})^2 + (\frac{2.405}{R})^2$

Fig. 1. Geometric buckling B^2 for various simple geometries. "Effective" dimensions have to be used, i.e. the actual dimensions must be increased by extrapolation lengths.

[7]) L. Cranberg and J. S. Levin, Phys. Rev. **109** (1958) 2063.

[8]) B. C. Diven, Geneva 1958 P/667.

[9]) W. M. Good, J. H. Neiler and J. H. Gibbons, Phys. Rev. **109** (1958) 926.

[10]) J. B. Marion and J. L. Fowler, Fast Neutron Physics (New York, 1960).

[11]) B. V. Rybakov and V. A. Sydorov, Fast Neutron Spectroscopy (New York, 1960).

[12]) G. F. v. Dardel and N. G. Sjöstrand, Progr. Nucl. En. **1**, 2 (1958) 183.

[13]) M. J. Poole, M. S. Nelkin and R. S. Stone, Progr. Nucl. En. **1**, 2 (1958) 91.

be exactly described by elementary diffusion theory and if the asymptotic neutron spectrum were a Maxwellian with the moderator temperature, the second term on the right side would correctly describe the effects of leakage on the decay constant, since D_0 is the average of the energy dependent diffusion coefficient $D(E)$:

$$D_0 = \frac{\int_0^\infty D(E)\; M(E)\; \mathrm{d}E \;^{\dagger}}{\int_0^\infty \frac{1}{v}\, M(E)\, \mathrm{d}E} \,. \tag{2.3}$$

Careful experimental and theoretical work however shows clearly that higher terms in B^2, especially a B^4 term, have to be considered with smaller dimensions of the moderator. This is due to

– transport theory corrections to elementary diffusion theory which become important at large B^2.

– the "diffusion cooling" of neutrons.

In a moderator with small dimensions the main effect which removes neutrons is leakage. Since a faster neutron will escape from the moderator more probably than a slower one, the moderator continuously loses neutrons which are "hotter" than the neutrons inside. This loss is partially compensated by the coupling through collisions between the neutron gas and the moderator. As a result of these two counteracting processes a shift of the neutron spectrum below the equilibrium Maxwellian occurs which will be the larger the worse the thermalisation properties of the moderator and the more pronounced the leakage effects are. This "diffusion cooling" reduces the leakage rate.

Nelkin[14]) has given an essentially exact treatment of the two above-mentioned effects for simple moderators. In restricting to terms of order B^4, he shows that the constant C can be written

$$C = C_{\mathrm{D}} + C_{\mathrm{T}} \tag{2.4}$$

where C_{D} describes the "diffusion cooling" and C_{T} the "transport theory" contribution to the B^4 term. Extrapolating from Nelkin's results it can be assumed that $C_{\mathrm{T}} \ll C_{\mathrm{D}}$ for most moderators of interest. In what follows we shall therefore identify C and C_{D}.

As Nelkin has further shown[15]), the diffusion cooling constant C can be correlated in an approximate manner to a quantity M_2 which is a kind of "mean squared energy loss per collision" and therefore a fundamental quantity characteristic for the thermalisation power of a moderator: If $D(E) \sim E^{\alpha}$, Nelkin finds

$$C = \frac{(\alpha + \frac{1}{2})^2 \sqrt{\pi}\, D_0{}^2}{v_0\, M_2} \tag{2.5}$$

with

$$v_0 = \sqrt{\frac{2\,kT}{m_n}}$$

and

$$M_2 = \frac{1}{(kT)^2} \int_0^\infty \int_0^\infty \Sigma_{\mathrm{s}}\, (E \rightarrow E')\, (E' - E)^2\, M(E)\, \mathrm{d}E\, \mathrm{d}E' \,. \tag{2.6}$$

The analysis of α vs. B^2 curves measured on pure moderators therefore yields

the absorption cross section

the average thermal neutron diffusion coefficient, which can be combined with the absorption cross section to obtain the diffusion length

the "thermalisation power" M_2.

An exact determination of these parameters is indispensable if the use of a moderator for a thermal reactor is considered.

For such an analysis, the geometric buckling of a particular assembly has to be computed using the method outlined in fig. 1. This is a straightforward matter if the extrapolation length is energy independent. For moderators with a strongly energy dependent transport mean free path special considerations are necessary, as for example these made for water by Gelbard[16]).

---

† $M(E) = \dfrac{E}{(kT)^2}\, \mathrm{e}^{-E/kT}$ (T: moderator temperature).

[14]) M. S. Nelkin, Nucl. Sci. Eng. **7** (1960) 210.

[15]) M. S. Nelkin, J. Nucl. En. **8** (1958) 48.

[16]) E. Gelbard, J. Davis and J. Pearson: Westinghouse Atomic Power Division (USA) Report WAPD–T–1065 (1959).

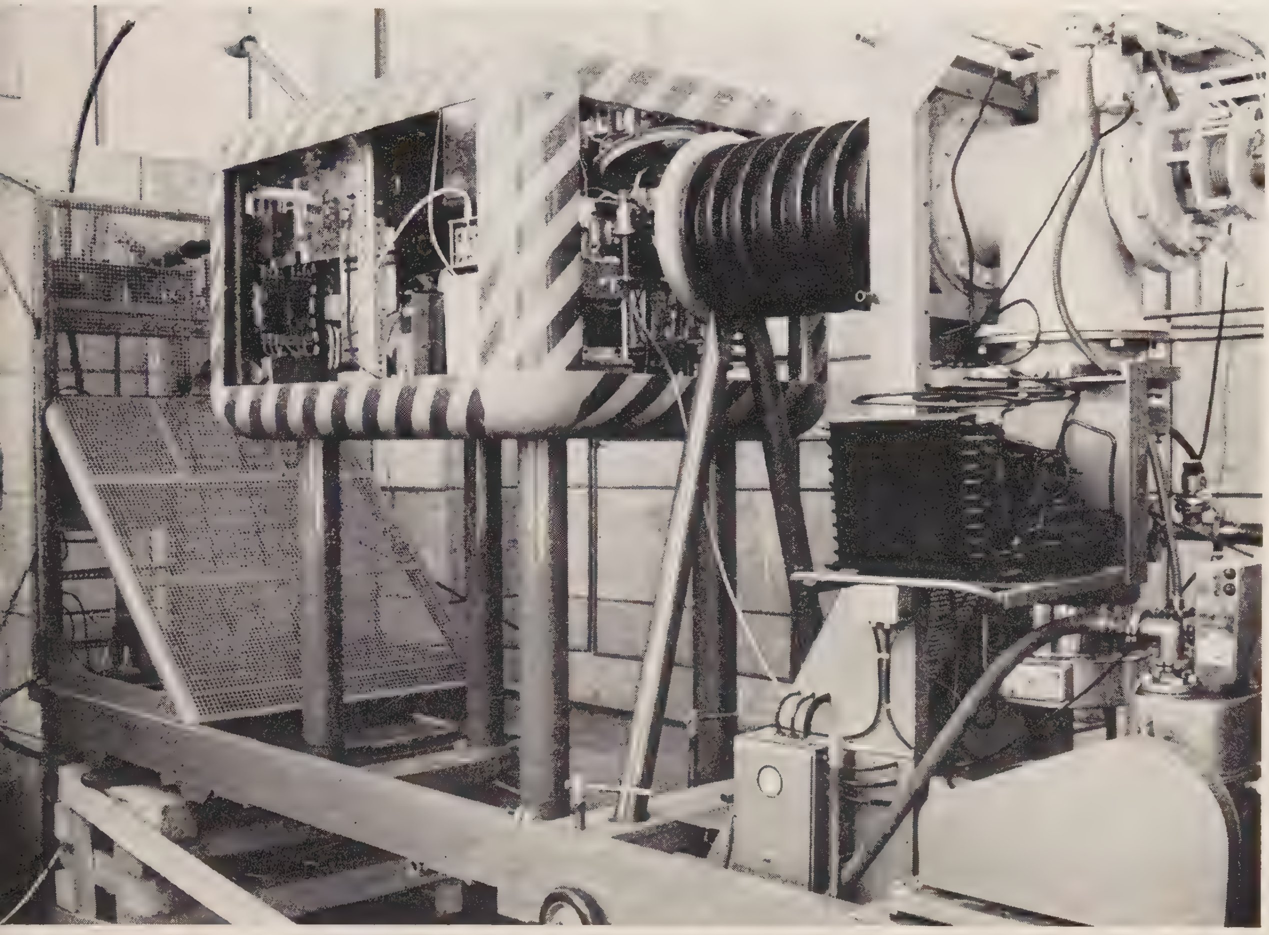

Fig. 2. Versatile 200 keV neutron generator at Karlsruhe.

2.2. INSTRUMENTATION†

The apparatus for α – measurements consists of a pulsed neutron source, neutron detectors and a suitable time analyzer. As pulsed sources it is nowadays customary to use low voltage, high current deuteron accelerators with pulsed ion sources. These accelerators give sufficient neutron intensities, especially when used with tritium targets, and can be made highly flexible. Requirements as to pulse length, yield and repetition rate are about as follows:

Repetition rate: Since α's between 100 and 10^5/sec have to be observed, and since one observation interval should be of the order of $10/\alpha$, the repetition rate should be variable between 10 and 10^4/sec.

Pulse length: The pulse length will normally be a fraction of α, at the maximum being equal to α, e.g. 10 millisec–10 μsec.

Intensity: In order to have reasonable statistics, the average neutron intensity should be at least 10^8–10^9/sec. It should however not exceed 10^{10}/sec since this will cause to high counting rates and corresponding counting losses. This problem has been carefully studied by Keepin[17]).

A typical pulsed neutron source has been developed by W. Eyrich at Karlsruhe (fig. 2). Deuterons from a r.f. ion source are accelerated to 200 keV in a horizontal one-stage acceleration tube. The source is easily movable on wheels and can be varied in height. Target extension tubes up to 4 meters length have been successfully

---

† see also 3.2. and 4.2.

[17]) G. R. Keepin, Symp. on Application of Pulsed Neutron Techniques, Berkeley (1958) (UCRL–5665).

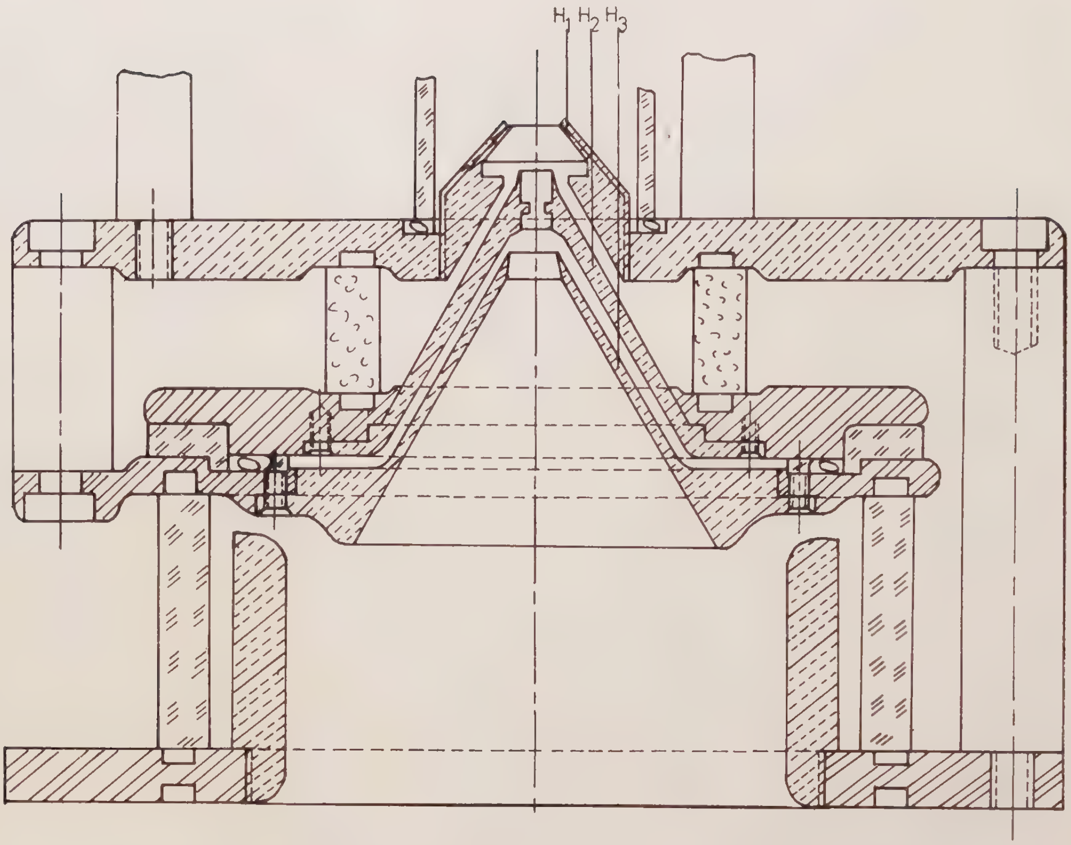

Fig. 3. Ion extraction system at the r.f. ion source of the generator from fig. 2.

used; this makes possible the use of the source with reactors where the shield has to be penetrated. Pulsing of the r.f. ion source is achieved by pulsing the extraction voltage. Details of the extraction system can be seen in fig. 3. The extraction electrode H_2 is normally on zero potential; during pulses it is driven up to — 15 kV. Ion currents up to 10 mA (measured at the target) have been obtained, the risetime of the ion pulse being about 0.5 μsec. Electrode H_3 is always + 1000 V positive against H_2. This is ineffective during pulse-on-time, however prevents ions from drifting into the acceleration tube during the pauses between bursts. In this way, a "background" current as low as 10^{-5} of the "normal pulse" current is obtained, which is very important for this type of work. Using tritium targets and a 1:10 duty ratio this source can furnish more than 10^{11} n/sec which is more than sufficient for most applications. The burst length is determined by an univibrator in the high voltage terminal which can be easily changed; the repetition rate is arbitrarily and determined by the frequency with which the optical transmission system is triggered.

A number of small pulsed accelerators are commercially available:

The PN 400 van de Graaff (High Voltage Engineering Corporation).

The 400 keV-Cockroft-Walton-Accelerator (Arco/HVEC).

Pulsed accelerators are also built by Häfely, Basel; Texas Nuclear Corporation, Austin; Sames, Grenoble; and others. We do not intend to review the properties of these and other accelerators here. Different types of ion sources and of pulsing systems have been used. A particularly interesting development is being carried out by Arco Corporation in collaboration with LASL for a very versatile accelerator to be used by LASL[17]).

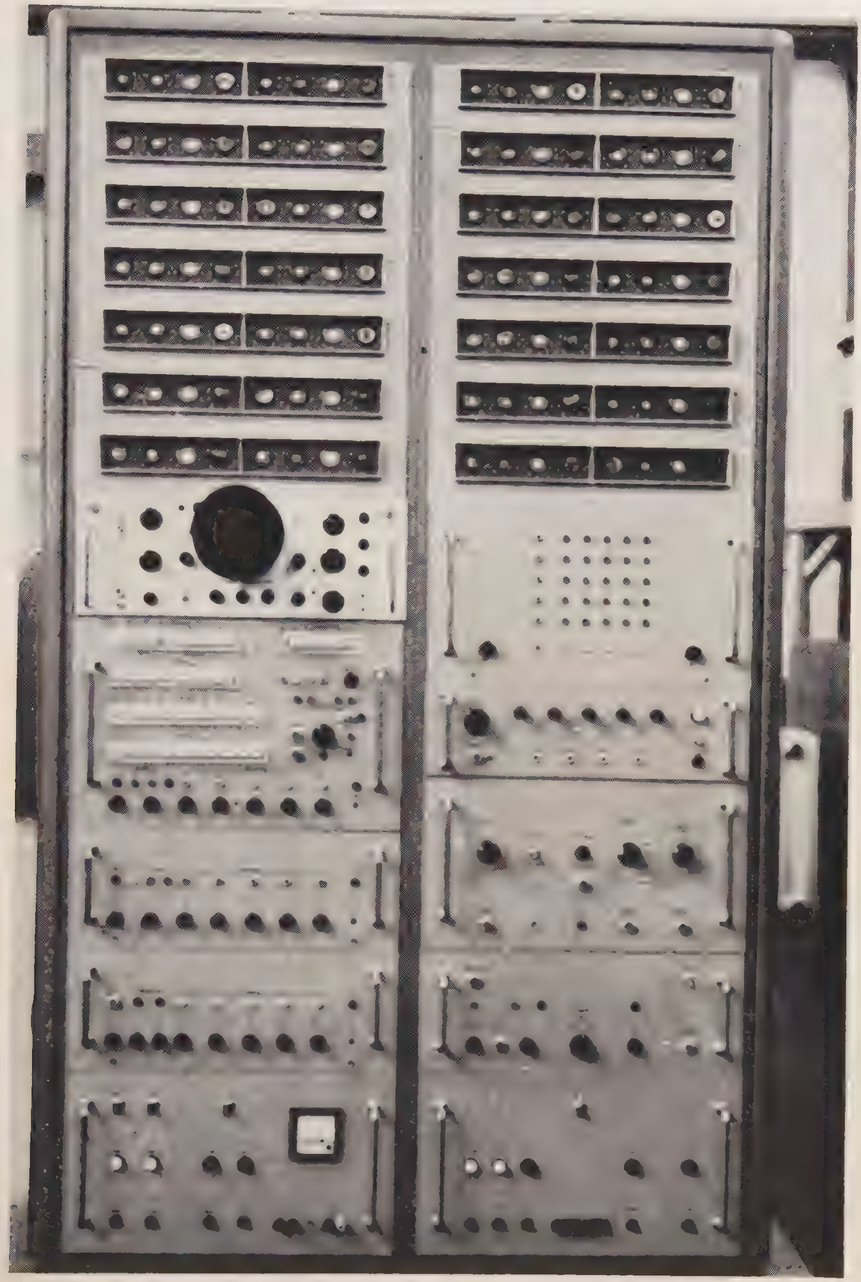

Fig. 4. 25 channel analyzer used a Karslruhe.

This facility will give pulsed beams of 350 keV deuterons with intensities up to 5 mA and yields, by different techniques, bursts from 10^{-8}–3×10^{-3} sec long with repetition rates from 3×10^{6} down to 10/sec.

Detectors for pulsed moderator work do not pose special problems. Most authors have used BF_3 gas counters which are commercially available in a variety of models. The Oak Ridge group[22]) has successfully used small Li^6 (Eu) scintillators. With the tendency to measure diffusion parameters up to very high moderator temperatures (i.e. up to 800° C in graphite and beryllium; up to 300–400° in organic moderators) the demand for a temperature-resistant prompt neutron detector arises. Fission detectors for temperatures up to 300° C are available commercially, and it may be necessary to use these in combination with suitable cooling techniques.

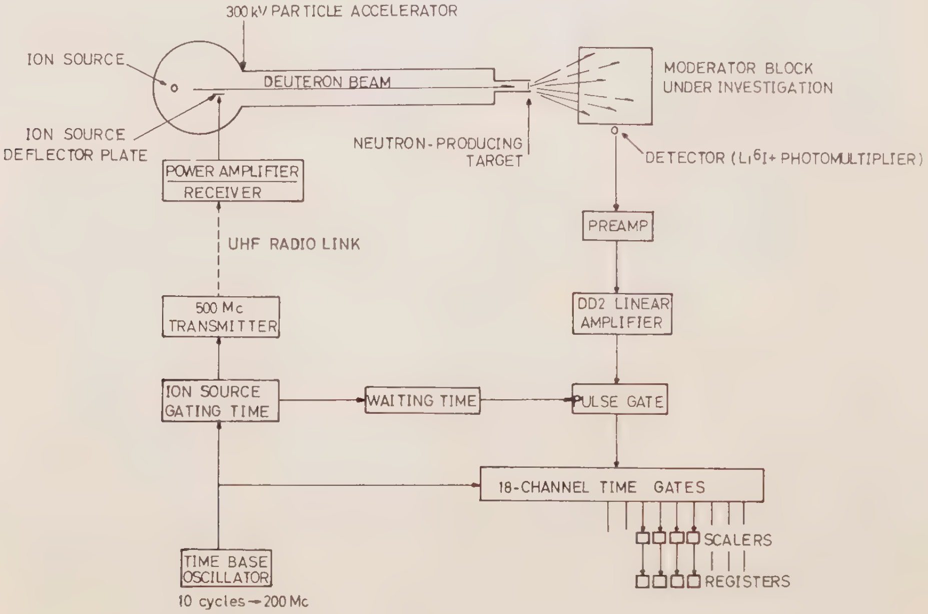
300 kV PARTICLE ACCELERATOR
ION SOURCE
DEUTERON BEAM
MODERATOR BLOCK UNDER INVESTIGATION
ION SOURCE DEFLECTOR PLATE
NEUTRON-PRODUCING TARGET
DETECTOR (Li6I+ PHOTOMULTIPLIER)
POWER AMPLIFIER RECEIVER
UHF RADIO LINK
PREAMP
500 Mc TRANSMITTER
DD2 LINEAR AMPLIFIER
ION SOURCE GATING TIME
WAITING TIME
PULSE GATE
18-CHANNEL TIME GATES
SCALERS
REGISTERS
TIME BASE OSCILLATOR
10 cycles → 200 Mc

Fig. 5. Block diagram of the equipment used by de Saussure and Silver[22]).

The time analyzer must be of the multichannel type and should have between 20–40 channels, each variable in width between 5 μsec and 5 msec. A number of strictly digital analyzers particularly designed for this type of work have been developed[18,19,20]). An important requirement for such an analyzer is a reasonably low deadtime which should be smaller than 5 μsec. A 25-channel analyzer with 1 μs deadtime now in use at Karlsruhe is shown in fig. 4. Each channel has a Burroughs beam switching tube scale of ten followed by several Dekatrons. The channel width is adjustable between 4 μsec and several seconds.

If counting rates are reasonably low the time analysis can be done by a time-to-height converter in connection with a multichannel pulse height analyzer. If this is done care must be taken in order to achieve sufficient linearity and stability. A system having high stability and being linear to better than 1 % has been recently described[21]).

2.3. A MEASUREMENT ON ROOM-TEMPERATURE BERYLLIUM

As an example of a moderator experiment with the pulsed source technique we consider the work on room temperature beryllium by de Saussure and Silver[22]). These authors followed the neutron decay from thirteen cubical blocks of beryllium having fundamental-mode bucklings ranging from 0.8×10^{-2} to 7.2×10^{-2} cm^{-2}. The general setup of their experimental equipment is shown in fig. 5. The pulsed source and the detector are located outside the moderator blocks, normally in the middle of adjacent side planes[†]. This arrangement minimizes the amount of "higher harmonics" contamination of the neutron flux decay. Figs. 6 and 7 show detailed

---

[18]) G. F. von Dardel, Appl. Sci. Res. B3 (1953) 209.

[19]) F. Glass, ORNL–2480 (1958) 22.

[20]) E. Gatti, Rev. Sci. Instr. **24** (1953) 345.

[21]) K. H. Beckurts, Nukleonik **2** (1960) 129.

[22]) G. de Saussure and E. G. Silver, ORNL–2641 (1959).

[†] Normally, the surfaces of moderator blocks are covered by a neutron absorber like cadmium in order to prevent room scattered neutrons from reentering the block. It is not clear whether this was done here.

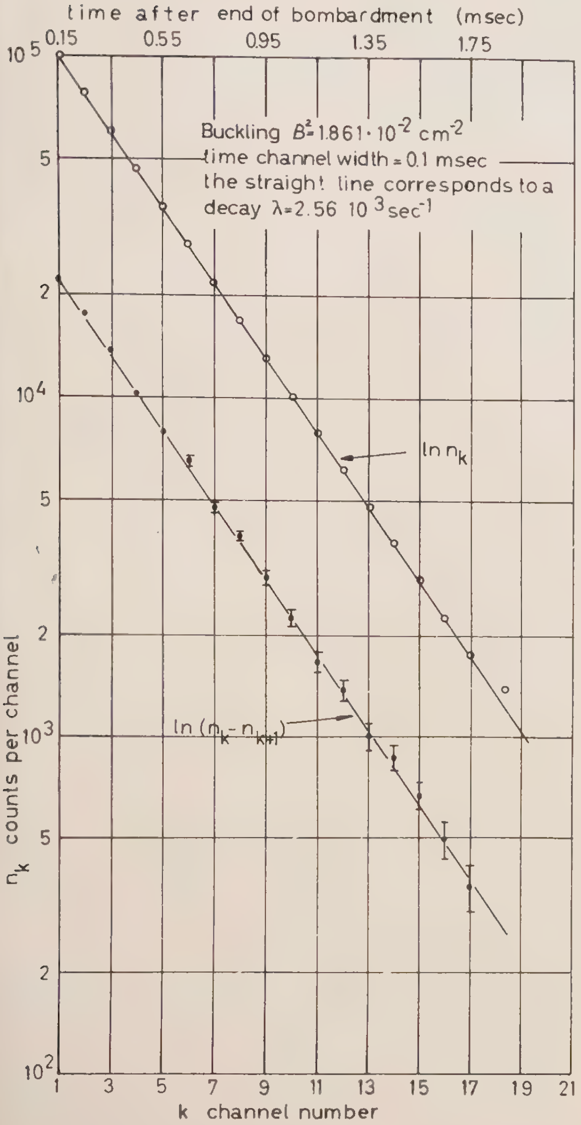

Fig. 6. Decay of the neutron flux in a beryllium assembly $14\frac{3}{8} \times 14\frac{3}{8} \times 16$ in. (from [22]).

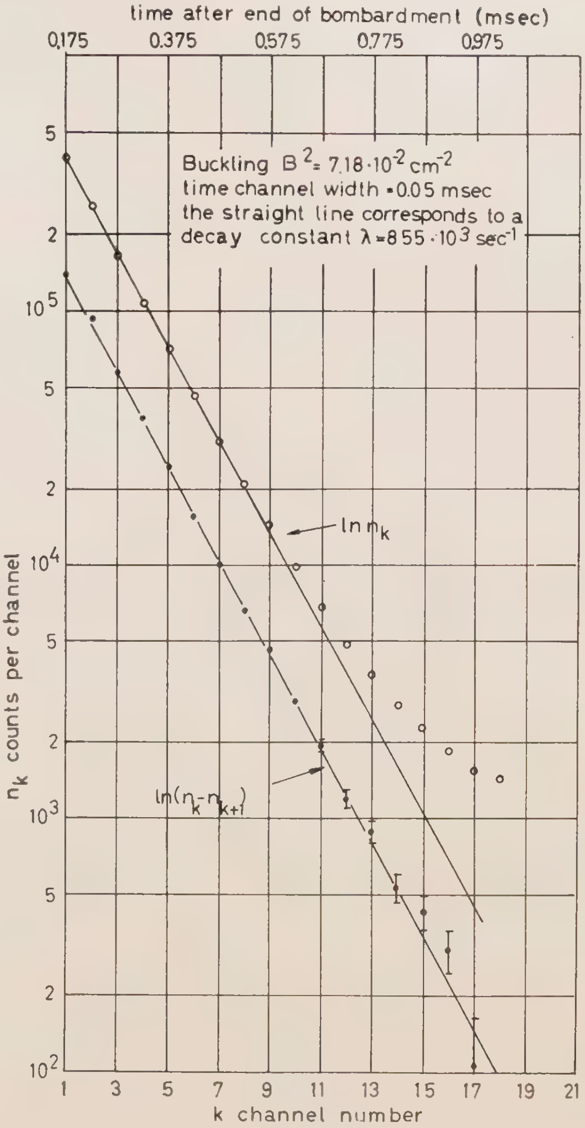

Fig. 7. Decay of the neutron flux in a beryllium assembly $5\frac{3}{4} \times 8 \times 8\frac{5}{8}$ in. (from [22]).

neutron flux decay curves obtained from the largest and the smallest assembly under investigation. While a very clean decay is observed from the large block, a considerable background of room scattered neutrons is observed in the case of the small assembly; this has to be eliminated before the decay constant can be determined. These authors used the Cornell[23a]) method for the α determination, while most other authors use the method of Peierls[23b]).

A plot of α vs B^2 as obtained from these measurements is shown in fig. 8. The curve shows clearly the deviations from the straight line which demonstrate the "diffusion cooling" effect. By a least squares fit, the following diffusion parameters are obtained (at a density 1.85 g/cm^3):

$$\alpha_0 = 288 \pm 60 \text{ sec}^{-1}$$
$$D_0 = (1.25 \pm 0.06) \times 10^5 \text{ cm}^2 \text{ sec}^{-1}$$
$$C = (1.40 \pm 1) \times 10^5 \text{ cm}^4 \text{ sec}^{-1} .$$

[23a]) R. G. Cornell, ORNL–2120 (1956).

[23b]) R. Peierls, Proc. Roy. Soc. Lond. A **149** (1935) 467.

TABLE 1

Results of pulsed experiments on beryllium (1.85 g/cm³)

Year	Author	α_0 (sec^{-1})	D_0 (cm^2 sec^{-1}) $\times$ 10^5	C (cm^4 sec^{-1}) $\times$ 10^5	B^2 range (cm^{-2})
1955	Antonov[26])	—	1.17 ± 0.05	2.93 ± 1.0	0.008 — 0.061
1956	Campbell and Stelson[27])	150	1.25	0	0.005 — 0.036
1958	Kloverstrom† [28])	270 ± 19	1.24 ± 0.04	3.90 ± 0.8	0.003 — 0.041
1959	de Saussure and Silver[22])	288 ± 60	1.25 ± 0.06	1.40 ± 1.0	0.008 — 0.072

The value of α_0 leads to a microscopic absorption cross section of 11 ± 2 millibarn which is only slightly higher than the cross section of pure Be[24]). The measured D_0 is close to the theoretical value 1.21×10^5 cm^2 sec^{-1} as calculated by Bhandari[25]). The diffusion cooling coefficient is in excellent agreement with the value 1.4×10^5 cm^4 sec^{-1} as calculated in an approximate manner by Nelkin[15]) who employed a Debye model for the lattice vibrations in beryllium.

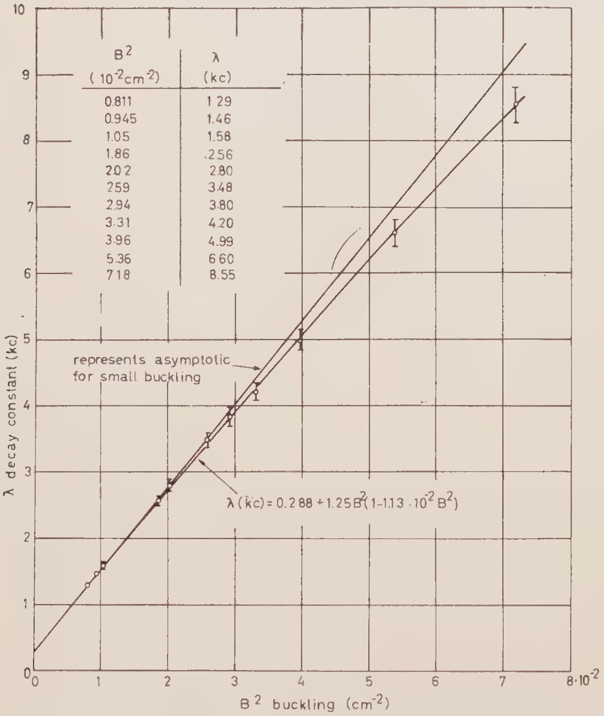

Fig. 8. Thermal neutron decay constant as a function of buckling for room temperature beryllium (from [22])).

It is interesting to compare these results with the results of other investigations on beryllium (table 1).

We can disregard the discrepancies in α_0 which may be due to different purity grades of the materials. There are, however, considerable discrepancies in the D_0 and particularly the C values. While de Saussure and Silver[22]) state that the older results probably involve errors in the interpretation of data, the discrepancies between the more recent ORNL and UCRL data still persists and cannot be explained. As we shall see later, the situation is very similar for other moderators.

De Saussure and Silver have also performed measurements on beryllium at temperatures

TABLE 2

Results of different pulsed experiments on graphite (1.6 g/cm³)

Year	Author	α_0 (sec^{-1})	D_0 (cm^2 sec^{-1}) $\times$ 10^5	C (cm^4 sec^{-1}) $\times$ 10^5	B^2 range (cm^{-2}) $\times$ 10^3
1955	Antonov[26])	82 ± 3	2.07 ± 0.03	12.5 ± 2.0	1.0 — 40
1956	Beckurts[31])	127 ± 1	2.13 ± 0.02	16.3 ± 2.5	0.7 — 5.5
1960	Starr and Price[32])	71.2 ± 0.9	2.06 ± 0.02	12.4 ± 2.2	1.6 — 27.5

---

† A more recent measurement by Andrews[29]) reconfirms these results.

[24]) D. J. Hughes and R. B. Schwartz, BNL–325 (1958).

[25]) R. C. Bhandari, J. Nucl. En. **6** (1957) 104.

[26]) A. V. Antonov *et al.*, Geneva 1955 P/661.

[27]) E. C. Campbell and P. H. Stelson, ORNL–2076 (1956) 32.

[28]) T. T. Komoto and F. Kloverstrom, Trans. Am. Nucl. Soc. **1** (1958) 1.

[29]) W. M. Andrews, Trans. Am. Nucl. Soc. **3**, 1 (1960) 161.

different from room temperature[30]). Fig. 9 shows the variation of the transport mean free path of beryllium with temperature as obtained from pulsed measurements between—46 and +511°C.

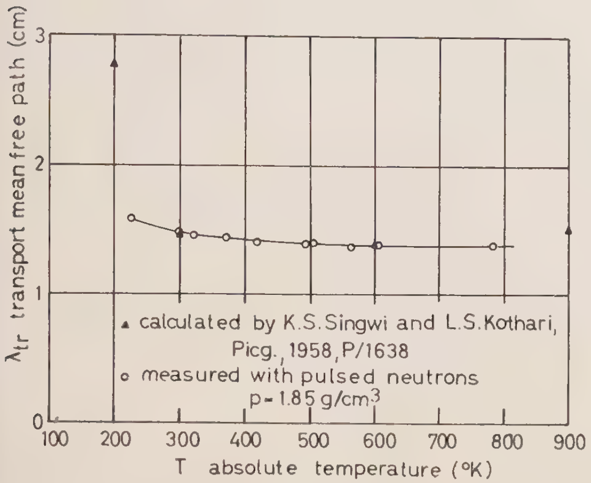

Fig. 9. Transport mean free path of thermal neutrons in beryllium as a function of temperature (from [30])).

2.4. RESULTS ON DIFFERENT MODERATORS

2.4.1. *Graphite*

Table 2 summarizes different results on room temperature graphite.

While these three determinations are in reasonable agreement, two recent measurements[33,34]) show a diffusion cooling coefficient which is larger by a factor of two. The reasons for these discrepancies are not yet understood. Possible causes for errors and discrepancies which have to be checked are

- the role of a B^6-term
- the importance of data evaluation schemes
- the effects of higher harmonics and of background neutrons.

It might also be possible that graphites manufactured by different methods have different diffusion parameters. Still much experimental and theoretical work has to be done in order to clear these discrepancies up. For graphite this is particularly important since the pulse method is sometimes used for routine measurements of absorption cross sections, where a high precision is desired. A more precise value for the diffusion cooling coefficient C is also important in order to check current thermalisation theories for graphite: The theoretical value for C, as computed by Nelkin[15]) in the Debye crystal approximation, is 14×10^5 cm^4 sec^{-1}.

2.4.2. *Water*

Results of various experiments on (ordinary) water are summarized in table 3.

It is seen that the values are in excellent agreement among each other; this holds especially for the two most recent determinations. Küchle's result yields 326 ± 6 millibarn for the proton capture cross section at 2200 m/sec and 2.72 ± 0.08 cm for the diffusion length, which compares very well with a directly measured value of 2.72 ± 0.03 cm[39]). From the diffusion

TABLE 3

Results of different pulsed experiments on water (22° C)

Year	Author	α_0 (sec^{-1})	D_0 (cm^2 sec^{-1})	C (cm^4 sec^{-1})	B^2 range (cm^{-2})
1954	v. Dardel and Sjöstrand[35])	4892	36340 ± 750	7300 ± 1500	0.1 — 0.7
1955	Antonov[26])	4831	35000 ± 1000	4000 ± 1000	0.09 — 0.93
1956	Bracci and Coceva[36])	4950	34850 ± 1100	3000 ± 1000	0.09 — 0.96
1959	Dio[37])	4808	35450 ± 600	3700 ± 700	0.09 — 0.87
1960	Küchle[38])	4785	35400 ± 700	4200 ± 800	0.11 — 0.75

---

[30]) G. de Saussure and E. G. Silver, ORNL–2842 (1959) 115.

[31]) K. H. Beckurts, Nucl. Sci. Eng. **2** (1957) 516.

[32]) E. Starr, G. A. Price, Trans. Am. Nucl. Soc. **2**, 2 (1959) 125.

[33]) M. Küchle, personal communication (1960).

[34]) G. Denielou, personal communication (1960).

[35]) G. F. v. Dardel and N. G. Sjöstrand, Phys. Rev. **96** (1954) 1245.

[36]) A. Bracci and C. Coceva, Nuovo Cim. **4**, X (1956) 59.

[37]) W. H. Dio, Nukleonik **1** (1958) 13.

[38]) M. Küchle, Nukleonik **2** (1960) 131.

[39]) K. H. Beckurts and O. Klüber, Zs. Natf. **132** (1958) 822.

cooling coefficient a value of 30 barn per hydrogen atom for M_2 can be derived. This is the same as would be computed for a gas of mass 18 nuclei and shows that the molecular rotations in water are strongly hindered.

A few measurements in water at elevated temperatures have been made. The variation of the diffusion coefficient in the temperature region 20–80° C thus obtained is shown in fig. 10.

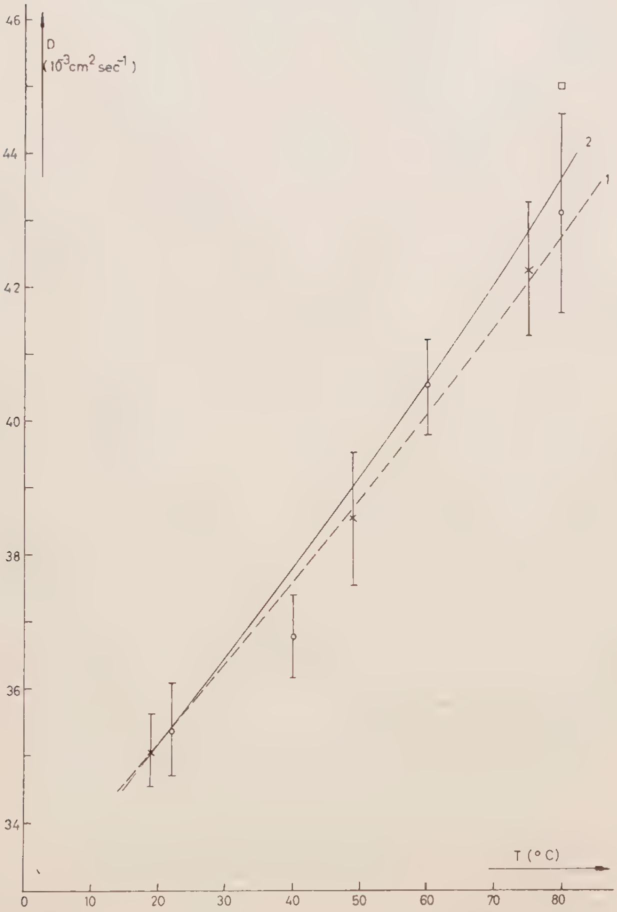

Fig. 10. Temperature dependence of the diffusion coefficient of thermal neutrons in water.
× : Dio[37]) □ : Antonov[26]) ○ : Küchle[38]).
The solid line is computed assuming a $1/v$ behaviour of the transport cross section in water.

The situation in water seems quite consistent so far. However, a very careful stationary measurement of the diffusion length has been recently published yielding $L = 2.859 \pm 0.018$ cm at 25.9° C[40]). Using $\sigma_a = 327$ millibarn, this would lead to a diffusion coefficient $D_0 = 38\,800$ cm^2 sec^{-1} at 22° C, i.e. a result 10% higher than all the values from the pulsed experiments!

2.4.3. *Other moderators*

Beryllium oxide has been investigated by Iyengar *et al.*[41]) who found the following results (for a density 2.96 g/cm^3)

$$\alpha_0 = 131.5 \text{ sec}^{-1}$$

$$\begin{aligned} D_0 &= 1.18 \times 10^5 \text{ cm}^2/\text{sec } (24° \text{C}) ; \\ & 1.36 \times 10^5 \text{ cm}^2/\text{sec } (80° \text{C}) ; \\ & 1.60 \times 10^5 \text{ cm}^4/\text{sec } (140° \text{C}) . \end{aligned}$$

$$\begin{aligned} C &= 3.85 \times 10^5 \text{ cm}^4/\text{sec } (24° \text{C}) ; \\ & 7.5 \times 10^5 \text{ cm}^2/\text{sec } (80° \text{C}) ; \\ & 12.4 \times 10^5 \text{ cm}^4/\text{sec } (140° \text{C}) . \end{aligned}$$

The reasons for the very strong increase of C with temperature are not very well understood.

As a typical organic moderator Dowtherm A (Diphyl) has been investigated by Küchle[37]). The results obtained between 20° C and 180° C are given in table 4.

The results for α_0 are consistent with a microscopic hydrogen absorption cross section of 333 ± 5 millibarn; this is higher than the pure hydrogen cross section due to impurities. The temperature dependence of the transport mean

TABLE 4
Diffusion parameters of Dowtherm A

	20° C	80° C	140° C	180° C
α_0 (sec^{-1})	2870 ± 40	2780 ± 40	2600 ± 60	2530 ± 70
D_0 (cm^2 sec^{-1})	49200 ± 600	60700 ± 700	74300 ± 1100	83800 ± 1300
C (cm^4 sec^{-1})	11900 ± 2100	12200 ± 2400	17700 ± 4500	22300 ± 5700

---

[40]) K.S. Rockey and W. Skolnik, Nucl. Sci. Eng. 8 (1960) 62.

[41]) S.B.D. Iyengar *et al.*, Proc. Ind. Acad. Sci. 45 (1957) 215.

free path as deduced from the measured D_0 is shown in fig. 11 in comparison to the calculations of Petrie *et al.*[42]). For M_2, a value of 50 barn per hydrogen atom can be deduced from the measured C values. This is somewhat higher than for water and indicates very good thermalisation properties of Dowtherm A.

The diffusion cooling coefficient for heavy water has been determined by Sjöstrand[43]) from measurements on very small assemblies. Employing the diffusion coefficient D_0 as known from other work[44]), he found $C = (3.5 \pm 0.8) \times 10^5$ cm^4 sec^{-1} at 20°C. This is considerably smaller than would be expected for a monoatomic gas with mass 20 nuclei.

A measurement of the thermal neutron diffusion parameters in plexiglas has been reported by Seemann[45]). By observing the neutron decay from different cylindrical assemblies ranging in buckling from 0.04037 to 0.7061 (cm^{-2}), the following diffusion parameters were determined:

$$\alpha_0 = 4.3 \times 10^3 \text{ sec}^{-1}, \qquad D_0 = 3.4 \times 10^4 \text{ cm}^2 \text{ sec}^{-1}.$$

C was found to be $(0.00 \pm 0.04) \times D_0$; it is very surprising that no diffusion cooling was observed in this experiment.

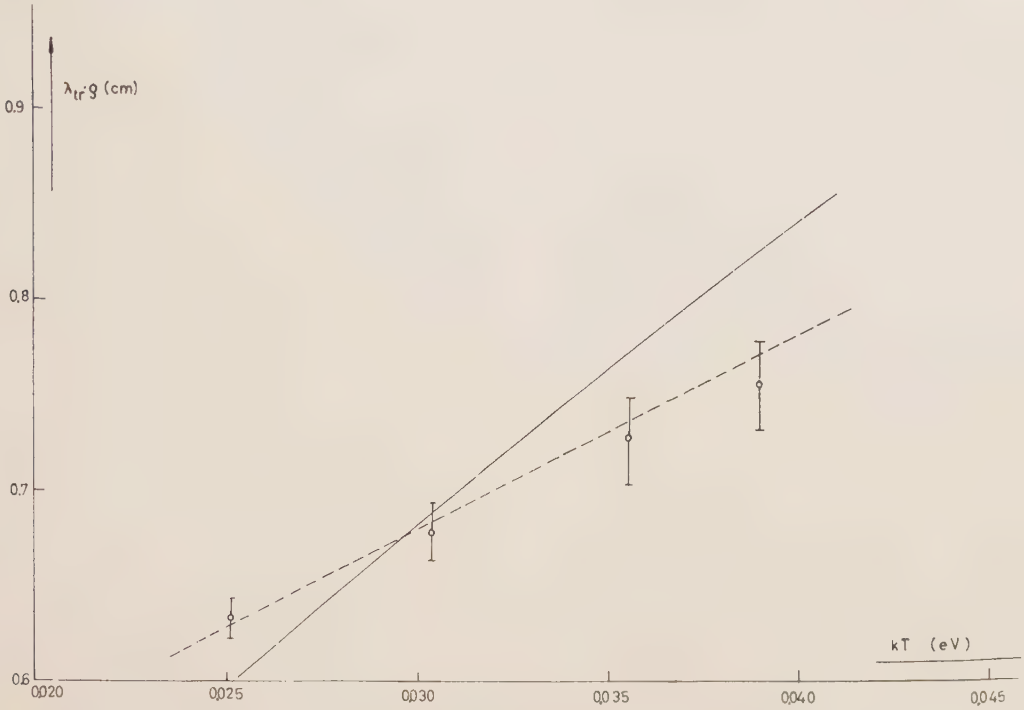

Fig. 11. Temperature dependency of the transport mean free path of thermal neutrons in Dowtherm A as measured by Küchle[38]). The solid line is computed using the method of Petrie *et al.*[42]), while the broken line assume a $1/v$ transport cross section.

2.5. MEASUREMENTS OF THE GEOMETRICAL BUCKLING

Hitherto we have considered only the case where the diffusion parameters are determined from α measurements on moderator assemblies of known, easily computable buckling. If the diffusion parameters —e.g. the α vs. B^2 curve— of a moderator are known, a measurement of α yields the buckling of the system under investigation. This can be used to determine bucklings of assemblies with complicated boundary conditions which are likely to occur in reactor physics. The method has first been used by Beckurts[46]) who measured the change in buckling which arises when a concentric ring of 4 absorbing rods is introduced into a moderator (graphite) of cylindrical shape. Sjöstrand *et al.*[47]) have employed this method to determine the geometrical bucklings of reactors having complicated shape and to study the extrapolation lengths at the surface of absorbing rods. Some studies of control rods in square shaped moderators have been done by the Oak Ridge group[48, 49]). We shall not go into the details of these measurements since no results of any general physical importance can be obtained. We want to stress however the great possibilities of the pulse method for buckling determinations with regard to problems arising in special situations.

---

[42]) C. D. Petrie, M. L. Storm and P. F. Zweifel, Nucl. Sci. Eng. **2** (1957) 728.

[43]) N. G. Sjöstrand, Arkiv för Fysik **15** (1958) 145.

[44]) S. W. Kash and D. C. Woods, Phys. Rev. **90** (1953) 564.

[45]) K. W. Seemann, Trans. Am. Nucl. Soc. 2, 1 (1959) 69.

[46]) K. H. Beckurts, Zs. Natf. **11a** (1956) 881.

2.6 CONCLUSIONS

It has been shown that the pulsed source method is a powerful tool for investigations on moderators, and that many careful investigations have been carried out. However, still much work has to be done in order to cover more moderating materials and to increase the accuracy. Additional determinations of diffusion parameters are desirable for

- heavy water at room temperature and at elevated temperatures
- light water at temperatures above room temperature (100–300°C)
- organic moderators like Santowax R (Terphenyl), especially at elevated temperatures
- graphite at temperatures up to 800°C.

Experiments in order to clarify discrepancies and to increase accuracy are necessary for

- graphite and beryllium in order to settle the diffusion cooling problem
- beryllium oxide as a reconfirmation of the strong dependence of C on temperature
- light water in order to clarify the discrepancy with the recent diffusion length experiment. A very interesting contribution to this question has quite recently been given by Lopez, Beyster *et al.*[50]). These authors have started a very careful remeasurement of the diffusion parameters in light water using an somewhat modified method: They inject fast neutron bursts into very large (up to $17\frac{1}{2} \times 17\frac{1}{2} \times 19\frac{1}{4}$ inch) water tanks and perform measurements of the time—dependent neutron flux at different detector positions inside the tank, using a small fission detector which can easily be inserted into the system. The resulting space- and time-dependent flux distribution is analyzed into the "fundamental mode" and "higher harmonic" contributions by means of a special IBM 704 code. In this way decay curves of isolated modes are obtained which yield α values definitely free of modal effects. The following preliminary values for the diffusion parameters have been obtained (at 22°C):

$$D_0 = 36\,800 \pm 400 \text{ cm}^2 \text{ sec}^{-1}$$
$$C = 4\,137 \pm 688 \text{ cm}^4 \text{ sec}^{-1}$$
$$\sigma_{\text{H}} = 326 \pm 2 \text{ millibarn}\,.$$

The values for σ_{H} and C are in excellent agreement with those obtained by Küchle (table 3), while D_0 is about 4% larger. The diffusion length deduced from these results is 2.78 cm and thus somewhat more consistent with the recent diffusion length results.

It should be interesting to follow these lines and to check whether modal effects have given rise to errors in previous experiments.

Apart from the work on pure moderators there are many possibilities of expanding the method. Much work in the field of buckling determinations has to be done; there are also many possibilities for heterogenous system (systems composed of different moderators, systems composed of moderators at different temperatures). We finally mention the possibility of absorption measurements by the change in α observed when the substance investigated is dissolved in water. This method has first been used to determine the boron cross section[51]) and still has many unexplored possibilities[52]).

[47]) N. G. Sjöstrand, J. Mednis and T. Nilsson, Arkiv för Fysik **15** (1959) 471.

[48]) R. P. Belles, G. de Saussure and E. G. Silver, Trans. Am. Nucl. Soc. **3**, 1 (1960) 155.

[49]) R. P. Belles, G. de Saussure and E. G. Silver, personal communication (1960).

[50]) W. M. Lopez, J. R. Beyster, R. E. Nather and J. L. Wood, Trans. Am. Nucl. Soc. **3**, 1 (1960) 199.

[51]) G. F. von Dardel and N. G. Sjöstrand, Phys. Rev. **96** (1954) 1566.

[52]) J. Meadows and J. Whalen, WASH–1026 (1959) 1.

3. Prompt Neutron Period Measurements on Reactor Assemblies

3.1. GENERAL

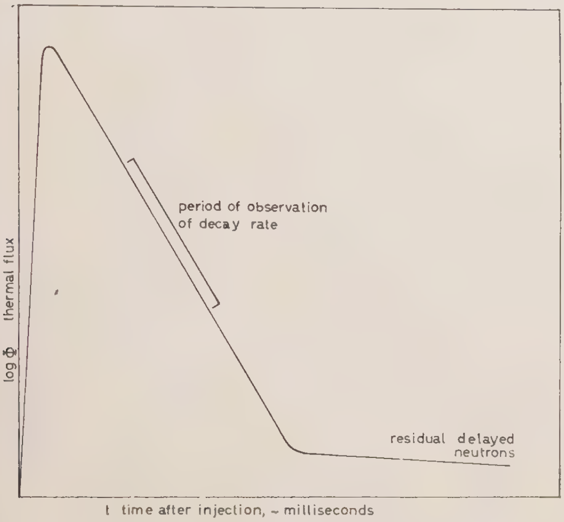

Fig. 12. Time behaviour of thermal flux following injection of a fast neutron burst (from[56]).

The general time behaviour of the thermal neutron flux in a multiplying medium after injection of a fast neutron burst is illustrated in fig. 12. After the burst injection a transition phase follows in which the thermal neutron population is established and the harmonic modes die out. In the next phase this initial thermal neutron population dies out exponentially with the prompt decay constant α of the system. After the decay of the prompt neutron group there remains a slowly decaying group due to residual delayed neutrons. The idea of pulsed experiments on reactor systems is to observe the prompt decay and to measure α, which can be correlated to other reactor data. Under certain simplifying assumption, the following relation holds for α† [54,55,56]:

$$\alpha = \frac{1}{l}\,[1 - (1 - \beta)\,K_{\text{eff}}]\,. \tag{3.1}$$

Here l is the mean generation time of the system, K_{eff} is the effective multiplication factor, and β the effective delayed neutron fraction ($\beta \approx 0.007$ for U^{235} systems). $K_{\text{eff}}\,(1 - \beta)$ is sometimes called K_p, the prompt multiplication factor.

Eq. (3.1) permits different interpretations. In the more fundamental one, systematic measurements of α as a function of B^2 are made over a wide range of subcritical systems. For these systems, l and K_{eff} are calculated using multigroup techniques. These measurements allow a systematical check of these reactor computing techniques by comparing calculated and measured α vs. B^2–curves.

The other application aims towards reactivity calibrations on existing reactors or critical facilities. If we define the reactivity

$$\rho = \frac{K_{\text{eff}} - 1}{\beta} \tag{3.2}$$

(in units "Dollar"), we have for systems close to critically

$$\alpha = \frac{\beta}{l}\,[1 - \rho]\,. \tag{3.3}$$

The quantity β/l can be determined by an α measurement on a system with known reactivity, particularly at delayed critical where we have $\rho = 0$ and therefore

$$\alpha = \alpha_c = \frac{\beta}{l}\,. \tag{3.4}$$

We thus have

$$\alpha = \alpha_c\,(1 - \rho)\,. \tag{3.5}$$

Eq. (3.4) and (3.5) show that measurements of α on systems with known reactivity yield the generation time, while an α measurement on a system once its α_c is known gives its reactivity directly in "Dollars". This method can be used to calibrate control and safety rods on reactors and to measure reactivity contributions of absorbers or fuel elements.

Fig. 12 showed the time behaviour after the injection of a single neutron burst into a "clean" system, that is a system which had no other neutron population than that caused by spontaneous fissions before the burst was injected. In an actual measurement it will be necessary to fire many bursts into the system before sufficient counting statistics have been reached. Periodic injection of neutron bursts into the system will however permit the long-living delayed neutron group to come into equilibrium thus causing a constant neutron background to build up. The ratio of the maximum neutron flux during the burst to the source-induced background is given by[55]

---

† We shall not deal here with the difficulties arising in reflected systems, nor shall we discuss the problems of "static" and "dynamic" reactivity[53]) interpretation of the experiments.

[53]) B. E. Simmons, Nucl. Sci. Eng. **5** (1959) 254.

[54]) S. C. Fultz, Nucl. Sci. Eng. **6** (1959) 313.

[55]) J. Bengtson *et al.*, Geneva 1958 P/1783.

[56]) B. E. Simmons and J. S. King, Nucl. Sci. Eng. **3** (1958) 595.

$$1 + \frac{[1-(1-\beta)\,K_{\text{eff}}]^2}{2\beta(1-\beta)\,K_{\text{eff}}}\,\frac{T}{l} \tag{3.6}$$

where T is the repetition period of the pulsed source. In order to have this ratio sufficiently high, it is necessary to keep the repetition rate of the source low.

3.2. INSTRUMENTATION

Pulsed sources for reactor work have to be highly flexible. In order to inject neutrons into reactors, it is necessary to pass channels through thick shields, sometimes under very restricting room conditions. The desirable pulse frequencies are very low—of the order of 1/sec—due to the above-mentioned condition for high signal-to-background ratio. The pulse intensities however must be high—of the order of 10^6–10^7 neutrons per burst—in order to perform measurements in reasonably short times, and to overcome any background source neutrons present in the system from previous operation (e.g. long-lived photoneutron sources in D_2O or beryllium systems). A source meeting these requirements is the "Pulsatron" pulsed neutron generator†. This generator, which is schematically shown in fig. 13, delivers 1–10 5 μsec-bursts each of 10^7 neutrons per second. The dimensions of the accelerator unit are 4″ O D × 18″ length, thus making it readily usable in situations where space is very restricted. Of course, most of the accelerators mentioned in section 2.2 can also be used for reactor work. Fig. 13a shows the PN 400—van de Graaff generator used as a pulsed neutron source for a subcritical assembly.

Due to the fact that pulsed experiments on reactors are done with low repetition rate but high intensity, the neutron detection and time analysis may become a difficult experimental problem. While some authors have used more conventional equipment like BF_3 counters or fission chambers, others have employed typical high resolution detectors. Simmons and King[56] have used a DuMont 6292 multiplier with a borated cathode[57]††. The α-particles from the B^{10} (n,α) Li^7 reaction enter into the Cs-Sb photocathode layer where they produce electron emission directly. This counter has high sensitivity and an extremely low deadtime (a small fraction of a microsecond). Keepin[58] has proposed the use of loaded plastic and liquid scintillators and particularly of noble-gas scintillation counters. The latter have the advantage that they are extremely insensitive to γ-radiation and can be made very fast.

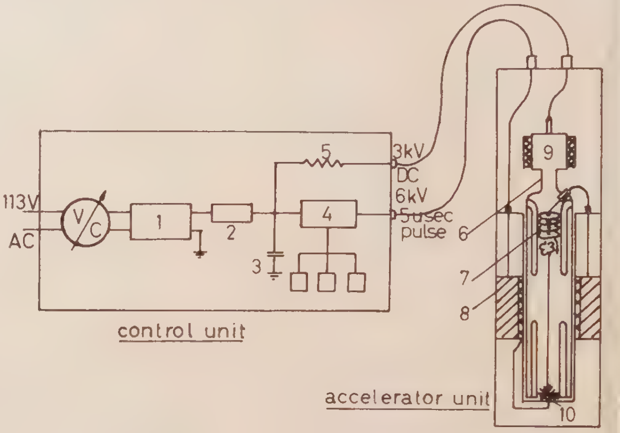

1. HV transformator
2. rectifier
3. energy storage capacitor
4. thyratron
5. dropping resistor
6. VN accelerator tube
7. ion source
8. 30–1 pulse tranformator
9. pump
10. target

Fig. 13.
The "Pulsatron" pulsed neutron generator (Kaman Nuclear).

A very suitable time analyzer for work on reactor systems is the TMC 256—Channel Analyzer in connection with the # 212 pulsed neutron plug in unit†, which is shown in fig. 14. This device has 256 analysis channels with a width adjustable between 10 and 2560 μsec. The input deadtime is of the order of 3×10^{-8} sec, thus making very high counting rates tolerable. The apparatus has facilities to register the preburst background and to introduce arbitrary delays between the source burst and the start of the registering period. Storage is done in a magnetic core memory. Read out is done by either a printer or a tape puncher. Another high-resolution analyzer has been developed at Los Alamos[17]) with fifty time channels (1 μsec-10 sec wide) and an input deadtime $< 5 \times 10^{-8}$ sec.

---

† Manufactured by Kaman Aircraft Co., Nuclear Division, Colorado Springs, Colo.

†† Such neutron detectors are now commercially available.

[57] G. F. Erickson, S. G. Kaufmann and I. F. Pahis, IRE Trans. on Nucl. Sci. NS-3, No. 3 (1956).

[58] G. R. Keepin, personal communication (1960).

Measurements on fast systems require special instrumentation. Neutron pulse lengths as short as several millimicroseconds are necessary due to the short decay times of these reactors. This can only be achieved by electrostatic deflection of ion beams[10]). The overall time resolution of the neutron detection system should be of the order of 1 millimicrosecond. A typical detection system developed for this type of work by Passell[55]) is shown in fig. 15.

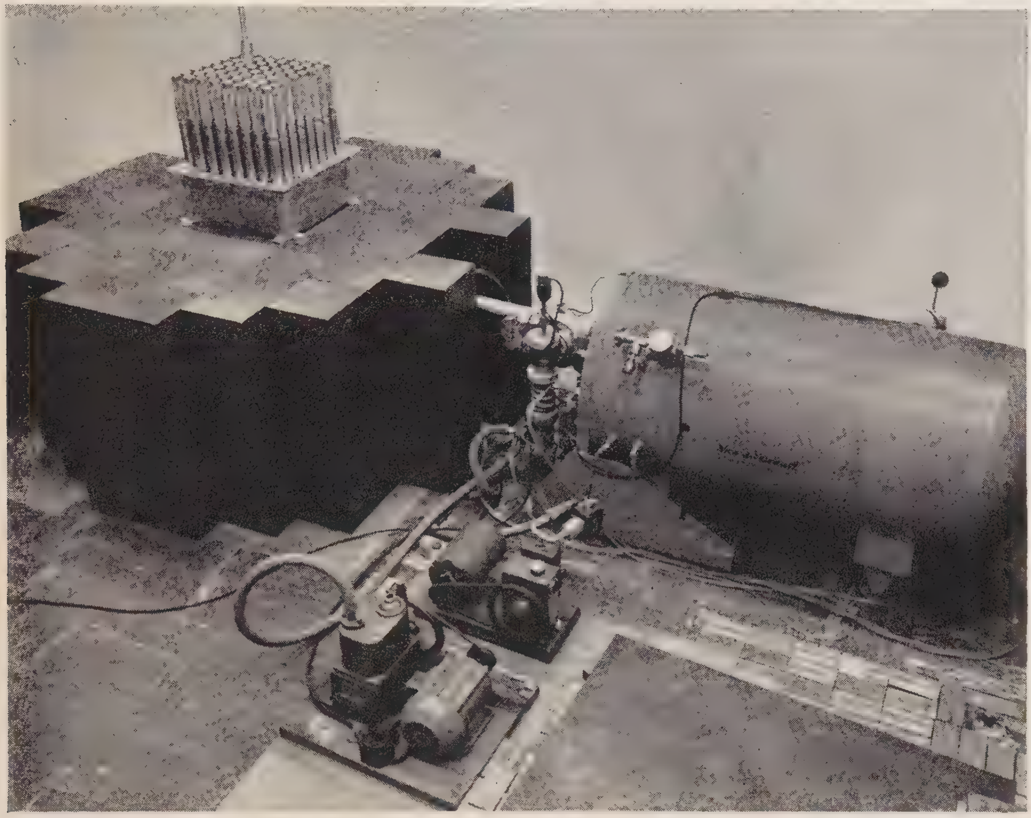

Fig. 13a: PN 400—Van de Graaff pulsed neutron generator used at Belgonucléaire, Brussels.

3.3. STUDIES OF DECAY RATES AS A FUNCTION OF BUCKLING

A very careful study of unreflected, nearly homogenous assemblies consisting of graphite and enriched (19.16%) uranium has been done by the Livermore group[59, 55, 54]). Various loadings were obtained by intermixing 0.001- and 0.002 inch thick uranium foils with 0.500-inch thick graphite plates. Carbon- to uranium atomic ratios were 1, 300, 600, 1200, 2340 and 9950:1 with an overall graphite density of

---

† Manufactured by Technical Measurement Corporation, North Haven, Conn.

[59]) F. A. Kloverstrom and E. Komoto, UCRL–5477 (1959).

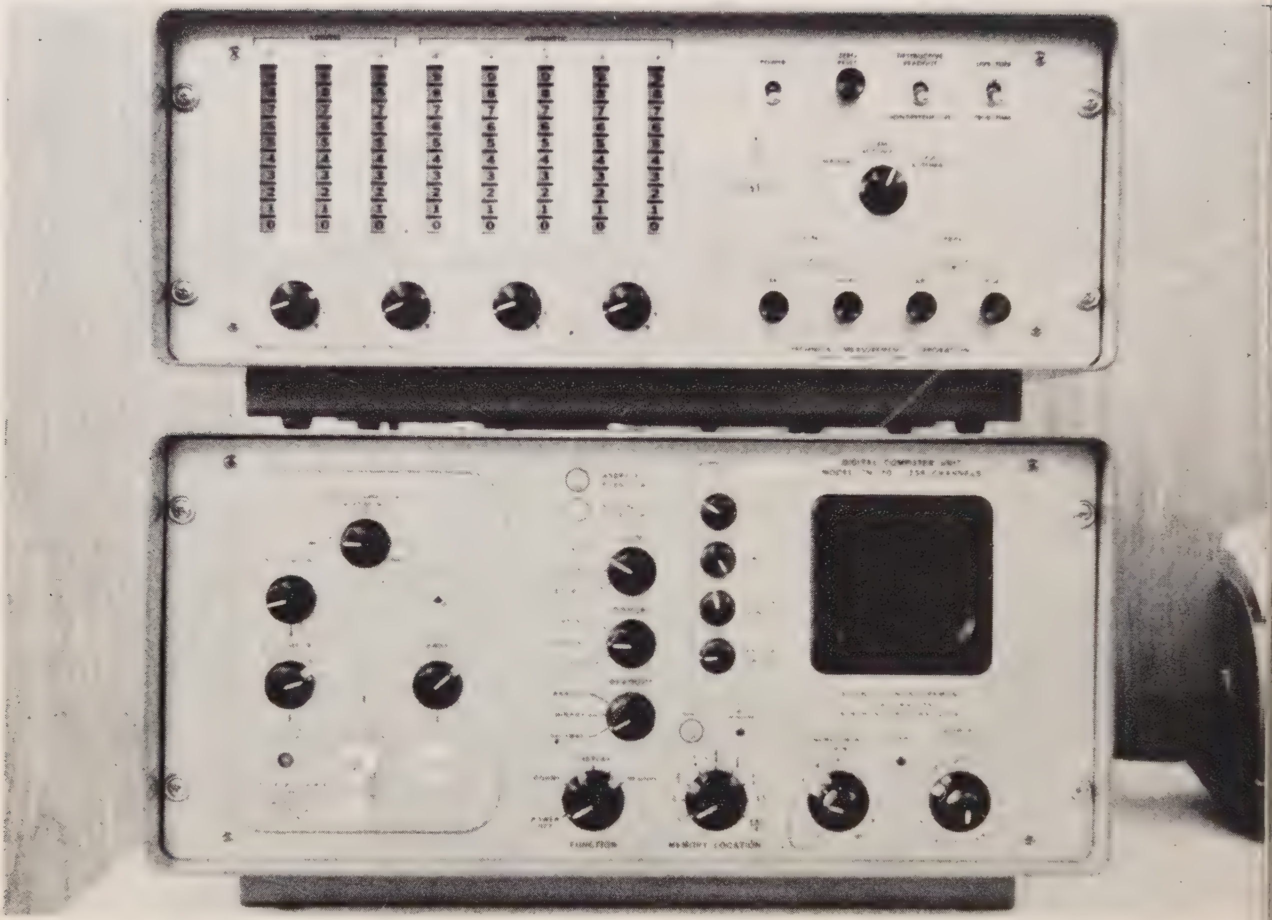

Fig. 14. The TMC–256-time analyzer with 212 "pulsed neutron" plug in unit.

1.645 g/cm^3. As an example of the resulting α vs. B^2 curves, fig. 16 shows the result for the 2340:1 system in comparison to an α vs. B^2 curve for pure graphite. At high bucklings, the decay constant of the composite system is considerably larger than that of graphite due to the excess absorption in uranium (fission neutrons are lost by leakage during slowing down) while at low B^2 the system decays slowlier than graphite due to the effect of neutron multiplication. The point

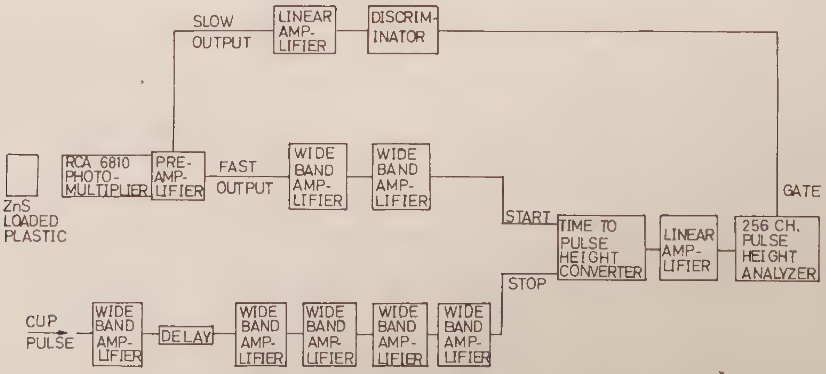
SLOW OUTPUT
LINEAR AMP-LIFIER
DISCRIM-INATOR
GATE
ZnS LOADED PLASTIC
RCA 6810 PHOTO-MULTIPLIER
PRE-AMP-LIFIER
FAST OUTPUT
WIDE BAND AMP-LIFIER
WIDE BAND AMP-LIFIER
START
TIME TO PULSE HEIGHT CONVERTER
LINEAR AMP-LIFIER
256 CH. PULSE HEIGHT ANALYZER
STOP
CUP PULSE
WIDE BAND AMP-LIFIER
DELAY
WIDE BAND AMP-LIFIER
WIDE BAND AMP-LIFIER
WIDE BAND AMP-LIFIER
WIDE BAND AMP-LIFIER

Fig. 15. Block diagram of the equipment used by Passell to study fast systems (from [55]).

where the curve intersects the abscissa defines the "prompt critical" buckling.

Fultz[54]) has tried an interpretation of the obtained α vs. B^2–curves by means of a simple 2-group theory (one group representing fast, the other one thermal neutrons). A comparison of theory and experiment for the system with a C:U ratio 9950:1 is shown in fig. 17 and shows a very good agreement. The agreement is not as good for the systems having lower C:U ratio. As stated by Fultz, this may be due to the fact that only the 9950:1 system is "thermal" while the other system investigated have a considerably harder energy spectrum. For these systems, it may be necessary to use other group constants, especially for the "thermal" group. Studies on aqueous solutions of enriched uranyl fluoride, containing 53.0 and 26.5 g U^{235} per liter, have been performed by Campbell and Stelson[60]).

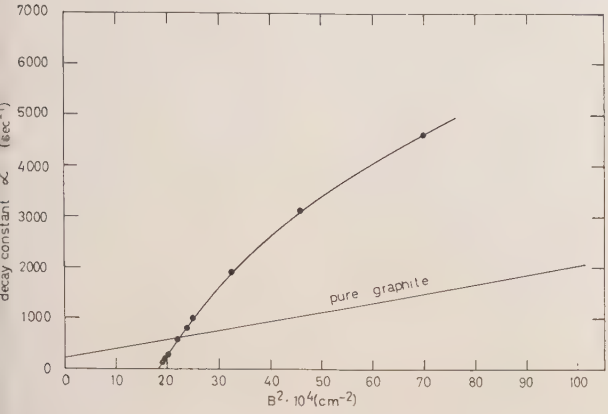

Fig. 16. Decay constant vs. buckling for graphite and for system with C: U^{235} = 2355:1 (from [55])).

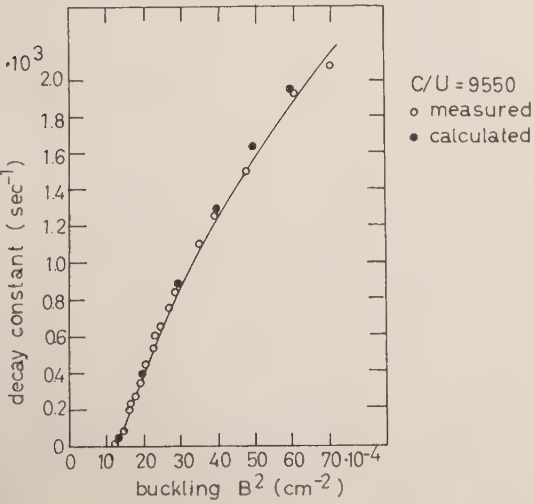

Fig. 17. Decay constant vs. buckling for a C:U ratio 9950:1, showing experimental and calculated points (from [54])).

3.4. REACTIVITY CALIBRATIONS ON COMPLETE REACTOR SYSTEMS

A calibration of the safety rods of the Swedish reactor R 1 and a measurement of the D_2O reactivity equivalent has been done by Sjöstrand[61]). Sjöstrand used a technique somewhat different from the one outlined in section 3.1; we shall not go into its details here. Calibrations of control rods on hydrogenous reactors have been done by Simmons and King[56]) and by the Oak Ridge group[62,63]). The latter group has also performed measurements of reactivity equivalents of fuel elements[64]).

As an example, we consider a control rod calibration which was done at the Bulk Shielding

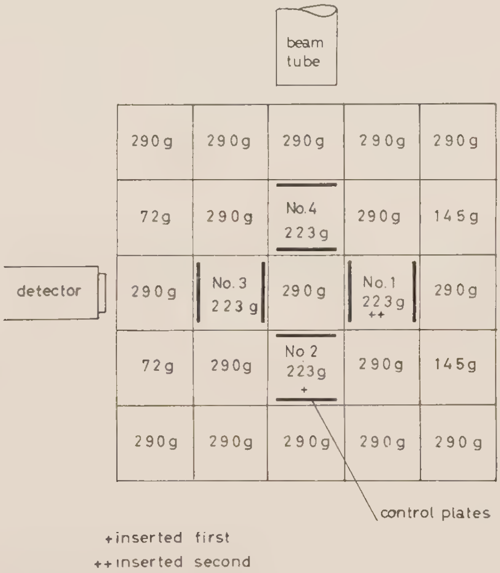

290g	290g	290g	290g	290g
72g	290g	No.4 223g	290g	145g
290g	No.3 223g	290g	No.1 223g ++	290g
72g	290g	No 2 223g +	290g	145g
290g	290g	290g	290g	290g

Fig. 18. BSR–II schematic core configurations for pulsed neutron measurement (from [62])).

---

[60]) E. C. Campbell and P. H. Stelson, ORNL–2204, 34 (1956).

[61]) N. G. Sjöstrand, Arkiv för Fysik **11** (1956) 233.

[62]) E. G. Silver *et al.*, ORNL–2842 (1959) 35.

[63]) E. G. Silver *et al.*, Trans. Am. Nucl. Soc. **3**, 1 (1960) 278.

[64]) G. de Saussure, K. M. Henry and R. P. Belles, Nucl. Sci. Eng. (in press).

Reactor (BSR II) at Oak Ridge[62]). The core of this "swimming pool' type reactor consists of 25 plate-type fuel elements as schematically shown in fig. 18. The control plate pairs to be calibrated are numbers 1 and 2 as shown in fig. 18. After α_c had been determined by independent measurements, the decay curves with one and with both control plate pairs inserted were measured, they are shown in fig. 19. With $\alpha_c = 3.13 \times 10^2\ \mathrm{sec}^{-1}$ and α (1 "in") $= (1.36 \pm 0.03) \times 10^3\ \mathrm{sec}^{-1}$; α (1 + 2 "in") $= (2.11 \pm 0.04) \times 10^3\ \mathrm{sec}^{-1}$ we find with eq. (3.5)

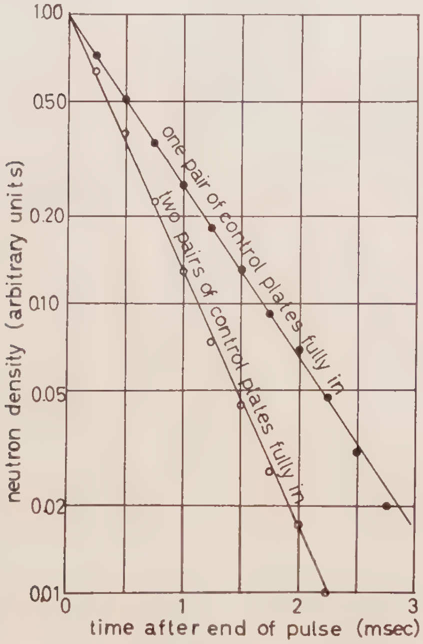

Fig. 19. Decay of the thermal neutron flux in the BSR–11 as a function of time after end of pulse for various subcritical conditions (after [62])).

$$\rho_{(1)} = -3.3 \pm 0.2\,\$\,, \quad \rho_{(1+2)} = -5.6 \pm 0.2\,\$\,.$$

Since for reasons of symmetry $\rho_1 = \rho_2$, we apparently have $\rho_{[1+2]} < \rho_{[1]} + \rho_{[2]}$ which shows mutual shielding effects between the two control plate pairs. Using stable period measuring techniques and the inhour formula, reactivities as large as several dollars cannot be accurately measured. It is a special advantage of the pulsed technique that it permits this type of measurement to be done with good accuracy.

3.5. FAST SYSTEMS; COMPARISON WITH ROSSI α METHOD

Investigations on fast systems have been performed by Passell *et al.*[55,65]) and by Bendt *et al.*[66]). The latter authors have studied prompt periods from the Godiva fast critical assembly at Los Alamos. The measurements were performed at two different positive reactivities between delayed and prompt critical, the reactivities being accurately determined from measurements of the (stable) reactor period. The resulting α values are plotted in fig. 20 as a function of reactivity, together with α-values independently determined by Orndorff[67]) using the "Rossi-α-method". This method, which has been frequently used for measurements on fast and intermediate reactor systems[55]), consists in a determination of α by analysis of time intervals between pairs of counts in a steady state, low power reactor system. A neutron detector placed in or near a chain-reacting system will present counts which are in part nonrandom due to the time correlation between neutrons having a

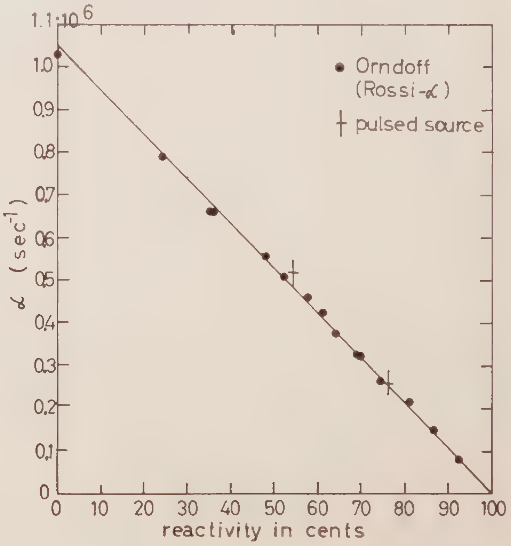

Fig. 20. α measurements on Godiva, plotted against reactivity (from [66])).

---

[65]) L. Passel, J. Bengston and D. C. Blair, UCRL–4808 (1957).

[66]) P. J. Bendt, H. J. Karr and F. R. Scott, Nucl. Sci. Eng. 4 (1958) 703.

[67]) J. D. Orndorff, Nucl. Sci. Eng. 2 (1957) 450.

common ancestor. The advantage of this method relative to the pulse method is apparently the fact that it does not involve a pulsed source, the equipment thus being much simpler and cheaper. The method is however only applicable in systems with a very short generation time which are close to criticality, otherwise the background problems will be increasingly difficult[55]). It is seen from fig. 20 that pulse method and Rossi-α-method give results which agree extremely well.

A comparison of the Rossi-α-method and the pulse method for a measurement of the neutron generation time in the Brookhaven Beam Research Reactor (BBRR) critical facility, a slightly undermoderated, enriched uranium – D_2O system, has been carried out by Price *et al.*[68]).

4. Measurements of Neutron Spectra in Moderators and Reactor Systems by the Time-of-Flight Method

4.1. GENERAL

Perhaps the most interesting application of pulsed neutron sources as far as physics is concerned is the study of neutron thermalisation processes in moderators and reactors. Such investigations yield information on the basic interaction processes between neutrons and bound atoms which are very important for solid state physics. On the other hand they make possible calculations of reactor spectra which have to be done in order to predict the long—term behaviour of power reactors.

If a fast neutron is born in a moderating medium it will successively pass through different stages of the slowing down and thermalisation process until it is finally thermalized, that means in an asymptotic state where its mean energy does not change with time. The following questions as to the thermalisation process arise:

a. What is the energy spectrum $\Phi(E,t)$ of the neutron as a function of time t?[†].

b. What especially is the asymptotic energy spectrum $\Phi_{as}(E)$ reached at the end of the thermalisation process?

c. What is the average spectrum of the neutron over its lifetime in the moderator?

Questions a. and b. are important mainly for the fundamental aspects of neutron thermalisation physics, while c. has a direct bearing on reactor spectra since it is the spectrum observed in a stationary assembly with steady neutron sources. All three questions can be answered by means of pulsed neutron sources. In each case, very intense neutron bursts are injected into the system under investigation, and neutrons from the moderator are allowed to enter into a neutron flight path about 10 meters long. Since the energy region of interest is about 10^{-2}–10^{2}eV, and since a 1 eV neutron has a flight time of 70 μsec/meter, sufficient resolution can be obtained when gate widths of $\leq$ 50 μsec are used.

Now in order to answer question a., a mechanical interrupter (slow chopper) is placed between the moderator and the flight path which is synchronized with the pulsed source in a way that it passes a short (a few μsec) burst of neutrons at a selected delay time t after the fast neutron burst injection. By varying t, $\Phi(E,t)$ can be completely determined. This is the principle of the elegant "neutron life history experiment" which was proposed by Poole[69]) and is currently being done at Harwell. Since t can be made large, the measurement can be extended into the asymptotic region, thus answering question b. also.

If it is desired to observe only the asymptotic spectrum a somewhat different technique can be used[70]). A "shutter" prevents neutrons from entering the flight path during the thermalisation process and opens only after complete equilibrium has been reached. We shall discuss this method and its application to water systems in section 4.

The method of taking the "average" spectrum depends on the neutron lifetime of the system. If this is short (of the order of 50–100 μsec) as in hydrogenous moderators, all the neutrons from the moderator are admitted to the time-of-flight analysis, the system thus performing the time integration itself. This method was first used by Poole[71] and will be reviewed in section 4.3. If the system has a long neutron lifetime like D_2O or graphite, this method cannot be used since unreasonably long flight paths would be necessary in order to achieve good resolution. For this case, a very interesting "sampling" technique has been developed by Beyster *et al.*[72] which we shall discuss later.

[†] The "energy spectrum" of a neutron can of course be only defined in the sense of an "average spectrum" if many neutrons have started at $t = 0$.

[68]) G. Price, personal communication (1960).

[69]) M. J. Poole, Symp. on Application of Pulsed Neutron Techniques, Berkeley (1958) UCRL–5665.

[70]) K. H. Beckurts, Internal Karlsruhe report (1960).

All these investigations use rather high neutron source intensities, the experimental equipment is almost one order of magnitude more complex and expensive than for the simple moderator studies outlined in section 2. However, before the arrival of these advanced techniques very nice experimental work has been done using low intensity neutron sources and a simple transmission method in order to study the time behaviour of the mean neutron energy during the thermalisation process. The reader is referred to the early work of von Dardel[73], which represents one of the most important contributions to pulsed neutron source research.

4.2. INSTRUMENTATION

Neutron spectra determinations by the time-of-flight technique require extremely high neutron intensities, at least of the order of 10^9–10^{10} per burst. Most work has therefore been done using high intensity electron linear accelerators. Two major facilities are in use now: The new Harwell accelerator[3] and the General Atomic accelerator[74]. Both have electron energies of the order of 25 MeV and deliver microsecond electron pulses with currents above 100 mA to neutron producing targets, the neutron yield thus exceeding 10^{10}/burst. Since the repetition rate of these accelerators is normally too high for spectrum observations, and since it is desired to operate other experiments simultaneously, pulsed beam deflection magnets are used which deliver selected electron pulses to the neutron target of the system under investigation.

We shall not go into the details of the construction of choppers which are sometimes used for these experiments, nor shall we deal with the problems of detectors and time analyzers since these are the same as used in standard slow neutron spectroscopy.

4.3. MEASUREMENT OF THE "INTEGRAL" SPECTRUM

Fig. 21 shows the arrangement used by Poole[71] for the investigation of neutron spectra from water and from boric acid solutions.

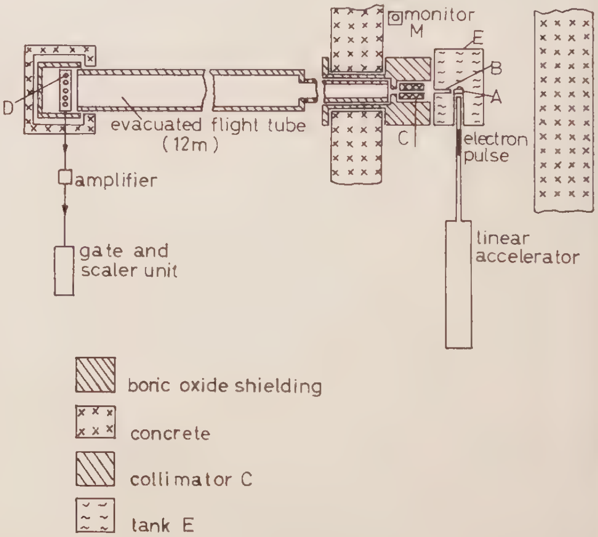

Fig. 21. The arrangement used by Poole for spectra measurements on water and boric acid solutions (from [71]).

Neutrons are extracted from the system by means of a reentrant channel. A very carefully designed collimator at the entrance of the flight path is of vital importance in order to prevent unwanted neutrons to enter. Also, great care has to be taken in shielding the flight path and the detectors against room-scattered neutrons. The neutron spectrum thus observed is the spectrum leaking at the end of the reentrant channel in one particular direction. Since the desired quantity is the spectrum averaged over all directions, it is necessary to apply corrections which

[71] M. J. Poole, J. Nucl. En. **5** (1957) 325.

[72] W. M. Lopez, J. R. Beyster, R. E. Nather, R. B. Walton and J. L. Wood, Trans. Am. Nucl. Soc. **3**, 1 (1960) 173.

[73] G. F. von Dardel, Trans. Roy. Inst. Technol., Stockholm **75** (1954).

[74] J. R. Beyster, J. L. Wood, W. M. Lopez and R. B. Walton, Trans. Am. Nucl. Soc. **3**, 1 (1960) 157.

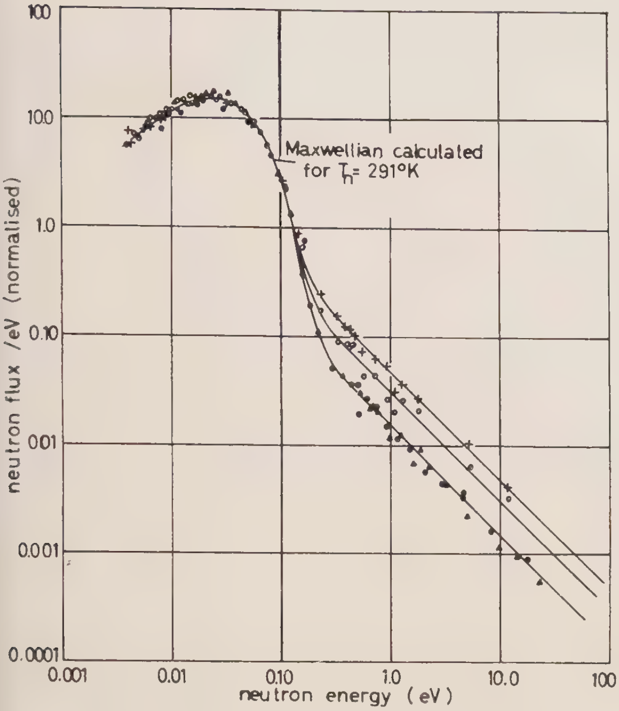

+ spectrum 2 cm from source
○ spectrum 5 cm from source
▲ spectrum 10 cm from source
● spectrum 12.5 cm from source

Fig. 22. Flux spectra in water of room temperature (from [71])

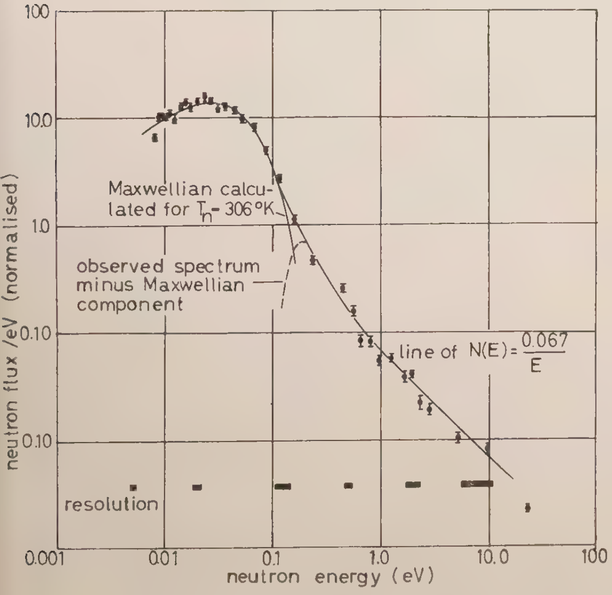

Fig. 23.
Flux spectrum in boric-acid solution at room temperature; 1.5 barn capture cross section per H-atom present (from [71])).

depend on the flux gradient at the observation point. Fig. 22 shows the flux spectrum obtained from pure water at different distances from the source. It is seen that at distances above 10 cm equilibrium is reached which indicates the presence of the "infinite homogenous medium spectrum". This spectrum can be decomposed into a Maxwellian region at low energies, a transition region and a $1/E$-tail extending to higher energies. Spectra obtained from two boric acid solutions are shown in figs. 23 and 24. It is seen that the "neutron temperature" of these spectra exceeds the moderator temperature considerably which is a consequence of the strong "hardening".

Beyster *et al.*[74]) have measured neutron spectra in different aqueous solutions in polyethylene and in zirconium hydride by the same technique. As an example we present from their recent work the spectra obtained from cadmium sulfate solutions (fig. 25). Since cadmium has a resonance at 0.18 eV, a bump is expected to appear in the spectra at this energy. This is indeed present, as seen especially at the higher cadmium concentrations. In fig. 25, the measured spectra are also compared to spectra calculated using two different "thermalisation kernels" for water. One of these is the "free hydrogen kernel" as derived by Wigner and Wilkins[75]) while the other, developed by Nelkin[76]) takes into account the chemical binding of hydrogen in water in an approximate manner. It is seen that the "bound hydrogen kernel" calculations give very good agreement with the measured spectra.

We cannot go further into the details of the experimental work nor can we discuss here the status of thermalisation theory in explaining the measured spectra. These questions, as of 1958, are extensively discussed in the above-mentioned review article[13]). However some remarks as to the intercomparison of these techniques to stationary chopper methods should be made: Neutron spectra can also be measured by exciting the assembly under investigation with neutrons from a reactor and by chopping the beam of emerging neutrons in order to perform a time-of-flight analysis. This method has been applied to water systems by Stone and Slovaczek[77]) who found results which are in general agreement with Poole's measurements. The pulse method has the disadvantage that it can be used only on systems with a short die-away time of the neutrons while the chopper method can be used for all systems. The advantage of the pulse method over chopper-reactor methods is that easily altered geometric and a large range of parameters can be used; since for a chopper method fluxes between 10^8 and 10^{10}/cm^2 sec are necessary, certain contamination problems arise, especially if the system under investigation contains nuclear fuel. It seems therefore reasonable to use the pulse method on as many systems as possible, eventually with flight path lengths up to 100 m and at the expense of intensity and resolution.

---

[75]) E. P. Wigner and J. E. Wilkins, AECD 2275 (1948).
[76]) M. S. Nelkin, General Atomic Report GA–1063 (1960).

An elegant solution to the problem of neutron spectrum measurements on long living assemblies consists in the use of a chopper which samples short neutron bursts from the decaying assembly. In order to take a correct average over the spectrum of the assembly the delay time between the burst injection and the chopper opening is varied in such a way that the chopper scans with equal probability all portions of the neutron die away history in the assembly. This has been achieved by Lopez, Beyster *et al.*[72]) who use the chopper window as a reference point in time and generate a time delay, based on the chopper angle, to trigger the accelerator. The system has been used for preliminary experiments on graphite so far. It may open the possibility of investigating all systems by the pulsed source method.

4.4. A STUDY OF THE "ASYMPTOTIC" SPECTRUM IN WATER

In order to prove the "diffusion cooling effect" (section 2.1.) directly by observations of spectra, Beckurts[70]) has performed measurements of the asymptotic neutron spectrum in pure water assemblies as a function of buckling. The experimental arrangement is shown schematically in fig. 26. A neutron source emits bursts of neutrons (10^8 neutrons/burst) into small water systems. During the slowing down and

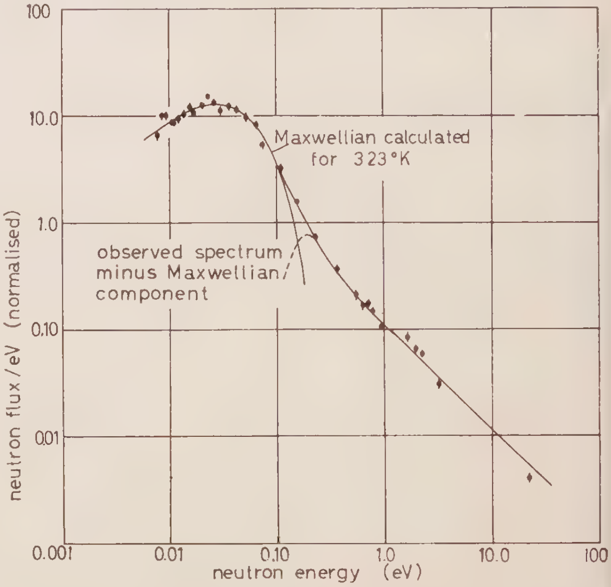

Fig. 24. Flux spectrum in boric-acid solution at room temperature; 2.9 barn capture cross section per H-atom present (from [71])).

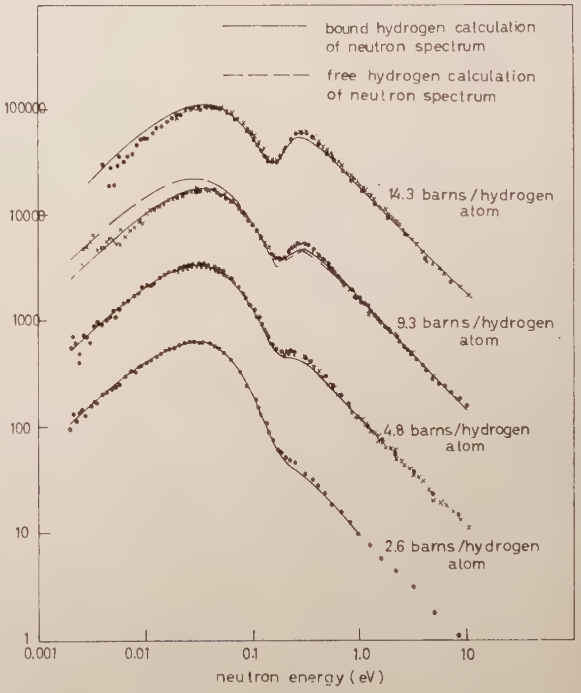

Fig. 25. Neutron spectra in water poisoned with cadmium sulfate of different concentrations (from [74]).

---

[77]) R. S. Stone and R. E. Slovaczek, Nucl. Sci. Eng. **6** (1959) 466.

thermalisation process, a shutter synchronized with the source prevents neutrons from entering the time-of-flight analyzer. It opens after the asymptotic state has been reached; since the thermal neutron population dies out successively in a time short compared to the neutron flight

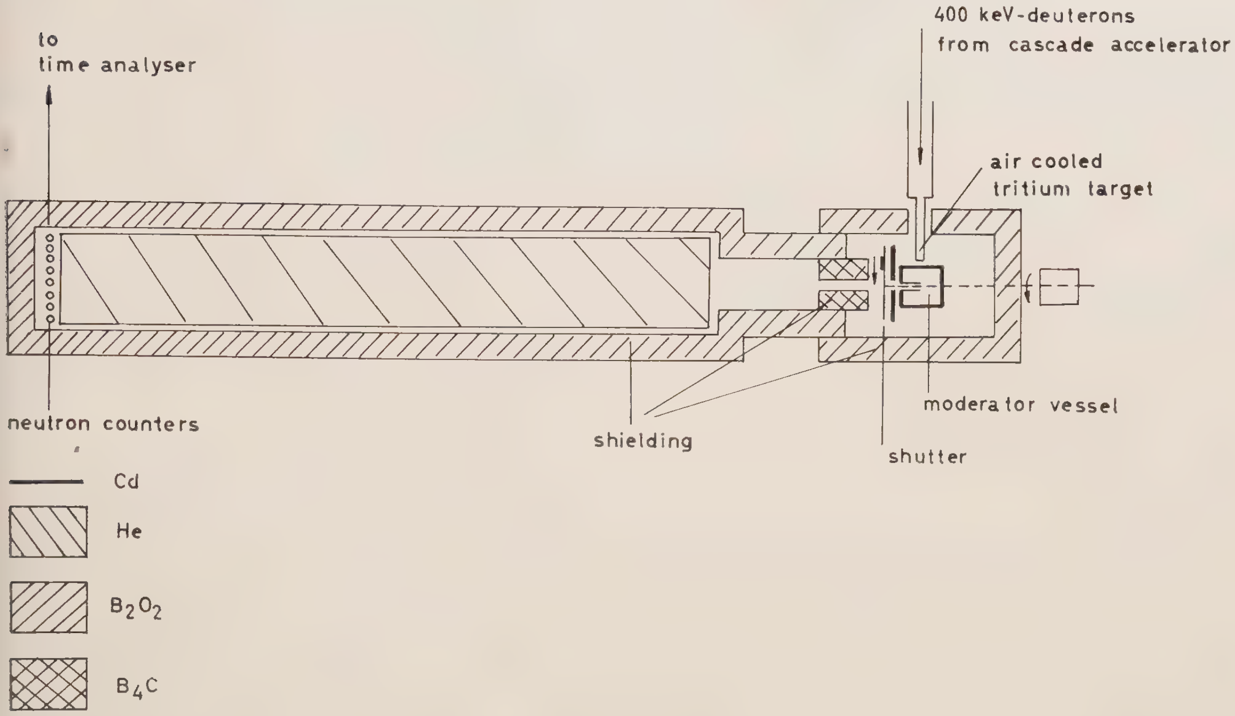
400 keV-deuterons
from cascade accelerator
to
time analyser
air cooled
tritium target
moderator vessel
neutron counters
shielding
shutter
Cd
He
B_2O_2
B_4C

Fig. 26. Arrangement for observation of "diffusion cooling" in water.

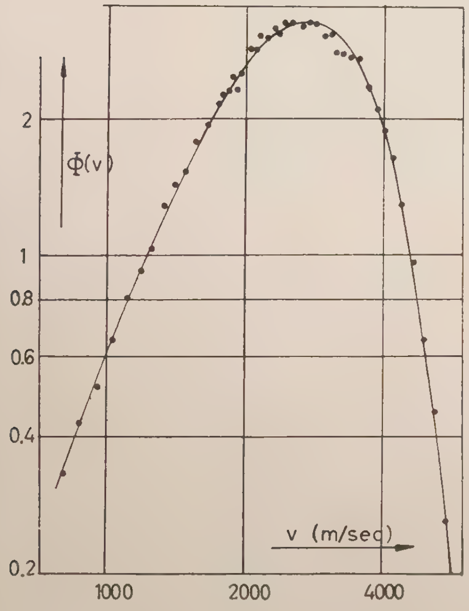

Fig. 27. The asymptotic spectrum from the center of a (15 cm)^3-water cube. Full curve: Maxwellian with moderator temperature.

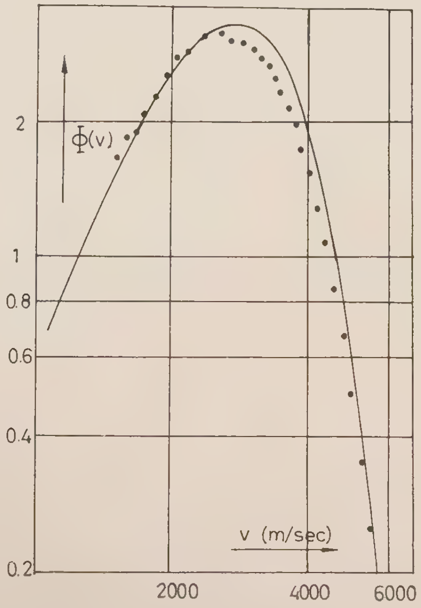

Fig. 28. The asymptotic spectrum from the center of a (5 cm)^3-water cube. Full curve: Maxwellian with moderator temperature.

time to the detector, the time spectrum observed can be immediately converted into the asymptotic energy spectrum.

Fig. 27 shows the neutron flux spectrum as extracted from the center of a large water cube, this is well represented by a Maxwellian distribution with moderator temperature as has to be expected. In fig. 28 however the same spectrum taken from a small moderator is shown. It is seen that a considerable "diffusion cooling" exists since the spectrum is shifted towards lower energies. Preliminary calculations show that the amount of shifting is consistent with calculations based on a $M = 18$-model of the water. The above-mentioned method has also been used to study leakage spectra energing from the surface of the moderator.

5. Conclusions

The pulsed neutron source technique can be used to solve many reactor physics problems. In most of its applications, it is superior to other methods since it allows normally more insight into the physics of a particular problem and gives more accurate results. Most work so far has been devoted to the study of diffusion parameters of pure moderators. Very noteworthy results have been obtained, however much work remains to be done in order to resolve discrepancies and to improve the accuracy. The field of reactivity measurements on reactor systems is still in its beginnings. It is expected that α vs. B^2 measurements on subcritical reactor systems can give a remarkable contribution to reactor physics and help to establish accurate reactor calculation methods. The possibility of neutron spectrum measurements with pulsed neutron sources has considerably accelerated the progress in neutron thermalisation physics. Many important results are still to be expected here, particularly by the combination of pulsed source and chopper techniques which is now performed in several laboratories.

The present article is to a very substantial part based on preprints and private information concerning unpublished work. The author wishes to express his gratitude to the members of the various research groups for communicating this information, particularly to Drs. W. M. Andrews (UCRL), J. R. Beyster and W. M. Lopez (General Atomic), G. de Saussure (ORNL), G. R. Keepin (LASL) and G. A. Price (BNL).

NUCLEAR INSTRUMENTS AND METHODS **11** (1961) 169–178; NORTH-HOLLAND PUBLISHING CO.

THE KS–3 MeV VAN DE GRAAFF INJECTOR OF THE FRASCATI ELECTRON SYNCHROTRON †

FERNANDO AMMAN

Laboratori Nazionali di Frascati

The modifications apported to a standard 3 MeV Van de Graaff, used as injector for the 1100 MeV Frascati synchrotron, are reported.

They concern the voltage stabilizer, a compensation circuit that takes care of the fast variations of the voltage at the belt frequency, and the Pierce type electron source.

A few data concerning the synchrotron operation in the period Jan. 1–Aug. 31, 1960, are added.

Finally it is shortly described the project of a storage ring for 250 MeV electrons and positrons which is being built in Frascati.

1. Introduction

The Frascati synchrotron is an electron accelerator with a maximum energy of 1100 MeV, an average intensity of 5×10^9 electrons accelerated per pulse and a repetition rate of 20 pulses per second.

The electron beam coming from the injector at an energy of 2.6 MeV, goes through a system of magnetic lenses, then past an electrostatic inflector, which injects it tangentially into the synchroton magnetic field; there the electrons are accelerated up to the final energy by two radio frequency cavities.

At the maximum energy, 23 milliseconds after the injection, the electrons strike a tantalum target, 0.5 mm thick, equal to 0.13 radiation lengths; the experiments use the γ-ray beam thus produced which has a continuous spectrum of energy, up to the maximum electron energy, and a half-width of 3.5 mrad at 1000 MeV.

Fig. 1 shows a view of the synchrotron room; one can see the injector, the pipe connecting the injector to the inflector, along which are two magnetic lenses and four coils for the beam positioning, the electrostatic inflector and the radio frequency cavities.

The injector is a standard KS–3 MeV Van de de Graaff of the High Voltage Engineering Corporation; a few modifications have been made, of course, and they are the subject of the following report.

I think that we must say, first of all, that these modifications have been limited as much as possible; our aim was to get, in a short time, a suitable injector for the synchrotron, whose prime requirement was reliability.

The modifications inside the tank have been confined to the cathode and its pulser; other modifications required a lot of time and experience that we do not have.

Unfortunately the time at our disposal to study the behaviour of the injector and the general problems of injection in the Synchrotron, has been very short indeed.

2. Injector Specifications

The specifications for the electron beam at the injector output fall into three classes:

2.1. Energy
2.2. Intensity
2.3. Optics

2.1. ENERGY

Because of the small acceptance in momentum of the inflector and the synchrotron, the electron energy must agree, within 0.1 %, with the inflector voltage and the synchrotron magnetic field. This means that a stability in energy of 0.1 % would be required, if the other two parameters were kept constant.

---

† Report of the Synchroton Staff, Laboratori Nazionali di Frascati, delivered by Fernando Amman.

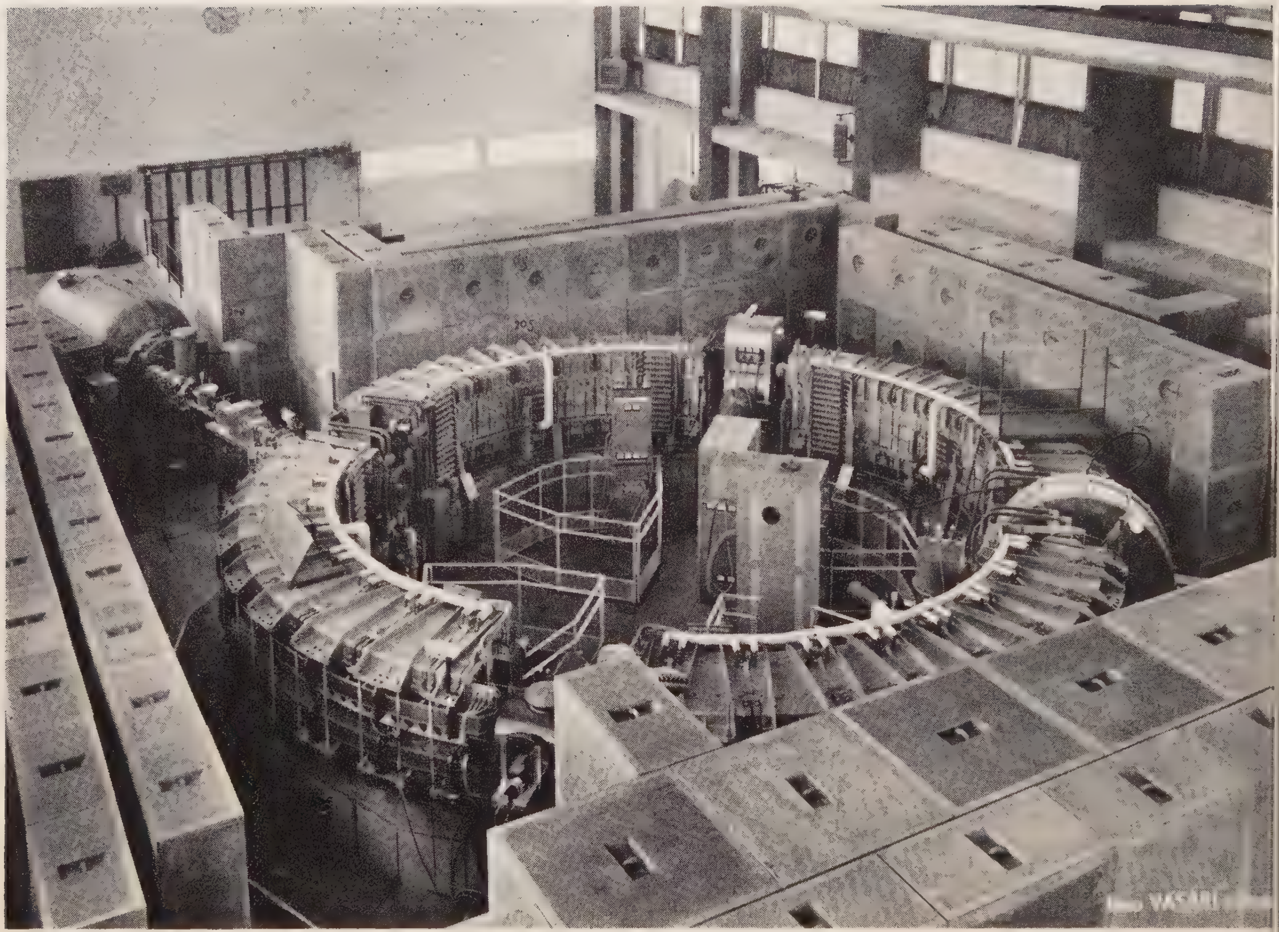

Fig. 1. The Frascati 1.1 GeV electron synchrotron. General view.

It is known that the voltage of a Van de Graaff has fast variations, with the belt frequency (their value depends on the belt). In the 3 MeV Van de Graaff it is usually between ± 0.5 % and ± 1 %.

The belt charge system at the base cannot of course take care of these variations at the belt frequency.

The corona stabilizer, used in positive machines, should be mounted on the high voltage terminal, and this produces a lot of problems.

Another easier system could be devised: to use the down belt charge, like a corona stabilizer, driven by a feedback signal transmitted to the high voltage terminal with a frequency-modulated light; but, as said before, we did not want to install anything inside the tank unless absolutely necessary.

Then, following more or less what had already been done at the Cornell University Synchrotron, we do not try to cancel the fast variations, but vary the other two parameters, namely the inflector voltage and the magnetic field at the injection time, in agreement with the injector voltage.

This compensation takes care of the fast variations of the injector voltage, with a frequency band from about 0.1 c.p.s. up to very high frequencies.

Besides this the injector needs a low frequency stabilizer to hold the mean voltage constant within 0.1 %, with a high gain in the frequency range from zero to 0.1 or 0.2 cycles per second.

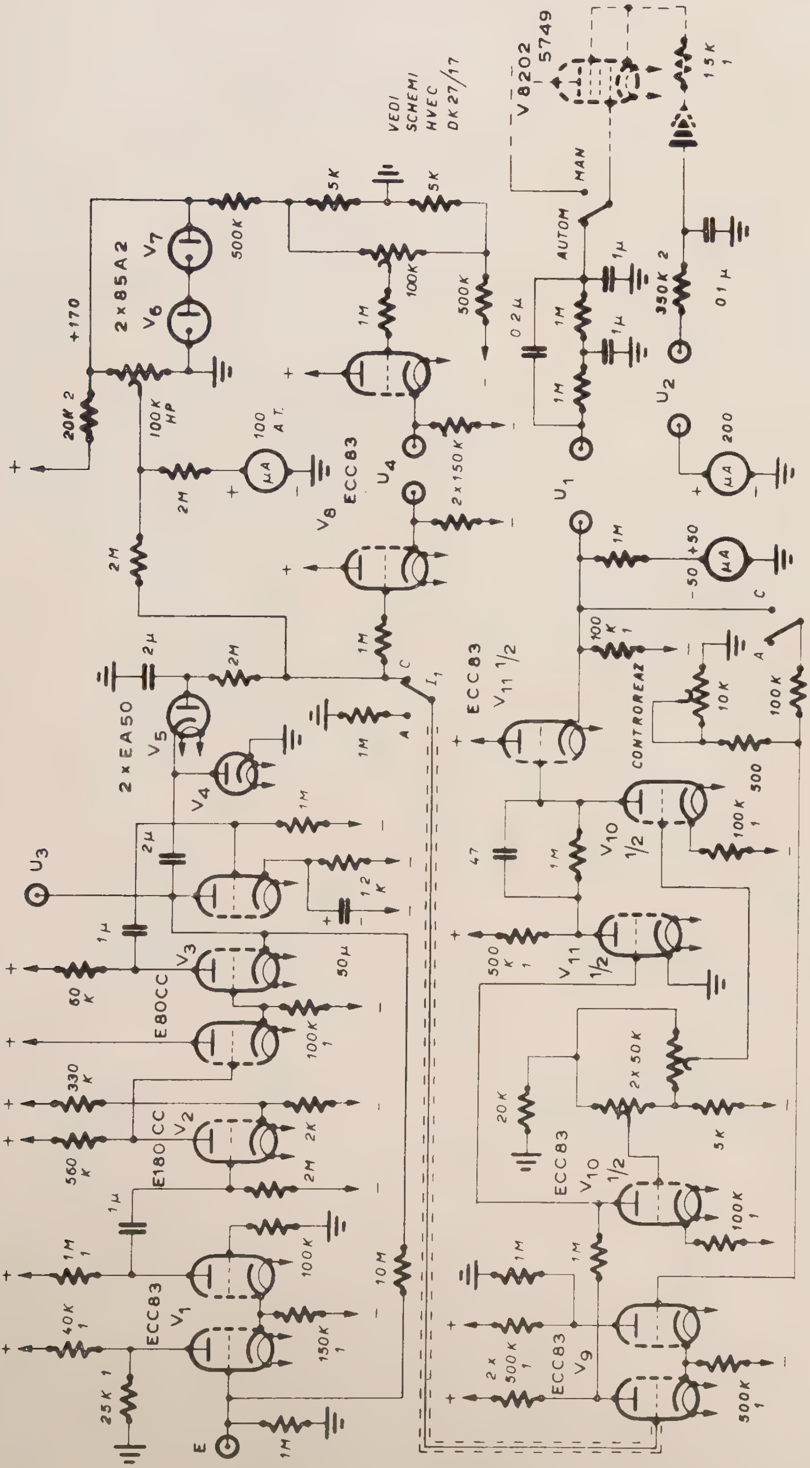
E
1M
25K 1
40K 1
1M 1
ECC83
V1
150K 1
100K
10M
1µ
560 K
330 K
E180CC
V2
2M
2K
E80CC
V3
60 K
1µ
50µ
100K 1
U3
2µ
1.2 K
1M
V4
2×EA50
V5
2µ
2M
1M
A
C
I1
2M
2M
20K 2
+170
100K HP
2×85A2
V6
V7
500K
100 AT.
µA
V8
ECC83
U4
2×150K
1M
100K
500K
5K
5K
VEDI
SCHEMI
HVEC
DK27/17
V8202
5749
MAN
AUTOM
1µ
1µ
0.2µ
1M
1M
U1
U2
350K 2
0.1µ
15K 1
200
µA
1M
+50
-50
C
A
100 K 1
10K
100K
CONTROREAZ
500
ECC83
V11 1/2
V10 1/2
47
1M
100K 1
500 K 1
V11 1/2
2×50K
20K
5K
ECC83
V10 1/2
100K 1
1M
1M
2× 500K 1
ECC83
V9
500K 1

Fig. 2. Low frequency stabilizer.

2.2. INTENSITY

A 100 mA beam, in pulses of 2 μsec, is required. The original cathode has been changed and a Pierce type source is used.

2.3. OPTICS

The beam coming from the injector must have small divergence, of the order of 10^{-3} rad, and a diameter not greater than 2 cm, to avoid the use of many magnetic lenses.

This requires a careful design of the source.

3. The Low Frequency Stabilizer

A very simple equivalent circuit of the Van de Graaff voltage generator can be assumed to consist of a current generator (the belt charge system), a fixed time delay (the time for the charges on the belt to travel from the base to the terminal) and a time constant RC, R being the loading resistor and C the capacity between the terminal and ground. The time delay is of the order of 0.1 sec and the time constant 2.3 sec.

The open loop frequency response of the generator up to 2.5 c.p.s. (the point at which there is a 180° phase shift between input and output) has been measured; it is in good agreement with the above mentioned simple equivalent circuit.

The original stabilizer did not meet the requirement of a mean stability within 0.1 %.

We have built a new stabilizer, whose diagram is shown in fig. 2.

The signal from the generating voltmeter goes to an amplifier, whose gain is about 2000; its output is fed back to the input, with a change in phase of 180°, through a resistance of 10 MΩ. The amplifier is used to match the impedance and to cancel the effects of stray capacitances.

The output signal depends on the rotation frequency of the generating voltmeter; we use a frequency-stabilized supply, we had already for other equipment, whose stability is better than 0.1 %.

This AC signal, whose amplitude is 150 V peak to peak for a terminal voltage of 3 MeV, is rectified and compared with the reference voltage. The difference signal is amplified by a factor of 30, and after a network, goes to the grid of the pentode of the belt charge circuit. The pentode has a negative feedback due to the high resistance in its cathode. The other parts of the charge circuit are unaltered.

The network at the pentode grid is like the one mounted on the original stabilizer, except for the maximum attenuation frequency, which is lower; this allows a greater phase margin, and therefore smaller overshoots.

The open loop static gain of the system is 120–130. This is enough to hold constant the mean voltage of the Van de Graaff within 0.1 %, as required.

4. The 'Pick Up Compensation'

As has been mentioned before (section 2), the fast disturbances introduced by the belt cannot be corrected by the stabilizer; the "pick up compensation", which changes the voltage of the inflector and the magnetic field at the injection time, takes care of them.

The necessary information is obtained from a signal induced on a pick up electrode, mounted in a hole in the tank: this signal is proportional to the terminal voltage variation. The compensation circuit diagram is shown in fig. 3. There is a preamplifier, whose first stage is an electrometer tube, and two amplifiers, one for the inflector, and the other one for the injection timing.

The system is AC coupled: the time constants are greater than 20 sec, to allow a good linearity from high frequency down to 0.05 c.p.s. With this "pick up compensation" the result is the same as if the fast variations of the terminal voltage were decreased by a factor greater than 10, while holding constant the other parameters (inflector voltage and magnetic field at the injection time).

On this subject, it may be interesting to mention a phenomenon which occurred at the beginning of the synchrotron operation.

When the injected current was high, the accelerated intensity oscillated from zero to a maximum, with a period of the order of 5 seconds.

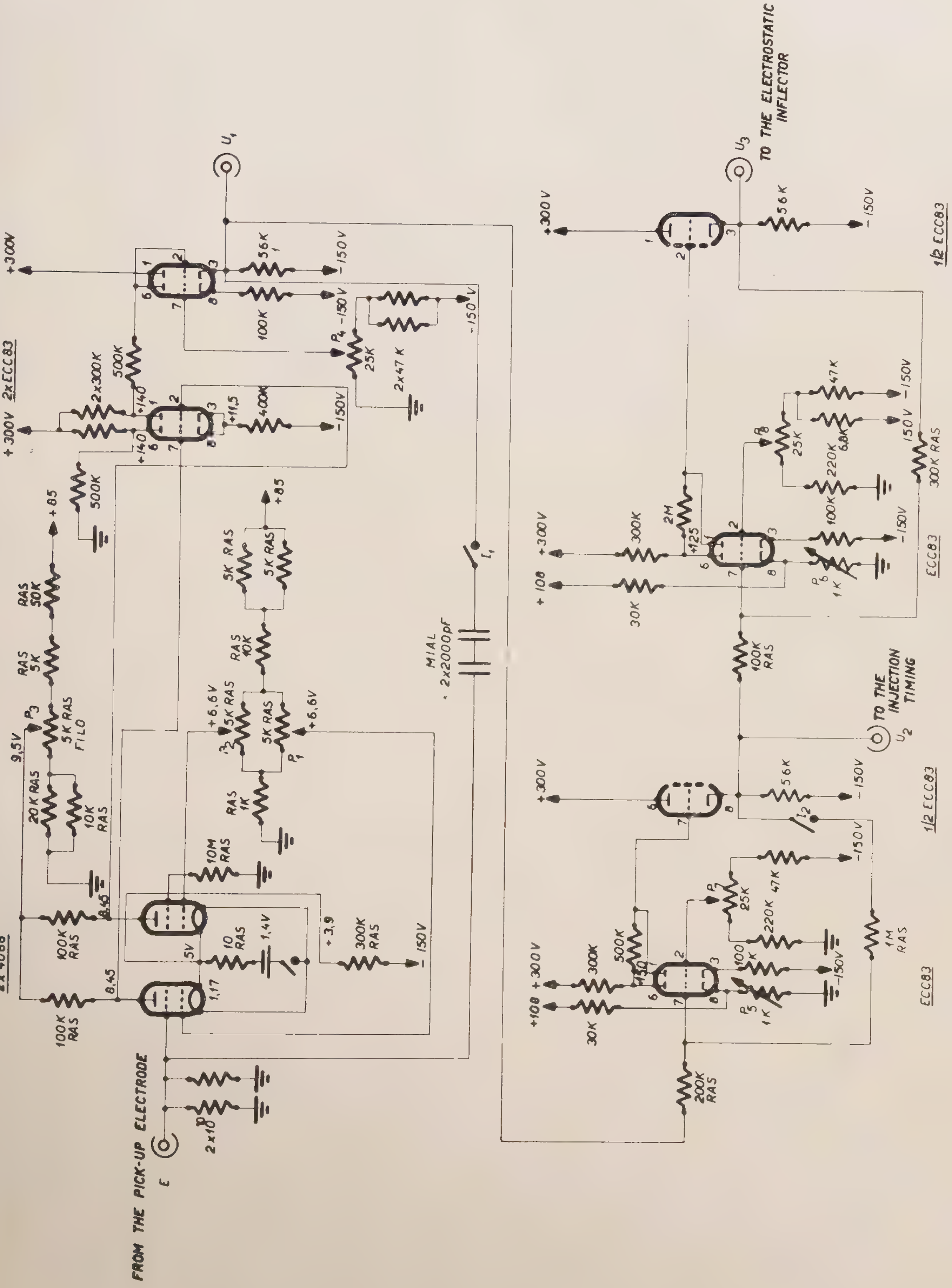
FROM THE PICK-UP ELECTRODE
E
2x10^8
2x 4066
100K RAS
100K RAS
8,45
1,17
5V
10 RAS
1,4V
+3,9
300K RAS
-150V
10M RAS
20K RAS
10K RAS
9,5V
P3
5K RAS FILO
RAS 5K
RAS 50K
+85
RAS 1K
5K RAS
P1
+6,6V
RAS 10K
5K RAS
+85
MIAL 2x2000pF
I1
500K
+300V
2xECC83
2x300K
500K
+140
+11,5
400K
-150V
P4
25K
2x47K
-150V
+300V
56K
100K
U1
+300V
-150V
U3
TO THE ELECTROSTATIC INFLECTOR
56K
1/2 ECC83
+300V
300K
30K
+108
2M
+125
P8
25K
47K
220K
6,8K
100K
300K RAS
P6
1K
ECC83
100K RAS
U2
TO THE INJECTION TIMING
+300V
56K
I2
-150V
1/2 ECC83
+108
+300V
30K
300K
500K
150
P7
25K
47K
220K
100K
P5
1K
1M RAS
200K RAS
ECC83

Fig. 3. Compensation circuit.

The pick up output had a similar behaviour, not justified by terminal voltage variations, because the signal from the generating voltmeter was regular.

This effect has been eliminated by shielding the Van de Graaff from the Synchrotron with concrete blocks, and the bushing of the pick up with lead.

We made the hypothesis that the effect was caused by a change in the characteristics of the dielectrics of the pick up (bushing and cable) in a strong radiation field, due to the high accelerated beam intensity. This change altered the behaviour of the compensation circuit, when the intensity was high, thus decreasing it to zero; at this point the compensation circuit recovered, the accelerated intensity increased up to a maximum, and the process repeated.

5. The Electron Source

The design of the source is based on the imposed condition that the electrons coming from the filament must keep parallel trajectories while they are accelerated.

With this condition we found a differential equation for the potential along the tube, which depends on the beam current density; this equation must be integrated numerically. However useful information can be drawn directly: the limiting value of the electric field in the tube when the kinetic energy approaches infinity always with the above mentioned condition of parallel trajectories, is given by:

$$E_\infty = \sqrt{\frac{\pi W_0}{\varepsilon_0 qc} J} = 2.43 \times 10^4 \sqrt{J}$$

where: E_∞ is the limiting value of the electric field, in V/m,

J is the beam current density, in A/m^2;

W_0 is the electron rest mass in energy units;

ε_0 is the vacuum permittivity;

c is the speed of light.

The value of the electric field given by this relation differs by 13 % at 1 MeV, and 7 % at 2 MeV from the exact value. From this we get that at a maximum energy of 2.6 MeV, corresponding to a mean electric field in the tube of 15.3 kV/cm, the upper limit of the current density for a parallel beam is 4×10^3 A/m^2.

We roughly evaluated the space charge effect on the electron beam, in the interval 100 keV–2.6 MeV, supposing it parallel at 100 keV, for current densities higher than the limit given above; at 10^4 A/m^2 we get a divergence of the order of 10^{-3} rad.

As this divergence is small enough, the source has been built so that the potential along the tube axis has the calculated values up to about 80 kV; from here on the field is practically uniform.

Using an electrolytic tank, we determined the voltages of the grid and the first three electrodes that gave the electric field we wanted on the tube axis.

The grid voltage is given by a pulser, which we will talk about later on; the electrodes voltage is determined by the resistors between the planes.

The results obtained with this source are sufficiently good; the beam divergence is of the order of $2–3 \times 10^{-3}$ rad at 50 mA.

A point we think must be improved, is the voltage distribution to the first electrodes; the resistors change in value with time and the optics get worse.

The source is composed of a Pierce-shaped tantalum electrode, equipotential with the filament; in its center, in a hole 6 mm in diameter, is the tantalum filament, which is shielded at the back to decrease the power radiated; at 8 mm from the filament there is the grid, with a hole 5 mm in diameter, supported by three ceramic spacers: the grid is made with very pure and polished aluminum. Fig. 4 is a view of the source mounted in the accelerating tube. The filament is made with tantalum wire, 0.5 mm in diameter, drawn to a cross-section of about 1×0.2 mm^2, arranged in a zig-zag shape within a circle 5 mm in diameter.

The zig zag has been preferred to the spiral, because with the spiral arrangement the electron beam had a hole in the center, due to the magnetic field of the heating current.

With these filaments we obtained 100 mA at the output of the Van de Graaff, with a power of about 40 W. Usually we work with 40 mA, and the heating power is 30–35 W.

The mean lifetime of the filaments is 300 hours; we prefer to change them every two weeks, which means 250 hours of active life, rather than to wait for their failure.

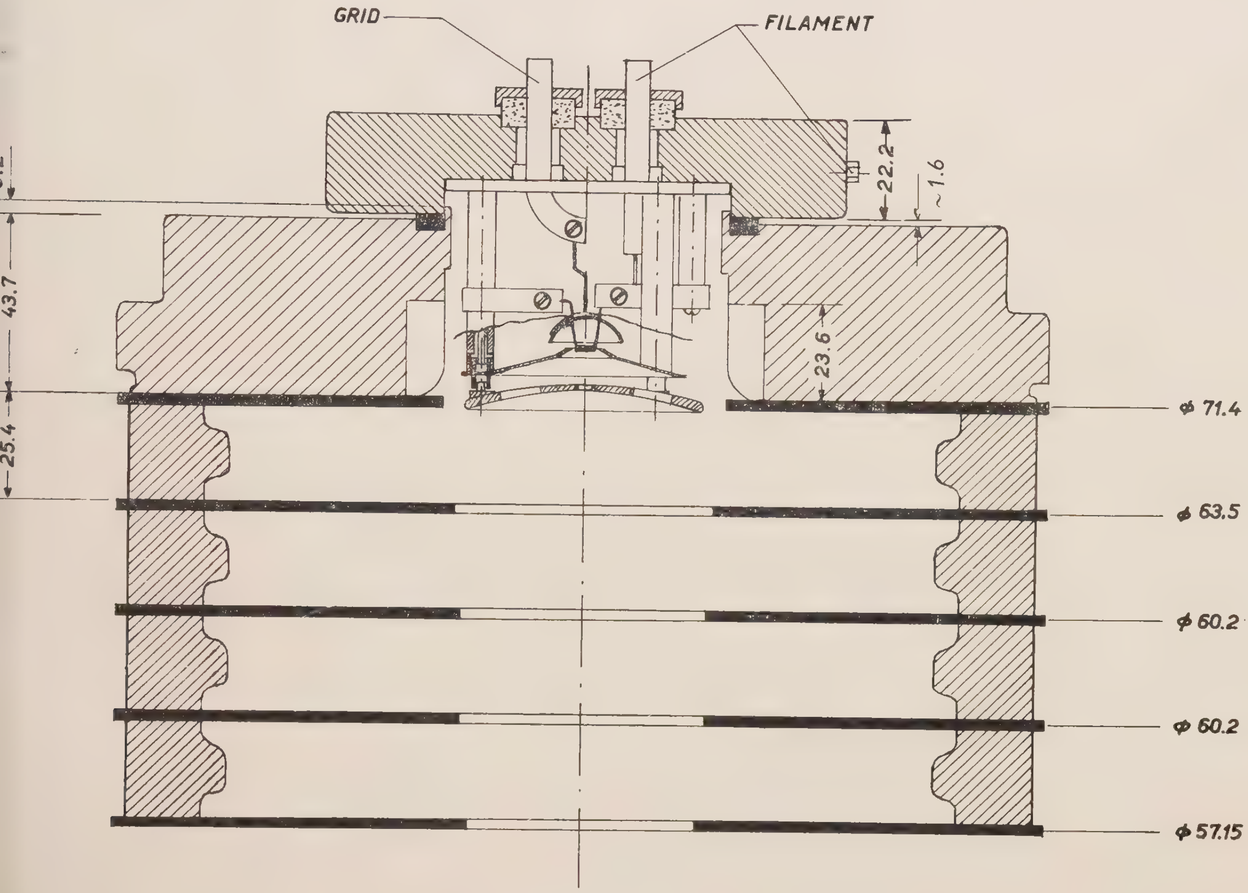

Fig. 4. Electron source.

The pulsed beam is obtained by swinging the grid, which is normally at —500 V with respect to the filament, up to +5000 V for 2 μsec. In fig. 5 is the circuit diagram of the pulser.

A light pulse from a neon (type GE-NE2) mounted inside the tank is transmitted with a light pipe to the terminal and detected by a 931-A photomultiplier, which drives the pulser; this includes an amplifier and a thyratron, at the plate of which there is a wave-shaping line which determines the pulse length.

The pulse, brought up to 6000 V by means of a pulse transformer, then goes to the grid.

The pulse height is variable from outside by changing the plate voltage of the thyratron. The grid pulse has a jitter smaller than 10^{-7} sec (of the order of 10^{-8} sec); this is obtained by keeping the neon lamp normally on and driving it, during the pulse, with a current 200 times larger than the rated current.

6. Injector and Synchrotron Operation

We think it useful to give here an idea of the operating conditions and performance of both the injector and synchrotron.

The schedule for approximately the last year has been as follows: 132 hours per week of operation, of which 126 are assigned to experiments, in shifts of 21 hours per day; on Mondays, 13 hours for the normal maintenance (this in-

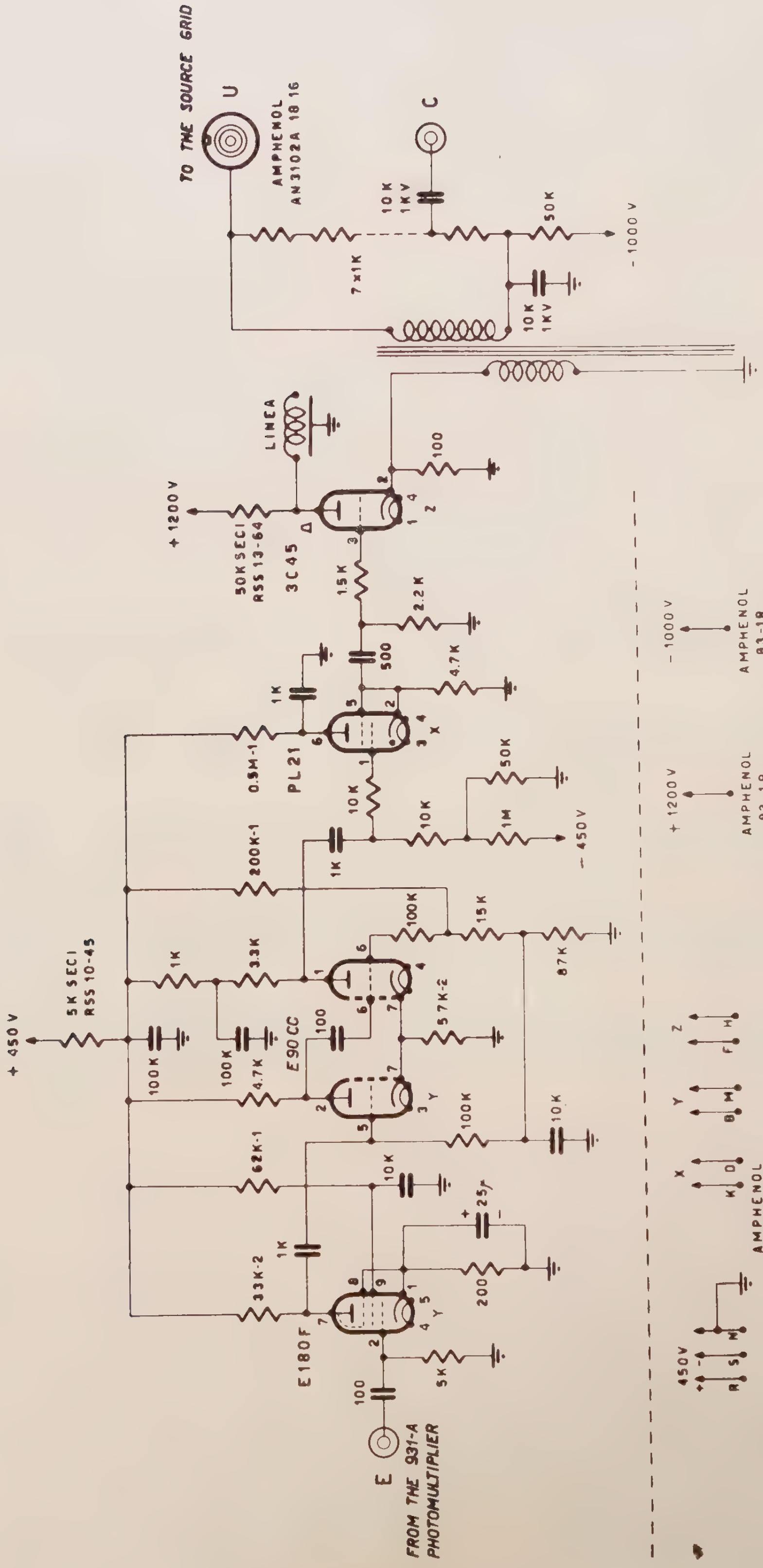
FROM THE 931-A PHOTOMULTIPLIER
E
100
E180F
5K
33K-2
1K
200
25μ
10K
62K-1
100K
4.7K
E90CC
100
100K
3.3K
1K
57K-2
10K
100K
15K
87K
200K-1
+ 450 V
5K SECI RSS 10-45
1K
10K
10K
1M
50K
- 450 V
0.5M-1
PL21
1K
500
4.7K
2.2K
1.5K
3C45
50K SECI RSS 13-64
+ 1200 V
LINEA
100
TO THE SOURCE GRID
U
AMPHENOL AN3102A 18 16
7 x 1K
10 K 1 KV
C
50K
10 K 1 KV
- 1000 V
450V
R S N
AMPHENOL AN3102A-20-29
X Y Z
K D B M F H
+ 1200 V
AMPHENOL 83-1R
- 1000 V
AMPHENOL 83-1R

Fig. 5. Electron source pulser.

cludes, once every two weeks, changing the injector cathode).

The running time in the period January 1–August 31, 1960, has been 4020 hours, 98 of them have been spent for the injector conditioning (something less than half an hour per day); the time lost for failures, in the same period, has been 434 hours, 170 of them for injector failures.

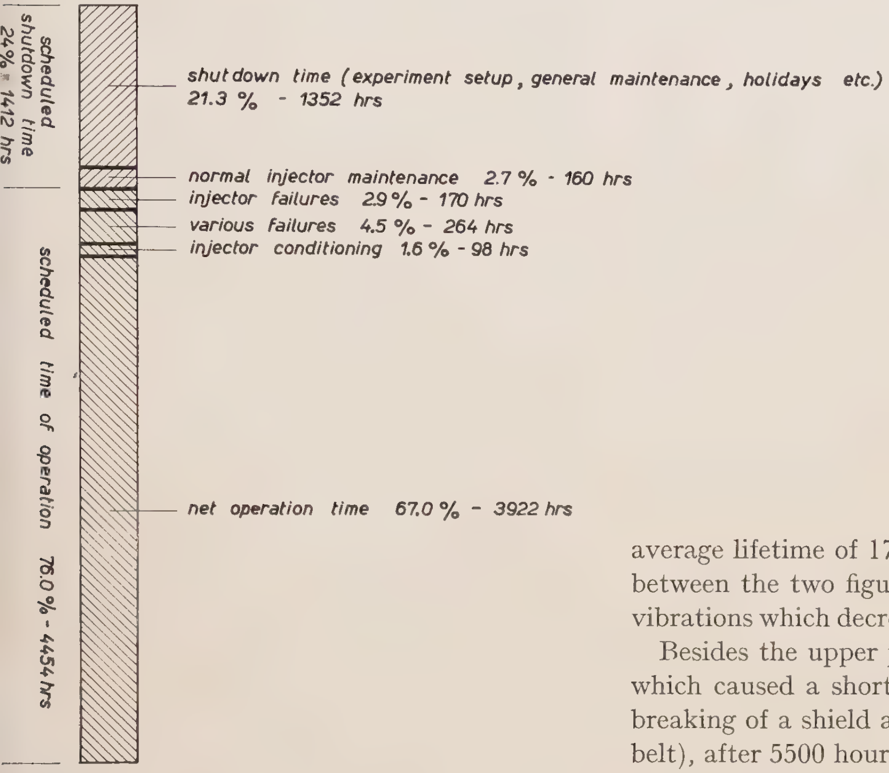

Fig. 6. Injector and synchrotron operation (period Jan. 1–Aug. 31, 1960).

For the injector, normal maintenance has amounted to 160 hours; the tank has been opened 20 times.

All these figures are displayed together in fig. 6; the net efficiency of the synchrotron has been 67.0 %; the efficiency with respect to the scheduled time of operation 88.2 %.

Before we examine the kind of failures we had to the injector, we must recall that our Van de Graaff runs at 2.6 MeV, with a very low average current (1–3 μA); therefore, as is actually the case, we should not expect many electrical faults.

The failures we have had up to now are mainly mechanical, and the weak point has been the bearings of the upper pulley.

With the rated load and speed, the average lifetime of the bearings used should be of the order of 8000 hours; in 7000 hours we had an average lifetime of 1750 hours; the discrepancy between the two figures is probably due to the vibrations which decrease the life of the bearings.

Besides the upper pulley failures (the first of which caused a short circuit to the motor, the breaking of a shield and, in consequence, of the belt), after 5500 hours the accelerating tube has been changed, because the first insulator towards the terminal had some tracks on the glass inside.

As far as the synchrotron as a whole is concerned, the maximum γ-ray beam obtained up to now is 8×10^{11} equivalent quanta per minute, which corresponds to about 6×10^{9} electrons accelerated per pulse, with an injected beam of 40 mA; up to this limit the accelerated intensity increases roughly linearly with the injected intensity. With higher injected current, the accelerated intensity does not increase; this is caused, at least in part, by a coupling between the two radio frequency cavities, due to the beam itself, which excites synchrotron oscillations and therefore sets a limit to the intensity.

However this is not, probably, the only cause; all accelerators show this "saturation" phenomenon.

A complete study of the problem would certainly require a long machine time; for the time being, we prefer to carry it on at odd moments because the intensity already obtained justifies the full effort being devoted to experiments.

7. A Storage Ring for Electrons and Positrons

It may be interesting, to spend a few words on a project on which part of the synchrotron staff is now working.

Following a proposal of Prof. Touschek, of the University of Rome, last March has been decided the construction of a small storage ring for 250 MeV electrons and positrons; it should be ready for operation at the beginning of the next year, 1961.

The magnet weights 8 tons; the equilibrium orbit radius is 58 cm; it is a weak focusing magnet with $n = 0.6$ and four quasi-straight sections; the stainless steel donut, in which are stored on the same orbit both the electrons and the positrons, has a cross section of 45 mm × 90 mm; the radiofrequency cavity, which takes care of the radiation losses (600 eV per turn at 250 MeV), is at 155 Mc/sec with 10 kV peak to peak.

The injection of electrons and positrons into the storage ring will be obtained with a double conversion, bremsstrahlung on an internal target in the synchrotron, and pair production on two converters in the storage ring.

First are injected, for instance, the electrons produced on one of the converters, for a certain number of synchrotron pulses; then the whole storage ring is moved, while the γ-ray beam stays at the same place, another converter is inserted in the storage ring and the positrons produced on this second converter are injected. Of the total number of electrons and positrons produced by the γ-ray beam in the two converters, a small part, within a certain energy range, around 250 MeV, and within a certain angle, will be accepted in the storage ring.

The factors affecting the beam lifetime are essentially the vacuum and the radio frequency voltage; in our case, with an RF voltage of 10 kV, the most limiting factor is the vacuum which gives a lifetime of 2 hours at 10^{-8} mm of Hg, and a factor of 100 longer at 10^{-10} mm of Hg.

With a vacuum of 10^{-8} mm of Hg (but we should get a better vacuum), we should, in principle, store up to 10^5 particles.

With these intensities it will be practically impossible to do high energy physics research, except, may be, with nuclear emulsions.

But what certainly can be done, is the study of the behaviour of the storage ring; using the irradiated light (about 10^7 photons per electron per second in the visible range at 250 MeV) we will be able to study a circulating beam of 100 electrons. The intensity necessary to study the interactions between e^+ and e^- (annihilation, π and μ mesons pair production, π^0 production) should be of the order of 10^8 particles, to get a reasonable counting rate for counter experiments (between 1 count/sec and 0.01 counts/sec).

We do not exclude, of course, if we will be able to find some way to improve the injection efficiency, to get the above mentioned intensity that will allow some high energy physics research with this storage ring; but we consider that its purpose will be achieved if it will allow a better understanding and a check of the theory of the particle storage process.

DISCUSSION

Speaker adressed: F. Amman (*Frascati*)

Question by: Kai Siegbahn (*Uppsala*)

Question: Did I understand you correctly that an increase in the injector current above 100 mA would not increase the output current of your synchrotron. What is then the reason for this?

Answer: The relationship between the injected current and the output current in our synchrotron has a non-linearity, which sets in for injected currents of the order of 30-40 mA; the increase of the injected current beyond this value does not increase the output current.

All the electron accelerators present this phenomenon, which, for the time being, has not yet been explained. We are trying to understand it, but we did not reach any conclusion up to now. We know that the time of the acceleration cycle in which the non linearity sets in is between the injection and about 5 μsec after it, and probably is connected with the radiofrequency capture.

NUCLEAR INSTRUMENTS AND METHODS **11** (1961) 179–184; NORTH-HOLLAND PUBLISHING CO.

ON ION SOURCES WITH HIGH EFFICIENCY AND INTENSITY

J. KISTEMAKER

F.O.M.-Laboratorium voor Massaspectrografie, Amsterdam, The Netherlands

The conditions determining the shape of the ion emitting plasma cap in ion sources are analysed. Dense plasmas ($n_i = 10^{14}$) give expanding caps like in the Von Ardenne source. Thin plasmas ($n_i = 10^{10}$) give inward bended caps like in all normal ion sources. This difference in shape means a difference in ion emission with a factor ten.

The problem of an ion source with a high material efficiency is solved by the magnetic type ion sources. The Von Ardenne source has a high density plasma ($n_i = 10^{14}$) in the emission region with an extremely high electron temperature Therefore hardly any neutral particles are available.

In the magnetic P.I.G. type sources the material efficiency is obtained by internal ion focusing. They run with low plasma density ($n_i = 10^{10}$). For the separation of microgram quantities of rare materials (radioactive or toxic like Pu) the P.I.G. type source should be preferred over the normally used arc source.

1. Discharge Boundary Conditions

To produce intense ion beams[1,2]) extracted from an exit opening at the end of the discharge chamber, it is necessary to create so many ions in front of this exit hole, that a space charge limited current of positive ions can be withdrawn. The emission of the ions from the plasma boundary can take place either thermally, as in all low voltage arcs at sufficiently high pressures, or using a selffocusing mechanism inside the discharge[10]).

The shape of a plasma boundary is determined by the geometry of the extracting electrodes, the ion density of the plasma and the applied potentials. Suppose that the ion current emitted per unit area of this boundary is given by

$$J_b = n_i e \left(\frac{kT_e}{m_i}\right)^{\frac{1}{2}}, \tag{1}$$

where n_i is the number of ions per cm^3 at the boundary inside the plasma, T_e is the electron temperature, m_i the mass of the ions and k the Boltzmann constant. On the other hand the space charge limited current from a flat emitter per unit area deduced via Poissons equation, for ideal vacuum is[11])

$$J_{\text{sp.ch.l.}} = \frac{1}{9\pi}\sqrt{\frac{2e}{m_i}}\,\frac{1}{d^2}\,V^{\frac{3}{2}}, \tag{2}$$

where d is the distance of the boundary to the extraction electrode, which has a potential difference V with the plasma boundary. The space charge limited current can only be withdrawn if J_b is high enough. The first requirement is therefore that

$$J_b \geq J_{\text{sp.ch.l.}}\,. \tag{3}$$

which leads to a minimum ion density $n_{i_{\text{min.}}}$ opposite the exit hole of

$$n_{i_{\text{min.}}} = \frac{\sqrt{2}}{9\pi}\,\frac{1}{d^2}\left(\frac{V^3}{ekT_e}\right)^{\frac{1}{2}}. \tag{4}$$

Example:

$V = 6 \times 10^4$ volts $= 200$ e.s.u.; $d = 1$ cm; $T_e = 10^4$, then $n_{i_{\text{min.}}} = 6 \times 10^{12}$ ions/cm^3 to give $J_{\text{sp.ch.l.}} = 800$ mA protons per cm^2 emitting area.

This is only true in case of a flat plasma boundary and if no ions with a higher mass than the proton mass are present. If this $n_{i_{\text{min.}}}$ is not present the plasma boundary will be pressed backwards until the electrical field strength at the plasma boundary just fits with a space charge limited current. This is the reason that inward bended plasma caps arise in most ion sources where $n_i = 10^8$ or 10^{10}.

In the case that $n_{\text{plasma}} > n_{i_{\text{min.}}}$ the plasma

---

[1]) W. A. S. Lamb and E. J. Lofgren, Rev. Scien. Instr. 27 (1956) 907.

[2]) M. von Ardenne, Tabellen der Elektronenphysik, Ionenphysik und Übermikroskopie I (1956) p. 544–549.

will flow out of the source opening A (fig. 1). The plasma behaves like a solid metal body if $n_{\mathrm{plasma}} = n_{\mathrm{i}}$ is large enough, and compresses the electrical equipotential surfaces ahead, actually increasing the field strength there.

To study more in detail at what place, or better at which electrical fieldstrength the plasma surface will be stopped we go closer to the famous plasma sheath, well known from classical gas discharge experiments on the border of electrodes and insulators. We consider an equipotential surface at distance d, with a potential difference respective to the plasma potential of V volts. Just take 100 volts as an example.

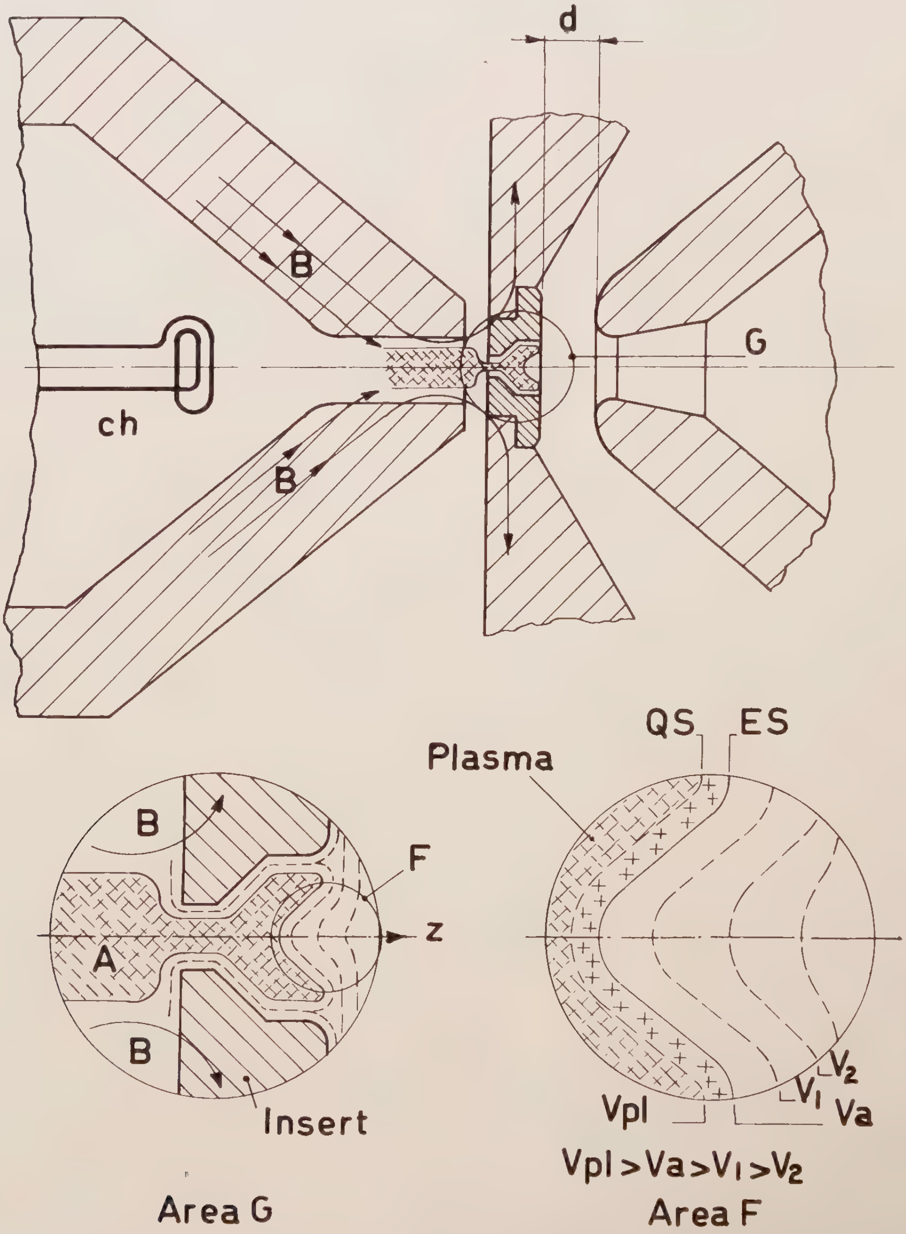

Fig. 1. Von Ardenne type duoplasmatron with protruding plasma cap. Ch is the discharge chamber; ES is the emitting surface at potential V_{a}; QS is the plasma surface at potential V_{pl}; The insert is of Mo or W and has a very special shape to reduce the penetration of the extraction field.

From

$$\tfrac{1}{4}\, e\, n_{\mathrm{i}}\, v_{\mathrm{i}} = \frac{1}{9\pi}\sqrt{\frac{2e}{m_{\mathrm{i}}}}\,\frac{V^{\frac{3}{2}}}{d^2}\,, \tag{5}$$

where now

$$v_{\mathrm{i}} = (2\, e\, V_{\mathrm{plasma\ therm.}}/m_{\mathrm{i}})^{\frac{1}{2}}\,,$$

we find

$$d^2 \approx \frac{10^6}{n_{\mathrm{i}}}\left(\frac{V^3}{V_{\mathrm{pl.\,th.}}}\right)^{\frac{1}{2}} \tag{6}$$

d in cm

V and $V_{\mathrm{pl.th.}}$ in volts

We see from table 1 that to keep up with the flow of positive ions from a plasma with density $n_{\mathrm{i}} = 10^{14}\ \mathrm{cm}^{-3}$, and with apparent mean particle energy inside the plasma of 300 electron volts, an electrical field strength E, short ahead of the plasma boundary, of 120 kilovolts/cm is necessary. This field strength is not available in the insert of Mo (see fig. 1). The penetration of the extraction field has been reduced by purpose to give the plasma the opportunity to flow out. The outflow of the plasma is only stopped at that surface where a space charge limited current just can be taken off, and eq. (5) is satisfied.

TABLE 1

Relation between d, V_{plasma} and n_{i}

n_{i}	V_{pl} (volts)	V (volts)	d (cm)	$E = V/d$ (volts/cm)
10^{10}	0.1	100	0.5	2×10^2
10^{13}	10.0	100	0.006	2×10^4
10^{14}	0.1	100	0.006	2×10^4
10^{14}	300.0	100	0.0008	1.2×10^5

It will also be clear now that working with too low accelerating voltage can have disastrous consequences, if the value of n_{i} in the source plasma is high. The plasma expansion goes too far and one gets a very diverging ion beam, with big losses against the electrodes.

The value of v_{i} in eq. (5) can be increased by the force exerted on the plasma because of the decreasing magnetic field B, corresponding with

$$K = -\frac{eV_{\mathrm{pl.th.}}}{B}\,\frac{\partial B}{\partial z}\ \text{(per particle)}\,.$$

In a strong magnetic lens this can give rise to an apparent doubling of the "thermal" speed with which the positive ions press against the electrical polarizing force.

The above considerations try to give an explanation of the very large currents/cm² exit area, which have been obtained with Von Ardenne type ion sources (100 Amps/cm², protons). The explanation is mainly that the emitting area is easily a factor 10 larger than the small exit area A, because of the protrusion. The real shape of the protruding plasma inside and just outside the insert is not yet clear, however[2,3,13,14]).

The expansion of the plasma from the arc sources in large electromagnetic isotope separators (calutrons) is from the cases 1, 2 and 3 from table 1, also clear[4]). In the normal case of $n_{\mathrm{i}} = 10^{10}$ the plasma is bended inward ($E = 200$ V/cm). However, if by some reason (pressure rise, or presence of easily ionisable atoms like Li) the n_{i} increases, the plasma comes out the exit slit and requires some $E = 10$ kV/cm to stop it. This can give rise to bad focusing, and therefore bad efficiency.

2. Concerning Ion Source Efficiency

If one studies the ratio of the quantity of ions leaving an ion source to the total quantity of gas consumed by the source (the gas efficiency γ), one finds for various sources practical data indicated in table 2.

Arc discharge ion sources are used in the large electromagnetic isotope separators in Oak Ridge, Harwell and Amsterdam[4,5,9]).

[3]) C. D. Moak, H. Reese and W. M. Good, Nucleonics **9** (1951) 18.

[4]) J. Kistemaker, P. K. Rol, J. Schutten and C. de Vries, Zeitschr. f. Naturf. **10a** (1955) 850.

[5]) J. Druaux et R. Bernas, Proceedings of the Harwell Conf. 1955, 30.

TABLE 2
Gas efficiency γ

Type of ion source	Experimental gas efficiency (%)	Operating pressure in source (mm Hg)
Arc discharge	2 — 10	10^{-3} — 3×10^{-2}
High frequency	5 — 10	10^{-2} — 3×10^{-1}
Magnetic (P.I.G.)	10 — 50	10^{-5} — 10^{-2}
Von Ardenne	up to 100	$\approx 10^{-2}$

High frequency sources are only used on particle accelerators. The Thonemann type is famous. Magnetic ion sources have been developed by ourselves (Kistemaker and Douwes Dekker), by Nielsen, and by many others[6,7,8,10,12].

One can try to get high efficiency sources by either:

ionising the gas at the plasma boundary to a high degree, or

using as low a pressure as possible in the source.

In both cases there is as extra requirement that the source body as a whole should be at high temperature to prevent recombination, adsorption and condensation inside the source body. Moreover trivial losses should be reduced, as for instance chemical decomposition of the charge material and bad focusing of the ion beam after leaving the source.

We will treat here only the main aspects of the ionisation of the gas, and a high gas economy (magnetic source).

2.1. HIGH DEGREE OF IONISATION

If the plasma at the boundary layer contains $n_i = n_e = n_{pl}$ charged particles per cm^3, and n_{gas} neutral particles the gas efficiency γ is determined by

$$\gamma = \frac{100\, n_i\, v_i}{n_i\, v_i + n_{gas}\, v_{gas}}$$

EXAMPLE

degree of ionisation

$$= \frac{100\, n_i}{n_i + n_{gas}} = 50\%$$

in H$_2$ gas

v_{gas} corresponds with 0.03 electron volts (eV$_{gas}$)

v_i corresponds with 30 electron volts (eV$_i$)

$$\gamma = \frac{100\, \sqrt{2}\, n_i\, \sqrt{V_i}}{\sqrt{2}\, n_i\, \sqrt{V_i} + n_{gas}\, \sqrt{V_{gas}}} \,. \tag{7}$$

We took $n_i = n_{gas}$, which gives:

$$\gamma = \frac{100\, \sqrt{2}\, \sqrt{V_i}}{\sqrt{2}\, \sqrt{V_i} + \sqrt{V_{gas}}}$$

$$= 98\% \text{ in this case .}$$

Conclusions

1. The degree of ionisation should be 10% or higher.

2. At the plasma boundary the plasma must flow out at a speed large in comparison with the mean thermal velocity of the gas particles.

To get the required degree of ionisation it is necessary that

$$\lambda_{\text{ionisation}} = (n_e\, \sigma_{\text{ionisation}})^{-1} < l \tag{8}$$

where $\lambda_{\text{ionisation}}$ and $\sigma_{\text{ionisation}}$ are respectively the free path length and the cross section of a neutral gas particle in the plasma with an electron density n_e and dimension l.

If $\sigma_{\text{ionisation}} = 10^{-15}$ cm^2, we see that

$$n_e\, l > 10^{15}$$

which shows why most gas discharges of low density have very low degrees of ionisation. Indeed l is always of the order of 1 cm, but electron densities of 10^{15}/cm^3 are never reached if normal arc currents are drawn. Such densities

---

[6] J. Sommeria-Klein, Ann. de Physique **13** (1956) 344.

[7] O. Almén and K. O. Nielsen, Proceedings of the Harwell Conf. 1955, 23.

[8] C. F. Barnett, P. M. Stier and G. E. Evans, Rev. Scien. Instr. **24** (1953) 394.

[9] D. Kamke, Handbuch der Physik **33** (1956).

[10] J. Kistemaker and H. L. Douwes Dekker, Physica **16** (1950) 198, 209.

[11] I. Langmuir and K. T. Compton, Rev. Mod. Phys. **3** (1931) 237.

[12] O. Almén and K. O. Nielsen, Nucl. Instr. **1** (1957) 302.

[13] H. Fröhlich, Nukleonik **1** (1958) 184.

[14] C. D. Moak *et al.*, Rev. Scien. Instr. **30** (1959) 694.

are only there if gas with an orginal pressure of 0.03 mm Hg is fully ionised. And the only way to keep such a gas highly ionised is to have an electron temperature $T_e > 10^5$°K, which corresponds with 10 eV_e.

Such extremely high temperatures have been reached in Von Ardennes[2]) ion source, working at gas pressures of more than 10^{-2} mm Hg in the following way.

1. *large potential differences* on both sides of the plasma region between A and the boundary (see fig. 1). Most electrons are accelerated over about 100 volts after their liberation.

2. *magnetic focusing* of the primary as well as the secondary electrons, causing a long lifetime and an excellent energy distribution over the electron sea inside the plasma via many electron-electron collisions.

This does not mean that the ion temperature should be the same.

2.2. HIGH GAS EFFICIENCY BECAUSE OF INTERNAL FOCUSING[10, 12])

In ion sources with an axial magnetic field of the Penning type (P.I.G.), as we have developed in Amsterdam, operating pressures of 10^{-3} to 10^{-5} mm Hg have been used. According to equation (8) this means that $\lambda_{\text{ionisation}}$ is between 10 and 1000 cm and in normal gas discharges this would mean a degree of ionisation lower than a few percent. Our measurements have shown however, that the axial magnetic field, combined with the electron reflection electrode F (see fig. 2), build up a negative space charge in the middle of the discharge tube. This negative trough makes it impossible for all positive ions, created in this tube, to reach the anode wall. They are all focused in the middle and fall from the potential mountain with the highest top in D (fig. 2), guided by the axial

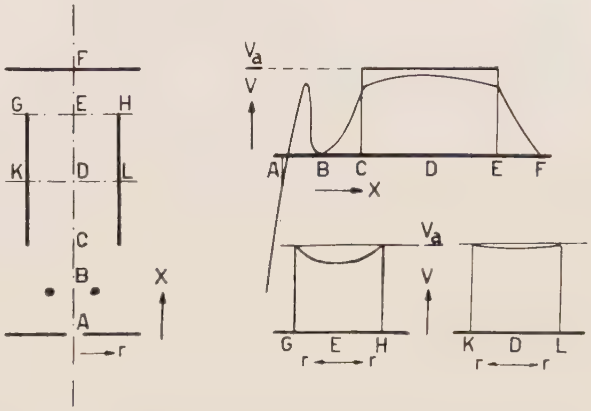

Fig. 2. Potential distribution in the discharge tube of a magnetic ion source.

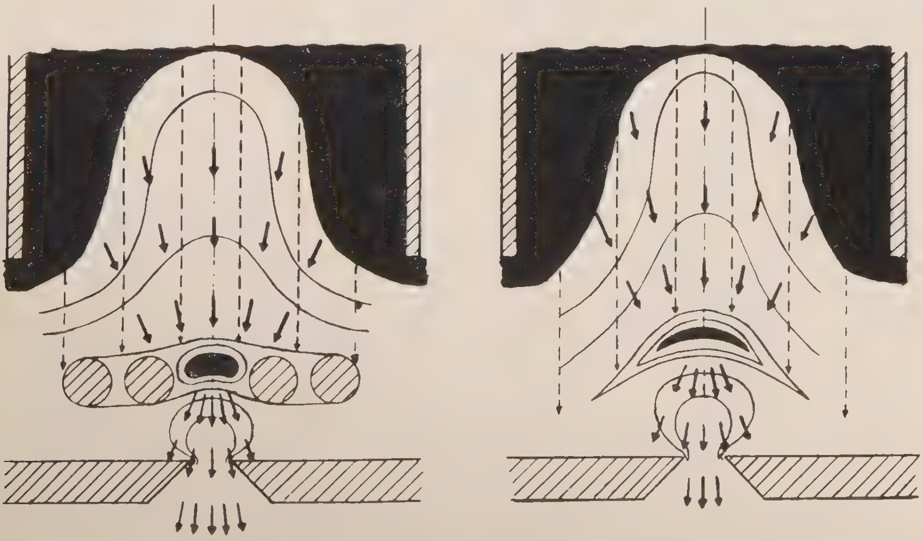

Fig. 3. Ion focusing inside the magnetic discharge chamber on the exit hole. Where the electrons are reflected a positive potential mountain might arise, sifting out low energy ions. These sources have therefore an amazing small energy spread (less than 10 eV).

magnetic field, to the exit opening A, where they have reached a speed corresponding with approximately $e(V_{\text{anode}} - V_{\text{cath}})$ which should be about 100 eV.

Half of the ions flows in the wrong direction and is lossed, neutralized at the end of the discharge chamber. If the chamber is hot they can evaporate again and be used again and again, until they escape via the exit hole A either in ionic or gaseous shape.

The optimum gas efficiency of this source is determined by

$$\gamma = \frac{100\,(n_{\text{i}}\,v_{\text{i}})_{\text{sp.ch.l.}}}{(n_{\text{i}}\,v_{\text{i}})_{\text{sp.ch.l.}} + \frac{1}{4}\,n_{\text{gas}}\,v_{\text{gas}}}$$

where

$$(n_{\text{i}}\,v_{\text{i}})_{\text{sp.ch.l.}} = \frac{\text{O}}{9\pi}\sqrt{\frac{2}{em_{\text{i}}}}\,\frac{V^{\frac{3}{2}}}{d^2}$$

(see eq. (5)).

The factor $\frac{1}{4}$ originates from the fact that the ions have all of them an axial direction and therefore no ion diffusion takes place, contrary to the gas.

The flow of ions inside the discharge to the orifice at A (fig. 2) is determined by

$$n_{\text{gas}}\,n_{\text{e}}\,\sigma_{\text{ionis}}\,\overline{v_{\text{e}}}\cdot\text{Volume}\,.$$

If the space charge limited current through the orifice with area O is not reached the gas efficiency decreases. An increasing γ value can be obtained then by increasing n_{e} or by improving the magnetic focusing on the exit hole A. Increasing n_{e} is usually done by increasing the arc current. Very high material efficiencies have been obtained with these ion sources in Copenhagen by Nielsen, Skilbreid and Sidenius[15]).

3. Conclusions

Today there are ion sources with very high material efficiencies *viz.* the Von Ardenne type and the Penning type (P.I.G.). Both can have efficiencies of 50% or perhaps even better. Both use an axial magnetic field in the direction of the ion extraction. The big difference between these two types is the shape of the plasma cap.

The P.I.G. ion source can produce ion currents (H^+) up to about 1 Amp/cm².

The Von Ardenne ion source reaches 100 Amp/cm². For the separation of microgram quantities of rare material (radioactive) the P.I.G. ion source is more elaborate and the extracted currents are enough. The Von Ardenne source seems especially of importance for the separation of bulky quantities of isotopes, and is certainly of importance for particle accelerators and plasma physics. Because of the very favourable material efficiency the pumping of the acceleration chamber is seriously reduced.

---

[15]) K. O. Nielsen, Skilbreid and Sidenius, to be published.

DISCUSSION

Speaker adressed: J. KISTEMAKER (*Amsterdam*)

Question by: KAI SIEGBAHN (*Uppsala*)

Question: Under the high plasma pressure and the great difference between electron- and ion temperature one would expect all sorts of plasma oscillations to be set up in an ion source of the von Ardenne type. This would lead to particle emission due to run away phenomena. Could this contribute essentially to the high emission yield, reported from this ion source?

Answer: What we have observed is that the so called "Hash" can be a limit for the extracted beam to build up space charge neutralization in field free space. This is especially true for gases with high ionization energy. Li on the other hand shows no oscillations in the source. The general problem is how to suppress the oscillations in the plasma in the source. Perhaps we will have to change our attitude to get other mechanisms of ionization.

PHYSICS AND RADIATION RESEARCH (II)

(October 6, 1960) pp. 185-253

RADIATION RESEARCH AND INDUSTRIAL APPLICATION

Chairman: A. Charlesby

Royal Military College of Science, England

CONTENTS

Otvos, John W., Guinn, V. P., Lukens, H. R. Jr. and Wagner, C. D.	Photoactivation and Photoneutron Activation Analysis	187
Baruch, P.	The Use of the Electron Accelerator in Solid State Physics	196
Huber, Wolfgang	High Energy Radiation for Research in Biochemistry and Microbiology	210
Pinner, S. H. and Davison, W. H. T.	The Development of Radiation Process Applications	227
Moore, D.	Neutron, Electron and X-ray Beams used for Radiation Research from a Van de Graaff Generator	238
Trageser, D. A.	Future Accelerators: Intense Sources for Processing	248

NUCLEAR INSTRUMENTS AND METHODS **11** (1961) 187–195; NORTH-HOLLAND PUBLISHING CO.

PHOTOACTIVATION AND PHOTONEUTRON ACTIVATION ANALYSIS

JOHN W. OTVOS†, V. P. GUINN, H. R. LUKENS, JR. and C. D. WAGNER

Shell Development Company, Emeryville Research Center

For the last two years the 3 MeV Van de Graaff electron accelerator at Shell Development Company, Emeryville, California, has been in routine use in neutron activation analysis. Over 30 elements can be analyzed for, some in the parts per million range and some in macro concentrations. The 3 kW electron beam produces bremsstrahlung in a gold target and the photons, in turn, liberate neutrons from a large (15 cm cube) beryllium block immersed in a moderator. The thermal neutron flux available in a volume of over 3 liters is more than $5 \times 10^7/\mathrm{cm}^2$ sec. Twenty-four samples of 25 ml each can be irradiated simultaneously. The activities produced are measured instrumentally in a scintillation counter using gamma ray spectroscopy. Several activities in the same sample may be distinguished by taking advantage of differences in half-life and gamma energy.

Recently it has been found possible to extend the scope of activation analysis by activating directly with photons. Eighteen metastable isomers of the stable nuclides have been produced, 7 for the first time by direct photoactivation. Bremsstrahlung from the gold target is allowed to act directly on the samples. Although sensitivities are lower, the method is more specific than neutron activation, and in many cases interferences in neutron activation can be eliminated by activating a sample with photons alone. Applications of photoactivation other than chemical analysis are (1) beam energy measurement and (2) dosimetry.

1. Introduction

At the Accelerator Conference in 1958 we mentioned that the 3 MeV Van de Graaff at Shell Development Company, Emeryville, was already being used routinely for instrumental neutron activation analysis. Since that time the analytical applications of the accelerator have been expanded and we have experimentally obtained the necessary sensitivities and gamma-ray spectra for the activation analysis of 27 elements. This work has been published in detail¹) including representative analyses of samples that are of interest in oil and chemical research. Therefore, as far as neutron activation is concerned, it will only be necessary here to recall the experimental arrangements and to summarize the results briefly.

Another technique, which we have found to be useful as a supplement to neutron activation analysis and which has other interesting applications also, is direct photoactivation with bremsstrahlung from the 3 MeV electron beam²). This technique grew unexpectedly out of an attempt to measure a small neutron flux in the vicinity of our gold target by the activation of indium.

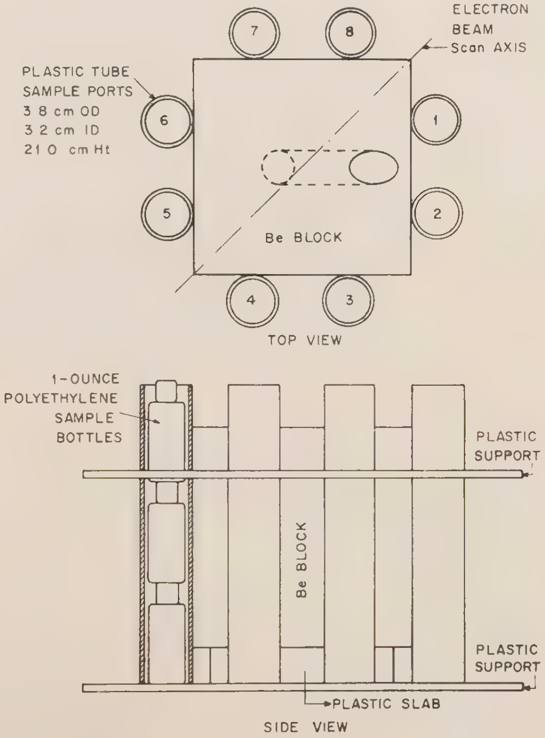

Fig. 1. Arrangement of sample ports scale.

---

† Temporary address: Koninklijke/Shell-Laboratorium, Amsterdam.

¹) V. P. Guinn and C. D. Wagner. Anal. Chem. **32** (1960) 317.

²) H. R. Lukens, J. W. Otvos and C. D. Wagner, in press.

The amount of activity produced was far too high for the neutron flux expected and indeed it turned out to be due not to In^{116}, the neutron capture product, but rather to In^{115m} from photon excitation of stable In^{115}. Later it was found possible to excite 17 other nuclides to their metastable states with varying efficiencies up to a specific activity of 1 μc per gram for hafnium. The photoactivation results are tabulated and discussed below and applications to analysis, beam energy measurement, and dosimetry are suggested.

2. Neutron Activation

2.1. SOURCE

The 1 milliampere, scanned beam of the 3 MeV electron accelerator is absorbed completely in a small, 3 mm thick, gold target. 5 cm below the target a 15 cm cube of beryllium metal is centered and the bremsstrahlung impinging on it produces neutrons ranging in energy from 0 to 1.2 MeV by the $Be^9(X,n)2He^4$ reaction. The block has 8 sample ports adjacent to it, as shown in figs. 1 and 2, and the assembly is immersed in a moderator, e.g. water or terphenyl. The flux in the ports ranges from 5–8 × 10^7 thermal neutrons/$cm^2 \cdot s$. This means that there is available a volume of about 3000 cm^3 in which the neutron flux varies by less than a factor of 2. Differences in flux from one position to another can be easily corrected for and as many as 24 samples can be irradiated at the same time. The moderator is surrounded by an aqueous mush of boric acid and the top of the block is covered with a boral sheet 6 mm thick. The boron shielding prevents neutrons from escaping into the room.

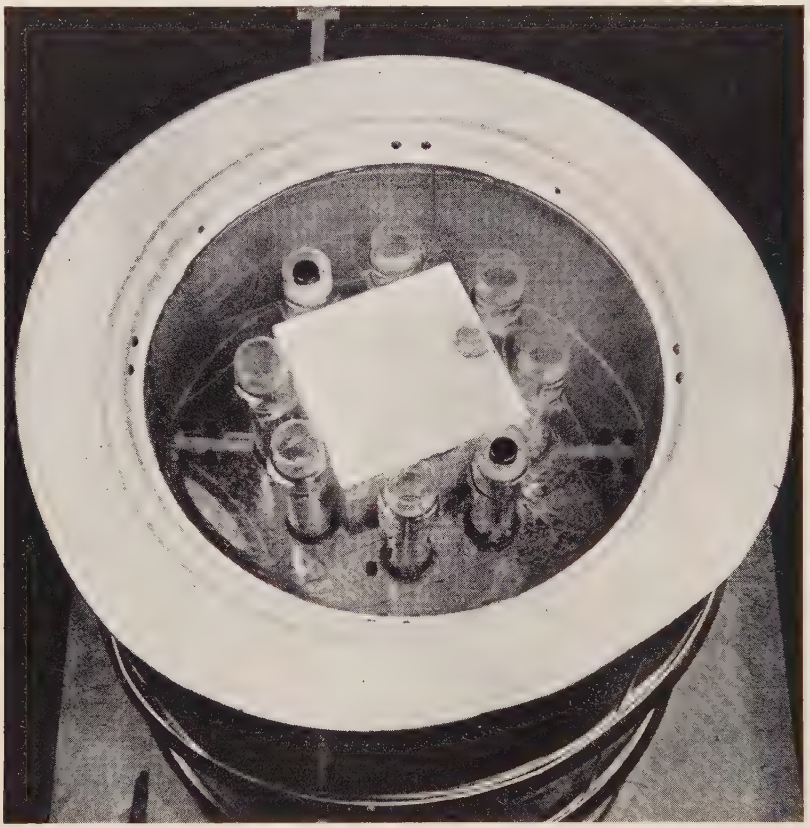

Fig. 2. View looking down into neutron generator. Beryllium cube is at center, surrounded by sample ports and water moderator. Annulus is a boric acid neutron shield.

TABLE 1
Theoretical and experimental detection sensitivities for 27 elements
(25-gram samples, 2-hour irradiation at 10^8 neutron flux)

Element	Radioisotope formed	Half life	p.p.m. detectable	
			Theory[a]	Exptl.[b]
Na	Na^{24}	15 h	5.2	6.4
Mg	Mg^{27}	9.5 m	80	82
Al	Al^{28}	2.3 m	1.3	2.4
Cl	Cl^{38}	37 m	6.8	6.8
K	K^{42}	12.5 h	220	150
Ca	Ca^{49}	8.7 m	220	270
Ti	Ti^{51}	5.8 m	72	40
V	V^{52}	3.8 m	0.12	0.20
Cr	Cr^{51}	27 d	3300	1300
Mn	Mn^{56}	2.6 h	0.11	0.12
Co	Co^{60m}	10.5 m	0.036	0.45[c]
Ni	Ni^{65}	2.6 h	180	320
Cu	Cu^{64}, Cu^{66}	13 h, 5.1 m	7	4
Zn	Zn^{69m}	14 h	460	370
As	As^{76}	27 h	7.6	5.2
Br	Br^{80}, Br^{82}	18 m, 36 h	3.4	1.4
Mo	Mo^{101}, Tc^{101}	15 m, 15 m	28	14
Ru	Ru^{105}, Rh^{105}	4.5 h, 37 h	32	38
Ag	Ag^{108}	2.3 m	3.8	1.2
In	In^{116}	54 m	0.012	0.081[d]
Sn	Sn^{123}, Sn^{125}	40 m, 9.5 m	65	40
Sb	Sb^{122m}	3.5 m	0.34	8.9[c]
I	I^{128}	25 m	3.3	1.0
Re	Re^{188m}, Re^{188}	20 m, 17 h	0.044	0.5[c]
W	W^{187}	24 h	5.1	3.5
Pt	Pt^{199}, Au^{199}	30 m, 3.1 d	80	17
Au	Au^{198}	2.7 d	1.1	1.3

[a] Defined as concentration in 25-gram sample that will give 1000 gamma d.p.m.
[b] Defined as concentration in 25-gram sample that will give 500 c.p.m. (equivalent to 1000 gamma d.p.m.).
[c] Discrepancy due to high degree of internal conversion of very soft gammas.
[d] Discrepancy due mostly to indium self-shielding.

2.2. MEASUREMENT OF ACTIVITY

Samples, usually in 30 ml polyethylene vials, were counted in a 7.5 cm sodium iodide, well-type scintillation counter, shielded by 7.5 cm of lead, and connected through an amplifier to a Penco 100-channel pulse height analyzer. The background counting rate of the unit was about 250 cpm. The spectra could be observed on an oscilloscope screen and printed out. Figs. 3 and 4 illustrate readout on a strip chart recorder.

2.3. RESULTS

Table 1 summarizes the calculated and experimentally measured sensitivities for 27 elements. Calculations are based on literature values of the cross-sections and other physical properties of the nuclides. Experimental results on known samples were extrapolated to 500 net counts per minute as the minimum accurately measurable counting rate. Agreement is usually quite good. Where there are significant discrepancies the reasons are noted in the table.

2.4. APPLICATION

In our use of neutron activation analysis we make no chemical separations. The sample is exposed to a neutron flux and then its gamma-ray spectrum is obtained. For quantitative work the spectrum is always compared with that of a standard sample of similar size and composition. The sample bottle need never be opened and so the analysis can be finished, if necessary, in a very short time. Thus, many isotopes of short half-life are useful. This is an essential point when an accelerator is used for other things besides analysis. Irradiation times must be kept short, and with the modest neutron flux attainable ($< 10^8$) it is impossible to generate significant amounts of long-lived activity.

If more than one activity is produced, then the gamma-ray spectrum offers a means for discrimination. Fig. 3 illustrates the type of resolution obtained in an actual analysis of sulfuric acid containing arsenic, manganese, and sodium impurities. When resolution on the basis of gamma energy is insufficient, then half-life can be used, as shown in fig. 4. During a short irradiation of the reforming catalyst, which contains platinum, chlorine, and aluminum, only the aluminum becomes appreciably activated, while after a long irradiation and long decay the Al^{28} disappears, leaving only the Pt^{199} and Cl^{38} activities. With a single irradiation this particular sample would have been impossible to analyze.

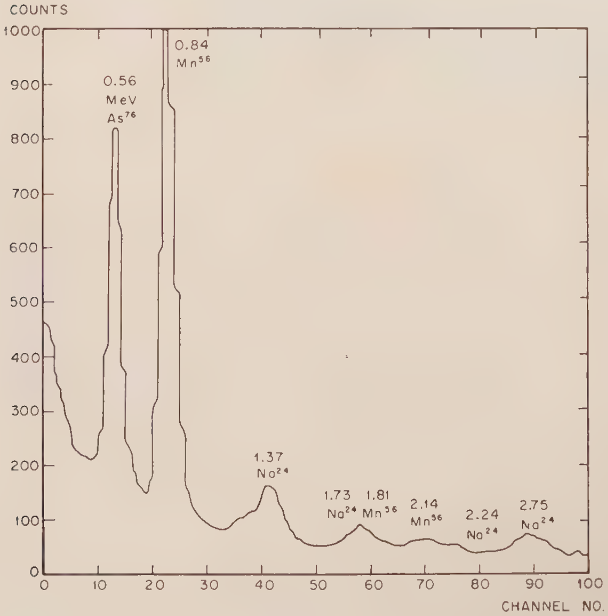

Fig. 3.
Gamma-ray spectrum of neutron-activated sulfuric acid.

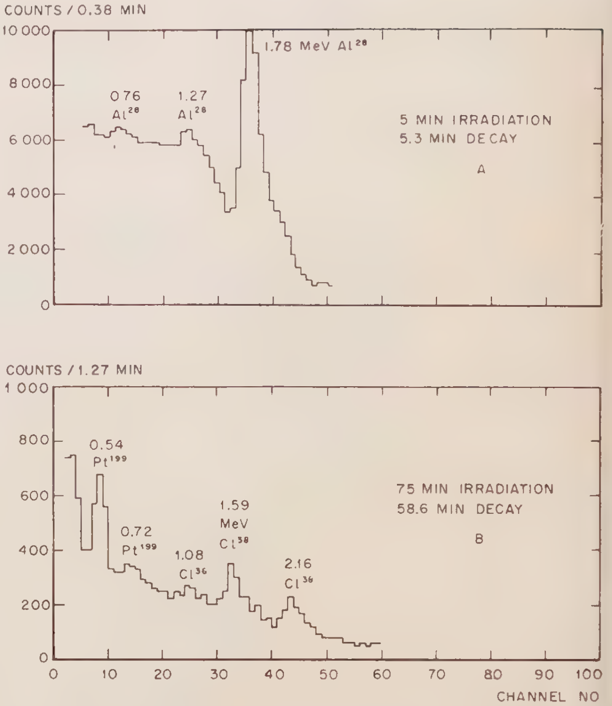

Fig. 4. Gamma-ray spectra of neutron-activated cracking catalyst at two decay times.

Another means of obtaining discrimination between isotopes is with coincidence spectrometry. Gamma rays of similar energy can be distinguished if one of them occurs in coincidence with another one. Still another method is by use of both fast and thermal neutrons, since, in general, the relative production rates of two isotopes will be different for the two kinds of irradiation. These are both obvious extensions of the instrumental activation analysis technique, but of course for the latter one a positive-ion accelerator is required that can produce fast neutrons via, say, the $H^3(H^2,n)He^4$ reaction.

One may regard the photoactivation method of analysis as still a further extension of the use of two kinds of bombarding particle. The extent to which neutrons and photons can be used to eliminate interferences between activities, and the extent to which photons are useful alone will become apparent from the experimental results on photoactivation described in the next section.

3. Photoactivation

We have estimated from standard bremsstrahlung formulae that the photon flux in the forward direction one centimeter from the gold target[3]) is $3 \times 10^{14}/\text{cm}^2 \cdot \text{s}$ when the electron beam is at full power, 3 MeV and 1 mA. The calculated energy distribution of bremsstrahlung from our target, taking into account the photon absorption in the gold, is shown in fig. 5. With such an intense photon source and with the possibility of irradiating large samples—0.1 gram-atom or more—it is possible to observe induced activities that have cross-sections for their production as low as $\approx 5 \times 10^{-10}$ mb. We therefore undertook to look for photoactivation of nuclei to metastable states and to determine whether analytical or other use could be made of such nuclear reactions.

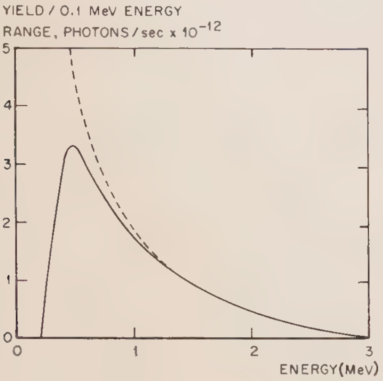

Fig. 5 Energy distribution and yield of bremsstrahlung photons. (Within 10° of beam axis.)

3.1. EXPERIMENTAL

Elements were irradiated in chemical forms that were available in high purity. The amounts

---

[3]) C. D. Wagner and V. A. Campanile. Nucleonics **17** [7] (1959) 99.

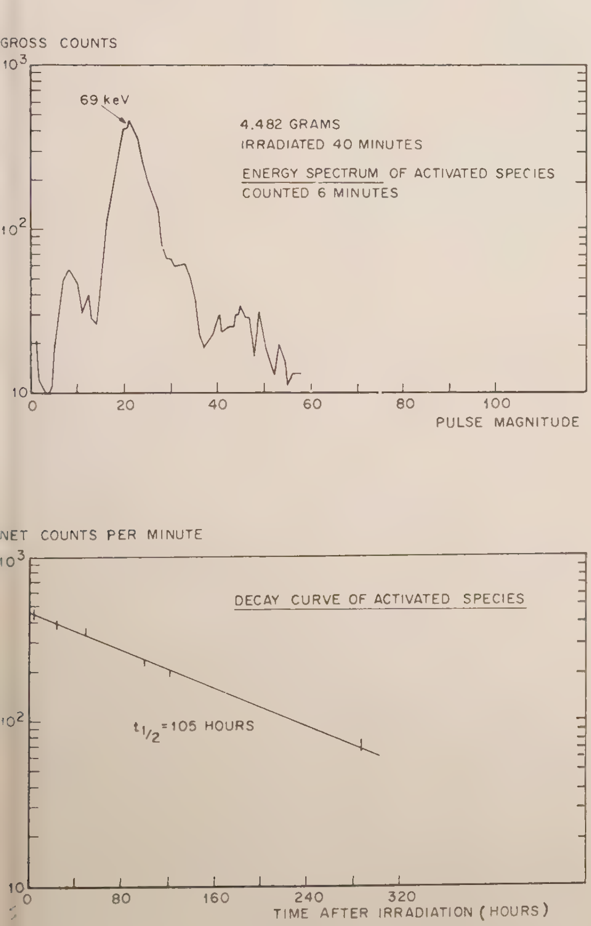

Fig. 6. Platinum activity.

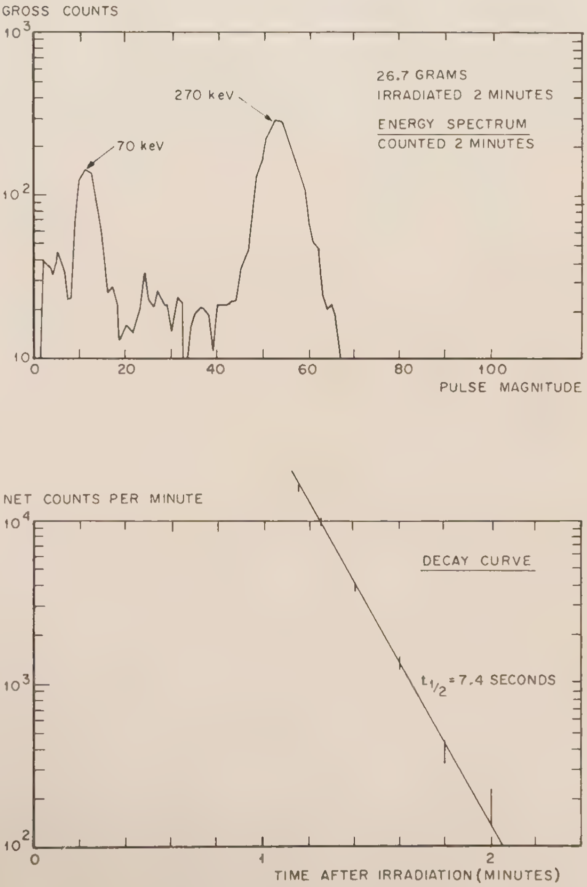

Fig. 7. Gold activity.

ranged from 1–250 grams, depending on availability and density. All of the stable elements were included in the study except $Z = 1, 2, 3, 4$ and the inert gases. Irradiations were done in polyethylene vials as close to the gold target as possible. Samples that produced little or no activity were irradiated for 30 minutes, others only as long as the induced half-lives required. Counting techniques were the same as in the neutron activation work. Whenever there was sufficient activity complete gamma-ray spectra were recorded and half-lives were determined. Figs. 6 and 7 shows graphs of typical data for long and short lived activities, respectively.

3.2. DISCUSSION AND RESULTS

The only mechanisms that can account for generated activity are (1) photoexcitation of stable nuclei to metastable states and (2) neutron activation, by means of neutrons generated from the deuterium in the cooling water of the target or from a beryllium impurity. Thresholds for other photon-excited nuclear reactions are too high to permit them to be induced by 3 MeV photons.

In table 2 there is a list of the metastable nuclides that were generated in these experiments. The third column shows how the nuclides were identified, whether by gamma-ray spectrum, half-life, or both, and the fourth column gives the calculated specific activity the element would have immediately after a 1 hour irradiation. The seven isomers marked with an asterisk were produced for the first time by photoactivation, although they had previously been obtained by other means such as coulomb excitation and decay from radioactive nuclides.

TABLE 2
Metastable isomers produced by bremsstrahlung from 3 MeV electron beam

Isomer	Half-life	Identification	Specific activity of element after 1 hour irradiation cpm/g
Se^{77m}	17.5s	A	140 000
Sr^{87m}	2.8h	B	9 500
*Y^{89m}	16s	A	47 000
Rh^{103m}	57m	C^4	100
Ag^{107m}	44s	A^1	210 000
Ag^{109m}	39s		
Cd^{111m}	49m	A	65 000
In^{113m}	1.9h	B^2	282 000
In^{115m}	4.5h	A	
*Sn^{117m}	14d	A	10
*Ba^{137m}	2.6m	A	1 600
*Er^{167m}	2.5s	C	2 800
Lu^{176m}	3.7h	A	3 700
*Hf^{179m}	19s	A^3	3 700 000
*Ir^{191m}	5s	A	1 000 000
*Pt^{195m}	3.5d	A^4	1 000
Au^{197m}	7.2s	A^3	370 000
Hg^{199m}	42m	B^3	2 200

Legend

A = by half-life and gamma-ray spectrum.
B = by gamma-ray spectrum only. Half-life was not measured.
C = by half-life only. Gamma-ray spectrum not conclusive.
* = isomer not previously produced by photoactivation.

Notes

[1]) The isomers of silver have such similar half-lives and gamma-ray spectra that they could not be resolved. Either one or both may be present.

[2]) The gamma-ray spectrum of indium was that of In^{115} but there was a shoulder on the high side of the photopeak indicating In^{115m}. The measured half-life of 4.2 hours also pointed to contribution by In^{113m}.

[3]) The K X-ray resulting from internal conversion was observed in addition to a gamma peak.

[4]) Only the K X-ray was observed.

It is interesting to note that there are only 33 stable nuclides (excluding Kr^{83}) that have isomers with half-lives greater than 1 second. Table 2 shows that 18 of them were produced in this survey. Of the other 15, ten have half-lives greater than 1 day and two have half-lives 5 seconds or shorter. These would be difficult to observe under our experimental conditions unless they had exceptionally high cross-sections for production. The remaining three are Os^{188m}, Os^{190m} and Pb^{204m}. Unfortunately we had less than 3 grams of osmium to irradiate and that may account in part for our failure to observe its isomers. Pb^{204}, on the other hand, has a natural abundance of only 1.4 % so the amount of target material again was very small. It appears, therefore, that direct photo-excitation to a metastable isomer is generally possible. In those instances where production failed there were experimental difficulties beyond our control. Given larger samples, longer irradiation times and better transfer facilities from gold target to counter it is quite likely that the entire list of 33 isomers could be made.

In addition to the nuclear isomers, there were weak activities produced in a number of the elements studied, but only in 4 cases, arsenic, bromine, molybdenum, and iodine, could they be identified by both half-life and energy. These four activities belonged to the neutron addition products As^{76}, Br^{80}, Mo^{101}–Tc^{101} and I^{128}. The neutrons, as mentioned earlier, are probably generated from natural deuterium in the cooling water by the (γ,n) reaction. They must be essentially unmoderated with energies extending up to 0.4 MeV and skewed strongly in favor of the lower energies.

The magnitude of the thermal neutron flux was estimated, from the very small, but measurable, activities induced in vanadium and manganese, to be only about 3–5/$cm^2 \cdot s$. These two elements are the most sensitive slow neutron detectors and their cross-sections for fast neutron capture (0.1–0.4 MeV) are smaller by a factor of 1000 than their thermal cross-sections. This small thermal flux, however, is not sufficient to account for the As, Br, Mo and I activities, which therefore must be due to fast neutron capture processes. Arsenic and iodine, the only ones for which data are available, have fast neutron (0.1 MeV) capture cross-sections of 2 and 0.4 barns, respectively. From their activities the flux of fast neutrons was calculated to be ca. 300–3000/$cm^2 \cdot s$.

Apparently the fast neutrons predominate and their effect in causing possible interferences in photoactivations should be borne in mind. However, the four elements, As, Br, Mo and I, seem to be the only ones with large enough cross-sections to be significant.

3.3. APPLICATIONS

Analytical

The most obvious application of photoactivation is in elemental analysis as a supplement to instrumental neutron activation analysis. Thus, direct irradiation followed by gamma-ray spectrometry can be used for quantitative estimation of several of the elements. Data from table 2 are used in table 3 to obtain sensitivity. It is assumed

TABLE 3
Sensitivity of photoactivation analysis

Element	Required[a] activity at irradiation end (cpm)	Specific[b] activity in one hour irradiation (cpm/g)	Minimum[c] weight determinable (mg)	Minimum concentration determinable (ppm)
Se	460	140 000	3.3	110
Sr	32	9 500	3.4	110
Y	460	47 000	9.8	320
Rh	50	100	500	16 670
Ag	300	210 000	1.4	47
Cd	64	65 000	1.0	33
In	32	282 000	0.11	3.6
Sn	32	10	3200	110 000
Ba	160	1 600	100	3 300
Lu	32	3 700	8.5	280
Hf	440	1 800 000[d]	0.25	8.3
Ir	1300	1 000 000	1.3	43
Pt	32	1 000	32	1 000
Au	1000	370 000	2.7	90
Hg	74	2 200	34	1 100

[a] For 10% standard deviation in sample count.

[b] From table 2.

[c] These numbers may be reduced by 50–70% if a smaller sample is used.

[d] Figure in table 2 divided by 2 to approximate activity from a 30 ml sample.

that a 30 ml organic or aqueous sample is irradiated for one hour (less if saturation is reached more quickly), and counted at irradiation end for counting periods of optimum length up to one hour. Sensitivity values are then the concentration of the element determinable to ± 10 % standard deviation. It is assumed that background counting rate is 300 cpm, determined accurately in a long count.

It is clear that the method is potentially useful for Se, Sr, Y, Rh, Ag, Cd, In, Ba, Lu, Hf, Ir, Pt, Au, and Hg. Although neutron activation analysis with the same accelerator is more sensitive for all these elements, sometimes by a factor of 1000, nevertheless photoactivation has potential usefulness by virtue of its greater specificity. Interferences that might occur in neutron activation analysis may often be eliminated.

For example, none of the elements between $Z = 5$ and $Z = 32$ can possibly interfere in photoactivation because they have no isomers with lifetimes greater than 1 second, nor do they have large enough (n,γ) cross-sections for epithermal neutrons.

Sensitivity in photoactivation is affected considerably by sample size, because of self absorption effects on low energy photons, both in activation and detection. With barium, for example, a 5 ml sample gave three times as high a specific activity as a 30 ml sample. With silver the ratio was 2. For optimum concentration sensitivity, a 30 ml sample size is generally correct. However, this figure must be modified for those elements having very low photon energies.

With aqueous or organic samples interferences might occur because of moderation of fast neutrons to produce thermal neutrons. This was checked by irradiation of a 50 % manganous nitrate solution and a sample of manganese dioxide. The Mn^{56} specific activity was 10 times as great in the aqueous solution.

Checking of Beam Energy

For a given position of an indium foil the induced specific activity is a sensitive function of electron beam energy. Thus, for a given experimental arrangement in equal irradiation time it was found that the specific activity at 3 MeV is 2.2 times that at 2.5 MeV. This corresponds to a slope at 3 MeV of 11 % per 0.1 MeV.

This sensitivity of activity to beam energy suggests the use of photoactivation in a beam calibration method when the electron beam is inaccessible for the more accurate partial absorption method4). Irradiation to about one megarad should provide sufficient accuracy to determine beam energy to ± 20000 volts. It should be more useful than the deuterium threshold method in that: (1) the determination is made at 3.0 MeV, and no extrapolation from 2.23 MeV is required, (2) extreme voltage stability is not required, since one is dealing with an average value and not a threshold, and (3) a single determination is sufficient once the standard curve is established.

Dosimetry

The measurement of indium activity can also be used as a dosimeter for bremsstrahlung, but care must be taken to keep the energy distribution of the bremsstrahlung constant. The dependence of the photoactivation response on photon energy distribution is shown in fig. 8. It was obtained by wrapping indium foils around small vials of ceric solution and irradiating with doses of several megarads, as measured by loss in ceric ion. Specific activity of the foil vs

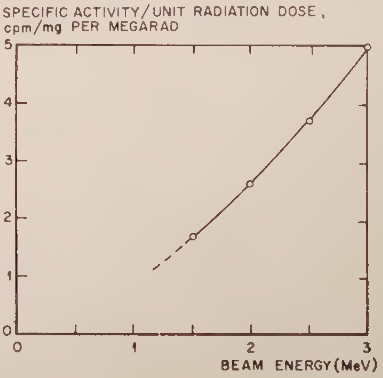

Fig. 8. Dependence of indium dosimeter for bremsstrahlung on energy of bombarding beam.

---

4) V. A. Campanile and C. D. Wagner, Nucleonics **17** [7] (1959) 74.

electron beam energy was then plotted for doses of one megarad (corrected for zero decay during irradiation). It is evident that the specific activity is rather sensitive to bremsstrahlung energy. Thus, the dosimeter's use would have to be restricted to bremsstrahlung produced in standard fashion, with little energy degradation by intervening materials.

DISCUSSIONS

Speaker adressed: J. W. Otvos (*Shell Dev. Corp.*)

Question by: E. H. Cornish (*Standarä Tel. Lab., Harlow*)

Question: What values of beam current at 3 MeV were used for the photo-activation experiments?

Answer: Because of the weakness of the induced activities we always used the full power of our accelerator for the photo-activation work: 1 milliampere at 3 MeV.

Speaker adressed: J. W. Otvos (*Shell Dev. Corp.*)

Question by: W. H. T. Davison (*Tube Investment*)

Question: What are the threshold values for these photo-activation reactions? If they are similar to those of Be, there should be a great increase in activity, using increased voltage, say 4 MeV.

Answer: We did not measure threshold values in most cases, however, the metastable levels are 0.1 to 1 MeV and presumably takes place via a state somewhat higher. Increase of voltage may very well lead to increase in activity.

Speaker adressed: J. W. Otvos (*Shell Dev. Corp.*)

Remark by: W. Minder (*Bern*)

Photo-activation can also be used for qualitative dosimetry, for instance for the evaluation of field distribution in radiation beams. We made some experiments of this kind with the γ-radiation of our 31 MeV-betatron, using the two radioactive Cu-isotopes produced by photoactivation.

Speaker adressed: J. W. Otvos (*Shell Dev. Corp.*)

Question by: D. A. Trageser (*HVEC*)

Question: While the photoneutron technique with a scanned beam permits a large sample volume to be activated, is indeed the result of a (p,n) or (d,n) a "point" neutron field?

Answer: The neutrons are emitted from a point, and although thermalization gives a rather uniform flux near the point, the fall-off with distance is quite rapid. In our set-up the bremsstrahlung is a line source and not a point source. Furthermore, the photons produce neutrons throughout a large volume of about 3.5 liters. Thus the fall-off of thermalized neutrons with distance from the block must be less severe than in the case of neutrons produced at a point with a positive ion-accelerator.

NUCLEAR INSTRUMENTS AND METHODS **11** (1961) 196–209; NORTH-HOLLAND PUBLISHING CO.

THE USE OF THE ELECTRON ACCELERATOR IN SOLID STATE PHYSICS

P. BARUCH

Laboratoire de Physique de l'Ecole Normale Supérieure, Paris (5è)

Among the many processes by which electrons in the energy range 300 keV to 3 MeV interact with matter, two are important for the physics of crystalline solids: ionization and nuclear recoils.

These processes and their secondary effects are reviewed. Examples are given of their importance:

1. The ionization creates in semiconductors electron-hole pairs in large excess; these extra carriers relax, their recombination laws are studied by various means, such as "electron-voltaïc" effect, excess conductivity decay, emission and decay of fluorescent light.

2. The nuclear recoils are the cause of radiation damage in most materials. The energy transfer in an electron collision is small, and the incident electron energy has to be greater than a certain threshold to produce permanent displacements, thus creating lattice defects. In electron irradiation these defects are simple point defects (vacancies and interstitials at low temperature, which can combine into simple associations by warming). Electron irradiation can then be used to obtain knowledge of interatomic forces to test the laws of displacement of atoms by radiation, or to introduce in a crystal point defects in a controllable way.

Examples are given such as measurement of threshold in metals, and study of lifetime in semiconductors. A curious phenomenon is the failure of the reciprocity law: the magnitude of damage in germanium is dependent not only on the total dose, but also on the dose rate.

Some emphasis is put on the experimental requirements for electron irradiation of solids: energy and intensity stability, beam steering and controlling, large range of beam currents, including pulsed operation. The design and mounting of samples are also discussed, specially for low temperature irradiation.

1. Electron Interactions in Solids

Electron accelerators in the energy range from about 300 keV to 3 MeV are now, frequently, if not widely, used for pure research work. This interest lies in the two different ways of interaction with the solid: electron interactions, which lead to ionization of the crystal, nuclear interactions which cause atomic displacements, leading to radiation damage.

All these interactions are summarized, in a schematic way, in tables 1, 2 and 3. A more detailed discussion has already been given by W. L. Brown at the First Accelerator Conference¹).

However, we want to stress some aspects of these effects which are directly relevant to the design of experiments.

1.1. IONIZATION DENSITY

In the above mentioned energy range all the energy of the electron beam, except a negligible part, is dissipated in electron excitation which ends up in ionization[†]. Consequently the ionization density is proportional to $\mathrm{d}E/\mathrm{d}x$, rate of energy loss: the number of pairs per electron per unit range is $(1/\varepsilon)(\mathrm{d}E/\mathrm{d}x)$, where ε is the energy required to create a pair (between 0.1 and 10 eV). Both factors are to be considered as constant: ε is a characteristic of the material, $\mathrm{d}E/\mathrm{d}x$ is almost constant in the energy range considered. The important result is that for a given material, with a thin sample (smaller than the range), the ionization density per electron per unit length is the same, immaterial of the electron energy. For example, in germanium, where $\varepsilon \simeq 3\,\mathrm{eV}$, $\mathrm{d}E/\mathrm{d}x = 1$ keV/micron, 300 pairs are created per micron. The total number of pairs created depends on the energy, it is simply E/ε.

[†] In all this text, the term ionization describes the existence of excess populations of electrons and holes, without excess kinetic energy: hole and electron populations are thermalized individually; this occurs after degradation into phonons, photons or secondary electrons, of the energy of the primary excited electron, this delay is of the order of 10^{-12} sec while the time for excess carrier concentration decay is much longer except in metals.

¹) W. L. Brown, Nucl. Instr. and Meth. **5** (1959) 234.

TABLE 1

Effect of electron beams on solids

(i) ELECTRON-ELECTRON INTERACTION:

Individual electron excitation → Thermal effects
Individual electron excitation → X-ray emission
Individual electron excitation → Ionization → secondary electrons
Ionization → transient effects
Ionization → *radiation damage in ionic and organic crystals*

Collective interaction → Plasma excitation
Collective interaction → Čerenkov radiation

(ii) ELECTRON-NUCLEUS ELASTIC INTERACTION:

Rutherford scattering → Atomic displacements → *radiation damage in metallic and covalent crystals*

(iii) BREMSSTRAHLUNG → Photo electrons, Compton electrons, Pair production
BREMSSTRAHLUNG → Photo fission, Photo disintegration

(iv) SPACE CHARGE EFFECTS IN INSULATORS

Dielectric breakdown

TABLE 2

Electronic interaction of fast electrons in solids.

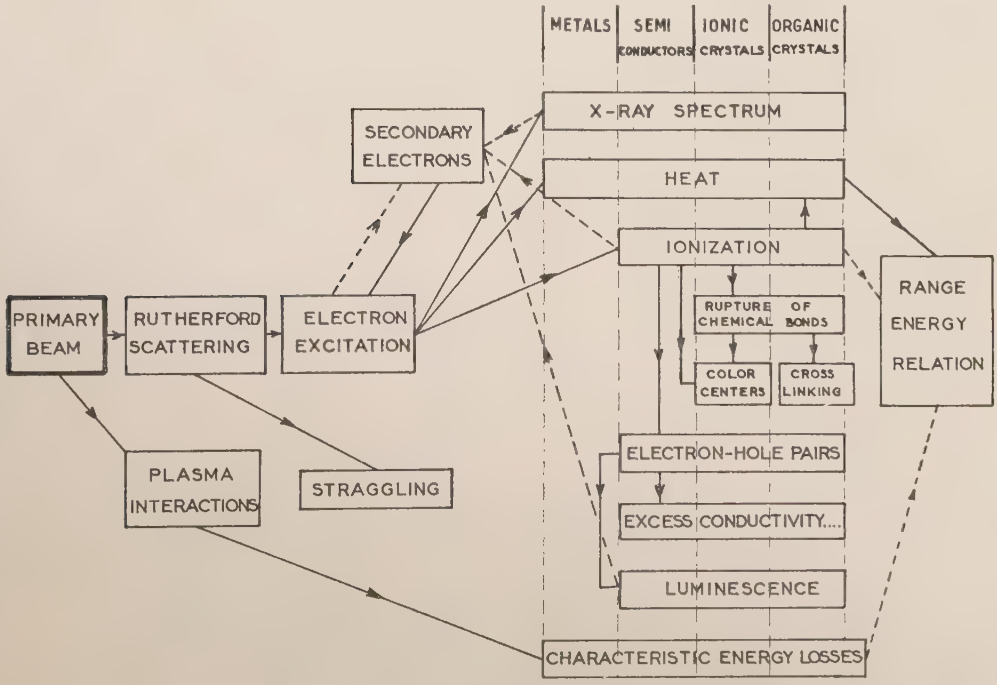
METALS
SEMI CONDUCTORS
IONIC CRYSTALS
ORGANIC CRYSTALS
SECONDARY ELECTRONS
X-RAY SPECTRUM
HEAT
IONIZATION
RANGE ENERGY RELATION
PRIMARY BEAM
RUTHERFORD SCATTERING
ELECTRON EXCITATION
RUPTURE OF CHEMICAL BONDS
COLOR CENTERS
CROSS LINKING
ELECTRON-HOLE PAIRS
PLASMA INTERACTIONS
STRAGGLING
EXCESS CONDUCTIVITY....
LUMINESCENCE
CHARACTERISTIC ENERGY LOSSES

1.2. RANGE ENERGY RELATIONS

From the preceding considerations, it results that the range varies approximately linearly with energy when the ionization losses are the only processes through which the electron energy is dissipated. This appears in the empirical relations (Katz and Penfold[2])) which gives the range as a function of energy:

$$R_{(\mathrm{mg/cm^2})} = 530\, E_{(\mathrm{MeV})} - 106$$

which is valid, within 10% above 0.5 MeV. For example, a 2 MeV electron penetrates about 1.8 mm in germanium and copper, and 4 mm in aluminium and silicon.

For radiation damage studies, where a threshold energy E_{T} for the onset of damage exists, an effective range R_{eff} could be defined as the distance, from the entrance surface, at which the average electron energy is lower than E_{T}. A rough estimate from Katz and Penfold formula would give:

$$R_{\mathrm{eff}\,(\mathrm{mg/cm^2})} = 530\,(E - E_{\mathrm{T}})\,.$$

1.3. RADIATION DAMAGE IN METALS AND SEMICONDUCTORS

The ability to produce radiation damage with electrons is connected with the efficiency of momentum transfer from electron to nucleus, in a Rutherford type collision. This efficiency is low: a 1.5 MeV electron transfers at most 100 eV in a head-on collision with a germanium atom, and the average energy is lower. Since the atom is bound by cohesion forces in the lattice, there exists a minimum energy which has to be imparted to it to cause permanent displacement; as a consequence, the electron beam must have an energy higher than a certain threshold E_{T} to cause radiation damage (see table 3).

TABLE 3
Displacements effects from fast electrons

PRIMARY COLLISION

Threshold energy E_{T} given by $2\dfrac{m}{M}E_{\mathrm{T}}\left(\dfrac{E_{\mathrm{T}}}{mc^2}+2\right) > E_{\mathrm{D}}$ displacement energy ($10\ \mathrm{eV} < E_{\mathrm{D}} < 50\ \mathrm{eV}$)

Electron energy $< E_{\mathrm{T}}$ No permanent effects

$> E_{\mathrm{T}}$ *Primary displacement*

DISPLACED ATOM

leaves a *lattice vacancy* at original site

stops as an *interstitial atom*

or initiates a chain of events (*replacement collisions, focussing collisions*) ending by one or more *Vacancy-Interstitial pairs* (*Frenkel defects*)

EFFECTS OF FRENKEL DEFECTS

Structural:	Lattice parameter changes, expansion X-ray or neutron line broadening Enhanced diffusion Stored energy, released by heating
Mechanical:	Internal friction, hardness, yield stress, etc.
Transport:	Mobility (conductivity in metals) decrease by increased scattering Thermal conductivity decrease
Electronic:	localized energy levels (in semiconductors and insulators): Variation in electron concentration (resistivity, Hall effect, etc.) Trapping centers → increased recombination, . . . spin resonance centers
Optical:	absorption lines (through energy levels), Color centers, . . .
Magnetic, etc . . .	

All these effects can be enhanced by association with other defects and impurities

---

[2]) L. Katz and A. S. Penfold, Revs. Mod. Phys. **24** (1952) 28.

For the same reason, the number of atoms displaced after a single collision is small for the usual energy values (below 3 MeV), the end result of irradiation is a small number of vacancies and interstitials dispersed in an otherwise undisturbed matrix. This is different from the damage caused by heavy particles, which can impart many kilovolts of energy in a single collision, cause cascades of thousand of displacements and result in heavily disordered regions.

These features: possibility of threshold measurements, creation of a simple type of defects, make the electron irradiation very attractive for the study of the mechanism of radiation damage and for determination of the properties of simple point defects.

The study of these point defects is made through a number of properties which are affected by their presence, such as mechanical properties, heat content, electronic energy structure, optical, magnetical properties, and others. We should mention specially the transport properties: the presence of point defects increases the scattering of conduction electrons and of phonons, leading to an increase in electrical and thermal resistivity. This is true in metals, where the number of conduction electrons is fixed. In semiconductors, this effect is often masked by larger changes in carrier concentration, as the newly created defects introduce localized energy levels, which are effective in trapping or releasing carriers. Another effect connected with the former, is the formation of spin resonance centers, the structure of which can be analyzed in detail and has given, up to now, the most detailed information about the existence of point defects and about their interaction with other defects and impurities in silicon[13]).

In fact, this picture of the radiation induced disorder is a static one, true at absolute zero. The disorder is thermodynamically unstable, and anneals out by thermal agitation. This is the other aspect of the research work on radiation damage: studying, after irradiation, the annealing processes and obtaining information about the mobility of defects, their annihilation mechanism, etc... We will not review this part of the work, but it has an important bearing on the experiments: the irradiation has to be made at a controlled temperature, and quite often at low temperature—liquid nitrogen, hydrogen or helium—to freeze the picture of defects before it can be blurred by thermal agitation, and the experimental set-up should allow, specially for low temperature irradiation, *in situ* measurements and temperature cycling.

Before describing any experiments, it is necessary to point out that all which has been said of electron irradiation is true for γ-ray irradiation, since γ-rays act through production of fast electrons, by photo effect, Compton effect or pair production. The advantage is the larger penetration of γ-rays, compared to that of electrons, the inconvenients are the very broad energy spectrum, and, mostly, the very low flux available from present sources.

2. The Experimental Problem in Electron Bombardment of Solids

The specific advantages of electron irradiation are: convenient penetration—much larger than protons and deuterons of the same energy, although much smaller than neutrons or γ-rays—high ionization efficiency, creation of a simple type of damage, absence of any induced radioactivity after irradiation, and also the other advantages of all other particle accelerators: easy means for controlling the dose and measuring it, facility of adjustment of the beam position, possibility of beam modulation, and the same drawbacks: all the energy is transformed into heat which has to be evacuated without heating the sample; also a heavy biological shielding is required and this implies a difficult access to the experiment and calls for remote controls and measurements.

We can then point out the various requirements for an electron irradiation experiment:

1. The beam, of known energy within a few per cent in the range 300 keV to 3 MeV, must hit a sample, giving a homogenous electron distribution on the sample area, of the order of 1 cm^2. The necessary means must be provided to steer, focus, homogeneize the beam, control its intensity and

know its position and size. As we shall see, means for pulsing the emission have a number of uses. The usual current density on the sample ranges from $1/10\ \mu A/cm^2$ to $100\ mA/cm^2$ (in pulse operation, with a good focussing).

2. Size and mounting of the sample are quite important: the thickness has to be smaller than the electron range, to ensure good homogeneity of ionization and damage; however this may be a cause of serious trouble when the surface interferes with the measurements (lifetime in semiconductors, low temperature conductivity in metals). The sample is mounted in good thermal contact with a heat sink which ensures a constant temperature. The heat power to be dissipated is minimized by allowing the beam to strike only parts which do not need temperature control, except, of course, the sample. For example, if the maximum heat input in a germanium sample $\frac{1}{10}$ mm thick is 1 watt, since the energy loss is 100 keV (see above), the maximum beam current will be $10\ \mu A$. If the energy is 2 MeV, 19 watts have to be dissipated in a back stop, which can be remote from the sample.

The sample mounting must also allow measurements to be made during or after irradiation, and during annealing; usually, except when injection effects are looked for, the irradiation is stopped during the measurements, to avoid interferences.

In the case of low temperature work, usually the annealing measurements have to be made *in situ* since it is not possible to remove, without warming, the sample from the irradiation chamber to a measuring set up. The sample holder has to be designed to allow a good thermal contact, during irradiation, with the refrigerant bath; during anneal, the sample will be thermally isolated from this bath, to allow fast cycles (pulse annealing) from the lowest temperature, used as a reference for measurement, to warmer and warmer temperatures. Difficult for liquid nitrogen, the problem is very complicated for liquid helium or hydrogen. Two different approaches are used: one is to circulate, around the sample, helium gas, the temperature of which is controlled by an external heat exchanger; in this case, the beam has to go through vacuum tight windows, and strikes the sample in a gaseous atmosphere, this can be troublesome for some experiments (energy degradation, deleterious effect of gas ionization). The other technique makes use of conduction cooling and of a thermal switch, such as a sapphire rod, or a helium chamber which can be evacuated. We shall see some examples of these techniques.

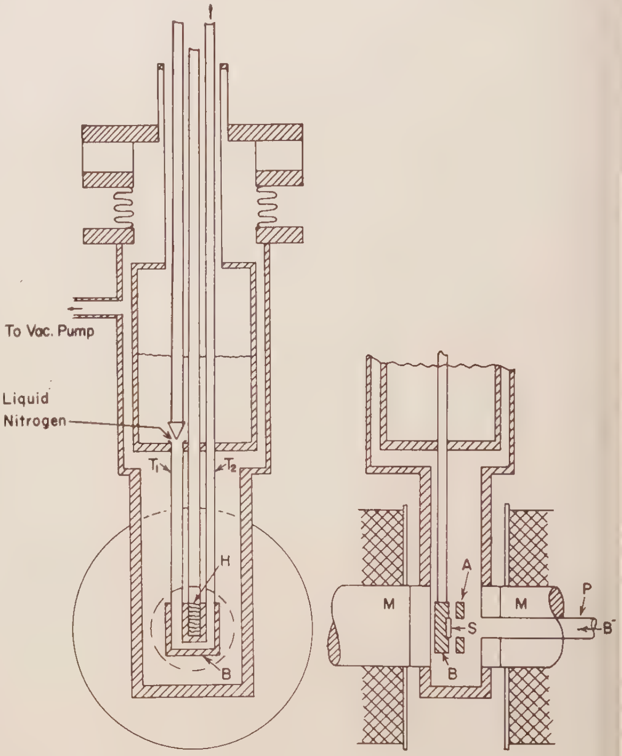

Fig. 1. Liquid nitrogen cryostat for electron irradiation, used at Purdue University (see text). (From Methods of Experimental Physics[3].)

3. Lastly, it is important to have a precise knowledge of the dose. Usually, the beam is calibrated with a precision Faraday cup, and then monitored by the current flowing to ground from different parts of the target.

An example featuring these experimental requirements is the cryostat (fig. 1) used at Purdue University[3]) for liquid nitrogen irradiations: this apparatus allows Hall effect measurements or annealing studies above liquid nitrogen temperature: the flow of liquid nitrogen to sample block B is interrupted by a stopper, the sample block is warmed by an auxiliary heater H. The electron beam enters by means of a tube P through pole piece M of Hall magnet. The beam current is measured by the charge collected on block B.

---

[3]) J. Mackay, Methods of Experimental Physics, Vol. 6A (Academic Press, 1959) p. 360.

3. Some Experiments Involving Ionization

Without narrowing the subject, we will describe only three experiments where ionization is used as a mean of detecting radiation damage.

3.1. ELECTRON VOLTAÏC EFFECT

A d–c beam is used both to create defects and to evaluate them. A semiconductor p–n junction is irradiated: the electron-hole pairs created are collected by the junction without external bias, a current flows in an external circuit and electrical power can be drawn; the operation is similar to that of a "solar cell." The short circuit current I_{cc} is proportional to the excess carrier concentration near the junction, or to the beam current I_B (ionization rate) and to the diffusion length in the semiconductor (collection efficiency). Since the lifetime is proportional to the square of the diffusion length, $(I_{cc}/I_B)^2$ varies as the lifetime. This lifetime is very sensitive to crystal imperfections, such as interstitials and vacancies, which act as recombination centers in a two step transition from conduction to valence band. For constant resistivity and temperature, lifetime is inversely proportional to the number of recombination centers. As a result, in first approximation, $(I_{cc}/I_B)^{-2}$ varies linearly with dose I_Bt, the short circuit current and conversion efficiency go down by irradiation. This technique, suggested by Loferski and Rappaport[4]) in 1955, has been used by them and others for threshold measurements in a number of simple and compound semiconductors; it is a very sensitive means of detection of the onset of radiation damage, less than 10^{12} defects per cm^3 can be detected[5,6]).

We have used this technique at E.N.S. to evaluate radiation damage on germanium at liquid nitrogen temperature, with the apparatus shown on fig. 2[7]), used in conjunction with a 2 MeV electron Van de Graaff.

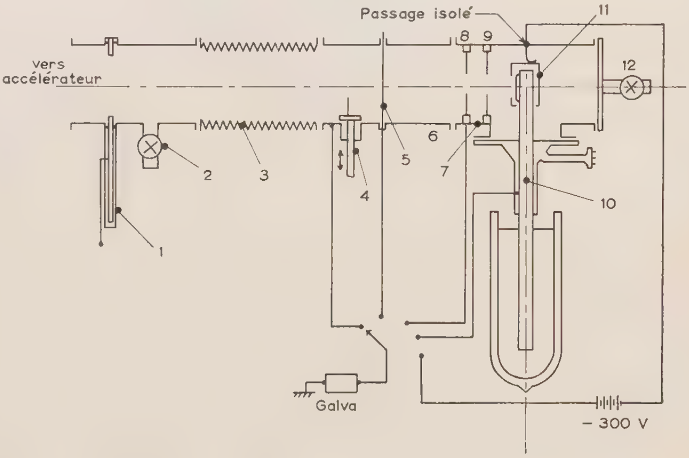

Fig. 2. Experimental set-up for 2 MeV electron irradiation, at Ecole Normale Supérieure (see text). (From Annales de Physique[7]).)

With respect to the preceding remarks, we can notice that the beam centering is done through adjustment of flexible bellows 3 and is controlled through the current on shutter 4; diaphragms 8 and 9 and secondary electron repeller 11 ensure that the current collected on sample and sample holder comes only from the useful part of the beam. When necessary, a thin ($\frac{5}{100}$ mm) aluminium foil scatters the beam and improves the homogeneity on the sample (no focussing coil was used). Temperature control is insured by the copper rod 10, to which the sample is soldered. This rod can be immersed in a constant temperature bath. This method is simple and efficient, but the thermal inertia is too large to allow pulse annealing (20 minutes from liquid nitrogen to room temperature). The fact that the total beam is absorbed in the sample and rod limits the beam intensity to about 1 μA at 2 MeV (2 watts). The adjustments are also rather tedious, by lack of remote control of beam

---

[4]) J. J. Loferski and P. Rappaport, Phys. Rev. 98 (1955) 1861.

[5]) Bauerlein, Z. f. Naturf. **14a** (1959) 1069.

[6]) J. Loferski, Private communication.

[7]) P. Baruch, Annales de Physique, Paris (in print); J. Phys. Chem. Solids **8** (1959) 153.

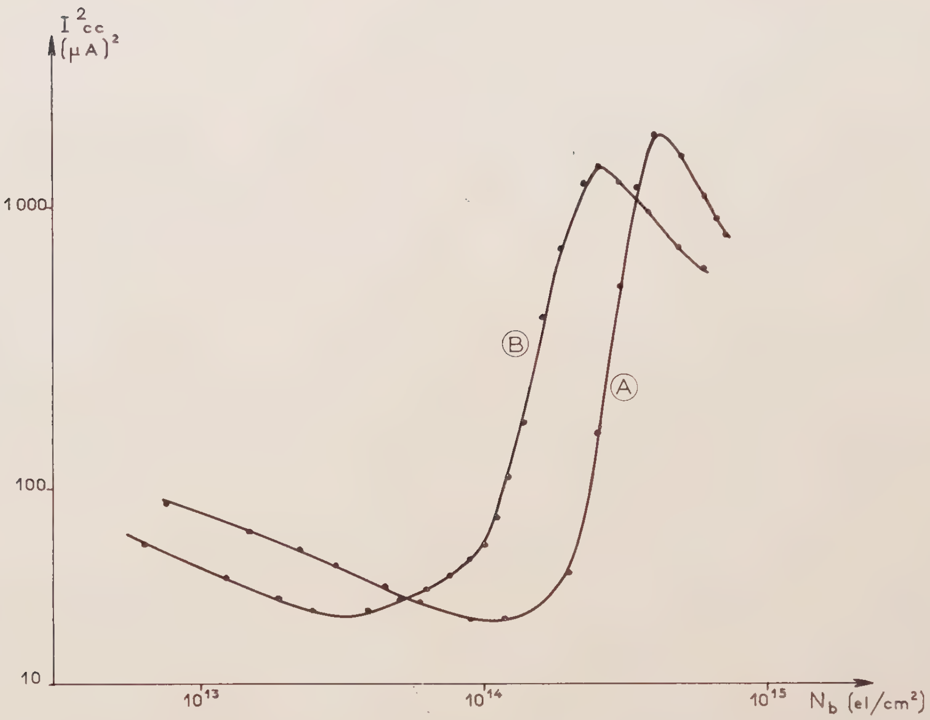

Fig. 3. Electron voltaïc short circuit current, as a function of integrated electron dose, in a p+–n junction at liquid nitrogen temperature. Curve A refers to the first irradiation with a beam current of 0.04 μA/cm²; Curve B to a second irradiation of the same sample, after a 15 minutes anneal at 100°C; the beam current, for B, was 0.033 μA/cm². (From Annales de Physique[7].)

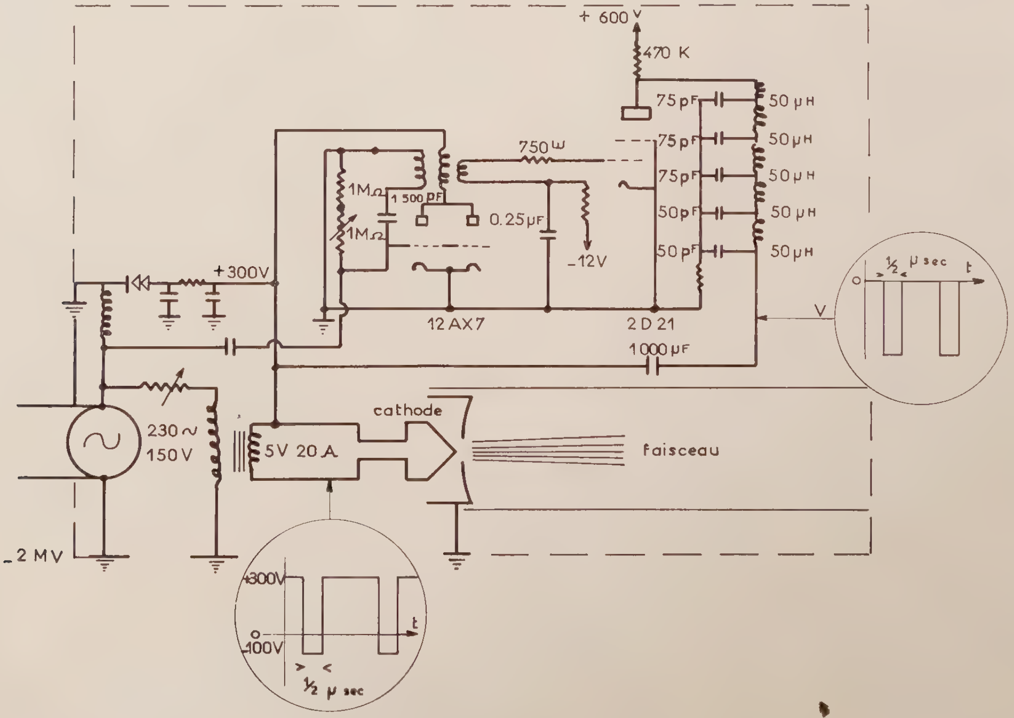
+ 600 V
470 K
75 pF
75 pF
75 pF
50 pF
50 pF
50 μH
50 μH
50 μH
50 μH
50 μH
750 ω
1 MΩ
1 500 pF
1 MΩ
0.25 μF
-12V
+300V
12AX7
2 D 21
1 000 μF
V
½ μ sec
t
o
cathode
faisceau
230 ~
150 V
5V 20 A
-2 MV
300V
o
100V
t
½ μ sec

Fig. 4. Pulse generator for the 2 MeV electron Van de Graaff at the Ecole Normale Supérieure. (From Annales de Physique[7].)

steering. A new experimental set up is being developed now.

The short circuit current of a germanium p^+-n junction was recorded, for a constant beam current. Curves of fig. 3 show the variation of I^2—i.e. of lifetime—versus dose. The lifetime decreases, as expected, at the beginning of irradiation, but goes through a minimum, and increases far above the initial value. This paradoxical effect can be attributed to the shift in Fermi level through irradiation: in semiconductors, radiation induced defects introduce localized energy levels: in n-type germanium, these levels are acceptor type, removing conduction electrons and driving n-type Ge to p-type Ge through intrinsic. The theory of recombination shows that the recombination efficiency of a given center is lower when the carrier concentration decreases, and is a minimum for the intrinsic semiconductor. The tendency to lifetime decrease through introduction of new centers is overbalanced by the change in carrier concentration, which can be, as in the experiment described, the most important factor.

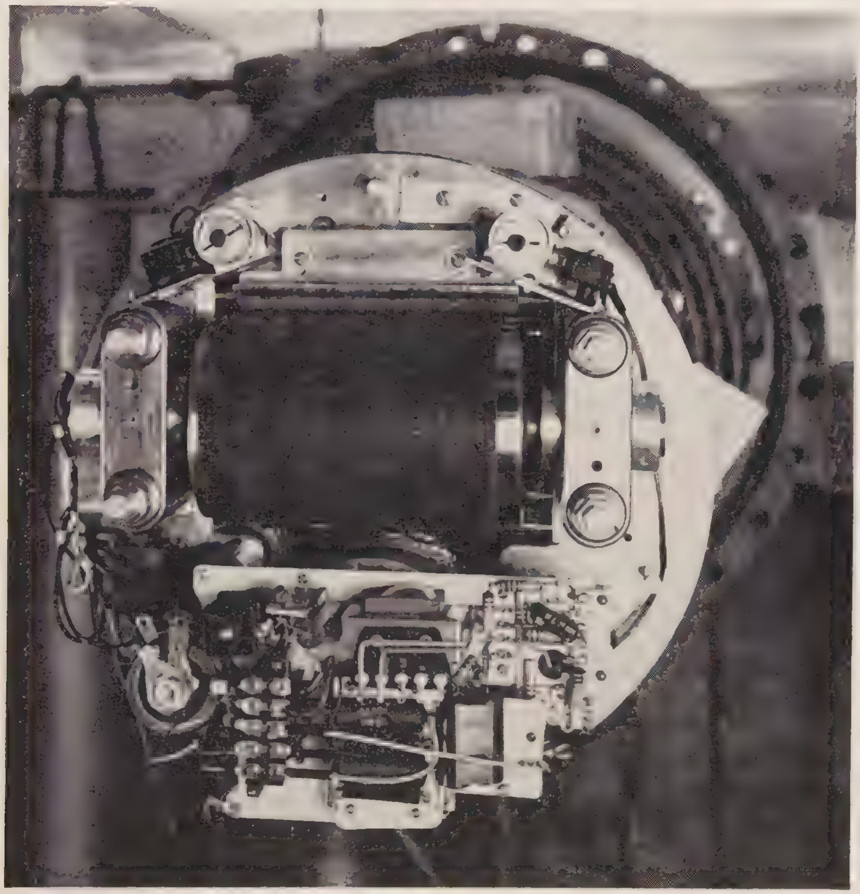

Fig. 5. Pulse generator for the 2 MeV electron Van de Graaff at the Ecole Normale Supérieure.

These experiments are disturbed by instabilities in the Van de Graaff beam current: these instabilities can come from cathode emission fluctuations, from stray magnetic fields, from mechanical (belt) vibrations. They can be overcome by d–c heating of the cathode, magnetic shielding, mechanical reinforcement.

It is also possible to cancel part of these drifts in electron voltaic measurements by a self balancing potentiometer giving directly the ratio I_{cc}/I_B[6]).

3.2. PULSE MEASUREMENTS

With the same experimental set-up we have measured the induced conductivity decay time, which is the effective lifetime of excess carriers, after a transient excitation by a short burst of high energy electrons. The accelerator beam was pulse modulated, with a pulse length ($\frac{1}{2}$ μsec) shorter than the expected decay time (2 to 100 μsec). The pulser was located in the high voltage terminal (figs. 4, 5); it is a simple delay line discharged through a thyratron fired by a blocking oscillator. The oscillator is synchronized with the alternator, to avoid as far as possible jitter due to the previously mentioned fluctuation. As usual, the cathode is biased + 300 V with respect to the cathode cup, so that the beam is at cut-off. The 400 V pulse biases the cathode to — 100 V, deblocking it. The current pulse in the beam has a total length of 0.5 μsec with rise and decay times 0.1 μsec; the peak current could be as high as 2 mA (fig. 6a).

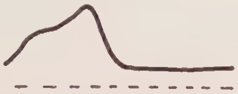

Fig. 6a. Pulse shape of the beam current with the fig. 4 pulses (0.1 μsec markers).

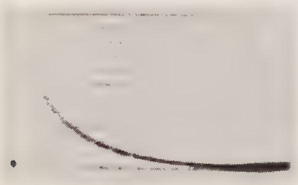

Fig. 6b. Display of excess conductivity of a germanium sample, after excitation by pulse of fig. 6a (markers 1 μsec). The lifetime of hole-electron pairs is this sample is 2.5 μsec.

The excess conductivity was observed by flowing a constant current through the sample, and observing on a fast oscilloscope the voltage transient (fig. 6b). The duty cycle of the beam was kept small enough so that no detectable damage was introduced in the sample. Fig. 7 shows the lifetime variation with irradiation, at

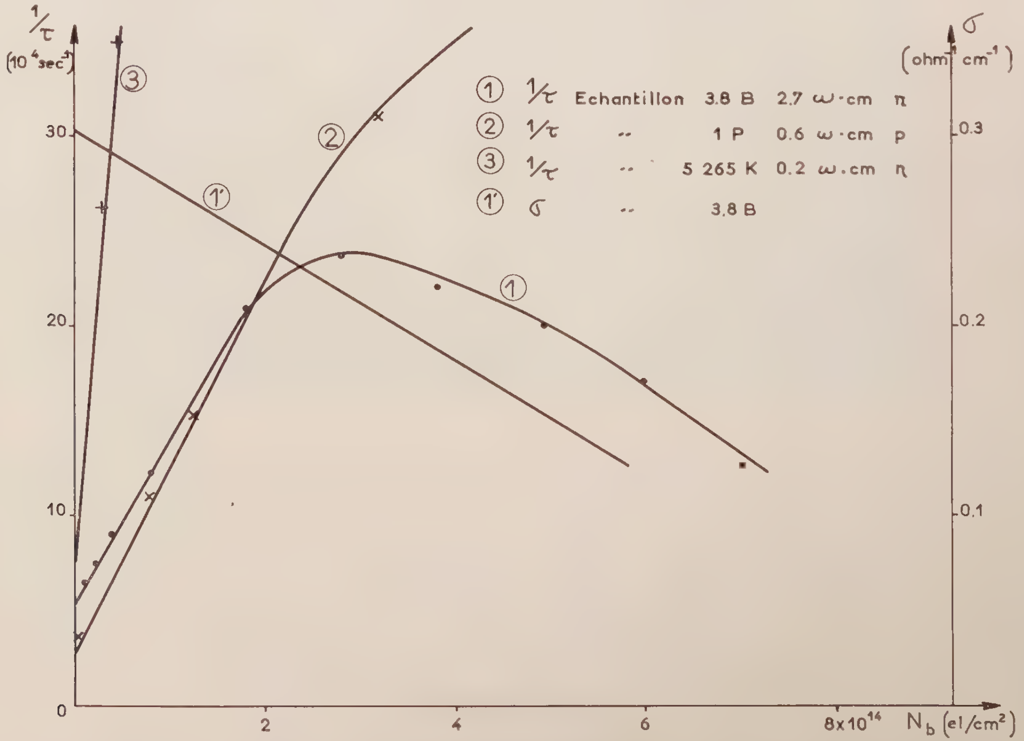

Fig. 7. Variation of inverse lifetime $1/\tau$ for three different samples during irradiation at room temperature. The conductivity σ is also displayed for sample 1; the turnover in the variation of $1/\tau$, for this sample, is related to the large conductivity variation. (From Annales de Physique[7].)

room temperature displaying, in certain conditions, the same minimum in lifetime as above.

A similar, but much more refined technique has been developed at Bell Telephone Laboratories by Wertheim and Augustyniak, using a fast mercury pulser[8]).

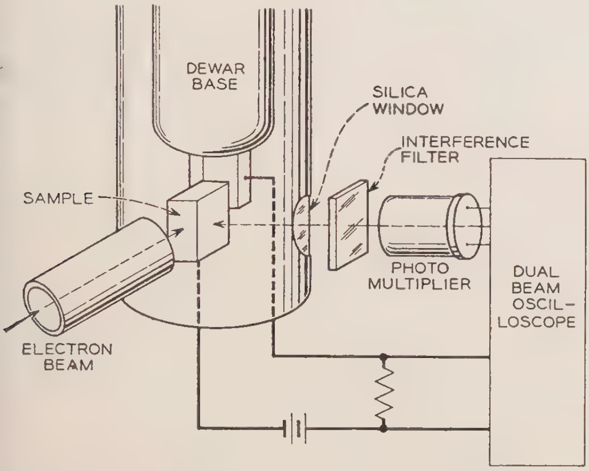

Fig. 8. Experimental apparatus for observing fluorescence decay in cadmium sulfide irradiated with a pulsed electron beam. (From J. of Appl. Phys.[9]).)

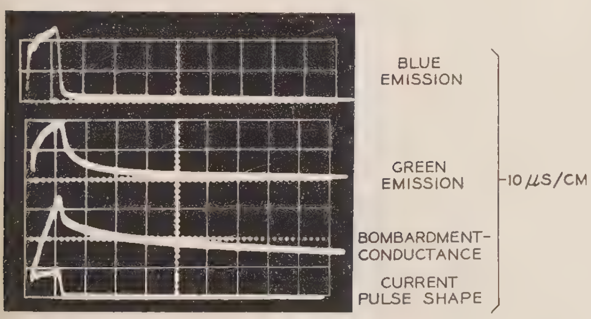

Fig. 9. Shape of fluorescence and excess conductance decays, in the apparatus of fig. 8; the beam pulse is also displayed. (From J. of Appl. Phys.[9]).)

3.3. OPTICAL MEASUREMENTS

Using the Bell Labs 1 MeV pulsed Van de Graaff, Collins has made a study of luminescence of cadmium sulfide[9]). The accelerator set-up which is a good example of a completely integrated system for electron irradiation, has been previous described by Brown[1]).

The experiment was to observe the decay time of blue and green fluorescence in CdS, using a pulsed beam and a photomultiplier (figs. 8 and 9). The blue fluorescence has a very short decay time (10^{-8} sec) and is attributed to exciton decay. The green emission has a longer decay time; this also holds for excess conductivity and shows that a free carrier is involved in this process; the green emission is also enhanced by electron irradiation, and this would prove that it is associated with a defect: Sulfur vacancy or interstitial, trapping a free carrier.

Similar experiments have also been carried out by other groups[10]), and help to understand both the mechanisms of fluorescence and of radiation damage in such compounds as CdS.

Another experiment, on the same lines, would be to push this emission of fluorescence light up to the point where the photon energy density in the crystal would be high enough to provoke coherent light emission ("maser" action). The injection by an electron beam, eventually pulsed to obtain the highest intantaneous ionization density, seems to be a promising approach. However, no such experiment has yet, to this date, been successfully performed.

4. Radiation Damage Experiments

4.1. ELECTRON IRRADIATION OF METALS

Corbett, Walker and others use a resonant transformer electron accelerator, at General Electric to irradiate metals, measuring damage thresholds and identifying defects by their annealing properties, after liquid hydrogen or helium irradiation[11,12]).

They use[11]) a low temperature irradiation cell of the gas-flow type (fig. 10). The sample is contained in a "pill-box" (fig. 11) through which helium or hydrogen evaporating from a cryostat is pumped. The geometry is carefully designed to avoid thermal losses, the beam is well collimated

---

[8]) G. K. Wertheim and W. M. Augustyniak, Rev. Sc. Instr. **27** (1956) 1062.

[9]) R. J. Collins, J. Appl. Phys. **30** (1959) 1135.

[10]) B. A. Kulp and R. H. Kelley, J. Appl. Phys. **31** (1960) 1057.

[11]) J. W. Corbett, J. M. Denney, M. D. Fiske and R. M. Walker, Phys. Rev. **108** (1957) 954.

[12]) J. W. Corbett and R. M. Walker, Phys. Rev. **117** (1960) 970; (See also R. M. Walker, to be published in the Proceedings of 1960 Summer School on Radiation Damage, Ispra Italy).

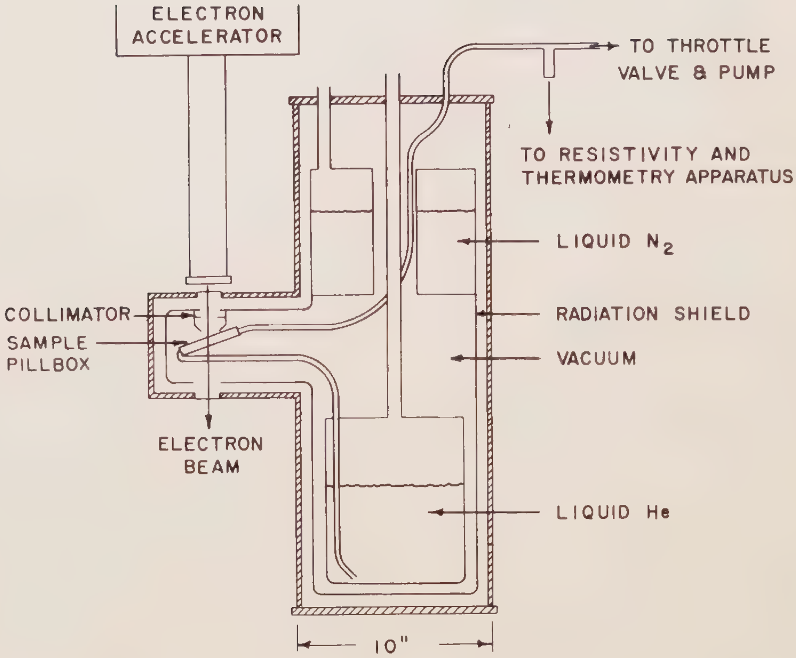
ELECTRON ACCELERATOR
TO THROTTLE VALVE & PUMP
TO RESISTIVITY AND THERMOMETRY APPARATUS
LIQUID N_2
COLLIMATOR
RADIATION SHIELD
SAMPLE PILLBOX
VACUUM
ELECTRON BEAM
LIQUID He
10"

Fig. 10. Cryostat used at General Electric Laboratories for liquid helium electron irradiation of metals. (From Phys. Rev.[11]).)

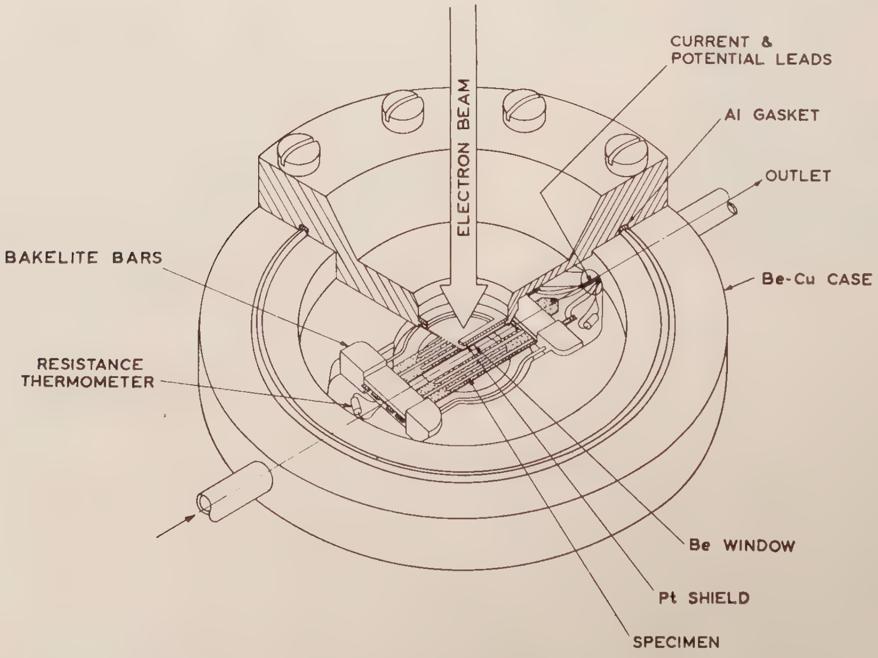
ELECTRON BEAM
CURRENT & POTENTIAL LEADS
Al GASKET
OUTLET
BAKELITE BARS
Be-Cu CASE
RESISTANCE THERMOMETER
Be WINDOW
Pt SHIELD
SPECIMEN

Fig. 11. Sample "pill box" in fig. 10 cryostat. The sample is double, half of it is a dummy, shielded from the beam by a platinum foil. (From Phys. Rev.[11]).)

to strike only the sample, while a dummy, cut from the same crystal, serves as a control. The system has a fast response time for temperature changes, which allows a fair control of temperature, and fast cycling for annealing.

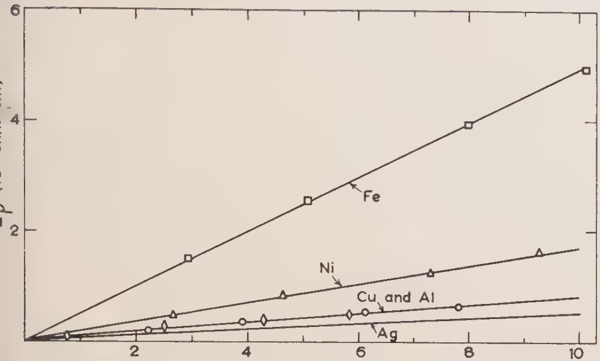

Fig. 12. Change of residual electrical resistivity in several metals bombarded at 20.4°K with 1.5 MeV electrons[12]).

The beam current and distribution is measured with a carefully designed Faraday cup in the same position as the sample and also by calorimetric measurements which can prove very accurate; the current is monitored by the current to an aluminium back stop behind the sample.

The parameter which is used as a measure of damage is the electrical resistivity at 4°K measured to 1 part in 5000. Fig. 12 shows a results for several metals, irradiated with 1.5 MeV electrons. From the change of resistivity it is possible, with assumptions on the scattering effect of vacancies and interstitials, to deduce the density of defects and the displacement rates. The defect concentration is of the order of 1 p.p.m. The variation of introduction rate with electron energy can be extrapolated, to give a threshold for onset of electron damage[11]). In this way displacement energies of 22 eV for copper, 30 eV for silver, over 40 eV for gold have been measured[12]).

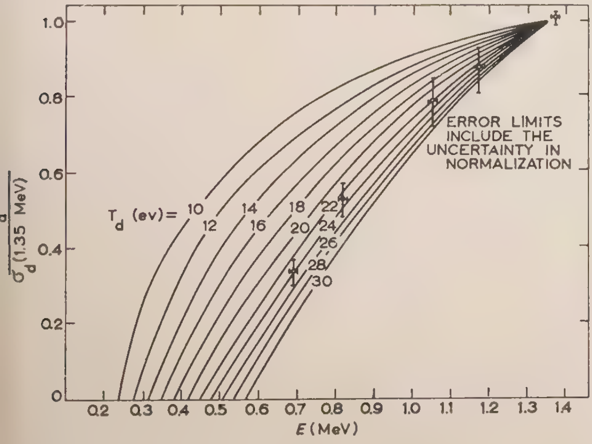

Fig. 13. Comparison of experimental data, for copper rradiated at 20° K, with theoretical curves of normalized displacement cross section *versus* bombarding electron energy. All the curves where calculated under the assumption that the displacement probability is a step function; the numbers refer to the assumed value of threshold energy. A good fit is obtained with $T_d = 22$ eV. (From Phys. Rev.[11]).)

It must be noticed that this technique gives an effective threshold and an average displacement energy, which can be used to compute damage rate at high energy. However. the energy threshold for the onset of damage, and the minimum displacement energy can be different, if the potential in which the atom sits is not a square well.

Other experiments include rate and energy dependance of low temperature annealing, and allow to give a good picture of electron damage in metals.

The same machine is also used for irradiation of semiconductors: through spin resonance measurements, a picture of the association of a vacancy with an oxygen impurity atom in silicon has been obtained[13]).

4.2. RATE EFFECT IN RADIATION DAMAGE IN GERMANIUM

The use of a pulsed beam allows very high peak currents, which are useful, as we mentioned above, in the study of ionization effects. They are useful too in the study of radiation damage, to know whether the nature and magnitude of damage is dependent only on the integrated dose of radiation or can be influenced by the irradiation rate. Indications that such an effect does exist can be inferred from results of MacKay[14]), at Purdue University: when using a microwave linear electron accelerator, he found a dependence of the introduction rate of acceptors

[13]) G. D. Watkins, J. W. Corbett and R. M. Walker, J. Appl. Phys. **30** (1959) 1198.

in germanium on the average current: in the microwave accelerator, the beam is pulsed in microsecond pulses, and each of these pulses is itself composed of a large number of microwave (2×10^{-11} sec) pulses, so that the peak current can be very high. This effect has recently been studied by W. L. Brown[1,15]) using a 1 MeV Van de Graaff accelerator.

With a careful focussing, a peak current of 2 mA, during 10^{-5} sec can yield a current density as high as 200 mA/cm^2 on the sample. For this heavy load, the Van de Graaff cathode has been changed to an L-type cathode; a grid has been added between the cathode and the cup; this grid is biased and pulsed to control the beam pulse in intensity and duration. With these conditions, a single impulsion of duration 10^{-5} sec introduces 10^{13} defects/cm^3 which are easily detected.

At 0.5 MeV, a peak current of 200 mA/cm^2 is more effective, by a factor seven, than a peak current of 20 mA/cm^2. Below 20 mA/cm^2, there is no visible rate effect. There is also a small, but definite influence of the pulse duration: the efficiency increases, in the rate dependent region, from the short (10^{-8} sec) to the long (10^{-5} sec) pulse.

The interpretation is difficult, but implies probably that the rate of damage depends on the intensity of ionization: the first interstitial position would be highly unstable, the interstitial could fall back in its original lattice site, or be liberated to go farther in the crystal. A high ionization would destroy the first possibility. This model of the interstitial has already been put forward to explain a decrease of displacement cross section at low temperature[16]), and there is also some good evidence that the mobility of a defect is dependent on its electrical charge.

Evidently, it would be most interesting to find out whether such a rate effect exists in metals, to ascertain the influence of ionization.

5. Conclusion

These few examples may give an idea of the way electron irradiation can be used in solid state physics, and of the technical problems involved. This is not, by far, a complete review, one could describe with more details the threshold experiments, the temperature and orientation dependence of the introduction rate, the impurity effects, the studies on annealing, recent work with higher energy (20 MeV) electrons, etc [17]).

A fair amount of knowledge about defect structure in metals and semiconductors can be obtained from these studies, but it is now evident that to obtain more precise information one has to turn to very low temperature work (4–20° K) although this can be a very challenging problem, at least from the experimental point of view.

I would like to thank W. L. Brown, J. W. Corbett, R. M. Walker, for interesting discussions and permission to use unpublished results.

[14]) J. Mackay, Private communication (to W. L. Brown.)

[15]) W. L. Brown, Private communication.

[16]) G. K. Wertheim, Phys. Rev. **115** (1959) 568.

[17]) See, for example, articles in the Aug. 1959 (T. 30, pp. 1117 to 1322) issue of the Journal of Applied Physics, reporting the Gatlinburg meeting on radiation damage in semiconductors. Van Lint and Roth's paper is a report of an experiment with a 20 MeV linear accelerator.

DISCUSSIONS

Speaker addressed: P. Baruch (*E.N.S., Paris*)

Question by: L. Lindner (*I.K.O., Amsterdam*)

Question: Would you please explain the meaning of a "focussing collision".

Answer: The term of "focussing collisions", coïned by Silsbee (Journal of Applied Physics **28** (1957) 1246, refers to a series of events, following a primary displacement, in which the kinetic energy of the primary displaced atom can be transferred, without any transfer of matter, along a row of atoms, for example a 110 direction on a closepacked lattice. Certain conditions have to be met: angle of the primary collision with respect to the row, correct values of the energy. It can then be shown that, even if the initial collision is at an angle with the row, this angle will decrease with successive collisions (hence the term "focussing") and the energy can propagate along hundreds of atoms up to the point where it is totally dissipated, or ending by displacing a weakly bound atom, for example when the "focusson" crosses a dislocation line. Experimental proofs have been found of such an effect (see: Leibfried, Journal of Applied Physics **30** (1959) 1388 and **31** (1960) 117; Thompson, Phil. Mag. **4** (1959) 139).

Speaker addressed: P. Baruch (*E.N.S., Paris*)

Question by: A. J. Swallow (*London*)

Question: What is the G-value i.e., number of events for 100 eV of energy absorbed, for the production of Frenkel defects by electrons?

Answer: The theoretical calculations of displacement cross-sections using the Mott-Rutherford scattering theory is not yet accurate enough in view of the large uncertainties about the elementary displacement processes, the shape of the interatomic potential, the number of secondaries per primary, the annealing effects, etc.... However, typical experimental values can be given: the number of defects per cubic centimeter introduced by one electron per sq.cm is 0.1 cm^{-1} ($G \simeq 10^{-6}$) at 800 keV, about 2 cm^{-1} ($G \simeq 2 \times 10^{-5}$) at 2 MeV, 5 cm^{-1} ($G \simeq 5 \times 10^{-5}$) at 5 MeV. See for example Brown and Augustyniak, Journal of Applied Physics **30** (1959) 1300; Cahn, Journal of Applied Physics **30** (1959) 1310.

Speaker addressed: P. Baruch (*E.N.S., Paris*)

Question by: H. Nauta (*Shell, Amsterdam*)

Question: How does the cross-section for atomic displacement produced by gamma rays compare with the one for electrons?

Answer: The displacement cross-sections from gamma rays could also be computed theoretically, knowing the displacement cross-sections for electrons of various energies, the creation rate for Compton or photo electrons, and the shape of the gamma spectrum. The calculations are difficult, and uncertain (see: Cahn, quoted above, and Oen and Holmes, Journal of Applied Physics **30** (1959) 1289). A typical value, also for germanium is 10^{-3} defect per incident electron per unit length with Co^{60} gamma rays.

NUCLEAR INSTRUMENTS AND METHODS **11** (1961) 210–226; NORTH-HOLLAND PUBLISHING CO.

HIGH ENERGY RADIATION FOR RESEARCH IN BIOCHEMISTRY AND MICROBIOLOGY

WOLFGANG HUBER

Biophysics Laboratory, Stanford University, Stanford, California, U.S.A.

The applications of accelerators to biological problems were initiated some thirty years ago and have since been increasing at an ever-growing rate. Today they are useful for applications requiring anywhere from a few electron volts to a few billion electron volts. In fact, intense beams of particles of homogeneous composition and uniform LET are available only from accelerators and these are becoming more and more standard tools for chemists and biologists alike.

Work during recent years has shown that an understanding of the enormously involved pattern of biochemical radiation effects may be obtained by approaching the subject indirectly through the study of the factors which modify radiation injury. It is this subject of parameters that are discussed to demonstrate the usefulness of high energy radiation as a research tool in biochemistry and microbiology.

The factors that have been recognized to influence the radiation response of biochemical systems include:

Linear Energy Transfer (LET)
Dose Rate
Composition of Surrounding Medium
Atmosphere (Oxygen Effect)
Temperature
Chemical Modifiers

These parameters can be classified rougly into two general groups; that is, those which are inherent to the radiation itself and those that are extraneous to the radiation but influence the radiation effect. All these parameters are discussed in detail.

1. Introduction

The applications of accelerators to biological problems were initiated some thirty years ago and have since been increasing at an ever-growing rate. Today they are useful for applications requiring anywhere from a few electron volts to a few billion electron volts. In fact, intense beams of particles of homogeneous composition and uniform LET are available only from accelerators and these are becoming more and more standard tools for chemists and biologists alike.

However, it was only shortly after the second World War that Lea[1]) made the first and very successful attempt to coordinate radio-biological knowledge into a comprehensive picture. Since then it has become widely recognized that those parts of radiation chemistry concerned with aqueous systems and macromolecules ought to have a special relevance to the problems of the actions of ionizing radiations on living systems. During the last fifteen years we have witnessed a tremendous expansion of research work in radiation chemistry and biology with the result that radio-chemical reactions and the mechanism of energy transfer are now far better understood. Precise methods of irradiating biological units with particles have yielded more definite notions of the effect on various cell structures, of the mechanism of gene action, cell division, and differentiation. Bond energy and atom migration have been recognized. The breakdown of ions and ion-molecule reactions may lead directly to some of the observed products. Triplet states may be important in radiochemical processes. Paramagnetic resonance measurements have been developed as an important tool for the determination of free radicals formed during a radio-chemical event.

Thus radiation as an investigational tool in chemistry and biology has established itself as a serious and vigorous field with a substantial literature that presently amounts to about 200 papers per year covering biological and related systems.

And yet the basic puzzle of radio-biology remains largely unsolved, that is, that such small doses of radiation should have such profound effects. While "deadly" if delivered in form of ionizing radiation, this amount of energy is harmless if spread throughout the cell by the normal processes of metabolism or if delivered by means such as light or radiant heat. The peculiar character of ionizing radiation to deliver its effect by concentration in a few thousand molecules selected at random throughout the cell creates this very different situation.

---

[1]) D. E. Lea, Actions of Radiations on Living Cells (Cambridge Univ. Press, London, 1957).

Work during recent years has shown that an understanding of the enormously involved pattern of biochemical radiation effects may be obtained by approaching the subject indirectly through the study of the factors which modify radiation injury. It is this subject of parameters that I would like to discuss to demonstrate the usefulness of high energy radiation as a research tool in biochemistry and microbiology.

The factors that have been recognized to influence the radiation response of biochemical system include:

Linear Energy Transfer (LET)
Dose Rate
Composition of Surrounding Medium
Atmosphere (Oxygen Effect)
Temperature
Chemical Modifiers

They can be classified roughly into two general groups, that is, those which are inherent to the radiation itself and those that are extraneous to the radiation but influence the radiation effect. To be sure each parameter will not be operative in altering the radiation response in every system, but the results indicate quite clearly that within the complicated maze that represents a biological unit every one of these factors can and often does contribute to the ultimate effect initiated by a given dose of ionizing radiation.

2. Radiation-Intrinsic Parameters

2.1. LINEAR ENERGY TRANSFER

The absorption of high energy photons (X-rays, gamma rays) and high speed particles (electrons, protons, alpha particles, etc.) in matter from an external source gives rise to electronically excited and ionized molecules of a variety of types and in a drastically inhomogeneous spatial arrangement. These "primary products" which are produced in close proximity of the track of a primary particle are nearly always extremely unstable and quickly undergo secondary reactions until the system is in thermal equilibrium. Fig. 1 is an attempt to illustrate the condition of the molecules within a few millimicrons of the track within about 10^{-16} seconds after the passage of the primary particle[2]. It shows ions as well as excited molecules and the well known "spurs" of the delta-rays jotting out perpendicularly from the main tract. The biological imprint of the radiation event becomes established by the disturbance of the chemical equilibrium which results in the formation of species which are different chemically from those originally present, and in the formation of free radicals.

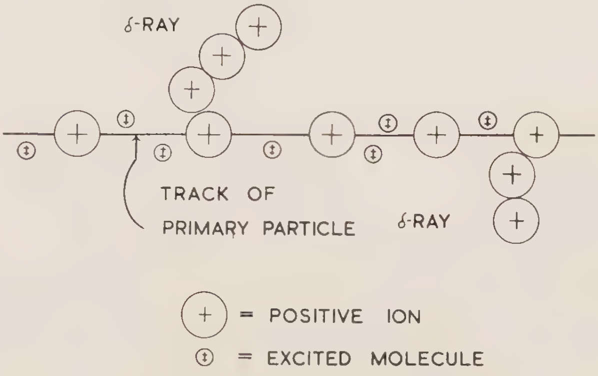

Fig. 1. Molecule distribution along track about 10^{-16} seconds after passage of primary particle (after Dainton[2]).

The term Linear Energy Transfer was introduced by Zirkle[3] in order to define the distribution of physical events along the track in terms of energy transferred rather than of ions formed. LET is expressed as thousands of electron volts per micron of track, in *all* biological events the track of course, being in tissue. It is always an *average* for the population of ionizing particles in a given absorber. This is important since approximately equal values of LET can therefore represent different populations of ionizing particles, which in some cases may differ significantly in their overall radiation effects. In order to deal

---

[2] F. S. Dainton, Chemical Effects of Radiation, Radiation Research (1959), Suppl. 1, 1.

[3] R. E. Zirkle, The Radiobiological Importance of the Energy Distribution Along Ionization Tracks, J. Cellular Comp. Physiol. **16** (1940) 221.

more simply with these highly complex problems it is generally assumed that the track effect for a given segment of particle track is characterised uniquely by the value of LET at that segment, and that the ultimate consequences of intermediate species are established during the chemical stage of radiation action[4]). This is not exactly true because the value of LET apart from being an average provides only a longitudinal measure of energy loss and that only approximately, for it disregards energy transport by secondary electrons. Obviously, the greater the LET the earlier will spatial factors tend to manifest themselves. The influence of transient heating and transient electrical fields is bound to show up in the overall results of track effects. It is now known that transient heating is a very important factor in the disordering of solids by ionizing radiation and the electrical field effect is known to be responsible for columnar recombination, the only track effect which occurs in gases.

Burch[5]) has attempted to extend the value of LET by an analysis of the more complex "indirect" effects and radiation quality. His calculations show that mean LET values in water are much higher for alpha particles than those calculated according to the methods of Gray[6]) and of Cormack and Johns[7]). In addition, the difference between "hard" radiation (25 MVp X-rays and cobalt-60 gamma rays) on the one hand and medium voltage X-rays (200 kVp) on the other hand, is smaller by a factor of 10 than those obtained previously.

In general, as the LET increases, the molecular yields increase and the radical yields diminish. However, the inequalities obtained at low average LET value are still preserved in the sense that the yield of hydrogen atoms is larger than the yield of hydroxyl radicals and both are larger than the yield of hydrogen peroxide. This is, of course, in accord with the expected effect of a higher LET favoring inter-radical recombinations at the expense of diffusion. Interestingly, it has been demonstrated that the fraction of radicals escaping from spurs is larger for heavy water[1]). It is not as yet clear why this is so but there is a possibility that the electron diffuses further from the tract in heavy water than in plain water because of the longer dielectric relaxation time.

It has, of course, been known for a long time that the same dose given by two different radiations can cause a different degree of biological effect. The "Relative Biological Efficiency" (RBE) is a conventionally used index for the measurement of such effects, and with the introduction of the concept of LET many attempts have been made to explain RBE in terms of different values for LET of a given type of radiation. However, it has become more and more apparent that it is hardly ever possible to state the relative biological efficiency of two radiations by a single parameter, even if limited to a given type of injury in a given cell. For example, Gray and Scholes[8]), as well as Kihlman[9]) have shown that the RBE of alpha-radiation versus X-radiation in inhibiting root growth will diminish from a value of 11.8 to a value of 4.5 when anoxia is replaced by oxygen. Experiments in which parameters other than LET were rigidly controlled have shown that RBE values for super-voltage radiation as contrasted with standard therapeutic X-radiation are much less dispersed than previously thought with super-voltage radiation being only slightly less than unity, i.e. 0.85 to 0.90[10]).

The work done at the Biophysics department of Yale University under the direction of E. C. Pollard provides a striking example how variation in LET can be utilized to determine fundamental biological properties[11]). The method is based on dose-effect relationships used for determination of a probability index or "cross section" which is related to the size of the area within which the biological entities are particularly sensitive to inactivation. Inactivation studies carried out with particles of different LET make it possible to derive approximations of the size and shape of the object studied. The method has been useful for the determination of size, shape, and active sites in a variety of viruses, enzymes and antibodies.

---

[4]) R. L. Platzman, The Physical and Chemical Basis of Mechanisms in Radiation Biology and Medicine, W. D. Claus Editor (Addison-Wesley, Reading, Mass., 1958).

[5]) P. R. J. Burch, Some Physical Aspects of Relative Biological Efficiency, Brit. J. Radiology **30** (1957) 524.

[6]) L. H. Gray, Problème des Relations entre le Rendement Radiochimique et les Aspects Physiques de la Qualité des Radiations, J. Chim. Phys. **52** (1955) 519.

[7]) D. V. Cormack and H. E. Johns, Electron Energies and Ion Densities in Water Irradiated with 200 keV, 1 MeV and 25 MeV Radiation, Brit. J. Radiol. **25** (1952) 369.

[8]) L. H. Gray and M. E. Scholes, The Effect of Ionizing Radiations on the Broad Bean Root, Brit. J. Radiol. **24** (1951) 82.

[9]) B. A. Kihlman, The Effect of Oxygen, Nitric Oxide and Respiratory Inhibitors on the Production of Chromosome Aberrations by X-rays Exp. Cell, Research **14** (1958) 639.

[10]) H. I. Kohn, The Relative Biological Effectiveness of External Beams of Ionizing Radiations: in Progress in Radiation Therapy, F. Buschke, Editor (Grune and Stratton, New York, N.Y., 1958).

Howard-Flanders[12]) has recently developed a quantitative treatment for microorganisms to describe the RBE of radiations of different LET. This "Track Segment Method" makes allowance for the oxygen effect. For a particular radiation the distribution of ions along a segment "*t*" of the track will be different. Plotting the reciprocal of the D-37 dose against LET (keV/micron) gives a measure of the effect with changing LET and thus an indication—as related to the injury caused—whether there are too few, the optimum number or a wasteful abundance of ions per track segment.

2.2. DOSE RATE

The effects of dose rate are intimately linked to the effects of LET inasmuch as a given energy distribution along a tract, at least in liquid and solid systems, can be influenced both by changing the quality of the radiation (LET) and the dose-in-time distribution. In any multi-component system the contribution of dose rates varying from seconds to hours often are overshadowed by the much more pronounced contribution of such parameters as oxygen, temperature, LET and the like. In short, during such time intervals dose rate is a parameter which may be only of minor importance. It appears, however that dose rate effects will become much more pronounced if total doses are applied in times of the order of milliseconds to microseconds. The very high intensity, short time pulses available from the newly developed L-band accelerators should prove particularly interesting and useful for further investigation in this area.

With individual chemical systems, particularly in dilute solutions, it can be readily demonstrated that the percentage destruction of a solute produced by a given dose will decrease as the dose-rate increases[13]). This is based on the well known competitive reaction between free radicals and solute molecules and between free radicals and other free radicals, and can be illustrated as follows:

$$M + \cdot OH \rightarrow M' + H_2O$$

$$H\cdot + \cdot OH \rightarrow H_2O\,.$$

Radical combination or recombination will be favored by increasing the instantenous concentration of radicals relative to that of solute molecules, that is, by increasing the dose rate. To a certain extent, an increase of dose rate will also decrease the probability of lightweight entities such as hydrogen atoms to escape from the "radiation cage". The radical recombination phenomenon will be further increased at very high dose rates where spurs from different tracts can overlap each other. That this is so has recently been shown by Sutton and Rotblat[14]) with the Fricke and the Cerric system. Using 1.3 microsecond pulses of 15 MeV electrons they were able to demonstrate that the *G*-values were markedly reduced with dose-rates above 10^8 rads per second. The linear accelerator used in this work permitted change in pulse-rate to an upper limit of 400 pulses per second. Within this range the results were unaffected by variation of the pulse rate. It is thus concluded that the lifetime of the radicals cannot exceed 2.5 milliseconds.

---

[11]) E. C. Pollard, W. R. Guild, F. Hutchinson and R. B. Setlow, The Direct Action of Ionizing Radiations on Enzymes and Antigens, Progr. Biophys. and Biophys. Chem. **5** (1955) 72.

[12]) P. Howard-Flanders, Injury of Cells by Ionizing Radiations, Adv. Biol. Med. Physics **6** (1958) 582.

[13]) A. Brasch, W. Huber and A. Waly, Radiation Effects as a Function of Dose Rate, Arch. Biochem. Biophys. **39** (1952) 245.

[14]) A. C. Sutton and J. Rotblat, Dose Rate Effects in Radiation-Induced Chemical Reactions, Nature **180** (1957) 1332.

Really pronounced dose rate effects can be expected wherever chain reactions occur. In an appropriate system a free radical can initiate as well as terminate a chain reaction.

$X\cdot + M \rightarrow X + M\cdot \; M \rightarrow MM\cdot \; M \rightarrow MMM\cdot$ etc.

$MMM\cdot + \cdot X \rightarrow MMMX$.

Increasing dose rate will increase the rate of formation of new radicals and hence increase the probability that a chain initiating reaction will be stopped by a chain terminating reaction based on radical action. The practical value of these effects is most pronounced in radiation-polymerization and depolymerization and I am sure Dr. Pinner in his paper will have to say a great deal about this. In biochemical systems the presence of numerous other entities that can act as potential chain terminators reduces the probability that dose rate dependent chain reactions will play an important role. However, the formation of trapped organic radicals inside the cage of a complex molecule such as a nucleoprotein, or along phase boundary lines such as between proteins and lipids may well initiate chain type reactions that could proceed over considerable lengths prior to being terminated by breakdown of the molecule or the interphase boundary layer. Such "captive" radicals may also in part be responsible for the "aftereffects" that have been observed by many investigators with a variety of biochemical materials including protein, fats, nucleic acids and enzymes.

In all systems where an increase in total dose changes the final effect by involvement of additional sites dose rate effects can be expected to be operative for one type of mechanism but not necessarily for another. Thus rats and mice die of X-ray doses of about 800 to 900 r by destruction of the hematopoietic system; above this dose level and about up to about 10000 r death occurs much faster and primarily because of damage to the intestinal tract; with further increases in dose up to about 150000 r death occurs almost instatenously and is primarily due to damage to the central nervous system. At very high dose rates, the effect on the central nervous system seems to be increased[10]).

Threshold value dependence in terms of damage to the molecule has been beautifully demonstrated by the inactivation of monolayers of bovine serum albumin[11]). The ability of this molecule to combine with its specific antibody is only destroyed after very serious damage to the molecular structure. Effects like these which involve threshold intensity values at given sites should clearly be responding to dose rate modification.

3. Radiation-Extrinisic Parameters

3.1. MEDIUM

Composition and physical state of the medium in which a radio-sensitive system is distributed have figured so prominently in radiobiological research because they are directly involved in the two major theories which have been developed for the explanation of biological radiation mechanisms. These are, of course, the so called "direct" and "indirect" effect. The direct effect postulates that the molecule undergoing change becomes ionized or excited itself by the passage through it of an ionizing particle. This concept was originated by Dessauer and expanded into the target theory by Lea[1]) and coworkers and extended lately by Pollard and associates[11,15]). It's by and large adequate to explain the radiation mechanisms in dry systems as well as in a sizeable number of solids.

Work by Risse, Fricke, Barron, Dale among others, clearly demonstrated that the tenants of the target theory were not applicable to the explanation of radiation effects in dilute aqueous systems[16]). This led to the concept of the "indirect" action of radiation which postulates that biological materials may be inactivated by chemically active intermediates formed from water by ionizing radiation. This concept is based on the assumption that these intermediates can diffuse through an aqueous medium and inactive a molecule at a distance from where the energy was originally absorbed, hence, the name

---

[15]) E. C. Pollard, The Action of Ionizing Radiation on Viruses, Advances Virus Res. **2** (1955) 109.

[16]) W. M. Dale, Survey of the Action of Ionizing Radiations in Aqueous Systems, Radiation Research Supplm. **2** (1960) 578.

"indirect effect". The magnitude of the indirect effect on a given substance depends partly on the inherent sensitivity of the substance to attack by the diffusible intermediates, and partly on the competition for the intermediates by other materials in the irradiated medium.

The role of water in the radiation effect upon living cells has been investigated with enough of a variety of materials to permit some generalizations[17]. Bacteriophage and other viruses are more sensitive in dilute than in concentrated suspension, more sensitive wet than dry, and more sensitive in the absence than in the presence of broth or certain chemical agents. Bacteria are more sensitive in aqueous suspensions than in the dry state. The sensitivity of fungus spores to X-ray inactivation is proportional to their relative water content and seeds mutate more easily in the wet (metabolizing) than in the dry (dormant) state. It seems that water where present exerts its influence whether it is intracellular or extracellular.

It is now quite clear that neither "direct" nor "indirect" action can be made solely responsible for the radiation effect on biochemical compounds, particularly in vivo. The available evidence supports the view that this holds true across the board i.e. for nucleic acids, nucleoproteins, enzymes, structural proteins, lipids, and carbohydrates alike.

The realization that the radiobiological end effect is a complex composite of direct and indirect action has initiated recent studies designed to determine the relative contribution of either in a given system. So far this work has been largely concentrated on nucleic acids and enzymes. In addition, several authors have attempted to determine the difference in radiation sensitivity, if any, for a given system extracellularly versus intracellularly. Hutchinson and his colleagues[18] have measured the inactivation of invertase, alcoholdehydrogenase (ADH) and coenzyme A (Co–A) in the living yeast cell as well as in the same cell after vacuum drying. After irradiation the enzymes were extracted from the cells and determined by standard methods. The doses needed to establish proper inactivation were large and varied from 1 to 1000 Mrads. The results show that the sensitivity wet versus dry was about 2 to 1 for invertase, 20 to 1 for ADH and 100 to 1 for Co-A. In other words, 2, 20 and 100 times as many molecules of the three enzymes respectively, were inactivated when the living cell was irradiated. Due to the difference in molecular weight of the three enzymes and the differences in G values (ADH, $G = 1$; invertase, $G = 0.053$) the contribution of chemically active intermediates formed by the radiations from the water in the wet cells is considerably less than indicated by these figures. The relative importance of this indirect effect is approximately inversely proportional to the size of the molecule. A later calculation by Hutchinson[19] which represents a refinement of a model previously proposed by Zirkle and Tobias[20] indicates the average distance which the free radicals produced by the radiation can diffuse, to be about 30 Å for all three enzymes. This value is based on the assumption that the free radicals will react with large biological molecules on every encounter. If this probability drops to as low as 0.001 diffusion will be of the order of a few hundred Å. In any case, these values are a small fraction of the dimensions of the cell and hence Hutchinson's data do not provide any support for a concept of indirect action which visualizes the effects of an ionization diffusing throughout a cell. Instead, the monotopic action of the target concept seems to be maintained, with a target which is somewhat blown up by surrounding water layers having hazy boundaries of thicknesses between tens and hundreds of angstroms.

---

[17] G. E. Stapleton and A. Hollaender, Biochemical and Cellular Effects; in Radiation Biology and Medicine, W. D. Claus, Editor (Addison-Wesley, Reading, Mass., 1958).

[18] F. Hutchinson, A. Preston and B. Vogel, Radiation Sensitivity of Enzymes in Wet and Dry Yeast Cells, Radiation Res. **7** (1957) 465.

[19] F. Hutchinson, The Distance That a Radical Formed by Ionizing Radiation Can Diffuse in a Yeast Cell, Radiation Res. **7** (1957) 473.

[20] R. E. Zirkle and C. A. Tobias, Effects of Ploidy and Linear Energy Transfer on Radiobiological Survival Curves, Arch. Biochem. Biophys. **47** (1953) 282.

In further extension of this work[21]), the inactivation of coenzyme A was recently determined in five different cells, namely, E. coli, S. cerevisiae, peas, beef heart, beef liver, and compared to the inactivation of pure, dry Co–A. Electrons were used at dose rates of about two Mrads per minute. The data show that the inactivation of coenzyme A in the five different cells requires surprisingly large doses of radiation. Radicals formed in water in the cell can migrate a distance of the order of 20 to 40 Å before reacting, which is also surprisingly small. On the assumption that the cell consists of 80% water and 20% large molecules and that the water is distributed evenly over the surface of the large molecules, the values are compatible with the assumption that indirect action of any effectiveness can be created only in the water layers directly surrounding the large molecules. With the exception of E. coli, Co–A appears to be present in the cells in two different states, one state being much less sensitive to the irradiation effect than the other state. The resistant state amounts to about 30% in yeast, to about 70% in peas, and in the heart and liver cells essentially all the activity is present in the radiation resistant state. The authors explain the high resistence in terms of lack of water surrounding the coenzyme in the respective cells. In view of the high radiation sensitivity of biological systems in the dry state found by others, the real reason rather may lie in the fact that the coenzyme in vivo is in a coupled state with substrate for extended periods of time, and that such coupled states can be more radiation sensitive or resistant than the uncoupled state.

The effect of one MeV electrons on DNA in pneumococcus cells has been determined in the dry state, in the wet anoxic state, in the wet aerobic state, and in the wet aerobic state in the presence of 1% of cysteamine[22]). The respective D-37 doses were 3.0 Mrad, 1.2 Mrad, 0.4 Mrad, and 1.2 Mrad. The effects were determined by measuring the transforming ability of the DNA extracted from the irradiated cells. The data in the dry state are consistent with a molecular weight of 247000 per unit of transforming activity, which is an excellent agreement with values obtained by other methods. The increase in radiosensitivity from the dry to the wet state would be equivalent to the diffusion of radiation produced radicals over a distance of the order of ten Å. The greatly increased sensitivity due to the presence of oxygen is somewhat surprising and will be discussed more fully below. The relative importance of indirect inactivation shown for the isolated long thread-like DNA molecule would be expected to be very great, in agreement with Butler's in vitro observation that at all concentrations down to 1%, the loss of structural integrity by DNA is as effectively brought about by energy deposited in the water as by energy deposited in the DNA itself[23]).

However, there is also evidence in vivo as well as in vitro, that the presence of water will *decrease* the radiosensitivity rather than increase it. Ehrenberg and co-workers[24]) as well as Caldecott and associates[25]) have shown this clearly in their intensive investigations on radiation effects on the cells of the embryo within the seed. The observation with seeds show a striking resemblence to observations made by Okada and associates[26, 27]) on the radiation inactivation of deoxyribonuclease and the susceptability of substrates to enzymatic degradation as represented by DNA, albumin, hemoglobin and cellulose. In the latter cases it was shown that on irradiation DNA becomes more readily depolymerized by nonirradiated deoxyribonuclease I, albumin and hemoglobin were more susceptable to tryptic digestion and cellulose was more susceptable to the action of cellulase. When albumin was irradiated in the dry state there was an increase in the rate of enzymatic digestion similar to that found in the irradiated solution. These effects indicate that the enzyme is either bound more strongly to the irradiated than to the non-irradiated substrate, or that the irradiated substrate has more active sites accessible to the enzyme. The latter might be the result of unfolding or of fragmentation of hydrogen bonds in the protein molecule.

---

[21]) F. Hutchinson and C. Norcross, Inactivation by Ionizing Radiation of Coenzyme A in Various Cells, Radiation Res. **12** (1960) 1.

[22]) F. Hutchinson and J. Arena, Destruction of the Activity of Deoxyribonucleic Acid in Irradiated Cells, Radiation Res. **13** (1960) 137.

[23]) J. A. V. Butler, Changes Induced in Nucleic Acids by Ionizing Radiations and Chemicals, Radiation Res. Supplm. **1** (1959) 408.

[24]) L. Ehrenberg, Radiobiological Mechanisms of Genetic Effects, Radiation Res. Suppl. **1** (1959) 114.

[25]) R. S. Caldecott, E. B. Johnson, D. T. North and C. F. Konzak, Proc. Natl. Acad. Sci. U.S. **43** (1957) 975.

[26]) S. Okada and G. L. Fletcher, Radiation Inactivation of Deoxyribonuclease in the Dry and Hydrated States, Radiation Res. **13** (1960) 92.

[27]) S. Okada, R. Kraunz and E. Gassner, Radiation Induced Change in the Susceptibility of Substrates to Enzymatic Degradation, Radiation Res. **13** (1960) 607.

In the irradiation of dry deoxyribonuclease I absorbed on cellulose, Celite and Dowex 50 it was found that the enzyme was more radiosensitive in the absorbed form than in the pure form. The enzyme dried with and absorbed on DNA however was protected to a considerable degree from the radiation inactivation. Wet enzyme containing about 50% water was less radiosensitive than the dry pure enzyme. Recent work of Butler and associates[28]) on the inactivation of chymotrypism with 15 MeV pulsed electrons demonstrates that the enzyme is about eight times more sensitive in the solid state than when it is in dilute aqueous solution. Both the protease and esterase activities are reduced equally.

One explanation of the seemingly contradictory results of irradiation in the wet state versus the dry state might rest in the fact that in certain systems specific inter- or intramolecular energy transfer systems may be more operative in the dry than in the wet state. The whole question of importance of indirect action and diffusion of active entities formed in the irradiated water to sites where the biological effect will take place has been questioned by Alper[29]). She presents an alternative hypothesis involving direct energy absorption in a biological target. This leaves the target itself in an activated state, free to react in several ways. The activated target molecule may react with oxygen resulting in inactivation, react with another molecule like itself, or return to the normal state. In this hypothesis water is involved only to the extent that it facilitates diffusion of the activated target molecule. In the absence of oxygen the probability is high that the activated target molecule can return to a normal state before interacting with oxygen or another molecule. Data by Howard-Flanders and Alper[30]) suggest that all activated targets may remain reactive for the order of several microseconds. No evidence is presented explaining the possibility of activated target molecules being located in areas where none of the effects suggested by Alper may take place for extended periods of time.

3.2. ATMOSPHERE—EFFECT OF OXYGEN AND OTHER GASES

The phenomenon now generally referred to as the Oxygen Effect appears to be universally involved in the degree of injury on cells brought about by ionizing radiation. It has also been demonstrated frequently with many individual chemical systems (enzymes, nucleic acids, structural proteins, carbohydrates, etc.). Work in this field prior to 1958 has recently been the subject of excellent and comprehensive reviews by Howard-Flanders [12]) and by Gray[31]).

Remarkably enough it has been found consistently that oxygen increases the effectiveness of X-irradiation or electron irradiation by a factor of 2 to 3 with a variety of cells, including bacteria, bean roots, insects and mamalian cells, particularly when the criterion of radiation injury is a failure of growth or colony formation. The degree of enhancement seems to be independent of temperature, at least between zero and 37°C and of the presence or absence of respiratory enzymes. As previously pointed out,

[28]) T. A. V. Butler, A. B. Robins and J. Rotblat, Inactivation of Chymotrypsin with 15 MeV Pulsed Electrons and 140 kV X-Rays, Meeting Faraday Soc. and Assoc. Rad. Res. Kings College, Univ. Durham, 23–25 March 1960.

[29]) T. Alper, The Modification of Damage Caused by Primary Ionization of Biological Targets, Radiation Res. **5** (1956) 573.

[30]) P. Howard-Flanders and T. Alper, The Sensitivity of Micro-organisms to Irradiation Under Controlled Gas Conditions, Radiation Res. **7** (1957) 518.

[31]) L. H. Gray, The Influence of Oxygen on the Response of Cells and Tissues to Ionizing Radiation, Lect. Sci. Basis of Medicine **7** (1957–58) 314.

dose rate has been shown to have some effect on the oxygen effect in vicia faba roots. Linear energy transfer is probably responsible for the fact that neutron radiation shows a much pronounced oxygen effect with the latter being least of all for alpha radiation. At temperatures well below zero when there is a reduction in the sensitivity of vegetative cells per se, the degree of the oxygen effect is also somewhat diminished[32]. In aspergillus spores the degree of enhancement due to the presence of oxygen decreases when transfer is made from suspension in water to thorough drying.

However, there are also exceptions to these rules. No oxygen effect has been found in the inactivation of either bacteriophages[33] or the transforming principle[34]. In contrast, the radiosensitivity of phagebacterial complex measured immediately after absorption, is decidely dependent upon oxygen[35].

That the degree of the oxygen effect may depend upon the presence in the cell of a particular biochemical system is supported by some recent work by Alper[36] where it is shown that freshly harvested haploid yeast cells exposed to 8 MeV electrons from a linear accelerator at dose rates of about 15000 rads per minute have an oxygen enhancement ratio twice as high (3.4) as the more resistant budding cells (1.6).

Radiation response of many individual organic substances is also modified due to an oxygen effect. However the picture here is much less clear cut than with cells. Of interest is the radiation induced cleavage of peptide chains[37]. In the presence of oxygen, a hydrogen atom is removed from the chain leaving a carbon nitrogen double bond which can subsequently be hydrolytically converted into a keto group. A variety of studies on the inactivation of enzymes in dilute solution surprisingly enough, failed to demonstrate an oxygen effect. The explanation to attribute the absence of the oxygen effect to the faster and predominant action of radical attack in dilute solutions seems rather untenable in view of the fact that there is a pronounced oxygen effect in the deamination of amino acids in dilute solution[38]. It might be useful to reinvestigate the oxygen effect on enzymes in solution in the presence of increasing amounts of substrate which, of course, would correspondingly reduce the severity of the attack by radicals formed from the water present.

In contrast, when enzymes are irradiated dry a marked oxygen effect has been observed both for lysozyme and ribonuclease. Alexander and co-workers[39] irradiated proteins in the solid state and explain the observed effects on the basis that a single ionization or cluster of ionizations brings about the breakdown of as many as several hundred hydrogen bonds, thus constituting the single primary event which discrupts the seondary structure over a large part of the protein molecule. The value of several hundred hydrogen bonds is appreciably in excess of the 15 to 20 hydrogen bonds previously postulated by Platzman and Frank[4] on the basis of theoretical considerations. The bovine serum albumin used, was evacuated prior to irradiation with two MeV electrons at a dose rate of one million rads per second. It seems possible that the much greater number of hydrogen bonds broken, might be due to oxygen occluded to the protein molecule and not removed by the evacuation procedure, particularly in view of the observation by Howard-Flanders and Alper[30]) that partial pressures as low as 8 to 16 millimeters Hg was all that was needed to demonstrate a pronounced oxygen effect in microorganisms.

---

[32] A. Hollaender and G. E. Stapleton, Fundamental Aspects of Radiation Protection from a Microbiological Point of View, Physiol. Res. **33** (1933) 77.

[33] H. B. Hewitt and J. Read, Search For an Effect of Oxygen on the Direct X-Ray Inactivation of Bacteriophage, Brit. J. Radiol. **23** (1950) 416.

[34] H. Ephrussi-Taylor and R. Latarjet, Inactivation par les Rayons X d'un Facteur Transformant du Pneumocoque, Biochim. et Biophys. Acta **16** (1955) 183.

[35] P. Howard-Flanders and P. Jockey, An Effect of Oxygen on the Sensitivity to Ionizing Radiation of the Early T2 Bacteriophage, E. Coli B Complex, Adv. Biol. Med. Physics **6** (1958) 563.

[36] T. Alper, Variability in the Oxygen Effect Observed with Microorganisms, Part I, Haploid Yeast: Single and Budding Cells, Int. J. Rad. Biol. **1** (1959) 414.

[37] M. E. Jayko and W. M. Garrison, Formation of $C = O$ Bonds in the Radiation Induced Oxydation of Protein in Aqueous Systems, Nature **181** (1958) 413.

[38] E. S. G. Barron, The Role of Free Radicals and Oxygen in Reaction Produced by Ionizing Radiation, Radiation Res. **1** (1954) 109.

[39] P. Alexander, L. D. G. Hamilton and K. A. Stacey, Irradiation of Proteins in the Solid State, I, Aggregation and Disorganization of Secondary Structure in Bovine Serum Albumin, Radiation Res. **12** (1960) 510.

The considerable work on the time relationship in the oxygen effect has conclusively shown that oxygen is effective only if present during the irradiation. In an admirably elegant experiment Howard-Flanders and Moore[40]) have demonstrated that the sensitivity of shigella flexneri lags behind a change in oxygen tension of the gaseous environment by something like less than 0.01 second. This was shown by mounting the bacteria on a shuttle which could be transferred from a compartment containing oxygen to one containing pure nitrogen and back within 0.01 second after the irradiation. If the sequence was irradiation in nitrogen followed by oxygen exposure this time limit failed to demonstrate any oxygen effect whatever. The irradiation was obtained with an electron beam of 1.2 MeV at a sufficiently high rate that the dose could be applied within about 0.007 seconds. The value of 0.01 second is only an upper limit, set by purely technical limitations. The availability from linear accelerators of microsecond pulses of sufficient intensity should make it possible to decrease this time limit by another one or two orders of magnitude. This should prove to be of interest since diffusion calculations indicate that the lifetime of the reactive condition responsible for the oxygen effect may be as low as 10^{-4} second.

Quantitatively the dependence of radio sensitivity on available oxygen is now usually expressed by the following formula.

$$\frac{D_0}{D} = \frac{K + m\,[O_2]}{m\,(K + [O_2])}$$

where D is the dose required to produce a given degree of biological injury, D_0 is the dose required to produce the same effect in oxygen; O_2 is the concentration of dissolved oxygen and K and m are constants. K is the concentration of gas required to raise the radio sensitivity to the level halfway between the anoxic and aerobic values; m is the ratio of doses required for a given effect under anoxia and in oxygen. The values determined by different workers in different systems are surprisingly close. For X-rays m is around 3 for bacteria and ascites tumor cells, and slightly less for yeast. For neutrons the value for m was found to be about $\frac{1}{2}$ of that for X-rays. The values for K in micro moles per liter are somewhere between 4.5 and 5.5[8,9,30,41]).

While the equation affords a consistent explanation for the systems investigated, it has not as yet sufficiently proven out to provide evidence for the mechanism that is actually at work. The same sort of scheme could be deduced for a different type of mechanism in which it is, for instance, assumed that oxygen is competing for particular sites on a surface or for reactive molecules.

Oxygen is a bi-radical and more strongly paramagnetic than any other gas. Almost all of the other common gases are diamagnetic. Oxygen owes these properties to the fact that in its most stable form two of the electrons of the molecule remain unpaired and are thus able to readily form attachments with other free radicals.

$$\mathrm{H\cdot + \cdot O - O\cdot \rightarrow H - O - O\cdot}$$

$$\mathrm{R\cdot + \cdot O - O\cdot \rightarrow R - O - O\cdot}$$

$$\mathrm{R - O - O\cdot + \cdot H \rightarrow R - O - O - H\,.}$$

Three other gases share with oxygen an unpaired electron valance and the realization of this fact induced Howard-Flanders[12]) to see whether the least toxic of the three, namely nitric oxide could replace oxygen by increasing radiobiological damage. Using X-rays it could indeed be shown that remarkably small concentrations of nitric oxide were equivalent to oxygen in sensitizing the radiation effect on completely anoxic bacteria. Others have recently demonstrated the same effect with bean roots9) and ascites tumor cells41). In each instance the nitric oxide raised the sensitivity to the aerobic level. While not the same type of metabolite in the ordinary sense as oxygen, nitric oxide is believed to be an intermediate in the metabolism of certain microorganisms and it can combine reversibly with hemoglobin and reduce cytochrome oxidase. Hence radiochemical as well as biochemical mechanisms could be responsible for its observed activity.

---

[40]) P. Howard-Flanders and D. Moore, The Time Interval Following Pulsed Irradiation within which Injury to Bacteria Can Be Modified by Dissolved Oxygen, Radiation Research **9** (1958) 422.

[41]) F. F. Deschner and L. H. Gray, Influence of Oxygen Tension on X-Ray Induced Chromosomal Damage in Ehrlich Ascites Tumor Cells irradiated in Vitro and in Vivo, Radiation Res. **11** (1959) 115.

That the bi-radical affinity of oxygen is not unequivocally operative under all conditions has been shown by the results of Ebert *et al.*42) in the irradiation of aerobic bean roots using inert gases under great pressure. Using xenon, krypton, argon, nitrogen, hydrogen and helium, they determined a critical pressure for each gas at which the aerobic response of the root could be reduced to the anaerobic level. The 50% values varied from 1.1 atmosphere for xenon to a maximum of 55 atmospheres for helium. The same effect was shown to hold also for ascites tumor cells. The inert gas under pressure does not seem to interfere with the entry of the oxygen into the cell and hence seems to represent a true competitive effect. The authors point out that the effectiveness of the different gases increases approximately in step with the distribution coefficient between lipid and water. Since these gases under pressure have a certain anaesthetic action on some animals, cyclopropane was tried with bean roots and found to be about as effective as argon or krypton. Cyclopropane, of course, has a very high lipid-water solubility ratio.

In the previously mentioned work by Hutchinson and Arena22) on the destruction of DNA in pneumococcus, cells irradiated in the presence of oxygen in saline, containing citrate, were shown to be more sensitive by a factor of 3 than in the anoxic wet state. While this factor is in excellent agreement with the experimental results on radiation inactivation of living cells in the aerobic state, the oxygen effect is somewhat surprising when tried to explain in terms of the transforming principle which was used as a test method in this investigation, since two investigators had previously reported the complete absence of an oxygen effect on the isolated transforming principle in dilute solution34, 43). On the other hand, an effect of oxygen on the radiation sensitivity of the transforming principle in the dry state has been reported, but the values would only account for one half of the effect observed when the transforming principle is irradiated in the intact cell. It seems quite possible that this is still another indication for the phenomonon observed with various enzymes and at different states of cell division, that the radiation sensitivity of a given biochemical entity can vary extensively depending upon its intracellular combination with other compounds.

3.3. TEMPERATURE EFFECTS

The use of low as well as elevated temperatures as a useful parameter in biochemical radiation research has not nearly received the attention than such other parameters as oxygen effect, LET, dose-rate, and chemical modifying agents. The original work in this field was largely prompted by practical considerations after it has been found that the radiosensitivity of spores was approximately the same in the frozen state than at room temperature, thus making it possible to reduce the effect on organic, structural components while the genetic effects still proceeded at about the same rate44). While appreciable changes in temperature above or below 37°C produces an abnormal habitat for any living cell, this does not mean that experiments in these regions are undesirable, particularly if it can be shown that the ratio of reaction rates of non-genetic and genetic material is of appreciably greater difference.

---

42) M. Ebert, S. Hornsey and A. Howard, Effect of Inert Gases on Oxygen Dependent Radiosensitivity, Nature **181** (1958) 613.

43) F. M. Defillipes and W. R. Guild, Irradiation of Solutions of Transforming DNA, Radiation Res. **11** (1959) 38.

44) W. Huber, A. Brasch and A. Waly, Effect of Processing Conditions on Foodstuffs Sterlized with High Intensity Electrons, Food Technol. **7** (1953) 109.

3.4. LOW TEMPERATURE

It is useful to remember that low temperature irradiation of biochemical systems in vivo or in vitro is bound to be effected to a considerable extent by the considerations that hold for solid aqueous systems[2]). While the LET remains the same as in liquid water the frozen water molecules are held relatively rigidly in a hydrogen bonded structure which precludes mass transfer of radicals but which may yet allow electron and excitation migration. Electron nuclear resonance measurements show the presence of fairly long lived trapped radicals which disappear rapidly on warming but *long before* melting[45]). This suggests either that hydrogen atoms are mobile or that they readily surrender electrons which can travel through a frozen lattice to react with radicals formed at other points and held there while the lattice structure is intact. Biologically important polymers are undoubtedly present in vivo in an arrangement that if anything is more closely related to the solid state than to an aqueous solution.

It has been shown by Magat[46]) that temperature plays a complex role. Increasing the temperature usually increases the rate of gas diffusion but at the same time also the rate of chain propagation and therefore of oxygen consumption. On the other hand, rates of radiation induced seissions also increase with temperature so that the total amounts of radicals or other intermediates is bound to be a complicated function of temperature. This being so, further experiments with biochemical compounds in the frozen state might well yield valuable results. The above mentioned rapid interaction of oxygen with radicals[30]) is such that it can well compete with the recombination reaction between two radicals even if only traces of oxygen are present. Low temperature experiments may therefore also shed new light on the efficiency of oxygen removal in dried or degased systems. The assumption that target reactions are solely operative once an aqueous dispersion of cells has been frozen, has undergone considerable adjustment. Experiments clearly indicate that indirect effects due to water take place in frozen cells. E-coli sensitivity to X-rays decreases by a factor of 3 between zero and — 22° C but still decreases by 17% at — 72° C and by 50% at — 196° C[32]). Wood and Taylor have shown that 9% of the total water content of yeast cells is still in the liquid state at — 72° C[47]). TP which is unusually susceptible to inactivations by indirect effects is protected by a factor of about 500 when irradiated in a frozen saline solution[48]). The addition of organic material such as yeast extract increases this resistivity in the frozen state even further. A similar increase in resistivity due to the presence of added organic material was noticed in the determination of the radiation sensitive volume of RNA of tobacco mosaic virus[49]). For several vegetative organisms it has been shown that the sensitivity in the frozen state is comparable to that of the dry organisms, suggesting that in this case the indirect effect has either been removed or very much reduced[50]).

For individual chemical compounds it has been demonstrated many times that indirect effects can be reduced sizeably by freezing[16, 51, 52]). That the elimination of the indirect effect is not complete is also quite evident. Often not enough attention has been given to doing the irradiation at low enough temperatures to assure solidification of the system throughout. Latarjet[48]) and co-workers have clearly demonstrated that freezing of aqueous solutions will protect the molecule totally from indirect effects only if it completely prevents the radicals formed in ice or in bound water from migrating to the molecule.

---

[45]) M. S. Matheson and B. Smaller, Paramagnetic Species Produced by Gamma Irradiation of Organic Compounds, J. Chem. Phys. **28** (1958) 1169.

[46]) M. Magat, Oxygen and Peroxide Effects in Organic Solids, Radiation Res. Supplement **1** (1959) 213.

[47]) T. H. Wood and A. L. Taylor, Dependence of X-ray Sensitivity of Yeast on Phase State and Anoxia, Radiation Res. 6 (1957) 611.

[48]) R. Latarjet, H. Ephrussi-Taylor and N. Rebeyrotte On the Target Site of a Transforming Factor based on X-Ray Inactivation, Radiation Res. Supplm. **1** (1959) 417.

[49]) A. Gierer and G. Schramm, Infectivity of Ribonucleic Acid from Tobacco Mosaic Virus, Nature **177** (1956) 702.

[50]) E. J. Lawton and W. D. Bellamy, Radiation Sterilization VIII, Problems in Using High-Voltage Electrons for Sterilization, Nucleonics **12**, No. 4 (1954) 54.

[51]) F. B. Traub, A. Brasch and W. Huber, The Effects of High-Intensity Electrons on Antibodies, J. Immunology **70** (1953) 366.

[52]) W. Huber, Cold Sterilization by Electron Beam as a Possible Tool for the Inactivation of the Virus of Homologous Serum Jaundice in Plasma, Annl. N.Y. Acad. Sc. **55** (1952) 536.

3.5. ELEVATED TEMPERATURES

Just as in the frozen state, elevated temperatures as a parameter are intimately connected with the oxygen effect and with radical effects, regardless whether they occur indirectly or directly. Elevated temperature, by changing the oxygen quotient, tends to increase the anoxic state of the system while with radicals both transport and reactivity may be facilitated due to the higher state of thermal excitation of the system per se.

Based on an early observation by Svedberg and Brohult with hemoglobin, Pollard and his associates[11]) in a series of papers were able to confirm and expand the rather surprising observation that temperature and particularly elevated temperature had a pronounced effect on irradiation sensitivity of dry materials in high vacuum. This temperature effect is uniformly observed at levels which are appreciably below the temperature where the heat inactivation rate becomes appreciable for the system in question. The enzymes invertase and catlase were found to be in excess of 50% more sensitive when irradiated at about 60° C, and this temperature dependence was found for electrons, deuterons, as well as alpha particles, and therefore seems to be associated with ionizing radiation in general. At temperatures above 90° C both enzymes show a cross section which is well above that of the molecule, which simply indicates that at this temperature an ionizing event *outside* of the molecule is already sufficient for inactivation.

No adequate theory has yet been offered to explain the temperature effects of ionizing radiation. The increased resistance at low temperature could qualitatively be explained by the decrease in bond lengths. Accelerated effects at elevated temperatures could be explainable on the assumption of some hypothetical energy transfer mechanism which is very temperature dependant.

Reports on the sensitivity of microorganisms treated with ionizing radiations while at elevated temperature are somewhat conflicting. In view of the pronounced heat sensitivity of most vegatative organisms per se, much of the work here has been done with spores. Edwards and associates[53]) claim that exposure of B. subtilis spores at elevated temperatures resulted in a decreased inactivation while Powers and associates[54]) working with Bacillus megaterium found an increasing radiation sensitivity between — 145° C to plus 35° C, while above 35° C the radiation sensitivity dropped and reached a minimum at about 80° C. Increased sensitivity to X-rays has been claimed for T-1 phage[55]).

However, it has been amply demonstrated that bacterial spores are more easily inactivated by heating *after* prior treatment with ionizing radiation[56]). It has been found that the F_0 for C botulinum spores can be reduced as much as four-fold by irradiation with X-rays or electrons, with doses varying between 200 000 and 500 000 rad. It is interesting to note that according to some literature references the same effect is observed following pretreatment with ultraviolet and even with visible light provided the latter is activated by a photosensitive dye[57]). This may represent an indication that effects on the secondary structure of complicated molecules such as proteins can be brought about by photochemical events appreciably below the 10 eV of a primary ionizing event.

---

[53]) R. B. Edwards, L. J. Peterson and D. G. Cummings, The Effect of Cathode Rays on Bacteria. Food Technol. **8** (1954), 284.

[54]) E. L. Powers, R. B. Webb and C. F. Ehret, Modification of Sensitivity to Radiation in Single Cells by Physical Means, In Progress in Nuclear Energy, Series VI, Vol **2** 189, J. C. Bugher, J. Coursaget and J. F. Loutit, Eds. (Pergamon Press, New York, 1959).

[55]) C. S. Bachofer, C. F. Ehret, S. Mayer and E. L. Powers, The Influence of Temperature upon the Inactivation of a Bacterial Virus by X-rays, Proc. Natl. Acad. Sci. U.S. **39** (1953) 744.

[56]) L. L. Kempe, Complementary Effects of Heat and Radiation on Food Microorganisms, Nucleonics **18**, No. 4 (2960) 108.

[57]) A. C. Giese and E. B. Crossman, Sensitization of Cells to Heat by Ultraviolet and Visible Light, J. Gen. Physiol. **19** (1946) 79, 193.

Fricke and associates[58]) have paid considerable attention to the degradation of irradiated proteins by heat treatment subsequent to the irradiation. This is based on the observation that injured configurations can be detected with subsequent heating because such structures are changed more easily to the denatured form than native protein. The serological activity of irradiated albumin was used as an indicator, with heating subsequent to the irradiation ranging from 25 to 68°C. The authors conclude that the observed changes essentially represent structural breakdown with unfolding of the peptide chain leading to disturbances in the spatial relationships of the specific combining groups. This is in keeping with the observations by Alexander and co-workers[39]) on the irradiation of proteins in the solid state, and the effect may initially have been a breakdown of hydrogen bonds as theoretically predicted by Platzman and Frank[4]).

In a recent paper Webb, Powers and Ehret[59]) attempt to explain the previously observed, decreased radiation sensitivity of bacillus megaterium spores above 35°C to be caused by anealment of long-lived X-ray induced states which damage the spores irreversibly when oxygen is present while the damage can be restored subsequent to anaerobic irradiation by heating at 90°C for 8 minutes. The authors coin the word "thermorestoration" for this phenomenon and find that in general it proceeds in a simple exponential fashion with time at any given temperature with an apparent energy of activation of about 16000 calories. Interestingly enough, they report also that the dry spore system can be partially restored by an exposure to nitric oxide after irradiation. The restoration period for nitric oxide can be extended for as long as two hours after irradiation provided anaerobic conditions are maintained. The application of heat subsequent to nitric oxide treatment did not cause an additional restoration. The results with nitric oxide are somewhat puzzling in view of the extensive data by Howard-Flanders[12]) on the interchangeability of nitric oxide and oxygen.

3.6. CHEMICAL MODIFIERS

The proof that extremely small amounts of certain chemcials when present during the irradiation can provide a significant measure of protection upon the test object is not much more than ten years old. The subject matter has recently been reviewed in an exemplary manner by Eldjarn and Pihl[60]) and it is recommended that this review be consulted for information on this field from its inception until the end of 1958.

The great mass of compounds investigated for their potential protective effect can be divided roughly as follows: (1) the sulfur compounds, particularly the sulfyhydryl compounds such as cysteine, cysteamine and the isothiouronium derivatives; (2) the amines, especially epinephrine and histamine, as well as a host of similar compounds of which many have a central nervous effect; (3) miscellaneous products which are chemically often completely unrelated to each other and which range all the way from sex hormones through carbohydrates such as fructose, to simple inorganic compounds, such as sodium cyanide.

It has been pointed out that the compounds of the amine type most probably are active by virtue of the fact that they are outoxidizable and thus can be quite efficient producers of anoxia. Hence their effect is simply the elimination or reduction of the oxygen effect. The compounds in class 3 in all probability, exert their effects primarily on the basis of radical scavenging and it can be shown that they are the more active the more pronounced the indirect effects are in any given system. Another reason for not classifying them as true chemical modifiers is the fact that in order to produce activity they have to be used generally in concentrations manifold those of the sulfhydryl compounds.

---

[58]) C. A. Leone, W. Landmann and H. Fricke, Structural Degradation of Gamma-Irradiated Ovalbumin, In Progress in Nuclear Energy, Series VI, Vol 2, 124, J. C. Bugher, J. Coursaget and J. F. Lutit, Eds. (Pergamon Press, New York, 1959).

[59]) R. B. Webb, E. L. Powers and C. F. Ehret, Thermorestoration of Radiation Damage in Dry Bacterial Spores, Radiation Res. **12** (1960) 682.

[60]) L. Eldjarn and A. Pihl, Mechanism of Protective and Sensitising Action; In Mechanisms in Radiology, Vol. **2**, 231, M. Errera and A. Forssberg, Eds. (Academic Press, New York, 1960).

Of the sulfhydryl type compounds cysteine, cysteamine (MEA) 2-aminoethylisothiouronium (AET), gluthathione and sodium hydrosulfite have all been found to be effective both in vivo and in vitro, in concentrations which are often as low as 0.1% calculated on the system to be protected. Electron spin resonance techniques[61, 62]) as well as precise chemical analysis have provided impressive evidence during the last few years that the "sulfhydryl" chemicals may protect against the action of ionizing radiation by becoming temporarily bonded to the target molecule so that the unpaired electron can be passed on. The unique position of these compounds is thus provided by the fact that they are protectors for the direct mechanism of irradiation.

Gordy and Miyagawa[63]) have recently reported a series of elegant experiments in which they dissolved small quantities of sulfhydryl compounds into zein, keratin, blood fibroin, ovalbumin, pepsin and liver prior to irradiation with doses ranging from 1 to 5 Mrad from a cobalt-60 source. Irradiations were carried out after thorough evacuation of the samples and the effects measured by determining electron spin resonance generally at 9000 Mc per second (X-band). The protectors were found to alter very markedly the form of the electron spin resonance, produced by the ionizing radiation in the protein. The results indicate that an electron hole can migrate through certain segments of the polypeptide chain of proteins to sites where the sulphur protectors form complexes with the proteins. The protecting effect of sulfhydryl compounds is also noticeable in the presence of air although the picture is much less clear cut. It appears that the oxygen effect is the more powerful agent in competition and therefore more pronounced, particularly since the change is brought about by it in protein appears to be irreversible. The protective effect, if any, in the presence of oxygen may be due to the fact that oxygen attack which damages the protein-cysteine complex may be of such nature that the damage may later be removed by metobalic processes leaving the protein itself intact.

Eldjarn and Pihl[60]) have obtained chemical evidence that cysteamine protects by forming a mixed disulfide linkage with the SH or SS groups of the protein. In addition, they point out that the ability of MEA to capture radiation induced free radicals in a biological medium is too low to explain its protective ability solely in terms of an indirect effect and they too emphasize that the available evidence indicates that the sulfur-containing agents are primarily active by the reduction of the immediate biological alteration (target effect) caused by the radiation. This is in keeping with the findings that oxidized glutathione, acetylglutathione, and cystamine are all void of protective action. Hence, an intact SH group seems a prerequisite for protection.

Braams[64]) has demonstrated that cysteine and glutathione are able to protect invertase, papain and urease in part, when irradiated in the dry form and in vacuum (0.0001 mm Hg) with neutrons, alpha particles or protons. The protective effect obtained at 0.1% concentration amounted to 50 to 100%. Invertase, papain and urease being SH enzymes, in the non-protected state might be more prone to give up an electron for migration through their free SH groups, thus causing irreversible damage in the molecule and thus in the activity of the enzyme. The blocking of the free SH-group by attachment of cysteine could thus provide a better chance for retention of activity.

The observation by Hutchinson and Arena[22]) that the addition of 1% cysteamine to pneumococcus cells reduced the radiation sensitivity against electrons from the wet aerobic state to

---

[61]) K. G. Zimmer, Evidence for Free Radical Production in Living Cells Exposed to Ionizing Radiation, Radiation Res. Supplm. **1** (1959) 519.

[62]) W. Gordy, Electron Spin Resonance of Free Radicals In Irradiated Biochemicals, Radiation Res. Supplm. **1** (1959) 491.

[63]) W. Gordy and I. Miyagawa, Electron Spin Resonance Studies of Mechanisms for Chemical Protection from Ionizing Radiation, Radiation Res. **12** (1960) 211.

[64]) R. Braams, Changes in the Radiation Sensitivity of Some Enzymes and the Possibility of Protection against the Direct Action of Ionizing Particles, Radiation Res. **12** (1960) 113.

that of the wet anoxic state is remarkable in the sense that the experiment was carried out in the presence of oxygen.

Recent work by Kunkel and Schubert[65]) has demonstrated that protective action of cysteine can also be operative when applied *after* irradiation provided that the initial state of radiation damage remained latent so that the protector could arrive at the site of injury in time to alter the damage. The authors demonstrated that this is so by a series of elegant experiments with hibernating dormice, dried beans, and bull sperm. The results indicate that there seems to be an unstable state in the cell immediately connected with the primary physical radiation event, which can be maintained over considerable periods of time under special circumstances such as reduced metabolism and low temperature and therefore can still be influenced with protectors at a later date. Under ordinary circumstances this latent phase must be of very short duration as shown by the previously mentioned experiments of Howard-Flanders and Moore[40]) on the oxygen effect. Chemical protectors also apparently show a decided difference in their protective effect on DNA, depending upon the stage of the synthesis that is influenced. The protective effect is much more pronounced in the presynthetic period and it seems that once a final template stage of DNA synthesis is in progress, much larger doses are required to reduce incorporation and it is much more difficult to show a clearly protective action of sulfhydryl compounds[66]).

In summary, it is evident that it is the sum total of a number of parameters which is involved in bringing about the primary biochemical radiation event as well as in determining the passway of what happens thereafter. It seems likely that the first action of irradiation is to form a radical at some point in some essential molecule M. The inactivation of this radical which most probably is associated with a carbon atom, will result if a second radical reacts at this point. The second radical may be oxygen or it may also be radiation induced. Since the unaltered retention of M is essential to normal function of the cell its irreparable impairment will bring about a non-physiological effect. In microorganisms this may be cell death and may result from a single ionization if oxygen is present or from a small number of ionizations acting together, in the anoxic state. The situation in higher cells and in dry materials is more complex as it appears that the inactivation of more than one nearby site within a structure is needed for effect. This is clearly shown by the many in vivo and in vitro studies on enzymes, antigens, nucleic acids, nucleoproteins, etc., which all demonstrate that it requires more than one ionization occuring *simultaneously* to remove the biological activity. The in vivo radiation effect is undoubtedly closely dependant on the combination of essential elements to specific substrates as shown by dividing cells (preprophase arrest), DNA-cell substrate combination, and the "hidden" radiation effects in enzymes[67, 68]).

In the evaluation of radiation effects it is well to remember that metabolic processes are very fast. For instance, it has been shown that labeled valine is removed from rat liver practically immediately and appears in the Ferritin molecule which has a molecular weight of about 400 000, in about two minutes. Assembly of secondary structures such as coiling disulfide and hydrogen bond formation, etc., appears to take a little longer, but even these rate determining stages are fast enough so that the whole process is being completed within a few minutes.

Looking at recent data on the mechanical composition of cells one cannot fail to be impressed by the high degree of order and structural integrity. Hence one might ask whether in the explanation of biological radiation effects

[65]) H. A. Kunkel and G. Schubert, The Influence of Total Body Irradiation on DNA Synthesis and the Protective Action of Cysteine, Radiation Res. 9 (1958) 141.

[66]) U. Hagen, Radiosensitivity of DNA Synthesis in Regenerating Liver; Modification by Protective Substances, Radiation Res. **9** (1958) 125.

[67]) L. Augenstine, Structural Correlation Between Esterase and Protease Activities of Trypsin, Science **129** (1959) 718.

[68]) L. A. Mounter, Studies on the Effects of Radiation on Enzymes I. Inactivation of Chymotrypsin and Chymotripsinogen by X-rays, Radiation Res. 12 (1960) 487.

[69]) K. Folkers, Vitamins, Perspectives and Prospectives, Perkin Medal Lecture, Chem. and Ind. (1960) 946.

we haven't been swayed somewhat too much by the impression that the systems essential for metabolism, respiration and cell division are more or less in solution or at best in form of a heavy suspension within their respective enclosures be it the cell wall itself or the membranes of mitochondria and nuclei. Considerations of solid state physics such as semi-conductor phenomena might well be applied usefully for the explanation of what happens in a biological system directly subsequent to the primary radiation event. Ionizing radiation is known to lead essentially to a production of impurities in solids thus changing their conductance qualities [70]. It seems not too far fetched to treat proteins and protein-lipid interphases in terms of semi-conductors which might become sensitive to changes in carrier concentration brought about by irradiation events. The sharp increase in resistivity of germanium when bombarded with electrons is a case in point.

Limit of time and the endeavor to present a coherent story have made it necessary to often abandon comprehensiveness and omit the mention of many interesting and exciting ideas, even at the risk that the experts among you may find my selection arbitrary, partial and personal.

---

[70]) R. Smoluchowski, Radiation Effects in Solids. Radiation Res. Supplem. **1** (1959) 26.

NUCLEAR INSTRUMENTS AND METHODS **11** (1961) 227–237; NORTH-HOLLAND PUBLISHING CO.

THE DEVELOPMENT OF RADIATION PROCESS APPLICATIONS

S. H. PINNER

BX Plastics Ltd., Lawford Place, Essex

and

W. H. T. DAVISON

T.I. Research Laboratories, Hinxton Hall, Cambridge

The patent literature provides a measure of applications for radiation processes. At present, there are well over 200 U.K. and U.S. patents, which can be classified into a. polymerisation, b. crosslinking of polymers, c. degradation of polymers, d. multicomponent polymers (graft and block copolymers), e. general chemical reactions and petroleum products, f. sterilisation, g. specific articles and shapes, h. uses for irradiated polymers, i. inorganic compounds, j. machines for generating radiation (including isotopes). Processes involving polymers account for more than 75% of these patents, so it can be fairly claimed that the major application of radiation will lie in the polymer field. The first polymerisation patent was granted in 1927 and the first crosslinking patent in 1933 but the first patent on multicomponent polymers was only granted in 1958 and this is the topic selected for detailed consideration in this paper.

The development of multicomponent polymers can be classified into a. direct grafting, b. indirect grafting, c. peroxidation grafting, d. block copolymers and e. attenuated network polymers. These methods are outlined and exemplified, by reference to continuous process techniques.

More recently, the application of radiation processes to polyvinyl chloride has attracted interest. This can be converted into infusible and insoluble rigid sheet with potential use as a solvent-resistant and corrosion-resistant structural material, by incorporating a plasticiser containing two or more olefinic double bonds and subjecting to radiation. The plasticiser is caused to polymerise and form a network which is attentuated by the polyvinyl chloride molecular chains.

The drawback to this material is its brittleness but recent work has shown this can be overcome by incorporating a small amount of a saturated elastomer. By inference, well-crosslinked materials are not necessarily brittle and this widens the scope for attenuated network copolymers in industrial applications.

1. Introduction

Over the years, there have been numerous assessments of the potentialities of ionising radiation in chemical technology. Based mainly on information released by public service or state-supported laboratories, these have tended to be somewhat speculative. Many radiation reactions were under close examination in industrial laboratories during this period but details were being withheld on security grounds. This situation has been transformed by the spate of patents during the past two years, and it is now possible to verify earlier claims of radiation process applications by reference to the patent literature. It would be imprudent in arguing a scientific case to rely entirely on the patent literature, since many patents contain insupportable claims and, as the cynic would say, many are designed to conceal rather than reveal information. Appraisal of the patent literature does however permit one to delineate the main fields of interest in industrial laboratories and it is relatively easy for those skilled in the art to discriminate between sound and unsound patent claims.

At the present time, there are well over 200 U.K. or U.S. patents, as shown classified by company in table 1. The number of separate processes is not as high as this as it is common to file the same process in a number of countries. For this reason it has not been considered important to review patents in other countries. Analysis of the subject matter of the U.K. and U.S. patents of table 1 suggested a breakdown into 10 categories, of which 6 categories deal strictly with polymers and 3 further categories deal with polymers in a borderline sense. The classification of patents in this way is shown in table 2.

TABLE 1

Classification of radiation patents by company

	UK patents	US patents	Total
General Electric Co.	23	17	40
Esso Research and Eng. Co.	15	7	22
High Voltage Eng. Co.	1	14	15
U.K. Atomic Energy Authority	14	1	15
Electronised Chem. Corp.	4	9	13
E.I. du Pont	11	1	12
Monsanto	11	0	11
British Insulated Callenders Cables	9	0	9
T.I. (Group Services)	7	0	7
Dow Chemical Co.	5	0	5
Others	34	20	54
Totals	134	69	203

TABLE 2

Classification of radiation patents by subject

	UK patents	US patents	Total
Polymerisation and copolymerisation	24	3	27
Crosslinking of polymers	33	16	49
Degradation of polymers	7	2	9
Multicomponent polymers (graft and block copolymers)	22	4	26
Specific articles and shapes (including dose control)	16	5	21
Uses for irradiated polymers	6	1	7
General organic reactions (including petroleum products)	16	12	28
Sterilisation	1	7	8
Machines for generating radiation (including isotopes)	6	18	24
Inorganic compounds	3	1	4

It may be asked why polymers figure so prominently in radiation process applications, and the reason lies in the simple formula expressing approximately the weight of material changed for a given dose,

$$w = 10^{-6}\,GMr$$

where w is the weight fraction of material of molecular weight M changed by a dose of r Mrad. In the polymer field, one has access both to high molecular weights in crosslinking processes and to high G values in chain reaction polymerisations, so that substantial amounts of material can be changed by relatively low doses of radiation. In grafting processes and the synthesis of multicomponent polymers, high values of M and G are available simultaneously making these processes still more economical of radiation. Although the cost of radiation has progressively decreased during recent years due to the introduction of more powerful electron accelerators, it is only natural that attention should have been given to processes requiring, say, less than 20 Mrads to give the desired products, and it turns out that over 75% of all radiation patents are concerned with polymer technology.

The proposed application of radiation in the polymer field is not solely of recent date. Indeed, considering that isotope sources and electron accelerators have only become freely available during the last decade, it is surprising to find patents dating back to the "pre atomic era". Perhaps we overlook the fact that radio-active emanations and X rays were discovered in the nineteenth century. The earliest U.K. patent was granted to H. Plauson in 1927 and is concerned with the polymerisation of impure ethylene and acetylene to liquid hydrocarbons1). Doubtless at that time, he would have been hard put to provide the necessary sources of radiation in sufficient amount and at an economic price!

An early interest was shown by I.C.I. in the radiochemical polymerisation of ethylene2). Much work on this topic3) was subsequently carried out by Dr. Roberts at Monsanto Chemicals Ltd. using facilities available at Harwell. This process was of considerable potential interest at the time. By avoidance of a thermal catalyst, the reaction could be conducted at moderate temperatures which reduced the

---

1) H. Plauson, U.K. Patent 309002 (1927).

2) I.C.I., U.K. Patent 714843 (1954).

3) Monsanto Chemicals, U.K. Patents 768666–70; 777847, 778225, 781035, 781421 (1957).

frequency of chain transfer and branching and enabled the formation of a more linear polythene with greater crystallinity. The yield was quite low unless the process was operated at substantial pressures. This itself was no obstacle because γ rays can penetrate autoclaves or high pressure lines, but it implied that the cost would not be substantially lower than the conventional high pressure method and the remaining advantage of a more linear polythene disappeared when the ionic polymerisation of ethylene was discovered and furthermore when free-radical catalysts for the high pressure process active at lower temperatures were discovered by I.C.I.

During the period 1950–5, a thorough study of radiochemical polymerisation was made principally by the French school headed by Magat and Chapiro[4]). This established the generality and theoretical principles of these reactions and had its industrial counterpart in patents issued to General Electric[5]), Esso Research and Engineering[6]) and other companies[7]). One drawback to the commercial exploitation of these processes was the limited availability of isotope sources. Because of the dependence of the rate of free-radical polymerisation on the radiation intensity, low intensity sources were favoured for giving the highest yield per unit dose. On this basis, high intensity electron sources, such as Van de Graaff accelerators or resonant transformers, though capable of providing the necessary output, were less efficient. This dependence of rate on the intensity of radiation does not apply to ionic polymerisations, as typified by the case of isobutene, which can be polymerised at a rate which is directly proportional to the average intensity[8]). Accordingly, the conversion per unit dose is independent of intensity, as shown in fig. 1. Unhappily, the yield falls off with increasing dose due to the simultaneous production by the radiation of an inhibitor, such that it is not possible to proceed to complete conversion except in the presence of an inorganic solid such as zinc oxide or glass powder[9]).

The finding that radiation could initiate polymerisation at very low temperatures has revived interest in low temperature polymerisation for producing stereospecific polymers from branched alkyl acrylates, for example, or obtaining unbranched polymers as in the case of polyvinyl chloride. Radiation is unique in its ability to initiate solid state polymerisation either at normal[10]) or at very low temperatures[11]) and this has important theoretical connotations but apart from the polymerisation of solid hexamethyl trisiloxanes[12]), there is little prospect of commercial application.

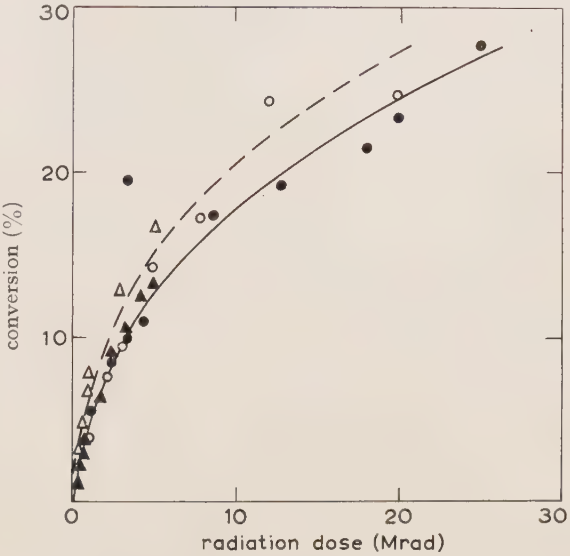

Fig. 1. Conversion of *iso*butene by irradiation at — 78.5°C. ○, △, – – – electron irradiation; ●, ▲, — γ-rays (^{60}Co).

In the field of polymer crosslinking, the first patent extant is that granted to B. F. Goodrich in 1933. This related to the vulcanisation of rubber, preferably in the absence of air, using 250 keV electrons from a cathode ray tube[13]). This patent had expired before Charlesby published his pioneering theoretical studies on polymer crosslinking: nevertheless, the application of radiation to the curing of rubber has resisted attempts to evolve sensitisers and special formulations[13a]) and has remained industrially elusive.

---

[4]) A, Chapiro, Ind. Plastiques Modernes **8** (Nov. 1956) 67; J. Chim. Phys **47** (1950) 747.

[5]) General Electric, U.K. Patent 762953 (1956).

[6]) Esso Research & Engineering, U.S. Patents 2803598–9, (1957), U.K. Patents 784624, 785507, 785611 (1957), 793575, 802082 (1958).

[7]) Allied Chemical & Dye Corp., U.K. Patent 783933 (1957); Centre National de la Recherche Scientifique, U.K. Patent 815305 (1959); Saint Gobain, U.K. Patent 830515 (1959).

[8]) W. H. T. Davison, S. H. Pinner and R. Worrall, Proc. Roy. Soc. A **252** (1959) 187.

[9]) A. Charlesby, S. H. Pinner and R. Worrall, Proc. Roy. Soc. (In press);

R. Worrall and S. H. Pinner, J. Poly. Sci. **34** (1959) 229.

[10]) A. J. Restaino *et al.*, J. Amer. Chem. Soc. **78** (1956) 2939;

H. Morawetz and T. A. Fadner, Die Makromol. Chemie **34** (1959) 162.

[11]) H. Sobue and Y. Tabata, J. Poly. Sci. **43** (1960) 459.

[12]) General Electric, U.K. Patent 810684 (1959).

Much work has been carried out during the past decade on the crosslinking of polythene[14]). This differs significantly from the curing of rubber inasmuch as polythene is a saturated polymer. Prior to the discovery of the radiation crosslinking of polythene, it had been deemed necessary to incorporate olefinic bonds or other reactive groupings into a polymer chain to provide sites for crosslinking and crosslinked saturated hydrocarbon polymers were not known. Uses were naturally found for these new structures and a large proportion of the patents on the crosslinking of polymers and the uses for irradiated polymers are concerned with irradiated polythene. It is now possible to produce crosslinked polythene via peroxide catalysts[15]) or by ultra violet irradiation in the presence of sensitisers[16]) but it remains true that the crosslinking of a saturated polyhydrocarbon was first realised by high energy radiation.

Radiation crosslinking has of course been extended to other elastomers and to other saturated polymers such as silicones, polyamides and poly (alkyl acrylates) and industrial progress may be expected with these as and when radiation costs are reduced to economic and competitive levels. In general, the crosslinking of polymers requires doses in the range of 5–50 Mrads.

Lower dose requirements serve for grafting reactions and for the production of multicomponent polymers. This is a more up-to-date process. Whereas the first polymerisation patent was granted in 1927 and the first crosslinking patent in 1933, the first patent on grafting was only granted in 1958. Because of topical interest, the remainder of this paper will be confined to this process.

2. Multicomponent Polymers

The term "multicomponent polymers" relates to structures in which different polymer chains are combined or connected. It covers graft copolymers, block copolymers and attenuated network polymers, all of which can readily be made through the use of high energy radiation. Five variations of the synthesis of multicomponent polymers can be discerned from the literature.

2.1. DIRECT GRAFTING

As the name implies, this process involves the direct irradiation of the polymer while in solution or while swollen or otherwise in intimate contact with the monomer[16a]). This promotes long branch chain growth. However, direct radiation initiation of the monomer may also occur, so the graft copolymer is usually contaminated with homopolymer, which may have to be removed by selective solvent extraction. In many cases however, especially when using high intensity radiation, such as electrons from a Van de Graaff accelerator, the amount of homopolymer formed is not serious[17]). This process also covers the direct irradiation of polymers in the presence of a non-polymerisable organic compound. Although the *G* value for such reactions is quite low, it may be possible nevertheless to obtain a useful modification to the surfaces of polymer films or fibres, especially when the organic modifier bears selected functional groupings and has a moderately high molecular weight[18]).

---

[13]) B. F. Goodrich Co., U.S. Patent 1906402 (1933).

[13a]) S. H. Pinner, Int. J. Appl. Radiation & Isotopes **5** (1959) 121;
G. Lamm, A. Lamm and H. Madelaine, Rev. Gen. Caoutchouc **36** (12) (1959) 1877.

[14]) U.K. Atomic Energy Authority, U.K. Patents 732047, 739709, 740899 (1955);
General Electric, U.K. Patents 773529, 774161, 784037 785505 (1957).

[15]) Godfrey L. Cabot, U.K. Patent 843617 (1960).

[16]) G. Oster, U.K. Patent 848414 (1960).

[16a]) CNRS, U.K. Patent 801528 (1959); Du Pont, U.K. Patent 820120 (1959).

[17]) A. Charlesby and S. H. Pinner, Ind. Plastiques Modernes **9** (Nov 1957) 43.

[18]) Du Pont, U.K. Patents 820120 (1959), 834557, 838412 (1960).

2.2. PRE-IRRADIATION GRAFTING

Designed to avoid homopolymer formation entirely, this process involves irradiation of the pure polymer in an inert atmosphere such as nitrogen or in vacuo. Bond fracture occurs and the resultant free-radicals remain trapped in the solid polymer. The irradiated polymer is immediately contacted with pure monomer, which swells the polymer, confers radical mobility and undergoes chain polymerisation[19]). Since the monomer is never exposed to radiation, the yield of homopolymer, theoretically, is zero. Some homopolymer could arise by chain transfer however and the yield of deposited polymer is often very low in this process due to the low concentration of trapped free radicals. In highly crystalline polymers, such as high density polythene, the trapped radical concentration and life-time may be greatly increased and good yields of grafted products have been obtained with this process[20]).

2.3. PEROXIDATION GRAFTING

This is another indirect grafting process differing from pre-irradiation grafting insofar as the irradiation of the pure polymer is conducted in an atmosphere containing oxygen[20a]) or in the presence of a fluid capable of releasing oxygen under irradiation[21]). Polymer free-radicals are again considered to result from bond-fracture but these mainly react with oxygen to form peroxy-radicals or peroxide or hydroperoxide groups and the reactive sites are thereby stabilised. The product can be stored for prolonged periods without undue deterioration but if then heated in monomer, the peroxide or hydroperoxide groups cleave thermally and act as polymerisation initiators. Although the process is designed to eliminate homopolymer, this is still formed in small amounts presumably because hydroperoxide groups may yield not only polymeric oxide radicals but also hydroxide radicals which can lead to non-grafted polymer chains. Recently it has been found possible to increase substantially the yield of graft at room temperature and also to reduce the proportion of homopolymer by adding to the monomer a redox agent such as ferrous acetyl acetonate or a polymeric imine[22]).

2.4. BLOCK COPOLYMERS

Both block copolymers and graft copolymers are long-sequence non-random copolymers, but whereas a "graft copolymer" implies a branched molecule with a distinct unbroken main "trunk", the term "block copolymer" connotes a consecutive arrangement of the sequences in an essentially unbranched chain. This structure would be expected on the irradiation of a mixture of two polymers each suffering main chain fracture. From the process standpoint, this differs from those mentioned above in that the radiation is applied to an intimate mixture of polymers either in solution in a mutual solvent[23]) or as a mechanical blend[23, 23a]) or where one of the polymers is applied to the other as a coating[24]). This process is less economical of radiation than grafting processes, the required dose range being comparable with that for polymer crosslinking.

2.5. ATTENUATED NETWORK COPOLYMERS

In terms of process, the formation of attenuated network copolymers closely resembles direct grafting. These structures arise during the radiation polymerisation of poly-functional monomers in the presence of a compatible polymer, which becomes involved in the resultant network. This is exemplified by the polymerisation of di-allyl or tri-allyl esters in the presence of polyvinyl chloride[25]). By virtue of the short propagation chain length in allyl polymerisation and the high chain transfer efficiency, the

[19]) Du Pont, U.K. Patent 801531 (1958); Union Carbide, U.K. Patent 823462 (1959).

[20]) Y. Shinohare and K. Tomioka, J. Poly. Sci. **44** (1960) 195.

[20a]) CNRS, U.K. Patent 809838 (1959).

[21]) Du Pont, U.K. Patent 809558 (1959).

[22]) L. Minnema, J. F. A. Hazenberg, L. Callaghan and S. H. Pinner, J. Appl. Poly. Sci. (In press).

[23]) T.I. (Group Services), U.K. Patent 805897 (1958).

[23a]) General Electric, U.S. Patent 2924559 (1960).

[24]) Du Pont, U.K. Patent 801479 (1958).

[25]) S. H. Pinner, Plastics (London) **25** (1960) 35;
S. H. Pinner and V. Wycherley, Symposium on Macromolecules, Wiesbaden, 1959, paper III, B. 9.

network becomes attenuated by the polyvinyl chloride chains. Crosslinked products with good resistance to heat and solvents thereby result and it is not necessary in this process for the polymer itself to be capable of radiation crosslinking. Even polymers which normally degrade on irradiation, such as cellulose acetate[26]) and polymethyl methacrylate[27]), can be converted into insoluble and infusible network polymers by this process. A diagrammatic representation of an attenuated network copolymer is given in fig. 2.

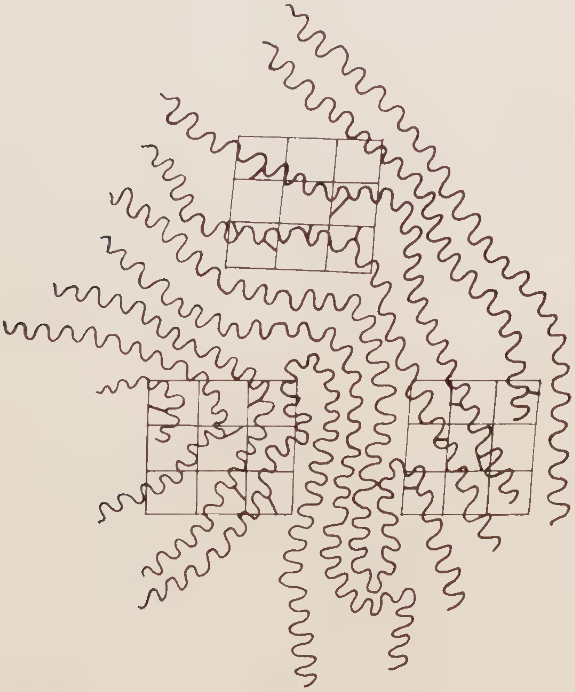

Fig. 2. Attenuated network copolymer.

3. Development of Radiation Processes

All the above techniques for the synthesis of multicomponent polymers have come under consideration in the authors' laboratories, particularly from the standpoint of designing economical continuous processes. This has entailed the solution of many problems not envisaged in the initial patents[16a, 20a]), which were exemplified by small scale batch experiments in glass apparatus. The direct grafting process can be illustrated by the irradiation of polytetrafluoroethylene films in the presence of vinyl acetate to render the surface receptive to adhesives. The apparatus shown in highly simplified form in fig. 3 could be used for this purpose. The P.T.F.E. film may be unwound from a roll and passed between the nip of a pair of rollers, of which the upper roller is a doublewalled cylinder, the annular space being fed with vinyl acetate from a storage vessel. The outer wall of this cylinder could be porous, such as of felt construction, so allowing vinyl acetate to permeate to the exterior of the roller and so impregnate one surface of the P.T.F.E. film as it passed through the nip. To prevent evaporation from the porous surface at other parts, the whole of the upper roller with the exception of the nip required enclosure with an impermeable sheath. The contact time was very short but this was not important in the present instance since P.T.F.E. does not swell in vinyl acetate nor in any other liquid. The film coated with monomer would then pass under a radiation source, then through a drying oven, then to winding up gear[28]). The radiation source preferentially is a low intensity, low voltage electron source, as P.T.F.E. suffers degradation on exposure to radiation and it is desirable to limit both the dose to below 0.5 Mrad and the penetration into the film to less than 0.002".

The pre-irradiation technique for the grafting of methyl methacrylate to polyvinyl chloride or of styrene to polythene film could be conducted continuously with the apparatus shown diagrammatically in fig. 4. The polymer film may be irradiated in nitrogen using high intensity electrons and on emergence from the radiation zone is caused to enter a tank of monomer and to festoon around a series of rollers wholly immersed in the monomer. The throughput speed should be such as to allow the requisite degree of swelling and grafting by the monomer and the gear train should be designed to allow slight tension on the film to be continuously exercised despite the change of dimensions consequent upon swelling. The film may be similarly festooned during passage through the forced draught drier and finally passed to the winding up gear.

---

[26]) S. H. Pinner, T. T. Greenwood and D. G. Lloyd, Nature **184** (1959) 1303.

[27]) S. H. Pinner and V. Wycherley, J. Appl. Poly. Sci. **3** (1960) 338.

[28]) T.I. (Group Services), U.K. Patent Appln. 26488/56.

The only modification to the apparatus of fig. 4 necessary for employment of the peroxidation technique is to allow oxygen to permeate the film during or after irradiation and before entering the bath of monomer. One arrangement utilising electrons would be to convey the polymer film round a sequence of rollers as shown in fig. 5. However, it is equally convenient to prepare peroxidised polymer film by storage in a cave where it is subjected to γ radiation from a cobalt source. Loose wrapping of the roll suffices for oxygen diffusion and replenishment of dissolved oxygen converted by the radiation into peroxide groups.

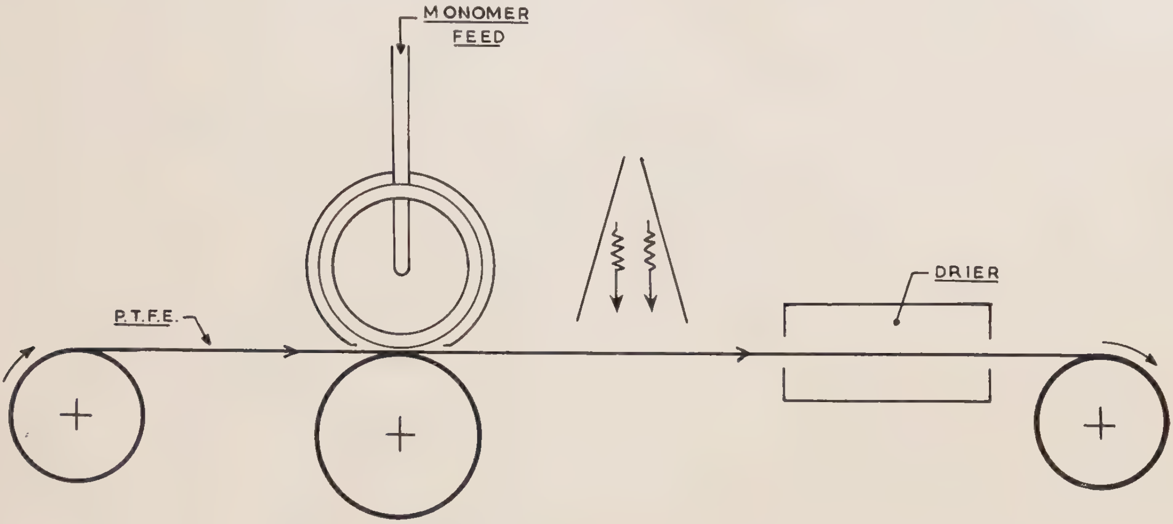

Fig. 3. Apparatus for continuous direct grafting.

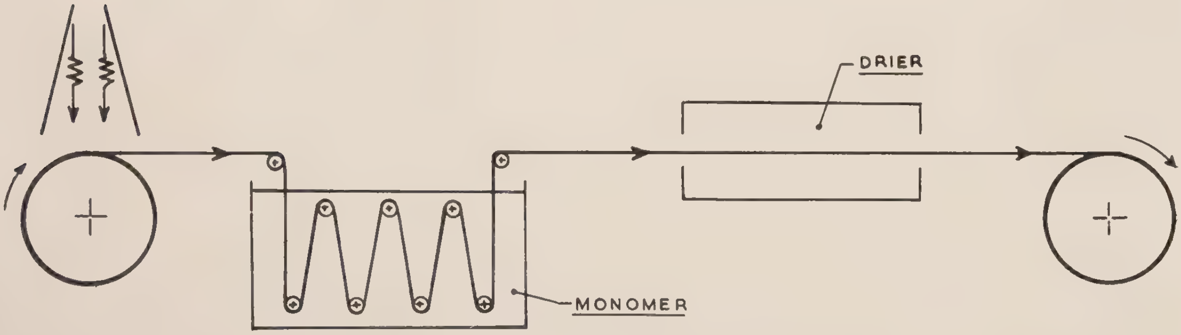

Fig. 4. Apparatus for continuous pre-irradiation grafting.

The synthesis of block copolymers by irradiation does not normally involve a chain polymerisation reaction and the apparatus requirements are accordingly less stringent. Any of the devices shown in figs. 3–5 may be used to deposit a surface layer of a polymer or of a non-volatile organic modifier upon the film or fabric and the coated web is then exposed to the radiation source. The mixture of polymers can also be prepared away from the radiation department and the problems of irradiation are solely those of controlling the amount and uniformity of the dose, just as in the case of polymer crosslinking[29]).

This is true also for the synthesis of attenuated network copolymers, provided the monomers employed are non-volatile and have a plasticising action on the polymer. These requirements are met, for example, with mixtures of polyvinyl chloride with di-allyl and tri-allyl esters[25]). In these instances, the main theme in development of the process is the constitution and composition of the polymer-monomer mixture and the nature and utilisation of the radiation source are of secondary importance.

---

[29]) General Electric, U.K. Patents 805818–9 (1958); British Insulated Callenders Cables, U.K. Patents 817033, 821669 (1959).

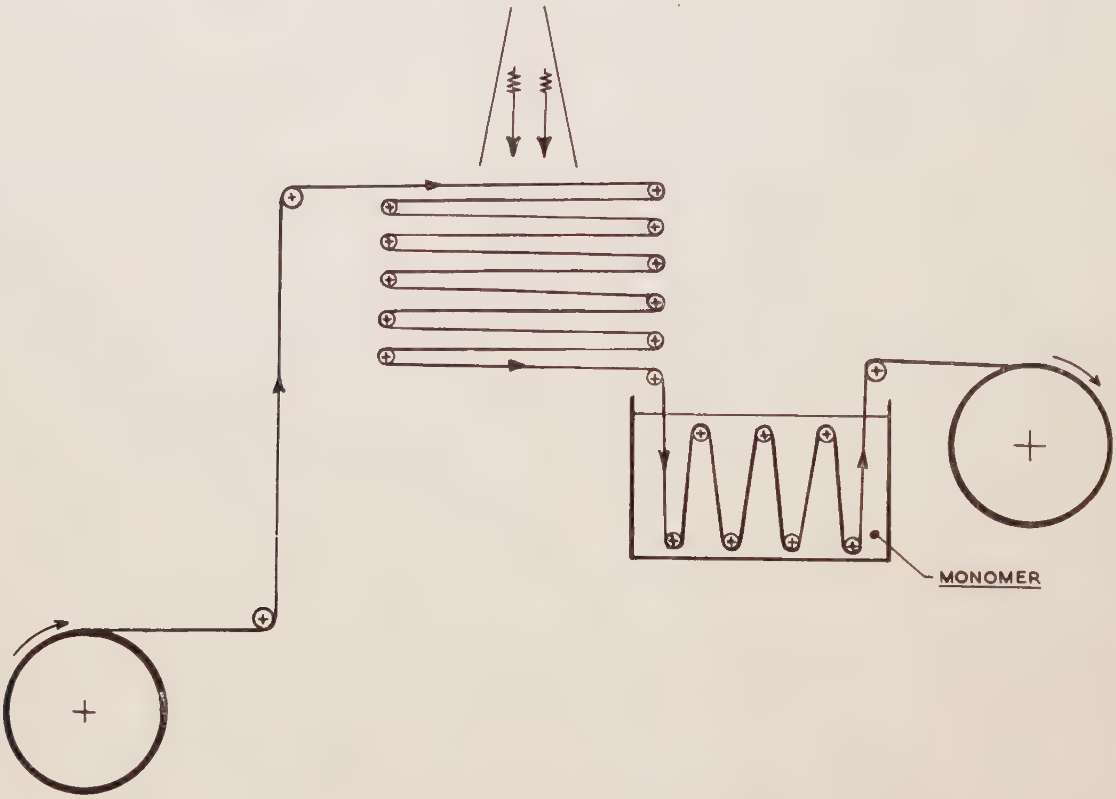

Fig. 5. Apparatus for continuous peroxidation grafting.

4. The Irradiation of Polyvinyl Chloride

Recently, the application of radiation processes to polyvinyl chloride has attracted interest. Early experience with this polymer was discouraging, inasmuch as relatively high doses of radiation were necessary to produce any useful degree of crosslinking and the polymer suffered dehydrochlorination and discoloration after mild radiation exposure[30]). This degradation is now considered to be due not to the immediate action of the radiation but to a slow dehydrochlorination chain reaction initiated by trapped free-radicals. By increasing the internal mobility of polyvinyl chloride, as by plasticisation, the radicals may disappear by mutual coupling and considerable doses of radiation can be absorbed without serious attendant discoloration. The same protective function is exercised by monomers[31,32]), allowing these to be grafted to polyvinyl chloride without deleterious side reactions.

It has been suggested that a mixture of p.v.c. with an aromatic monomer, such as styrene, and an unsaturated ester, such as dioctyl maleate, might serve for the production of articles with great resistance to radiation degradation[31]). In point of fact, the composition becomes rigid due to loss of the volatile styrene and to radiation induced polymerisation, and the mixtures

[30]) A. Chapiro, J. Chim. Phys. **53** (1956) 895.

[31]) U.S. Rubber, U.K. Patent 833610 (1960).

[32]) Dow Chemical Co., U.K. Patent 829512 (1960).

are more usefully regarded as raw materials for radiation grafting.

For this purpose, it is preferred to select a monomer which has a plasticising action on the polyvinyl chloride and which contains two or more double bonds per molecule. As indicated above, the use of non-volatile plasticising monomers avoids problems of "wet" irradiation and enables the polymer-monomer mixture to be worked up and shaped with normal processing equipment and stored till required. The irradiation process becomes a separate operation affording no more difficulty than the irradiation of pure polymers. By the use of appropriate monomers, the dose required for crosslinking can be reduced to the range 0.1–2 Mrad, which is much lower than that required for the crosslinking of pure polymers. One of the most radiation sensitive crosslinking monomers is ethylene glycol dimethacrylate[32]. This can be used alone or in combination with long chain methacrylates such as lauryl methacrylate. A composition containing 70% polyvinyl chloride and 30% ethylene glycol dimethacrylate, for example, can be rendered insoluble with a dose of 0.1 Mrad delivered by a Van de Graaff accelerator, which is remarkably low in view of the low efficiency of high intensity electrons in polymerisation reactions.

Ethylene glycol dimethacrylate is sensitive to thermal polymerisation as well as to radiation and this limits the storage life of compositions made with this monomer, unless inhibitors are incorporated. Allyl monomers, in contrast, are stable thermally and can be used to make plasticised compositions by hot milling. The radiation dose required to render insoluble is naturally increased but only to a moderate extent as shown in table 3. Continued irradiation leads to essentially hard and rigid compositions, the dose depending on the nature of the monomers used as shown in table 4.

The physical properties of irradiated compositions containing convertible monomers improve with the number of double bonds in the molecule, the distinction being brought out particularly by measurement of tensile strength at elevated temperatures[25].

TABLE 3
Crosslinking efficacy of various monomers in polyvinyl chloride[32]

Monomer	Dose to render insoluble mixture of 80 % p.v.c. and 20 % monomer (Mrad)
Ethylene glycol dimethacrylate	0.25
Allyl methacrylate	0.25
Glycerol trimethacrylate	1
Diallyl itaconate	0.5
Triallyl aconitate	3
Triallyl cyanurate	3
Diallyl maleate	3
Triallyl phosphate	3

The tensile strength of a composition containing 30 parts of dioctyl fumarate per hundred of p.v.c. and given 15 Mrad was 400 lbs/sq.in. measured at 100° but a composition containing triallyl cyanurate in place of dioctyl fumarate and given the same dose had a tensile strength at 100° of 3300 lbs/sq.in.

Accordingly, the grafting process allows the benefits of crosslinking to be extended to polyvinyl chloride, leading to infusible and insoluble rigid sheet with potential use as an acid-resistant and solvent-resistant structural material[25]. The drawback to this material is its brittleness but recent work has shown that this can be overcome by exploiting the "alloying" technique with rubbers, which has been so successful in creating tough materials from normally brittle thermoplastics[33]. The reason for the toughening action of rubbers on brittle resins is not clearly understood, but is associated with the arrest of crack propagation at the particle interfaces in a two-phase matrix. Such two phase structures can also be created in polyvinyl chloride attenuated network copolymers by the incorporation of selected elastomers in definite proportions. The improved notched impact strength of such compositions is evident from table 5, indicating that a highly crosslinked material is not necessarily brittle.

[33] N. E. Davenport *et al.*, Brit. Plastics **32** (1959) 549.

TABLE 4

Effect of radiation on p.v.c. compositions

Monomer	P.h.r.a)	Gel quality	Dose to render hard and tough
Diallyl sebacate	55	Flexible	Above 25 Mrad
Diallyl sebacate Triallyl cyanurate	25.5 25.5	Flexible	Above 25 Mrad
Triallyl cyanurate	67	Flexible	Above 25 Mrad
Polyoxyethylene dimethacrylate (M.G.I.)	55	Flexible	2 Mrad
M.G.I. Triallyl cyanurate	25.5 25.5	Flexible	4 Mrad
M.G.I. Vinyl toluene	25.5 25.5	Stiff	1 Mrad
M.G.I. Diallyl sebacate	25.5 25.5	Flexible	4 Mrad
Lauryl methacrylate	55	Flexible	10 Mrad
Divinyl benzene	110	Very soft	Above 10 Mrad

a) Parts by weight per 100 parts of p.v.c.

TABLE 5

Physical properties of rubber-modified crosslinked polyvinyl chloride

	Units	Viniplus Aa)		Viniplus Ba)		Normalb) p.v.c.
Dose	Mrad	10	15	10	15	0
Residual monomera)	%	15	11.8	14.3	11.2	0
Tensile strength	lb/sq.in	7000	8000	7000	7800	7600
Elongation	%	30	20	30	25	75
Stiffness modulus	lb/sq.in × 10^{-4}	35	38	34	37	41
Tensile strength at 160°	lb/sq.in	530	760	330	580	0
Impact strength notched	ft.lb/in. notch	0.44	0.33	0.50	0.36	0.20
Impact strength, drop-weight unnotched	ft.lb	5.7	1.45	7.1	3.6	12
Softening point	°C					
30° Deflection		70.5	133	85	131	74
45° Deflection		77.5	> 145	98.5	> 145	82

a) Samples initially contained A) 28.0% triallyl cyanurate and 4.7% elastomeric reinforcing agent and B) 26.8% triallyl cyanurate and 4.5% elastomer. The value for residual monomer is based on a spectroscopic measurement of the allyl absorption peak at 2.15–2.05 μ, and is expressed as % triallyl cyanurate. It does not follow that this triallyl cyanurate is present in unreacted form, as 33% removal of allyl bonds suffices theoretically to bind the hexafunctional monomer into the network.

b) Control sample containing no elastomer and no triallyl cyanurate.

In this review of the development of applications for radiation processes, especially in polymer technology, it has only been possible to touch briefly on some of the highlights and a more detailed study of the patent literature should be rewarding for those concerned with estimating the future potential for radioactive isotopes or radiation from electrical machines.

Acknowledgement

The authors thank the Managing Director of BX Plastics Ltd. and the Chairman of Tube Investments Ltd. for permission to publish.

NUCLEAR INSTRUMENTS AND METHODS **11** (1961) 238–247; NORTH-HOLLAND PUBLISHING CO.

NEUTRON, ELECTRON AND X-RAY BEAMS USED FOR RADIATION RESEARCH FROM A VAN DE GRAAFF GENERATOR

D. MOORE

Medical Research Council, Experimental Radiopathology Research Unit,
Hammersmith Hospital, Ducane Road, London, W. 12

The Van de Graaff generator of the Medical Research Council at Hammersmith Hospital, has been used for radiation research for the past ten years. Details of its special design are given. The accelerator provides neutron, electron and X-radiations up to energies of 2 MeV. High intensity outputs are possible with beam currents of several hundred microamperes. The conversion from an output of neutrons to an output of X-rays is accomplished within a few minutes.

Methods of dosimetry are discussed for the delivery of defined doses of either of these radiations for studies in chemical, biological and pathological research. Examples of the versatility of the accelerator output, together with some of the published work are included.

1. Introduction

The Van de Graaff generator of the Experimental Radiopathology Research Unit, Medical Research Council at Hammersmith Hospital has been in almost continuous use for radiation research for the past ten years. The design was influenced by the needs of chemical and biological research. The generator, which is large compared with modern 2 megavolt machines is mounted vertically. The high intensity outputs are produced with beam currents of several hundred microamperes. An accelerating tube of 25 cm internal diameter is constructed of porcelain segments cemented to stainless steel electrodes. The tube is 2½ meters long and normally kept at a vacuum of 3×10^{-6} millimeters of mercury. It withstands a voltage of 2×10^6 and is used for accelerating both positive ions and electrons. Focussing of positive ions and electrons from a few hundred kilovolts to over 2 megavolts is made possible by a graded resistance column[1]). Charge is sprayed over 48 cm of a belt 53 cm wide and carried to the terminal at about 1000 meters per minute. The amount of charge of opposite sign sprayed on to the down run of the belt can be varied at the control desk. This is necessary to produce stable running for the different load conditions. A pressurized deuterium supply is installed in the high voltage terminal. This feeds the low power ion source[2]) from which deuterons are extracted and injected into the accelerating tube. The ion source can produce more than 1 mA of deuterons. An electron gun is also mounted on the upper end of the accelerating tube. The accelerated particles are focussed on to a target at the lower end of a field free tube below the accelerator. In the target chamber is an X-ray target which can be moved to intercept the beam when required. This is possible through a rotating vacuum seal from the outside.

With these facilities the polarity of the machine can be changed within a few minutes, to produce either neutrons or X-rays—a desirable feature in biological research. The additional requirement of not increasing significantly the background of scintillation counters within the hospital area, made it necessary to reduce the reverse current of negative particles accelerated up the tube when running on positive potential.

The object of this communication is to describe the dosimetry carried out with the machine to meet efficiently the requirements of a radiation research team, covering such

[1]) P. Howard-Flanders, *Nature* **170** (1952) 744.

[2]) P. Howard-Flanders, Ph. D. Thesis, Univ. of London, 1956.

divergent fields as chemistry, biology and radiopathology.

2. Neutron Irradiations

Normally the reaction $Be^9(d,n)B^{10}$ is used for the production of fast neutrons at Hammersmith. Deuterons with an energy of 1.8 MeV produce an energy spectrum of neutrons up to 6 MeV with a mean energy of 2 MeV. This spectrum has little contamination from slow neutrons as shown in fig. 1, which is of considerable importance for radiation chemical and radiation biological work since it is difficult to assess the LET of slow neutrons in an irradiated medium and dosimetry becomes virtually impossible. The radiation is filtered through the Be target, 0.43 cm thick, 0.15 cm of cooling water and 1.2 cm of a tungsten loaded alloy 11.3 g per cm³. The d on Be reaction produces a γ-component of radiation. The filtration reduces this component in the forward direction.

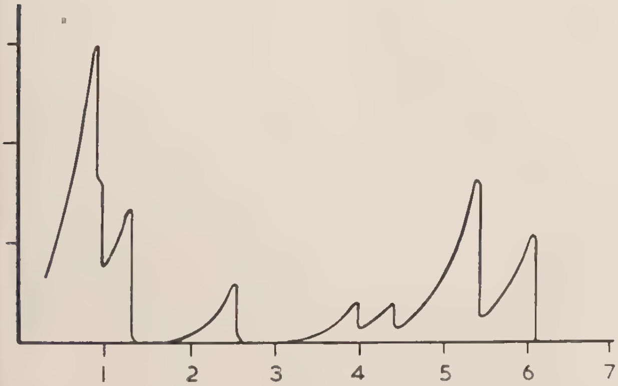

Fig. 1. Neutron energy spectrum obtained by 1.8 MeV deuterons in the reaction $Be^9(d,n)B^{10}$. Abscissa: neutron energy in MeV. Ordinate: Number of neutrons in the forward direction.

A few measurements have been made with deuterons on a heavy ice target. The measurements indicated an improvement in the neutron to γ dose ratio. The γ-component is approximately 50 % of that with the Be reaction. The neutron yield from the target per microampere beam current is however lower by 40 %. No attempt was made to solve the engineering problems associated with an ice target. The great difficulty is to prevent the target from evaporation and maintain a good accelerator tube vacuum with high beam currents.

A BF_3 counter mounted permanently at a distance of 5 m from the Be target is used to monitor the radiation from the accelerator. The monitor is routinely checked by exposure to the radiation from a Ra-Be source. The output of the accelerator is measured with condenser ionization chambers to be described below. This measurement is related to the BF_3 monitor reading. Since the BF_3 calibration remained constant within 2 % over six years, these measurements are a check on the whole of the measuring equipment.

3. Field Below the Target

Red phosphorus mixed with "Araldite" can easily be cast into plaques of desired dimensions. Si^{31} is formed on exposure to fast neutrons. The induced radioactivity is therefore a measure of the neutron flux. These plaques are useful relative dosimeters to explore the general characteristics of the intensity distribution of fast neutrons around the target. It was shown that the intensity of the beam falls off in the forward direction almost inversely proportional to the square of the distance from the target. This suggests that the deuteron beam is well collimated and strikes the Be target fairly centrally. The intensity is a maximum in the forward direction and falls with increasing angle to a minimum at an angle of 65° beyond which a slight increase in intensity is evident.

4. Ionization Chambers

Condenser ionization chambers are used to estimate the neutron dose delivered to an irradiated specimen. Two types of condenser ionization chamber shown in fig. 2 are in continuous use at Hammersmith. The electrodes are formed by the opposite walls of the cavity and are insulated by amber. The two types shown, differ mainly in their wall materials. One chamber has its measuring air cavity surrounded mainly by Duraluminium, whereas the other has the cavity set mainly in tissue-equivalent

---

[3] H. H. Rossi, Radiology 61 (1953).

plastic, kindly supplied by Dr. H. Rossi[3]). Tissue equivalent plastic is now commercially available. The air-gaps are 0.5 mm and 1 mm respectively, and fulfill a condition of the cavity chamber theory[4]). The chamber made of Duraluminium responds mainly to γ-radiation, and is relatively insensitive to neutron radiation. In contrast, the second chamber with the cavity surrounded by material containing 10.1 % H, 82.7 % C, 3.5 % O and 3.7 % N is almost equally sensitive to both neutrons and γ-radiation.

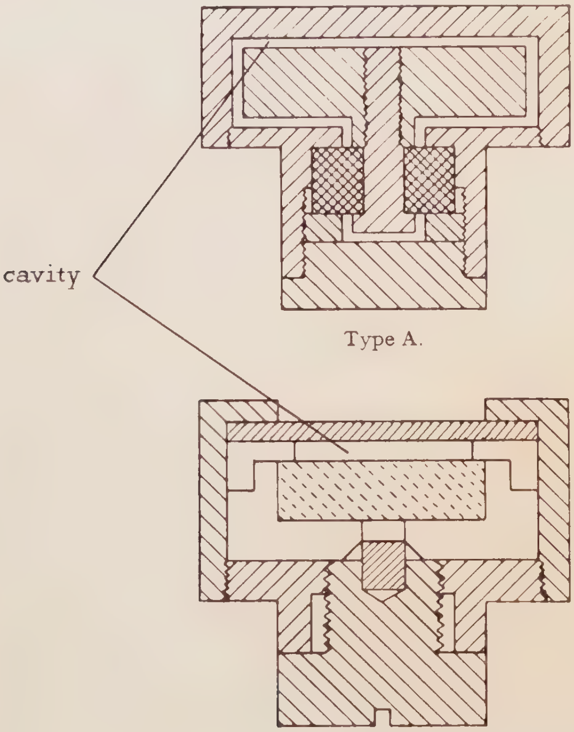

Type A.

Type B.

Fig. 2. Condenser ionization chambers: Type A: aluminium chamber. Type B: Plastic chamber.

The response to γ-radiation of these chambers can briefly be described as follows. The electrically insulated inner electrode is charged to a potential of 220 V with respect to the outer walls. Gamma quanta produce secondary electrons in the walls which traverse the cavity and ionize the gas. The resulting loss of charge produces a measurable potential drop. This potential drop is related to the energy absorbed by the wall material according to the Bragg-Gray theory[4]) which states that the ratio of energy absorbed per unit mass of the wall material, E_{w}, to that absorbed per unit mass of air, E_{air}, is equal to the ratio of the mass stopping powers of the wall to that of the air for electrons, S_{w} to S_{air}, respectively:

$$\frac{E_{\mathrm{w}}}{E_{\mathrm{air}}} = \frac{S_{\mathrm{w}}}{S_{\mathrm{air}}}.$$

The energy absorbed in air is defined by the product of the number of ion pairs produced, J, and the mean energy required to produce an ion pair, W. W is taken to be 32.5 eV for fast electrons. J is measured by the loss of charge from the condenser chamber. Therefore,

$$E_{\mathrm{w}} = J\,W\,\frac{S_{\mathrm{w}}}{S_{\mathrm{air}}}.$$

The response of the condenser ionization chambers to neutrons is similar to that of γ-rays except for the mode of energy absorption. Neutrons with energies between 20 keV and 20 MeV lose their energy mainly by elastic collision with nuclei. H nuclei have the highest collision cross-section for neutrons. The proton receives more energy from a neutron than any other nucleus and since almost $\frac{2}{3}$ of the nuclei in biological tissue are hydrogen, about 90 % of neutron energy transferred to tissue is via recoil protons. It is the number of recoil protons from the wall material in the gap of the condenser ionization chamber which is measured by the potential drop of the chamber. W for recoil protons is taken to be 35 eV.

The neutron beam has a γ-component to which both chambers are sensitive and the ionization in the cavities will therefore be the sum of both secondary electrons and recoil protons and can be written as:

$$J = \left(\frac{E_{\mathrm{w}}}{W}\,\frac{S_{\mathrm{air}}}{S_{\mathrm{w}}}\right)_{\mathrm{protons}} + \left(\frac{E_{\mathrm{w}}}{W}\,\frac{S_{\mathrm{air}}}{S_{\mathrm{w}}}\right)_{\mathrm{electrons}}$$

for each chamber.

When both chambers are exposed simultaneously to the radiation from the Van de Graaff generator two different readings of J are obtained, J_{plastic} and $J_{\mathrm{aluminium}}$. The conversion

[4]) L. H. Gray, Proc. Roy. Soc. (London) A **156** (1936).

of these readings to the absorbed dose in rads received by the wall material requires a knowledge of (a) the mass stopping power ratios, (b) the collision cross-sections and (c) the energy expended in these collisions for each constituent of the wall material[2,5,6]). Thus the readings can be written as:

$J_{\text{plastic}}\ (= J_{\text{pl.}}) = 0.96\ E_N + 0.967\ E_\gamma$

$J_{\text{aluminium}}\ (= J_{\text{al.}}) = 1.43\ E_N + 1.12\ E_\gamma$

E_N = energy absorbed per unit mass of material from neutron radiation.

E_γ = energy absorbed per unit mass of material from gamma radiation.

To convert these readings to the absorbed dose in rads received by tissue, it is necessary to have a knowledge of the above for the constituents of tissue, so that the energy absorbed in tissue from the γ-radiation becomes

$$E_\gamma = 1.026\ J_{\text{al.}} - 0.078\ J_{\text{pl.}}\ \text{rads}$$

and the energy absorbed in tissue from neutron radiation becomes

$$E_N = 1.175\ J_{\text{pl.}} - 1.018\ J_{\text{al.}}\ \text{rads}\ .$$

The volume and sensitivity of the ionization chambers is determined by exposure to radiation from a 100 mg Ra-Be source which had been compared with similar sources, calibrated by the N.P.L. and was further checked by simultaneous exposure with a Baldwin-Farmer sub-standard cable ionization chamber to 8 MeV X-rays from a linear accelerator. The Ra-Be calibration of the chambers has remained constant within 2 % for ten years.

It was found that the absorbed dose in tissue from the radiation of the Van de Graaff generator operated at 1.8 MeV contained a 12 % contribution from γ-radiation. This low γ-ray content makes the study of the effects of neutrons possible.

5. Experimental Assemblies

An assembly used for neutron exposures of liquid samples consists of three glass cells mounted in a stack under the target. These cells are 3.7 cm diameter and 1.2 cm deep and have an optically flat base. The drop in intensity vertically downwards, as determined by P^{32} activation analysis and by ionization chamber measurements is given in fig. 3 together with the expected drop on the basis of the inverse square fall off with distance. The relative dose delivered to solutions of 3 ml each in the three vessels was determined by counting the induced radioactivity in H_3PO_4 solutions and checked with 10^{-3} *M* Fe^{++} in 0.1 *N* H_2SO_4. This chemical dosemeter shows a linear response to dose up to more than 5×10^4 rads.

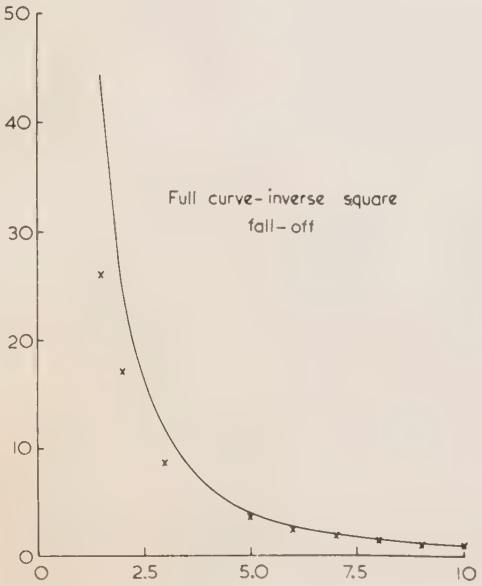

Fig. 3. Intensity fall-off below the target. Abscissa: distance in cm below the target. Ordinate: relative intensities. Full curve: Inverse square fall-off. Crosses: measured values.

The dose to the centre of the surface of a liquid in a vessel at a distance "*x*" from the target with a radius "*r*" can be estimated from the dose "*d*" measured at a standard distance of 10 cm along the beam axis. A correction factor "*f*" for the departure of the field from the inverse square law is obtained from fig. 3. The mean surface dose "*D*" is calculated from purely geometrical considerations. Thus "*D*" becomes:

$$D = \frac{d}{x^2} \times 10^2 f \frac{x^2}{f^2} \log_e \left(1 + \frac{r^2}{x^2}\right).$$

---

[5]) I.C.R.U. Handbook **62** (1956).

[6]) T. J. Thompson, University of California Radiation Laboratory Report, U.C.R.L. 1910 (1952).

The 3-vessel assembly is used for the irradiation of liquids and suspensions as required for chemical and microbiological work with dose rates of 300 rads per minute. Layers of solid material, if their H content is known, can also be given predetermined doses in this assembly.

Some radiobiological experiments, however, require controlled gas conditions during irradiation. For this purpose, the three vessels can be enclosed in a metal box with a 1 mm thick perspex lid. Little radiation is absorbed in the perspex. Continuous equilibration of the suspensions with gas, is achieved by tilting and rotating the whole assembly. Under these conditions, dosimetry is carried out with a chemical dosimeter, which can be calibrated in a subsequent exposure against an ionization chamber in the standard three-vessel set-up.

A Be target built into an extension tube and surrounded by 2.0 cm of lead had been constructed to provide a large radiation field in the horizontal plane of the target. This is desirable when animals are given whole-body irradiation. At a radius of 20 cm from the target a neutron dose-rate of 10 rads per min is obtained with an accompanying γ dose-rate of 1.2 rads per min. This radiation field has been used to expose rats to doses of a few hundred rads. It is possible to irradiate simultaneously eight animals arranged in aluminium cylinders in a circle of 20 cm radius. An accurate estimate of dose to the rats is made by inserting condenser ionization chambers into a wooden rat phantom. The radiation is attenuated by 35 % in the body of a rat of 150 g. For this reason, half the required dose is given from each side of the rat by reversing the cylinders, thus reducing the dose variation.

A collimated beam of neutrons is obtained by surrounding the extension tube target with two circular slabs of absorbing material, spaced vertically 2.5 cm apart as shown in fig. 4. The slabs with a radius of 28 cm are made of a borax-loaded paraffin wax and surrounded by 1.5 cm of lead. The lead improves the neutron to γ dose ratio from 1:1 to 2.7:1. The radiation from the target is filtered by 2 cm of lead.

Mice mounted in cages secured to the 1.5 cm lead filter on the periphery of the slabs have had their tails, or tumours in their hind legs irradiated. The intensity to the limbs of the mice was 2.5 rads per minute, whereas the shielded body of the mice received only 0.3 rad, i.e. 12.5 % of this figure.

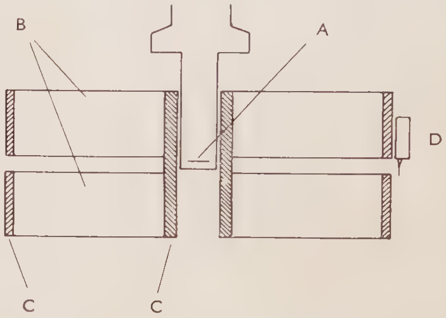

Fig. 4. Assembly for collimated neutron beam. A: target; B: paraffin; C: lead; D: mice.

6. Electron Irradiations

Electrons with energies from 300 keV to 1.8 MeV pass through an aluminium window at the lower end of the field free tube below the accelerator. This window is 13 mg/cm^2 thick and has a diameter of 4 cm. A monitoring ionization chamber to be described later is mounted below the window. Secured to the chamber is as low speed mechanical shutter.

The position and focussing of the electron beam can be shown by exposing a piece of paper close to the aluminium window. The paper becomes discoloured or even charred, and thus indicates the centre of the beam. Also, exposed sodium chloride crystals show a graded brown discolouration which gives the same information. A more quantitative method is to give short exposures to bromide photographic paper. After normal processing, a picture of the beam and the fall of intensity from its centre is seen.

A parallel-plate ionization chamber[7]) having thin foil electrodes is suitable for monitoring or measuring the dose of a beam of fast electrons. Such a chamber is shown in fig. 5.

---

[7]) J. W. Boag, Radiation Dosimetry, edited by G. J. Hine and G. L. Brownell (Academic Press, New York, 1956) Ch. 4.

The foils are made of aluminium 13 mg/cm^2 thick. Amber pegs insulate the centre foil from the outer two which are earthed by the case. Connection to the centre foil is made through a co-axial cable. A circular diaphragm may be used to define the electron beam to the central region of the chamber. A voltage is applied between the centre foil and the outer foils to collect the ions produced in the coin shaped cavities. A field strength of about 100 V/mm is used to collect the ionization[7]). The ion current is a measure of the dose-rate in the air of the chamber and if integrated a measure of the total dose in air. The dose is calculated from the volume defined by the diaphragm and the foil spacing. For very low dose-rates, chambers with large spaces between the electrodes are used. The maximum dose-rate which can be measured with accuracy is 5 × 10^4 r/sec. Dose-rates higher than 5 × 10^4 r/sec have been measured by collecting the electron beam on an electrode and recording the current.

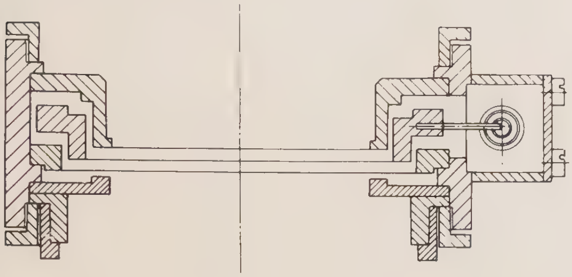

Fig. 5. Parallel plate ionization chamber.

7. Experimental Assemblies

It seemed desirable to develop a dose-measuring system which would be applicable to any experiment involving irradiation of liquid samples. The assembly most commonly used at Hammersmith consists of the thin foil ionization chamber mounted 5 cm below the shutter and an irradiation vessel in a determined position below it. It is the integrated ionization current of the chamber which has to be related to the dose in rads received by a sample in the irradiation vessel. Therefore, the electron beam was investigated always with reference to this chamber. Measurements below this chamber which will be called chamber 1 were taken with other ionization chambers or with a chemical dosimeter in solution.

Fig. 6 is a plot of the ionization observed in the chamber versus the thickness of absorbing material above. This was measured keeping the distance between chamber 1 and the measuring chamber 2 constant and placing aluminium foils on the surface of chamber 2. The three curves plotted are for three initial electron beam energies of 1.0, 1.1 and 1.2 MeV. Extrapolation of these curves indicates the mean range of electrons in aluminium. The tail of the curves is a measure of the bremsstrahlung ionization current produced in a chamber when the electron beam is stopped in 3 mm of Al. It amounts to 0.5 % of the current recorded when the unattenuated beam traverses the chamber. It can thus be concluded that the dose-rate in the chamber, when the beam is stopped in the shutter, is of this magnitude and therefore quite negligible for the experiments envisaged.

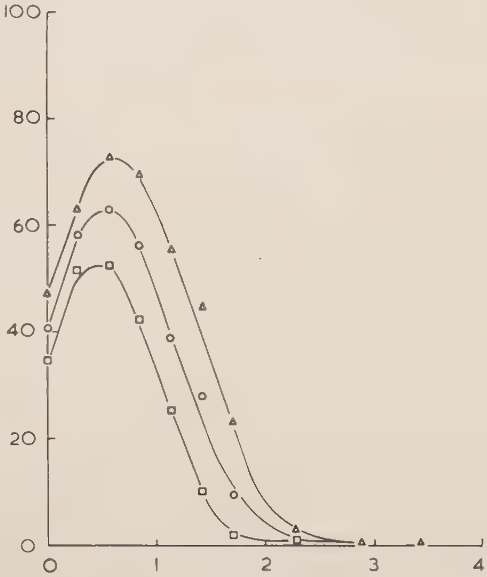

Fig. 6. Absorption curves of electrons in aluminium. Abscissa: thickness of aluminium in mm. Ordinate: relative ionization below the aluminium. △ curve for 1.2 MeV electrons; ○ curve for 1.1 MeV electrons; □ curve for 1.0 MeV electrons.

The radial variation of intensity of the electron beam in the area covered by the irradiated sample in a glass dish below chamber 1 was measured by a small ionization chamber which could be moved across the field. The relative ionization current in this small chamber is plotted against distance from the axis in fig. 7. This shows a maximum variation of dose-rate of about 30 % for a diameter of 3.6 cm. The mean dose-rate for the surface of a disc 3.6 cm in diameter is 88 % of the dose-rate at the centre.

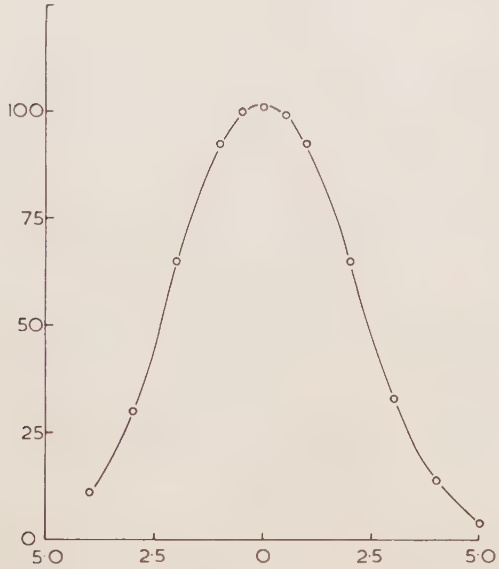

Fig. 7. Radial distribution of electron intensity below chamber 1. Abscissa: distance from beam axis in cm. Ordinate: relative ionization.

The fall-off of ionization intensity in air along the vertical axis was measured over the range 0.3 cm–1.0 cm below chamber 1 and it was found to be approximately 2.6 % per mm. This range was chosen since it covered the positions occupied by solutions to be irradiated and indicated the error introduced by incorrect positioning.

With the preceding three measurements a fairly clear picture is obtained of the changes of ionization intensity in the whole area below chamber 1. This allows the dose-rate in air to be defined by the ionization current measured in chamber 1 provided no additional scattering material is present. The introduction of an irradiation vessel containing liquid affects the response of chamber 1 by scattering of electrons. The measurements reported next, deal with such distortions of the response of chamber 1.

Fig. 8 shows the assembly used for this investigation. Chambers 1 and 2 were fixed relative to one another. An Al diaphragm designed to give minimum multiple scatter into chamber 2 defined the electron beam to a diameter of 5 mm. Chamber 2 was then backed by a variety of materials ranging from air to lead. It was assumed that the reading in chamber 1 was not affected, and only chamber 2 responded to the varying conditions. Fig. 9 summarizes the results by plotting the ionization current of chamber 2 against the atomic number of the backing material. When chamber 2 was backed by Al foils as used in the construction of the chambers an increase of 1.6 % in ionization current was observed for each foil. Since similar

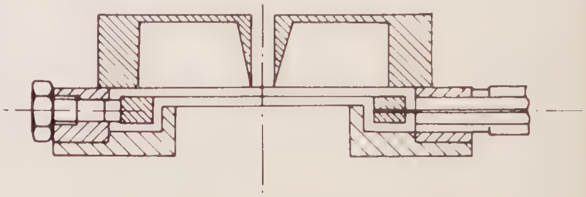

Fig. 8. Assembly for measuring backscatter.

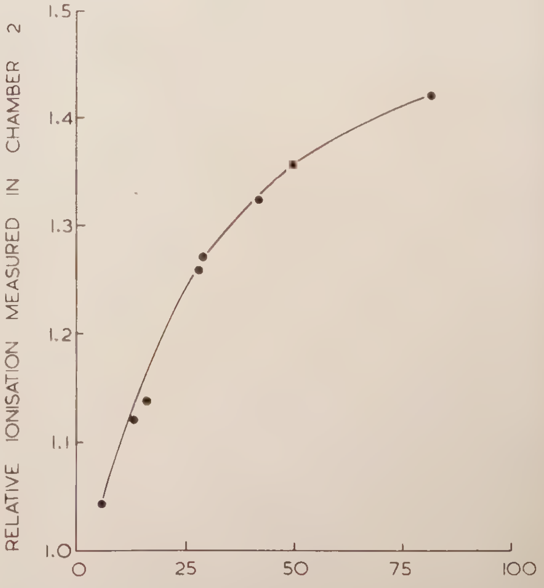

Fig. 9. Backscatter from different materials. Abscissa: atomic number of material used. Ordinate: relative ionization measured in chamber 2.

backscatter occurs within the chambers from two foils, the absolute value for the dose-rate in air is taken to be 3 % lower than the measured value.

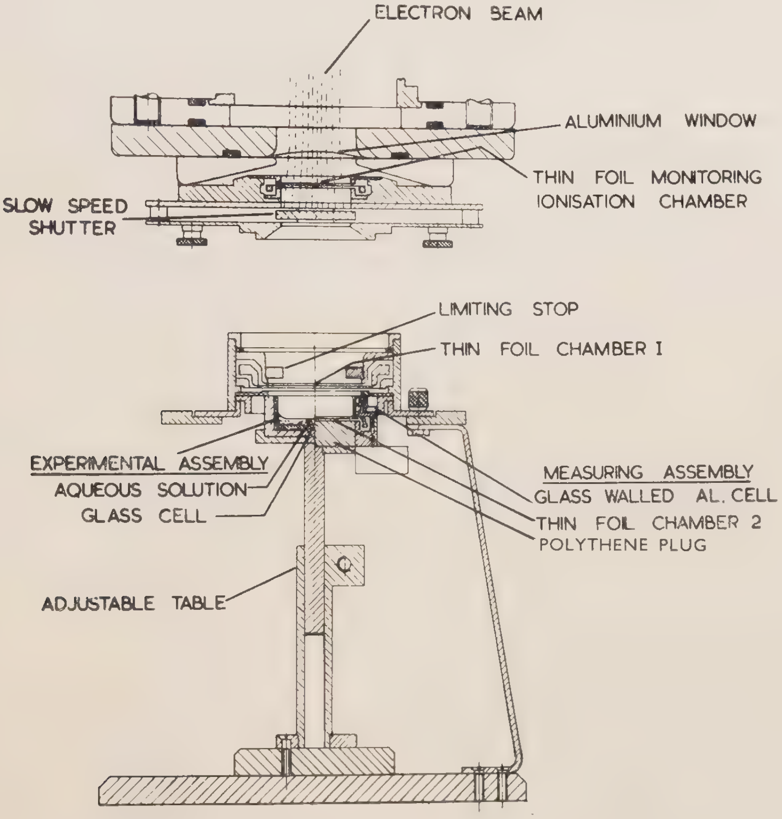
ELECTRON BEAM
ALUMINIUM WINDOW
THIN FOIL MONITORING IONISATION CHAMBER
SLOW SPEED SHUTTER
LIMITING STOP
THIN FOIL CHAMBER I
EXPERIMENTAL ASSEMBLY
AQUEOUS SOLUTION
GLASS CELL
MEASURING ASSEMBLY
GLASS WALLED AL. CELL
THIN FOIL CHAMBER 2
POLYTHENE PLUG
ADJUSTABLE TABLE

Fig. 10. Assembly for irradiating liquids with the electron beam. The left section shows the vessel and solution; the right section of the diagram shows chamber 2 and backing material.

Fig. 10 shows the lower end of the field free tube, the aluminium window, below which is mounted a monitor chamber and the slow speed mechanical shutter. Chamber 1 is mounted 5 cm below the shutter. The lower part of the diagram is divided in two halves, the left side shows the sample vessel in the irradiation position. The right side shows chamber 2 on which is mounted a glass walled vessel which has a thin mica base. Chamber 2 is backed by polythene. A solution can be put into the glass-mica vessel and the distance between chamber 1 and the surface of the solution can be kept constant. The influence of the solution on the ionization current in chamber 1 was measured under conditions of constant monitor chamber current. The cylindrical part of the glass-mica vessel was made in two pieces so that the upper piece remained in position as the vessel was lowered to keep the surface level constant. This was to present as near a constant backscatter environment to chamber 1 as was possible. A maximum correction of 1.2 % was necessary to compensate for the effect of scatter from the solution. As was to be expected, the backscatter from H_2O and from a 10^{-3} M ferrous ammonium sulphate solution in 0.2 N sulphuric acid were not distinguishable.

In the same experimental assembly it was possible to estimate the electron dose-rate distribution in the volume of a liquid. This was measured by comparing the ionization current in chamber 2 with that in chamber 1 for varying depths of solution. Fig. 11 shows the changing ionization current in chamber 2 with increasing depths of H_2O and Fe^{++} solution. This curve indicates the maximum depths of solution which can be irradiated with a relatively uniform dose-rate.

Similar measurements can give an estimate of dose when the ionization currents are integrated and the solution is a chemical dosimeter. For a constant integrated current measured by chamber 1, a constant integral dose is received by any material below it. In the absence of any solution, this dose is received by the backing material of chamber 2. The integral dose is therefore shared between the solution above chamber 2 and the backing material of chamber 2. At a depth of 5 mm, all the dose is absorbed by the solution. Fig. 12 shows these results. The ordinate is in rads and the abscissa in millimetres of material. Curve A is the increasing dose to the ferrous sulphate solution with increasing depth, and curve B the calculated dose received by the backing material as if this were the same material. Curve C is the sum of these two doses. Curve A was computed with a G-value for Fe^{++} of 15.7 ions of Fe^{++} oxidized per 100 eV absorbed. This shows that for 3.5 mm depth of solution the departure from the estimated dose by physical measurements is less than 5 %. Consequently all solutions and suspensions irradiated at Hammersmith have been confined to less than this depth—i.e. 4 ml of solution.

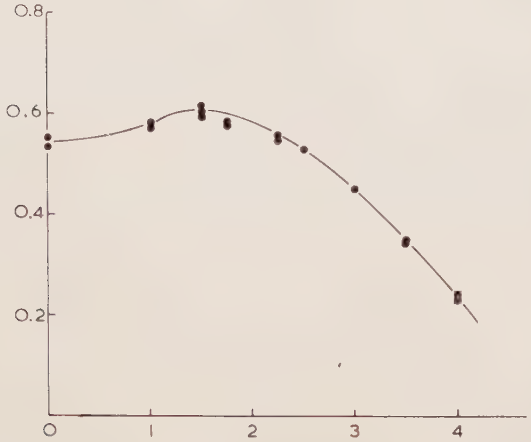

Fig. 11. Depth dose curve in water and ferrous ammonium sulphate solution. Abscissa: ml of $10^{-3}M$ $Fe_2(NH_4)_2SO_4$ in 0.2 N HSO_4 or H_2O in irradiation vessel. Ordinate: relative ionization measured in chamber 2.

8. X-Irradiation

X-rays are produced in the gold-plated copper target which can be swung into position above the aluminium window or the Be target. It is thus possible to have two types of radiation, either electrons and X-rays, or neutrons and X-rays in quick succession, a requirement for studies into the effects of changes in LET.

The X-radiation is monitored with an ionization chamber mounted near the X-ray target. The construction of this chamber is similar to the thin foil ionization chambers described previously. "Foil" electrodes of 1.5 mm thick perspex discs coated with colloidal graphite are used. The characteristics of the X-ray field below the target will be described for the case of X-rays produced by the target above the Al window. Commercially available X-ray cable-type ionization chambers have been used to explore the field below the target. The fall-off in intensity with distance follows closely an inverse square relationship.

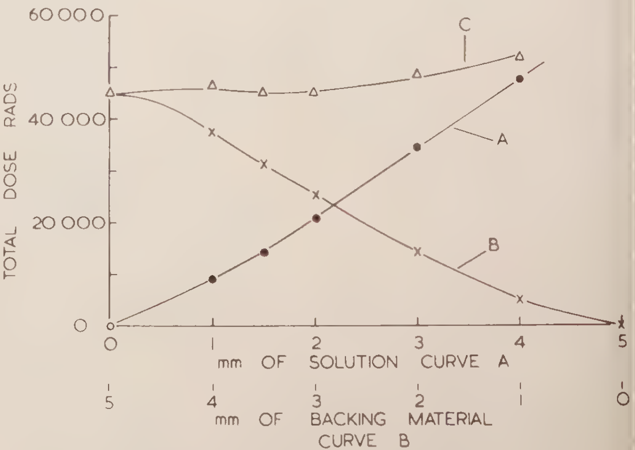

Fig. 12. Comparison of doses to the solution and backing material. Abscissa: mm of solution (Curve A). mm of backing material (Curve B). Ordinate: Total dose in rads. Curve A: dose received by solution. Curve B: estimated dose to backing material. Curve C: sum of A and B.

The absorbed dose is estimated by a condenser ionization chamber described in the section dealing with neutron doses. When biological tissue is irradiated, the measurements are carried out with ionization chambers made from tissue-equivalent plastic.

With a target current of 200 μA and a beam energy of 1.5 MeV, a dose-rate of 2600 rads per minute is obtained at 10 cm from the target with added filtration of 0.3 cm of lead, 0.15 cm of copper and 0.15 cm of aluminium. When X-rays are used with the Be target in position, the radiation is filtered by the target assembly, including the tungsten alloy filter. This reduces the dose-rate from 2600 rad/min to 1000 rad/min at 10 cm and generally hardens the spectrum. The monitoring of the beam and measurement of dose is the same as before.

For irradiations of liquids and suspensions, similar assemblies as described for neutron exposures can be used. By spacing a greater number of vessels in the field, one exposure allows the irradiation of many experimental solutions to different doses. The estimate of dose is usually carried out by chemical dosimetry

Whole-body exposures of animals are easily performed at convenient dose-rates. When rats are irradiated, at a distance of 100 cm at about 12 rads/min, the attenuation of the intensity throughout the body amounts to $7\frac{1}{2}\%$ as measured in a wooden phantom.

9. Conclusions

The paragraphs dealing with dosimetry for neutron, electron and X-irradiations, each include some examples of their application. It is felt that these methods cover the range of useful radiations which the machine can produce. In fact these methods have been used in many studies of radiation effects in chemistry of foods[8]), bacteriophage[9]), bacteria[10]), mammalian tissues[11]), plant material[12,13,14]), cancer cells[15]), pathology[16]), chemical studies[17,18,19]), immunity of monkeys[20]), etc. Only a selection of published experiments has been quoted as an indication of the variety of investigations which were made possible by comprehensive dosimetry carried out around the target of a versatile Van de Graaff generator.

Acknowledgements

The methods described were developed over many years and are mainly dues to Dr's. J. W. Boag and P. Howard-Flanders on whose knowledge and experience I have drawn freely, and to whom I am greatly indebted. I also wish to thank Dr. M. Ebert for his interest shown in this work.

---

[8]) R. S. Hannan and H. J. Shepherd, Trans Farad. Soc. Brit. J. Rad. **49** (1953) 326.

[9]) P. Howard-Flanders and T. Alper, Rad. Res. **7** (1957).

[10]) P. Howard-Flanders and D. Moore, Rad. Res. **9**, No. 4 (1958).

[11]) A. Glücksmann, Lea Memorial Lecture (1953).

[12]) M. B. E. Godward, Ed. Ralph Lewes. (Acad. Press.) In press.

[13]) D. A. Barber and M. Ebert, In press.

[14]) M. B. E. Godward, Nature. **185**, No. 4714, 706.

[15]) S. Hornsey, P. Howard-Flanders and D. Moore, Int. J. Rad. Biol. **2** No. 1 (1960).

[16]) P. Howard-Flanders and E. Wright Nature, **175** (1955) 1.

[17]) M. Ebert and J. Boag, Farad. Soc. Dis. **12** (1952).

[18]) M. Ebert, P. Howard-Flanders and R. J. Shalek, Rad. Res. **3** (1955).

[19]) M. Ebert, P. Howard-Flanders and D. Moore, Rad. Res. **4**, No. 2 (1956).

[20]) D. J. Perkins, unpublished (1956).

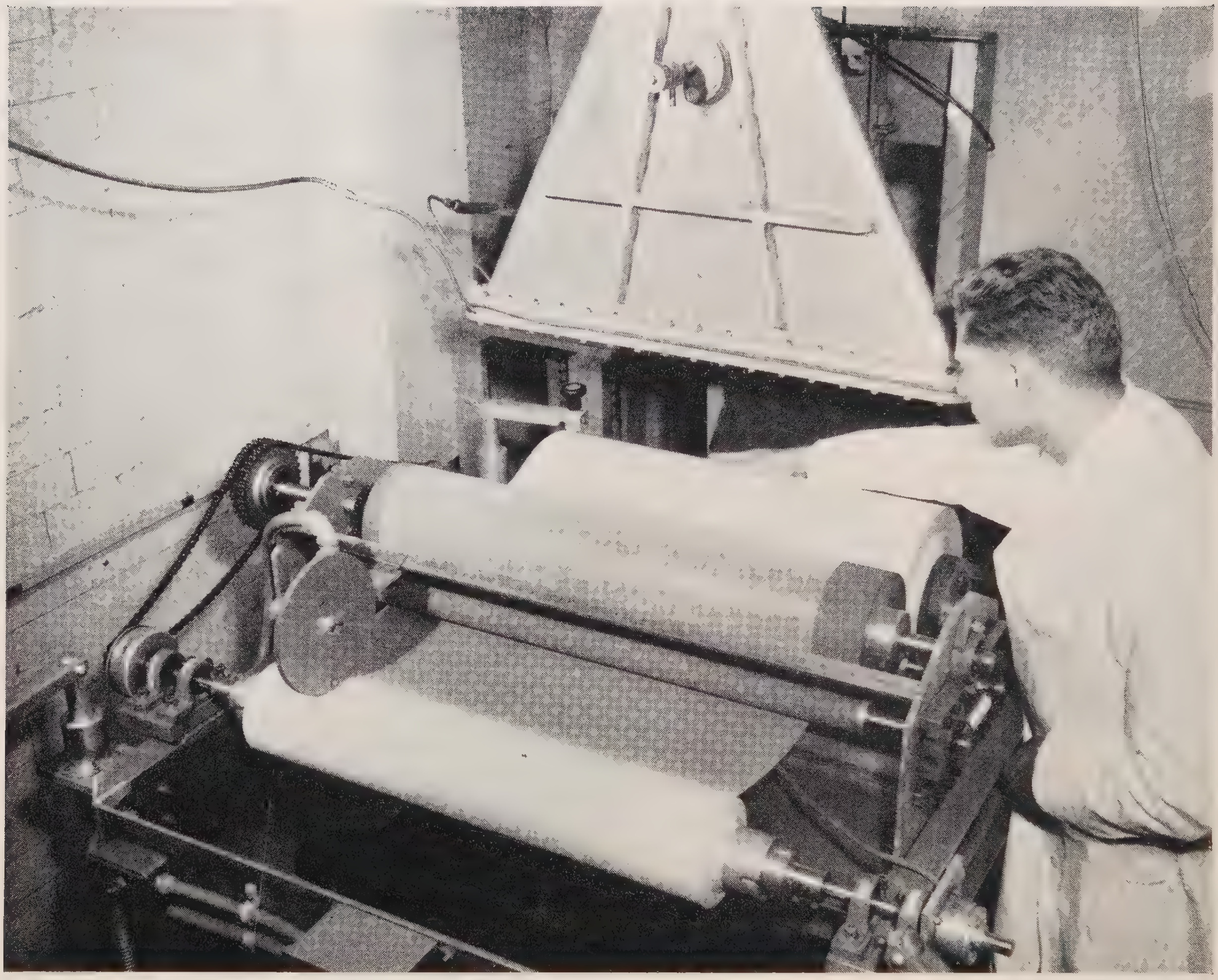

Fig. 2. 75-cm linear scanner for film handling.

Transformer, a sustained d-c beam current of 20 milliamperes has been accelerated to an energy of 1 MeV. This unit is shown in fig. 1.

While the prototype is large and involves expensive materials, the important principle of an insulating core has been proven. The idea can now be adapted immediately to produce a smaller unit at low frequency with cheaper core material and cheaper rectifiers at energies of 0.3 and 0.6 MeV and at a beam current of 8 milliamperes initially.

Whatever the method of voltage generation all direct accelerators have similar acceleration-tube systems. Thus, long past experience at low current with the various sizes of the Van de Graaff electron accelerator has provided background for the present work on (1) cathodes at 100 mA. (2) tubes at 20 mA and (3) "windows" at 0.4 mA per cm of linear scan. Reliability is the primary criterion of design. This involves the achievement of a low failure rate of components, predictability of failure where possible, and ease of replacement.

Several concepts of use make easier the design of acceleration-tube systems at high beam intensities. The first is an extension of existing techniques of beam deflection or diffusion. These techniques permit more efficient use of the beam because a uniform surface dose is realized. Also, by spreading the beam over a greater surface area of the accelerator's "window", a higher beam current can be used without increasing the power density absorbed by the "window". For example, the maximum power limit for an unscanned beam with a diameter of one centimeter might be several hundred watts. But with a linear scan of 38 centimeters, this limit is increased to about 20 kilowatts. Work was completed recently at High Voltage Engineering Corporation on a 75-cm line scanner. It has been used successfully with a 1.5 MeV Van de Graaff accelerator for the uniform coverage of wide film (fig. 2).

It doubles the power-absorbing capacity of the window to 40 kilowatts. It can be extended to greater lengths. Those products, other than film, which cannot be conveniently assembled for movement transverse to the direction of scan, can be conveyed at oblique angles. Extremely narrow objects or fluids could be processed in line with the direction of scan.

Another concept of processing is required in the use of very intense sources. The economy of large packages can only be realized by transmitting super-voltage power from one generator through insulated piping to independent, multiple acceleration tubes, each of which draws an increment of the total power. The accelerated beams would be applied in a series of steps on one processing line, or to parallel lines, as shown in fig. 3.

There are several additional reasons for separating the tube from the generator:

1. Maintaining continuity of the process in the event of failure of an accelerators tube. Standby tubes can be available for immediate use.

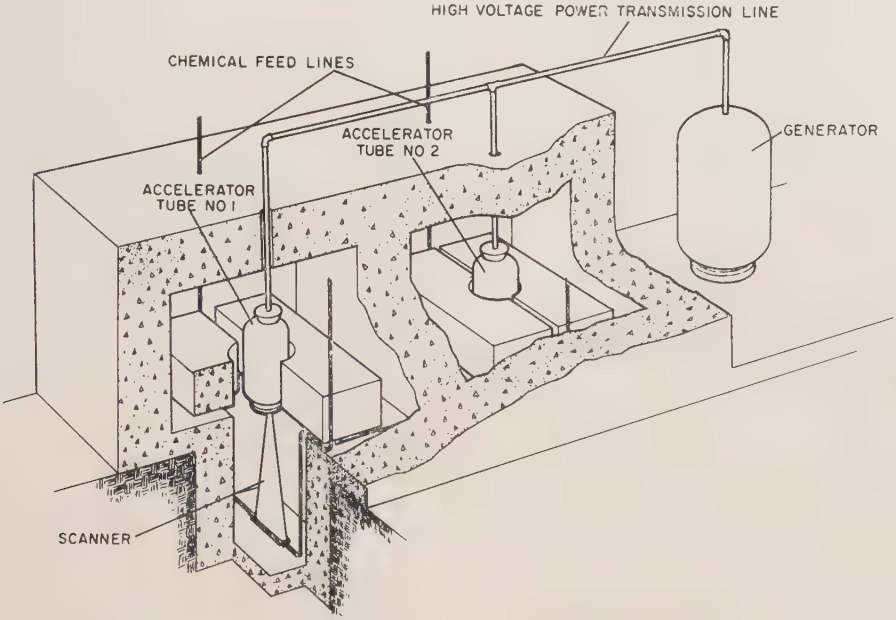

Fig. 3. Transmission system to multiple acceleration tubes.

2. Reducing the area of radiation shielding. The power source and transmission line require voltage insulation only.

3. Covering wide sheet or applying the beam to a re-entrant geometry.

The concept is more applicable to d - c power On the basis of known technology flexible cable can be used up to about 300 kV, rigid solid dielectrics could be used for power transmission up to a level of about one million volts, pressurized gas above.

This concept is also applicable to microwave linear accelerators by waveguide transmission of the r - f power to independent accelerator tubes.

In summary, all four elements of the direct accelerator are being designed in concert to meet the wide needs of future applications. These elements are the generator, the tube, the cathode, and the window, The guideposts are initial cost, life, replacement time, and replacement cost.

3. Linear Accelerators

In linear accelerators the same guideposts apply. Two of the elements are also the same: the cathode and the window. There is an additional requirement on the cathode over d - c direct accelerators-pulsed duty is required. There is a reduced current-density requirement on the window.

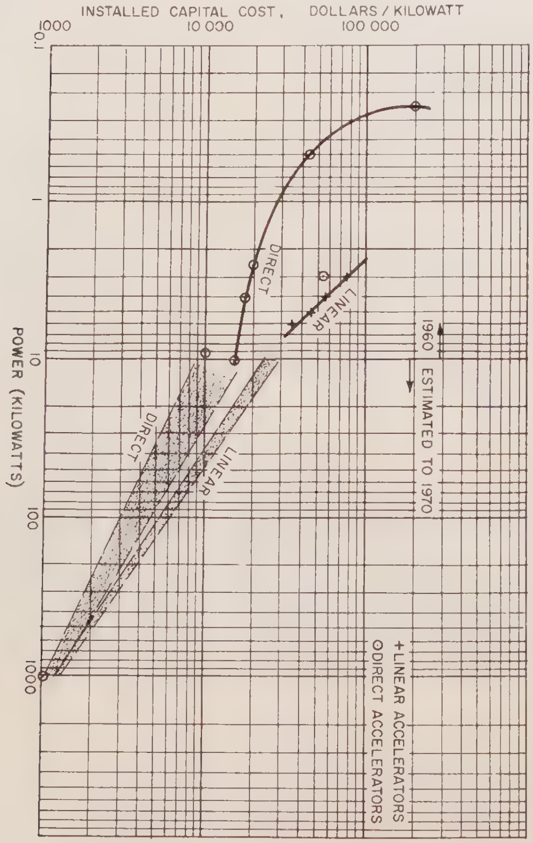

Fig. 4. Effect of power on capital cost.

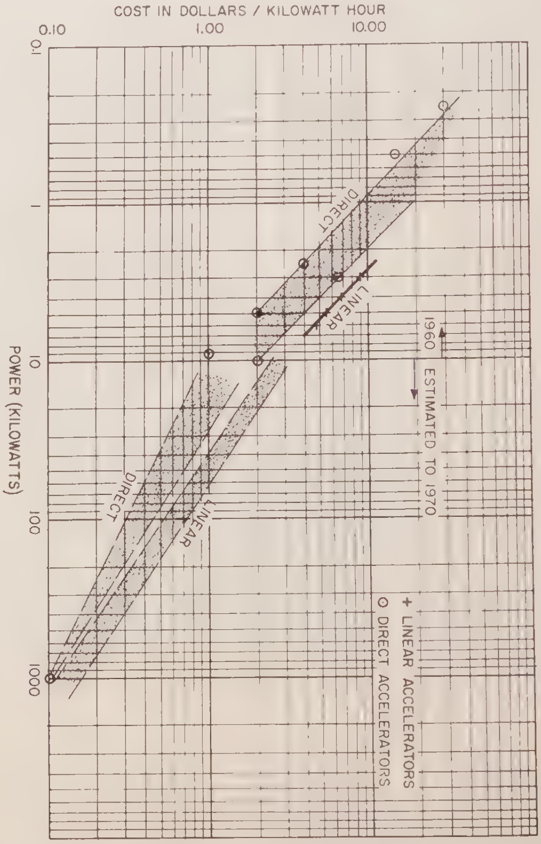

Fig. 5. Effect of power on operating cost.

Two other elements are analogous to two in the direc accelerator: the r - f power source to the generator, and the waveguide to the acceleration tube. The waveguide is long-lived as compared with the acceleration tube and contributes very little to the operating cost. It also will be a minor factor in original cost in the future, over the processing energy range, as design becomes standardized. Recent developments include a 1.5-meter design for peak power at 6 MeV and a 3-meter design for peak power at 6 MeV,and a 3-meter design for 12 to 14 MeV.

The r - f power source, like the generator of the direct accelerator, excerts a strong influence on unit capital cost by its rating. But in addition, it is the most importance element of operating cost. These two factors are related because the life expectancy of the power tube depends on its rating. One single combination should produce minimum overall cost. As new tubes at higher power are produced the emphasis is shifting to life expectancy.

There has been a steady improvement in both the peak power ratings and efficiencies of tubes. Only three years ago the best available rating was about 4 kilowatts of average r - f power from 2 Megawatts of peak power. A year later this increased to 5 kilowatts from 10 megawatts. Our present designs are based on either (1) 20 kilowatts from 10 megawatts at the L-band frequency of 1300 megacycles per second or (2) 15 kilowatts from 3 megawatts at the S-band frequency of 2856 megacycles per second. The latter is produced by the current model of the Amplitron. It is undergoing bench tests now at higher power levels.

The S-band linac is at present a more economical source of average electron power than the L-band linac. Operation at high frequency results in smaller cross sections of waveguides. At the L-band frequency waveguides are capable of transmitting greater peak powers, and the larger acceleration structures can store more microwave energy and support greater peak beam currents. This is not of prime importance, however, for industrial processing.

Other tubes at S-band, L-band, and at a band below 1000 Mc/sec are under test for radar programs. These should produce average electron power of 50 to 100 kilowatts. A large demand in radar use, when declassified, will favor low costs for use in linear accelerators. Whereas the use costs of the tube on warranty are about $1 (U.S.) per kilowatt-hour today, the power divisor and the life expectancy factor should produce improvement by a factor of ten in the future.

In unit capital cost, the power divisor has already produced a twofold reduction. A 6 MeV, 7 kW linear accelerator now costs about $20000 per kilowatt. Tubes with larger power will result in accelerator costs below $10000 per kilowatt at all energies in the processing range.

4. Summary

All of these future improvements in both direct accelerators and linear accelerators have been assessed in formulating cost projections. First, installed capital cost, which includes shielding, is shown in fig. 4.

We believe that the power range can be extended if needs arise by the magnitude shown with principles we now have in development. Multiple-tube use is essential for very high power.

Estimates of operating cost are shown in fig. 5.

Although great strides must be made beyond the limits of present accelerators, we are optimistic that the wide range of needs can be met under conditions and costs which will satisfy more industrial applications. A small amount of industrial operating experience has already indicated that use-costs can be reduced significantly by an improvement in reliability under conditions of continuous use. Surprisingly, recent demands in physics research create new design approaches and sustain a development program which has multiple purposes. Indeed, not only are the tools of the physicist useful for chemical or biochemical purposes, but his expanding need provides a staying power until the reluctant chemist is ready to adopt a more fundamental, and hence classical, solution to his problems.

VAN DE GRAAFF ACCELERATORS†

(INSTALLED OR ON ORDER FROM HIGH VOLTAGE ENGINEERING CORP.)

Location	Energy (MeV)	Beam current (micro-amperes)	Particles and radiation
Atomics International	0.35	—	
U.S. Air Force Institute	0.4	150	d
Case Institute of Technology	0.4	150	d
Northwestern University	0.4	150	d
U.S. Naval Research Laboratory	0.4	150	d
U.S. Naval Ordnance Laboratory	0.4	150	d
National Institutes of Health	0.4	150	d
University of Michigan	0.4	150	d
General Motors	0.4	150	d
Edgerton, Germhausen, and Greer	0.4	150	d
Southern Methodist University	0.4	150	d
University of New Hampshire	0.4	150	p,d,α
University of Toledo	0.4	150	d
Boston College	0.4	150	d
Comitato Nazionale Ricerche	0.4	150	d
University of Florence	0.4	150	d
AEC of Greece	0.4	150	d
University of Sao Paulo	0.4	150	d
Royal Military College	0.4	150	d
Magnolia Petroleum Company	0.5	250	p,d
Wells Surveys Inc.	0.5	250	p,d
Bell Telephone Laboratories	1	250	e,X-rays
University of Virginia	1	50	p,d,α
Yale University	1	250	e
Chicago Bridge & Iron Co.	1	250	X-rays
Arnold Green Testing Laboratory	1	250	X-rays
Westinghouse Electric Corp.	1	250	X-rays
Cooper Alloy Corp.	1	250	X-rays
Massachusetts Institute of Technology	1	250	e
Bell Telephone Laboratories	1	250	e
University of California	1	150	p,d
Radio Corporation of America	1	250	e
U.S. Army Quartermaster Corps	1	50 p 250 e	p,d,n,e
Union Carbide Nuclear Corp.	1	50 p 250 e	p,d,n,e,α
Babcock and Wilcox	1	250	X-rays
Austenall Inc.	1	250	X-rays
Pratt and Whitney Aircraft	1	250	X-rays
Oak Ridge National Laboratory (2)	1	250	X-rays
University of California (2)	1	250	X-rays
Rensselaer Polytechnic Inst.	1	50	p,d
New York University	1	50	p,d,n
Brookhaven National Laboratory	1	50	p,d,n
North Carolina State College	1	50	p,d,n
Georgia Institute of Technology	1	50	p,d,n
California Institute of Technology	1	50	p
University of Connecticut	1	50	p,n
Syracuse University	1	50	p,n
Duke University	1		p,n
Texas University	1	50	p
University of Purdue	1 (injector)	250	e
Wright Patterson AFB	1	250	e
Argonne National Laboratory	1	50	d
Dow Chemical Co.	1	250	e,X-rays
Space Technology Laboratory	1	250	e
Bundesforschungsanstalt für Lebensmittelfrischhaltung	1	250	X-rays
Atomic Energy of Canada Ltd.	1	50	α
Physikalisches Institut der Universität Giessen	1	50	p,d,n
CERN	1.5	injector	e

Location	Energy (MeV)	Beam current (micro-amperes)	Particles and radiation
Harper Hospital	2	250	X-rays
Temple University Hospital	2	250	X-rays
Strong Memorial Hospital	2	250	X-rays
S. California Cancer Center	2	250	X-rays
Mt. Sinai Hospital	2	250	X-rays
U.S. Naval Medical Center	2	250	X-rays
University of Chicago	2	50	p
University of Notre Dame	2	100	e,X-rays
Massachusetts Institute of Technology	2	250	e,X-rays
Westinghouse Electric Corp. (2)	2	50 p 250 e	p,d,e, X-rays
Oak Ridge National Laboratory	2	250	e,X-rays
General Electric Company	2	250	e
General Electric Company	2	50	p,d
Stanford Research Institute	2	50	p,d
Evans Signal Laboratory	2	50 p 250 e	p,d,e
Foster Wheeler Corporation	2	250	X-rays
Wright-Patterson Airforce Base	2	50	p
Cornell University	2	250	e
Magnolia Petroleum Company	2	50	p,e
Watertown Arsenal, U.S. Army	2	50	p
U.S. Naval Radiological Defense Laboratory	2	250 e 50 p	p,d,e
U.S. Naval Postgraduate School	2	250 e 50 p	p,d,e
U.S. Naval Research Laboratory	2	250 e 50 p	e,p
Dow Chemical Co.	2	50	p,d,e
W. R. Grace & Co.	2	250	e
Ethicon Company, Div. of Johnson & Johnson	2	250	e
Brookhaven National Laboratory	2	250	e
Shell Development Co.	2	50	p,d
National Bureau of Standards	2	50	p,d
Humble Oil and Refining Co.	2	250	e,X-rays
DuPont de Nemours, Inc.	2	250	e
Union Carbide and Carbon Co.	2	250	e
Ramo Wooldridge-Thompson Products	2	250	e
Texas Nuclear Corp.	2	50	p,d
Socony-Vacuum Oil Co.	2	250	e,X-rays
U.S. Rubber Company	2	250	e,X-rays
Monsanto Chemical Company	2	250	e
Chicago Bridge & Iron Co.	2	250	X-rays
Dow Chemical Co.	2	250	e
U.S. Army Redstone Arsenal	2	50 p 250 e	p,d,e
Thiokol Chemical Corp.	2	250	e,X-rays
Sandia Corp.	2	50 p 250 e	p,d,n,e
American Chain and Cable Co.	2	250	X-rays
University of California	2	250	X-rays
Worcester Polytechnic Inst.	2	50	p,d,n
Watertown Arsenal, U.S. Army	2	250	X-rays
Dow Chemical Co.	2	250	e
National Physical Lab.	2	250	X-rays
Sheffield Nat. Center for Radiotherapy	2	250	X-rays
École Normale Supérieure	2	50 p 250 e	p,d,e
Westminster Hospital, London	2	250	X-rays
Royal Marsden Hospital, London	2	250	X-rays
Royal Infirmary, Edinburgh	2	250	X-rays
Univ. of Bologna	2	250	X-rays
National Univ. of Mexico	2	50 p 250 e	p,d,e

General Electric Co.	2	250	e
Nuclear Propulsion-Brookhaven N.L.	2	250	e,X-rays
Upjohn Co.	2	250	e,X-rays
Massachusetts General Hospital	2	250	X-rays
Tumor Institute, Swedish Hospital	2	250	X-rays
Pondville State Hospital	2	250	X-rays
Lemuel Shattuck Hospital	2	250	X-rays
Baylor University Coll. of Medicine	2	250	X-rays
University Hospital of Cleveland	2	250	X-rays
E. Talmadge Memorial Hospital	2	250	X-rays
Radiation and Medical Research Foundation of the Southwest	2	250	X-rays
Charity Hospital of Louisana	2	250	X-rays
St. Joseph Infirmary	2	250	X-rays
Johns Hopkins Hospital	2	250	X-rays
Hospital of the University of Pennsylvania	2	250	X-rays
Mary Fletcher Hospital	2	250	X-rays
University of Missouri Hospital	2	250	X-rays
Grace New Haven Community Hospital	2	250	X-rays
University of Oklahoma Hospital	2	250	X-rays
Mellon Institute	3	200 p 1000 e	e,p,n,d
Argonne National Lab.	3	200	p,d
Johns Hopkins University	3	200	p,d
Princeton University	3	pulsed	p
American Cyanamid Co.	3	1000	e,X-rays
Aberdeen Proving Ground	3	200	p,d
Case Institute of Technology	3	200	p,d
University of Maryland	3	200	p,d
Florida State University	3	1000	e
U.S. Air Force Cambridge Research Center	3	200	p,d
Stanford University	3	200	p,d
Chance-Vought Aircraft	3	200	p
Duke University	3	200	p,d
N.I.R.S., Japan	3	200	p,d
Weizmann Institute of Science	3	200	p,d
Associated Electrical Industries	3	200	p,d
Canadian Dept. of Defense Production	3	1000	e
Ontario Cancer Institute	3	200	p,d
University of Bonn	3	1000	e
Tsing-Hua University	3	200 p 1000 e	p,d,e
Dept. of Scientific and Industrial Research, New Zealand	3	200 p 1000 e	p,d,e
University of Utrecht	3	200	p,d
University of Algiers	3	200 p 1000 e	p,d,e
Sumitomo Atomic Energy Comm.	3	200 p 1000 e	p,n,d,e
University of Hamburg	3	200	p,d
Laboratori Nazionali de Frascati, University of Rome	3	Pulsed Injector	e
University of Neuchatel	3	200	p,d,n
Shell Amsterdam	3	1000	e,X-rays
Institut für Metalphysik, Aachen	3	400	p
University of Texas	3	200	p
Duke University	4	50	p,d
Brookhaven National Laboratory	4	Injector	p,d,He^3
Centre d'Études Nucléaires de Saclay	4	Injector	p,d
Los Angeles Tumor Institute	2	250	X-rays
University of Oregon Hospital	2	250	X-rays
Memorial Hospital N.Y.C.	2	250	X-rays

Canadian Defense Research Board	2	50	p,d
British Insulated Callenders Cables	2	250	e
Tube Investments Research Lab	2	250	e,X-rays
Badische Anilin und Soda Fabriken	2	250	e
Junta de Energia Nuclear, Lisboa	2	50 p 250 e	p,d,e
Japan Atomic Energy Research	2	50 p 250 e	p,d,e
Compagnie Française de Raffinage	2	250	e
Japanese Chemical and Fibre Assoc.	2	250	e,X-rays
Pirelli	2	250	e,X-rays
University of Reading	2	250	e
University of Lyon	2	50 p 250 e	p,d,e
Electronized Chemical Corp.	2	250	e
École Polytechnique, Paris	2	50 p 250 e	p,e
Comm. Énergie Atomique, Paris	2	50 p 250 e	p,e
Shell Development Co.	3	1000	e,X-rays
Gulf Research and Development Co.	3	1000	e,X-rays
Lockheed Aircraft Company	3	200	p,d
E. I. du Pont de Nemours & Co.	3	1000	e,X-rays
Eli Lilly & Co.	3	1000	e
The Texas Company	3	1000	e
Oak Ridge National Laboratory	5.5	25	p,d
Rice Institute	5.5	25	p,d,t,He^3
Columbia University	5.5	25	p,d
Pennsylvania State University	5.5	50	p,d
Atomic Energy Research Inst., Japan	5.5	20	p,d
Atomic Weapons Research Establishment, England	5.5	20	p,d
University of Strasbourg	5.5	20	p,d
Tata Institute of Fundamental Research, Bombay	5.5	20	p,d
Physikalisches Institut der Universität Freiberg, Germany	5.5	20	p,d
Physikalisches Institut der Universität, Zürich	5.5	20	p,d
A.B. Atomenergi, Stockholm	5.5	20	p,d
University of Padova	5.5	20	p,d
University of Laval	5.5	20	p,d,He
University of Frankfurt	5.5	20	p,d
Tandems			
University of Wisconsin	12	1.5	p
Florida State University	12	1.5	p
Rice Institute	12	1.5	p
California Institute of Technology	12	1.5	p,He
Oak Ridge National Laboratory	12	1.5	p
Argonne National Laboratory	12	1.5	p,He
University of Pennsylvania	12	1.5	p,
Atomic Energy of Canada, Ltd.	12	1.5	p,He
Australian National University	12	1.5	p,He
Physikalisches Institut der E.T.H., Zürich	12	1.5	p
Max-Planck-Institut für Kernphysik, Heidelberg	12	1.5	p
Institut for Teoretisk Fysik, Copenhagen	12	1.5	p
University of Liverpool	12	1.5	p
University of Texas	17	(with 5.5 MeV injection)	p

† These lists of accelerators were compiled and edited by the High Voltage Engineering Corporation and are presented as "News form Industry".

MICROWAVE LINEAR ELECTRON ACCELERATORS

(INSTALLED OR ON ORDER)

Location	Energy (MeV)	Peak pulse current	Radiation power (kW)
Ethicon, Inc., Somerville, N.J.	6		3.75
Ethicon, Inc., Somerville, N.J.	6		7
Elizabeth Steel Magee Hospital, Pittsburg, Pa.	6		0.5
Phillips Petroleum Co., Bartlesville, Okla.	6		4.5
Texas Co., Beacon, N.Y.	6		4.5
Shannon Memorial Hospital, W. Texas	6		0.5
A. O. Smith Corp.	8		3
Thiokol Chemical Corp., Brigham City, Utah	8		5
Osaka Isotope Center, Japan	8.5	200	7.75
Midwestern Irradiation Center, Rockford, Illinois	10		6
Cornell Synchrotron Laboratory	10.7	200	—
Argonne National Laboratory	14	200	—
J.A.E.R.I., Japan	19	160	3.2
Cambridge Electron Accelerator, Cambridge, Mass.	20	250	—
General Atomic, San Diego, Calirfornia	20	200	4.5
Lawrence Radiation Laboratory University of California	26	400 600	—
Rensselaer Polytechnic Institute	35	800	48
Yale University	40	700	28
U.S. National Bureau of Standards	102	242	40

CROCKROFT-WALTON ACCELERATORS

(INSTALLED OR ON ORDER FROM APPLIED RADIATION CORP.)

Location	Energy (MeV)	Beam current (micro-amperes)	Particles accelerated
University of Arkansas	0.4	700	p and d
Phillips Petroleum	0.4	700	p
Los Alamos Scientific Laboratory	0.350	1500	p
Sandia Corp.	0.250	500	p
Army Chem. Center	0.7	1000	p
Ames Laboratory	0.06	10000	p
Ames Laboratory	0.2	10000	p

ISOTOPE SEPARATORS

Mass 1–400 On order for: Brookhaven National Lab.
10–100 mA Argonne National Lab

Mass spectrograph/spectrometers for Chalk River Lab AEC of Canada, Ltd.
Lockheed Aircraft Corp.
University of Strasbourg
Pennsylvania State University
Egyptian Atomic Energy Program
University of Leval, Canada

POWER SUPPLIES

0.6 MeV 8000 microamperes for Brookhaven National Lab.

HIGH VOLTAGE ENGINEERING CORPORATION

BURLINGTON, MASS., U.S.A.

Affiliates

APPLIED RADIATION CORPORATION WALNUT CREEK-CALIF.
ELECTRONIZED CHEMICALS CORPORATION BURLINGTON-MASS.
GLASS GRINDING CORPORATION WHITMAN-MASS.
GOODRICH-HIGH VOLTAGE ASTRONAUTICS, INC. BURLINGTON-MASS.
HIGH VOLTAGE ENGINEERING (EUROPA) N.V. AMERSFOORT – THE NETHERLANDS

Representatives outside the United States

AUSTRALIA
NEW ZEALAND
Watson Victor Ltd.
Watson House, 9–13 Bligh Street
Sydney

BELGIUM
Belgonucléaire S.A.
35, Rue des Colonies
Brussels
(For neutron sources)

GERMANY AUSTRIA
SWITZERLAND
Leybold Hochvakuum Anlagen G.m.b.H.
Bonner Strasse 504
Köln/Bayental

ISRAEL
Eastronics Ltd.
22 Rothschild Boulevard
P.O. Box 2554,
Tel Aviv

ITALY
Alfa Beta Gamma S.r.l.
Via por Santa Maria 8
Florence

JAPAN
Marubeni-Iida Company Ltd.
P.O. Box 595
Tokyo

PORTUGAL
Equipamentos de Laboratorio Lda.
Apartado 458
Lisbon

UNITED KINGDOM EIRE
High Voltage Servicing Co. Ltd.
60 Carpenters Wood Drive
Chorley Wood. Herts. England

SOUTH AFRICA MOZAMBIQUE
Protea Holdings Ltd.
7 Newton Street, Wemmer
P.O. Box 7793
Johannesburg

SWEDEN FINLAND
NORWAY DENMARK
LKB-Produkter
Fabriksaktiebolag
P.O. Box 12220. Stockholm 12

We are pleased to supply on request literature describing the fields of accelerator application

INDUSTRIAL RADIOGRAPHY
ELECTRON-BEAM PROCESSING
PHYSICS RESEARCH
CANCER THERAPY
RADIOBIOLOGICAL RESEARCH
RADIATION CHEMISTRY
NEUTRON ACTIVATION ANALYSIS

Van de Graaff®
Accelerators
0.4 to 15 Mev Energy
Electrons:
up to 1 ma at 3 Mev
Positive Ions:
up to 400 μa at 3 Mev
Neutrons:
up to 10^{12} n per sec

For Research
In Nuclear Physics
Biology & Medicine
Solid State Physics
Radiation Chemistry
Reactor Kinetics

For Application
In Polymerization
Sterilization — Therapy
High Energy Radiography
Catalysis
Nuclear Engineering
and Teaching

LINACS
Microwave Linear Electron Accelerators
4 to 150+ Mev Energy
Peak Pulse Current:
up to 1 ampere
in 0.3 μsec pulses
Neutrons:
up to 10^{16} n per sec
during pulse

160 cm
Electromagnetic Isotope Separator
10 μa of most abundant
isotope in mass range 1 to 400
(Resolving Power: 400)
Ion Sources
Duoplasmatron—200 ma protons
Neutral and Negative
Ion Sources

Cockcroft-Walton
Accelerators
40 to 800 kev Energy
Beam Current:
up to 2 ma
Neutrons:
up to 10^{11} n per sec
Electromagnetic Accelerator
100 to 600 kev Energy
Current Capacity:
up to 8 ma

Beam Pulsing Equipment
Van de Graaff:
1.0 millimicrosecond
up to millisecond
Linacs:
0.1 to 30 μsec pulses

Magnetic Beam Analyzing, Stabilizing and Switching Systems
Ion Lens Systems
Electron Scanners
5″ to 30″

Mass Spectrograph/ Spectrometers
for energy analysis of protons,
deutrons, alpha particles
(Resolving Power: 10^{-3})

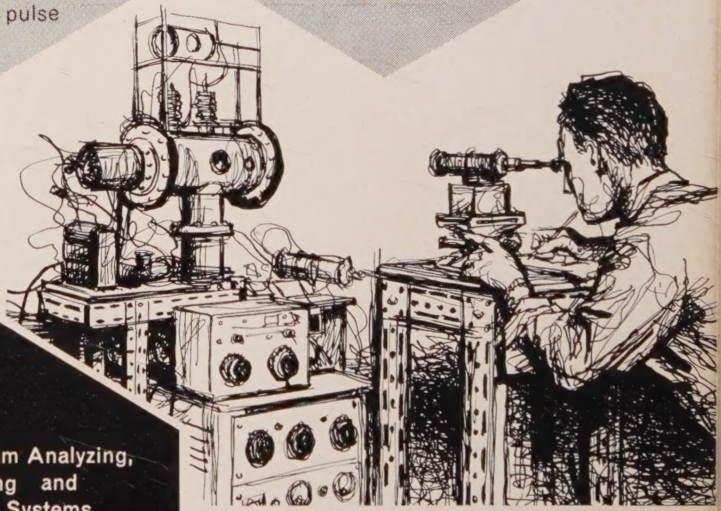

PERFORMANCE SPECIFICATIONS
ALWAYS GUARANTEED

More than 275 particle accelerators by High Voltag
Engineering Corporation and Applied Radiation
Corporation are now installed world-wide

HVEC arc

HIGH VOLTAGE ENGINEERIN
CORPORATION
BURLINGTON, MASSACHUSETTS • U.S.A.

APPLIED RADIATION CORPORATION
WALNUT CREEK, CALIFORNIA, U. S. A.

HIGH VOLTAGE ENGINEERING (EUROPA
AMERSFOORT, THE NETHERLANDS